Springer Series in Optical Sciences 201

V.V. Apollonov

High-Energy Molecular Lasers

Self-Controlled Volume-Discharge Lasers and Applications

Springer

Springer Series in Optical Sciences

Volume 201

Founded by

H.K.V. Lotsch

Editor-in-Chief

William T. Rhodes, Georgia Institute of Technology, Atlanta, USA

Editorial Board

Ali Adibi, Georgia Institute of Technology, Atlanta, USA
Theodor W. Hänsch, Max-Planck-Institut für Quantenoptik, Garching, Germany
Ferenc Krausz, Ludwig-Maximilians-Universität München, Garching, Germany
Barry R. Masters, Cambridge, USA
Katsumi Midorikawa, Saitama, Japan
Herbert Venghaus, Fraunhofer Institut für Nachrichtentechnik, Berlin, Germany
Horst Weber, Technische Universität Berlin, Berlin, Germany
Harald Weinfurter, Ludwig-Maximilians-Universität München, Munchen, Germany

Springer Series in Optical Sciences

The Springer Series in Optical Sciences, under the leadership of Editor-in-Chief William T. Rhodes, Georgia Institute of Technology, USA, provides an expanding selection of research monographs in all major areas of optics: lasers and quantum optics, ultrafast phenomena, optical spectroscopy techniques, optoelectronics, quantum information, information optics, applied laser technology, industrial applications, and other topics of contemporary interest.

With this broad coverage of topics, the series is of use to all research scientists and engineers who need up-to-date reference books.

The editors encourage prospective authors to correspond with them in advance of submitting a manuscript. Submission of manuscripts should be made to the Editor-in-Chief or one of the Editors. See also www.springer.com/series/624

Editor-in-Chief

William T. Rhodes
School of Electrical and Computer Engineering
Georgia Institute of Technology
Atlanta, GA 30332-0250
USA
e-mail: bill.rhodes@ece.gatech.edu

Editorial Board

Ali Adibi
School of Electrical and Computer Engineering
Georgia Institute of Technology
Atlanta, GA 30332-0250
USA
e-mail: adibi@ee.gatech.edu

Theodor W. Hänsch
Max-Planck-Institut für Quantenoptik
Hans-Kopfermann-Straße 1
85748 Garching, Germany
e-mail: t.w.haensch@physik.uni-muenchen.de

Ferenc Krausz
Ludwig-Maximilians-Universität München
Lehrstuhl für Experimentelle Physik
Am Coulombwall 1
85748 Garching, Germany *and*

Max-Planck-Institut für Quantenoptik
Hans-Kopfermann-Straße 1
85748 Garching, Germany
e-mail: ferenc.krausz@mpq.mpg.de

Barry R. Masters
Cambridge
USA

Katsumi Midorikawa
Saitama
Japan

Herbert Venghaus
Fraunhofer Institut für Nachrichtentechnik
Heinrich-Hertz-Institut
Einsteinufer 37
10587 Berlin, Germany
e-mail: venghaus@hhi.de

Horst Weber
Optisches Institut
Technische Universität Berlin
Straße des 17. Juni 135
10623 Berlin, Germany
e-mail: weber@physik.tu-berlin.de

Harald Weinfurter
Sektion Physik
Ludwig-Maximilians-Universität München
Schellingstraße 4/III
80799 München, Germany
e-mail: harald.weinfurter@physik.uni-muenchen.de

More information about this series at http://www.springer.com/series/624

V.V. Apollonov

High-Energy Molecular Lasers

Self-Controlled Volume-Discharge Lasers and Applications

Springer

V.V. Apollonov
General Physics Institute of the Russian
Academy of Sciences
Moscow
Russia

ISSN 0342-4111 ISSN 1556-1534 (electronic)
Springer Series in Optical Sciences
ISBN 978-3-319-33357-1 ISBN 978-3-319-33359-5 (eBook)
DOI 10.1007/978-3-319-33359-5

Library of Congress Control Number: 2016941323

© Springer International Publishing Switzerland 2016
This work is subject to copyright. All rights are reserved by the Publisher, whether the whole or part of the material is concerned, specifically the rights of translation, reprinting, reuse of illustrations, recitation, broadcasting, reproduction on microfilms or in any other physical way, and transmission or information storage and retrieval, electronic adaptation, computer software, or by similar or dissimilar methodology now known or hereafter developed.
The use of general descriptive names, registered names, trademarks, service marks, etc. in this publication does not imply, even in the absence of a specific statement, that such names are exempt from the relevant protective laws and regulations and therefore free for general use.
The publisher, the authors and the editors are safe to assume that the advice and information in this book are believed to be true and accurate at the date of publication. Neither the publisher nor the authors or the editors give a warranty, express or implied, with respect to the material contained herein or for any errors or omissions that may have been made.

Printed on acid-free paper

This Springer imprint is published by Springer Nature
The registered company is Springer International Publishing AG Switzerland

To the blessed memory of my teacher and colleague—Acad. A.M. Prokhorov

This book is dedicated to the great man of XX century Nobel prize winner and my teacher Acad. A.M. Prokhorov. The research presented in this book was done together and scientific influence of A.M. Prokhorov was very intense and helpful. The following is my reminiscence about him.

Preface

The goal of the present book is to introduce the investigation that was carried out to improve understanding of the formation characteristics of a self-controlled volume discharge for the purposes of pumping molecular lasers, i.e. self-sustained volume discharge (SSVD), which involved a preliminary filling of a discharge gap by an electron flux from an auxiliary-discharge plasma. We found that this method was suitable for large inter-electrode gaps, that distortion of the electric field in the gap by the space charge of the electron flux played an important role in the formation of the discharge and that the electrodes could be profiled dynamically during propagation of an electron flux through the discharge gap and an SSVD could form in systems with a strongly inhomogeneous field. High power SSVD-based CO_2 laser systems with an output of up to 30 kJ have been created, investigated and discussed in the book.

The second chapter of the book is devoted to another type of SSVD without pre-ionization, i.e. a self-initiated volume discharge (SIVD), in non-chain HF lasers with SF_6-C_2H_6 mixtures. We have established that, after the primary local electrical breakdown of the discharge gap, the SIVD spreads along the gap in directions perpendicular to that of the electric field by means of the successive formation of overlapping diffuse channels under a discharge voltage close to its quasi-steady state value. It is shown that, as new channels appear, the current following through the channels formed earlier decreases. The volume occupied by the SIVD increases with increase in the energy deposited in the plasma and, when the discharge volume is connected with a dielectric surface, the discharge voltage increases simultaneously with the increase in the current. The possible mechanisms to explain the observed phenomena, namely the dissociation of SF_6 molecules and electron attachment SF_6 molecules, are examined. A simple analytical model, which makes it possible to describe these mechanisms at a qualitative level, was developed. High power SIVD-based HF(DF) lasers with an output of up to 1 kJ have been developed, tested and evaluated.

The third part of the book discusses a wide spectrum of short pulse laser systems and investigations of different methods of high-power nanosecond pulses selection

from large-aperture CO_2 oscillators. In particular, we discuss a regenerative CO_2 amplifier of a nanosecond pulse train, nanosecond pulse transmission of buffered SF_6 at 10.6 μm and 20 J nanosecond locked oscillator (pulse CO_2 laser system based on an injection mode). Creation of N_2O laser pumped by an SSVD and experimental problems of high efficiency for an electric-discharge N_2 laser are based on the same technology of sophisticated electric discharge and are also included in this part of the book.

The final, fourth part of the book is devoted to a set of different applications for high energy molecular lasers, such as stimulation of a heterogeneous reaction of decomposition of ammonia on the surface of platinum by CO_2 laser radiation. A number of interesting investigations are discussed in this part, including the influence of the pumping regime on lasing of an He-Xe optical-breakdown plasma; formation of the active medium in lasers with rare-gas mixtures pumped by optical breakdown; low-threshold generation of harmonics and hard X-ray radiation in laser plasma. Interaction of CO_2 laser nanosecond pulse train with the metallic targets in optical breakdown regime and probe investigations of close-to-surface plasma produced by CO_2-laser nanosecond pulse train are of particular interest. Finally, the wide aperture picosecond CO_2 laser system and new applications of short pulse laser systems conclude this chapter.

This book will be of very high interest to a wide audience, including students, scientists, teachers, and those with an intellectual interest in the area.

Moscow, Russia V.V. Apollonov

A Talented Person is Talented in Everything

I was lucky to work with A.M. Prokhorov for more than 32 years and, every time revealing new facets of his many talents; I was always amazed by the genius of this great man. What, above all, comes to my mind about this extraordinary man now that he is no longer with us? His incredibly developed sense of intuition; his striking ability to find the right solutions quickly; his heightened sense of the new that would be fundamentally significant for a leap into the future; and his humaneness. I believe that the feeling of being at the front edge of science and its development trends are perhaps the most important characteristics of this phenomenal scientist! Anyone who had a chance to work and communicate with A.M. Prokhorov, even for a short time, was blessed with this feeling.

The Institute, at the stage of its formation, was lucky to have a leader like this. Even at most difficult times, this feeling did not leave those who, despite all the hardships, continued to work actively. The constant state of extreme stress to find the only right solution could turn, by an experienced hand of the Master, into unbridled joy, witticism or a joke. If during a meeting at a seminar one did not burst into laughter at a witty word used to relax the situation, it meant that he did not understand something, that he was not in shape. Loud laughter from the office, from time to time heard even in remote parts of the corridor, said: Everything is OK. We continue to move forward. We live.

A.M. Prokhorov did not like jokes that were not to the point. His style was when the joke was in one sentence, touching upon an important issue with a master's hand. Let me remind you of the interview given to NTV correspondent Pavel Lobkov about the causes of failure of Russian candidates for the Nobel Prize. Pavel pondered indecently long over the meaning of the appropriate final sentence voiced by A.M. Prokhorov in defense of V.S. Letokhov. The phrase "he who pays the piper calls the tune" was certainly about the role of America in decision making of the Nobel committee. A.M. Prokhrov's colleagues at the Institute got accustomed to good humor, which was undoubtedly to his credit.

Fig. 1 Acad. A.M. Prokhorov and author of the paper at the meeting (30th of December 2001)

The ability to take a decision, even in an insanely difficult situation when one gives up the fight, is also what he taught us to do. It was important for him to think, first of all, about the common cause rather than about himself, and he wanted us not to be afraid of making a mistake. Any mistake can be corrected, but the time lost to the cause will never come back. A good example here is a series of decisions made during the Perestroika Years. Here is one of them. In the most difficult moment, when the science "was just thrown overboard", it was necessary to quickly interpret the phrase "one can do anything that is not prohibited by law". "Where to get money for science in order to be useful tomorrow when once again the Motherland will become aware of the greatness of scientific progress?"—That was what we had to think about, standing on the ashes of the former Soviet Union. The solution was simple and effective: freedom was given to departments and laboratories to conduct foreign economic activity via contracts and grants. And it was in those times when neither accounting nor planning departments simply had specialists for 'shoveling' piles of papers written in all sorts of foreign languages. Several dozens of world-famous scientists from the Institute, who traveled around the world and clearly understood how the capitalist-world economy with its mostly contractual form of science financing works, quickly adapted to the changing situation and ensured a smooth transition. Now, when everybody understands everything and gives 'valuable' advice to others, much seems trivial. But then, it was necessary to find an effective way out of the situation and to take the right decision, which now produces significant results.

Now, a few words about acad. A.M. Prokhorov as an educator. In fact, A.M. Prokhorov was an outstanding educator of young and not so young talents. But what rules did he follow? Democratic approach to everything and a sense of fairness and equity to everybody. Even his son, who now works at the Institute, often caught it from his father. No privileges! Everybody at the Institute knew that he would be listened to and supported. One cannot carve the future on regalia and merits of the past, which is why we had to prove our rightness every day, because the fact that you were right yesterday did not matter. Everyday someone was wrong in a dispute, but that was not a reason to mock at. Tomorrow things could change. Everybody knew that we need to work and everything will be fine. Prokhorov's casual question: "What's new?"—And, almost at once, his answer with a smile on his face —"Nothing!" It was a usual, very conventional phrase to start a conversation the next day. Yes, last night we all went home, and this morning there could and should be news of scientific nature, of course. The Institute is the Shrine of Science, where research is a continuous process.

In our lives we spend too much time in the laboratory, often losing touch with reality and with small things, of which our life outside the laboratory, in general, consists. We often need to do something for our child, to help our mother or to give a supporting hand to a close relative, etc. At the same time, there are very serious situations when help is most needed. And here (moreover, it was well known in the scientific world), the best solution was to ask A.M. Prokhorov. His heart will be open for you. Not only colleagues from our Institute but also from other Institutes asked him for help. And everybody knew that he will not refuse. And everybody knew that if there is an opportunity to help, he will certainly do it. I do not know whether time will come when it is no longer necessary to help people, but I know for sure that Prokhorov's office is not spacious enough to accommodate all those whom he helped.

A natural easiness to communicate with others is another distinguishing feature of A.M. Prokhorov. He always showed patience and respect, no matter if his interlocutor was a student or a government bureaucrat. Communication with him was inspiring. Of importance was intelligence—intrinsic essence of civilization development—of the interlocutor. No wonder that in such situations people felt at ease, finding new opportunities for self-expression and having a surge of creative forces, which they really liked themselves.

I remember an interesting meeting of A.M. Prokhorov with Mr. M. Shikaya, the Tokyo Metropolitan governor, in Japan. I was fortunate to be part of this meeting. The Japanese, who had already got a feel of visitors from Russia, instructed our delegation for a few minutes about things they considered appropriate for their century-old principles and rules of good manners in their homeland. We found out that we could talk about flowers, nature and health. All other topics of conversation could be construed as improper. You should have seen the faces of these instructors a few minutes after a conversation between Prokhorov and Shikaya started. They talked as if they had known each other since childhood and they were incredibly happy with the possibility of communicating with each other. In this life, when eternity is born in the hands of such people, to spend time talking about flowers and

bows just means not to respect each other. Apparently, this protective form of communication is introduced in Japan in the event of visitors from Russia, who can talk only about credits and dividends on favorable terms, which, of course, is extremely important today. This is humanly understandable, though still not to all.

A.M. Prokhorov was not only a scientist by profession. He was, as they say, a physicist to the bone. Moreover, his habits were even physically correct. Here is one of them: He loved it when it is warm, even hot (so hot that I would compare it with the Sahara Desert) in his office. "Why to warm the office with the warmth of human bodies? What is the average temperature of a normal person? 36.6 °C! So, here we are!" It was almost physically impossible to linger in his office for a long time. Heaters stood at the window, directly behind the visitor and quite close to the visitor's back. Thus, for someone it was thermodynamic equilibrium, but for someone it was nothing but thermal screening of the boss. However, it was only the smallness of the space surrounding him, because no space could accommodate the greatness of this man.

Now a few facts about intuition of this great scientist. I would say about his great intuition! I will not talk about his anticipation of the laser era. Much has already been said about it and even much more will be written by those who were next to him at that crucial period of his life. I should talk about things I witnessed myself and about projects I directly participated in.

It is difficult to overestimate the importance of lasers in solving the problems of medicine and biology. Even at the dawn of laser revolution, when military men were overexcited about possible applications of lasers in the country's defense, A. M. Prokhorov began to actively introduce into the consciousness of the Institute staff and civilians the ideas about the effective use of laser methods of treatment of patients and the use of lasers in biological research. Today, in our country and abroad well-known are the methods of laser treatment of urolithiasis, laser eye surgery, bloodless laser surgery, TB treatment, diagnosis and treatment of skin diseases, laser hair removal, etc. Now it is impossible to imagine how doctors could treat patients without lasers and laser methods of diagnostics and therapy.

One more example directly concerns military applications. Lasers can be used and actively applied in solving military tasks, and this fact is no longer a secret. They cut, melt, reduce the mechanical stability of structures, allow the transfer of mechanical momentum and provide a power regime of destruction of military equipment. Moreover, lasers can do all these things at considerable distances. No wonder that the attention of professionals from the Ministry of Defense was drawn to the prospect of the use of lasers for military purposes. To solve the problem of ballistic missile warhead interception in the framework of the Strategic Defense Initiative, our country and the USA spent a huge amount of money. To a large extent, this stage of confrontation with the United States undermined our economy and led to the collapse of the Soviet Union. But there is another regime of destruction of military equipment, i.e., functional impact regime (the Americans call it "smart" impact), which is, in fact, today the main one in research and applications. There is no need to "cut" or "drill holes", which requires a lot of energy and is totally ineffective. All you need is the timely laser impact on a target, which in a

large number of cases will be sufficient to disrupt the mission. Prokhorov wrote about it in his letter to the Minister of Defense of the USSR. And just imagine, it was in 1973, i.e., 12 years before the beginning of Reagan's "Strategic Defense Initiative". If only the society were ready for it, if only ... On the contrary, our country got involved in this senseless race and lost a lot. Americans also lost. But they were much richer and it saved them.

Now about Prokhorov's fame in the world and his role in the development of mankind and in pushing the society forward, which are the main goals of geniuses, who are born, once in a while, on the planet Earth.

The Nobel Prize is a recognized indicator of outstanding abilities of a particular individual. But we all well know that "not all yogurts are created equal". Among the several hundred Nobel laureates there are geniuses of mankind, who received this award for the revolutionary transformation of life on the Earth. The Nobel Prize for laser and maser principles of generation and amplification of electromagnetic radiation with the effect of stimulated emission in quantum transitions of atomic and molecular systems is one of them. Today, it is impossible to imagine our life without lasers and their wide range of applications. This discovery stands in one line with the electron's discovery, electromagnetism, nuclear energy, penicillin, evolutionary principles of biological life on earth, chemical transformations of elements, transistors (basic elements of electronics, computers), etc. Nevertheless, it is simply impossible to work out a kind of a unified scale of values of certain discoveries. Moreover, it is difficult to take on the function of an arbitrator in this competition. Here I want to resort to the help of the Internet—a highly respected tool in the hands of the scientific world. We will google "who is who" in the world, at least on the basis of a small sample of widely cited scientists, artists and politicians. On the April 2003, this list of several prominent figures with a coefficient of "scientific fertility" looked like this:

(1) Aleksandrov A.P.—108
(2) Basov N.G.—700
(3) Brezhnev L.I.—611
(4) Gorbachev M.S.—548
(5) Yeltsin B.N.—19
(6) Keldysh M.V.—715
(7) Primakov E.M.—151
(8) Prokhorov A.M.—2160!!!
(9) Pugacheva A.B.—8
(10) Stanislavsky K.S.—159
(11) Townes Ch.—1190
(12) Chubais A.B.—100

This is a certain projection of the view on the problem, and nothing more, but rather indicative and informative I should say. Having looked through all the pages related to one or another known name on the Internet you become fully aware of the role of the individual in history and of the range of his creative interests. But do not overestimate the role of this kind of projection. Evaluation, of course, must be

multi-faceted and it is the business of historians. Nevertheless, I believe that sooner or later the situation will improve, and the role of science and its geniuses will occupy its rightful place in our country, where even today the hierarchy of values is still unfortunately significantly oriented towards those, who squander public property, natural resources and give practically nothing in return to their Motherland.

A talented person is talented in everything! It is well known that "we should step back for better observation". As time goes by, we go further from the point of parting with our teacher and friend. The sharp pain of loss softens, and small, insignificant details, which are totally unimportant in the image of this giant of humanity, disappear. What is left is an increasingly growing, irresistible sense of the continuing impact of this GREAT MAN on us and on the development of physical science, to which we—his disciples and associates—continue to faithfully serve today. And yet the soul overflows with gratitude to Fate for being for many years with this rock of a man, an outstanding naturalist of the 20th century and a patriot of Russia—Academician Aleksandr Mikhailovich Prokhorov.

Fig. 2 11th of July 1996—Jubilee of A.M. Prokhorov V.V. Apollonov presents his painting to A.M. Prokhorov.

Intuition. Step in the Universe. 11th of July 1996

On the top. 11th of July 1991

Where you are my scholars? 11th of July 2001

During long period of time a few jubilees of our leader took place and my paintings prepared for that particular events are represented here in the book.

Acknowledgements

The author expresses his gratitude to N. Akhunov, G.G. Baitsur, V.I. Borodin, S.A. Chetkin, S.I. Derzhavin, K.N. Firsov, K.Kh. Kazakov, I.G. Kononov, V.N. Motorin, V.V. Ostanin, S.A. Savranskii, A.G. Safronov, S.K. Semenov, Yu.A. Shakir, S.F. Sholev, V.A. Shurygin, A.A. Sirotkin, V.R. Sorochenko, G.V. Vdovin, Yu.P. Voinov, V.A. Yamshchikov, S.I. Zienko. During the work in the field of high energy molecular lasers and important new applications, the author of this book was the scientific supervisor and scientific advisor of separate studies conducted in conjunction with the above researchers.

The author also believes it important to note the fruitful cooperation with A.J. Alcock, A.A. Aliev, A.I. Artemyev, O.D. Baklanov, H.A. Baldis, A.I. Barchukov, A.A. Belevtsev, R.E. Beverly III, V.D. Borman, F.V. Bunkin, G.V. Bush, Yu.I. Bychkov, P.B. Corkum, A.V. Ermachenko, M.V. Fedorov, B.A. Frolov, A.E. Hill, D.S. Joins, Yu.L. Kalachev, N.V. Karlov, S.Yu. Kazantsev, V. Khmelev, V.I. Konov, I.N. Konovalov, O.B. Kovalchuk, V.V. Kralin, A.A. Kuchinsky, B.B. Kudabaev, N.V. Kudrov, G.P. Kuzmin, V.F. Losev, G.A. Mesyats, V.R. Minenkov, J.-C. De Miscault, P.I. Nikitin, B.I. Nikolaev, V.F. Oreshkin, S.S. Pel'tsman, N.V. Pletnyev, D.A. Polukhin, A.M. Prokhorov, N.A. Raspopov, R.E. Rovinskii, V.E. Rogalin, A.V. Saifulin, A.A. Sazykin, B.V. Semkin, B.G. Shubin, V.M. Sobolev, E.A. Sviridenkov, A.G. Suzdaltsev, V.F. Tarasenko, R.S. Taylor, V.I. Troyan, I.S. Tsenina, V.P. Tomashevich, E.E. Trefilov, N.D. Ustinov, D.M. Velimamedov, Yu.M. Vas'kovskii, R. Walter, A. Watanabe, A.V. Yushin, N.S. Zakharov and M.I. Zhavoronkov, all of whom made significant contributions to the development of high energy molecular lasers and new important applications.

Moscow, Russia V.V. Apollonov

Contents

Part I High Energy Pulsed CO_2 Lasers

1 Carbon Dioxide Laser with an Output Energy of 3 kJ, Excited in Matched Regime 3
References 7

2 SSVD in Long Gaps Containing CO_2–N_2–He Mixtures 9
References 13

3 Carbon Dioxide Laser with a Variable Output Pulse Duration 15
References 18

4 Efficiency of Utilization of Certain Readily Ionized Substances for Discharge Stabilization in CO_2 Lasers 19
References 23

5 Electric Discharge CO_2 Laser with a Large Radiating Aperture 25
5.1 Introduction. 25
5.2 General Propositions 26
5.3 Experimental Part. 27
5.4 Experimental Results and Discussion 29
References 32

6 Formation of an SSVD with Intense Ultraviolet Irradiation of the Cathode Region 35
References 41

7 High-Energy Electric-Discharge CO_2 Laser with Easily Ionizable Substances Added to the Mixture. 43
7.1 Introduction. 43
7.2 Apparatus 44
7.3 Volume Discharge Characteristics 44

7.4 Optimization of Laser Output Characteristics 46
7.5 Conclusions 48
References 48

8 Formation of a Spatially Homogeneous Discharge in Large-Volume CO_2–N_2–He Gas Mixtures 49
References 51

9 Stability of an SSVD in a CO_2–N_2–He Gas Mixture with Easily Ionizable Additives 53
References 56

10 Formation of an SSVD for the Pumping of CO_2 Lasers 57
10.1 Introduction. 57
10.2 Experimental Setup 58
10.3 Model of Propagation of an Electron Flux. 60
10.4 Results of Experiments and Discussion 63
10.5 Conclusions 70
References 71

11 Mechanism of Formation of an SSVD Initiated by a Barrier Discharge Distributed on the Surface of a Cathode 73
References 77

12 Formation of an SSVD for Pumping of Gas Lasers in Compact Electrode Systems 79
References 81

13 Large-Aperture CO_2 Amplifier 83
References 85

14 Dynamic Profiling of an Electric Field in the Case of Formation of an SSVD Under Conditions of Strong Ionization of the Electrode Regions. 87
References 90

15 Small-Signal Gain of CO_2 Lasers Pumped by an SSVD 91
References 94

16 Feasibility of Increasing the Interelectrode Distance in an SSVD by Filling the Discharge Gap with Electrons 97
References 100

17 Influence of Easily Ionizable Substances on the Stability of an SSVD in Working CO_2 Laser Mixtures 101
References 106

18 Dynamics of Population of the $A^3\Sigma_u^+$ Nitrogen Metastable State in an SSVD of a Pulsed CO_2 Laser 107
References 111

19 High-Energy Molecular Lasers Pumped by an SSVD 113
19.1 Introduction. 113
19.2 Discharge Stability 114
19.3 Initial Electrone Concentration. 119
19.4 Dynamic Profiling in the Discharge Gap 122
19.5 CO_2 Lasers Pumped by the Discharge 127
19.6 Characteristics of an Active Medium and Scalability 127
19.7 N_2O Lasers 128
19.8 Conclusions 132
References 132

20 N_2O Laser Pumped by an SSVD 135
References 138

21 CO_2- and N_2O-Lasers with Preliminary Filling of the Gap by Electrons 139
21.1 Necessary Conditions for Preionization and Field Enhancement. 140
21.2 Discharge Preionization and Ignition Model 141
21.3 Method of Solution and Rate Data 144
21.4 Discharge Ignition Phenomena. 146
21.4.1 CO_2 Lasers 146
21.4.2 N_2O Lasers 149
21.5 Discussion and Conclusions 151
References 152

22 Modeling of Large-Aperture CO_2-Lasers 155
22.1 Excitation Waveform Requirements 156
22.1.1 Single-Pulse Waveforms 156
22.1.2 Double-Pulse Waveforms 157
22.1.3 Minimum Ignition Voltage 158
22.2 Coupled-Particle Kinetics-Equivalent Circuit Model 158
22.3 Pulsed Power Systems 161
22.4 Computational Results 162
22.4.1 Single-Pulse Excitation Without Quasi-DC Bias. 162
22.4.2 Single-Pulse Excitation with Quasi-DC Bias 164
22.4.3 Double-Pulse Excitation 167
22.5 Conclusions 169
References 170

Part II High Energy HF/DF Lasers

23 Non-chain High Radiation Energy Electric-Discharge HF(DF) Lasers 173
References 177

24 SIVD in Nonchain HF Lasers Based on SF_6-Hydrocarbon Mixtures 179
24.1 Introduction. 179
24.2 Experimental Apparatus 180
24.3 Experimental Results 182
24.4 Discussion of the Results 191
24.5 Conclusions 194
References 194

25 Discharge Characteristics in a Nonchain HF(DF) Laser 197
References 201

26 Ion–Ion Recombination in SF_6 and in SF_6–C_2H_6 Mixtures for High Values of E/N 203
26.1 Introduction. 203
26.2 Experimental 204
26.3 Results of Measurements 206
26.4 Discussion of Results 207
26.5 Conclusions 212
References 213

27 SSVD Instability of Nonchain HF(DF) Laser Mixture 215
27.1 Introduction. 215
27.2 Experimental Setup 216
27.3 Experimental Results 218
27.4 Results and Discussion 220
27.4.1 Nonlinear Mechanism of Ionization Development in Active Media of HF/DF Lasers 4.1. 220
27.4.2 Self-Organization of SSVD Plasma upon Laser Heating of SF_6-Based Mixtures 223
27.4.3 Mechanism of Evolution of Conducting Channels in SF_6 and Its Mixtures. 224
27.5 Conclusions 224
References 225

28 Dynamics of a SIVD in Mixtures of Sulfur Hexafluoride with Hydrocarbons 227
28.1 Introduction. 227
28.2 Experimental Investigation 228
28.3 Conclusion 230
References 230

29 High-Energy Nonchain HF(DF) Lasers Initiated by SSVD 231
29.1 Introduction. 231
29.2 Features of SSVD in the Mixtures of SF_6 with Hydrocarbons or with Deuterocarbons 232
29.2.1 Possibility of Obtaining an SSVD Without Preionization 232
29.2.2 Obtaining an SSVD in a System of Electrodes with High Edge Nonuniformity 237
29.2.3 SSVD Stability in Mixtures of SF_6 with Hydrocarbons or Deuterocarbons 239
29.3 Scaling of Nonchain HF/DF Laser 240
29.4 Conclusion 242
References 242

30 SSVDs in Strongly Electronegative Gases 243
30.1 Introduction. 243
30.2 Experimental Investigation 244
30.3 Conclusions 246
References 246

31 High-Energy Pulse and Pulse-Periodic Nonchain HF/DF Lasers 247
31.1 Introduction. 247
31.2 SIVD—a New Form of an SSVD 248
31.2.1 What Is an SIVD? 248
31.2.2 The Mechanisms of Restriction of a Current Density in Diffuse Channels of SIVD in SF_6 and Mixtures of SF_6 with Hydrocarbons and Deuterocarbons 255
31.2.3 Stability and Uniformity of SIVD 259
31.3 Nonchain HF(DF) Lasers Excited by an SIVD. 262
31.3.1 The Operation Features of Pulse and Pulse-Periodic Nonchain HF(DF) Lasers with Small Apertures and Active Medium Volumes 262
31.3.2 Wide Aperture Nonchain HF(DF) Lasers Excited by SIVD. 266
31.4 Conclusions 266
References 268

32 UV-Preionization in Nonchain HF Lasers with a SSVD to Initiate Chemical Reaction 271
32.1 Introduction. 271
32.2 Experimental Setup 272
32.3 Experimental Results 273

32.4 Discussion 276
32.5 Conclusion 278
References 278

Part III Short Pulse Laser Systems

33 Selection of High-Power Nanosecond Pulses from Large-Aperture CO_2 Oscillators 281
References 285

34 Nanosecond Pulse Transmission of Buffered SF_6 at 10.6 μm 287
34.1 Introduction. 287
34.2 Experimental Procedure 288
34.3 Results and Discussion 289
34.4 Laser Applications 294
34.5 Conclusions 295
References 296

35 20-J Nanosecond-Pulse CO_2 Laser System Based on an Injection-Mode-Locked Oscillator 299
References 304

36 Numerical Simulation of Regenerative Amplification of Nanosecond Pulses in a CO_2 Laser 305
References 309

37 Regenerative CO_2 Amplifier of a Nanosecond Pulse Train 311
37.1 Introduction. 311
37.2 Experimental Set up 315
37.3 Conclusion 317
References 318

38 Regenerative CO_2 Amplifier with Controlled Pulse Duration 319
References 323

39 Efficiency of an Electric-Discharge N_2 Laser 325
References 332

Part IV Applications

40 Stimulation of a Heterogeneous Reaction of Decomposition of Ammonia on the Surface of Platinum by CO_2 Laser Radiation 335
References 339

41 Influence of the Pumping Regime on Lasing of an He-Xe Optical-Breakdown Plasma 341
41.1 Introduction. 341
41.2 Apparatus 342
41.3 Experimental Results 343
41.4 Discussion of Results 346
References 348

42 Formation of the Active Medium in Lasers with Rare-Gas Mixtures Pumped by Optical Breakdown 349
References 352

43 Low-Threshold Generation of Harmonics and Hard X-Ray Radiation in Laser Plasma 353
43.1 Experimental Results and Discussion 353
43.2 Conclusion 357
References 357

44 Probe Investigations of Close-to-Surface Plasma Produced by CO_2-Laser Nanosecond Pulse Train 359
44.1 The Experimental Set up. 360
44.2 Experimental Results 362
References 365

45 Interaction of CO_2 Laser Nanosecond Pulse Train with the Metallic Targets in Optical Breakdown Regime 367
45.1 Introduction. 367
45.2 Numerical Calculation of Regenerative Amplification 368
45.3 Experimental Set up 371
45.4 Measurements of the Breakdown Thresholds 374
45.5 The Results of Investigations of the Electric Field and Current 374
45.6 The Investigation of Laser-Target Energy Transmission 376
45.7 Conclusion 377
References 377

46 Wide Aperture Picosecond CO_2 Laser System 379
46.1 Introduction. 379
46.2 New Approach to the CO_2–HPA Construction. 380
46.3 Description of the Laser System 381
46.3.1 Master Oscillator 381
46.3.2 High Pressure CO_2 Amplifier. 383
46.4 Discharge Pump Pulsed High-Voltage Generator 384
46.5 Estimation of the Individual Pulses Duration in the Train 386
46.6 Prospect of the Laser System Upgrading. 388
46.7 Conclusions 390
References 390

47 Lasers for Industrial, Scientific and Ecological Use 393
47.1 Introduction: The New Era of High Energy Lasers 393
47.2 Comparison of Some Types of Lasers That Can Be Scaled up to the Average Power Level >100 kW 395
47.3 Mobile CO_2-AMT GDL 396
47.4 Efficiency Increase of the AMT GDL by Additional Chemical Pumping 399
47.5 High Repetitive Pulsed Regime of the AMT GDL 399
47.6 New Approach to High Energy Lasers—Mono-Module Disk Laser 399
47.7 Conclusions 405
References 405

48 Generation of a Submillimeter Half-Cycle Radiation Pulse 407
References 412

49 High Power CO_2-Laser Radiation Conversion with $AgGaSe_2$ and $AgGa_{1-x}In_xSe_2$ Crystals 413
49.1 Introduction 413
49.2 Crystal Samples Investigation 413
49.3 Calculations 415
49.3.1 Phase Matching Characteristic 415
49.3.2 Efficiency of Difference Frequency Generation 416
49.3.3 Half-Cycle Pulse 418
49.4 Conclusion 418
References 418

50 Subtraction of the CO_2 Laser Radiation Frequencies in a $ZnGeP_2$ Crystal 421
References 424

51 Self-controlled Volume Discharge Based Molecular Lasers Scaling 425
References 429

Index 431

About the Author

V.V. Apollonov is the leading specialist in the area of basic principles of creation and the development of high power laser systems and high power laser radiation interaction with matter. He has made an outstanding input into the creation and development of new branches of science, including work in the following areas: physical and technical fundamentals of high power laser optics and adaptive optics; investigation of physical processes in a high volume self-controlled volume discharges; creation of high power continuous wave; pulsed and high repetition rate pulse-periodic laser systems; high intensity laser radiation interaction with matter; high power laser application for an effective protection of valuable objects; and water surface cleaning from oil films and medical applications for UV lasers.

Recent results of his investigations relating to the laser diode arrays phase-locking, mechanisms of shock waves merging for a rockets launch by high repetition rate pulse-periodic laser light, super long conductive channel based on the electrical breakdown in a dust plasma produced by mechanism of ablation, high repetition rate optical pulsating discharge applications, space debris elimination by laser, scalable mono-module disk laser and high power laser applications in the Arctic are under very intensive implementation in Russia and abroad. He is the author of more than 1300 publications (14 books, 359 presentations and 147 patents, 750 articles (Research Gate)).

V.V. Apollonov is a high profile scientist and is well known all over the world. Spanning more than 45 years, he has participated and organized more than 58 international conferences, symposiums and workshops, prepared more than 32 candidates and doctors of physics and mathematics. For the last 5 years, his scientific group has fulfilled more than 60 R&D contracts with customers from Japan, UK, Germany, France, China, Korea, Singapore and USA. www.gpi.ru/hpl He is the General Director of "Energomashtechnika" Ltd.

V.V. Apollonov is the member of European and American Physical Society, SPIE, AIAA, American Society for QE and the member of specialized scientific council of Russia. He is a full member of Russian Academy of Natural Science and Academy of Engineering Sciences, member of the Presidium RANS. He is the laureate of State Prize of USSR (1982) and of Russia (2002).

Introduction

The widespread use of pulsed gas lasers in various fields of science and engineering accounts for their extensive investigation over many years. In electroionization devices with apertures as large as 30 cm, maximum radiation loads on the optical elements were already attained by the mid-1970s. Any further increases in laser output energies were presumably related to larger apertures. However, solving the problem of limitations on output by operating several lasers in parallel presents great technical difficulties. An alternative method is to enlarge the aperture of a single molecular laser. The electroionization approach to the problem proved impracticable because the voltages on the accelerator were too high and because the critical restriction imposed on the transverse dimensions of the discharge zone by the discharge-induced magnetic field affected the trajectory of accelerated electrons.

To better understand all features of non-SSVD, an investigation of a CO_2 laser with pulsed pumping of a gas cell in the matched regime was carried out and described. The total energy of the output radiation was 3 kJ when the pressure of the mixture was 2 atm and the active volume was 50 l. When the active volume was 12 l, the energy deposited in a mixture of the CO_2:N_2:He = 1:2:2 composition was 0.6 kJ l^{-1} atm^{-1} and the radiation energy was $\sim$80 J l^{-1} atm^{-1}.

This restriction on the discharge zone transverse dimensions is removed if a CO_2 laser is pumped by an SSVD. It is, however, far less stable than a non-SSVD. Furthermore, the actual scalability of the aperture is limited by the difficulty involved in reaching the required concentrations of primary electrons at long electrode separations, as well as by the size and shape of electrodes. According to the notions that were generally adopted in the early 1980s, these difficulties could not be eliminated in gas lasers pumped by an SSVD. Primary electrons in the discharge gap were believed to be the result of gas ionization caused either by radiation or by fast particles, while uniform excitation of the laser active medium was thought to be possible only in a uniform electric field set up by electrodes of specific shapes.

It is known that an SSVD can be established in a gas by creating primary electrons, the density of which should exceed a certain minimum value n_{min} throughout the discharge gap. Various methods for preionization of a gas in the

discharge gap have been developed for this purpose. Primary electrons are created by these methods directly in the discharge gap, which sometimes causes difficulties in the establishment of conditions necessary for the formation of an SSVD. For example, high voltages are needed for the formation of an initial plasma when the preionization source and the active medium are combined in the same volume, whereas preionization with ultraviolet radiation may be ineffective because of strong absorption of such radiation in a medium, and if soft x rays are used, it is necessary to ensure rigid synchronization of the x-ray and pump sources.

In mixtures of gases typical of CO_2 lasers, losses of electrons due to trapping are relatively small: at low values of E/p (E is the electric field intensity and p is the gas pressure) the trapping coefficient is considerably less than the absorption coefficient of ultraviolet radiation for the same mixtures. It follows that, in principle, it should be possible to create primary electrons in a density needed for the formation of an SSVD at a considerable distance from an ionization source and then transport the electrons to the gap by drift in an electric field. This possibility was confirmed experimentally. A method for forming an SSVD by filling the discharge gap with a flux of electrons drifting in an electric field, without preliminary ionization of the whole discharge volume, was proposed and implemented. The source of electrons was a plasma formed in an auxiliary discharge initiated under a grid cathode. This method also made it possible to establish an SSVD in a system of electrodes with a strongly inhomogeneous electric field in the discharge gap.

In the present book we have considered, in detail, a one-dimensional model of the propagation of an electron flux in the discharge gap, analyzed the influence of distortions of the electric field by the space charge of the electron flux on the formation of an SSVD in the real geometry of the gap, and reported on studies of the main types of the auxiliary discharge suitable for the creation of an electron flux with the necessary characteristics.

The main mechanisms of instabilities in an SSVD were identified by investigating the influence of easily ionizable substances and of other impurities on the duration of stable burning of such a discharge in N_2 and in CO_2–N_2 mixtures, when the initial electron density depended weakly on the gas composition. The results obtained demonstrated the dominant role played by multistage ionization in the development of instabilities in SSVD in working CO_2 laser mixtures, as well as the need to use easily ionizable substances for the suppression of these instabilities.

An investigation was carried out into suitable conditions for the preliminary filling of a discharge gap with electrons and the dynamic profiling of the electric field in a discharge gap in the process, forming an SSVD in the case of large interelectrode distances d in CO_2–N_2–He gas mixtures at atmospheric pressure. An SSVD was established in systems of electrodes without any special surface profile and the characteristics of an active medium were calculated for a distance of d = 70 cm. The method of generation of an SSVD in a system of two plane electrodes of identical size and with sharp edges was proposed and tested experimentally. This method provided means for controlling the energy distribution over the super large aperture of a CO_2 laser with such electrodes.

A special study was made of the mechanisms of formation of an SSVD in CO_2–N_2–He gas mixtures initiated by an auxiliary barrier discharge distributed on the surface of a cathode. The volume discharge was initiated when the discharge gap was filled by an electron flux formed from the barrier discharge plasma in the course of a smooth rise of the voltage across the electrodes. Measurements were made of the small-signal gain confirming the model of formation of an SSVD and demonstrating that a discharge of this kind could be used to amplify nanosecond light pulses. Intracavity laser spectroscopy was used to study the dynamics of population of the v = 2–8 vibrational levels of the $A^3\Sigma_u^+$ state in order to establish the possible influence of multistage ionization on the evolution of instability in an SSVD in CO_2 laser active mixtures. The populations of the nitrogen vibrational levels N_v were calculated taking into account the real output pulse profile of a dye laser. It was found that multistage ionization can only influence the duration of stable operation of an SSVD by increasing the growth rate of the spark channel in the discharge gap. This is why the addition of readily ionized substances to the gas that reduce the electron energy and therefore lower N_v can substantially improve the stability of the SSVD, and increase the active volume and output energy of a lasers.

The basic principles that underline the initiation of an SSVD, which is to be used for pumping N_2O lasers, are presented in the book. The experimental results for discharge stability, optical homogeneity, and scalability of the laser active medium are discussed. Characteristics of CO_2 lasers with apertures of up to 70 cm and active volumes of up to 400 l as well as of N_2O lasers with apertures of up to 20 cm and active volumes of up to 60 l, are presented in the book.

The second part of this book is devoted to an SSVD without preionization, i.e. an SIVD, in nonchain HF lasers with SF_6–C_2H_6 mixtures. It was established that, after the primary local electrical breakdown of the discharge gap, the SIVD spreads along the gap in directions perpendicular to that of the electric field by means of the successive formation of overlapping diffuse channels under a discharge voltage close to its quasisteady state value. It is shown that, as new channels appear, the current flowing through the channels formed earlier decreases. The volume occupied by the SIVD increases with increase in the energy deposited in the plasma and, when the discharge volume is confined by a dielectric surface, the discharge voltage increases simultaneously with increase in the current. The possible mechanisms that explain the observed phenomena, namely the dissociation of SF_6 molecules and electron attachment SF_6 molecules, are also examined in the book. A simple analytical model, which makes it possible to describe these mechanisms at a qualitative level, was developed and discussed.

Scaling problems are also considered in Part II of the book for non-chain HF (DF) laser operating on mixtures of SF_6 and hydrocarbons (deuterocarbons) in which a chemical reaction is initiated by self-sustained volume discharge. The possibility of obtaining a volume discharge in SF_6 and in corresponding mixtures without preionization, i.e., SIVD, is a new qualitative result in solving the scaling problem for non-chain lasers. The dynamics of SIVD evolution has been investigated. The possibility of obtaining SIVD (including the systems with plane

electrodes that have highly enhanced electric field at the edges of the discharge gap) is determined in SF_6 by mechanisms that limit the density of current, are related to specific energy release, and prevent the total energy from flowing through a single channel. A simple model is developed for calculating the discharge characteristics in non-chain lasers. The model is supported by experimental data. The obtained energy of a non-chain HF-laser is 407 J and that of a DF-laser is 325 J with the electric efficiency 4.3 and 3.4%, respectively. On the basis of the experimental data obtained, the possibility of creating non-chain HF(DF) lasers with the output energy of the order of few kilojoules and higher is discussed.

Part III is devoted to the problem of regenerative generation and amplification of a nanosecond pulse in the active volume CO_2 laser. Recent advances in injection mode locking and high-power 10.6 μm pulse selection have been incorporated into a high-power CO_2 laser system built around a single 5 l TEA CO_2 gain module. A pulse selected from a line-tuned [to *P*(20)] injection-mode-locked oscillator was amplified to produce a 20 J, 3 ns pulse with a main-pulse-to-prepulse contrast ratio of $>10^7$:1. Regenerative amplification of a nanosecond pulse train in the 50 l active volume CO_2 laser has been investigated both numerically and experimentally. The area in which RA takes place was determined when varying the injected radiation parameters. The nanosecond pulse train utilization as an injected radiation instead of a monopulse was shown to significantly broaden the injection time "window" and to enable variation of an individual pulse time structure in the output train.

The 10.6 μm transmission properties of SF_6 were measured using nanosecond-duration pulses for various buffer gases and buffer gas pressures up to 3 atm. The addition of a buffer gas strongly increased the SF_6 absorption at moderate energy fluences without significantly altering the high fluence pulse transmission. For pressures above 1 atm, the transmission behavior appeared independent of the pulse duration over the range of parameters investigated in this experiment. The implication of these results for CO_2 nanosecond pulse laser applications is discussed in detail in the chapter.

Electric-discharge lasers based on transitions in the nitrogen molecule as a promising source of near-UV radiation is a further topic of discussion in Chap. 3. Such lasers are widely used in the microelectronics industry, in medicine, in laser chemistry, as pump sources of organic lasers, as well as in spectroscopy, and in laser diagnostics of plasmas, etc. The design of these lasers is relatively simple and the active medium is chemically inert. Moreover, in some applications, the nitrogen laser wavelength is the most effective.

Chapter 4 looks at the different applications for high-power molecular lasers for technological and industrial needs, including:

- Stimulation of heterogeneous catalytic reactions involving decomposition of vibrationally excited ammonia molecules on the surface of platinum after absorption of a CO_2 laser photon. This stimulated dissociation of HN_3 on Pt was attributed to radiative excitation of the vibrational levels of the ammonia molecule.

- An experimental investigation of an optical-breakdown plasma lasing in an He–Xe gas mixture exposed to CO_2 laser radiation. A wide range of pump pulse energies and durations and active mixture pressures was used. Lasing was realized on four Xe I transitions (λ = 2.03, 2.65, 3.4, and 3.65 μm). The pump pulse duration was found to exert a strong influence on the lasing characteristics of the optical breakdown plasma. The role of gasdynamic processes in the interaction of the CO_2 laser radiation, with the gas close to a target during the buildup of inversion, was analyzed. A quasi-cw lasing regime of the recombination laser in the optical breakdown plasma was observed and investigated.
- Generation of hard x-ray radiation possessing multi-spike structure (HXRMS) in a CO_2-laser plasma had been observed at low intensity of the heating radiation. The possibility of applying the principle of low-threshold ($q < 10^{10}$ W/cm^2) generation of hard x-ray radiation (HXR) in single-spike operation resulting from the development of parametric instability (PI) within a homogeneous plasma with the characteristic size $L > 1.3$ mm was shown experimentally. The schematic of the set-up, plasma parameters and estimates of laser radiation intensity are presented in the book.
- Investigations of currents in close-to-surface plasma, produced by CO_2 laser radiation of different temporal structures are also described in the chapter. The character of evolution of the registered currents in temporal structures at growing energy densities was different when the target was irradiated in air versus in a vacuum by the train of short pulses (τ = 2.5 ns). Experiments in vacuum have revealed that the transit from smooth single mode pulse to the nanosecond pulse train of the same total energy was followed by a considerable decrease in plasma formation energy thresholds and by the increase in amplitudes of currents induced by plasma. The current pulses from the target were registered after finishing the laser irradiation; their appearance was probably connected with cumulation effects, caused by the ring form of the irradiated area. Many phenomena accompaning the air optical breakdown (in particular, the electric fields and currents arising in breakdown plasma) sufficiently depend on the temporal parameters of laser radiation. For example, utilization of two successive laser pulses results in a considerable increase of the magnetic fields and currents.
- The results of investigations into the electric fields and currents in the air breakdown plasma produced by a train of CO_2 laser nanosecond pulses near the surface of uncharged metallic targets are presented. The breakdown thresholds as well as efficiency of plasma-target heat transmission for different temporal parameters of CO_2 laser radiation are measured and observed.
- Regenerative amplification (RA) enables the transformation of free running mode laser pulses into the train of nanoseconds with varied duration of the individual pulse and time interval between the pulses. This is why we have used RA for carrying out the experiments presented in the book. The numerical

calculations made it possible to predict the influence of RA scheme parameters upon the temporal structure of the nanosecond pulse train and thus facilitate realization of the experimental set up.

- The construction of CO_2 laser system generating a train of subnanosecond laser pulses with total train energy up to 5 J is reported. *A* record *level* of laser energy was obtained due to utilization of unique 5 x 5 cm^2 aperture, 6 atm x-ray preionized CO_2 amplifier. The estimations of individual pulses durations in the train are given. The prospect of upgrading the present configuration of laser system towards shortening laser pulse duration and increasing the pressure of the working gas mixture of the amplifier and its efficiency are discussed.
- A technique for obtaining of the repetitively pulsed operating regime in high-power wide-aperture lasers is proposed and experimentally realized. In this regime, the laser emits a train of pulses with duration of 100–150 ns and a pulse repetition rate of several tens of kilohertz. The main properties of the pulsed regime are theoretically analyzed and the proposed technique is tested in detail, employing a test-bench gas-dynamic laser. The results of the test confirmed the conclusions of the theoretical analysis. The possibility of a repetitively pulsed regime in high-power wide-aperture lasers without significant reduction in the average output power was demonstrated experimentally.

Part I
High Energy Pulsed CO_2 Lasers

In electroionization devices with apertures as large as 30 cm, maximum radiation loads on the optical elements were already attained by the mid-1970s. Any further increases in laser output energies were presumably related to larger apertures. However, solving the problem of limitations on output by operating several lasers in parallel presents great technical difficulties. An alternative method is to enlarge the aperture of a single molecular laser. The electroionization approach to the problem proved impracticable because the voltages on the accelerator were too high and because the critical restriction imposed on the transverse dimensions of the discharge zone by the discharge-induced magnetic field affected the trajectory of accelerated electrons.

This restriction on the discharge-zone transverse dimensions is removed if a CO_2 laser is pumped by an SSVD. It is, however, far less stable than a non-SSVD. Furthermore, the actual scalability of the aperture is limited by the difficulty involved in reaching the required concentrations of primary electrons at long electrode separations as well as by the size and shape of electrodes. According to the notions that were generally adopted in the early 1980s, these difficulties could not be eliminated in gas lasers pumped by an SSVD. Primary electrons in the discharge gap were believed to be the result of gas ionization caused either by radiation or by fast particles, while uniform excitation of the laser active medium was thought to be possible only in a uniform electric field set up by electrodes of specific shapes.

Transverse-discharge excitation of large-aperture CO_2 lasers places demanding and unusual constraints on the pulsed power supply. Stable discharges with interelectrode gaps as large as $g = 70$ cm were achieved using pulsed power supplies that satisfy specific requirements imposed by volume preionization and discharge ignition. The supply must initially apply a quasi-dc or slow-rise voltage to affect preliminary filling of the gap with electrons from an auxiliary discharge, followed by application of a controlled rise voltage to ignite an SSVD. A coupled particle kinetics-equivalent circuit model has been developed to simulate discharge behavior for the various pulsed power configurations. Computational results are compared with experiments involving very-large-aperture and large-volume devices.

Chapter 1
Carbon Dioxide Laser with an Output Energy of 3 kJ, Excited in Matched Regime

Abstract An investigation was carried out into a CO_2 laser with a pulsed pumping of a gas cell in the matched regime. The total energy of the output radiation was 3 kJ when the pressure of the mixture was 2 atm and the active volume was 50 L. When the active volume was 12 L, the energy deposited in a mixture of the CO_2:N_2:He = 1:2:2 composition was 0.6 kJ L^{-1} atm^{-1} and the radiation energy was $\sim$80 J L^{-1} atm^{-1}.

In the most powerful laser systems excited by an electric discharge and stabilized by an electron beam, the discharge is supplied with power from a storage capacitor connected to a laser gap [1, 2] or by a pulse voltage generator [3, 4]. In the former case, the energy stored in a capacitor is considerably more than the energy deposited in the discharge so that after the end of an excitation pulse a high voltage remains for a long time (compared with the excitation pulse duration) on the electrodes. The advantage of such a nonmatched operation is that the voltage on the electrodes of a gas does not vary significantly during the pumping time. However, a residual voltage on the electrodes of a laser cell hinders—because of discharge contraction—attainment of a high field intensity in the gap and prevents deposition of large energies, particularly in the case of mixtures with low helium concentrations. When a pulse voltage generator is used to supply a gap, only part of the stored energy is deposited in the gas during the action of an electron beam [3, 4] and this imposes restrictions on the total efficiency and gives rise to a residual voltage on the electrodes.

The use of matched pumping of a CO_2 amplifier with a characteristic excitation time of $\sim$1 μs was first reported in [5], but in this case the specific input energy did not exceed 200 J/L and the output energy characteristics were not given.

Our aim was to investigate the possibility of excitation of a CO_2 laser in the matched regime so as to ensure a high specific input energy and a high output energy in pulses of $\sim$1μs duration.

Our laser system consisted of a gas cell, a power supply, and an electron accelerator. The active medium was excited by a non-SSVD. The maximum active volume of the chamber was 50 L (20 × 20 × 125 cm). The chamber could be operated at pressures up to 2.5 atm. Experiments were carried out on an active volume of 50 L and also on a reduced active volume of 12 L (8 × 12 × 125 cm).

© Springer International Publishing Switzerland 2016

V.V. Apollonov, *High-Energy Molecular Lasers*,
Springer Series in Optical Sciences 201, DOI 10.1007/978-3-319-33359-5_1

The electron accelerator provided an electron beam current of density ~ 0.5 A/cm^2 in the gas chamber and an acceleration voltage of ~ 300 kV in a vacuum diode. Oscillograms of the acceleration voltage across this diode and of the electron beam current in the gas chamber were recorded (Fig. 1.1a, b). A special feature of the selected operation regime was the fact that the duration of the electron beam pulses was twice the duration of the discharge current pulses. The discharge in the chamber was delayed by −0.3 μs relative to the electron-beam current. Thus, the discharge occurred under conditions of constant electron-beam current density and constant electron energy, which was an important factor tending to increase the stability of the discharge, because it was possible to eliminate the low-energy electrons formed during the rising and falling parts of the acceleration voltage.

We used LC correction in a pulse voltage generator supplying the vacuum diode, so that the beam current pulses were nearly rectangular (Fig. 1.1b).

The gas chamber was supplied with a Marx pulse generator consisting of three parallel branches with five steps in each. This generator utilized IK-100/0.4 capacitors and the LC correction circuit contained IMN-100/0.1 capacitors. The equivalent capacitance of the pulse generator was 0.24 μF and its wave impedance was $p = 3.3\ \Omega$; when the charging voltage was $U = 58$ kV, the energy stored in the pulse generator reached 10 kJ. Spark gaps (through which dry air was blown) were employed in the generator and this ensured a high triggering stability (±20 ns) and made it possible to synchronize the discharge current and beam current pulses.

The discharge current in our electrical circuit can be described using the following equation:

$$f(t) = (U_0/\omega L)\exp(-Rt/2L)\sin\omega t. \tag{1.1}$$

where $\omega = (L/C - R^2/4L^2)^{1/2}$ is the oscillation frequency of the circuit; R is the active resistance included in the circuit. In our case, R is the resistance of the discharge plasma, which can be regarded (with a good approximation) as linear and constant in time because there is no change in the electron beam current during the discharge. The matched load condition is $R = (\mathrm{LC})^{1/2} = \rho$ and it then follows from (1) that the discharge current pulse has the following parameters:

$$t_p = 2\pi(\mathrm{LC}/3)^{1/2};\quad t_m = 2\pi(\mathrm{LC}/27)^{1/2},\quad I_m = [U_0(\mathrm{LC})^{1/3}]\exp(\pi/3\sqrt{3}), \tag{1.2}$$

where U_0 is the open-circuit voltage of the generator; t_p is the duration of the current pulses at the base; t_m is the time needed to reach the maximum value of the current; I_m is the maximum discharge current.

In practice, there is no need to satisfy the exact equality $R = \rho$ because for $0.75\,\rho \le R \le 2\rho$, the reduction in the peak power does not exceed 10 %. It is worth noting that an increase in R from 0.75 ρ to 2 ρ alters the voltage across the plasma from $0.47U_0$ to $0.74U_0$. This should be allowed for in order to ensure the maximum efficiency of the laser. In the laser described above with the maximum active volume of 50 L for a mixture of the composition CO_2:N_2:He = 1:2:2 at a pressure of 2 atm the plasma resistance was $R = 3.8\ \Omega$. For a charging voltage of

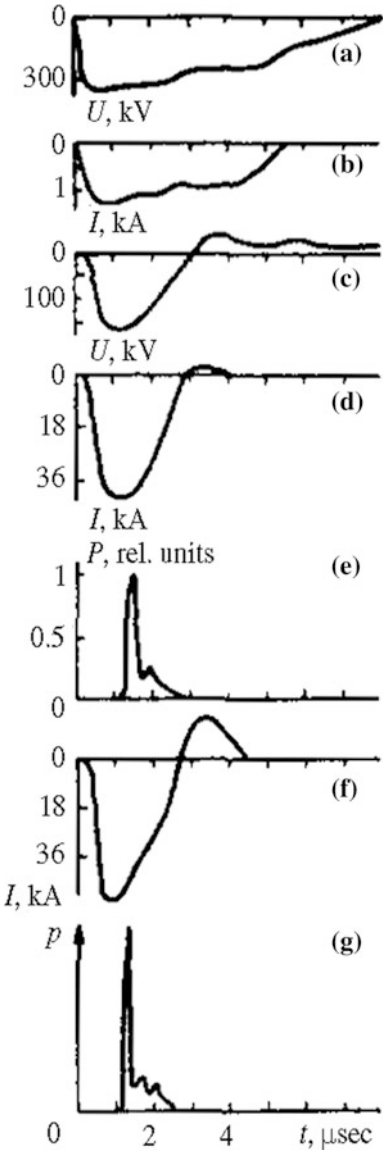

Fig. 1.1 Oscillograms of the voltage (**a**) and current (**b**) pulses in the accelerator, voltage across the gap (**c**), current in the chamber (**e**, **f**), and radiation pulses (**d**, **g**). The charging voltage of the pulse generators supplying the cell was 58 kV and the mixture has the composition CO_2:N_2:He = 1:2:2. The pressure was p = 2 atm and the volume was 50 L (**c**–**e**) and 12 L (**f**, **g**)

U = 58 kV the oscillograms of the voltage across the plasma, discharge current, and radiation pulse had the form shown in Fig. 1.1c–e. The dependence of the total radiation energy on the energy stored in the pulse generator was determined for this case (Fig. 1.2a), The transverse distribution of the radiation in the output beam was nonuniform and the center of the energy density reached 15 J/cm^2; at this energy density, the exit window was damaged. The total radiation energy reached 3 kJ and the efficiency was ~21 %. The radiation energy was measured by scanning a laser

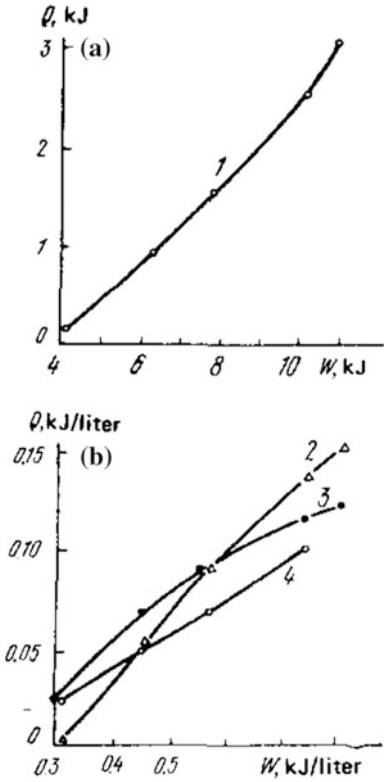

Fig. 1.2 Dependences of the total radiation energy on the input energy for an active volume of 50 L (**a**) and the specific output energy plotted as a function of the specific input energy when the active volume was 12 L (**b**). Composition CO_2:N_2: He = 1:2:2, pressure p = 2 atm [1–3] and 1.2 atm [4]; exit window made of KRS (*1*, *3*, *4*) and of NaCl (*2*)

beam with an IKT-lM calorimeter, from which the sapphire window in the detection head was removed.

The possibility of attaining high input energies in the matched regime was investigated by reducing the active volume of 12 L (8 × 12 × 125 cm). In the case of the 50 L volume, this could not be done because of the limited energy stored in the pulse generators supplying the gap. The plasma resistance then decreased to 2.5 Ω. Oscillograms of the discharge current and radiation pulse were also recorded for this case (Fig. 1.1f, g). The energy deposited during the second half-period did not exceed 10 %, so that the conditions could be regarded as practically matched. The amplitude of the voltage across the plasma was 136 kV (E/p = 8.5 kV*cm^{-1}*atm^{-1}) and the maximum input energy exceed 0.6 kJ*L^{-1}*atm^{-1}. The dependences of the radiation energy on the input at pressures of 2 and 1.2 atm in the mixture and also in various resonators were determined using exit mirrors in the form of NaCl and KRS plates (Fig. 1.2b). The maximum radiation energy obtained from the 12 L volume was 1.8 kJ. An increase in the input energy reduced the lasing efficiency, in agreement with the results of [3].

Our experimental study thus showed that it should be possible to achieve high specific energy inputs in large volumes if the matched regime is used.

References

1. Y.I. Bychkov, E.K. Karloav, N.V. Karlov, B.M. Koval'chuk, G.P. Kuz'min, Y.A. Kurbatov, V. T. Manykov, G.A. Mesyats, V.M. Orlovskii, A.M. Prokhorov, A.M. Rubalov, Pis'ma Zh. Tekh. Fiz. **2**, 212 (1976) [Sov. Tech. Phys. Lett. **2**, 81 (1976)]
2. V.A. Adamovich, V.Y. Baranov, R.K. Bevov, Y.B. Smakovskii, A.P. Strel'tsov, Pis'ma Zh. Tekh. Fiz. **4**, 988 (1978) [Sov. Tech. Phys. Lett. **4**, 398 (1978)]
3. C. Cason, G.J. Dezenberg, R.J. Huff, Appl. Phys. Lett. **23**, 110 (1973)
4. A.M. Orishich, A.G. Ponomarenko, V.G. Posukh, R.I. Soloukhin, S.P. Shalamov, Pis'ma Zh. Tekh. Fiz. **3**, 39 (1977)
5. Status Report on Laser Program ot LASL, Report LA-5251- PR, July-December (1972)

Chapter 2
SSVD in Long Gaps Containing CO_2–N_2–He Mixtures

Abstract Strong ultraviolet radiation and easily ionizable impurities made it possible to achieve stable SSVD using voltage (pump) pulses of 2 μs minimum duration and specific deposited energy of at least 200 J/l in discharge gaps up to 25 cm filled with CO_2–N_2–He mixtures with the molecular gases representing up to 50% of the total content. The minimum voltages required from a pump source to initiate a stable discharge did not exceed 255 kV.

CO_2 lasers and amplifiers pumped by an SSVD with preionization by ultraviolet radiation are used extensively in various branches of science and technology because of their simplicity and reliability, particularly in systems designed for investigating the interaction of intense radiation with a plasma [1–3]. However, up to now, the available CO_2 amplifiers pumped by an SSVD have been incapable of replacing systems pumped by a bulk nonself-sustained discharge controlled by an electron beam in the output stages of systems of this kind. This has been primarily due to the difficulty of ensuring an SSVD in gaps of considerable length d and in volumes comparable with the typical volume of electron-beam-controlled systems. Strong ultraviolet radiation and fast (in the form of pulses shorter than 1 μs) pumping had made it possible to achieve stable bulk self-sustained discharge across gaps of length d = 30 cm [4] and 20 cm [5]. However, the minimum voltage needed for initiation of a stable bulk self-sustained discharge U_{min}, was found to be 280 kV, even for a mixture with the molecular gas content p_o = 20% in a gap d = 30 cm long, and the length of the active medium in both cases did not exceed 30 cm. Clearly, construction of electric discharge CO_2 amplifiers capable of competing with electron-beam-controlled systems would require a reduction in U_{min} and at the same time an increase in the proportion of molecular gases in the mixture as well as an increase in the length of the active medium to at least 1 m. The first requirement may be satisfied using certain substances, which become readily ionized in a Penning discharge as a result of collisions with N_2 molecules [6–8]. However, a simultaneous reduction in the pump voltage and an increase in the length of the active medium for a constant specific deposited energy W would increase the energy evolution time, which again would make it difficult to achieve a

© Springer International Publishing Switzerland 2016

V.V. Apollonov, *High-Energy Molecular Lasers*,
Springer Series in Optical Sciences 201, DOI 10.1007/978-3-319-33359-5_2

stable SSVD. Estimates indicate that for a pump source voltage of 300 kV and a specific deposited energy W = 300 J/l, the minimum time τ for energy evolution (representing the duration of a half-period of a short-circuit current found allowing for the inductance of the leads and for the intrinsic conductance of the discharge) in a zone of 25 × 25 × 100 cm dimensions would be ~2 μs. Our aim was to investigate the possibility of attaining an SSVD for this value of r in a system with a long discharge gap employing strong ultraviolet radiation and easily ionizable admixtures.

A discharge was struck between two disk aluminum electrodes 350 mm in diameter, with rounded edges. The distance between the electrodes was varied and ranged from 5–25 cm. The cathode was a ring with an internal diameter 190 mm in its aperture, covered by a brass grid of ~80 % transparency. A high-voltage pulse was applied to a gap from a five-stage Arkad'ev-Marx voltage generator based on IK-0.25–100 capacitors with a maximum output voltage of 300 kV. The time r was varied by connecting an additional inductor in the discharge circuit.

A system providing ultraviolet radiation was located directly below the grid cathode and it was similar to that employed in [9], but the use of a high-permittivity ceramic reduced the working voltage (10–17 kV as against 50–70 kV in [9]). The specific energy density recorded on the surface of the ultraviolet preionizer did not exceed 0.1 J/cm^2. Preliminary experiments established a high reliability and efficiency of the preionizer. In this way, it was possible to achieve a stable SSVD in the region of 10 × 10 × 50 cm dimensions for τ ~ 1 μs and W = 250 J/l in the case of mixtures with a molecular gas content of up to 50% but free of other additives. The delay of the main discharge relative to the preionization discharge was varied within the range 0–20 μs, subject to an error of ±100 ns.

The easily ionizable additives were 3-n-propylamine and 3-ethylamine at vapor pressures of 1–1.5 Torr. These additives had approximately the same effect on a bulk self-sustained discharge and, depending on the composition of the mixture, they could reduce the voltage U_{min} by 40–50 %.

The results of our experiments are presented in Table 2.1. In the calculation of U'_{min} (U'_{min} is the value of U_{min} for "pure" mixtures, i.e., mixtures free of additives, calculated using data from [9, 10]) we assumed that the empirical dependence taken from [4] also applied to mixtures with $K = p_{N_2}/p_{CO_2} \neq 1$, where p_{N_2} and p_{CO_2} are the partial pressures of the two molecular gases. We can see from Table 2.1 that stable SSVDs were achieved for large values of d and τ using several mixtures with the molecular gas content p_0 < 50 % and with the parameter 1; the value of W was at least 200 J/liter. One should also note that a considerable reduction in U_{min} was recorded as a result of the presence of easily ionizable additives. For τ = 2 μs and $p_{CO_2} > 20\,\%$ of the total pressure in the mixture in a gap d = 20 cm long and for $p_{CO_2} > 16\,\%$ in a gap of d = 25 cm it was found that a stable bulk self-sustained discharge was obtained when a peaking capacitance C = 1375 pF was connected in parallel with the gap. A characteristic "oscillatory" regime of energy deposition in the plasma of the discharge was then observed (Fig. 2.1) and it was found that U_{min} < 160 kV even for d = 25 cm and p_0 = 50 %. This regime could be of

Table 2.1 The results of our experiments

CO_2:N_2:He (1 atm.)	τ (μs)	U_{min} (kV)	U^p_{min} (kV)	W (J/l)
d = 20 cm				
10:10:80	2.0	<140	190	>300
8:32:60	0.95	180	–	>300
8:32:60	2.0	200	–	300
5:35:60	2.0	190	–	350
16:24:60	2.0	220	–	270
[a]20:20:60	2.0	<140	300	~200
16:32:52	1.5	230	420	290
d = 25 cm				
10:10:80	2.0	<140	238	250
8:32:60	2.0	252	–	250
5:35:60	2.0	235	–	270
[a]16:32:52	2.0	156	525	220

[a]A stable SSVD was obtained when a peaking capacitance C = 1375 pF was connected in parallel to the discharge gap

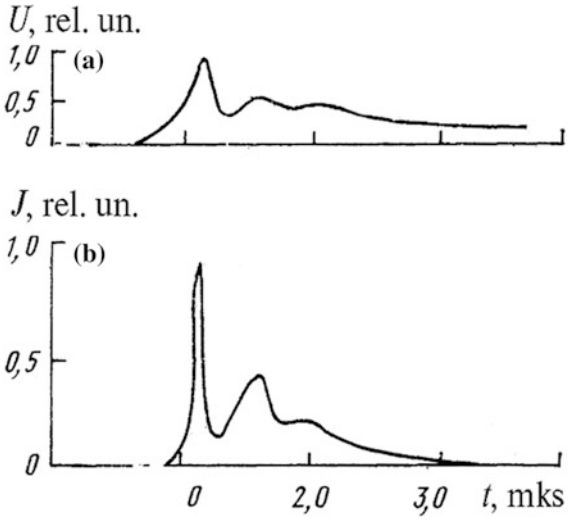

Fig. 2.1 Oscillograms of the voltage (**a**) and current (**b**) pulses recorded for a bulk self-sustained discharge in a mixture of the CO_2:N_2: He = 20:20:60 composition inside a gap d = 20 cm long, in the presence of a peaking capacitance C = 1375 pF

intrinsic interest for the excitation of large volumes of mixtures containing easily ionizable additives.

The efficiency of excitation of the active medium by long pump pulses was monitored by measuring the small-signal gain of the $P(20)$ line in the region of the 10.6 μ wavelength. For d = 25 cm, τ = 2 μs, and W = 210 J/l, its value for the CO_2:N_2:He = 16:32:52 mixture was 3.9 m^{-1}. These findings were in good

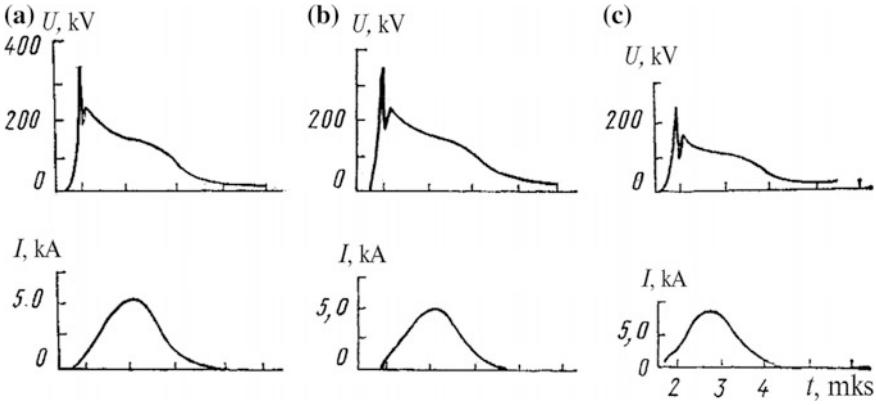

Fig. 2.2 Oscillograms of the voltage U and current I pulses obtained for an SSVD in CO_2:N_2: He = 8:32:60 (**a**), 5:35:60 (**b**), and 10:10:80 (**c**) mixtures characterized by τ = 2 μs

agreement with the results of measurements of the gain of mixtures containing 3-n-propylamine, which were characterized by small values of d and τ [8].

A further feature of SSVDs with mixtures containing easily ionizable additives and characterized by large values of τ should also be discussed. Oscillograms of the voltage and current pulses for such discharges were obtained for mixtures of different composition and τ = 2 μs (Fig. 2.2). In contrast to an SSVD characterized by $\tau \sim 1$ μs [6, 8], in our case a voltage pulse had a very flat step, which was more characteristic of SSVD in pure mixtures and its shape did not depend strongly on the parameter K. This was due to the fact that at vapor pressures of the easily ionizable additives in the range LV-1–1.5 Torr, which is needed for a significant reduction in U_{min}, practically all the metastable electron states of N_2 excited during the initial stage of the bulk self-sustained discharge became deactivated in a time shorter than 1 μs [11]. Next, the excess of electrons formed in the Penning discharge decreased because of recombination and trapping and, if τ was sufficiently long, the ratio E/p rose to a value governed by the characteristics of the pure mixture. This circumstance could limit a further increase in the duration of SSVD.

At high values of τ, it was preferable to reduce the concentration of the easily ionizable admixtures, especially as in this case for d = 20–25 cm the maximum yield of photoelectrons was obtained at optimal pressures of the vapors of the easily ionizable components (for example 3-n-propylamine), which were in the range 0.05–0.2 Torr [12].

We were thus able to achieve stable SSVDs in mixtures with the molecular gas content up to 50% and with a specific deposited energy of at least 200 J/l when the discharge gap was up to 25 cm long and the minimum duration of the period needed to deposit the energy in the discharge plasma was $\sim$2 μs. These results indicated that, in principle, it should be possible to construct large-aperture electric-discharge CO_2 amplifiers with active media of considerable length.

References

1. G.H. McCall, Abstracts of Papers presented at Twelfth European Conference on Laser Interaction with Matter, Moscow, 1978
2. V.A. Adamovich, V.N. Anisimov, E.A. Afonin, V.Y. Baranov, V.L. Borzenko, S.M. Kozochkln, D.D. Malyuta, Y.A. Satov, A.Y. Sebrant, Y.B. Smakovskil (Smakovskl), A.N. Starostin, A.P. Streltsov (Streltzov), V.M. Petryakov, S.F. Chaikin, Appl. Opt. **19**, 918 (1980)
3. V.V. Apollonov, F.V. Bunkin, et al., Proc. Ninth Intern. Congress "Interkamera". Prague **2**, 297 (1981)
4. M.C. Richardson, A.J. Alcock, K. Leopold, P. Burtyn, IEEE J. Quantum Electron. QE **9**, 236 (1973)
5. V.Y. Baranov, V.M. Borisov, Y.A. Satov, Y. Y. Stepanov, Kvantovaya Elektron. (Moscow) **2**, 2086 (1975) [Sov. J. Quantum Electron. **5**, 1139 (1975)]
6. V.V. Apollonov, A.I. Barchukov, S.I. Derzhavin, I.G. Kononov, A.M. Prokhorov, et al., Pis'ma Zh. Tekh. Flz. **3**, 1073 (1977) [Sov. Tech. Phys. Lett. **3**, 441 (1977)]
7. V.V. Apollonov, N.G. Akhunov, et al., Abstracts of Papers presented at Tenth Siberian Conference on Spectroscopy, Tomsk, 1981 [in Russian] Tomsk State University (1981), p. 94
8. V.V. Apollonov, F.V. Bunkin, et al., Kvantovaya Elektron. (Moscow) **6**, 1176 (1979) [Sov. J. Quantum Electron. **9**, 694 (1979)]
9. A.M. Orlshlch, A.G. Ponomarenko, R.I. Solovkhtn, Do!d. Akad. Nauk SSSR **212**, 1099 (1973) (Sov. Phys. Dokl. **18**, 671 (1974)]
10. A.K. Zhigalkin, Y.L. Sidorov, Zh. Tekh. Flz. **48**, 1621 (1978) [Sov. Phys. Tech. Phys. **23**,918 (1978)]
11. V.V. Apollonov, N.G. Akhunov, et al., Lectures presented at Symposium 0ptika-80 (Budapest, 1980), p. 91
12. Z. Rozkwitalski, M. Grodel, J. Appl. Phys. **51**, 2267 (1980)

Chapter 3
Carbon Dioxide Laser with a Variable Output Pulse Duration

Abstract We report here on the construction of a CO_2 laser in which the exciting discharge was stabilized by adding readily ionized organic substances to the mixture. The temporal characteristics of the laser emission pulses were investigated for a wide range of active mixtures and pulse durations from 10 μs to 150 ns. Improvements in the output energy distribution over the beam cross section are discussed.

The aim of the present work was to make an electric-discharge atmospheric pressure CO_2 laser with high energy characteristics and a uniform radiation distribution over the cross section of the beam, offering the possibility of varying the laser pulse duration over a wide range.

The CO_2 laser described consisted of three standard amplifier modules of the "Polinom" apparatus [1], pumped by Arkad'ev-Marx two-stage voltage pulse generators. The modules were mounted in a single 3 m long resonator, formed from an aluminum mirror of radius of curvature $R = 19$ m and a plane-parallel NaCl plate.

The total volume of the active medium was 3 dm^3. The transverse dimensions of the output beam were 5×4 cm. To a considerable extent, the energy characteristics of the laser depended on the synchronism in actuating the voltage pulse generators. Two ignition units were used to synchronize the generators with ignition pulse peaking [2], and, as a result, the time spread in actuating the voltage pulse generators did not exceed 30 ns.

The temporal characteristics of the laser output pulses were investigated as a function of the excitation conditions and the composition of the active medium. In [3] and [4], the influence of the active mixture components in CO_2-N_2-He mixtures on the shape of the CO_2 laser emission pulses was analyzed. It was shown that a laser pulse consisted of an initial spike and a long tail, the energy ratio of which (other things being equal) was determined by the composition of the gas mixture, with the presence of the long tail being primarily a consequence of the energy transfer from the N_2 molecules. Thus, by varying the CO_2-N_2-He mixture composition, it is possible to change the shape and duration of the pulses. For a laser with a non-SSVD, controlled by an electron beam, there is no special difficulty in

© Springer International Publishing Switzerland 2016

V.V. Apollonov, *High-Energy Molecular Lasers*,
Springer Series in Optical Sciences 201, DOI 10.1007/978-3-319-33359-5_3

changing the mixture composition in view of the high stability of a non-SSVD [5]. In electric-discharge CO_2 lasers, achieving a stable bulk discharge with different active media was associated with some difficulty. In the present experiments, the discharge was stabilized and the operating range increased in terms of the pump energy and the active medium composition by introducing readily ionized alkyl amine additives: tri-n-propylamine (TPA), triethylamine, dimethylamine, and dibutylamine.

Figure 3.1 shows oscillograms of the laser emission pulses obtained using atmospheric-pressure active media with different nitrogen concentrations, but with a constant ratio of the combined content of both molecular gases to the atomic gas content. On reducing the ratio p^$Jpco_2$ >, the energy of the initial spike decreased relative to that of the tail of the pulse and the pulse duration also decreased.

In the present work we succeeded, by changing the active mixture composition, in varying the pulse duration from 10 μs for a CO_2:N_2:He = 1:7:12 mixture to 150 ns overall duration for CO_2:N_2:He = 9:1:15. In the latter case, the 25 J output pulse did not exhibit the characteristic tail. The maximum output energy of ~100 J was obtained for a CO_2:N_2:He = 1:1:3 mixture, the pulse having a typical form with an initial ~150 ns spike and a ~1.5 μs tail. All the experiments were carried out using tri-*n*-propylamine and triethylamine (at 1.5 and 1 Torr, respectively) as the readily ionized additive, which provided conditions close to optimal for obtaining a bulk discharge.

Special attention was paid to ensuring a homogeneous energy distribution over the cross section of the output beam. In such lasers, this is mainly determined by the homogeneity of the distribution of the gain q over the aperture. This characteristic depends directly on the distribution of the pump energy over the discharge cross section, which is determined by the profile of the electrodes and (when the

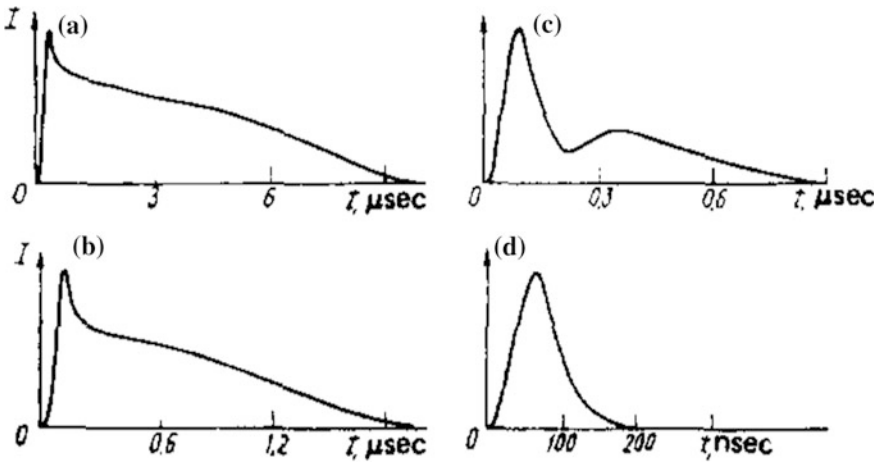

Fig. 3.1 Laser emission pulse oscillograms for active mixtures: CO_2:N_2:He = 1:7:12 (**a**), 1:1:3 (**b**), 8:2:15 (**c**), and 9:1:15 (**d**), at atmospheric pressure

preionizers are mounted laterally) by the distance from the latter to the discharge region, as well as by the gas mixture composition and by the pressure of the readily ionized vapor material. Since the gas mixture composition (the molecular gas content) and the pressure of the added organic vapor *Ptpa* were specified by the condition for obtaining the maximum gain and efficiency, the preionizer was used to vary the input energy distribution over the discharge cross section. Electrodes of the Chang profile [6] were used and their curvature parameters were $K = 0.027$ and 0.0554. Under conditions where the input energy distribution was strongly inhomogeneous over the electrode width, characteristic of electrodes with a large curvature ($K = 0.0554$), the q distribution profile over the aperture also depended on the total pump energy. The total pump energy ε was increased by changing the voltage U_0. On increasing ε, the profile broadened considerably and became smoother, i.e., the distribution of q became more uniform. This resulted from a nonlinear dependence of q on the input energy so that the gain distribution became saturated on the optic axis before it did so at the edges of the optical aperture.

The conditions for a discharge to develop in a gas depend on the initial field distribution, determined by the electrode shape, and on the distribution of the preionization electron density n_{e0} distorting the initial field distribution [7]. Therefore, for a given electrode profile, the geometrical preionization parameters and the characteristics of ultraviolet absorption in the gas mixture and vapor exert a strong influence on the width of the discharge. Figure 3.2 gives the profiles of the q distribution over the aperture as a function of the distance δ between the preionizers. In the system with electrodes of large curvature, an improvement was observed in the distribution of the optical characteristics over the cross section of the discharge region on decreasing δ, accompanied by an increase in the nonuniformity of the n_{e0} distribution and a corresponding broadening of the discharge. In the system with small-curvature electrodes and with the specified admixture concentrations, a dip was observed in the gain profile near the optic axis because of the absorption of the ultraviolet radiation in the vapor of the readily ionized

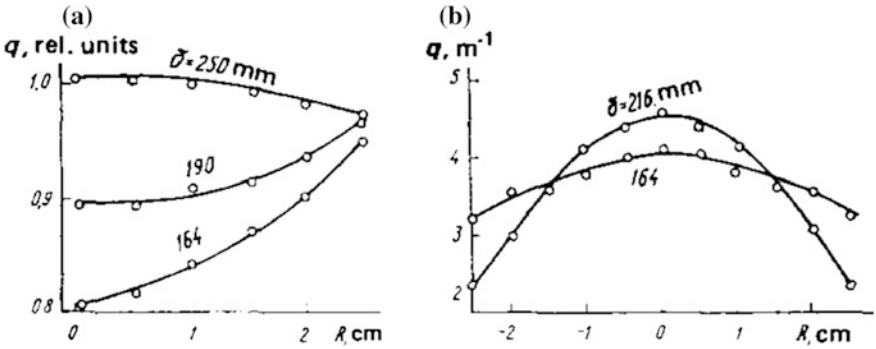

Fig. 3.2 Spatial distribution profiles of the gain q, as a function of δ, in systems with small ($K = 0.027$) (**a**) and large ($K = 0.0554$) (**b**) electrode curvature: $p_{TPA} = 1.5$ Torr; gas mixture CO_2:N_2:He = 3:3:4 (**a**) and 1:1:3 (**b**); $U_0 = 100$ (**a**) and 95 kV (**b**)

admixture. In this case, an improvement in the gain profile distribution was achieved with a decreased degree of inhomogeneity of n_{e0} over the discharge cross section by increasing δ.

In the final version of the laser, electrodes were used with a curvature parameter $K = 0.0554$, a distance between the preionizers of 164 mm, and an input energy of at least 400 J ($U_0 = 90$ kV); this made it possible to obtain the energy distribution over the beam cross section given in Fig. 3.2b.

Thus, a pulsed CO_2 laser was created with a high degree of homogeneity of the output radiation distribution over the beam cross section and a maximum output energy of ~ 100 J. In addition, it was possible to vary the pulse duration over a wide range by changing the active mixture components.

References

1. V.V. Apollonov, F.V. Bunkin et al., Izv. Akad. Nauk. SSSR Ser. Fiz. **42**, 2488 (1978)
2. H.B. Gibson, Rev. Sci. Instrum. **50**, 1489 (1979)
3. O.R. Wood II, Proc. IEEE **62**, 355 (1974)
4. K.R. Manes, H.J. Seguin, J. Appl. Phys. **43**, 5073 (1972)
5. G.P. Kuz'min, Radiotekh. Elektron. **18**, 1533 (1973)
6. T.Y. Chang, Rev. Sci. Instrum. **44**, 405 (1973)
7. J.M. Meek, J.D. Craggs, *Electrical breakdown of gases* (Clarendon Press, Oxford, 1953)

Chapter 4
Efficiency of Utilization of Certain Readily Ionized Substances for Discharge Stabilization in CO_2 Lasers

Abstract An investigation was conducted into the use of some alkyl amine substances with ionization potentials from 7.14–8.24 eV as readily ionized additives to stabilize the discharge in an ultraviolet-preionized CO_2 laser. The main attention was devoted to the processes resulting from the Penning ionization of the additives in a self-sustained discharge. It was established that the magnitude of the effect associated with ionization of the additives by the Penning process increases with the decrease in the ionization potential φ of the substance in the range $7.6 < \varphi < 8.24$ eV, and is independent of φ when $\varphi < 7.6$ eV. The best output energy results were obtained using tri-*n*-propylamine and triethylamine.

It is well known that the efficiency of CO_2 lasers with an active mixture containing readily ionized additives, pumped with a pulsed SSVD initiated by ultraviolet radiation, is mainly determined by two ionization processes: photoionization of the readily ionized substances [1, 2] and their ionization by the Penning process through metastable electronic states of nitrogen [3, 4]. The first mechanism can increase the initial electron density in the gas with additives compared with its value in a pure mixture, as well as improve the homogeneity of the SSVD, and also increase the efficiency of systems with insufficiently powerful ultraviolet illumination sources [5, 6]. However, since the density of photoelectrons is much less than that of electrons in a self-sustained discharge plasma, this mechanism does have an important influence on the current–voltage characteristics of an SSVD and on the electron energy distribution function. Consequently, the photoionization of readily ionized substances cannot—for fundamental reasons—improve the output characteristics of a CO_2 laser relative to those obtained using a pure mixture and intense ultraviolet illumination. The ionization of readily ionized substances by the Penning process enables the quantity E/p (where E is the electric field strength and p is the gas pressure) in the quasisteady-state phase of an SSVD, $(E/p)_{qs}$, to be reduced. This makes it possible to extend the ranges of pump source voltages, gas mixture compositions and input energies in which an SSVD is stable, and also to increase the gain and output energy of the CO_2 laser [3, 4, 7, 8]. However, currently, a marked reduction in the quantity $(E/p)_{qs}$ has been observed only when

© Springer International Publishing Switzerland 2016

V.V. Apollonov, *High-Energy Molecular Lasers*,
Springer Series in Optical Sciences 201, DOI 10.1007/978-3-319-33359-5_4

using tri-*n*-propylamine and dimethylaniline [4, 9, 10]. In the present work, for the purposes of seeking other readily ionized substances—the use of which would enable the quantity $(E/p)_{qs}$ to be substantially reduced—and also to study the fundamental laws governing this phenomenon as a function of the ionization potential φ of the readily ionized substance, a comprehensive investigation was carried out into a number of alkyl amines: triethylamine (φ = 7.59 eV), trimethylamine (φ = 7.82 eV), dimethylamine (φ = 8.24 eV) and dibutylamine (φ = 7.69 eV). For convenience of comparison, data are given for tri-*n*-propylamie (φ = 7.23 eV) and dimethylaniline (φ = 7.14 eV), which are also alkyl amines.

The Penning ionization efficiencies of different readily ionized substances were compared by measuring the quantities $(E/p)_{qs}$ and $(E/p)_{sb}$, the latter being the value of E/p for static breakdown, on adding a readily ionized substance to the active mixture. The vapor pressures p_{ti} of the readily ionized substances did not exceed 0.4 Torr and this made it possible to reduce the influence on the results of electron attachment to the additive molecules. A standard amplifier, similar to that described in [11], was used to study the influence of readily ionized substances on the self-sustained discharge characteristics as well as on the laser output parameters. The dependences of $(E/p)_{qs}$ and of the minimum value of E/p for igniting a stable SSVD, $(E/p)_{min}$, on p_{ri} were plotted for reduced pressures (0.4 atm) and for input energies of $\sim$60 J l^{-1} atm^{-1}, and this made it possible to obtain the initial values of these quantities for pure mixtures. The influence of the readily ionized substances on the output characteristics was investigated for mixtures at atmospheric pressure and input energies of $\sim$200–250 J/l. A chamber with an interelectrode gap of 1 cm was used in a study into the dependences of $(E/p)_{sb}$ on p_{ri} and φ. The readily ionized substances were admitted by evaporation into a previously evacuated chamber. Substances with a low boiling point were dissolved to form aqueous (dimethylamine) or alcohol (trimethylamine) solutions and then frozen; they were evaporated into the chamber through a potassium hydroxide trap as they slowly thawed. The value of p_{ri} was measured with an oil manometer and a system of calibrated chambers.

The addition of all the readily ionized substances listed above to the mixture led to a marked reduction in the values of $(E/p)_{qs}$, $(E/p)_{sb}$, and $(E/p)_{min}$ and to an increase in the SSVD current. Figure 4.1 gives the dependences of $(E/p)_{sb}$ in nitrogen on p_{ri} for a number of substances. Figure 4.1 shows that the quantity $(E/p)_{sb}$ saturates with an increase in the parameter p_{ri}. The dependences of $(E/p)_{qs}$ and $(E/p)_{min}$ on p_{ri} are of a similar form. According to the nature of the curves in Fig. 4.1, the readily ionized substances can be divided into two groups. When $\varphi < 7.6$ eV (tri-*n*-propylamine, triethylamine, and dimethylaniline), the experimental points lie close to a single curve and this indicates that the Penning ionization cross sections of these substances are similar, despite the considerable differences in the values of φ. When $\varphi > 7.6$ eV, there is a general tendency toward a reduction in the value of p_{ri} at which point, saturation of $(E/p)_{sb}$ is observed on increase in φ. In addition, the maximum values of the relative decrease $\Delta(E/p)_{sb}$ of

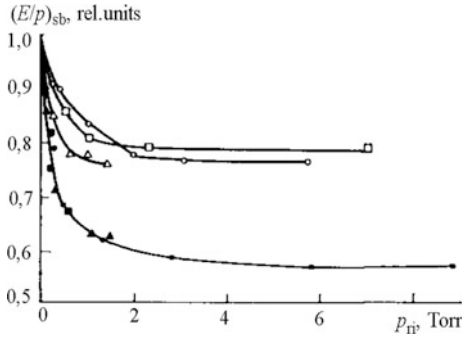

Fig. 4.1 Dependences of $(E/p)_{sb}$ on p_{ri} (0.25 atm) for dimethylaniline (■), triethylamine (•), tri-*n*-propylamine (A), dibutylamine (Δ), dimethylamine (□), and diethylamine (○)

$(E/p)_{sb}$ for the second group of substances do not exceed 22% (compared with 40% for the first group), and this can evidently be explained by the process of strong electron attachment to the molecules of these additives. For the same reason, the relative decrease $\Delta(E/p)_{qs}$ of $(E/p)_{qs}$ for the readily ionized substances in the second group does not exceed 17%, which, for similar conditions, is considerably less than the maximum value of $\Delta(E/p)_{qs}$ (by roughly 40% for tri-*n*-propylamine and triethylamine), determined by complete deexcitation of the metastable electronic states of nitrogen in collisions with the additive molecules [4, 7].

Figure 4.2 gives the dependences of $(\Delta E/p)_{qs}$ in a CO_2:N_2:He = 7:10:23 mixture (at 0.4 atm) and of $(\Delta E/p)_{sb}$ in nitrogen (at 0.25 atm) on φ for p_{ri} = 0.4 Torr. It can be seen that for $\varphi < 7.6$ eV, the values of $(\Delta E/p)_{qs}$ and $(\Delta E/p)_{sb}$, are independent of φ. It was shown experimentally in [12], when studying readily ionized substances having $\varphi > 9$ eV, that the Penning cross section saturates when the condition $E_i - \varphi > 1$ eV is satisfied, where E_i is the excitation potential of the metastable level. In the case considered here, this condition is satisfied for E_i = 8.6 eV, which approximately corresponds to the excitation potential of the $a_1\pi_g$ level of N_2 (E_i = 8.55 eV) through which, according to [3], the Penning ionzation of readily ionized substances can take place in the active mixture of a CO_2 laser. Thus, the curves in Fig. 4.2 reflect qualitatively the dependences on φ of the ionization cross section of the substances readily ionized by the Penning process via the $a_1\pi_g$ metastable electronic state of N_2. A basic consequence of this result is that the magnitude of p_{ri} corresponding to the maximum value of $(\Delta E/p)_{qs}$ also saturates with the parameter φ. This magnitude, normally 1–1.5 Torr, for large separations of the discharge zone from the ultraviolet illumination source ($d > 5$ cm), is considerably higher than that which corresponds to the maximum photoelectron yield for the given separation [13, 14], and this prevents the advantages associated with the photoionization of readily ionized substances from being fully ultilized. The lack of coincidence between the optimal values, in terms of the parameter p_{ri}, for the two ionization processes is particularly marked when using substances that have $\varphi > 7.6$ eV, which can only undergo photoionization by short-wavelength ultraviolet radiation in the neighborhood of the CO_2 $\lambda \sim 120$ nm transmission window, where the readily ionized substances possess large photoabsorption cross sections [15]. Thus,

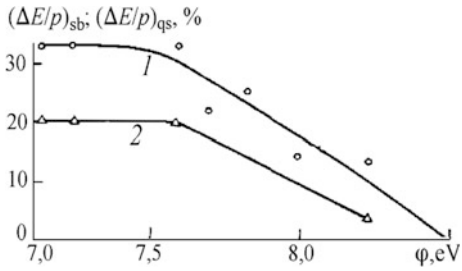

Fig. 4.2 Dependences of $(\Delta E/p)_{sb}$ in N_2 (0.25 atm, *curve 1*) and $(\Delta E/p)_{qs}$ in a CO_2:N_2:He = 7:10:23 mixture (0.4 atm, *curve 2*) on φ for p_{ri} = 0.4 Torr

Table 4.1 Laser output energies obtained using the different readily ionized substances

CO_2:N_2:He mixture	Readily ionized substance	p_{ri}, Torr	Output energy, J/l
1:2:3	tri-*n*-propylamine	1.0	28.5
1:2:3	triehylamine	0.9	27.6
1:1:3	dibutylamine	0.6	24.8
1:1:3	dimethylamine	2.0	15.8

when tri-*n*-propylamine and triethylamine were used in the present work, no appreciable deterioration was observed in the quality of the discharge on varying p_{ri} in the range 0.5–4 Torr. However, on using dimethylamine, for example, the SSVD changed to a streamer discharge for $p_{ri} > 3$ Torr (input energy $\sim$250 J/l, CO_2:N_2:He = 1:1:3 gas mixture). For comparison, Table 4.1 gives the output energies obtained using the different readily ionized substances. The gas mixture composition and the value of p_{ri} were chosen for each of these substances so as to achieve the maximum output energy. It can be seen from Table 4.1 that the output energy decreases with increasing φ. This is a result both of a lowered density of photoelectrons with a corresponding deterioration in the quality of the SSVD, and of a reduction in the magnitude of $(\Delta E/p)_{qs}$.

Let us consider the characteristics of triethylamine in more detail. It can be seen from Table 4.1 that similar output energy results were obtained when using triethylamine and tri-*n*-propylamine, although the former was more convenient to use since it has a high saturated vapor pressure and causes less contamination of the internal surface of the chamber compared with the latter. Figure 4.3 shows the dependences of $(E/p)_{qs}$, $(E/p)_{sb}$, and $(E/p)_{min}$ on the triethylamine pressure p_{TEA} in a CO_2:N_2:He = 7:10:23 mixture. There are characteristic minima in the graphs of the dependences of $(E/p)_{qs}$ and $(E/p)_{min}$ on p_{TEA}, the quantities $(E/p)_{qs}$ and $(E/p)_{min}$ rising considerably more rapidly than $(E/p)_{sb}$ with increasing p_{7TA} at large values of the latter. The increase in $(E/p)_{min}$ and $(E/p)_{qs}$ in the range $p_{TEA} > 3$ Torr is evidently caused not only by the electron losses resulting from electron attachment to the additive molecules, but also from a lowering of the excitation efficiency of the metastable electronic levels of nitrogen at high concentrations of the readily ionized substance, due to a rapid reduction in E/p during the formation stage of the SSVD.

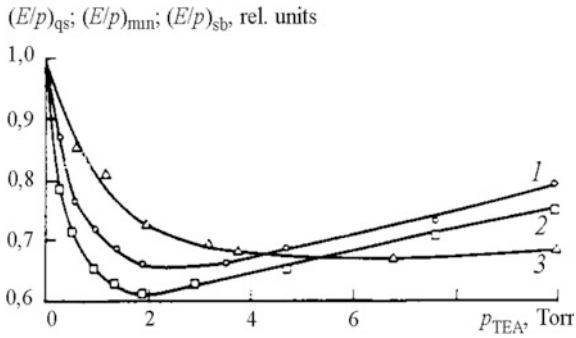

Fig. 4.3 Dependences of $(E/p)_{qs}$ (*curve 1*), $(E/p)_{min}$ (*curve 2*), and $(E/p)_{sb}$ (*curve 3*) in a CO_2:N_2:He = 7:10:23 mixture (0.4 atm) on p_{TEA}

It can also be seen from Fig. 4.3 that, in contrast to SSVD in pure mixtures [16], in the present case, the equality of $(E/p)_{qs}$ and $(E/p)_{sb}$ fails to be satisfied since they have different dependences on p_{TEA}.

We carried out a study on a number of alkyl amines with ionization potentials between 7.14 and 8.24 eV, which acted as readily ionized additives in stabilizing the discharge in a CO_2 laser. It was established that the magntitude of the effect associated with the Penning ionization of the readily ionized substances increases on decreasing φ in the range $7.6 < \varphi < 8.24$ eV, but is independent of φ for $\varphi < 7.6$ eV. The best output energy results were obtained using tri-*n*- propylamine and triethylamine. The use of dimethylaniline was not favored, since (on account of its low saturated vapor pressure) this substance strongly contaminates the internal surface of a discharge chamber. Neither was it advisable to use readily ionized substances with $\varphi > 7.6$ eV due to their small influence on the value of $(E/p)_{qs}$ and their large photoabsorption cross section in the neighborhood of the CO_2 transmission window.

References

1. D.C. McKen, H.J. Seguin, J. Tulip, IEEE J. Quantum Electron. QE **12**, 470 (1976)
2. H.J.J. Seguin, D. McKen, J. Tulip, Appl. Phys. Lett. **29**, 110 (1976)
3. B.J. Reits, J. Appl. Phys. **48**, 3697 (1977)
4. V.V. Apollonov, F.V. Bunkin et al., Kvantovaya Elektron. (Moscow) **6**, 1176 (1979), [Sov. J. Quantum Electron. **9**, 694 (1979)]
5. C. Grigoriu, H. Brinkschulte, Phys. Lett. A **42**, 347 (1973)
6. K.J. Andrews, B. Bhatnagar, P.E. Dyer, G. Salvetti, Opt. Commun. **26**, 228 (1978)
7. V.V. Apollonov, N. Akhunov et al., *Abstracts of Papers presented at Tenth Siberian Meeting on Spectroscopy* (Tomsk, 1981) (in Russian), p. 134
8. V.V. Apollonov, N. Akhunov et al., *Symposium Optika-80* (Budapest, 1980), p. 94
9. V.V. Apollonov, S.I. Derzhavin, et al., Pis'ma Zh. Tekh. Fiz. **5**, 1518 (1979), [Sov. Tech. Phys. Lett. **5**, 643 (1979)]
10. V.V. Apollonov, N. Akhunov, et al., Pis'ma Zh. Tekh. Fiz. **6**, 1047 (1980), [Sov. Tech. Phys. Lett. **6**, 450 (1980)]
11. V.V. Apollonov, F.V. Bunkin et al., Izv. Akad. Nauk SSSR Ser. Fiz. **42**, 2488 (1978)

12. L.A. Taranenko, V.Yu. Orlov, Khim. Vys. Energ. **7**, 73 (1973)
13. Z. Rozkwitalski, M. Grodel, J. Appl. Phys. **51**, 2267 (1980)
14. M.F. Borisov, V.B. Znamenskii, T.P. Uvarova, Zh. Tekh. Fiz. **50**, 1257 (1980), [Sov. Phys. Tech. Phys. **25**, 722 (1980)]
15. D.F. Grosjean, P. Bletzinger, IEEE J. Quantum Electron. QE-13, 898 (1977)
16. A.K. Zhigalkin, Y.L. Sidorov, Z. Tech. Fiz. **48**, 1621 (1978), [Sov. Phys. Tech. Phys. 23, 918 (1978)]

Chapter 5
Electric Discharge CO_2 Laser with a Large Radiating Aperture

Abstract The use of intense bilateral ultraviolet illumination and of readily ionized organic substances established a stable SSVD in an 18-liter chamber with an interelectrode separa-tion of 20 cm, a maximum voltage of 240 kV, and a molecular gas content of up to 40%. A specific output energy of 34 J/l was achieved for an overall system efficiency of 17%.

5.1 Introduction

The possibility of obtaining an SSVD, initiated by ultraviolet radiation in CO_2-N_2-He mixtures at atmospheric pressure with interelectrode separations d of up to 30 cm, was demonstrated some time ago [1, 2]. However, currently, only a few reports [3–5] have been published of large-aperture electric discharge systems (d = 15 cm: [3, 4]; and d = 20 cm: [5]), the specific input and output energies for these systems being considerably inferior to those of small devices. The lowering of the specific characteristics of electric-discharge CO_2 lasers on increase in d and in the total volume is mainly due to the limits on the stability of the SSVD throughout the energy deposition process and also due to the high values of E_{min}, the minimum electric field intensity required to initiate the discharge (here and henceforth we shall be discussing CO_2 lasers with an atmospheric-pressure active mixture). In conjunction with the difficulty of creating a sufficiently high photoelectron density n_0 for a high molecular gas content in the mixture, this means that low-efficiency mixtures [6] with a helium content of 90–70% must be used for large values of d. There are also difficulties that are purely technical.

In [8, 9], we indicated the possibility of realizing an SSVD with d = 25 cm, a specific input energy of up to 300 J/l, and a pump pulse duration of $\sim$2 μs by adding readily ionized substances to the active medium and employing an efficient ultraviolet illumination system. The electrodes described in [8, 9] did not have a special profile, while the value of E_{min} for mixtures with a 40% molecular gas

© Springer International Publishing Switzerland 2016

V.V. Apollonov, *High-Energy Molecular Lasers*,
Springer Series in Optical Sciences 201, DOI 10.1007/978-3-319-33359-5_5

content did not exceed 10 kV/cm. In the present work, we investigated the characteristics of an electric-discharge CO_2 laser with an active volume of 20 × 20 45 cm. The aim was to show that by optimizing the preionization and pumping conditions, it is possible to achieve specific output energies and efficiencies which, for large values of *d,* are not inferior to the corresponding characteristics obtained with small devices.

5.2 General Propositions

It is well known that n_0 must be higher than some critical value throughout the entire active volume for the establishment of an SSVD [10–12]. In the case of unilateral illumination from the cathode side, this requirement is equivalent to the need to provide the necessary conditions for n_0 over the surface of the anode (see, for example, [5]). In systems with large values of *d,* this leads to an unjustified increase in the energy of the preionization source and a reduction in the overall efficiency of the system. Thus, in the work of [5], the energy consumed in preionization reached 45% of that dissipated in the main discharge. It is evident that, despite certain technical difficulties, employment of bilateral illumination is justified for large values of *d* [33, 34]. It is also advisable to position the illumination sources as near as possible to the electrode surfaces in order to reduce the ultraviolet radiation losses and it is also necessary to make the distribution of the illumination intensity highly uniform over the preionizer surface. Among the presently known radiation sources, those utilizing a multichannel "creeping" surface discharge in an electrode system with a high normal component of the electric field [8, 9, 13–16] most closely satisfy these requirements. The ultraviolet radiation sources that employ such a surface discharge, used in the work of [1–3] and [5], do not provide a sufficiently uniform illumination. In addition, their use close to an electrode runs into difficulties due to the danger of electrical breakdown.

Let us briefly dwell on the special features of using readily ionized substances in large-aperture systems. As a rule, for unilateral illumination from the cathode side, the admixture concentration is chosen so as to give the maximum increase in n_0 in the vicinity of the surface of the opposite electrode. For $d > 10$ cm, this concentration does not usually exceed 0.1 Torr. For example, when $d = 15$ cm, the concentration of readily ionized substances (optimized according to this reasoning) is ~ 0.04 Torr [3, 4], only the photoionization mechanism being involved in ionizing the readily ionized substance. In the case of bilateral illumination, it is appropriate to choose the concentration of the readily ionized substance in such a way so as to ensure the maximum increase in n_0 in the vicinity of both electrodes (under the condition that n_0 will not fall below the critical value in the remaining volume), i.e., to optimize its value for distances corresponding to that from the surface of the preionizer to the surface of the nearest electrode. For distances of the order of 1 cm from the ultraviolet radiation

source to the electrode surface, the optimal concentration of the readily ionized substance (for example, tri-*n*-propylamine) is 1–1.5 Torr [13]. At such high admixture concentrations (for readily ionized substances having ionization potentials of $\varphi < 7.6$ eV, two ionization processes are simultaneously efficiently ultilized: photoionization and Penning ionization [14, 15]. The action of the latter mechanism makes it possible to substantially lower not only the electric field intensity E_{qs} in the quasisteady-state phase of the SSVD [14–16], but also the value of E_{min} [15–17], and this is of special importance for large-aperture systems. It is worth mentioning that in [7] and in the case of unilateral illumination (from the cathode side), the best results in terms of the stability of an SSVD with $d = 25$ cm were obtained for concentrations of the readily ionized substance of 1–1.5 Torr. This is in agreement with the conclusions of [8] on the primary need to optimize the preionization conditions in the vicinity of the cathode.

5.3 Experimental Part

Rectangular electrodes were employed in the present work: their overall dimensions were 46 × 70 × 6 cm and they were rounded off along the perimeter (radius 10 cm), so that the dimensions of the plane part were 30 × 53 cm. Windows of dimensions 27 × 53 cm were cut in the electrodes in order to mount the preionization sources. The electrodes were sheathed with a brass mesh made of 0.5 mm diameter wires with a 3 × 3 cm mesh size, and were placed in a 60 cm internal diameter, 100 cm long dielectric tube. In the experiments, the interelectrode distance was varied over the range 10–20 cm, the dimensions of the illumination window being 15 × 50 cm for $d = 10$ and 15 cm and 20 × 20 and 15 × 45 cm for $d = 20$ cm. The electric field inhomogeneity factors, roughly estimated from the ratio of the voltages of the quasisteady-state discharge phase and of the static breakdown, were 1.2, 1.45 and 1.6, respectively for $d = 10$, 15 and 20 cm. For the purposes of increasing the breakdown delay time in the inhomogeneous electric field region when $d > 15$ cm, the electrodes outside the illumination zone were coated with nitrocellulose lacquer. The cathode surface was then covered with a 3 mm thick polyethylene sheet in which a 27 × 50 cm window had been cut. The ultraviolet radiation source took the form of a "creeping" discharge over the surface of a ceramic of high permittivity ε. This type of discharge was first proposed for this purpose in [25, 26].

The electrical circuit of the preionizer used for illumination from the cathode 1 is shown in Fig. 5.1. Under the mesh 2 was mounted a plane electrode 5 to whose surface were bonded eight plates of a ceramic with $\varepsilon = 1100$, with dimensions of 13 × 13 × 1 cm. The body of the preionizer 4 was encased in an epoxy resin 6 along its edges in order to eliminate breakdown from the high-voltage electrode 5 to

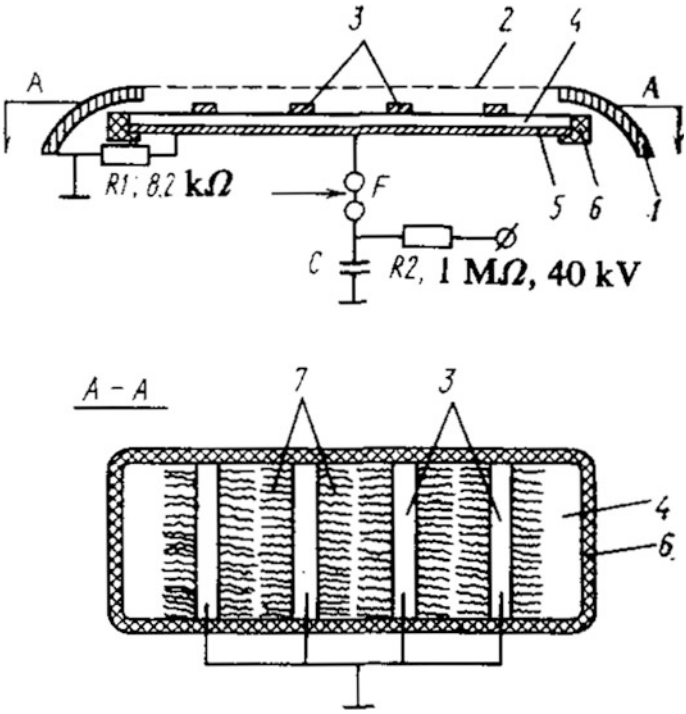

Fig. 5.1 Electrical circuit of the cathode preionizer

grounded electrodes 3. A high-voltage pulse was applied to the preionizer from a $C = 0.1$ μF capacitor, which was charged to 40 kV when a spark gap F was triggered. A discharge 7 of length ~2 cm with five to seven channels per 1 cm width of the discharge gap then developed over the ceramic surface. The discharge filled 75–80% of the total surface area of the preionizer for a specific discharge input energy of less than 0.07 J/cm^2. The system employed made it possible to bring the preionizer surface to within 1 mm of the mesh, although this distance was increased to 1 cm in order to improve the uniformity of illumination.

For illumination from the anode side, a preionizer produced a discharge over the surface of a ceramic with $\varepsilon = 900$, using the normal arrangement [13, 14]. The overall preionizer dimensions were 42.8 × 10.7 × 0.7 cm. A multichannel surface discharge developed in eight parallel 3.5 cm long discharge gaps. A high-voltage pulse was applied to the preionizer from a 0.1 μF capacitor charged to 40 kV. The number of channels per 1 cm width of the discharge was then two to three, with a specific discharge input energy of less than 0.17 J/cm^2. The preionizer was mounted at a distance of 5 cm from the anode surface. Both preionizers were driven from a single high-voltage source and triggered simultaneously with an accuracy of ± 20 ns.

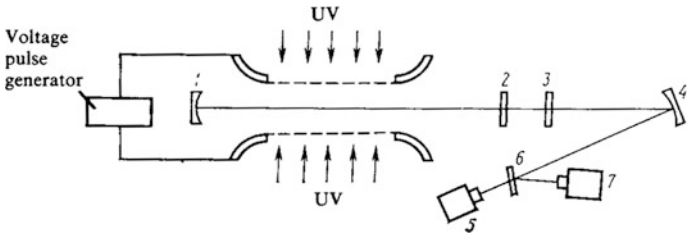

Fig. 5.2 Electrical and optical arrangement of the apparatus

The preionization efficiency was increased and the values of E_{min} and E_{qs} were reduced by adding the readily ionized substances triethylamine and tripropylamine, and a mixture of them, to the active gas. Measurements of the photoelectron concentration, made using an electrostatic probe, showed that in a mixture having a CO_2 content of <10% and at a vapor pressure of the readily ionized substance of ~ 1 Torr the value of n_0 at the cathode surface reached $\sim 10^{12}$ cm^{-3}.

In all the regimes in which the apparatus was operated the energy consumed in preionization did not exceed 5% of that dissipated in the main discharge. This discharge was pumped with an Arkad'ev-Marx voltage pulse generator constructed from IK-100–0.25 capacitors. For d = 10, 15, and 20 cm, the voltage pulse generator consisted of two, three and four stages, respectively, with each stage having a 0.5 μF capacitance.

The current–voltage characteristics of the SSVD and of the preionization discharge were monitored with a resistive divider and coaxial shunts [27]. The signals were recorded using an S8-2 storage oscilloscope.

In Fig. 5.2, the 1 m long laser resonator was formed by a spherical mirror (1) with a 230 mm diameter and a radius of curvature R = 24 m, and a plane dielectric-coated germanium mirror (2), with a 150 mm diameter and reflection coefficient $\sim 80\%$. The mirrors were mounted directly on the ends of the discharge chamber. The laser output energy was measured with a TPI-2-5 calorimeter (5). For this measurement, the beam was focused, after having been attenuated with a set of calibrated filters (3), by a copper mirror (4) (R = 10 m) onto the calorimeter surface in a 45 mm diameter spot. The shape of the output radiation pulse was recorded with an FP-5 photodetector (7) after having been reflected from an NaCl plate (6).

5.4 Experimental Results and Discussion

The use of the preionization and pumping arrangements described previously made it possible to obtain an SSVD in a wide range of gas mixture compositions, having a molecular gas content of up to 40% with input energies of up to 250 J/l. The maximum input energy was limited by the amount of energy stored in the voltage pulse generator.

It was established that the use of bilateral illumination enabled the quality of the SSVD to be improved and the service life of the active gas to be lengthened. For unilateral illumination (from the cathode side) and input energies above 200 J/l, in mixtures with a molecular gas content exceeding 25%, partial streamers were already developing in the anode region for d = 15 cm. For unilateral illumination from the anode side and for d = 10 cm, a similar picture was observed in the cathode region, i.e., an instability formed on the electrode remote from the illumination source. In subsequent experiments on systems with d > 10 cm, bilateral illumination was employed. It was established that the anode preionizer played a secondary role. Removing it to a distance of up to 7 cm from the electrode surface had practically no effect on the structural quality of the self-sustained bulk discharge or on the quality of the output radiation. In the final variant of the system the anode preionizer was positioned at a distance of 5 cm from the electrode surface and this enabled sufficiently intense and uniform illumination to be provided while at the same time eliminating the influence of illumination from the anode side on the area occupied by the SSVD on the cathode.

For d = 10 and 15 cm, despite the high peripheral inhomogeneity of the electric field in the electrode system employed in the present work, because of the high photoelectron density on the cathode surface, the discharge developed only in a region bounded by the dimensions of the illumination zone and was stable for molecular gas contents in the mixture of up to 40% and a specific input energy to the SSVD plasma of up to 250 J/l. For d = 20 cm, a spark breakdown always developed in the zone of maximum electric field inhomogeneity at a time 1–1.2 μs after the start of the diffuse phase of the SSVD. Only the special measures mentioned above, which were taken in order to increase the delay time of this breakdown, enabled a stable discharge to be formed with characteristics that did not differ from those of an SSVD with d = 15 cm. The maximum values of the specific input energy for mixtures with a molecular gas content of up to 40% were 200 J/l, for dimensions of the cathode illumination zone of 20 × 45 cm, and ~260 J/l when the width of this zone was reduced to 15 cm. In mixtures with a molecular gas content of 20–25%, we were able to form up to 40 stable discharges for one charge of active gas without any appreciable reduction in the output energy. In mixtures containing more than 25% of molecular gases, the number of stable SSVDs was reduced to roughly 20.

Figure 5.3 shows characteristic oscillograms of pulses of the voltage and current for an SSVD, of the preionizer current, and of the laser radiation in a CO_2:N_2:He = 8:16:76 mixture with d = 20 cm for a voltage pulse generator output of 240 kV. As can be seen from Fig. 5.3, practically all the energy stored in the capacitors of the voltage pulse generator was transferred to the discharge plasma. It must be mentioned that in all the regimes investigated, for which a stable discharge was formed on account of the presence of the readily ionized substance in the mixture, not less than 90% of the energy stored in the capacitors was coupled into the SSVD plasma. Figure 5.3 shows the optimal relative timing of the preionizer current and pump-voltage pulses. A change in the delay between them by +0.5 μs

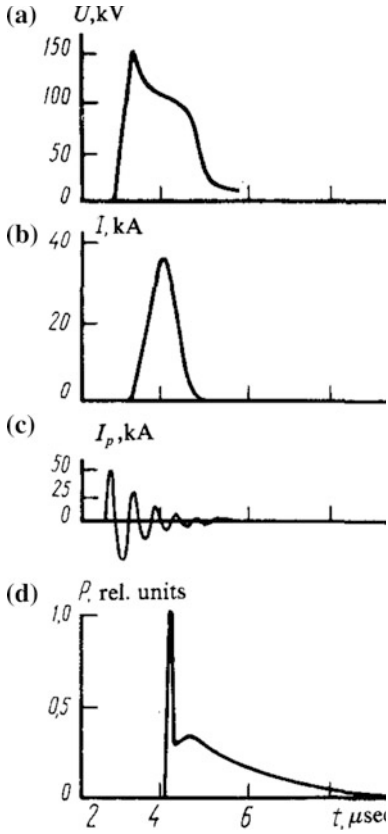

Fig. 5.3 Oscillograms of pulses of the voltage ***U*** (**a**) and current ***I*** (**b**) for an SSVD, of the preionizer current $\boldsymbol{I_F}$ (**c**), and of the laser output power ***P*** (**d**)

was not critical with regard to the stability of the SSVD. It can also be seen from Fig. 5.3 that the radiation pulse had the usual form expected for CO_2 lasers.

The results of measurements of the laser output energy for a number of mixtures with d = 15 and 20 cm are given in Table 5.1 (no optical measurements were made for d = 10 cm). For purposes of comparison, Table 5.1 also gives the values of E_{qs}. The E_{min} values were not determined in the present work since, for low charging voltages of the voltage pulse generator, spark breakdown developed outside the illumination zone due to the residual voltage on the electrodes. It can be seen from Table 5.1 that, as is usually the case [16], the efficiency and output energy increased on raising the fraction of the molecular gases in the mixture. For identical values of the input energy, the maximum specific output energies and efficiencies were practically the same for d = 15 cm and d = 20 cm. The maximum specific output energy for d = 20 cm was 41 J/L, with an efficiency of 15.4% (for a volume of 20 × 15 × 45 cm). For a discharge volume of 20 × 20 × 45 cm, the specific output energy was 34 J/L and the efficiency was 17%. In this case, a radiation energy of 270 J was coupled with a 15 cm diameter mirror aperture. The total energy that could be extracted from the discharge zone was estimated by measuring

Table 5.1 The results of measurements of the laser output energy for a number of mixtures with d = 15 and 20 cm

Mixture CO_2:N_2: He	Specific input energy W_p (J/L)	Specific output energy W_L (J/L)	Efficiency (%)	Volume (cm^3)	E_{qs} (kV/cm)
d = 15 cm					
10:10:80	208	26.2	12.5	15 × 15 × 50	4.95
10:20:70	208	33.8	16.3	15 × 15 × 50	6.02
10:20:70	248	37.4	15	15 × 15 × 50	6.02
8:32:60	248	39.7	16	15 × 15 × 50	6.7
d = 20 cm					
6:14:80	200	24.8	12.4	20 × 20 × 45	
8:16:76	168	28.6	17	20 × 20 × 45	5.28
10:20:70	200	30.5	15.2	20 × 20 × 45	5.83
6:24:70	187	30.5	16.3	20 × 20 × 45	5.28
8:32:60	200	34	17	20 × 20 × 45	6.6
8:32:60	267	41	15.4	20 × 15 × 45	6.6

the radiation energy distribution over the discharge cross section on parallel displacement of a resonator formed by 30 mm diameter mirrors. These measurements showed the radiation to be distributed uniformly, to an accuracy of 10%, over a 20 × 20 cm cross section, i.e., for an input energy of 200 J/L, it is possible to obtain an energy of ~600 J from a 20 × 20 × 45 cm discharge zone. The results given in the present work suggest that this is not the ultimate value.

It must be mentioned that in terms of its specific characteristics, the total output energy and efficiency, the apparatus that was built is superior to the presently known electric-discharge systems with apertures of greater than 10 cm [5, 6], and, in terms of its specific characteristics, it is negligibly inferior to systems with apertures of less than 10 cm [18, 28–32], exceeding many of these in terms of its efficiency.

References

1. M.C. Richardson, K. Leopold, A.J. Alcock, IEEE J. Quantum Electron. QE-9, 934(1973)
2. V.Y. Baranov, V.M. Borisov, Y.A Satov, Y.Y. Stepanov, Kvantovaya Elektron. (Moscow) **2**, 2086 (1975) [Sov. J. Quantum Electron. **5**, 1139 (1975)]
3. J. Domey, Rev. Sci. Instrum. **46**, 811 (1975)
4. Y. Ohwadano, T. Sekiguchi, Jpn. J. Appl. Phys. **19**, 1493 (1980)
5. Technical data from the firm Lumonics, 1980
6. J.J. Lowke, A.V. Phelps, B.W. Irwin, J. Appl. Phys. **44**, 4664 (1973)
7. V.V. Apollonov et al., Kvantovaya Elektron. (Moscow) **10**, 1458 (1983) [Sov. J. Quantum Electron. **13**, 947 (1983)]

8. V.N. Karnyushin, R.I. Soloukhin, *Macroscopic and Molecular Processes in Gas Lasers (in Russian)* (Atomizdat, Moscow, 1981)
9. A.J. Palmer, Appl. Phys. Lett. **25**, 138 (1974)
10. J.I. Levatter, S.-C. Lin, J. Appl. Phys. **51**, 210 (1980)
11. Yu.I. Bychkov, D.Yu. Zaroslov, N.V. Karlov, G.P. Kuz'min, V.V. Osipov, A.M. Prokhorov, V.A. TePnov, Kvantovaya Elektron. (Moscow) **9,** 1718 (1982) [Sov. J. Quantum Electron. **12**, 1105 (1982)]
12. E.P. Bel'kov, P.N. Dashuk, G.L. Spichkin, Zh. Tekh. Fiz. **52,** 1979 (1982) [Sov. Phys. Tech. Phys. 27, 1216 (1982)]
13. Z. Rozkwitalski, M. Grodel, J. Appl. Phys. **51**, 2267 (1980)
14. B.J. Reits, A.H.M. Olbertz, Appl. Phys. Lett. **27**, 24 (1975)
15. V.V. Apollonov, A.I. Barchukov et al., Pis'ma. Zh. Tekh. Fiz. **3**, 1073 (1977) [Sov. Tech. Phys. Lett. **3**, 441 (1977)]
16. V.V. Apollonov, F.V. Bunkin et al., Kvantovaya Elektron. (Moscow) **6**, 1176 (1979) [Sov. J. Quantum Electron. **9**, 694 (1979)]
17. A.A. Kuchinskii, V.A. Rodichkin, Zh Tekh, Fiz. **53**, 563 (1983) [Sov. Phys. Tech. Phys. **28**, 352 (1983)]
18. I.K. Krasyuk, N.I. Lipatov, P.P. Pashinin, Kvantovaya Elektron. (Moscow) **3**, 2384 (1976) [Sov. J. Quantum Electron. **6**, 1298 (1976)]
19. E.I. Azarkevich, Y.A. Kotov, Prib. Tekh. Eksp. **6**, 119 (1976)
20. D.A. Goryachkin, V.M. Irtuganov, V.P. Kalinin, Y.T. Mazurenko, Y.A. Rubinov, Izv. Akad. Nauk SSSR Ser. Fiz. **46**, 1877 (1982)
21. Y.A. Anan'ev, D.A. Goryachkin, V.M. Irtuganov, V.P. Kalinin, O.I. Pashkov, V.A. Solov'ev, Kvantovaya Elektron. (Moscow) **5**, 1381 (1977) [Sov. J. Quantum Electron. **8**, 792 (1978)]
22. V.F. Basmanov, V.S. Bosamykin, V.V. Gorokhov, V.I. Karelin, A.I. Pavlovskii, P.B. Repin, A. Ya, Kharchenko. Zh. Tekh. Fiz. **52**, 128 (1982) [Sov. Phys. Tech. Phys. **27**, 85 (1982)]
23. V.Y. Baranov, V.M. Borisov, A.M. Davidovskii, O.B. Khristoforov, Kvantovaya Elektron. (Moscow) **8**, 77 (1981) [Sov. J. Quantum Electron. **11**, 42 (1981)]

Chapter 6
Formation of an SSVD with Intense Ultraviolet Irradiation of the Cathode Region

Abstract An investigation was made into the influence of the voltage rise time on the characteristics of an SSVD in CO_2-N_2-He mixtures. When the region near the cathode was subjected to intense and prolonged ultraviolet irradiation, the use of a pumping regime with a deliberately prolonged voltage rise time made it possible to obtain an SSVD in an electrode system with a highly inhomogeneous electric field at its edges, and to raise the CO_2 laser efficiency.

It is well known that the feasibility of an SSVD in dense gases is governed not only by the initial electron density and electric field intensity [1, 2], but also by the rate of rise of the electric field in the discharge gap [3–5]. In view of this, it is normally recommended that the active media of gas lasers should be excited by pulses with a short voltage rise time. However, it is evident that the voltage rise time τ can be increased if the initial electrons are produced (to be specific, we shall consider the case of ultraviolet preionization) by a high-power source that is applied for a sufficiently long time. The rate of loss of electrons from the regions near the cathode by drift must then not exceed their rate of formation by ultraviolet radiation.

Our aim for this chapter of the book was to investigate the characteristics of an SSVD under conditions of intense ultraviolet irradiation of the region near the cathode, the effects of different forms of the voltage rise on the electrodes, and efficient regimes for pumping the active media of CO_2 lasers. The following regimes were employed: a short voltage rise time ($\tau < 0.2$ μs); a short voltage rise time with previous application of a dc voltage to the gap; and a deliberately prolonged voltage rise time ($\tau > 0.5$ μs).

The experiments were performed on a CO_2-N_2-He gas mixture at atmospheric pressure containing 10% of CO_2, up to 50% of N_2, and the readily ionized substances tripropylamine and triethylamine. Two electrode systems were used. In the first of these, the electrodes had a Rogowski profile, while in the second they had 4 cm radius rounded edges. The electric field inhomogeneity coefficients, for an interelectrode gap of $d \sim 10$ cm, were ~ 1.05 and 1.4 respectively. Radiation from "creeping" discharges over ceramic surfaces passed through a window in the cathode covered with a brass mesh. Energy was liberated in the "creeping"

© Springer International Publishing Switzerland 2016

V.V. Apollonov, *High-Energy Molecular Lasers*,
Springer Series in Optical Sciences 201, DOI 10.1007/978-3-319-33359-5_6

discharge in a total time of ~2 μs. The maximum electron density at a distance of 5 cm from the cathode reached a value of $10^8 \sim 10^9$ cm^{-3}: according to [7], this corresponded to the density $n_0 = 10^{11}$–10^{12} cm^{-3} at a cathode. The prolonged voltage rise time regime was produced by a Fitch generator (having no spark gap at its output) and the short voltage rise time regime was produced by an Arkad'ev-Marx generator. To be specific, the values of r are given for open-circuit operation.

A stable discharge could be obtained in all regimes with the Rogowski electrode system, but inhomogeneities in the form of 2 cm long bright channels were observed near the cathode for the short voltage-rise time regime with input energies of >180 J/l. Figure 6.1 shows typical oscillograms of the radiation source current and also of the voltage and current in an SSVD in the prolonged-rise time regime (τ = 2.5 μs) and in the short voltage rise time regimes with and without a preapplied dc voltage. It is worth highlighting that in the prolonged voltage-rise time regime, the irradiation began during the voltage rise. It can be seen from Fig. 6.1, that the discharge characteristics in the three regimes differ only during the formation phase of the SSVD. In the short voltage riset ime regime, the maximum voltage (the ignition voltage U_j of the discharge) is roughly a factor of 1.6 higher than in the prolonged voltage rise time regime, while the current and voltage in the quasisteady-state phase of the discharge are practically independent of the regime. The short voltage rise time regime with a preapplied dc voltage occupies an intermediate position between the other two regimes to regard to U_i. The small differences in the amplitude and duration of the current in Fig. 6.1b, c result from differences in the discharge circuit inductances of the Fitch and Arkad'ev-Marx arrangements. It was established that in the case of intense irradiation, the value of U_i is considerably less than the breakdown voltage U_b for an unirradiated gap and that the ratio U_b/U_i increases with τ. Thus, for the optimal delay time between the main and auxiliary discharges in the prolonged voltage-rise time regime characterized by τ = 2.5 μs, this ratio reached ~1.42 while in the short voltage rise time regime it did not exceed 1.2. A characteristic feature was that in the short voltage rise time regime the ignition voltage of the SSVD was only a weak function of the radiation intensity and of the delay between switching it on and operating the pump source. Neither did it change on reversing the pump source polarity, this being equivalent to reducing n_0 at the cathode by roughly three orders of magnitude [7]. We were not able to obtain an SSVD in the regime with a short voltage rise time and a preapplied dc voltage, nor was it possible to obtain an SSVD with a prolonged voltage rise time when the radiation came from the anode side, since the ultraviolet radiation intensity at the cathode was insufficient in this case to replace the electrons leaving the cathode region by drift in the electric field. This was in agreement with the work of [3–5].

In the short voltage rise time regime with a preapplied dc voltage, the conditions during the formation phase of an SSVD were similar to those in the prolonged voltage-rise time regime since, in both cases, the photoplasma was formed after the electric field had been applied. In the former of these regimes, a monotonic reduction was observed (by a maximum of 15%) on increasing the dc voltage up to

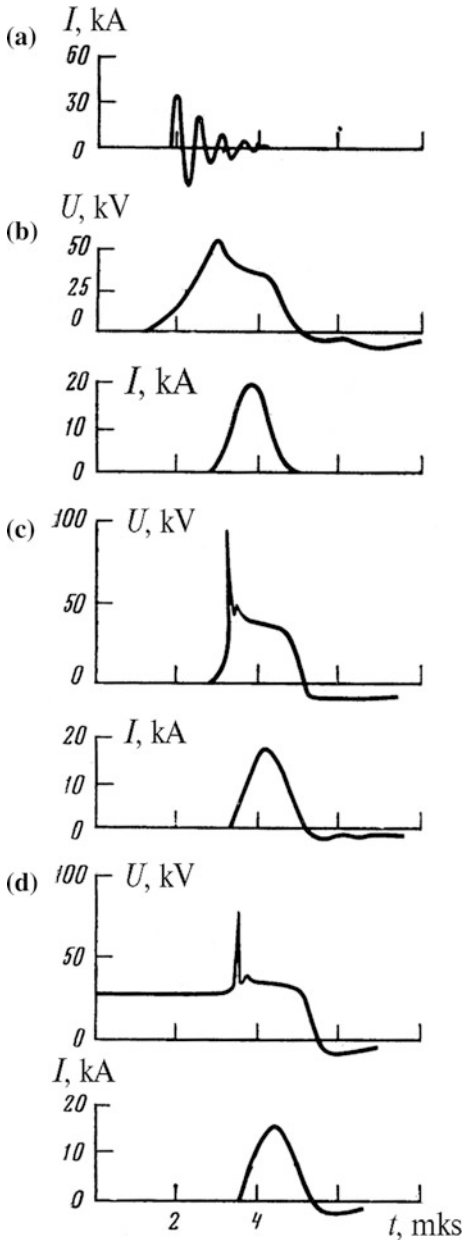

Fig. 6.1 Oscillograms of pulses of the radiation-source current (**a**) and of the SSVD voltage and current obtained in the prolonged voltage rise time regime (**b**), the short voltage rise time regime (**c**), and the short voltage rise time regime with preapplied DC voltage (**d**)

the static breakdown value U_{st}, and this was accompanied by a marked improvement in the homogeneity in the zones near the electrodes and by an increase in the service life of the active mixture.

The dependences on r of the influence of irradiation on the ignition voltage of an SSVD indicate the possibility of effectively separating the irradiated region of the gas and obtaining an SSVD with large edge-inhomogeneity coefficients of the electric field by using the short voltage-rise time regime with preapplied dc voltage or the prolonged voltage-rise time regimes with large values of τ. In actuality, the possibility of realizing a self-sustained volume discharge in an unprofiled electrode system was strongly dependent on τ. For $\tau < 1$ μs, an SSVD always terminated with spark breakdown at the electrode edges (outside the irradiated zone), delayed relative to diffuse breakdown in the irradiated zone by 1–1.2 μs. For $\tau > 1.3$ μs, the SSVD was localized within the irradiation window on the cathode. The same SSVD characteristics were obtained in the regime with the short voltage rise time and preapplied dc voltage when the latter was close to U_{st}. For $1 < \tau < 1.3$ μs, the discharge was also diffuse, but it developed in both the irradiated zone and outside it (evidently due to a corona discharge from the mesh points) and had numerous structural defects in the form of incomplete streamers localized mainly outside the irradiation window.

We therefore find that in the case of intense and sufficiently prolonged irradiation of the region near the cathode an increase in τ does not lead to a loss of stability of an SSVD, but it makes the latter considerably easier to achieve in a system of unprofiled electrodes.

It follows from the results given that during the formation phase of an SSVD, under the experimental conditions considered, a mechanism associated with the irradiation acts to increase the electric field in the irradiated region relative to the external field, and this makes it possible to reduce the influence of edge inhomogeneity on the discharge development. This effect is reinforced in the case when the irradiation lasts a sufficiently long time after the voltage has been applied to the gap. It is reasonable to assume that such a mechanism involves a distortion of the field in the gap due to the polarization of the dense photoplasma and subsequent redistribution of the space charge.

Let us use the following quantitative model to interpret the results presented. Let us assume that an external field E_0 is switched on after a photoplasma with an initial density $n - f(x)$ has been formed in the gap (the X axis being directed from the cathode to the anode). For simplicity, let us assume that $f(x) = n_0\exp(-x/L)$. Owing to polarization of the photoplasma, the field E will be expelled from a region close to the cathode and will be strengthened in the remaining part of the gap, reaching a maximum at the electrodes and a minimum on the interface between the positive and negative space charges ($x = 5$). Assuming that the polarization of the photoplasma occurs in a short time during which the form of the spatial charge density distribution remains substantially constant (the short voltage-rise time regime), it is possible to readily obtain an expression for $E(x)$ from Poisson's equation, and the dimensions of the region where $E < E_0$ can be estimated. For the values of $L/d = 0.1$–0.2, which characterize the experimental conditions considered [7], and for $8 < L$, the dimensions of this region are $\sim 2L$.

The lowering of the field at the charge interface will prevent any further expansion of the zone depleted of electrons, while its strengthening in the region

where $x > 2L$ must lead to a reduction in U_t on account of the nonlinear dependence on E of the collisional ionization coefficient. This was observed experimentally. If in a time r the negative space charge in the region where $x > 5$ cannot be significantly redistributed over the gap, the expressions for the maximum values of <5 and for the field intensities at the cathode and anode $E_c \sim E_a$, determined by the condition E (x = <5) = 0, are of the form

$$\delta_{\max} = \varepsilon_0 E_0/[en_0(1 - L/d)]; \tag{6.1}$$

$$E_c^{\max} = E_0/(1 - L/d), \tag{6.2}$$

where e is the electronic charge and e_0 is the permittivity. Expression (2) for E is also valid when the irradiation is from the anode side. It also follows from this expression that in the short voltage-rise time regime E™** is independent of n_0. This also explains the experimentally observed weak dependence of U_t in this regime on the radiation intensity and on the polarity of the pump source. For values L/d = 0.1–0.2, we find that E™*/E_0 = 1.11–1.15, and this is close to the measured value of the ratio U_b/U_j for the short voltage rise time regime. According to (1), it is appropriate to increase n_0, since this will reduce the dimensions of the zone near the cathode, which is depleted of electrons and will lower the probability of the development of an instability accompanying the formation of a cathode layer [3].

If the photoplasma is formed after the voltage has been applied (the prolonged voltage rise time and short voltage rise time with a preapplied dc voltage regimes), then for intense and prolonged irradiation a considerable distortion of the electric field in the gap may be achieved (even in its initial phase), while the field will be subsequently strengthened at the electrodes as a result of a redistribution of the space charge as it moves to the anode. Therefore, a greater relative lowering of U, under the action of ultraviolet irradiation is observed in regimes with long values of r compared with the case of the short voltage rise time regime. It must be mentioned that no depletion of the zone near the cathode occurs in these regimes since some minimum electron density at the cathode is maintained by the ultraviolet radiation source over the entire formation period of the SSVD (Fig. 6.1). In addition, since in the present case (in contrast to that for the short voltage rise time regime), a photoplasma is created and remains in the field for an extended time until the SSVD is ignited, two positive effects are realized: the photoelectron losses up to the moment of ignition of the volume discharge are reduced owing to an increase in the effective ionization coefficient; and the electrons from the region near the cathode, where their density is high, are transported into the gap. The experimentally observed improvement in the homogeneity of SSVDs in regimes with large values of r can evidently be explained by the combined action of these factors, and by the fact that in the prolonged voltage rise time and short voltage rise time with a preapplied dc voltage regimes, an SSVD is formed at a lower average electric field intensity in the gap than in the short voltage rise time regime and, as a result of this, the current density gradients caused by local electric field gradients at the cathode are reduced when the cathode layer is formed.

Let us now consider yet another characteristic feature of the regimes in which the region near the cathode is subjected to intense and prolonged irradiation after switching on the electric field. It is probable that, in this case, a cathode layer may form during the irradiation phase as a result of the field being distorted. Indirect confirmation of this suggestion is provided by the oscillograms of voltage and the current of an SSVD given in Fig. 6.2. These were obtained under conditions when the gap voltage was below the minimum value at which SSVD ignition can occur in the short voltage rise time regime [2]. If the irradiation takes place before the field has been switched on (Fig. 6.2a), the discharge terminates with spark breakdown, evidently due to the fact that during the time in which the electron density rises in the gap (owing to distortion of the field by a redistribution of the negative space charge over the gap), the cathode region can become considerably depleted and an instability occurs when the cathode layer is formed. The discharge becomes diffuse if the radiation is switched on after the gap voltage has reached its maximum (Fig. 6.2b). A similar picture is observed if the radiation is switched on when the gap voltage is 5 U_{st} (Fig. 6.2c). It can be assumed that in the latter two cases, an intense collisional ionization process due to distortion of the field first develops in the regions of higher field intensity (i.e., near the anode and cathode), a cathode layer is formed, and then the electron density becomes uniform over the gap, reaching an estimated value of $\sim 10^{12}$ cm^{-3}. If an electron-emitting cathode layer does not form during the irradiation, then in instances that characterize the regime of Fig. 6.2c, the cathode region will be depleted of electrons and the situation depicted in Fig. 6.2a occurs. It should be mentioned that the regime of Fig. 6.2c can be used to prepare conditions in the gap for coupling in the main pump energy.

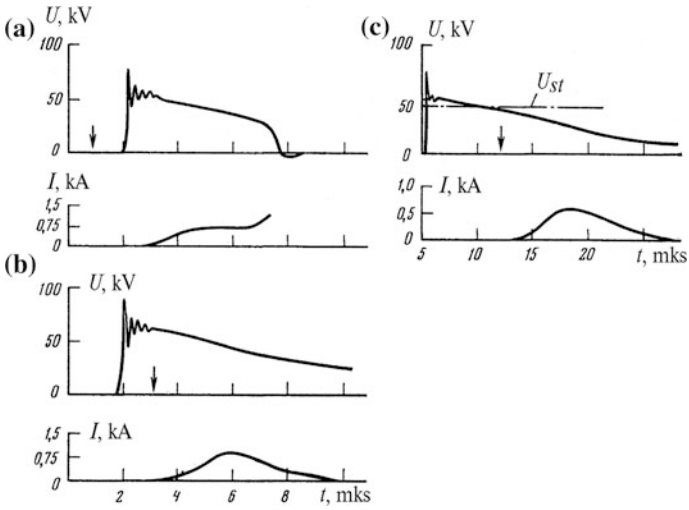

Fig. 6.2 Oscillograms of voltage and current pulses for cases when irradiation was applied before (**a**) and after (**b**) the voltage maximum, and also for a voltage near U_{st} (**c**). *Arrows* indicate the start of irradiation

An improvement in the homogeneity of an SSVD in the prolonged voltage rise time and short voltage rise time with a preapplied dc voltage regimes should be accompanied by a rise in the CO_2 laser efficiency. In fact, we observed that for input energies of 200–300 J/l, an increase in the output energy of a CO_2 laser by approximately 30%, compared with that for the short voltage rise time regime. In the case of low input energies, there was an insignificant change in the efficiency on transitioning from the short voltage rise time regime to the regimes with larger values of τ.

It is important to mention that an increase in the duration of the voltage rise time was utilized in one of the first CO_2 laser models employing a transverse discharge [8, 9] in order to provide a delay between the auxiliary and main discharges. However, in these studies and in later publications devoted to investigating this system, the processes considered in the present work were not discussed.

Our results show that in the case of intense irradiation of the region near the cathode, an important factor influencing the formation and development of SSVDs is the distortion of the electric field in the gap due to polarization of the photoplasma. When the duration of the irradiation is sufficiently long, it is appropriate to employ a pumping regime for obtaining an SSVD in which the voltage rise time is artificially prolonged. This makes it possible to improve the homogeneity of the discharge, to reduce the demands on the accuracy of the electrode profiles, and to increase the CO_2 laser efficiency.

References

1. A.J. Palmer, Appl. Phys. Lett. **25**, 138 (1974)
2. V.N. Karnyushin, R.I. Soloukhin, *Macroscopic and Molecular Processes in Gas Lasers (in Russian)* (Atomizdat, Moscow, 1981)
3. J.I. Levatter, S.-C. Lin, J. Appl. Phys. **51**, 210 (1980)
4. D.B. Gurevich, M.A. Kanatenko, T.D. Sidorova, Zh Tekh, Fiz. **53**, 68 (1983) [Sov. Phys. Tech. Phys. 28, 38 (1983)]
5. M.A. Kanatenko, Pis'maZh. Tekh. Fiz. **9**, 214 (1983) [Sov. Tech. Phys. Lett. *9*, 94 (1983)]
6. V.V. Apollonov, N. Akhunov et al., Kvantovaya Elektron. (Moscow) **10**, 1458 (1983) [Sov. J. Quantum Electron. *13*, 947 (1983)]
7. Z. Rozkwitalski, M. Grodel, J. Appl. Phys. **51**, 2267 (1980)
8. R. Dumanchin, J. Rocca-Serra, C.R. Acad, Sci. Ser. B. **269**, 916 (1969)
9. Yu-Li Pan, A.F. Bernhardt, J.R. Simpson, Rev. Sci. Instrum. **43**, 662 (1972)

Chapter 7
High-Energy Electric-Discharge CO_2 Laser with Easily Ionizable Substances Added to the Mixture

Abstract Optimization of the pumping regime and of the resonator parameters, as well as the correct choice of easily ionizable additives to the active mixture of a CO_2 laser excited by an SSVD ensured a specific output energy of 51 J/l and a conversion efficiency of electrical into optical energy of 22 % in an active medium volume of 16 l.

7.1 Introduction

In recent years, pulsed CO_2 lasers pumped by an SSVD initiated by ultraviolet radiation have become highly popular in laboratory investigations. The following basic requirements are imposed on such lasers: simplicity of construction, reliability, high efficiency, small overall dimensions, reasonably low operating voltages, uniformity of the radiation energy distribution over the beam cross section, and the possibility of varying the output parameters over a wide range. One of the difficulties arising with large-aperture systems is the need for accurate profiling of the electrodes, the transverse electrode dimensions considerably exceeding the interelectrode separation (e.g., by a factor of 3–4 in the case of a Rogowski profile). A compact electrode system was proposed in one of the first studies [1] devoted to a transverse-discharge CO_2 laser. In [2, 3], a uniform radiation energy distribution was obtained in a design of this type over an aperture of 10×10 cm, with a specific output energy of ~ 35 J/l, by using easily ionizable substances; the cathode width (10 cm) was equal to the interelectrode separation.

In the present work, the parameters of the laser described in [2] were optimized. The aim was to show that the correct choice of the easily ionizable substances, of the mirror reflection coefficients, and of the regime for coupling energy into the active gas makes it possible to obtain efficiencies as well as specific output energies from a system with a simple and compact construction of the electrodes, pumped by an SSVD, which are not inferior to the corresponding characteristics of electron beam-controlled lasers.

© Springer International Publishing Switzerland 2016

V.V. Apollonov, *High-Energy Molecular Lasers*,
Springer Series in Optical Sciences 201, DOI 10.1007/978-3-319-33359-5_7

7.2 Apparatus

A four-section CO_2 laser was used in our experiments; it was similar to that described in [2] and the discharge zone of each section had the dimensions 10 × 10 × 40 cm. All the sections were fed from independent pump sources and could be switched on either simultaneously or in any given sequence. Two-stage Arkad'ev-Marx voltage pulse generators served as the pump sources, having a discharge capacitance C_1 = 0.25 μF and a maximum voltage of U = 120 kV, discharged through an inductance of L = 15–20 μH into an IMN-100-0.1 capacitor of value C_2 = 0.1 μF connected in parallel with the discharge gap. The voltage pulse generators were assembled using IK-100 × 0.25 commercial capacitors. The 75-Ω resistors, which served to prevent spark breakdown of the gap following the passage of the main pump pulse, were also connected in parallel with the gap The inductance in the discharge circuit of C_1 across the gap was ~1 μH.

The experiments were performed on CO_2–N_2–He atmospheric pressure gas mixtures with a 50% molecular gas content. The results are provided below for a CO_2:N_2:He = 1:4:5 mixture, which gave the maximum specific output energies in the presence of easily ionizable substances. Tripropylamine and triethylamine were mainly used as the latter. The results were compared with the data on metaxylene given in [2]. Calibrated resistance dividers and shunts were employed for monitoring the discharge characteristics.

A 3 m long laser resonator was formed by a 40 m radius concave copper mirror and an interchangeable plane-parallel exit mirror. A single-crystal plate of Ge, antireflection-coated on the exit surface (reflection coefficient K = 0.36), Ge plates with antireflection-coated exit surfaces and reflecting coatings on the working surfaces (K = 0.25, 0.7 and 0.8), and uncoated plates of Ge (K = 0.51) and NaCl (K = 0.08) were employed as exit mirrors.

Part of the output radiation was deflected by wedges made of NaCl so that its parameters could be measured. The energy was monitored with a TPI2-5 calorimeter, and the shape and duration of the pulses were determined with an FP-5 photodetector.

The signals were recorded with S8–14 and S8–11 oscilloscopes.

7.3 Volume Discharge Characteristics

In order to obtain a stable volume discharge, providing homogeneous excitation of the active medium, it is important to choose the easily ionizable substance correctly. The two known ionization processes that enable the characteristics of a CO_2 laser to be improved on introducing easily ionizable substances into the active gas are photoionization [4] and the Penning ionization of this substance [5, 6]. The form of the additive and its concentration must be chosen in such a way that both of these processes are utilized maximally. It was shown in [7, 11] that these requirements are satisfied by the alkyl amine class of substances such as tripropylamine and

triethylamine. They have the largest Penning ionization cross sections and also are efficiently ionized by ultraviolet radiation in the region of both of the CO_2 transmission windows (110 and 160 nm, see [4]). As a result, a photoelectron density sufficient to ignite an SSVD can be created not only near the ultraviolet radiation source (in the present arrangement, directly on the cathode surface), but also at large distances from it, even at vapor pressures of the easily ionizable substance that exceed 1.5 Torr [8].

Let us consider the operation of the pump system in more detail. Its special feature, compared with the usual systems for producing an SSVD, [9] is the long risetime τ of the gap voltage. Under these conditions, the discharge conductivity and, consequently, also the input energy (for a constant voltage on the pulse generator) were substantially determined by the nature of the easily ionizable substance and its concentration in the mixture. Maximum input energies of 250 J/l were achieved in mixtures with added tripropylamine and triethylamine, while in those with added metaxylene they did not exceed 150 J/l.

It was also established that the discharge homogeneity is improved on increasing τ, the optimal conditions for the discharge being obtained for $\tau \sim 4$ μs. Oscillograms of the discharge voltage and current pulses for a CO_2:N_2:He = 1:4:5 mixture are given in Fig. 7.1, together with an oscillogram of the laser output pulse.

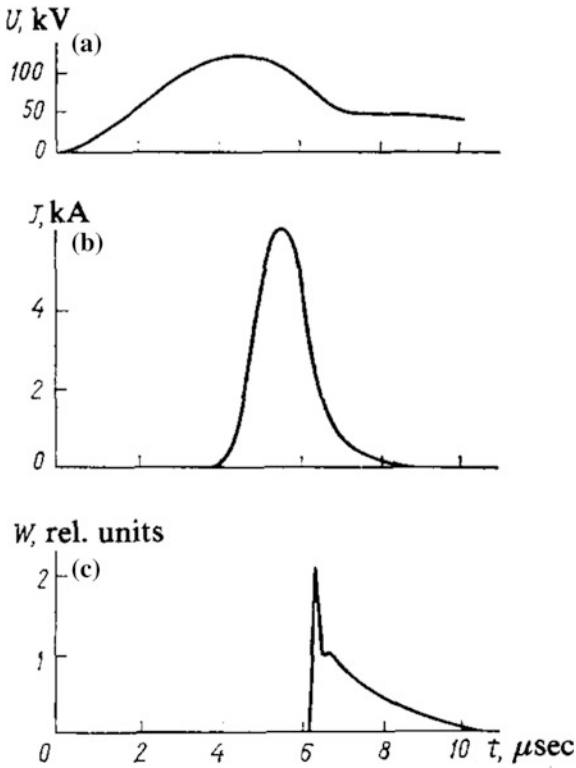

Fig. 7.1 Oscillograms of the discharge voltage (**a**) and current pulses (**b**) and of a radiation pulse (**c**)

The discharge characteristics for large values of τ can be seen in Fig. 7.1. There is no sharp decay on the voltage oscillogram, corresponding to breakdown of the gap; the discharge is formed at a gap voltage lower than that in the case of a short voltage risetime by a factor of 1.5–2; the current begins before the voltage reaches a maximum. It is quite evident that it is the long voltage risetime that is responsible for these characteristics of the discharge.

In view of this, it is necessary to consider the process of the formation of an SSVD with large values of τ. It is a widely held view (see, for example, [10]) that one must prolong the voltage risetime in the system of [1] in order to provide an automatic delay between the main and auxiliary discharges, thereby allowing an accumulation of the photoelectrons at the cathode or attaining the maximum electron density in the auxiliary corona discharge. No account is taken of the obvious fact that the photoplasma in this system is formed by the illumination source during the entire voltage risetime, i.e., when there is an electric field in the gap. Consequently, if τ = 2–4 μs, the photoelectrons are fundamentally unable to accumulate at the cathode, but will drift in the electric field toward the anode. In this case, the focus should not be on the accumulation of electrons at the cathode, but rather on their transport during the voltage risetime from the cathode region into the discharge gap. The resultant space charge formed will distort the electric field in the gap up to the onset of electron multiplication by ionization. It will increase the field at the electrodes and reduce it on the interface of the positive and negative space charges. Thus, on account of the polarization of the photoplasma the field can be increased in separate regions of the gap and ionization processes can develop at a reduced voltage during its risetime. The characteristic features of the discharge behavior observed for large values of r, as indicated above, are a consequence of this.

The experimentally observed improvement in the discharge homogeneity on increasing r is also easily explained once the fact is considered that there is a simultaneous lowering of the average field value at which a discharge is formed and, consequently, owing to the strong nonlinear dependence of the ionization coefficient on the electric field, a lowering of the current density gradients including those resulting from the cathode structure.

7.4 Optimization of Laser Output Characteristics

For the purposes of optimizing the laser output characteristics, an investigation was carried out into the dependences of the laser output energy both on the active medium length and on the reflection coefficient of the exit mirror. They were plotted (for tripropylamine and triethylamine) for an input energy of 235 J/l when no appreciable discharge inhomogeneities were observed in the region near the cathode. The dependences of the laser output energy on the reflection coefficient of the exit mirror are given in Fig. 7.2, for different active medium lengths l. It can be seen that for $l > 80$ cm the optimal output is observed for $K = 0.36$. Figure 7.3 gives the dependences of the output energy on l, obtained using triethylamine and

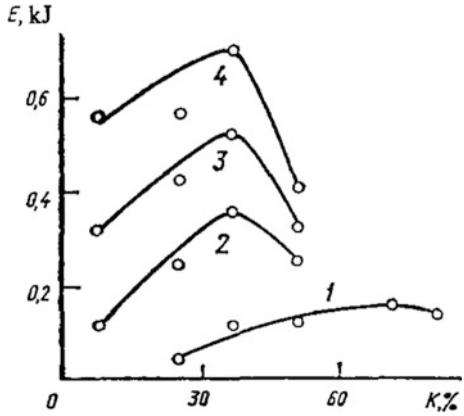

Fig. 7.2 Dependences of the laser output energy *E* on the exit mirror reflection coefficient *K*, for *l* = 40 (*1*), 80 (*2*), 120 (*3*), and 160 cm (*4*)

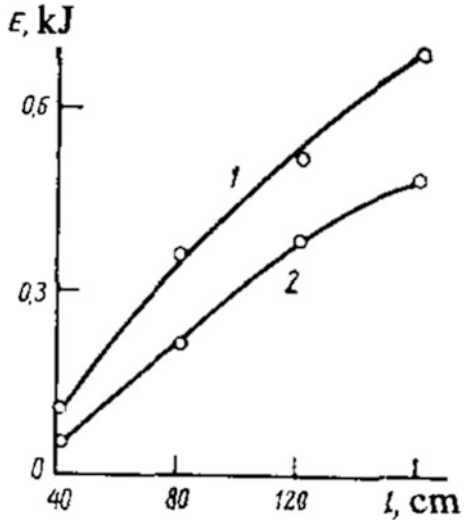

Fig. 7.3 Dependences of the laser output energy *E* on the active medium length *l*, for triethylamine (*1*) and metaxylene (*2*)

metaxylene as the readily ionizable substance. It can be seen that the use of a substance with a lower ionization potential made it possible to increase the output energy by a factor of ~1.5, compared with that reported in [2]. In the case of tripropylamine, the same energy was obtained as in the case of triethylamine.

Estimates from the data of Figs. 7.2 and 7.3 show that the maximum specific output energy reached 45 J/l and the efficiency of conversion of the electrical energy dissipated in the discharge plasma into radiation energy was ~19%. The overall efficiency of the device was then ~11%. A voltage pulse generator discharge capacitance equal to that connected in parallel with the gap could be employed to increase efficiency. However, this would require the pulse generator voltage to be increased.

The output energy was further raised (to 820 J) and the conversion efficiency of electrical energy into radiation energy was further increased (to 22%) by using a mixture of tripropylamine and triethylamine as the easily ionizable substance. The overall efficiency then reached 13% and the specific output energy was 51 J/l. These figures indicate highly homogeneous pumping of the active medium in the system used in the present study.

7.5 Conclusions

The correct choice of the easily ionizable substances and of the pumping regime, and also optimization of the resonator, can thus ensure that the efficiencies and specific output energies obtained for a CO_2 laser excited by an SSVD are not inferior to the characteristics of the corresponding electron beam-controlled systems. The laser described in the present chapter has an extremely compact electrode construction and does not require low-inductance capacitors in the pump circuit.

References

1. R. Dumanchin, J. Rocca-Serra, C.R. Acad, Sci. Ser. B **269**, 916 (1969)
2. Z.I. Ashurly, Y.M. Vas'kovskiY, I.A. Gordeeva, L.V. Malyshev, R.E. Rovinskii, A.A. Kholodilov, Kvantovaya Elektron. (Moscow) **7**, 1456 (1980) [Sov. J. Quantum Electron. **10**, 838 (1980)]
3. V.V. Apollonov, N. Akhunov et al., *Abstracts of Papers presented at Tenth Siberian Meeting on Spectroscopy* (Kuibyshev State University, Tomsk, 1981) [in Russian], p. 134
4. H.J. Seguin, J. Tulip, D.C. McKen, IEEE J. Quantum Electron. **QE-10**, 311 (1974)
5. B.J. Reits, A.H.M. Olbertz, Appl. Phys. Lett. **27**, 24 (1975)
6. V.V. Apollonov, F.V. Bunkin et al., Kvantovaya Elektron. (Moscow) **6**, 1176 (1979) [Sov. J. Quantum Electron. **9**, 694 (1979)]
7. V.V. Apollonov, N. Akhunov et al., *Abstracts of Papers presented at Fourth All-Union Conf. on Laser Optics* (Vavilov State Optical Institute, Leningrad, 1984) [in Russian]
8. Z. Rozkwitalski, M. Grodel, J. Appl. Phys. **51**, 2267 (1980)
9. V.N. Karnyushin, R.I. Soloukhin, *Macroscopic and Molecular Processes in Gas Lasers [in Russian]* (Atomizdat, Moscow, 1981)
10. E.P. Velikhov, VYu. Baranov, V.S. Letokhov, E.A. Ryabov, A.N. Starostin, *Pulsed CO_2 Lasers and Their Application to Isotope Separation [in Russian]* (Nauka, Moscow, 1983)
11. A.A. Aliev, V.V. Apollonov et al., Kvantovaya Elektron. (Moscow) **11**, 735 (1984) [Sov. J. Quantum Electron. **14**, 497 (1984)]

Chapter 8
Formation of a Spatially Homogeneous Discharge in Large-Volume CO_2–N_2–He Gas Mixtures

Abstract A three-dimensional SSVD was established in a large-volume ($F \sim 100$ l) CO_2–N_2–He gas mixture at atmospheric pressure. It was found that the regime of a slow rise of the voltage together with the use of easily ionizable substances made it possible to form stable discharges between electrodes separated by large gaps ($d \sim 40$ cm) under relatively low voltages ($U < 300$ kV) from a pulse generator.

It was shown in [1, 2] that high-intensity fairly long ($\tau \geq 1$ μs) ultraviolet illumination, used to increase the stability of an SSVD, should be combined with a deliberate reduction in the rate of rise of the voltage applied to the electrodes, i.e., the regime of a slow voltage rise should be used. In this regime, the photoelectrons drifting in an electric field may be transported over considerable distances from an ultraviolet radiation source before the beginning of the avalanche multiplication process. Such a regime is of interest in the formation of SSVDs in systems with large distances between the electrodes.

In this chapter, we plan to report the results of our investigations of an SSVD's characteristics in a chamber with a gap up to 0.4 m and with a discharge volume of up to 100 l.

The discharge took place in a CO_2–N_2–He mixture of gases at atmospheric pressure. We used electrodes of shape close to the Chang profile [3] designed for a discharge gap with $d = 0.25$ m. In our experiments, the value of d was varied from 0.2–0.4 m. Illumination with ultraviolet radiation was provided from both sides (from the cathode and the anode) and the sources were based on a creeping surface discharge on a ceramic, similar to that described in detail in [4]. The maximum dimensions of the discharge zone on the electrodes were governed by the dimensions of the illuminated window on the cathode and they amounted to 0.25×1 m. This preliminary ionization of the gas mixture required not more than 3% of the energy stored in the capacitors of a pulse voltage generator feeding the main discharge. The preliminary ionization sources were switched on after a delay relative to the pulse generator supplying the discharge gap and this made it possible to match the duration of illumination with the leading edge of a voltage pulse and

© Springer International Publishing Switzerland 2016

V.V. Apollonov, *High-Energy Molecular Lasers*,
Springer Series in Optical Sciences 201, DOI 10.1007/978-3-319-33359-5_8

prevent the loss of the initial electrons created near the cathode. The process of photoionization was enhanced and the working voltage was reduced by introducing ionizable substances (tripropylamine and triethylamine) into the mixture.

The maximum energy stored in the pulse-generator capacitors was 15 kJ when these capacitors were subjected to a voltage of 300 kV. For these parameters and optimal delays between the moment of switching on the auxiliary and main sources of excitation, it was found that a three-dimensional SSVD was stable in mixtures with the maximum concentration of the two molecular gases (K = 50, 35 and 25%; and d = 0.2, 0.3 and 0.4 m, respectively). The percentage content of CO_2 in the mixture reached 10%. The value of K was limited by the maximum voltage supplied by the pulse generator. For example, for d = 0.4 m and K = 30% it was found that a spark breakdown of the gap usually occurred during the residual voltage stage in 5–6 μs from the end of the diffuse stage of the discharge. For a constant composition of the mixture and a given input energy, a variation of d did not alter significantly the visible homogeneity of radiation emitted by the discharge, of the small-signal gain, and of the distribution of the spots on the electrodes.

Oscillograms of the current and voltage in the discharge obtained in the regime of a slow rise of the voltage for d = 0.4 m and CO_2:N_2:He = 4:16:80 mixture are shown in Fig. 8.1. These oscillograms differed considerably from those obtained typically for three-dimensional SSVDs: the duration of stable burning of the discharge exceeded 5 μs; for a relatively low initial overvoltage across the gap, over 90% of the energy stored in the pulse generator capacitors was deposited in the plasma; a high current began to flow through the gap before the voltage reached its maximum value. These last two circumstances indicated that the formation of such a discharge was affected by the distortion of the electric field in the discharge gap because of polarization of the photoplasma and because of the enhanced (in the regime of a slow rise of the voltage) shift of a negative space charge toward the anode [1, 2].

It should be noted that matching of the duration of the ultraviolet illumination to the leading edge of the voltage pulses in the cathode region of the investigated system did not give rise to inhomogeneities typical of systems with short duration of the action of a preliminary ionization source when the rate of rise of the voltage on the electrodes was not sufficiently high [5]. It is known [6, 7] that the development of such inhomogeneities due to the loss of electrons from the cathode

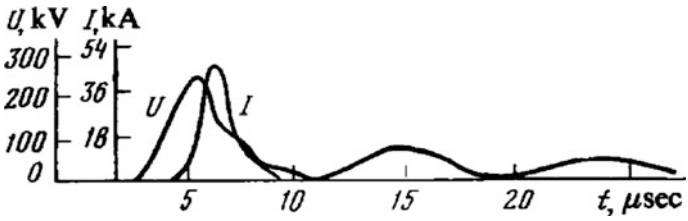

Fig. 8.1 Oscillograms of the current and voltage in the discharge

region before avalanche multiplication is one of the main factors that limit the stability of three-dimensional SSVDs.

In conclusion, it should be pointed out also that the use of easily ionizable substances makes it possible to form such discharges at considerably lower values of the voltage from the source of preliminary ionization and from the generator of voltage pulses feeding the main discharge, compared with the corresponding values obtained earlier [8] for comparable to specific input energies and comparable values of the parameters d and K.

References

1. V.V. Apollonov et al, *Abstracts of Papers presented at Second All-Union Conference on Physics of Electric Breakdown of Gases,* [in Russian] (Publ. by Tartu State University, Tartu, 1984), p. 360
2. V.V. Apollonov, V.R. Minenkov, A.M. Prokhorov et al., Kvantovaya Elektron. (Moscow) **11**, 1327 (1984) [Sov. J. Quantum Electron. **14**, 898 (1984)]
3. T.Y. Chang, Rev. Sci. Instrum. **44**, 405 (1973)
4. V. V. Apollonov, N. Akhunov et al, Kvantovaya Elektron. (Moscow) **11,** 1241 (1984) [Sov. J. Quantum Electron. **14,** 835 (1984)]
5. S.A. Genkin, K.A. Klimenko, A.V. Kozyrev, Y.D. Korolev, G.A. Mesyats, Y.N. *Novoselov, Abstracts of Papers presented at Second All-Union Conference on Physics and Electric Breakdown of Gases,* [in Russian] (Tartu State University, Tartu, 1984), p. 321
6. J.I. Levatter, S.C. Lin, J. Appl. Phys. **51**, 210 (1980)
7. M.A. Kanatenko, Pis'ma Zh. Tekh. Fiz. **9**, 214 (1983) [Sov. Tech. Phys. Lett. **9**, 94 (1983)]
8. A.I. Pavlovskii, V.F. Basmanov, V.S. Bosamykin, V.V. Gorokhov, V.I. Karelin, P.B. Repin, *Abstracts of Papers presented at Second All-Union Conference on Physics of Electric Breakdown of Gases*, [in Russian] (Publ. by Tartu State University, Tartu, 1984), p. 330

Chapter 9
Stability of an SSVD in a CO_2–N_2–He Gas Mixture with Easily Ionizable Additives

Abstract It was found experimentally that the stability of an SSVD ignited in a CO_2–N_2–He mixture at large distances from an ultraviolet radiation source could be increased by adding mixtures of easily ionizable substances with different ionization potentials and partial pressures.

The possibility of reducing operating voltages in CO_2 lasers pumped by an SSVD initiated by ultraviolet radiation [1–3] when some easily ionizable substances are added to the gaseous mixture is of interest in the construction of large-aperture electric-discharge systems [4, 5]. However, a considerable reduction in the ignition voltage of an SSVD due to the Penning ionization of easily ionizable (EI) substances [6, 7] is attained only at fairly high partial pressures of these substances $p_{EI} \sim 1$–1.5 Torr [2, 3]; the strong absorption of ultraviolet radiation in impurity vapors may reduce the density of photoelectrons n_0 at large distances from the radiation source to a value less than in the pure gas [8, 9]. Therefore, the disagreement between the optimal values of the pressures of easily ionizable substances p_{EI} in the Penning ionization and photoionization processes may limit the usefulness of easily ionizable substances.

Consequently, a method must be found to separate and independently optimize the processes under discussion. Here, we report on a study investigating the possibility of using a mixture of two easily ionizable substances with different ionization potentials φ at different partial pressures. We shall assume that when the difference between the ionization potentials of easily ionizable substances is sufficiently large, photoionization of the substance (EI_1) with the lower value of φ and the lower partial pressure will occur at wavelengths that are weakly absorbed by the second easily ionizable substance (EI_2) and that EI_2 and its partial pressure are selected to ensure the maximum yield of electrons in the Penning process [10]. Essentially, EI_1 becomes an easily ionizable additive to EI_2.

The success of this approach is indicated by the results reported in [11], where an increase in the maximum input energy to the plasma of an SSVD was achieved by adding a mixture of triethylamine and diethylaniline to a gas. However, these experiments were carried out in a system with a small gap between the electrodes

© Springer International Publishing Switzerland 2016

V.V. Apollonov, *High-Energy Molecular Lasers*,
Springer Series in Optical Sciences 201, DOI 10.1007/978-3-319-33359-5_9

(1.25 cm) and the source of the initiating radiation was located near the discharge zone; as such, the results reported in [11] could not be applied directly to systems with large apertures.

Therefore, we carried out a study in which we tried to show that the use of a mixture of easily ionizable substances with suitably selected ionization potentials should make it possible to increase the range of action of ultraviolet radiation sources and yet retain low working voltages.

We determined the dependences of the upper and lower limits U_{max} and U_{min} of the range of ignition voltages of SSVD on voltage U_c applied to the capacitor in the power supply of the radiation source, which qualitatively reflected the dependences of the voltage limits on n_0. Since the initial electron density affected U_{max} much more than U_{min} [12], variation of the partial composition of the easily ionizable substances caused by variation of U_{max} (keeping U_c constant) could be used to study the changes in n_0 and the deviation of U_{min} from its value for the pure gas indicated the contribution of the Penning ionization to the formation of an SSVD.

An SSVD was ignited in the CO_2:N_2:He = 1:2:3 mixture between two specially shaped *A* 1 electrodes located at a distance of 20 cm from an ultraviolet radiation source, using a system similar to that described in [4]. A voltage pulse with a leading edge not exceeding 20 ns was applied to the electrodes of a C = 8850 pF capacitor charged to its maximum voltage of 48 kV approximately 2.5 μs after switching on the radiation source. The discharge zone dimensions were 1.1 × 2.2 × 40 cm. The easily ionized substances used in the present investigation were selected in accordance with the recommendations formulated in [10]. The results given below were obtained for two widely used easily ionizable substances: tripropylamine (TPA, denoted here by EA_1 with an ionization potential φ = 7.23 eV) and triethylamine (TEA; EA_2, φ = 7.59 eV).

Figure 9.1 shows the dependences of U_{max} and U_{min} on U_c obtained for an SSVD in a gas containing one of the easily ionized substances. The discharge was stable in the range of pump source voltages $U_{min} < U < U_{max}$ for $U_c > U^\circ_c$, where U°_c is the value of U_c corresponding to $U_{max} = U_{min}$. Curve 1 was obtained for a pure gas. The range of stable ignition of the discharge became considerably wider on introduction of small (near-optimal for a given distance) amounts of an easily ionizable substance to the gas (curves 2 and 3); for a constant value of U_c, the voltage U_{max} was affected more than U_{min}. For the same partial pressures of the easily ionizable substance the discharge in the gas containing TPA (curve 2) occurred at a lower value of U°_c than in the gas containing TEA, which reflected the difference between the ionization potentials of these substances. An increase in the partial pressure of the easily ionizable substance (specifically, TEA) caused the range of the stable ignition of the discharge to narrow (curve 4) and at $p_{EI} > 0.35$ Torr the discharge was obtained only at values of U_c higher than U°_c for the pure gas (curve 5). When the partial pressure of TEA was higher than 0.8 Torr, the discharge could not be ignited anywhere in the range of U_c (up to 48 kV). In the case of TPA, the corresponding pressure was $\sim$1 Torr.

Figure 9.2 shows the dependences of U_{max} and U_{min} on U_c for an SSVD in a gas containing admixtures of two easily ionizable substances. The two curves in this

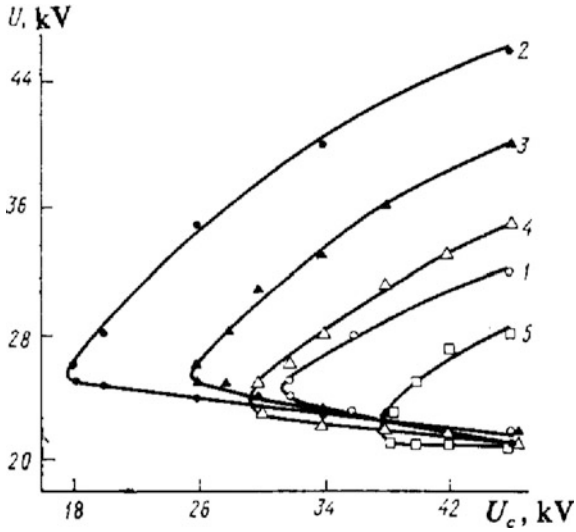

Fig. 9.1 Dependences of U_{max} and U_{min} on U_c: (*1*) pure gas; (*2*) 0.12 Torr TPA; (*3*) 0.12 Torr TEA; (*4*) 0.24 Torr TEA; and (*5*) 0.53 Torr TEA

figure were obtained at partial pressures of EI_2 exceeding the maximum value of p_{EI} in Fig. 9.1. The pressures of the TPA vapor for curves 2, 6, and 7 in Figs. 9.1 and 9.2 were approximately the same. A comparison of these curves indicated that the partial pressure of TEA in an easily ionizable mixture had a slight influence on the position of the upper limit of ignition of the discharge, i.e., on the value of n_0 corresponding to given U_c, whereas U_{min} decreased considerably on increase in the partial pressure of TEA because of the Penning ionization.

These results indicated that TPA was indeed ionized by radiation in the range of frequencies that did not coincide with the absorption band of TEA. The weak dependence of U_{max} on the partial pressure of EI_2 indicated that it should be

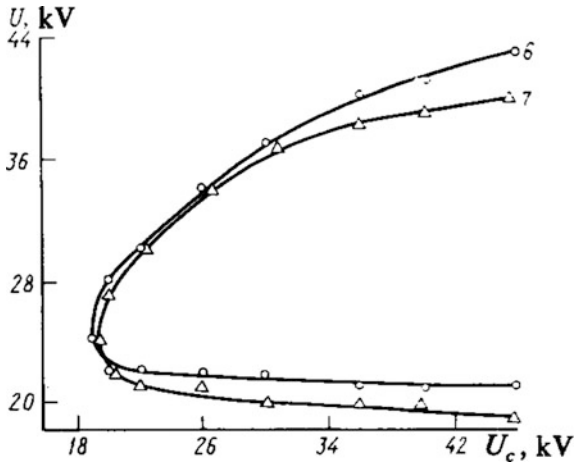

Fig. 9.2 Dependences of U_{max} and U_{min} on U_c for mixtures with 0.1 Torr TPA + 0.59 Torr TEA (*6*) and 0.1 Torr TPA + 1.12 Torr TEA (*7*)

possible to independently optimize the partial pressure of EI_1 so as the ensure the value of n_0 necessary for the ignition of the discharge at large distances from the radiation source. The results obtained were not in agreement with those reported in [13], according to which the absorption cross sections of TPA and TEA of ultraviolet radiation of wavelengths in the region of 160 nm were approximately the same, i.e., under the conditions described above the replacement of TPA with a mixture of easily ionizable substances (keeping the total vapor pressure constant) should not have expanded the range of stable ignition of an SSVD.

We shall conclude by noting that the use of a mixture of TPA and TEA, instead of one of these substances, made it possible to increase the maximum input energy of the system described in [14] by a factor of about 1.5 and to enhance the efficiency of a CO_2 laser by 15 % [15].

References

1. V.V. Apollonov, A.I. Barchukov et al., Pis'ma Zh. Tekh. Fiz. **3**, 1073 (1977) [Sov. Tech. Phys. Lett. **3**, 441 (1977)1
2. V.V. Apollonov, F.V. Bunkin et al., Kvantovaya Elektron. (Moscow) **6,** 1176 (1979) [Sov. **J.** Quantum Electron. **9,** 694 (1979)]
3. A.A. Kuchinskii, V.A. Rodichkin, Zh. Tekh. Fiz. **53**, 563 (1983) Sov. Phys. Tech. Phys. **28**, 352 (1983)]
4. V.V. Apollonov, N. Akhunov et al., Kvantovaya Elektron. (Moscow) **11**, 1241 (1984) [Sov. J. Quantum Electron. **14**, 835 (1984)]
5. V.V. Apollonov, G.V. Bush et al., Kvantovaya Elektron. (Moscow) **11**, 2149 (1984) [Sov. J. Quantum Electron. **14**, 1435 (1984)]
6. B.J. Reits, A.H.M. Olbertz, Appl. Phys. Lett. **27**, 24 (1975)
7. V.J. Reits, J. Appl. Phys. **48**, 3697 (1977)
8. Z. Rozkwitalski, M. Grodel, J. Appl. Phys. **51**, 2267 (1980)
9. M.F. Borisov, V.B. Znamenskii, T.P. Uvarova, Zh. Tekh. Fiz. **50**, 1257 (1980) [Sov. Phys. Tech. Phys. **25**, 722 (1980)]
10. A.A. Aliev, V.V. Apollonov, N. Akhunov et al., Kvantovaya Elektron. (Moscow) **11**, 735 (1984) [Sov. J. Quantum Electron. **14**, 497 (1984)]
11. N. Tho Vuong, Z. Puzewicz, Kvantovaya Elektron. (Moscow) **9**, 145 (1982) [Sov. J. Quantum Electron. **12**, 92 (1982)]
12. V.N. Karnyushin, A.N. Malov, R.I. Soloukhin, Kvantovaya Elektron. (Moscow) **5**, 555 (1978) [Sov. J. Quantum Electron. **8**, 319 (1978)]
13. D.R. Grosjean, P. Bletzinger, IEEE J. Quantum Electron. **QE-13**, 898 (1977)
14. V.V. Apollonov et al., Kvantovaya Elektron. (Moscow) **10**, 1458 (1983) [Sov. J. Quantum Electron. **13**, 947 (1983)]
15. V.V. Apollonov et al., Kvantovaya Elektron. (Moscow) **12**, 5, Sov. J. Quantum Electron. **15**, 1 (1985)

Chapter 10
Formation of an SSVD for the Pumping of CO_2 Lasers

Abstract An investigation was carried out into the characteristics of the formation of an SSVD for the pumping of CO_2 lasers, which involved a preliminary filling of a discharge gap by an electron flux from an auxiliary-discharge plasma. It was found that this method was suitable for large interelectrode gaps. Distortion of the electric field in the gap by the space charge of the electron flux was found to play an important role in the fomiation of the discharge. In addition, the electrodes could be profiled dynamically during propagation of an electron flux through the discharge gap and an SSVD could form in systems with a strongly inhomogeneous initial distribution of the electric field between the electrodes.

10.1 Introduction

It is well known that an SSVD can be established in a gas by creating primary electrons the density of which should exceed a certain minimum value $n_{\min}$ throughout the discharge gap [1–3]. Various methods for preionization of a gas in the discharge gap have been developed for this purpose [4–7]. Primary electrons are created by these methods directly in the discharge gap, which sometimes causes difficulties in the establishment of conditions necessary for the formation of an SSVD. For example, high voltages are needed for the formation of an initial plasma when the preionization source and the active medium are combined in the same volume [8, 9], whereas preionization with ultraviolet radiation may be ineffective because of strong absorption of such radiation in a medium, and if soft x-rays are used, it is necessaiy to ensure rigid synchronization of the x-ray and pump sources [10].

In mixtures of gases typical of CO_2 lasers, losses of electrons due to trapping are relatively small [1]: at low values of E/p (E is the electric field intensity and p is the gas pressure) the trapping coefficient is considerably less than the absoiption coefficient of ultraviolet radiation for the same mixtures [10]. It follows that, in principle, it should be possible to create primary electrons in a density needed for the formation of an SSVD at a considerable distance from an ionization source and then transport the electrons to the gap by drift in an electric field. This possibility

© Springer International Publishing Switzerland 2016

V.V. Apollonov, *High-Energy Molecular Lasers*,
Springer Series in Optical Sciences 201, DOI 10.1007/978-3-319-33359-5_10

was confirmed experimentally in [12]. A method of formation of an SSVD by filling the discharge gap with a flux of electrons drifting in an electric field, without preliminaiy ionization of the whole discharge volume, was proposed and implemented in [13]. The source of electrons was a plasma formed in an auxiliary discharge initiated under a grid cathode. This method made it possible also to establish an SSVD in a system of electrons with a strongly inhomogeneous electric field in the discharge gap.

This chapter reports on a continuation of an earlier investigation [13]. We shall consider in detail a one-dimensional model of the propagation of an electron flux in the discharge gap, analyze the influence of distortions of the electric field by the space charge of the electron flux on the formation of an SSVD in the real geometry of the gap, and report studies of the main types of the auxiliary discharge suitable for the creation of an electron flux with the necessary characteristics.

10.2 Experimental Setup

The formation of an electron flux and its characteristics were studied using a setup shown schematically in Fig. 10.1a. The source of electrons was an auxiliary discharge (1) initiated under a grid cathode (2). An electron flux was formed by the application of an electric field to the auxiliary-discharge plasma (a voltage U, was applied between the discharge gap cathode and an auxiliary electrode [3]). Under the action of this field, some of the electrons were driven to the discharge gap, where the electron flux was maintained by a bias voltage U_0 applied to an anode (4).

The electron flux current in the discharge gap was deduced from the voltage drop across a resistor R. The charge carried by the flux was found from the change in the voltage across a capacitor C for $R = 0$. The contribution to the gap conductance made by the photoionization of the gas in the gap by the auxiliary-discharge radiation was estimated from the charge of the positive ions fonned in the gap (these measurements were carried out by applying a negative bias voltage U_0).

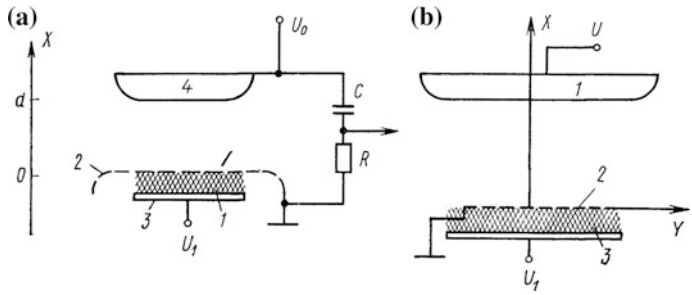

Fig. 10.1 Discharge systems with profiled (**a**) and nonprofiled (**b**) electrodes

The following types of an auxiliary discharge were investigated.

1. A barrier discharge [14] in which a wire insulated with polyethylene was used as the electrode.
2. A corona discharge initiated by a multipin electrode, stabilized by limiting the current through the pins by a ballast resistor [15].
3. A volume discharge between a grid (discharge gap cathode) and a metal cathode, initiated as described in [16].
4. A volume discharge between a semiconductor cathode (carbon-filled rubber with a bulk resistivity of $\rho = 2 \times 10^5$ Ohm cm) [17] and a grid (discharge gap cathode) initiated without preionization [18].
5. A multichannel discharge on the surface of a high-permittivity insulator limited by the insulator capacitance [19].
6. A multichannel discharge on the surface of a semiconductor (carbon-filledrubber, $\rho = 3 \times 10^4$ O cm) [17] limited by the semiconductor resistance (this auxiliary discharge was realized in the same way as a multichannel discharge on the surface of a ceramic described in [19]).

In all these auxiliary discharges, an electric field was applied to the auxiliary-discharge plasma; a special auxiliary electrode was not essential. We understand here the auxiliary electrode to be the one that is used to apply the voltage pulse to ignite the auxiliary discharge.

The characteristics of the formation of an SSVD by filling the discharge gap with an electron flux were investigated using a system of electrodes with an initially homogeneous distribution of the electric field (the anode had the Chang profile [20] and the cathode was a planar grid) with a discharge gap d = 6–10 cm. In these experiments, we used the configuration shown in Fig. 10.1a with values U_0 lower than the static breakdown voltage of the discharge gap U_{st}, as well as a configuration with pulsed application of a voltage higher than U_{st} to the discharge gap. In the latter case, filling the discharge gap with electrons from the auxiliary-discharge plasma occurred either by the application of a preliminary bias to the gap, analagous to the method in [21], or by a deliberate increase of the duration of the leading edge τ_{ph} of the voltage pulse applied to the discharge gap [21, 22]. The value of τ_{ph} was selected so that electrons could reach the anode before the onset of ionization processes in the discharge gap.

Investigations into the conditions for the formation of an SSVD in the presence of a strong inhomogeneous initial electric field in the discharge gap were carried out using apparatus shown schematically in Fig. 10.1b. The electrode system (d = 10 cm) was formed by a planar anode (1) (representing a rectangular plate of 18 × 50 cm dimensions rounded along the perimeter to a radius of 10 mm) and a cathode (2) with sharp edges (brass grid of rectangular shape and 10 × 40 cm dimensions). The area occupied by the auxiliary discharge (3) under the grid was slightly greater than the cathode area.

The working voltages were reduced [23, 24] and the duration of SSVDs was increased [25, 26] by adding easily ionizable substances (tripropylamine and triethylamine at vapor pressures of ~ 1 Torr) to the investigated mixtures.

We determined experimentally the lowest voltage $U_{\min}$ needed to ignite an SSVD (this was deduced from the voltage of tine pump source) and the stability limit of such a discharge considered as a function of the composition of a CO_2-N_2-He gas mixture and the input energy. The homogeneity of the volume discharge was checked visually by examination of photographs of a section of a discharge and also on the basis of the small-signal gain and its distribution over the aperture of an amplifier.

10.3 Model of Propagation of an Electron Flux

The process of propagation of an electron flux in the discharge gap (one-dimensional case) in the absence of ionization and multiplication is described by the following system of equations and boundary conditions for the electric field $E(x,t)$, electron density $n(x,t)$, and concentration of negative ions $N_t(x,t)$ [27]:

$$\partial n/\partial t + \partial(n\mu E)/\partial x = -\alpha n\mu|E|, \tag{10.1}$$

$$\partial N_{\mathrm{i}}/\partial x = \alpha n\mu|E|, \tag{10.2}$$

$$\partial E/\partial x = -(N_{\mathrm{i}} + n)e/\varepsilon_0, \tag{10.3}$$

$$\int_0^d E dx = -U_0, \tag{10.4}$$

$$n(0,t) = \mathrm{const} = n(0), \tag{10.5}$$

$$N_{\mathrm{i}}(x,0) = 0, \tag{10.6}$$

$$n(x,0) = 0 \quad \text{for} \quad x > 0, \tag{10.7}$$

where α, μ, and e are the trapping coefficient, mobility, and charge of electrons, respectively; ε_0 is the permittivity. The X axis is directed from the cathode ($x = 0$) to the anode ($x = d$); the electron density at the cathode surface $n(0)$ is assumed to be constant in time (the loss of electrons from the cathode to the region occupied by the bias field is compensated by the arrival of new electrons from the auxiliaiy-discharge plasma). The mobility of negative ions in Eqs. (10.1)–(10.7) is assumed to be negligible.

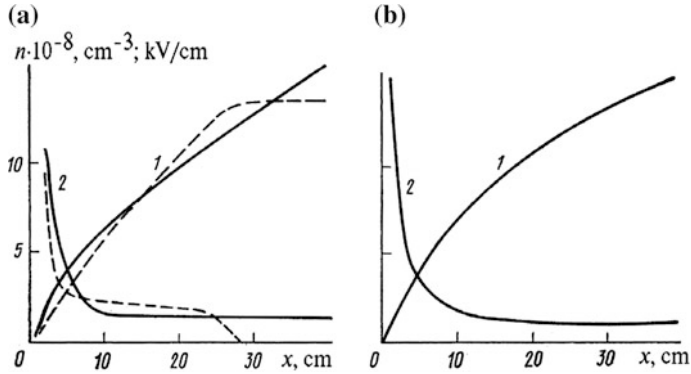

Fig. 10.2 Calculated dependences $E(x)$ (curves denoted by *1*) and $n(x)$ (curves denoted by *2*): (**a**) $t = 2$ μs (*dashed curves*) and 4–6 μs (*continuous curves*); (**b**) $U = 400$ kV, $\tau_{ph} = t = 8$ μs, $n(0) = 10^{10}$ cm^{-3}

The system of Eqs. (10.1)–(10.7) was solved on a computer employing an explicit difference scheme [27]. The calculations were simplified by assuming that α = const.

The dependences $n(x)$ and $E(x)$ calculated for different moments on the assumption that $U_0 = 400$ kV, $d = 40$ cm, $\mu = 10^3$ cm^2 V s, $\alpha = 0$; and $n(0) = 10^9$ cm^{-3} are plotted in Fig. 10.2a. We can see the absence of electron losses due to trapping; steudy state distributions $n(x)$ and $E(x)$ are established in the discharge gap after a time $t > t_0 = d/E_0\mu$, where in $E_0 = U_0/d$.

If $\alpha \neq 0$, then a space charge of negative ions preventing the propagation of the electron flux accumulates in the discharge gap. Calculations different values of α and d indicate that at the moment $t = t_0$ the electron densities near the anode $n_\alpha(d)$ (for $\alpha \neq 0$) and $n(d)$ (for $\alpha = 0$) are related by

$$n_\alpha(d) \approx n(d)e^{-\alpha d}. \qquad \delta = 3\varepsilon_0 E_0/4en(0)d << 1, \tag{10.8}$$

is of the form [28]

$$E(x) = \frac{3}{2}E_0\sqrt{\frac{x}{d} + \delta^2}; \tag{10.9}$$

$$n(x) = \frac{3}{4}\frac{\varepsilon_0 E_0}{ed}\sqrt{\frac{d}{x + \delta^2 d}}; \tag{10.10}$$

$$j = \frac{9}{8}\mu\varepsilon_0\frac{E_0^2}{d}(1 - 3\delta^2). \tag{10.11}$$

In atmospheric-pressure CO_2-N_2-He mixtures usually employed in CO_2 lasers, the values of α for $E_0 < 3$ kV/cm do not exceed 10^{-2} cm^{-1} [11]. Consequently, if $d < 1$ m and $E_0 < 3$ kV/cm, the loss of electrons due to trapping has no significant influence on the propagation of an electron flux and the ultimate potentialities of the proposed discharge can be analyzed in a steady-state electron flux model ($\alpha = 0$ and $t > t_0$).

An approximate steady-state solution of the system (10.1)–(10.7) for high values of $n(0)$, when where j is the current density in the electron flux.

We shall now obtain some estimates. We shall assume that $E_0 = 1$ kV/cm and $d = 50$ cm; then, Eq. (10.10) shows that $n(d) \approx 10^7$ cm^{-3} is clearly greater than $n_{\min}$ required for the formation of an SSVD [2] The condition (10.8) is then satisfied already for $n(0) = 10^8$–10^9 cm^{-3}. We shall show that such low electron densities at the cathode can be provided by practically any type of auxiliary discharge.

These estimates therefore confirm that a primary electron density necessary for the formation of a self-sustained volume discharge can be established at sufficiently large distances from the cathode by filling the discharge gap with an electron flux. We shall now point out some features of this method that follow from the above simple model.

It is clear from the expression (10.10) that at some distance from the cathode ($x \gg \delta^2 d \approx 10^{-3} d$ for $E_0 = 1$ kV/cm, $d = 40$ cm, and $n(0) = 10^9$ cm^{-3}) when the condition (10.8) is obeyed, the value of $n(x)$ is no longer dependent on $n(0)$. Therefore, the discharge gap will be filled uniformly with electrons (in a plane perpendicular to x) even in the case of a strong inhomogeneity of the distribution $n(0)$ over the cathode area, which makes it possible to form an SSVD avoiding small-scale inhomogeneities (typical of ultraviolet preionization and due to the shadow formed in the discharge volume by the grid cathode) [29] and to increase the small-signal gain as well as the efficiency of CO_2 lasers.

It is clear from Eq. (10.9) that, in spite of the relatively low density of the primary electrons in the discharge region, the presence of an uncompensated negative charge of the electron flux distorts considerably the electric field in the discharge gap. Consequently, the ionization processes begins first at the anode where the electric field may be 1.5 times higher than E_0. The ionization at the cathode is hindered because the field here is close to zero as a result of the screening of the cathode by the space charge of the electron flux. Clearly, this screening of the cathode as a result of filling of the discharge gap with electrons should also be manifested in the real geometry of the discharge gap. Consequently, it would be desirable to find the conditions for the formation of an SSVD in systems with unprofiled electrodes, because this would simplify greatly the construction of electric-discharge lasers.

The distortion of the electric field in the discharge gap by the space charge of the electron flux should reduce the voltage at which an SSVD can be established and this is a clear advantage of the proposed method. However, when a preliminary bias U_0 is used to fill the discharge gap with electrons and this is followed by the application of a voltage pulse of amplitude U to the discharge gap, the degree of enhancement of the electric field at the anode (compared with U/d), defined as

$K_e = 1 + U_0/2U$, may be small, because it is not always permissible to increase U_0 to values close to U_{st}. The degree of distortion of the field can be increased by deliberate delay of the leading edge of the voltage pulse [22]. Figure 10.2b gives the results of a numerical solution of the system of equations (10.1)–(10.3) and (10.5)–(10.7) for $n(x)$ and $E(x)$, obtained for the case when $\alpha = 0$ subject to the boundary condition

$$\int_0^d E dx = -\frac{U}{2}\left(1 - \cos\frac{\pi t}{\tau_l}\right), \tag{10.12}$$

which corresponds to the rate of rise of the voltage in a discharge gap selected for this case. A complete filling of the discharge gap with electrons also requires that the condition $\tau > 2d^2/\mu U$ be satisfied. It is clear from Fig. 10.2b that for $t = \tau = 2d^2/\mu U$ as in the case of a static bias across the discharge gap, the value of $E(d)$ is enhanced compared with $LZ\ U/d$ factor of 1.5 and the value of $E(0)$ is reduced several fold.

10.4 Results of Experiments and Discussion

a. Conditions for the Formation of an Electron Flux

Figures 10.3a, b show oscillograms of the electron charge $q(t)$ extracted from the discharge gap and of the voltage $U(t)$ between the gap cathode and the auxiliary-discharge electrode, recorded for a mixture of N_2 with tripropylamine obtained for the case when $d = 2$ cm and $U_0 = 6$ kV, and the electrode area was $S = 200$ cm^2. The auxiliary discharge was a multichannel discharge on the surface of a ceramic (with the permittivity $\varepsilon = 2000$), limited by the capacitance of the ceramic itself [19]. The shape of $U(t)$ was set by the parameters of a special $R\ C$ circuit. A comparison of the $q(t)$ oscillograms recorded for different polarities of the voltage $U(t)$ indicated that the main rise of $q(t)$ occurred in the region where $dU/dt < 0$. When a negative bias voltage was applied to the discharge gap, the form of the $q(t)$ oscillograms was independent of the sign of dU/dt. In accounting for these results, it is important to bear in mind that the sign of the electric field in the gap between the ceramic surface and the discharge gap cathode was the same as the sign of dU/dt. Therefore, for $dU/dt < 0$ some of the electrons were expelled from the auxiliary-discharge plasma into the discharge gap across the grid cathode and drifted toward the anode in the bias field ($U_0 > 0$). For $dU/dt > 0$ or $U_0 < 0$, it was not possible to drive electrons beyond the grid and the flow of the current in the discharge gap was then entirely due to the photoionization of the gas by the auxiliary-discharge radiation.

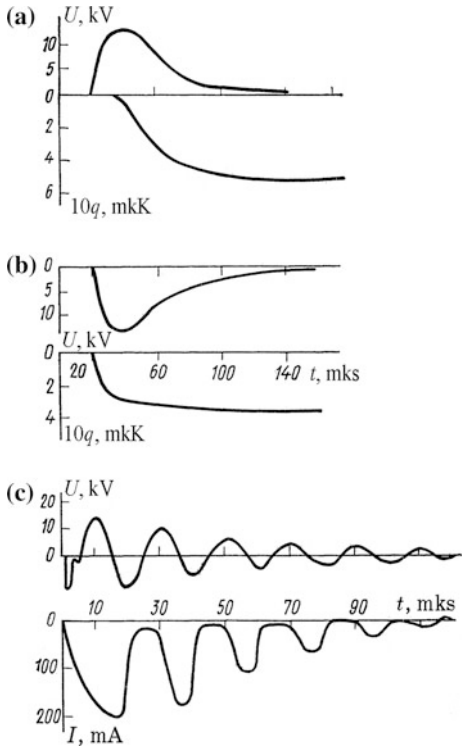

Fig. 10.3 Oscillograms of the voltage $U(\tau)$ on the auxiliary electrode, of the electron charge $\varrho(\tau)$, and of the electron flux current ‘L (τ) in tlie case of positive (**a**) and negative (**b**) polarities, and also in the case of oscillatory nature of the voltage $U(t)$ (**c**)

Figure 10.3c shows the oscillograms of the voltage $U(t)$ and of the electron current in the discharge gap $I(t)$ for an oscillatory form of the voltage $U(t)$. It is clear from these oscillograms that a considerable current in the discharge gap was recorded only for $dU/dt < 0$, irrespective of the sign of $U(t)$.

It should be stressed that we investigated long-duration auxiliary discharges in order to identify the conditions for the formation of an electron flux from the auxiliary-discharge plasma itself. Under these conditions, in spite of the presence of an easily ionizable substance in the gas, the contribution to the discharge gap conductance of the electrons arriving from the auxiliary-discharge plasma was (for suitable signs of dU/dt and U_0) approximately ten times higher than the contribution made by the photoionization of the gas by the auxiliary-discharge radiation, even when the latter was of the surface type. Under these conditions, the contribution of the photoionization to the charge of the electrons crossing the gap did not exceed 10% of the contribution of the electron flux for a corona discharge and it was not greater than 1% in the case of barrier volume discharges (these values were obtained for $d = 6$ cm, $U_0 = 30$ kV, mixture of N_2 with tripropylamine, and $p = 1$ atm) and the presence of an easily ionizable substance in the gas had practically no influence on I and q.

When the auxiliary discharge pulse was shortened (by reducing the inductance or the active resistance in the circuit of this discharge), the contribution of the photoionization to the discharge-gap conductance increased and, in principle, it was possible to form an electron flux from a plasma created by the ultraviolet radiation of the auxiliary discharge in the cathode region (and also from a plasma on the surface of a plasma cathode or a barrier discharge plasma in systems described in [16]).

b. Main Requirements in Respect of the Auxiliary Discharge Characteristics

As already highlighted, the homogeneity of an SSVD could be improved by selecting the auxiliary discharge characteristics in such a way as to satisfy the condition (10.8). Naturally, one would then have to ensure a certain minimum density of the electron current in the auxiliary gap. The possibility of igniting an SSVD in the gap was also governed by the condition $\tau_{ad} > t_0$ (τ_{ad} is the duration of the auxiliary discharge); in the opposite case, the cathode zone could lose electrons before the onset of ionization processes in the discharge gap.

Figure 10.4a shows oscillograms of the electron flux current $I(t)$ and of the auxiliary discharge current I_{ad} (this was a volume type of discharge) obtained for a mixture of gases of the CO_2:N_2 = 1:3 composition at a pressure of p = 0.3 atm when the gap was d = 6 cm and the applied bias voltage was U_0 = 12 kV. The distance between the auxiliary discharge electrodes was 1 cm and the area of the

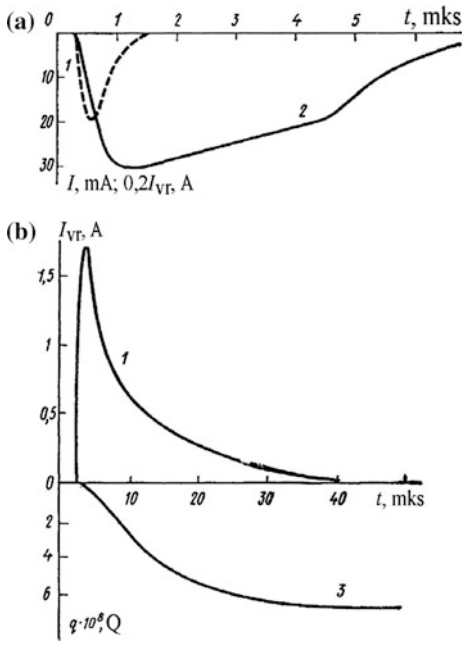

Fig. 10.4 Oscillograms of the volume auxiliary discharge current (*1*) from metal (**a**) and semiconductor (**b**) electrodes, of the electron flux current (*2*), and of the charge carried by this flux (*3*)

auxiliary electrode was S = 200 cm^2. It is clear from Fig. 10.4a that a change in the auxiliary discharge current I_{ad} by an order of magnitude altered $I(t)$ by just 10%, indicating that the condition (10.8) was satisfied. Measurements indicated that the saturation of $I(t)$ occurred when

$$I_{ad}/S = j_{ad} \geq (20-30)j_{max} = (20-30)\varepsilon_0 \mu E_0^2/d, \tag{10.13}$$

where j_{max} is the maximum density of the electron flux current obtained from Eq. (10.11), when the condition (10.8) is satisfied. The condition (10.13) is an empirical criterion equivalent to the condition (10.8). It should be noted that it was easier to satisfy these criteria as d was increased.

The condition (10.13) was also easily satisfied when a corona discharge was used as the auxiliary discharge. However, the maximum duration of stable operation of the corona and volume auxiliary discharges, in the case when the condition (10.13) was satisfied, did not exceed 5–10 μs unless special measures were taken.

Both volume and corona discharges could be stabilized by utilizing electrodes made of semiconductor materials [18]. Figure 10.4b shows oscillograms of the volume discharge current in a mixture of gases of the CO_2:N_2:He = 8:32:60 composition with an admixture of triethylamine at p = 1 atm, ignited without a preliminaiy ionization between a semiconductor material cathode (which was a disk 5 cm in diameter and 2 cm thick) and a grid (discharge gap cathode); it also includes an oscillogram of the charge $q(t)$ of the electrons extracted from the discharge gap in the case when U_0 = 5 kV, d = 8 cm, and the distance between the auxiliary discharge electrodes was 1 cm. The density of the auxiliary discharge current obtained in this way was ~50 in A/cm^2 and the duration of the stable burning of the discharge in gas mixtures of various compositions exceeded 30 μs.

In the case of a discharge of the surface of an insulator, which was limited by the capacitance of the insulator itself, our measurements indicated that the electron current in the gap between the insulator surface and the grid was an order of magnitude less than via an auxiliary electrode. Therefore, Eq. (10.13) was equivalent to the condition

$$|\mathrm{d}U/\mathrm{d}t| \geq (2-3)\cdot 10^2 \mu E_0^2 \varepsilon_0/dC_i, \tag{10.15}$$

The condition (10.15) was easily satisfied for $\tau_{ad} = t_0$ and $C_i \sim$ 100 pF/cm (C_i is the specific capacitance of the insulator).

When the condition (10.13) was satisfied, stable long-term burning of the discharge was also achieved for a multichannel auxiliary discharge on the surface of a semiconductor material, which was limited by the resistance of the material itself, when the charging capacitor was suitably selected.

It therefore follows that when special measures were taken, all the types of the auxiliary discharge discussed above would be capable of forming an electron flux with the maximum parameters specified by Eq. (10.11).

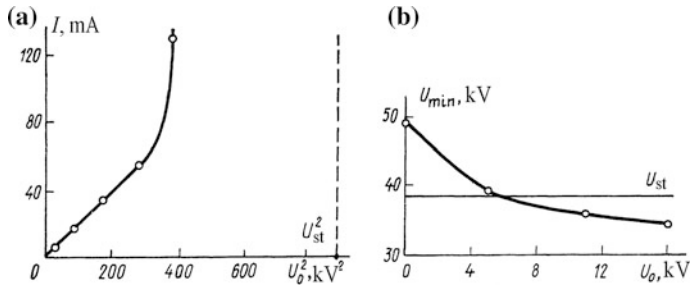

Fig. 10.5 Dependences of the amplitude of the electron flux ament (**a**) and of the minimum ignition voltage of an SSVD (**b**) on U_0

c. Formation of an SSVD When the Gap Is Filled with an Electron Flux

Figure 10.5a shows the dependence of the electron flux current $I(U_0)$, recorded under the same conditions as the oscillograms in Fig. 10.4a. Clearly, at low values of U_0 this dependence $I \sim U_0^2$ in agreement with Eq. (10.11). When U_0 exceeded a certain minimum value, the current I rose steeply and this was accompanied by volume radiation in the discharge gap, indicating the onset of the ionization processes and the formation of an SSVD. This minimum value of U_0 amounted to (2/3) U_{st} as expected on the basis of Eq. (10.10), according to which the electric field at the anode was enhanced by the space charge of the electron flux by a factor of 1.5 compared with E_0. We could assume that the possibility of igniting an SSVD at a voltage lower than U_{st}, mentioned in [30, 31] and [21], was also due to distortion of the electric field by the space charge of the electron flux. In addition, in [21], this flux could be formed both from an auxiliary-discharge plasma under the cathode or from the photoplasma in the cathode region, because the discharge on the surface of a ceramic used in [21] was of relatively short duration ($\sim$1.5 μs).

The influence of the distortion of the electric field on the conditions of formation of a self-sustained volume discharge is manifested also by the results in Fig. 10.5b, which gives the dependence of the minimum voltage for the ignition of such a discharge U_{min} on U_0 in a circuit with a preliminary bias of the discharge gap. The sign of this bias was opposite to the sign of U_0 in order to avoid formation of an electron flux on application of a voltage pulse to the discharge gap. In this case, the auxiliary discharge was of the barrier type. Experiments were carried out on a mixture of the CO_2:N_2:He = 1:1:3 composition and the other parameters were d = 6 cm and p = 0.5 atm. A voltage pulse was applied to the discharge gap after the delay $\tau = t_0 = d^2/\mu U_0$ relative to the beginning of the auxiliary discharge. It is clear from Fig. 10.5b that U_{min} decreased monotonically on increase in U_0 in accordance with the above model, and became less than U_{st}.

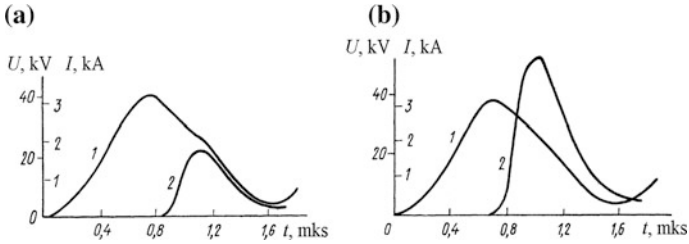

Fig. 10.6 Oscillograms of the voltage U (curves denoted by *1*) and of the current I (curves denoted by *2*) for an SSVD when the condition (10.8) is not satisfied (**a**) and when it is satisfied (**b**)

At low overvoltages across the discharge gap, the distortion of the electric field by the space charge of the electron flux had a considerable influence on the conditions of energy deposition in the plasma of the SSVD and on the residual voltage across the gap after the end of the discharge.

Figure 10.6a gives oscillograms of the voltage $U(t)$ and current $I(t)$ in an SSVD formed when the density of the electron flux current was too low for a significant distortion of the field and the condition (10.8) was not obeyed (d = 6 cm, gas mixture of the CO_2:N_2:He = 1:1:3 composition, p = 0.5 atm, charging voltage U_d = 45 kV, delayed leading edge, τ = 0.8 μs). Figure 10.6b shows oscillograms of $U(t)$ and $I(t)$ recorded under the same conditions as in Fig. 10.6a but, in this case, the condition (10.8) was satisfied. A comparison of Figs. 10.6a, b indicated that distortion of the electric field by the space charge of the electron flux resulted in some reduction in the amplitude of the voltage pulse across the discharge gap and also increased the amplitude of the current in the SSVD; it also increased the energy deposited in the discharge by a factor of approximately 2. This could be important under conditions when it would be difficult to establish a high overvoltage across the discharge gap.

All the forms of the auxiliary discharge that we investigated using a system of profiled electrodes made it possible to form an SSVD when up to 300 J/L of energy was deposited. The content of CO_2 in CO_2-N_2-He gas mixtures (with the addition of easily ionizable substances) at atmospheric pressure reached 40% when the total content of all the molecular gases was up to 70%, whereas in helium-free mixtures, it was up to 30%. We also established an SSVD in atmospheric air (p = 0.4 atm, d = 10 cm) by the addition of triethylamine, which was evidence of the high efficiency of the method of formation of an SSVD by filling the discharge gap with an electron flux. This was also true of gases characterized by strong electron trapping.

The best characteristics of an SSVD in a system of nonprofiled electrodes (Fig. 10.1a) did not differ from the characteristics of the corresponding discharge observed when the initial distribution of the electric field in the discharge gap was homogeneous. The discharge formed using such electrodes could be ignited employing any of the listed types of the auxiliary discharge, with the exception of a volume discharge utilizing metal electrodes (this type of the auxiliary discharge was

difficult to realize using nonprofiled electrodes because of the inhomogeneity of the electric field in the auxiliary gap). The investigated system was characterized by a strongly inhomogeneous initial distribution of the electric field in the discharge gap, which was close to the field distribution between one of the electrodes and a plane of symmetry in a parallel-plate capacitor of limited size (as shown in cross section in Fig. 10.1b); the field on the anode decreased monotonically along the normal to the symmetry axis of the discharge gap, whereas the field on the cathode increased reaching its maximum at the edge. Consequently, the static breakdown voltage U_{st} in the system with nonprofiled electrodes was approximately half the corresponding voltage in the quasisteady phase of an SSVD. When the discharge gap was subjected to a voltage pulse of amplitude $U > U_{st}$ (representing the regime with a deliberately delayed leading edge of the voltage pulse), a spark breakdown at the cathode edge was observed in the absence of an auxiliary discharge. When the auxiliary discharge was started and the static voltage was in the range $U_{st} < U < 1.8\ U_{st}$, a spark did not appear during the period τ_{ad} even when the formation of such a spark in the absence of an auxiliary discharge was less than τ. A weak electron flux current was then observed in the discharge gap. When the amplitude of the voltage pulse exceeded 1.8 U_{st} and an auxiliary discharge was started simultaneously with the leading edge of the pulse ($\tau > 2$ μs), a volume discharge appeared in the gap.

It therefore follows that the distortion of the initial distribution of the electric field by the space charge of the electron flux in the case of nonprofiled electrodes resulted, in an increase (as opposed to the reduction observed with profiled electrodes) of the pulsed breakdown voltage of the discharge gap and the breakdown was of volume nature. A strongly inhomogeneous initial distribution of the electric field in the presence of nonprofiled electrodes was collected in the process of filling the discharge gap with electrons, i.e., a dynamic profiling of electrodes by the space charge of the electron flux took place. We shall now qualitatively consider this phenomenon.

Screening of the cathode by the negative charge of electrons reduced the electric field on the cathode surface severalfold, compared with the average field $U(t)/d$ in the discharge gap at a given moment, so that ionization processes could not develop near the sharp edges of the cathode. The field at the anode was then enhanced and the relative magnitude of the enhancement should be highest at the center of the electrode, since the electron flux spread in the course of propagation in a discharge gap as a result of the electrostatic repulsion between the electrons. With initial distribution of the field in the discharge gap borne in mind, we concluded that the ionization processes began to develop simultaneously from the anode to the cathode and from the center to the edges of the discharge gap, i.e., the propagation of an ionization wave, which formed a cathode layer when it closed the discharge gap, was not governed by the initial configuration of the electric field but by that configuration which was formed with the participation of the space charge of the electron flux. This made it possible to prevent spark breakdown and to form, in a system with nonprofiled electrodes, an SSVD with a deposited energy distribution typical of such nonprofiled electrodes. Measurements of the small-signal gain at

low pump energies, which represented the distribution of the energy deposited in the discharge in a plane perpendicular to the optic axis, demonstrated that the gain decreased away from the optic axis to the electrode edges. This provided an indirect confirmation of the above description of the formation of an SSVD.

It should be stressed that a change in the voltage on the electrodes resulted in a redistribution of the electric field in the discharge gap at a finite rate governed by the electron mobility. Therefore, the condition for screening the cathode by the space charge of the electron flux $E_0 \ll U/d$ (where U/d is the instantaneous value of the field) could be disturbed if the voltage across the discharge gap rose too rapidly. In fact, it was not possible to create an SSVD using nonprofiled electrodes when the voltage was applied abruptly to the electrodes and this was true even when the application of a bias resulted in a preliminary filling of the discharge gap with electrons. Sparks were observed at the corners of the cathode, i.e., in the regions with the maximum concentration of the electric field in the absence of screening. The discharge was stable in the case when the leading edge of the voltage pulse was delayed deliberately [21, 22] so that the duration of this edge was $\tau > 2$ μs for $d = 10$ cm.

A classical example of nonprofiled electrodes with a strongly inhomogeneous initial distribution of the electric field in the discharge gap was the first transversely excited CO_2 laser. The present experiments indicated that the electron flux in such a system was formed by a barrier discharge plasma created directly on the cathode surface and this made it possible to readily satisfy the saturation [Eq. (10.8)] and screening conditions. It should also be stressed that an increase in the stability of an SSVD [22] in systems of the type described in [16] and considered in the present study, which was observed when easily ionizable substances were added to the gas mixtures, was not caused by photoionization of these additives. This is apparent because in the case of regimes used to form an SSVD by filling the gap with an electron flux, the contribution of the photoionization to the conductance of the discharge gap during the filling process was unimportant compared with the contribution of the electron flux from the auxiliary-discharge plasma. This was true of the majority of the auxiliary discharges.

10.5 Conclusions

We investigated the formation of an SSVD in CO_2-N_2-He mixtures by preliminary filling of the gap with an electron flux from an auxiliary-discharge plasma. This method was suitable for large distances between the electrodes. A study was carried out into the characteristics of some of the discharges that could be used as auxiliary discharges. It was established that the formation of an SSVD was affected significantly by the distortion of the electric field due to the presence of a space charge of the electron flux. Dynamic profiling of electrons was found to be possible and an SSVD was attained in systems with a strongly inhomogeneous initial distribution of the electric field in the gap.

The simplicity of the proposed methods is very promising for their applications in CO_2 lasers. Although the main results of the present investigation were obtained for CO_2-N_2-He gas mixtures, the methods can clearly be applied to other gases as well.

References

1. V.Y. Baranov, V.M. Borisov, A.A. Vedenov, S.V. Drobyazko, V.N. Knizhnikov, A. P. Napartovich, V.G. Niz'ev, A.P. Strel'tsov, Preprint No. 2248 [in Russian] (Institute of Atomic Energy, Moscow, 1972)
2. A.J. Palmer, Appl. Phys. Lett. **25**, 138 (1974)
3. V.N. Kamyushin, A.N. Malov, R.I. Soloukhin, Kvantovaya Elek-tron. (Moscow) **5**, 555 (1978) [Sov. J. Quantum Electron. *8*, 319 (1978)]
4. H. Seguin, I. Tulip, Appl. Phys. Lett. **21**, 414 (1972)
5. A.F. BelyatskiT, D.B. Gurevich, M.A. Kanatenko, I.V. PodmoshenskiT, Pis'ma Zh. Tekh. Fiz. **6**, 73 (1980) [Sov. Tech. Phys. Lett. *6*, 32(1980)]
6. S.C. Lin, J.I. Levatter, Appl. Phys. Lett. **34**, 505 (1979)
7. A.I. PavlovskiT, V.S. Bosamykin, V.I. Karelin, V.S. Nikol'skii, Kvantovaya Elektron. (Moscow) **3**, 601 (1976) [Sov. J. Quantum Electron. 6,321 (1976)]
8. A.I. Pavlovskii, V.F. Basmanov, V.S. Bosamykin, V.V. Gorokhov, V.I. Karelin, P.B. Repin, Abstracts of Papers presented at Second All-Union Conference on Physics of Electric Breakdown in Gases, Tartu, 1984 [in Russian], p. 330
9. R.V. Babcock, I. Liberman, W.P. Partlov, IEEE J. Quantum Electron. QE-12,29(1976)
10. A.V. Koz^{A}rev, Y.D. Korolev, G.A. Mesyats, Y.N. Novoselov, A.M. Prokhorov, V.S. Skakun, V.F. Tarasenko, S.A. Genkin, Kvantovaya Elektron. (Moscow) **11**, 524 (1984) [Sov. J. Quantum Electron. **14**, 356(1984)]
11. O.P. Judd, J. Appl. Phys. **45**, 4572 (1974)
12. V.V. Apollonov, N. Akhunov, A.M. Prokhorov, in *Proceedings of the Eighteenth International Conference on Phenomena in Ionized Gases*, Budapest, vol. 2 (1985), p. 887
13. V.V. Apollonov, G.G. Baitsur, A.M. Prokhorov et al., Pis'ma Zh. Tekh. Fiz. **11**, 1262 (1985) [Sov. Tech. Phys. Lett. 11, 521 (1985)]
14. A.K. Laflamme, Rev. Sci. Instrum. **41**, 1578 (1970)
15. A.J. Beaulieu, Appl. Phys. Lett. **16**, 504 (1970)
16. R. Dumanchin, J. Rocca-Serra, C.R. Acad, Sci. Ser. B **269**, 916 (1969)
17. V.P. Gorelov, N.N. Minakova, V.A. Chagin, Elektrotekh. Promst Ser. Elektrotekh. Mater. **5**, 20 (1972)
18. P.A. Belanger, R. Tremblay, J. Boivin, G. Otis, Can. J. Phys. **50**, 2753 (1972)
19. V.V. Apollonov, N. Akhunov, A.M. Prokhorov et al., Kvantovaya Elektron. (Moscow) **11**, 1241 (1984) [Sov. J. Quantum Electron. 14, 835 (1984)]
20. T.Y. Chang, Rev. Sci. Instrum. **44**, 405 (1973)
21. V.V. Apollonov, A.M. Prokhorov et al., Kvantovaya Elektron. (Moscow) **11**, 1327 (1984) [Sov. J. Quantum Electron. 14, 898, (1984)]
22. V.V. Apollonov et al., Kvantovaya Elektron. (Moscow) **12**, 5 (1985) [Sov. J. Quantum Electron. 15, 1 (1985)]
23. V.V. Apollonov et al., Pis'ma Zh. Tekh. Fiz. **3**, 1073 (1977) [Sov. Tech. Phys. Lett. 3, 441 (1977)]
24. V.V. Apollonov, S.I. Derzhavin et al., Pis'ma Zh. Tekh. Fiz. **5**, 1518 (1979) [J. Sov. Tech. Phys. Lett. 5,643 (1979)]
25. V.V. Apollonov, N. Akhunov et al., Kvantovaya Elektron. (Moscow) **10**, 1458 (1983) [Sov. J. Quantum Electron. 13, 947(1983)]

26. A.A. Kuchinskii (Kuchinsky), B.V. Lyublin (Ljublin), V.F. Shanskii (Shansky), V.A. Sheverev, in *Proceedings of the Sixteenth International Conference on Phenomena in Ionized Gases, Dusseldorf*, (ed. by W. Botticker, H. Wenk, E. Schulz-Gulde), Contributed Papers, vol. 2, publication by the Conference Committee (undated) (1983), p. 200
27. A.L. Ward, J. Appl. Phys. **36**, 2540 (1965)
28. A.H. von Engel, *Ionized Gases* (Clarendon Press, Oxford, 1955)
29. I.L. Kamardin, A.A. Kuchinskii, V.A. Rodichkin, V.F. Shanskii, Abstracts of Papers presented at Third All-Union Conference on Laser Optics, Leningrad (1982) [in Russian], p. 64
30. S.I. Andreev, N.M. Belousova, P.N. Dashuk, D.Y. Zaroslov, E.A. Zobov, N.V. Karlov, G.P. Kuz'min, S.M. Nikiforov, A.M. Prokhorov, Kvantovaya Elektron. (Moscow) **3**, 1721 (1976) [Sov. J. Quantum Electron. **6**, 931 (1976)]
31. A.V. Melekhov, Abstracts of Papers presented at Second Ail-Union Conference on Physics of Electric Breakdown of Gases, Tartu (1984) [in Russian], p. 357

Chapter 11
Mechanism of Formation of an SSVD Initiated by a Barrier Discharge Distributed on the Surface of a Cathode

Abstract A study was carried out into the mechanisms of formation of an SSVD in CO_2–N_2–He gas mixtures initiated by an auxiliary barrier discharge distributed on the surface of a cathode. The volume discharge was initiated when the discharge gap was filled by an electron flux formed from the barrier discharge plasma in the course of a smooth rise of the voltage across the electrodes. Measurements were made of the small-signal gain, confirming the model of formation of an SSVD and demonstrating that a discharge of this kind could be used to amplify nanosecond light pulses.

In models of formation of an SSVD in dense gases, a high homogeneity of the electric field in the discharge gap and a high rate of rise of the voltage pulse are among the principal requirements [1–3]. These requirements are clearly not satisfied in a CO_2 laser in which an SSVD is initiated by a barrier discharge distributed on the cathode surface [4]. In a system of this kind, an SSVD appears in a strong inhomogeneous field (similar in its configuration to the field between an infinite plane and a rectangular plate representing the cathode) and the discharge is obtained only if the leading edge of a pulse τ_l, is lengthened deliberately [5]. There are also contradictions in the treatment of the mechanisms of formation of primary electrons in the discharge gap given in [4]: the main mechanisms are postulated to be both the photoionization of the gas by the radiation from a barrier discharge [6] and the initiation of an SSVD on the cathode directly by electrons from the barrier discharge plasma [7].

A later investigation [8] of a CO_2 laser, essentially similar to the laser described in [4], yielded a specific output energy of the laser radiation of up to 50 J/l with an efficiency of 20%. The use of pumping pulses characterized by large values of τ_l in systems with other types of auxiliary discharge made it possible to increase the electrode gap d to 40 cm as in [9] and to dispense with special shaping of the electrodes as in [10]. Studies of the mechanisms of formation of an SSVD in a system of this kind and resolution of these contradictions were the aims of the present study.

© Springer International Publishing Switzerland 2016

V.V. Apollonov, *High-Energy Molecular Lasers*,
Springer Series in Optical Sciences 201, DOI 10.1007/978-3-319-33359-5_11

Our electrodes were constructed in a manner similar to that described in [11]. The main mechanism of the formation of primary electrons was identified using N_2 with the addition of easily ionizable substances, i.e., under conditions that were most favorable for the photoionization. We then used the method of [12]: we recorded the charge q flowing through the gap on application of the same bias voltages U_0 but of different polarities (relative to the electrode involved in the barrier discharge) when the barrier discharge was triggered by voltage pulses of different profiles. An SVD was observed using a pump system [5, 8] of the type described in [8] and characterized by $\tau_l \geq \tau_e$, where τ_e is the time taken by an electron to drift across the discharge gap. A barrier discharge voltage was supplied from the anode via a capacitance divider. Our experiments were carried out on gaps of d = 4–12 cm width in CO_2–N_2–He gas mixtures containing easily ionizable substances in the form of tripropylamine and triethylamine ($\sim$1 Torr).

Figure 11.1a shows an oscillogram of q for N_2 with the addition of triethylamine obtained for p = 1 atm, d = 8 cm, U_0 = −10 kV when the duration of the voltage pulses across the barrier discharge was $\sim$1 μs, which was less than $\tau_e \sim 10$ μs. Clearly, the time for the accumulation of a charge q was close to the drift time of positive ions across the discharge gap ($\sim$7 ms). An oscillogram showed a region of a rapid ($\sim \tau_e$) rise of q, which was observed for the negative polarity of U_0 when the density of photoelectrons n_e in the discharge gap was sufficiently high. Estimates indicated that in this experiment, the average photoelectron density in the discharge gap was $n_e \sim 10^7$ cm^{-3} and in spite of the presence of the easily ionizable substance in the gas, it did not exceed 10^{-2} of the concentration of the positive ions that were extracted from the barrier discharge plasma. When a positive voltage U_0 was applied, the charge q rose rapidly (in a time $\sim \tau_e$) owing to the accumulation of the electron charge supplied by the barrier discharge plasma.

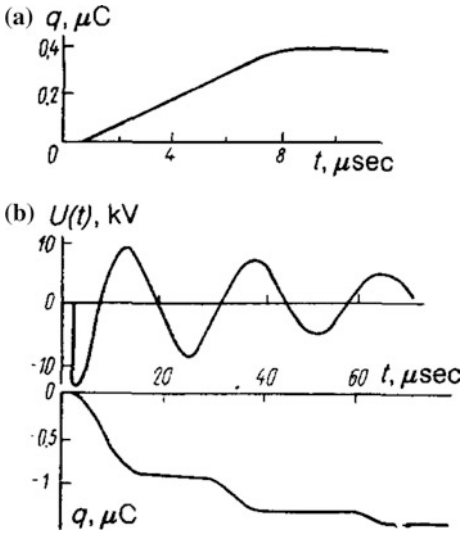

Fig. 11.1 Oscillograms of q recorded for negative (**a**) and positive (**b**) polarities of the continuous electrode; $U(t)$ is the voltage across the barrier discharge

Figure 11.1b shows oscillograms of q and of the voltage across the barrier discharge $U(t)$ for an oscillatory voltage $U(t)$, obtained for N_2 at $p = 1$ atm, when the gap was $d = 8$ cm and the static voltage was $U_0 = 10$ kV. Clearly, the penetration of electrons into the discharge gap was possible only for $dU/dt > 0$, owing to the construction of the cathode unit [11] and due to the associated distribution of the electric field around the electrode covered by an insulator.

These results indicated that the main source of electrons in the study reported in [4], before the onset of the ionization processes in the discharge gap, was not the photoplasma created by the barrier discharge radiation, but rather directly the plasma of the barrier discharge itself. Electrons were pulled into the discharge gap only when $dU/dt > 0$ [10] (in the conventional electric circuit of [4] the electron flux was formed at the leading edge of the voltage pulse). When a photoplasma with $n_e \sim 10^7$ cm^{-3} was present in the discharge gap, an SSVD could be initiated in a homogeneous field, [1] but its polarization could not result in compensation of the edge inhomogeneity. In fact, in the system of [4], irrespective of the delay between the main and auxiliary discharges in the regime with a short leading edge of the voltage across the barrier discharge ($\tau_l \ll \tau_e$), typical of systems with ultraviolet preionization, [1] a spark breakdown always occurred for $dU/dt < 0$.

For $\tau_l > \tau_e$ and $dU/dt > 0$, the electric field in the discharge gap was greatly distorted by a negative space charge of the electron flux: it was reduced by a large factor at the cathode and enhanced at the anode in the ratio U_i/d (U_i is the instantaneous value of the voltage) and because of the electrostatic repulsion between electrons in the flux, the maximum enhancement of the field could be expected in the central part of the anode. Therefore, it was here and not near the cathode edge that ionization began and this was why an SSVD could form. In this process, the condition for the slow rise of the voltage across the discharge gap was of fundamental importance, because in the opposite case the density of electrons in a flux could not follow the changes in the external field and the screening of the cathode was ineffective.

The redistribution of the electric field in the discharge gap by such a space charge and the formation of an SSVD affected the spatial distributions of the energy deposited in the discharge and the small-signal gain α.

Figure 11.2 shows the distribution of the gain a across the aperture [4] in a plane parallel to the electrode surfaces, recorded in the present experiments at low pump energies when a was proportional to the specific input energy [13]. It is clear from Fig. 11.2 that the specific input energy at the center of the discharge zone was approximately twice as high as at the edge of the zone, and this edge was very well defined. The shape of the edge should repeat the shape of the lines of force of the electric field. Measurements of a and photographs of the radiation emitted by an SSVD indicated that the discharge zone was in the shape of a rectangular parallelepiped, which once again was different from the distribution of the electric field in [4] for an SSVD from the distribution set by the electrode profiles.

This configuration of the discharge zone was obtained clearly because during the quasisteady phase of an SSVD the absolute value of the field E in the positive column was governed, at a given pressure, by the composition of the mixture [14]

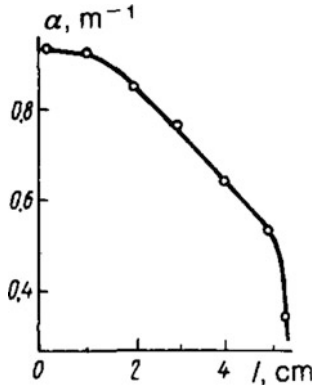

Fig. 11.2 Distribution of the gain over the aperture of the system

and was independent of the spatial coordinate. Therefore, the condition $U' = \int E \cdot \mathrm{d}l$ (integration along the lines of force of the field) was satisfied throughout the barrier discharge only when the lines of force of the field were perpendicular to the electrode surfaces everywhere. The shape of the discharge zone was reproduced when an SSVD was initiated for the second time. We recorded (Fig. 11.3) oscillograms of the SSVD voltage and current obtained under the same conditions as in [4], followed by the application to the barrier discharge of a second voltage pulse delayed relative to the first. The operation was stable (irrespective of τ_l and the polarity of the second pulse) if the average plasma concentration in the discharge gap at the moment of application of the second pulse exceeded 10^{11} cm^{-3}.

We thus found that an SSVD in laser systems of the type described in [4] formed as a result of filling the discharge gap with a flux of electrons pulled out from the plasma of a barrier discharge as well as a result of a redistribution of the field in the gap because of a space charge in such a way that the ionization processes began at the anode. Ultraviolet radiation from the barrier discharge did not play a significant

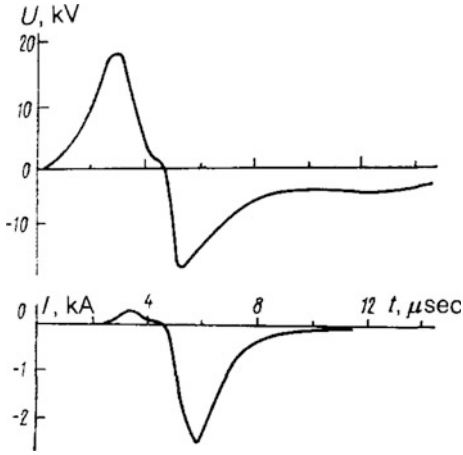

Fig. 11.3 Oscillograms of the voltage U and the current I for an SSVD

role and the use of easily ionizable substances under these conditions was desirable because of the reduction in the voltage and the increase in the duration of stable operation of an SSVD with the aid of such substances, irrespective of the photoionization process [15].

In conclusion, it should also be mentioned that when the specific input energy was ~250 J/l (d = 10 cm) the measured value of the small-signal gain α for a mixture of the CO_2:N_2:He = 1:1:2 composition reached 5 m^{-1}. A system of this kind is thus likely to be an efficient amplifier of nanosecond light pulses.

References

1. V.N. Karnyushin, R.I. Soloukhin, *Macroscopic and Molecular Processes in Gas Lasers [in Russian]* (Atomizdat, Moscow, 1981)
2. J.I. Levatter, Shao-Chi Lin, J. Appl. Phys. **51**, 210 (1980)
3. M.A. Kanatenko, Pis'ma Zh. Tekh. Fiz. **9**, 214 (1983) [Sov. Tech. Phys. Lett. **9**, 94 (1983)]
4. R. Dumanchin, J.C. Farcy, M. Michon, J. Rocca-Serra, *Paper Presented at Sixth Intern* (Quantum Electronics Conf, Kyoto, Japan, 1970)
5. Y.L. Pan, A.F. Bernhardt, J.R. Simpson, Rev. Sci. Instrum. **43**, 662 (1972)
6. Y.T. Mazurenko,Y.A. Rubinov, Kvantovaya Elektron. (Moscow) **3**, 610 (1976) [Sov. J. Quantum Electron. **6**, 328 (1976)]
7. E.P. Velikhov, VYu. Baranov, V.S. Letokhov, E.A. Ryabov, A.N. Starostin, *Pulsed CO_2 Lasers and Their Applications in Isotope Separation [in Russian]* (Nauka, Moscow, 1983)
8. V.V. Apollonov et al., Kvantovaya Elektron. (Moscow) **12**, 5 (1985) [Sov. J. Quantum Electron. **15**, 1 (1985)]
9. V.V. Apollonov, G.V. Bush et al., Kvantovaya Elektron. (Moscow) **11**, 2149 (1984) [Sov. J. Quantum Electron. **14**, 1435 (1984)]
10. V.V. Apollonov et al., Pis'ma Zh. Tekh. Fiz. **11**, 1262 (1985) [Sov. Tech. Phys. Lett. **11**, 521 (1985)]
11. Z.I. Ashurly, Y.M. Vas'kovskiY, I.A. Gordeeva, L.V. Malyshev, R.E. Rovinskii, A.A. Kholodilov, Kvantovaya Elektron. (Moscow) **7**, 1456 (1980) [Sov. J. Quantum Electron. **10**, 838 (1980)]
12. H. Raether, *Electron Avalanches and Breakdown in Gases* (Butter-worths, London, 1964)
13. E.A. Ballik, B.K. Garside, J. Reid, T. Tricker, J. Appl. Phys. **46**, 1322 (1975)
14. J.J. Lowke, A.V. Phelps, B.W. Irwin, J. Appl. Phys. **44**, 4664 (1973)
15. V.V. Apollonov, N. Akhunov et al., Preprint No. 212 [in Russian], Institute of General Physics, Academy of Sciences of the USSR, Moscow (1985)

Chapter 12
Formation of an SSVD for Pumping of Gas Lasers in Compact Electrode Systems

Abstract The method of generation of an SSVD in a system of two plane electrodes of identical size and with sharp edges was proposed and tested experimentally. This method provided means for controlling the energy distribution over the aperture of a CO_2 laser with such electrodes.

Efficient pumping of gas lasers by an SSVD makes it necessary to ensure a near homogeneous distribution of the input energy delivered to the active medium. This is usually achieved by a special geometry of the electrodes, the profiles of which are designed to ensure a homogeneous distribution of the electric field in the discharge zone [1–3].

A different method for the profiling of the electric field in a discharge gap was proposed in [4]: this is a dynamic method that makes it possible to excite an SSVD in a system of electrodes consisting of a plane anode (with rounded edges) and a smaller plane rectangular cathode with sharp edges: the discharge is initiated over the whole of the cathode surface. Breakdown at the edges is avoided by screening the cathode (before the onset of ionization processes in the discharge gap) by the negative space charge of the flux of electrons formed from the plasma of an auxiliary discharge.

We developed the dynamic profiling method still further. We considered the possibility of exciting a self-maintained volume discharge in a system of two identical planar electrodes with sharp edges, i.e., in a system characterized by extreme compactness. By analogy to [4], it is natural to assume that this should be feasible if the electric field intensity is reduced deliberately on the electrode surfaces if they are screened by a space charge.

Our experiments were carried out for an interelectrode gap of d = 6–10 cm in CO_2–N_2–He gas mixtures at an atmospheric pressure containing additives in the form of easily ionizable elements. The system is shown schematically in Fig. 12.1. Rectangular electrodes of 8 × 40 cm dimensions were made from a brass grid. They were subjected to voltage pulses of U_m = 60–80 kV amplitude and a leading edge of 2 μs; simultaneously with the beginning of this pulse, an auxiliary discharge was excited under a cathode C, in the same way as in [4], and an ultraviolet

© Springer International Publishing Switzerland 2016

V.V. Apollonov, *High-Energy Molecular Lasers*,
Springer Series in Optical Sciences 201, DOI 10.1007/978-3-319-33359-5_12

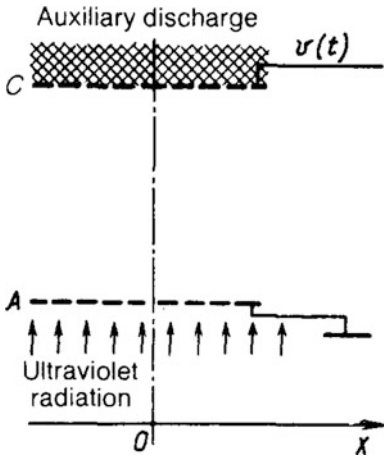

Fig. 12.1 Scheme of laser system

radiation source placed behind an anode A was triggered. During the rise time of the anode voltage, the loss of photoelectrons from the discharge gap resulted in accumulation of an excess space charge of low-mobility positive ions and the cathode became screened by the space charge of an electron flux emerging from the plasma of the auxiliary discharge and filling the discharge gap.

The screening of the anode by a positive charge due to the loss of photoelectrons from the discharge gap occurred when $n_0 \lambda e/\varepsilon_0 \gg U_0/d$, where n_0 is the photoplasma density near the anode, $\lambda \ll d$ is the depth of penetration of ultraviolet radiation into the gas, and U_0 is the voltage across the discharge gap. For typical parameters $\lambda \approx 1$ cm, $U_0/d \sim 10$ kV/cm, this condition was satisfied for $n_0 > 10^{10}$ cm^{-3} by spark sources of ultraviolet radiation.

We shall now consider the processes that occurred in the discharge gap in greater detail. For a given electrode geometry, the static breakdown voltage in the discharge gap U_{st} was ~ 0.5 of the voltage across the plasma in the SSVD during the quasistatic stage U_{qs} (which was close to the static breakdown voltage in a homogeneous field). For $U_{\mathrm{m}} > U_{st}$ in the case when the auxiliary discharge or the ultraviolet radiation source was switched off, spark breakdown of the discharge gap occurred at the leading edge of a voltage pulse. Under normal operating conditions when $U_{st} < U_{\mathrm{m}} < U_{\mathrm{qs}}$ this spark breakdown was delayed by 6–10 μs relative to the maximum of the voltage across the discharge gap, whereas for $U_{\mathrm{m}} > U_{\mathrm{qs}}$ a space charge completely covering the electrode surfaces was observed. The input energy delivered to the plasma of the SSVD reached 200 J/l. A smooth rise of the voltage across the discharge gap resulted in maintenance of a close to zero space charge of electrons at the cathode (at least at its edges) and these electrons arrived from the secondary discharge plasma [4]. Photoelectrons were simultaneously lost to the anode, which reduced the electric field near the anode surface (compared with the average over the whole discharge gap) and the edges became screened by the excess positive charge. If $\lambda \ll d$, the processes of screening of the cathode and anode occurred independently. The process of modification of the conditions so that they

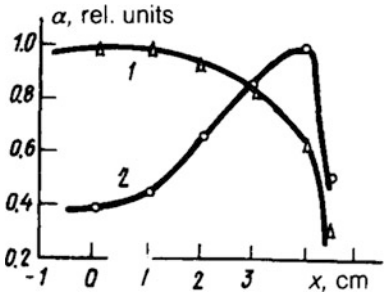

Fig. 12.2 Distributions of the small-signal gain over the aperture

became favorable for an SSVD was completed when the discharge gap was filled with electrons from the auxiliary discharge plasma. Up to that moment, the electric field in the discharge gap was distorted, so that its maximum was located in the region within the discharge gap and not at the electrode edges. Therefore, the ionization began, not at the electrode edges, but in the region of the strongest enhancement of the field. Ionization shifted the charge of the newly formed electrons to the anode; anode- and cathode-directed ionization waves were formed; and, when these waves reached the electrodes, the process of formation of an SSVD was finished.

This qualitative account of the formation of an SSVD is supported by the results in Fig. 12.2, which gives distributions of the small-signal gain α over the aperture of the investigated system (in a plane parallel to the electron surfaces) for low input energies (when α was proportional to the specific input energy). In the case of photoionization of a gas distributed uniformly over the electrode area in the anode region, it was found that the maximum enhancement of the field occurred on the symmetry axis of the system and this was responsible for the lowering of α at the edges of the discharge gap (curve 1). Maxima of $\alpha(x)$ for the illumination of the anode only along its perimeter also corresponded to maxima of the degree of enhancement of the field (curve 2).

References

1. N. Felici, Rev. Gen. Electr. **59**, 479 (1950)
2. F.M. Bruce, J. IEE Part II **94**, 138 (1947)
3. T.Y. Chang, Rev. Sci. Instrum. **44**, 405 (1973)
4. V.V. Apollonov et al., Pis'ma Zh. Tekh. Fiz. **11**, 1262 (1985) [Sov. Tech. Phys. Lett. **11**, 521 (1985)]

Chapter 13
Large-Aperture CO_2 Amplifier

Abstract A report is given of construction of a CO_2 amplifier with an aperture of 40 cm, pumped by an SSVD with a system of electrodes without a special profile. The SSVD formed as a result of filling the discharge gap with a flux of electrons from the plasma of an auxiliary discharge initiated under a grid cathode with sharp edges. The small-signal gain on the optic axis was 3.3 m^{-1} and its distribution over the aperture was nearly uniform.

The feasibility of using an SSVD for the pimping of large-aperture CO_2 amplifiers is seriously limited by the difficulty of achieving the threshold density of the primary electrons throughout the gap between the electrodes, and the need for careful profiling of the electrodes to ensure the maximum homogeneity of the electric field in the discharge gap.

A method for the formation of an SSVD involving filling of a discharge gap with a flux of electrons from the plasma of an auxiliary discharge, which made it possible to dispense with special profiling of the electrodes, was proposed in [1] and tested experimentally. Estimates indicate that it should be possible to use this method in CO_2–N_2–He mixtures when the gap between the electrodes d is large.

We would like to report the results of an investigation of the characteristics of a CO_2 amplifier with a 40-cm aperture in which an SSVD was formed in this way. Figure 13.1a is the circuit of the apparatus. An anode A is an A1 plate of 80 × 140 cm dimensions rounded along the perimeter to a radius of 15 mm. A cathode C is a brass grid of rectangular shape and 35 × 97 cm dimensions with sharp edges. An auxiliary multichannel discharge was initiated on the surface of a ceramic and limited by its intrinsic capacitance [2]. A flux of electrons formed in the gap between the ceramic surface and the grid in an electric field created as a result of the voltage drop across the surface discharge channels. Under the action of this field, some of the electrons were driven into the discharge gap and traveled to the anode because of the application of a bias voltage provided by a special pump system comprising an eight-stage Arkad'ev-Marx generator with a 0.25 μF capacitance per shot (the discharge voltage was varied within the range 30–55 kV) and a peaking 0.2 μF capacitor, which was in the fonn of a two-stage pulse generator.

© Springer International Publishing Switzerland 2016

V.V. Apollonov, *High-Energy Molecular Lasers*,
Springer Series in Optical Sciences 201, DOI 10.1007/978-3-319-33359-5_13

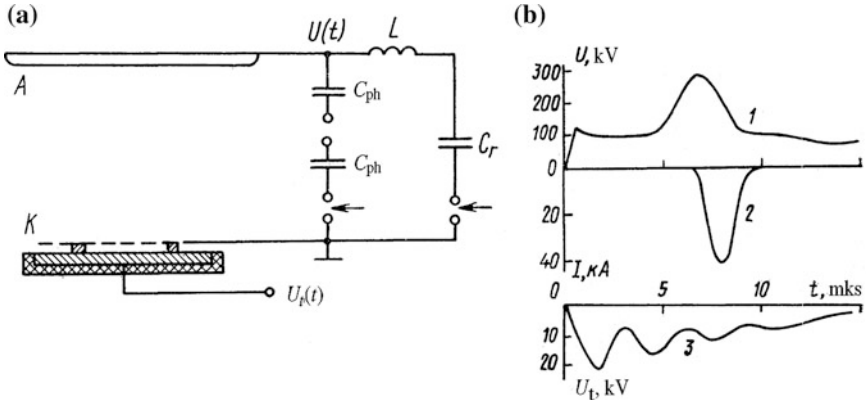

Fig. 13.1 Circuit of the apparatus (**a**) and oscillograms of U (*curve 1*), I (*curve 2*), and U_t (*curve 3*) (**b**)

The experiments were carried out using systems with $d = 20–40$ cm and atmospheric-pressure gas mixtures containing an easily ionizable substance (triethylamine). The energy needed to create an electron flux did not exceed 1% of the energy dissipated in the main discharge.

The possibility of formation of an SSVD in this system of electrodes was due to the fact that in the process of filling the gap with electrons, the electric field, due to a negative space charge, decreased severalfold at the cathode and increased at the anode compared with its average value U/d across the gap *(U is* the instantaneous value of the voltage across the gap). In view of the repulsion between electrons in a flux, the maximum enhancement of the field should occur in the central part of the anode. It was here and not near the sharp edge of the cathode that the ionization processes began. The voltage across the gap should not rise too rapidly, because otherwise the density of electrons in the flux could not follow changes in the external field and the screening of the cathode edge would be ineffective.

Figure 13.1b shows typical oscillograms of the voltage U and the current I in an SSVD, and also of the voltage across the electrodes of the auxiliaiy discharge U_t. The SSVD was stable when the time delay between the moments of application of a voltage to the auxiliary discharge and the onset of the ionization processes in the main gap was sufficient to fill the whole gap with electrons. When this condition was not obeyed, inhomogeneities in the form of bright partial channels were observed.

This qualitative description of the formation of an SSVD was supported by the distributions of the small-signal gain a across the aperture. Figure 13.2 shows the distributions of a in a plane parallel-to the electrode surfaces obtained in the case of weak saturation of a in respect of the specific input energy in small-signal gain. Clearly, the gain and, consequently, the specific input energy decreased from the center to the edges of the discharge zone, providing an indirect confirmation of the

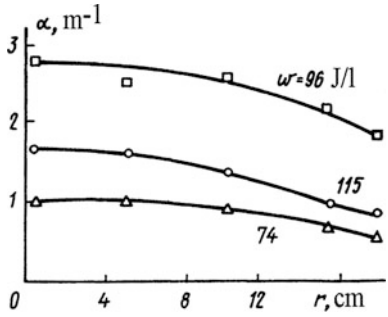

Fig. 13.2 Distributions of the small-signal gain over the aperture, obtained for CO_2:N_2:He = 15:15:70 (□), 6:24:70 (O), find 4:16:80 (Δ) mixtures using different specific input energies *w*

model of formation of an SSVD described above when the discharge gap was filled by an electron flux.

When the input energy was increased, the distribution of a over the aperture became nearly uniform as a result of saturation and the value of a corresponding to d = 40 cm on the optic axis in a mixture of the CO_2:N_2:He = 15:15:70 composition was 3.3 m, so that this system could be used in the output stages of high-power laser amplifiers operating in the nanosecond range.

References

1. V.V. Apollonov et al., Sov. Tech. Phys. Lett. **11**, 521 (1985)
2. V.V. Apollonov, N. Akhunov et al., Sov. J. Quantum Electron. **14**, 835 (1984)

Chapter 14
Dynamic Profiling of an Electric Field in the Case of Formation of an SSVD Under Conditions of Strong Ionization of the Electrode Regions

Abstract It was found that an SSVD could be ignited in a system of two electrodes with sharp edges under conditions of strong ionization of the electrode regions. The conditions for such ignition were determined. A discharge of this kind could be used in compact CO_2 lasers with apertures of up to 30 cm and specific output energies of up to 48 J/l, when preionization was provided by radiation from commercial flashlamps with quartz bulbs.

It was shown in [1–3] that an SSVD was ignited without special profiling of the (in order to establish a homogeneous electric field in the discharge gap) [4]. The method of formation of an SSVD proposed in [1, 2], where the necessary initial conditions in respect of the density of primary electrons and the distribution of the electric field were achieved as a result of motion of space charges in the discharge gap, could be called the method for dynamic profiling of the electric field. This method made it feasible to form an SSVD in a system of very compact electrodes composed of two identical rectangular plates with sharp edges. Since a redistribution of the space charge occurs at a finite rate, the method of dynamic profiling imposes restriction on the rate of rise of the voltage across the discharge gap [1, 2]. However, if a homogeneous plasma column is formed in advance along the anode-cathode direction in a system of electrodes with sharp edges and the density of electrons in the column is $n_e \sim 10^{10}$–10^{11} cm^{-3}, it is permissible to apply voltage pulse to the discharge gap, which can have a leading edge as short as necessary [3]. This electron density n_e can be the minimum value in the plasma column inside in discharge gap needed to ignite an SSVD in a system of electrodes with sharp edges.

It would be also of interest to find the conditions for achieving an SSVD in a system of compact electrodes in a situation typical of systems with ultraviolet preionization when the interelectrode distances d are high and when a fairly intense plasma with $n_e \sim 10^{10}$ cm^{-3} can be created only in narrow regions near the electrodes.

We investigated the feasibility and conditions for ignition of an SSVD in a system of electrodes with sharp edges in the case of strong ionization of the

© Springer International Publishing Switzerland 2016

V.V. Apollonov, *High-Energy Molecular Lasers*,
Springer Series in Optical Sciences 201, DOI 10.1007/978-3-319-33359-5_14

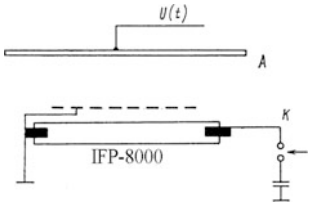

Fig. 14.1 Schematic diagram of the apparatus

electrode regions with ultraviolet radiation. Our experiments were carried out in CO_2–N_2–He gas mixtures at atmospheric pressure containing an easily ionized substance (triethylamine) at a pressure of 1–2 Torr when the discharge gap was d = 20–30 cm. We used the arrangement shown in Fig. 14.1. The anode was a steel sheet of 50 × 60 cm dimensions rounded along the perimeter to a radius of 0.3 cm. The cathode was a plane brass grid of rectangular shape with 20 × 30 cm dimensions and sharp edges. Ultraviolet radiation was provided by flashlamps with quartz bulbs [5]. The discharge gap was illuminated using twelve IFP-8000 flashlamps located at a distance of 1 cm from the grid and supplied from a shared 0.7 μF capacitor under a voltage of 20–30 kV. Under these conditions, the photoelectron density at the cathode was $\sim 2 \times 10^{10}$ cm^{-3} and at a distance of 20 cm from the flashlamps it was 10^8 cm^{-3} (this was true of a mixture of the CO_2:N_2:He = 1:1:8 composition containing 1.5 Torr of triethylamine; the average absorption coefficient of ultraviolet radiation was $k_r \sim 0.3$ cm^{-1}).

The power supply unit of an SSVD was a six-stage generator of voltage pulses with a 0.16 μF capacitance per shot and a maximum voltage of U_0 = 240 kV. The leading edge of the voltage pulses was selected to be either short (τ_{ed} = 200 nsec; short leading edge: SLE) or it was extended deliberately to 4–6 μs (long leading edge: LLE).

An SSVD was achieved both in the SLE and LLE cases when the average energy delivered to the discharge plasma was $W \sim 300$ J/l. The content of the molecular gases in the working mixture, limited by the value of U_0 was then 40 and 20% for d = 20 and 30 cm, respectively. Oscillograms of the discharge current and voltage obtained in the SLE and LLE cases did not differ from those reported earlier [6] for the same cases.

An SSVD was also achieved in an extremely compact system with two identical grid electrodes using flashlamps. In all cases, an SSVD was established when the initial electron density was $\sim 10^{10}$ cm^{-3} not throughout the discharge gap, as in [7], but simply near the sharp-edged electrodes. The energy characteristics of the active medium were investigated by increasing its length to 1 m when the discharge gap was d = 20 cm. A telescopic unstable resonator with a magnification of M = 2 and a concave mirror with a diameter of 20 cm was used in these experiments and it was found that the stimulated radiation energy was 1.5 kJ, the specific output energy of the laser radiation was 48 J/l, and the energy efficiency was 15%, measured relative to the plasma in an SSVD.

We shall now qualitatively consider the formation of an SSVD. Let us assume that a photoplasma is created in the discharge gap and the electron density in this plasma is

$$n(x) = n_0 \exp(-\lambda x) \tag{14.1}$$

The X-axis is directed from the cathode ($x = 0$) to the anode. The application of a voltage pulse $U(t)$ to the discharge gap creates an electron-depletion region near the cathode [4]. We can easily show that if

$$n_0 \gg U_0 \varepsilon_0 / d\lambda e \tag{14.2}$$

the size of this region x_0 is governed by the condition that the electric field $E(x)$ should vanish at its boundary [6].

It is particularly important to stress that the value of X_0 in the case of polarization of a dense photoplasma considered here is independent of tire rate of rise of the voltage across the discharge gap [6]. The ionization processes begin in the high-field regions near the cathode (of length $\sim x_0$) and near the anode ($\sim d/2$). The number of photoelectrons created by ultraviolet radiation and the degree of their ionization-induced multiplication near the cathode are small because of the smallness of x_0 The flux of electrons reaching the low-field region in the vicinity of the point x_0 is low and it does not alter significantly n and E in this region. The cathode is screened from the discharge gap by this low-field region. The distribution $E(x)$ in the range $x > x_0$ is qualitatively similar to that obtained as a result of dynamic profiling with a space charge of the electrons themselves, so that—as in [2]—the formation of an SSVD is completed after the passage of an ionization wave directed toward the cathode [11]. It also follows from this analysis that the formation of an SSVD in the case of illumination from both sides does not differ from that described in [3].

This qualitative model is valid for practically any leading edges τ_{ed}, that are used in practice. In fact, in the case of the parameters $U_0/d = 10$ kV/cm and $n_e = 2 \times 10^{10}$ cm^{-3} typical of our experiments with a short leading edge, the displacement of the initial distribution $n(x)$ by a distance of $x_0 \sim 0.25$ cm could be ensured by making $\tau_{ed} = 50$ ns, whereas in the case of a long leading edge, a complete depletion of electrons of this narrow region was impossible because of the long operation of the ultraviolet radiation source. On the other hand, the slow rise of the voltage across the discharge gap resulted in a lower average field intensity during the formation of a VSD in the LLE case than in the SLE case, so that the conditions for the overlap of electron avalanches in the LLE case were satisfied at a lower electron density at the anode [4].

The advantage of the LLE case is also the additional increase in the electron density in the discharge gap at considerable distances from the cathode when the initial distribution $n(x)$ is shifted toward the anode in a time τ_{ed}, which is important when d is increased [6]. Clearly, a considerable increase in d is also possible in the case of illumination with ultraviolet radiation from both sides.

We thus investigated the conditions for ignition and attainment of an SSVD in a system of electrodes with sharp edges in the case of strong ionization of the electrode regions. It was found that CO_2 lasers with large apertures and high energy characteristics could be constructed with initiation of an SSVD by radiation from flashlamps with quartz bulbs. Clearly, the adopted approach should make it possible to achieve an SSVD for pumping other gas lasers, and also for any other method of ionization of the gas ensuring an electron density of 10^{10} cm^{-3} near sharp-edged electrodes.

References

1. V.V. Apollonov, G.G. Baitsur et al., Pis'ma Zh. Tekh. Fiz. **11**, 1262 (1985) [Sov. Tech. Phys. Lett. **11**, 521 (1985)]
2. V.V. Apollonov et al., Kvantovaya Elektron. (Moscow) **14**, 135 (1987) [Sov. J. Quantum Electron. **17**, 76 (1987)]
3. V.V. Apollonov et al., Kvantovaya Elektron. (Moscow) **13**, 1960 (1986) [Sov. J. Quantum Electron. **16**, 1294 (1986)]
4. E.W. McDaniel, W.L. Nighan, (eds.), Gas Lasers. Academic Press, New York (1982) [Applied Atomic Collision Physics, vol. 3]
5. J.S. Levine, A. Javan, Appl. Phys. Lett. **22**, 55 (1973)
6. V.V. Apollonov, A.M. Prokhorov et al., Kvantovaya Elektron. (Moscow) **11**, 1327 (1984) [Sov. J. Quantum Electron. **14**, 898 (1984)]
7. V.V. Apollonov et al., Kvantovaya Elektron.(Moscow) **13**, 2538 (1986) [Sov. J. Quantum Electron. **16**, 1680(1986)]

Chapter 15
Small-Signal Gain of CO_2 Lasers Pumped by an SSVD

Abstract A study was carried out into small-signal gain α of CO_2 lasers excited by a volume self-sustained discharge at pump energy densities up to 700 J l^{-1} atm^{-1}. Initiation of the discharge by a beam of accelerated electrons and previous filling of the discharge gap with electrons in the case of a long leading edge of the voltage pulses ensured more homogeneous pumping of the active medium compared with preionization by ultraviolet radiation in the case of voltage pulses with a short leading edge. It was established that the maximum value of a for an SSVD exceeded 5 m and was actually α = 8.2 m.

The small-signal gain α is one of the most important characteristics of the active media of CO_2 lasers. It was shown in [1] that the maximum value of α for electron-beam-controlled lasers can reach 12 m^{-1}; whereas for systems pumped by an SSVD, it does not exceed 5 m^{-1}. The difference between these two maximum values of α is explained in [1] by the inefficiency of the excitation of laser levels at high values of E/p (E is the electric field intensity and p is the pressure) needed to ignite and maintain an SSVD. However, an analysis of the experimental conditions in [1] demonstrated that the high initial values of E/p were mainly due to the need to deposit a large amount of energy in the active medium in the limited time of stable SSVD.

When properly selected easily ionizable substances are added to the working mixtures used in CO_2 lasers, the value of E/p can be reduced considerably and at the same time the duration of stable operation of an SSVD as well as a can be increased [2–7]. Naturally, it would be of interest to find the maximum value of α for mixtures containing easily ionizable substances when such mixtures are excited by an SSVD. This was the task set in the present investigation.

Our experiments were carried out using pumped pulses of $\tau > 1$ μs duration, typical of large-volume amplifiers [7–9]. The highest possible specific input energies ($Q \sim$ 800 J l atm^{-1} was reported in [1]) could be achieved for pulses of this duration τ, even in the case of mixtures containing easily ionizable substances, but at the expense of the homogeneity of the medium during all stages of the discharge. The homogeneity is largely determined by the method of formation of an SSVD. In

© Springer International Publishing Switzerland 2016

V.V. Apollonov, *High-Energy Molecular Lasers*,
Springer Series in Optical Sciences 201, DOI 10.1007/978-3-319-33359-5_15

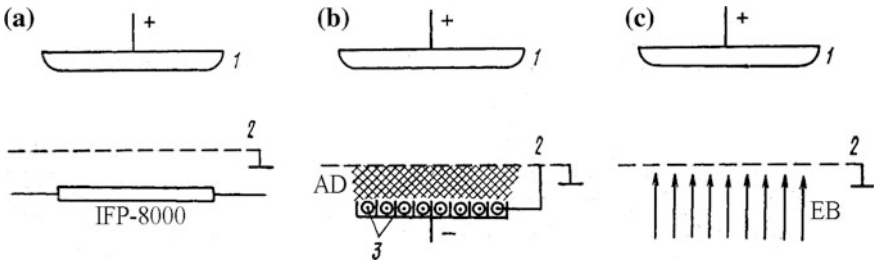

Fig. 15.1 Systems used in the excitation of an SSVD: **a** preionization of the active medium by ultraviolet radiation; **b** preliminary filling of the discharge gap with electrons; **c** preionization by an electron beam (*EB*); anode (*1*); cathode (*2*); auxiliary discharge (*AD*; *3*) electrodes

systems with ultraviolet, radioisotope, and X-ray preionization, one of the main reasons for the deterioration of homogeneity of the medium and for limitations on the duration of the volume phase of the discharge is the formation of incomplete channels at the cathode because of the flow of electrons out of the cathode zone before branch multiplication resulting from the drift during the leading edge of a voltage pulse [9–11]. We shall consider the methods of formation of an SSVD that can overcome the difficulty.

In the case of CO_2 lasers with ultraviolet preionization on the cathode side, the homogeneity of the cathode zone could be improved considerably by introducing easily ionizable substances into the active mixture. This is related to an increase in the concentration of a photoplasma near the cathode and activation of mechanisms of distortion of the electric field in the discharge gap (due to polarization of the photoplasma) preventing the escape of electrons from the cathode zone [12]. In our experiments, the ultraviolet radiation source was in the form of IFP-8000 flash-lamps and a VSD was ignited in a volume of 1–20 l in a conventional manner using voltage pulses with a short leading edge. The configuration used is shown in Fig. 15.1a.

In the method of formation of an SSVD by preliminary filling of a discharge gap with electrons (in contrast to preionization) in the case of a deliberately lengthened leading edge of the voltage pulse, there is no depletion (at least in principle) of electrons in the cathode zone [13, 14]. In this case, a reduction in the electric field at the cathode by the space charge and low overvoltages across the gap as a whole also reduce the probability of formation of inhomogeneities owing to the cathode structure [14]. An amplifier with an SSVD formed in this way (with a volume of 2–12 l) is shown in Fig. 15.1b. The source of electrons used to fill the main gap was an auxiliary low-current volume discharge ignited under a grid cathode as a result of initiation with a barrier discharge [6, 14].

The problem of inhomogeneities in the cathode zone can also be avoided by ensuring a high initial electron density (10^{12} cm^{-3}) created by initiation of an SSVD with a low-current beam of accelerated electrons [7, 15]. In this case, there is practically no overvoltage across the gap and the energy is deposited in the

discharge plasma, while the value of *E/p* remains quasisteady (because it is governed by the gas composition) and the duration of stable operation of an SSVD, which is ~10 μs in this method [7]. In our experiments, the density of the electron beam current in the gas chamber was 15 mA/cm^2 and the active volume was 16 l. The configuration used in this case is depicted in Fig. 15.1c.

The majority of our experiments was carried out using helium-free mixtures at a pressure p = 0.5 atm. The easily ionizable substance was triethylamine 1 Torr. The medium was assumed to be sufficiently homogeneous when a stable SSVD was maintained for an average input energy of ~600 J l^{-1} atm^{-1}. The gain was measured for the $P(20)$ line in the 10.4 μm band.

In all the methods of formation of an SSVD, the optimal conditions that maximized α were obtained for mixtures of the CO_2:N_2 = 1:1 composition. The dependences of α on Q were determined for mixtures containing triethylamine (Fig. 15.2). For the sake of comparison, we included in this figure the corresponding dependence for a Lamberton-Pearson system of 1 l volume (curve 4). In the amplifiers shown in Fig. 15.1, we found that in the investigated range of input energies, the value of the gain α increased on increase in Q reaching saturation at Q ~ 500–600 J l^{-1} atm^{-1}. In the Lamberton-Pearson configuration, the value of α reached its maximum at Q ~ 400 J l^{-1} atm^{-1} and it decreased on further increase in Q. A comparison of curves 1–4 clearly demonstrated the advantages of initiation of an SSVD by an electron beam and by preliminary filling of the gap with electrons as a result of deliberate lengthening of the leading edge of the voltage pulses, compared with the widely used method of initiation with ultraviolet radiation when short leading edges of the voltage pulses are used.

The maximum value of α = 8.2 m^{-1} was obtained for the configuration with preionization by an electron beam of a mixture containing triethylamine. Under these conditions, we found that α = 7.5 m^{-1} for a mixture that did not include triethylamine. When the composition was CO_2:N_2:He = 1:2:3 and the deposited

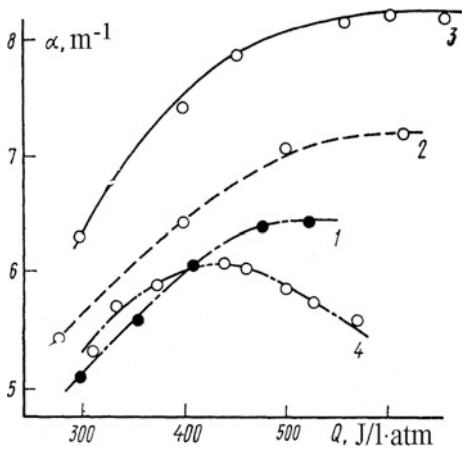

Fig. 15.2 Dependences $\alpha(Q)$ obtained for a mixture of the CO_2:N_2 = 1:1 composition (p = 0.5 atm) with the addition of triethylamine (p = 1 Torr) using amplifiers shown in Fig. 15.1a–c (curves *1–3*, respectively) and for a Lamberton-Pearson system (*4*)

energy was Q = 350 J/l, the gain was α = 6 m^{-1}. An increase in the total duration of the pump pulses from 3–9 μs reduced α by no more than 20%.

These results demonstrated that even in the case of long pulses pumping pure mixtures or those containing an easily ionizable impurity, including the mixtures containing helium, the small-signal gain α considerably exceeded the value 5 m^{-1}, regarded as the maximum for CO_2 lasers excited by an SSVD. The discrepancy between the results of [1] and those reported above is clearly due to the fact that, under the conditions of [1], a spark channel did not form because of a short duration of the current, but inhomogeneities created at high overvoltages across the gap [12, 16] could significantly reduce α. Moreover, under the conditions of [1], up to 30 % of the total energy was deposited in the plasma at high values of *E/p,* which were not effective from the point of view of excitation of the laser levels. The methods used in the present study made it possible to improve the homogeneity of the discharge, reduce the overvoltage across the gap, and optimized the conditions for energy deposition in the discharge plasma.

We thus demonstrated that in the case of sufficiently homogeneous excitation of the medium, the maximum small-signal gain of CO_2 amplifiers pumped by an SSVD would exceed 5 m^{-1}, irrespective of the initiation method. The value of α = 8.2 m^{-1} was obtained and this was close to the maximum gain achieved in systems pumped a nonself-sustained discharge in smaller active volumes [1, 17, 18].

References

1. A.M. Orishich, A.G. Ponomarenko, R.I. Soloukhin, V.N. Tishchenko, Gas Lasers [in Russian], Nauka, Novosibirsk (1977), pp. 290, 304
2. V.V. Apollonov, A.I. Barchukov et al., Pis'ma Zh. Tekh. Fiz. **3**, 1073 (1977) [Sov. Tech. Phys. Lett. **3**, 441 (1977)]
3. V.V. Apollonov, N. Akhunov, et al., Symposium 0ptica'80 (Lectures), Cologne, 1980, p. 94
4. V.O. Petukhov, V.V. Churakov, Kvantovaya Elektron. (Moscow) II, **835** (1984) [Sov. J. Quantum Electron. **14**, 565 (1984)]
5. V.V. Apollonov, N. Akhunov et al., Kvantovaya Elektron. (Moscow) **10**, 1458 (1983) [Sov. J. Quantum Electron. **13**, 947(1983)]
6. V. V. Apollonov et al, Kvantovaya Elektron. (Moscow) **13**, 2538 (1986) [Sov. J. Quantum Electron. **16**, 1680(1986)]
7. V.V. Apollonov, I.G. Kononov et al., Pis'ma Zh. Tekh. Fiz. **12**, 401 (1986) [Sov. Tech. Phys. Lett. **12**, 163(1986)]
8. V.V. Apollonov, G.V. Bush et al., Kvantovaya Elektron. (Moscow) **11**, 2149 (1984) [Sov. J. Quantum Electron. **14**, 1435 (1984)]
9. A.V. Kozyrev, Y.D. Korolev, G.A. Mesyats, Y.N. Novoselov, A.M. Prokhorov, V.S. Skakun, V.F. Tarasenko, S.A. Genkin, Kvantovaya Elektron. (Moscow) **11**, 524 (1984) [Sov. J. Quantum Electron. **14**, 356(1984)]
10. M.A. Kanatenko, Pis'ma Zh. Tekh. Fiz. **9**, 214 (1983) [Sov. Tech. Phys. Lett. **9**, 94 (1983)]
11. J.I. Levatter, S.C. Lin, J. Appl. Phys. **51**, 210 (1980)
12. V.V. Apollonov, et al., Kvantovaya Elektron. (Moscow) **11**, 1327 (1984) [Sov. J. Quantum Electron. **14**, 898 (1984)]

13. V.V. Apollonov et al, Pis'ma Zh. Tekh. Fiz. **11**, 1262 (1985) [Sov. Tech. Phys. Lett. **11**, 521 (1984)]
14. V.V. Apollonov, G.G. Baitsur et al., Kvantovaya Elektron. (Moscow) **14**, 135 (1987) [Sov. J. Quantum Electron. **17**, 76(1987)]
15. D.A. Goryachkin, V.M. Irtuganov, V.P. Kalinin, L.N. Malakhov, V.P. Yashchukov, Zh. Tekh. Fiz. **49**, 2656 (1979) [Sov. Phys. Tech. Phys. **24**, 1499(1979)]
16. D.A. Goiyachkin, V.M. Irtuganov, V.P. Kalinin, YuT Mazurenko, YuA Rubinov, Izv. Akad. Nauk SSSR Ser. Fiz. **46**, 1877 (1982)
17. N.G. Basov, E.M. Belenov, V.D. Danilychev, O.M. Kerimov, I.B. Kdvsh, A.S. Podsosonnyi, A.F. Suchkov, Zh. Eksp. Teor. Fiz. **64**, 108 (1973) [Sov. Phys. JETP **37**, 58 (1973)]
18. C.H.H. Carmichael, R.K. Gamsworthy, L.E.S. Mathias, Appl. Phys. Lett. **24**, 608 (1974)

Chapter 16
Feasibility of Increasing the Interelectrode Distance in an SSVD by Filling the Discharge Gap with Electrons

Abstract An investigation was made of the conditions of suitability of methods for preliminary filling of a discharge gap with electrons and dynamic profiling of the electric field in a discharge gap in the process of formation of an SSVD in the case of large interelectrode distances d in CO_2–N_2–He gas mixtures at atmospheric pressure. A SSVD was established in systems of electrodes without anyspecial surface profile and the characteristics of an active medium were calculated for a distance of d = 60 cm.

This chapter is devoted to an investigation of the conditions of suitability of methods for preliminary filling of a discharge gap with electrons and dynamic profiling of the electric field in a discharge gap in the process of formation of an SSVD in the case of large interelectrode distances d in CO_2–N_2–He gas mixtures at atmospheric pressure. An SSVD was established in systems of electrodes without any special surface profile and the characteristics of an active medium were calculated for a distance of d = 60 cm.

A new approach to the problem of formation of an SSVD in the case of large interelectrode distances d was developed in [1, 2]. It is based on the hypothesis that the necessary electron densities can be reached and the required electric field distribution can be established in a system of electrodes without any special surface profiles by filling the discharge gap with electrons supplied from the plasma of an auxiliary discharge. The conditions for the formation of an SSVD in the case when the cathode had sharp edges, formulated in [1, 2] and confirmed experimentally in [3], are

$$\frac{\mu}{d}\int_0^{t_b} U(t)\mathrm{d}t \geq d, \tag{16.1}$$

$$j_{\mathrm{ad}} \geq j_0 \quad \text{for} \quad 0 < t < t_{\mathrm{b}}, \tag{16.2}$$

where j_{ad} is the current density in the auxiliary discharge; t_{b} is the time in which the voltage across the discharge gap $U(t)$ rises from zero to the breakdown value; μ is

© Springer International Publishing Switzerland 2016

V.V. Apollonov, *High-Energy Molecular Lasers*,
Springer Series in Optical Sciences 201, DOI 10.1007/978-3-319-33359-5_16

the electron mobility; $\mu_0 = f(d, \mathrm{d}U/\mathrm{d}t)$ is the electron current density in the discharge gap needed for screening the sharp edges of the cathode.

We shall investigate the validity of these conditions on further increase in d in amplifying modules of laser systems designed for investigating the interaction of radiation with matter at ultra high radiation intensities [4].

Our experiments were carried out for d = 60 cm using CO_2–N_2–He gas mixtures at atmospheric pressure, containing an easily ionizable substance in the form of triethylamine (1–2 Torr). Power was supplied to the discharge by charging a 0.2 μF shaping capacitor from an eight-stage Arkad'ev-Marx generator producing pulses of amplitude up to 400 kV and characterized by a 0.25 μF capacitance per shot; the power was supplied in t_f = 3–20 μs [3]. The shaping capacitor was a generator with an abrupt or continuous rise of the voltage from zero to 80–100 kV. The anode was a rectangular plate of 100 × 160 cm dimensions made of A1 and rounded along the perimeter to a radius of 3 cm. The experiments were carried out for two variants of the cathode.

In the first variant, the cathode was a rectangular grid of 35 × 100 cm dimensions with sharp edges and the source of electrons was a multichannel discharge on the surface of a ceramic of high permittivity, limited by its internal capacitance and described in [3]. An SSVD was attained in mixtures with molecular gas concentrations of up to 15%. Oscillograms of the discharge voltage U and of the voltage across the surface-discharge electron source U_{sd} are shown in Fig. 16.1. These oscillograms did not differ from those reported in [3] for the case when d = 40 cm.

The surface discharge was an effective source of ultraviolet radiation, so that in the course of filling of the discharge gap the front of electrons arriving from the surface discharge plasma was preceded by electrons formed as a result of photoionization of the gas. This made it possible to increase the effective length of the electron-filled part of space by 15–20 cm and to ensure the density of electrons at the anode necessary for the formation of an SSVD, in spite of the fact that the condition (16.1) could not be satisfied formally because of the limited duration of the auxiliary discharge.

However, the absorption of ultraviolet radiation in the gas mixture made it necessary to limit the CO_2 content to a maximum of 4% for d = 60 cm. The condition (16.2) was then satisfied by a large margin, since the cathode edges were screened by electrons extracted by the electric field from the plasma in the spark channels on the ceramic surface, which projected beyond the edge of the grid.

In the second variant, the cathode was a rectangular plate of 30 × 70 cm dimensions made of Al; the electron source was a barrier discharge struck between the surface of this plate and a conductor insulated with polyethylene [5]. In contrast

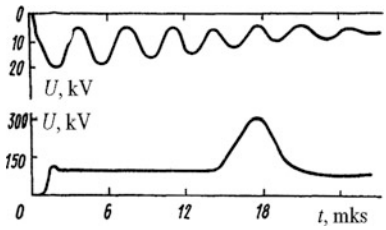

Fig. 16.1 Oscillograms of the voltage U across an SSVD and of the voltage across a surface-discharge electron source U_{sd}

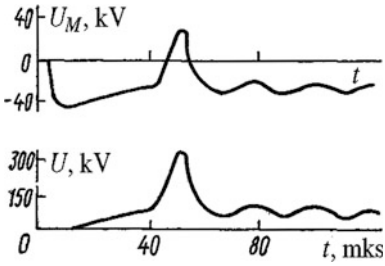

Fig. 16.2 Oscillograms of the voltage of an SSVD U and of the voltage across a barrier-discharge electron source U_M

to [5], in the present study, a conductor that was 4 mm in diameter was pressed tightly against the smooth surface of the cathode. An SSVD was obtained in gas mixtures with the content of the molecular components up to 20%. Oscillograms of the discharge voltage U and of the voltage across the barrier-discharge electron source U_{bd} are shown in Fig. 16.2.

Since the photoionization of gas by the radiation from a barrier discharge was ineffective; [5] in contrast to the surface discharge considered earlier, we observed formation of an SSVD in its pure form under conditions when the discharge gap was filled with electrons and this required that the condition (16.1) be rigorously satisfied. There was also an additional requirement in respect to the sign of the derivative of the voltage across the barrier-discharge electron source ($dU_{bd}/dt > 0$), necessary to ensure that electrons arrived from the barrier-discharge plasma in the discharge gap [5]. Even a brief (~ 1 μs) failure to satisfy this condition strongly increased the field at the edge of the cathode, and this created a streamer corona and resulted r subsequently in spark breakdown. "The screening of the cathode on increase in the voltage across the electrodes should be ensured by a corresponding increase in the space charge of electrons arriving in the gap from the barrier discharge plasma." However, the "productivity" of the barrier-discharge electron source was limited, so that it was necessary to limit dU/dt in order to satisfy the condition (16.2) and this was the reason for the selection of the voltage across the discharge gap shown in Fig. 16.2. The minimum time τ_f governed by these factors in the case of $d = 60$ cm was 12 μs. The energy was practically completely delivered to the plasma of the SSVD in a mixture of gases of the CO_2:N_2:He = 1:1:8 composition already when the voltage across the pump generator was ~ 340 kV. It should be pointed out that when the barrier-discharge electron source was used, the variation of the composition and pressure in the mixture was generally only limited by the voltage across the pump generator, in contrast to the case of the surface-discharge electron source. For example, for $d = 32$, 40, and 50 cm, we attained an SSVD in mixtures of the compositions CO_2:N_2:He = 1:1:2, 1:2:3 and 1:2:7, respectively, to which triethylamine was added and which were kept at atmospheric pressure.

The distributions of the small-signal gain across the aperture of the amplifier of the laser system were basically similar (irrespective of the nature of the electron source) to that described in [3] for the case when $d = 40$ cm. The absolute value of the gain on the optic axis was 3 m^{-1} for the interelectrode distance of $d = 60$ cm

and a specific input energy of ~ 130 J/l delivered to a mixture of the CO_2:N_2: He = 1:1:8 composition.

Our study therefore experimentally demonstrated the feasibility of scaling up the interelectrode distance in laser amplifiers when an SSVD was initiated by filling the discharge gap with electrons.

References

1. V.V. Apollonov, et al., Pis'ma Zh. Tekh. Fiz. **11** 1262 (1985) [Sov. Tech. Phys. Lett. **11**, 521 (1985)]
2. V.V. Apollonov, et al., Kvantovaya Elektron. (Moscow) **14**, 135 (1987) [Sov. J. Quantum Electron. **17**, 76 (1987)]
3. V.V. Apollonov, et al., Kvantovaya Elektron. (Moscow) **14**, 220 (1987) [Sov. J. Quantum Electron. **17**, 134 (1987)]
4. V.V. Apollonov, F.V. Bunkin, et al., Abstracts of Papers presented at Tenth International Intercamera Congress, Prague, 1981 [in Russian], p. 297
5. V.V. Apollonov, et al., Kvantovaya Elektron. (Moscow) **13**, 2358 (1986) [Sov. J. Quantum Electron. **16**, 1680 (1986)]

Chapter 17
Influence of Easily Ionizable Substances on the Stability of an SSVD in Working CO_2 Laser Mixtures

Abstract The main mechanisms of instabilities in an SSVD were identified by investigating the influence of easily ionizable substances and of other impurities on the duration of stable burning of such a discharge in N_2 and in CO_2–N_2 mixtures when the initial electron density depended weakly on the gas composition. The results obtained demonstrated the dominant role played by multistage ionization in the development of instabilities in SSVDs in working CO_2 laser mixtures and the need to use easily ionizable substances for the suppression of these instabilities.

The main mechanisms of instabilities in an SSVD were identified by investigating the influence of easily ionizable substances and of other impurities on the duration of stable burning of such a discharge in N_2 and in CO_2–N_2 mixtures when the initial electron density depended weakly on the gas composition. The results obtained demonstrated the dominant role played by multistage ionization in the development of instabilities in SSVDs in working CO_2 laser mixtures and the need to use easily ionizable substances for the suppression of these instabilities.

The feasibility of ignition and maintenance of a stable SSVD in dense gases depends both on the initial conditions during the formation of the discharge and on the nature of the kinetic processes that govern the rates of creation and loss of charged particles in a plasma. The majority of investigations into the stability of such discharges in gas mixtures employed in CO_2 lasers, including those containing easily ionizable additives, have been carried out using ultraviolet preionization, [1] but in this case the interpretation of the experimental results is complicated by a strong influence of the composition of the mixture on the initial-electron density n_e. For example, it is traditionally assumed that an increase in the stability of an SSVD discharge as a result of additionally ionizable substances to gas mixtures is a consequence of an increase in n_e because of the photoionization of the admixtures (see, for example, [2]). However, the results of [3, 4] obtained under conditions when the photoionization made no significant contribution to n_e as well as spectroscopic measurements reported in [5], demonstrated that the main effects of the introduction of easily ionizable substances are due to changes in the electron energy distribution function. Therefore, in studies investigating the stability of SSVDs in

© Springer International Publishing Switzerland 2016

V.V. Apollonov, *High-Energy Molecular Lasers*,
Springer Series in Optical Sciences 201, DOI 10.1007/978-3-319-33359-5_17

mixtures of variable composition, we have to separate the factors associated with the initial conditions and those related to the kinetics of the gas-discharge plasma.

We identified the main mechanisms of instabilities by investigating the influence of easily ionizable substances and of other impurities on the duration r of stable burning of SSVDs in N_2 and in CO_2–N_2 mixtures when n_e depended weakly on the gas composition. This was achieved by the formation of an SSVD involving preliminary filling of the discharge gap with electrons [6] (instead of preionization), which was known to ensure the requirements that n_e had to satisfy near the anode. When the gas composition was varied in the experiments described below, the electron density did not change by more than a factor of 1.5 (and this was due to a change in the discharge ignition voltage [6]), which made it possible to assume that the initial conditions were practically constant.

Our experiments were carried out in a chamber of 4 × 5 × 50 cm dimensions at a gas pressure of $p = 0.3$ atm using the apparatus shown schematically in Fig. 17.1a. The electron source used to fill the discharge gap was barrier discharge, because weak ultraviolet radiation generated in this discharge had little effect on n_e [4]. This discharge was ignited on the cathode K by using part of the voltage from the anode A applied across a capacitor C_1. The discharge gap was filled with electrons during the leading edge of a voltage pulse, which was deliberately lengthened by discharging a capacitor C_2 through a resistor R_1 to a capacitor C_3. The pump power was varied by altering a resistance R_2 and the charging voltage across C_2. The circuit parameters were selected so that the VSD always terminated with a spark breakdown of the discharge gap.

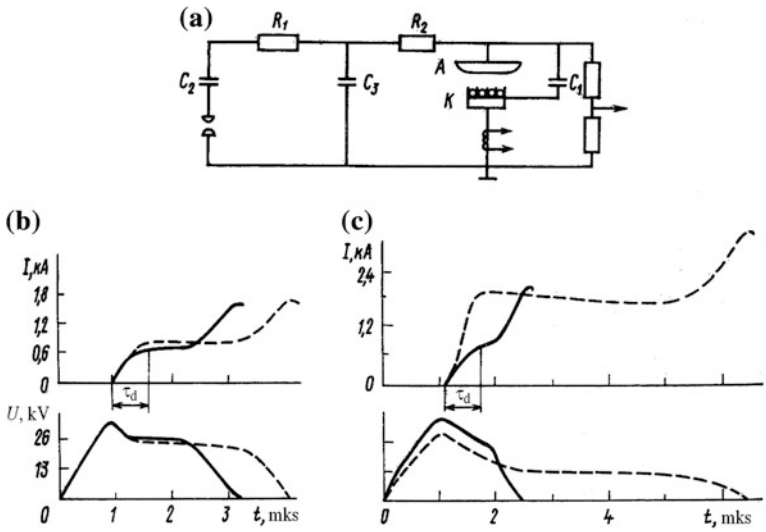

Fig. 17.1 Schematic diagram of the apparatus (**a**) and oscillograms of U and I obtained for discharges in CO_2 (**b**) and N_2 (**c**). The continuous curves represent SSVD in pure gases, whereas the dashed curves represent discharges in gases containing an easily ionizable substance (1.4 Torr of triethylamine)

Figure 17.1b, c show typical oscillograms of the voltage C_1 and of the current 7 for SSVDs in CO_2 and N_2, respectively. The time τ was taken to be the interval from the beginning of flow of the VSD current to the moment corresponding to the onset of an abrupt change in U from its quasisteady value because of growth of a spark channel and contraction of the VSD current inside this channel. τ_d is the time for U to decay from the quasisteady value to 0 as a result of growth of the spark channel in the resultant short-circuiting of the discharge gap (in the oscillograms we show also a time τ_c governed by the circuit parameters).

It is clear from Figs. 17.1b, c that in the case of pure CO_2 the inequality $\tau_d > \tau_c$ was obeyed and the decay time was practically unaffected by the addition of an easily ionizable substance (triethylamine), although τ then increased. In the case of N_2 we found that τ_d/τ_c, but the decay time increased considerably together with r on addition of an easily ionized durable substance reaching $\sim 3\tau_c$. These oscillograms demonstrated that the kmization processes goveming the rate of growth of the spark channel were different for N_2 and CO_2 and there was also a change in the nature of ionization in the mixture of N_2 with triethylamine.

Figure 17.2a shows the dependences of τ obtained for CO_2–N_2 gas mixtures without triethylamine on the relative content of CO_2 in the mixture $K = p_{CO_2}/(p_{N_2} + p_{CO_2})$. The following features were characteristic of the VSD in mixtures without the easily ionizable additive: when the specific pump power was $Q > 20$ MW l^{-1} atm^{-1} the stability of the discharge in CO_2 was higher than in N_2; for all the values of Q that were investigated (5–100 MW l^{-1} atm^{-1}), the time τ was considerably longer for the CO_2–N_2 mixtures than for either of the gases separately; there was an optimal value of τ, regarded as a function of K, which shifted toward higher K on increase in Q.

The nature of the dependence $\tau(K)$ was influenced greatly by the addition of triethylamine to the mixture (Fig. 17.2b): the stability of the VSD increased monotonically on reduction in K. The rise of τ because of the introduction of

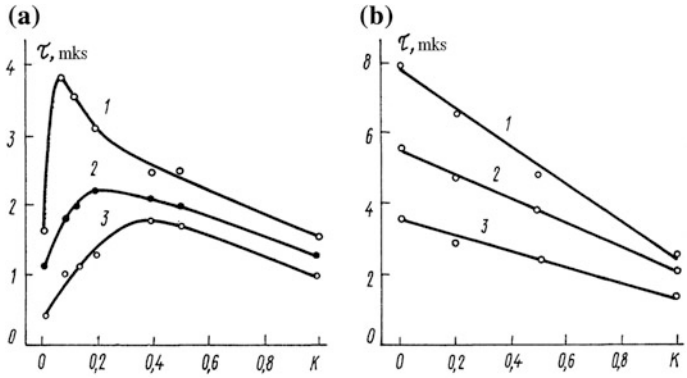

Fig. 17.2 Dependences $\tau(K)$ obtained for CO_2–N_2 mixtures (**a**) and for CO_2–N_2 mixtures including an easily ionizable substance (1.4 Torr of triethylamine). Q(MW l^{-1} atm^{-1}): 20 (*1*); 50 (*2*);100 (*3*)

triethylamine was observed for all values of K, including the case of pure CO_2, which in no way could be related to an increase in n_e.

We shall now try to identify the most probable processes responsible for the development of instabilities of the SSVD in N_2, which are slowed down by the addition of easily ionizable substances. The results plotted in Fig. 17.2a clearly cannot be explained by the overheating-ionization mechanism, because the growth time for this type of instability should decrease or a mixture of N_2 with CO_2 due to an increase in the IT relaxation rate, [7] which did not occur in practice.
Oscillograms in Fig. 17.1b, c provide indirect evidence of a different mechanism, mainly of an instability associated with multistage ionization of N_2 via two electron states $A^3\Sigma_u^+$ and $B^3\Pi_g$ [8] excited effectively in the SSVD plasma because of the high values of E/N. According to [8], when this ratio $E/N = 10^{-15}$ V cm^2, typical of the quasisteady stage of the SSVD in N_2 (Fig. 17.1), the contribution of this process to the ionization flux should become significant for $n_e \sim 5 \times 10^{11} - 10^{12}$ cm^{-3}, but because of inhomogeneities of the SSVD in the cathode zone, which grow from cathode spots, it should be observed at lower volume-average electron densities. In fact, it is shown in [9] that multistage ionization increases the rate of growth of the spark channel. This is clearly manifested by the difference in τ_d for N_2 and CO_2 in Fig. 17.1, whereas the increase in τ and τ_c on the addition of triethylamine to N_2 is a consequence of a reduction in the multistage ionization contribution to the ionization flux because of lowering of the electron energy (as a result of inelastic losses due to collisions with impurity molecules and reduction in E/N due to the Penning ionization of triethylamine [10]) and corresponding reduction in the rate of population of higher electron states.

We shall therefore assume that the instability associated with the multistage ionization process is the main factor which limits the duration of the volume phase of the SSVD in N_2. It is natural to also assume that an increase in τ observed for CO_2–N_2 mixtures, compared with pure N_2, is due to collisional quenching of the electron states of N_2 by the CO_2 molecules and partial compensation of the multistage ionization process by electron attachment. Then, the shift of the optimum of τ, considered as a function of τ in the direction of higher values of K on increase in Q can be explained by the need to increase the rate of depopulation, because of an increase in the multistage ionization contribution that is not proportional to 2, to the overall balance of charged particles in the SSVD plasma [2]. However, the efficiency of this mechanism of suppression of the instability is limited by an increase in the electron energy in N_2–CO_2 mixtures, compared with pure N_2 [11], and is clearly affected by a change in the nature of the development of the instability at high values of N_2 because of the accumulation of negative ions in the SSVD plasma [12]. An increase in the VSD stability in CO_2 and in mixtures with a high proportion of carbon dioxide on addition of an easily ionizable substance can also be attributed to a reduction in the electron energy and a corresponding reduction in the rate of dissociative attachment [11].

The collisional mechanism of suppression of the SSVD instability in N_2 on addition of CO_2 is supported by the analogous nature of the influence of the

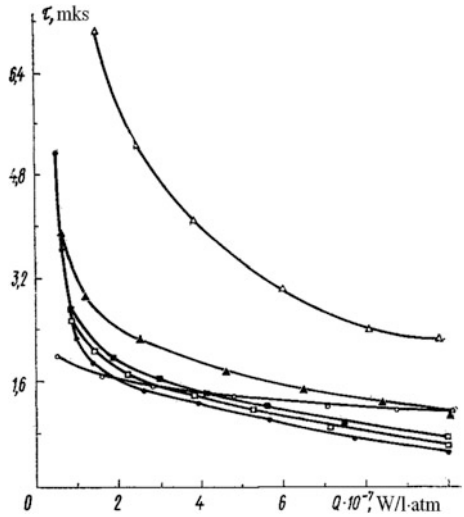

Fig. 17.3 Dependences $\tau(Q)$ for CO_2(O), N_2 (O) with 5 Torr O_2 (n), and 15 Torr (A) of CO_2, and NH_3 with 1.4 Torr

addition of other gases on τ. Figure 17.3 shows the results of measurements of τ for N_2 containing small amounts of O_2 and NH_3. This figure includes, for the sake of comparison, the dependences $\tau(Q)$ obtained for N_2, CO_2, and a mixture of the CO_2: N_2 = 1:14 composition. It is clear from Fig. 17.3 that all the additives (including O_2) made it possible to considerably increase the value of τ and the change produced in this way increased on increase in the rate of depopulation of the metastable molecular state $A^3\Sigma_u^+$ of the additive (the depopulation rates were estimated on the basis of [13]).

When the partial pressure of NH_3 (characterized by the highest rate of quenching of the $A^3\Sigma_u^+$ + state of N_2) was 3.5 Torr and the specific power was Q= 100 MW l^{-1} atm^{-1} the time τ reached the same value as for a mixture of N_2 with triethylamine (Fig. 17.2a). However, in contrast to triethylamine, the addition of NH_3 did not change the electron energy distribution function, which was manifested by a constancy of the parameter E/N and by a weak influence of N on the stability of the SSVD in mixtures with high CO_2 concentrations. We could therefore assume that suppression of the instability of the SSVD in N_2 by the addition of NH_3 was due to collisional quenching of the excited electron states. On the other hand, electron attachment had a negative influence on the stability. This was demonstrated, for example, by a comparison of τ for N_2–O_2 and N_2–CO_2 mixtures with the same (small) concentration of electronegative components (Fig. 17.3). At low rates of collisional quenching of the stated $A^3\Sigma_u^+$ of N_2 by the CO_2 and O_2 molecules, the value of τ was greater for the N_2–CO_2 mixture where the attachment process was less important.

Therefore, the results of the present investigation obtained under conditions of a weak influence of the gas composition on the initial electron density provided an indirect confirmation of the fundamental role played by multistage ionization in

limiting the duration of stable burning of a VSD in N_2. They also directly demonstrated the need to use easily ionizable substances in order to increase the duration of stable burning τ in working mixtures used in CO_2 lasers, irrespective of the method used to initiate the SSVD.

References

1. L.E. Kline, L. Denes, M.J. Pechersky, Appl. Pliys. Lett. **29**, 574 (1976)
2. W. McDaniel, W.L. Nighan (eds.), *Gas Lasers* (Academic Press, New York, 1982)
3. V.V. Apollonov, I.G. Kononov et al., Pis'maZh. Tekh. Fiz. **12**, 401 (1986), [Sov. Tech. Phys. Lett. **12**, 163 (1986)]
4. V.V. Apollonov et al., Kvantovaya Elektron. (Moscow) **13**, 2538 (1986), [Sov. J. Quantum Electron. **16**, 1680 (1986)]
5. A.A. Kuchinskiff, B.V. Lyublin, V.A. Shevere, Z. P. J. Spektrosk. **45**, 364 (1986)
6. V.V. Apollonov et al., Kvantovaya Elektron. (Moscow) **14**, 135 (1987) [Sov. J. Quantum Electron. 17, 76(1987)]
7. E.P. Velikhov, V.D. Pis'mennyi, T.A. Rakhimov, Usp. Fiz. Nauk **122**, 419 (1977), [Sov. Phys. Usp. **20**, 586 (1977)]
8. V.A. Pivovarand, T.D. Sidorova, Zh. Tekh. Fiz. **55**, 519(1985) [Soy. Phys. Tech. Phys. **30**, 308 (1985)
9. Q.M. Bulashenko, Abstracts of papers presented at seventh ail-union conference on low-temperature plasma physics, Tashkent 1987 [in Russian], p. 269
10. V.V. Apollonov, A. Barchukov et al., Pis'ma Zh. Tekh. Fiz. **3**, 1073 (1977), [Sov. Tech. Phys. Lett. 3, 441 (1977)]
11. A.N. Lobanov, A.F. Suchkov, Kvantovaya Elektron. (Moscow) **1**, 1527 (1974) [Sov.1. Quantum Electron. **4**, 843 (1975)]
12. W.J. Wiegand, W.L. Nighan, Appl. Phys. Lett. **26**, 554 (1975)
13. J.W. Dreyer, D. Pemer, C.R. Roy, J. Chem. Phys. **61**, 3164 (1974)

Chapter 18
Dynamics of Population of the $A^3\Sigma_u^+$ Nitrogen Metastable State in an SSVD of a Pulsed CO_2 Laser

Abstract Intracavity laser spectroscopy was used to study the dynamics of population of the v = 2–8 vibrational levels of the $A^3\Sigma_u^+$ state in order to establish the possible influence of multistage ionization on the evolution of instability in an SSVD in CO_2 laser active mixtures. The populations of the nitrogen vibrational levels N_v were calculated taking into account the real output pulse profile of a dye laser. It was found that multistage ionization can only influence the duration of stable operation of an SSVD by increasing the rate of growth of the spark channel in the discharge gap. This is why the addition of readily ionized substances to the gas that reduce the electron energy and therefore lower N_v can substantially improve the stability of the volume discharge and increase the active volume and output energy of a CO_2 laser.

The scope for scaling up the active volume and radiation energy of electric-discharge CO_2 lasers is, in many respects, limited by the instability of the volume discharge (both SSVD and non-SSVD) used to excite the active medium [1]. Consequently, studies of the main types of instability and the search for methods of suppressing these are topical problems. It was assumed in [1] that one of the main factors limiting the duration of stable operation of a non-SSVD in active mixtures of a CO_2 laser is the evolution of instability due to multistage ionization of N_2 via metastable electronic states. According to calculations, [2] multistage ionization should also make an appreciable contribution to the ionization flux when N_2 is excited by an SSVD, indicating that this type of instability may develop in N_2 and in active mixtures of a CO_2 laser with a high nitrogen content.

No $A^3\Sigma_u^+$ excited states of N_2 were observed in a non-self-sustained microwave discharge, although the sensitivity threshold of the intracavity laser spectroscopic technique used (10^{14} cm^{-3}) was substantially lower than that predicted from calculations of the population [3].

Some $A^3\Sigma_u^+$ excited states of N_2 were recorded in an SSVD plasma in [4] using diode laser spectroscopy [5], but owing to the narrow spectral tuning range of the diode laser in these experiments, the absorption was detected only due to a single

© Springer International Publishing Switzerland 2016

V.V. Apollonov, *High-Energy Molecular Lasers*,
Springer Series in Optical Sciences 201, DOI 10.1007/978-3-319-33359-5_18

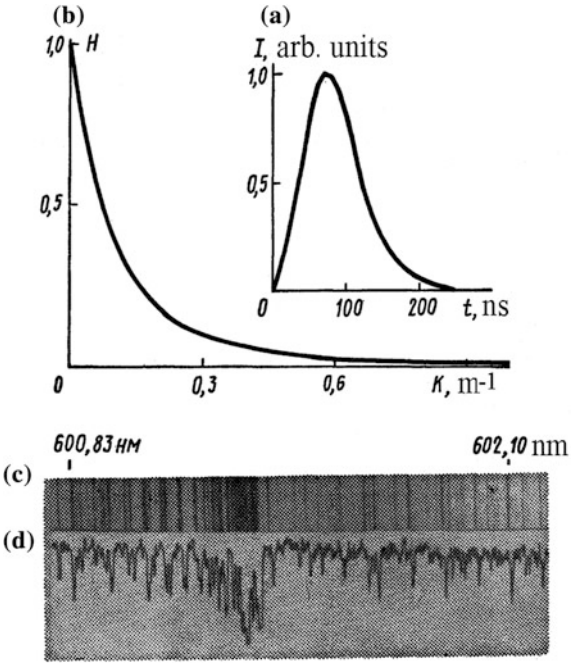

Fig. 18.1 Laser output pulse profile $I(t)$ (**a**), calculated curve to determine the absorption coefficient K from the exposure H (**b**), part of the absorption spectrum of the $v' = 7$, $v'' = 3$ band of the I^+ system of N_2 (**c**), and spectrogram of this part of the spectrum (**d**)

electronic-vibrational transition, $A^3\Sigma_u^+ - B^3\Pi_g$, so that it is not possible to estimate the total population of the electronic level.

We investigated the dynamics of population of the v = 2–8 vibrational levels of the $A^3\Sigma_u^+$ state of N_2 in an SSVD plasma in order to obtain quantitative data on the total population of this state and to establish any influence of multistage ionization on the evolution of SSVD instability in the active mixtures of CO_2 lasers.

A flashlamp-pumped pulsed laser utilizing a solution of rhodamine 6G in isopropanol with a half-height pulse duration $\tau r = 80$ ns (Fig. 18.1a) and a lasing wavelength tunable in the 575–610 nm range was used in the present study. A discharge chamber with a $4 \times 5 \times 50$ cm active volume filled with nitrogen at a pressure p = 0.3 atm was inserted in a laser resonator of length L_r = 130 cm. The discharge module was similar to that described in [6]. A spectrograph based on an UF-90 autocollimating tube with a diffraction grating had a resolution of 0.1 cm^{-1}. The absorption spectra I^+ of the N_2 system ($A^3\Sigma_u^+ - B^3\Pi_g$ transition) were recorded on photographic film at various times relative to the beginning of the SSVD current in order to obtain the time dependence of the vibrational level population (Fig. 18.1c).

The vibrational level populations N_t, were determined from the integrated absorption coefficient of the electronic-vibrational-rotational line $\int K(\omega)\mathrm{d}\omega$ using a standard method [7], since under these experimental conditions an equilibrium distribution function in terms of rotational levels with a temperature equal to that of

the neutral gas is established within a time comparable to the translational relaxation time [8]. The population of the $B^3\Pi_g$ electronic state was assumed to be zero.

The optical density D_1, within the absorption line and outside this line D_2 was determined in order to find the absorption coefficient $K(\omega)$ from the spectrogram (Fig. 18.1d). These data were fed into a computer where the exposures H_1 and H_2 corresponding to these optical densities were calculated taking into account the optical density curve of the photographic film in the yellow part of the spectrum. Since the light traveled the path $L_{\text{eff}} = K(\omega)cTL_c/L_r$ between the resonator mirrors during the lasing pulse time T (where c is the velocity of light, L_c = 50 cm is the length of the discharge zone), the exposure at the frequency ω was

$$H(\omega) = \int_0^T I(t)\exp[-K(\omega)ctL_c/L_r]\mathrm{d}t,$$

where $I(t)$ is the profile of the lasing pulse. Outside the absorption line it found that $K(\omega) = 0$ so that the solution of the equation

$$\int_0^T I(t)\exp[-K(\omega)ctL_c/L_r]\mathrm{d}t \Big/ \int_0^T I(t)\mathrm{d}t = \frac{H_1}{H_2} \tag{18.1}$$

was used to find the absorption coefficient $K(\omega)$ corresponding to the measured ratio H_1/H_2. The solutions of (18.1) for a specific lasing pulse profile $I(t)$ were tabulated by computer. Subsequently, $K(\omega)$ was determined purely by a graphical method (Fig. 18.1b). The neutral gas temperature T_g used in the following calculations of the vibrational level populations was determined from the values of $K(\omega)$ for the lines of the highest intensity Q_1 branch for the J = 1–25 rotational levels of the $v' - v''$ = 7–3 and 8–4 bands. The value T_g = 300 ± 20 K remained constant within the time interval 0–3 μs relative to the beginning of the SSVD current owing to the slow vibrational translational relaxation in N_2 [9].

Figure 18.2 shows an oscillogram of the SSVD current and also the time dependences of the electron density n_e and $N_{v''=3}$. It can be seen that the maximum of $N_{v''=3}$ is reached by the end of the SSVD current, its total duration being ~0.8 μs. A typical decay time of the metastable state $N_{v''=3}$ is ~0.5 μs. The time dependences of $N_{v''}$ for other vibrational levels of the $A^3\Sigma_u^+$ state are similar. Figure 18.3 shows the distribution of the population of the $A^3\Sigma_u^+$ state in terms of vibrational levels for two times. A similar distribution of N_v—was obtained in [10] for a cw discharge in low pressure nitrogen. The maximum total population for seven vibrational levels is

$$\sum_{v''=2}^{v''=8} N_{v''} = 6.4 \times 10^{14}\ \text{cm}^{-3},$$

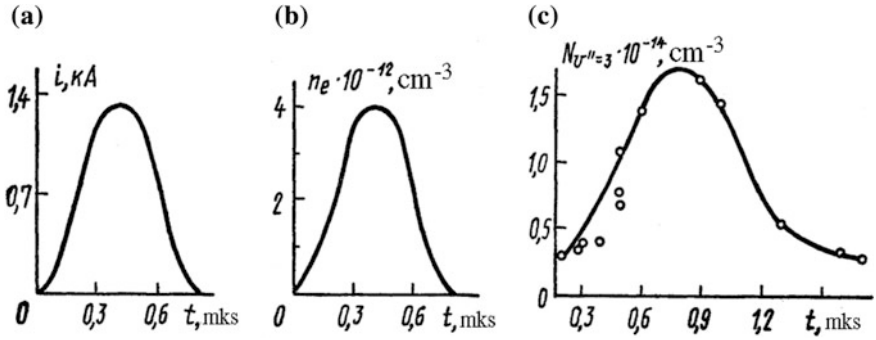

Fig. 18.2 Oscillogram of an SSVD current pulse i (**a**) and also time dependences of the electron density n_e (**b**) and the density of mctastable states $N_{v''=3}$ in an SSVD plasma (**c**)

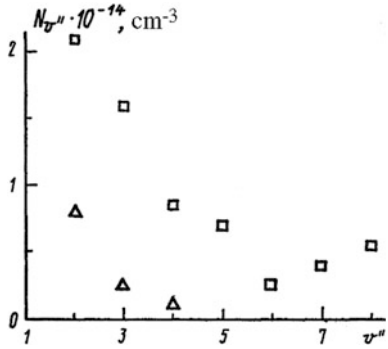

Fig. 18.3 Distribution of the population of the $A^3\Sigma_u^+$ state of N_2 in terms of vibrational levels at t = 0.7 (□) and 1.6 μs (Δ) relative to the beginning of the SSVD current pulse

which is substantially higher than the maximum electron density $n_e = 4 \times 10^{12}$ cm^{-3}.

Simple estimates show that, in the case under study, the contribution made by multistage ionization to the ionization flux (in the SSVD column) is negligible compared with the contribution of direct ionization of N_2. Thus, this process can only influence the SSVD stability by increasing the rate of growth of the channel [12], where the electron density at the head is substantially higher than that in the SSVD column [11]. The results of [13] indicate this mechanism for contraction of an SSVD in N_2 and in active mixtures of a CO_2 laser. Consequently, readily ionized substances that can reduce the electron energy and therefore lower the rate of population of the N_2 electronic states must be added to the active mixture to improve the stability of the SSVD and increase the output characteristics of CO_2 lasers [4].

References

1. E.P. Velikhov, V.D. Pis'menny, A.T. Rakhimov, Sov. Phys. Usp. 20, 586 (1977)
2. V.A. Pivovar, T.D. Sidorov, Sov. Phys. Tech. Phys. **30**, 308 (1985)
3. N.A. Bogatov, M.S. Gitlin, S.V. Golubev, S.V. Razin, Sov. Phys. Tech. Phys. **32**, 118 (1987)
4. V.V. Apollonov et al., Sov. Tech. Phys. Lett. **13**, 570 (1987)
5. Y.V. Kosichkin, A.I. NadezhdinskiT, Izv. Akad. Nauk SSSR Ser. Fiz. **47**, 2037 (1983)
6. V.V. Apollonov et al., Sov. J. Quantum Electron. **16**, 1680 (1986)
7. L.A. Kuznetsova et al., *Transition Probabilities in Diatomic Molecules [in Russian)* (Nauka, Moscow, 1980)
8. V.N. Ochkin, SYu. Savinov, N.N. Sobolev, Tr. Fiz. Inst. Akad. Nauk SSSR **157**, 6 (1985)
9. R.L. Taylor, S. Bitterman, Rev. Mod. Phys. **41**, 26 (1969)
10. G. Cernogora, C.M. Ferreira, L. Hochard, M. Touzeau, J. Loureiro, J. Phys. B **17**, 4429 (1984)
11. Y.I. Bychkov, YuD Korolev, G.A. Mesyats, *Injection Gas Electronics* (Nauka, Novosibirsk, 1982)
12. O.M. Bulashenko, V.V. Buchanov, E.I. Molodykh, *Abstracts of Papers presented at Seventh All-Union Conference on Physics of Low-Temperature Plasmas*, (Tashkent, 1987), p. 269
13. V.V. Apollonov et al., Sov. I. Quantum Electron. **18**, 351 (1988)

Chapter 19
High-Energy Molecular Lasers Pumped by an SSVD

Abstract The basic principles that underlie the initiation of an SSVD, which is to be ueed for pumping CO_2 and N_2O lasers, are disryssed. The experimental results for discharge stability, optical homogeneity, and scalability of the laser active medium are reported. Characteristics of CO_2 lasers with apertures of up to 70 cm and active volumes of up to 400 L, as well as of N_2O lasers with apertures of up to 20 cm and active volumes of up to 60 L, are presented.

19.1 Introduction

The widespread use of pulsed gas lasers in various fields of science and engineering accounts for their extensive investigation over many years. In electroionization devices with apertures as large as 30 cm, maximum radiation loads on the optical elements were already attained by the mid-1970s. Any further increases in laser output energies were presumably related to larger apertures. However, solving the problem of limitations on output by operating several lasers in parallel presents great technical difficulties [1]. An alternative method is to enlarge the aperture of a single molecular laser.

The electroionization approach to the problem proved impracticable because the voltages on the accelerator were too high and because the critical restriction imposed on the transverse dimensions of the discharge zone by the discharge-induced magnetic field affected the trajectory of accelerated electrons [1].

This restriction on the discharge-zone transverse dimensions is removed if a CO_2 laser is pumped by an SSVD. It is, however, far less stable than a non-SSVD. Furthermore, the actual scalability of the aperture is limited by the difficulty involved in reaching the required concentrations of primary electrons at long electrode separations as well as by the size and shape of electrodes. According to the notions that were generally adopted in the early 1980s, these difficulties could not be eliminated in gas lasers pumped by an SSVD. Primary electrons in the

© Springer International Publishing Switzerland 2016

V.V. Apollonov, *High-Energy Molecular Lasers*,
Springer Series in Optical Sciences 201, DOI 10.1007/978-3-319-33359-5_19

discharge gap were believed to be the result of gas ionization caused either by radiation or by fast particles, while uniform excitation of the laser active medium was thought to be possible only in a uniform electric field set up by electrodes of specific shapes.

When we began our studies in 1981, the maximum electrode separation that admitted an SSVD with UV preionization was 30 cm. The Canadian company Lumonix made a 20 cm aperture CO_2 laser whose characteristics were quite inferior to those of similar systems with apertures of several centimeters. In 1984, it was announced in the USSR that Korolyov and co-workers had succeeded in initiating a discharge by x-ray preionization at a 20 cm electrode separation, while Pavlovsky and his group [3] were able to initiate a discharge directly in a 280 L volume at a 35 cm electrode separation.

The development of preionization techniques alone could not solve the entire array of the problems related to enlargement of CO_2 laser apertures.

Therefore, it seemed relevant to search for an alternative approach to SSVDs in systems with apertures exceeding 30 cm. The feasibility of such an alternative approach was suggested by the existence of efficient CO_2 lasers without electrodes of a special shape, lasers whose operating principles could not be explained in terms of the theory available at that time. We refer to the French system that originated with Dumanchin, [4] who initiated the volume discharge by using an auxiliary barrier discharge, and to the plasma-electrode lasers proposed by Baranov et al. and Andrew et al. [5].

Our goal was to seek ways to create CO_2 and N_2O lasers with large (larger than 30 cm) apertures, pumped by an SSVD. To attain this goal, we had to accomplish the following:

1. Ensure discharge stability in the excitation of large active volumes of CO_2 and N_2O lasers;
2. Establish new principles of discharge initiation for wide electrode separations;
3. Obtain mechanisms of discharge initiation in systems with conventional electrodes and, in the limit, with similar flat sharp-edged electrodes;
4. Show the advantages of the new principles of discharge initiation and prove the scalability of CO_2 laser characteristics for larger apertures and active volumes.

19.2 Discharge Stability

Many authors noted that in UV preionization systems, the discharge becomes more stable if low-ionized additives (LIAs) are introduced into a mixture. This fact was attributed to the increased initial concentration of electrons caused by additive photoionization, i.e., to a particular mechanism of discharge initiation. We also

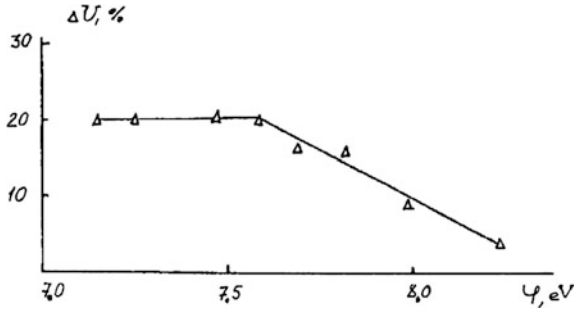

Fig. 19.1 Relative drop in breakdown voltage ΔU versus ionization potential φ of additives

relate the superior discharge stability in LIA-containing mixtures to the significant changes in the kinetics of discharge plasmas that take place in the presence of LIAs. To verify this presumption, and to verify the maintainability of stable discharges for long enough to excite large active volumes, we undertook multiple studies of the discharge contraction mechanisms in LIA-containing mixtures. The experiments were conducted with initial electron concentrations that were only slightly dependent on the gas mixture composition.

It was essential, first of all, to establish criteria for choosing LIAs to be introduced for discharge stabilization and to specify the limits of discharge stability [6]. For large-aperture lasers, the choice is obviously dictated by a maximum possible drop in the breakdown voltage through the Penning ionization of the additive. This condition is met by substances whose ionization potential is less than 7.6 eV, which is evident from the plot in Fig. 19.1. The figure shows the relative drop in the breakdown voltage as a function of the ionization potentials of substances that fall into a class of alkylamines. Qualitatively, the drop is a function of the Penning ionization cross section. We have verified by experiment that if this criterion is satisfied, the longest stable discharge is attained. So this criterion is helpful in choosing LIAs for discharge stabilization in CO_2 lasers.

To establish the limits of discharge stability in large-aperture systems, we examined the contraction of an SSVD for electrode separations in excess of 20 cm [7]. Since the growth rate of a spark channel is a nonlinear function of its length, discharge stability will not increase when the electrode separation exceeds 20 cm. This point is illustrated by Figs. 19.2 and 19.3, which show the stable discharge time versus electrode separation and the time dependence of the spark channel length, respectively. The maximum duration of the stable discharge proves to be 10 μs for a 20 cm electrode separation in CO_2 lasers with a mixture at typical atmospheric pressure that contains 50% molecular gases and LIAs with an input energy of 200 J/L. As can be seen from Fig. 19.2, this time is also maximal for apertures larger than 20 cm. Straightforward estimates have revealed that 10 μs is sufficient to pump a 1 m^3 single-discharge unit.

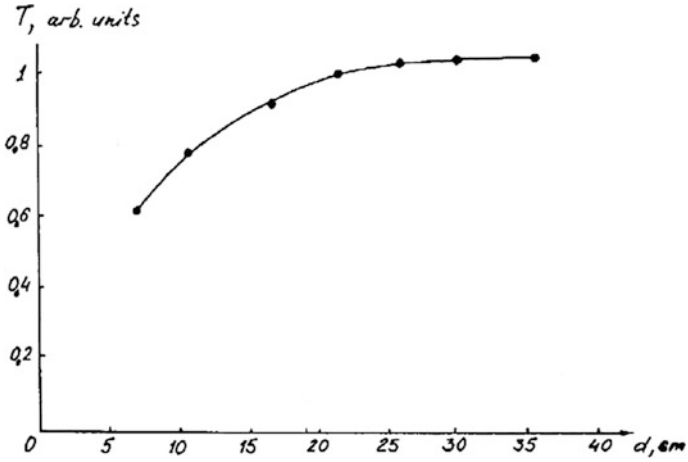

Fig. 19.2 Stable discharge time *T* (in arbitrary units) versus electrode separation *d* (centimeters)

We were the first, to our knowledge, to study an SSVD in mixtures of CO_2 and N_2 with Ar and H_2O as buffer gases in the presence of LIAs. Unlike the conventional CO_2:N_2:He systems, the above mixtures have their characteristics only slightly altered in the course of laser operation. Time was estimated by the vibration half-period of an electric circuit that was fabricated on a base of contemporary elements.

The established mechanisms that account for the SSVD instability in CO_2 laser active media and for the LIA contribution to their stability were confirmed by the findings for the spark channel dynamics and by the spectroscopically measured populations of N_2 electron states in a discharge plasma. [8, 9] The mechanism of discharge instability in N_2-containing gas mixtures that is due to stepwise ionization was first suggested in [10] for an electron-beam-controlled discharge. Later it was claimed to also be important in regard to SSVD. When instability of the discharge is controlled by stepwise ionization, a correlation is expected to exist between the stable discharge time and the electronic level population in N_2 that contains an LIA or other admixtures. This feature was observed in experiments [8, 9].

Figures 19.4a, b show oscillograms of the discharge voltage and current in pure CO_2 and N_2, respectively, as well as in their mixtures with the LIA triethylamine. The presence of the latter markedly increases the time of stable discharge, including that for the CO_2 case, which has nothing to do with the variations in the initial electron concentration under the specified experimental conditions. In pure N_2 the discharge contracts much faster than it does in pure CO_2. However, when triethylamine is introduced, the opposite is true. This response indicates that different ionization processes are responsible for the channel growth in N_2 and CO_2 and that there is a different nature for the ionization in a N_2-triethylamine mixture. Figure 19.5 shows plotted time dependencies of the channel length *H* in pure N_2 and in N_2 that contains triethylamine. The slowing down of the growth rate of a

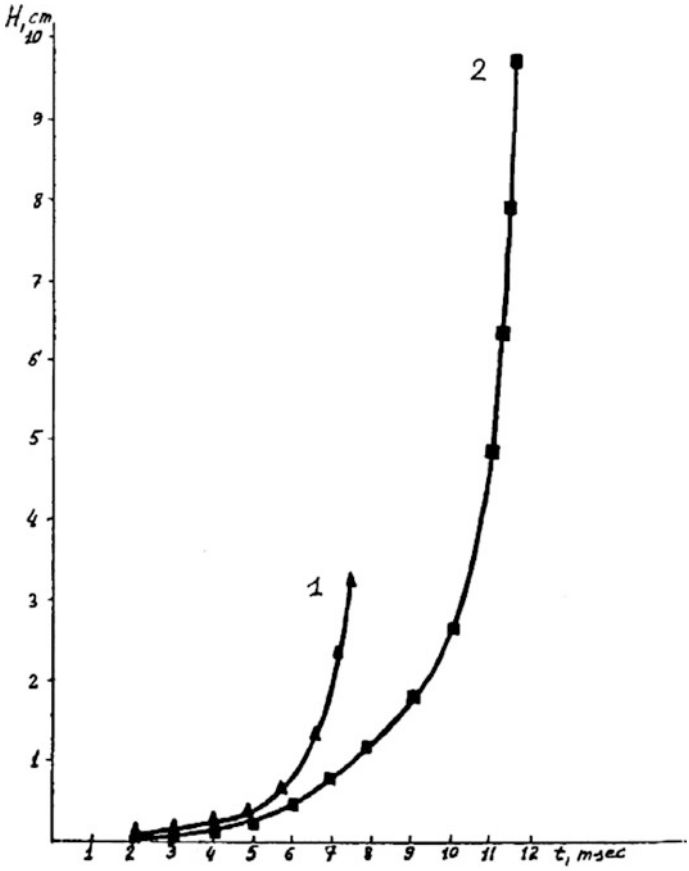

Fig. 19.3 Time dependence of spark channel length *H*: *1*, *d* = 6.4 cm; *2*, *d* = 30 cm

spark channel in LIA-containing mixtures supports our hypothesis that discharge stability is related to the LIA effect on the kinetics of gas discharge plasmas, rather than on the variations in its initial conditions.

Figure 19.6 depicts time dependencies of the population of a vibrational level of the $A^3\Sigma_u^+$ metastable state of N_2 in plasmas of N_2 and of its mixtures. As a matter of fact, the metastable state population correlates with the stable discharge time. The population of an N_2-triethylamine mixture proves to be lower than the discrimination threshold in intracavity spectroscopy. Thus, the results shown in this figure are in conflict with the claim that discharge contraction in N_2 and high N_2 mixtures is most likely to occur through instability arising from stepwise ionization [9].

The cause of reduced electronic level populations in LIA-containing gases is evident from Fig. 19.7, which shows part of the absorption spectra for pure N_2 and triethylamine-containing N_2 in the $A^3\Sigma_u^+ - B^3\Pi_g$, band for a 100 ns pulse of discharge current. The sharp decrease in absorption, corresponding to the level of

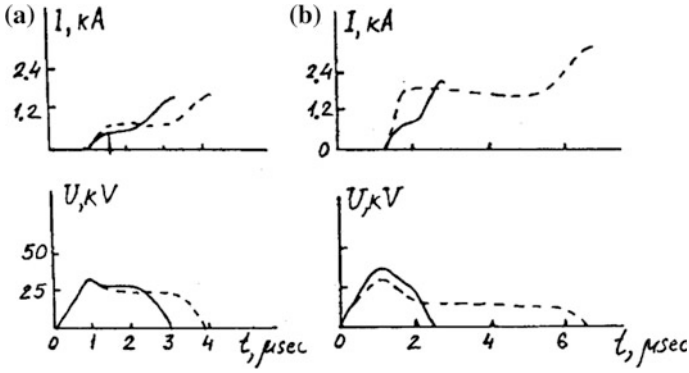

Fig. 19.4 Oscillograms of current I and discharge voltage V in (**a**) CO_2 and (**b**) N_2 (*solid curves*) and in their respective mixtures with the LIA triethylamine (*dashed curves*)

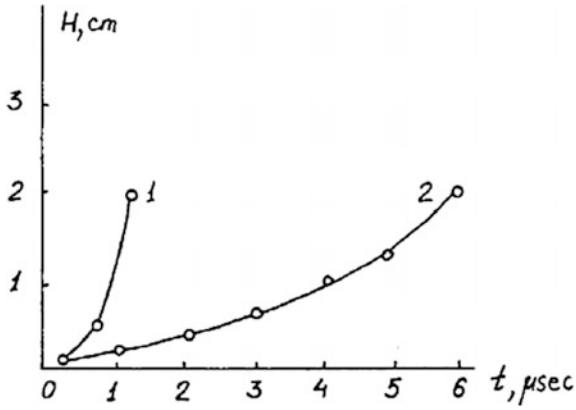

Fig. 19.5 Time dependencies of channel length H in pure N_2 (*curve 1*) and in triethylamine-containing N_2 (*curve 2*)

population reduced by a factor of 20 or more within 100 ns cannot be attributed to collisional deexcitation, even with the assumption of the highest values of its known rate constants. Therefore, the electron state populations in LIA-containing gases are essentially reduced through depletion of the electron energy as a result of the changed function of electron energy distribution. Accordingly, the observed discharges that are stable for longer periods of time in LIA-containing CO_2 are accounted for by the electron energy loss and hence by the slower rates of dissociative electron attachment to CO_2.

Thus, LIAs help to obtain stable discharges that are capable of exciting large volumes of CO_2:N_2:He gas mixtures, whatever discharge initiation technique may be used.

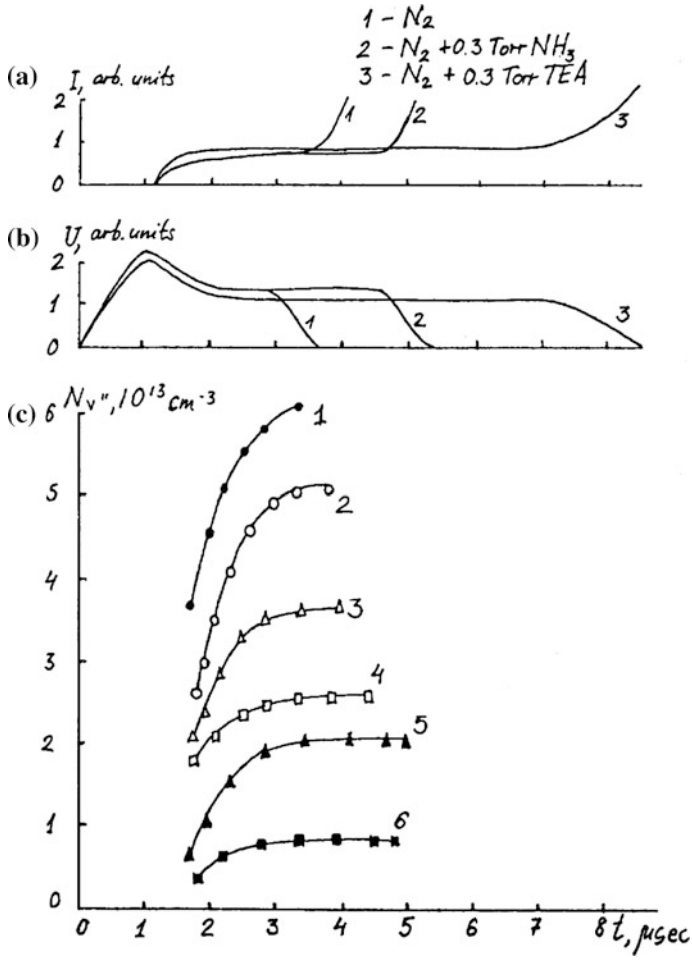

Fig. 19.6 Time dependencies of channel length *H* in pure N_2 (*curve 1*) and in triethylamine-containing N_2 (*curve 2*)

19.3 Initial Electrone Concentration

Since UV radiation is absorbed by additive vapors under a discharge stable for the maximum length of time, no discharge will be initiated by this radiation at electrode separations in excess of 30 cm.

To increase the range of action of UV radiation, we suggest that a mixture of two LIA components (rather than a single one) with different ionization potentials and partial pressures optimized for the Penning and the photoionization processes, respectively, should be used. In addition, photoelectrons should be transported in the electric field. It is known that the UV radiation absorption coefficient markedly

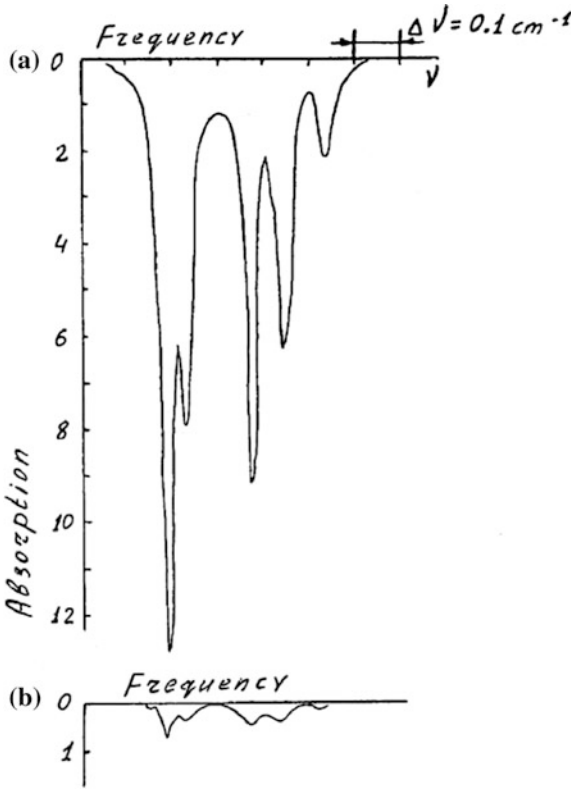

Fig. 19.7 Absorption spectra (in arbitrary units) **a** for pure N_2 and **b** triethylamine-containing N_2 in the $A^3\Sigma_u^+ (V = 2) - B^3\Pi_g$ (V = 3) band

exceeds the coefficient of electron attachment. Therefore, transportion of electrons from the source over great distances by drifting in the electric field is more advantageous than their production at the same distances by photoionization. The schematic diagram of the experimental arrangement is shown in Fig. 19.8. The discharge gap (1) is between mesh electrodes (2), which are supplied with a bias voltage, 20 cm from the UV radiation source (3). The upper and lower ignition limits of a stable discharge were recorded versus voltage across the UV source for two values of the bias voltage V and delay time τ between the instants at which the source was switched on and the voltage pulse was applied to the gap (Fig. 19.9). Evidently, the range of discharge stability is extended on application of a bias voltage, which indicates a higher initial concentration of electrons in the gap. In our arrangement, it is equivalent to a longer range of action of the UV radiation Source. An optimal delay time is determined from the electron drift velocity ($\tau_{\text{opt}} = d/V_{dr}$).

Under actual conditions, enlargement of the CO_2 laser aperture by transportion of initial photoelectrons is limited by the short emission time of the radiation sources in the vacuum UV. Hence, the possibility of discharge initiation by the gas preionization method is rejected, and the required initial concentration of electrons in the discharge gap is reached by prefilling it with electrons that are extracted

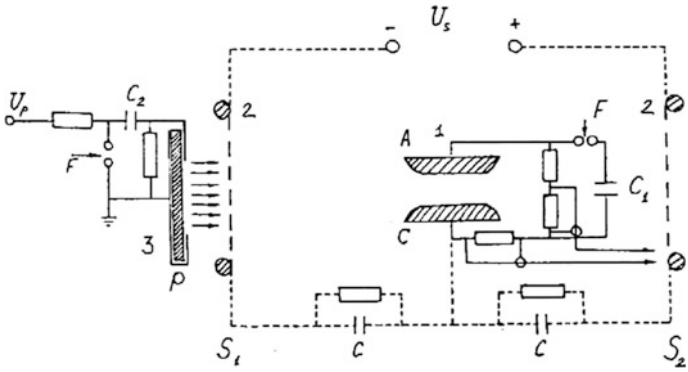

Fig. 19.8 Schematic diagram of experimental arrangement used to study limits of discharge stability: discharge gap (*1*); mesh electrodes (*2*); UV radiation source (*3*); charged voltages of capacitors C_1 and C_2, (*U, U_p*,, respectively); bias voltage (U_s,); anode (*A*); cathodes (*C*); radiation source (*P*); spark gaps (*F*); meshes (S_1, S_2)

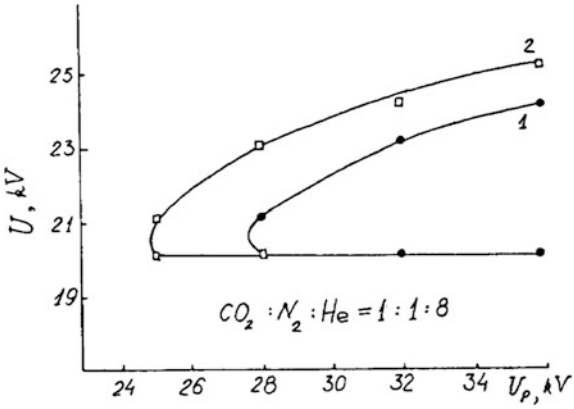

Fig. 19.9 Limits and V_{max} and V_{min} of discharge stability for different values of the bias voltage U_b and delay time τ : 1 – $U_b = 0$, $\tau = 1.5$ μs, 2 – $U_b = 30$ kV, $\tau = 5.5$ μs, U, U_p, charged voltage of capacitors C_1 and C_2, respectively (see Fig. 19.8)

directly from an auxiliary discharge plasma [11]. The relevant experimental setup is shown in Fig. 19.10. The auxiliary discharge is ignited under or on the surface of a mesh cathode, (2). The electrons are extracted by the discharge field and fill the gap while drifting in the bias field. For avoidance of discharge inhomogeneities in the near-cathode zone, the filling time, which is governed by the drift velocity, should not exceed the auxiliary discharge time.

The capabilities afforded by the filling technique are readily estimated within a one-dimensional stationary model. At high electron concentrations at the cathode

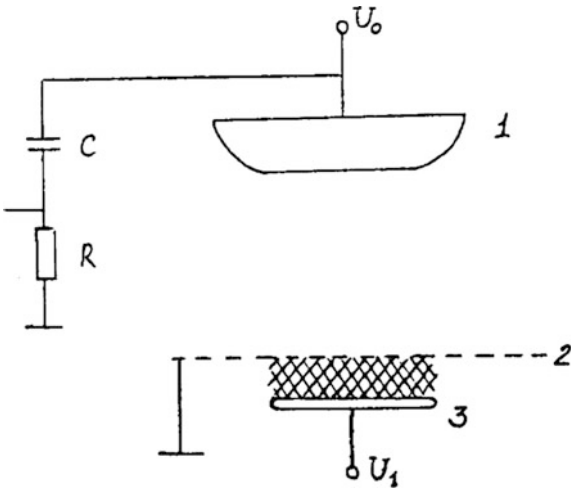

Fig. 19.10 Experimental setup for prefilling the discharge gap with electrons: anode (*1*); cathode (*2*); auxiliary electrode (*3*); capacitor (*C*); *R*, resistor (*R*)

$n_0 \gg E_0\varepsilon_0/ed$ the field strengths at the cathode, $E(0)$, at the anode, $E(d)$, and the electron concentration at the anode, $n(d)$, are

$$\begin{aligned} E(0) &= g/8\varepsilon_0 E_0^2/edn_0 \ll E_0, \\ E(d) &= 3/2E_0, \\ n(d) &= 3/4\varepsilon_0 E_0/ed, \end{aligned} \tag{19.1}$$

where E_0 is the mean strength of the bias field, U_0/d.

For typical values $E_0 = 2$ kV/cm, we have $d = 1$ m and $n(d) = 10^7$ cm^{-3}, which definitely exceeds the minimum concentration required for discharge initiation. It is remarkable that high concentrations at the cathode are already achieved with $n(0) \sim 10^8$ to $n(0) \sim 10^9$ cm^{-3}. This value is easy to obtain with any weak-current auxiliary discharge within the time required for electrons to fill the gap. By prefilling the gap with electrons, it is possible to reach concentrations sufficient for discharge initiation in large-aperture CO_2 lasers.

19.4 Dynamic Profiling in the Discharge Gap

Expressions (19.1) imply that as electrons fill the gap, the electric field becomes highly distorted by a negative space charge [12]. The same situation occurs if the gap is filled during the rise time of a cosine voltage. Figures 19.11 and 19.12 give the values of electron distribution and electric field strength calculated for various instants. Typically, the field at the cathode is nearly zero, since it is screened by a negative space charge throughout the filling phase. Meanwhile, the field at the anode is enhanced by a factor of 1.5, as compared with its mean value through the

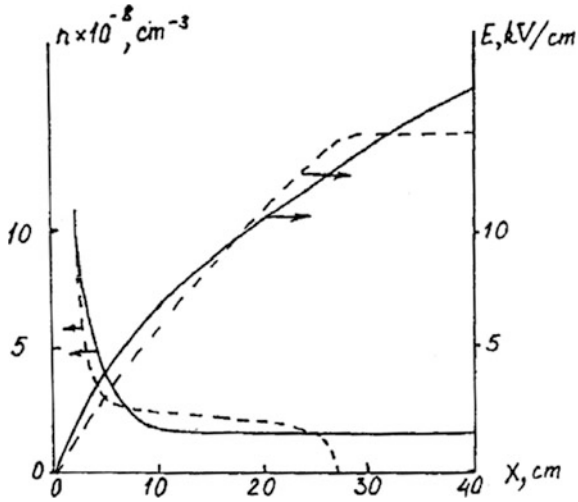

Fig. 19.11 Calculated values of electron distribution n and field strength E for two different rise times of cosine voltage $t = 2$ μs (*dashed curves*) and $t = 6.8$ μs (*solid curves*)

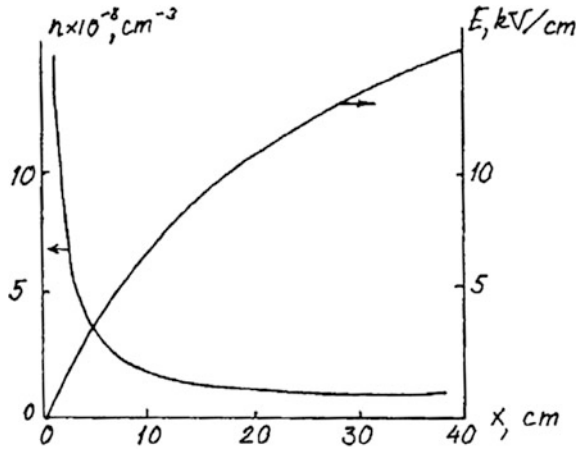

Fig. 19.12 Calculated values of electron distribution n and field strength E for U_0 = 400 kV, cosine voltage rise time $t = 8$ μs, $n(0) = 10^{10}$ cm^{-3}

gap at a given instant. The screening effect will naturally manifest itself in the gap geometry. Figure 19.13 shows a system of electrodes with an extremely compact cathode (made in the form of a sharp-edged plate) that is used for discharge initiation. Ionization at the cathode is hindered because of the small electric field. As the voltage increases, ionization processes are induced in the vicinity of the anode where the field is strongest, particularly near its central part where the field is created by the electrostatic repulsion of electrons that fill the gap. From this point, an ionization wave propagates simultaneously to the cathode and to the discharge gap edges. As soon as the wave closes the gap, a discharge column is formed.

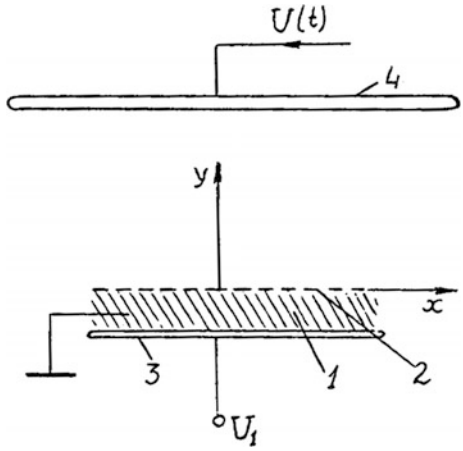

Fig. 19.13 Schematic diagram of experimental setup with extremely compact cathode: auxiliary discharge (*1*); cathode (*2*); auxiliary electrode (*3*); anode (*4*)

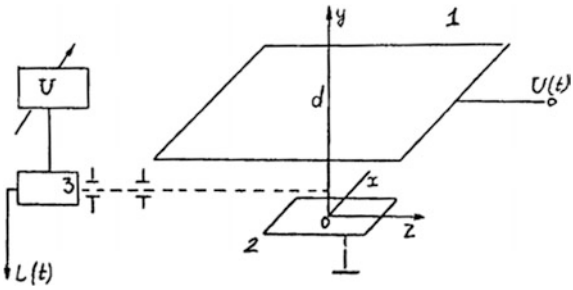

Fig. 19.14 Schematic diagram of experimental setup for investigation of dynamics of discharge initiation: anode (*1*); cathode (*2*); photomultiplier (*3*)

To verify the above qualitative sketch of the process, the glow intensity distribution over the discharge gap was measured at various instants of discharge initiation [13]. A photomultiplier was made to move along the x and y axes in a plane normal to the optic axis (Fig. 19.14). The glow-intensity distributions in the cathode-anode direction (along the y axis) for $x = 0$ are represented in Fig. 19.15.

Initially, the glow is seen near the anode. A discharge column is formed after two distinct glow waves that correspond to the ionization waves have traversed the gap. A similar pattern that is not delayed in time is observed near the gap edge. Thus, the active medium is excited at one time over the whole discharge volume, and this is reflected in the distribution of the small signal gain (Fig. 19.16). The gain is smaller with increased distance between the center and the edge of the discharge gap. Qualitatively, this distribution of the gain does not differ from those observed in systems with uniform fields.

In our scheme, the conditions for discharge initiation are determined by the configuration of the field that is formed by space charges introduced into the discharge gap, rather than determined by the field configuration that is specified by the shape of the electrode. In other words, we deal with dynamic profiling of the electric field in the discharge gap. Having experimentally verified the qualitative picture of

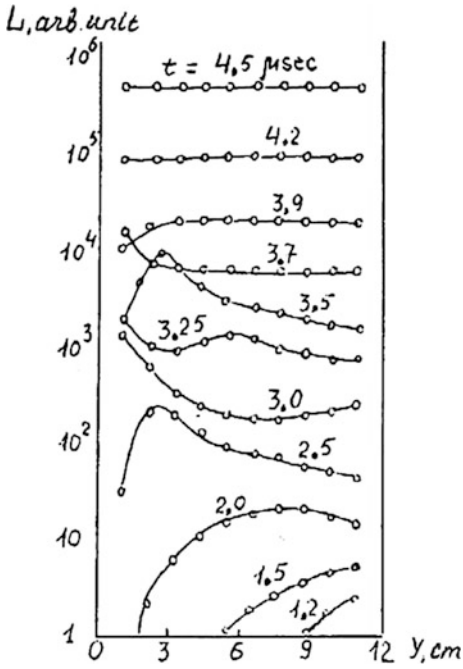

Fig. 19.15 Glow intensity (L) distributions in the center of the gap ($x = 0$) at various instants

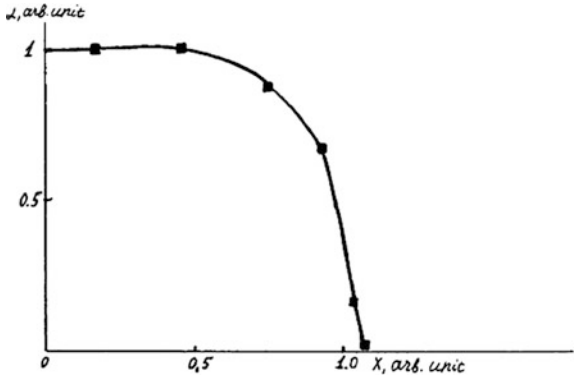

Fig. 19.16 Small signal gain distribution in a compact-cathode system: $x = 0$, center of electrode; $x = 1$, edge of electrode

discharge initiation by filling the gap with electrons, we suggest that dynamic profiling of the electric field is a general method for obtaining an SSVD in electrode systems with a markedly nonuniform initial distribution of the electric field. To this end, during discharge initiation, the field at the sharp-edged electrode should be reduced by introducing a space charge with the sign of the electrode into the gap.

Figure 19.17 is a schematic diagram of two identical sharp-edged flat electrodes that are used to initiate a discharge [14]. Just as in the previous case, the cathode is screened by the space charge of electrons that fill the gap. The anode is screened by

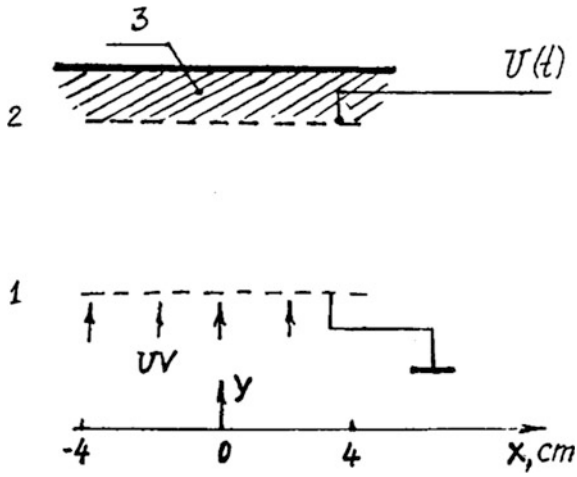

Fig. 19.17 Schematic diagram of experimental setup for discharge initiation in a compact-electrode system: anode (*1*); cathode (*2*); preliminary discharge (*3*)

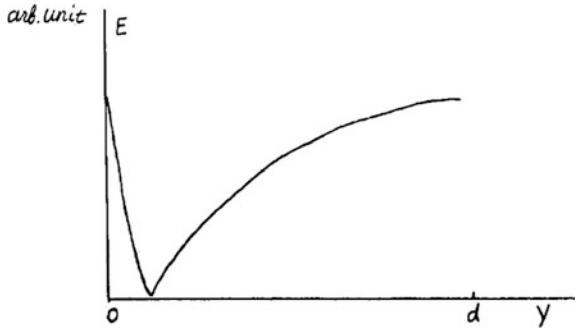

Fig. 19.18 Electric field distribution during discharge initiation under intense UV ionization of the near-cathode region

the positive-ion space charge formed on electron extraction from the photoplasma produced near the anode. The electric field distribution before the onset of ionization in the gap is depicted in Fig. 19.18. A similar profile of the field is achieved in a system of extremely compact electrodes that are exposed simultaneously to the intense UV radiation. To initiate a volume discharge, the photoplasma concentration at the sharp-edged electrode should exceed 10^{10} cm^{-3}. The field distribution over the gap is as shown in Fig. 19.18.

The electric field distortion by the space charge is a mechanism that permits discharge initiation in systems that have no specially shaped electrodes. Our concept of the dynamics of discharge initiation, involving space charges and the suggested methods, provide a new approach to the problem of CO_2-laser pumping by an SSVD. Employing it, we have succeeded in initiating a discharge in a system with a 70 cm electrode separation. The results obtained furnish an explanation of the previously unknown operating principles of systems in which the volume discharge is initiated by an auxiliary barrier discharge and of plasma electrode systems.

Table 19.1 Efficiencies of CO_2 Laser pumped by self-sustained versus electron-beam-sustained discharge

Discharge initiation	Electron-beam current density (A/cm^3)	Electron-beam current duration (ms)	Electron-beam energy (keV)	Laser output energy (kJ)	Efficiency (%)
Self-sustained	10^{-2}	1	140–200	2.5	25
Electron-beam sustained	0.5–1	6	300	2.7	27

19.5 CO_2 Lasers Pumped by the Discharge

The applicability of an electron beam to SSVD initiation in large volumes of active media is of partucular interest, since the beam penetrates deep into the gas and has a high ionizing power. The initiation of an SSVD does not call for electron concentrations so high as those needed for maintaining non-SSVD ignition under electroionization conditions. As such, the beam current density and the electron energy can be considerably reduced. For a beam current density of several milliamperes per square centimeter, initial electron concentrations of 10^{11} cm^{-3} are reached in CO_2-laser active media. Therefore, it is expected that a discharge will be obtained in systems of electrodes of no specific shape. In our experiments we used extremely compact electrodes for SSVD initiation. [15] Table 19.1 lists the results of a straightforward comparison of the data observed under electroionization and SSVD pumping conditions in a 60 L active volume CO_2 laser. For the latter, the beam current density is more than an order of magnitude smaller, while the electron energy is nearly twice as low as in the former. The extracted laser output energy is 2.5 kJ at an efficiency of 25%, which is not worse than the values obtainable under electroionization conditions.

19.6 Characteristics of an Active Medium and Scalability

In our approach to discharge initiation, the loss of initial electrons near electrodes is virtually precluded. The discharge is initiated in a relatively weak mean electric field. This contributes to good optical homogeneity of an active medium, which must affect the laser output energy, efficiency, radiation divergence and small signal gain values. Under the actual conditions of prefilling the gap with electrons, the output energy per unit volume was 50 J/L with an efficiency of 22% (V = 161). The radiation divergence at a half energy level in a laser with a 20 cm aperture unstable resonator was $\theta_{0.5} = 3 \times 10^{-3}$ rad, which is only 'N' times the diffraction-limited value. However, the main indicator that adequately characterizes an active medium is the small signal gain value. Figure 19.19 shows the gain in He-free LIA-containing mixtures of CO_2:N_2, prepared in a 1:1 proportion, as a function

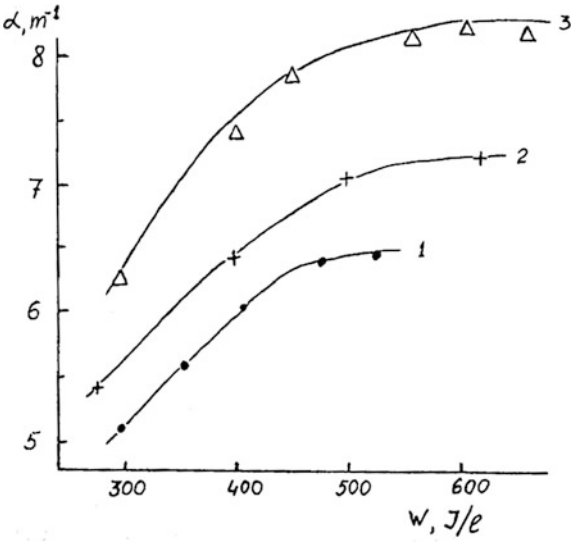

Fig. 19.19 Small signal gain α versus input energy per unit volume W for CO_2:N_2 = 1:1 [P = 456 Torr (0.6 atm) with 1-Torr triethylamine] under discharge initiation through intense UV ionization of the near-electrode regions (*1*), prefilling the gap with electrons (*2*), electron-beam preionization of the gap (*3*)

of the input pump energy per unit volume. The curves were plotted for discharges initiated by an electron beam, with the gap prefilled with electrons, by intense UV ionization of the near-cathode zone. Figure 19.19 also shows a curve that was recorded in a conventional system with weak preionization. The maximum value of the gain is more than 8 m^{-1}, which greatly exceeds the previously accepted upper limit of 5 m^{-1}. For a non-SSVD in a pure mixture, a gain of up to 7.5 m^{-1} was measured. Thus, the developed methods of discharge initiation provide a highly homogeneous active medium.

We have established that the small signal gain is scalable, i.e., it is preserved with increasing aperture. This implies the scalability of other characteristics of a CO_2 laser in the presence of appropriate optical elements. The experimental data needed for estimating the laser output energy and efficiency are compiled in Table 19.2. The data were obtained for 20 cm aperture systems with the output energy extracted from the total discharge volume.

19.7 N_2O Lasers

N_2O systems are second only to the highest power CO and CO_2 lasers and it is this fact that led to our interest in them, and encouraged investigations. We noted that the maximum output energy per unit volume and the efficiency of the NO_2 laser pumped by an SSVD, which was constructed earlier, were far lower than those of the recently created electroionization N_2O system [1]. A group from Lebedev [16] attributed this fact to the nonoptimal excitation of N_2O molecules because of the high value of the *E/P* parameter in an SSVD plasma. We showed (see Sect. 19.6)

Table 19.2 Parameters of experimental CO_2 devices

Type device	Electrode separation (cm)	Active volume (L)	Small signal Gain (m^{-1})	Output energy (kJ)	Efficiency (%)
SSVD	70	150	–	–	–
Amplifiers	40	320	3.9	–	–
	60	200	3.3	–	–
Lasers	10	16	–	0.8	22
	20	40	–	1.9	15
	20	20	–	0.6	1.7
	20	60	–	2.5	25
	40	100	–	2.5	16

that if the discharge is initiated by the techniques that ensure highly homogeneous active media in CO_2 lasers, then their output characteristics virtually do not differ from those of electroionization CO_2 systems. By employing these techniques, we anticipated a considerable increase in the efficiency and output energy of SSVD-pumped N_2O lasers.

Using the procedure developed for the CO_2 laser, we optimized the gas mixture composition with a view toward achieving a maximum homogeneity and duration of a stable discharge and demonstrating the feasibility of N_2O lasers with large active volumes. Dissociative electron attachment was compensated for by incorporating CO into the active medium.

In Fig. 19.20 shows plots of stable discharge time T versus the input pump power per unit volume for various ratios of CO and N_20 partial pressures, K. For $K \leq 6$, the time T increases with the K value, provided that the pump power is

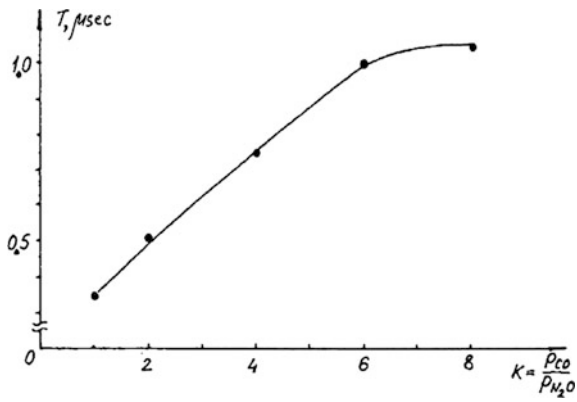

Fig. 19.20 Stable discharge time T versus input pump power per unit volume times unit pressure for various ratios of CO_2 and N_2O partial pressures $K = P_{CO}/P_{N_2O}$: $P_M = 114$ Torr (0.15 atm); $P = 380$ Torr (0.5 atm); $Q = 0.11$ MW/L Torr (80 MW/L atm)

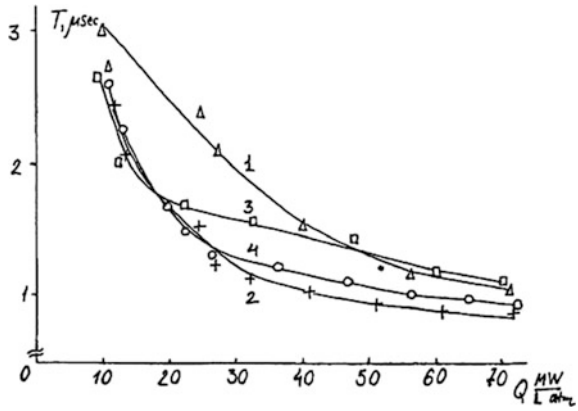

Fig. 19.21 Stable discharge time *T* versus input pump power per unit volume times unit pressure for various values of the *K* parameter: CO_2:N_2:He = 6:24:70 (1); N_2O:CO:He = 6:24:70 (2); N_2O:CO:He = 1:6:17 (3); N_2O:CO:N_2:He = 3:10:10:27 (4)

maintained at the same level. For $K \geq 6$, this time is barely dependent on the *K* value, and during a steady-state discharge, the value of *E/P* goes to its minimum, i.e., the loss of electrons through attachment is nearly completely compensated for. For pump power per unit, volume times unit pressure Q = 0.92 MW/L Torr (70 MV^L atm), the time *T* of stable discharge in a N_2O:CO:He mixture is close to that in an LIA-free CO_2:N_2:He mixture with the same proportion of molecular gases (Fig. 19.21). This result offers an opportunity for creating lasers with active volumes as large as tens of liters. When the discharge was initiated in a 10 L volume (10 cm × 10 cm × 100 cm) by prefilling the gap with electrons, or in a 60 L volume (20 cm aperture) by a weak-current electron beam, it was stable at the maximum input energies and the gas mixture proportions cited in Table 19.3. The operating pressure and proportions of molecular components were limited by maximum voltages (144 and 275 kV, respectively) of the pump sources. The shapes of the pump current and emitted laser pulses are typical of pulsed CO_2 and N_2O lasers.

Table 19.3 Parameters of laboratory N2O self-sustained discharge systems

Initiation technique	Proportions N_2O:CO: N_2:He	Partial pressure of molecular gases [Torr (atm)]	Total gas pressure [Torr (atm)]	Output energy (J)	Output energy [J/L MTorr (J/L atm)]	Efficiency (%)
Filling the discharge gap with electrons	4:16:0:30	152 (0.2)	380 (0.5)	60	16.6 (12.6)	6.7
	4:16:0:50	152 (0.2)	404 (0.7)	72	14.2 (10.8)	5.5
	3:10:10:27	97.3 (1.128)	304 (0.4)	53	18.4 (14.0)	6
	3:10:10:47	97.3 (0.128)	456 (0.6)	66	15.3 (11.6)	6.7
Accelerated electron beam	5:20:0:35	190 (0.25)	456 (0.6)	432	21.6 (16.4)	5.6
	5:20:0:45	190 (0.25)	404 (0.7)	465	19.9 (15.1)	5.3

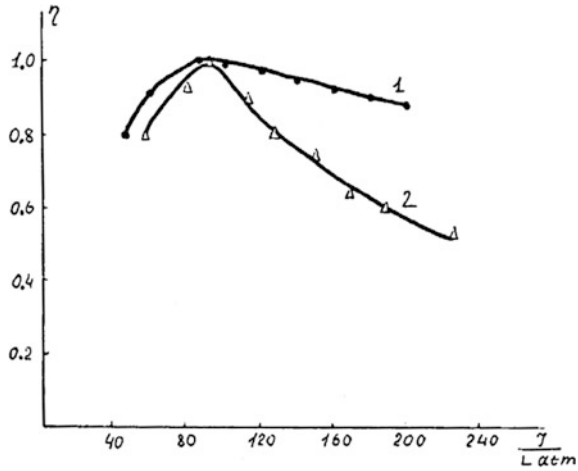

Fig. 19.22 Laser efficiency η (in relative units) versus pump energy per unit volume times unit pressure in the following mixtures: CO_2:N_2: He = 6:24:70 (1); N_2O:CO: He = 6:24:70 (2)

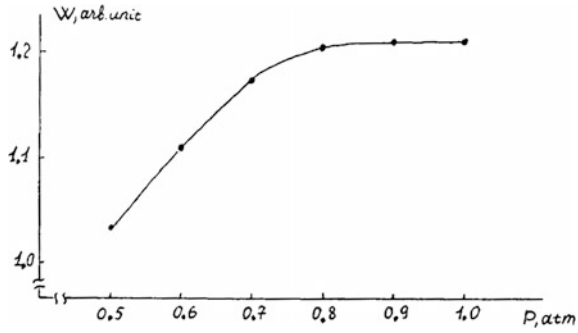

Fig. 19.23 Laser output energy W (in arbitrary units) versus total gas pressure P in a N_2O:CO:He mixture

In an N_2O device lasing took place simultaneously on four lines, $P(19)$, $P(29)$, $P(21)$, and $P(22)$ of the (00°1–10°0) transition of the N_2O molecule, with a maximum on the $P(21)$ line. Simultaneous laser action was also observed on the transitions of the CO_2 and N_2O molecules in a four-component mixture.

Figure 19.22 compares the relationships of the N_2O and CO_2 laser efficiencies (in relative units) to their pump energies per unit volume times unit pressure. Evidently, for N_2O the efficiency decrease with increased pump energy is more substantial.

The presence of He in a mixture contributes to the laser output energy and efficiency (Fig. 19.23). The requirements imposed on the population of the low-lying laser level in the active media are more stringent for N_2O than for CO_2 lasers.

Table 19.3 compiles efficiencies, output energies per unit volume per unit pressure, and total laser output energies for the most effective mixtures in N_2O lasers with 10 L and 60 L active volumes. To our knowledge, the observed efficiencies and output energies per unit volume exceed all the previously known

values for SSVD-pumped N_2O lasers, while the total laser output energy extracted is higher than any yet reported for N_2O lasers. Therefore, the previously observed modest (compared with electroionization systems) efficiency of N_2O lasers pumped by SSVDs is the result of insufficient uniformity of the active medium excitation rather than of the high E/P values in a discharge plasma.

19.8 Conclusions

The basic principles that underlie the initiation of an SSVD, which is to be used for pumping CO_2 and N_2O lasers, are presented in this part of the book. The experimental results for discharge stability, optical homogeneity and scalability of the laser active medium are reported. Characteristics of CO_2 lasers with apertures of up to 70 cm and active volumes of up to 400 L, as well as of N_2O lasers with apertures of up to 20 cm and active volumes of up to 60 L, are presented.

The suggested techniques for obtaining a discharge for pumping gas lasers make it possible to create high-power, compact, and simple pulsed CO_2 and N_2O lasers with large apertures. Our experiments have revealed that the developed approach is applicable to discharge initiation in any molecular gas that does not experience a marked loss of electrons because of attachment or permit the use of effective detachers, just as in the case of N_2O lasers.

References

1. Y.I. Bychkov, Y.P. Korolev, G.A. Mesyats, *Injection Gas Electronics* (Nauka, Novosibirsk, 1982), p. 238
2. S.A. Ghenkin, K.A. Klimenko, A.V Kozyrev, Y.D. Korolev, G.A. Mesyats, Y.N. Novoselov, Volume self-sustained discharge at long electrode separations initiated by soft x-rays, in *Proceedings of the Second SU Conference on Physics of Electric Breakdown in Gases* (University of Tartu, Tartu, USSR, 1984), pp. 63–65
3. A.I. Pavlovsky, V.F. Basmanov, V.S. Bosamykin et al., Electric discharge excited CO_2 laser with a 0.28 m^3 active volume. Kvantovaya Elektron. (Moscow) **14**, 428–430 (1987)
4. R. Dumanchin et al, High power density pulsed molecular laser, in *The Sixth International Quantum Electronic Conference*, Kyoto, Japan (1970)
5. V.Y. Baranov, V.M. Borisov et al., Formation of uniform discharge for large volume pulse CO_2 laser. Kvantovaya Elektron. **2**, 2086–2088 (1975)
6. A.A. Aliev, V.V. Apollonov, N. Akhunov et al., Efficiency of application of some low ionized additives to discharge stabilization in CO_2 lasers. Kvantovaya Elektron. **11**, 735–739 (1984)
7. V.V. Apollonov et al., Contraction of a SSVD at long electrode' separations. Pis'ma Zh. Eksp. Teor. Fiz. **14**, 1662–1667 (1988)
8. V.V. Apollonov et al., Dynamics of population of the $A^3\Sigma u^+$ metastable state of nitrogen in a SSVD of a pulsed CO2 laser. Kvantovaya Elektron. **16**, 269–271 (1989)
9. A.V. Ermachenko, V.I. Lozovoy et al., Relationship of the stable combustion time of a SSVD in active media of a CO_2 laser to the population of the $A^3\Sigma u^+$ metastable state of nitrogen. Pis'ma Zh. Tekh. Fiz. **15**, 7–11 (1989)

10. E.P. Velikhov, V.D. Pis'menny, A.T. Rakhimov, Non-SSVD pumping a CW CO_2 laser. Usp. Fiz. Nauk **122**, 419–434 (1977)
11. V.V. Apollonov et al., Initiation of a SSVD in dense gases at long electrode separations. Pis'ma Zh. Tekh. Fiz. **11**, 1262–1266 (1985)
12. V.V. Apollonov et al., SSVD initiation for CO_2 laser pumping. Kvantovaya Elektron. (Moscow) **14**, 135–145 (1987)
13. V.V. Apollonov et al., Dynamics of glow discharge formation in the gap pre-filled with auxiliary discharge electrons. Pis'ma Zh. Tekh. Fiz. **13**, 558–563 (1987)
14. V.V. Apollonov et al., SSVD initiation in a compact-electrode system for gas laser pumping. Kvantovaya Elektron. (Moscow) **13**, 1960–1962 (1986)
15. V.V. Apollonov et al., High-power CO_2 laser pumped by a SSVD initiated by an electron beam. Pis'ma Zh. Tekh. Fiz. **12**, 401–405 (1986)
16. A.A. Ionin, A.F. Suchkov, K.K. Frolov, Electroionization N_2O laser. Kvantovaya Elektron. (Moscow) **15**, 1967–1987 (1988)

Chapter 20
N_2O Laser Pumped by an SSVD

Abstract An investigation was carried out into the parameters of an N_2O laser pumped by an SSVD with the aim of improving the output characteristics of this laser. The discharge was ignited as a result of a preliminary filling of the discharge gap with electrons and preionization of the gas in the gap by a low-current beam of accelerated electrons. In this way, it was possible to reach an output energy up to 465 J, a specific output energy up to 16.4 J L atm and an efficiency of 6.7%, all of which exceeded the earlier values reported for N_20 lasers pumped by an SSVD.

A further important investigaton into N_2O laser parameters pumped by an SSVD with the aim of improving the output characteristics of that type of laser was also carried out by our team. The discharge was ignited as a result of a preliminary filling of the discharge gap with electrons and preionization of the gas in the gap by a lo-current beam of accelerated electrons. In this way, it was possible to reach an output energy of up to 465 J, a specific output energy of up to 16.4 J L atm and an efficiency of 6.7%, all of which exceeded the earlier values reported for N_2O lasers pumped by an SSVD. The highest values of the specific output energy and of the efficiency of N_2O electron-beam-controlled lasers (16 J L atm and 7% for a total output radiation energy of 8 J) achieved to date [1, 2] are much better than the corresponding characteristics of N_2O lasers excited by a transverse SSVD with ultraviolet preionization of the gas (4.8 J L atm and 1.8% for a total energy of 0.42 J) [3]. This was attributed in [1, 2] to nonoptimal excitation of the N_2O molecules in an SSVD plasma because of the high values of the parameter *E/p*.

Our earlier investigations demonstrated that when certain conditions for the formation of an SSVD were obeyed and the spatial homogeneity of the discharge was ensured, the output characteristics of CO_2 lasers pumped by an SSVD were, in practice, not inferior to the characteristics of electron-beam-controlled CO_2 lasers. The high spatial homogeneity of the active medium was achieved by initiation of an SSVD involving preliminary filling of the discharge gap with electrons or preionization of the gas with a low-current beam of accelerated electrons. These methods for initiating the SSVD made it possible to considerably increase the efficiency and output energy of the N_2O laser. This was the subject of the present investigation [3].

© Springer International Publishing Switzerland 2016

V.V. Apollonov, *High-Energy Molecular Lasers*,
Springer Series in Optical Sciences 201, DOI 10.1007/978-3-319-33359-5_20

Experiments were carried out using two configurations. In the first (which we shall label L_1), an SSVD was established in an active volume of 9.5 L (10 × 9.5 × 100 cm) filling the discharge gap with electrons from a barrier discharge plasma distributed over the cathode surface. In the second configuration (L_2), described in detail ih [4, 5], an SSVD was initiated by an electron beam with a current density of 15 mA/cm^2 and an electron energy of 180 keV in a volume of 44 L (18 × 19.5 × 125 cm). In both cases, the output mirrors of the optical resonators were plane-parallel Ge plates (transmission coefficient: 34%).

The energy lost as a result of dissociative attachment to the N_2O molecules was compensated, as in [6–9], by the addition of CO to the working mixture used in the N_2O laser. Optimization of the composition of the mixture to ensure the maximum SSVD stability was achieved in the configuration L_1 by a method described in [10, 11]. This was achieved by recording the dependences of the duration T of stable burning of an SSVD in N_2O-CO-N_2 mixtures on the specific pump power Q and on the ratio $K = [CO]/[N_2O]$ of the partial pressures of CO and N_2O. Figure 20.1 shows a typical dependence $T(K)$ obtained for a constant value of β. Clearly, it is strongly increased with K in the range $K < 4$ or depended weakly on K when $K > 4$. The minimum value of the parameter E/p of these N_2O-CO-N_2 mixtures was obtained for K = 4, close to the quasi-steady phase of the SVD and the value of this parameter was close to E/p (20 kV/cm atm) [12] for pure N_2, indicating almost a complete compensation of the electron losses due to attachment.

Figure 20.2 shows the dependences $T(Q)$ obtained for pure N_2 (curve 1) and for N_2 containing small amounts (i.e., less than 5%) of N_2O and CO (curve 2). In the case of the latter, the stability of the SSVD was considerably higher. This was obviously due to the higher rate of collisional quenching of the electronic states of N_2 by the N_2O molecules, [12] which reduced the probability of an SSVD instability due to multistage ionization of N_2 [10, 11]. For the same reason the addition of easily ionizable substances to the N_2O-CO-N_2 mixture did not affect the stability and the burning voltage of the SSVD, which was in contrast to CO_2-N_2 mixtures.

Operating characteristics of the lasers were investigated for N_2O-CO-He and N_2O-CO-N_2 mixtures. As in [1, 2], lasing occurred simultaneously at the wavelengths of four lines $P(19)$, $P(20)$, $P(21)$, and $P(22)$ of the (00°1–10°0) transition in the N_2O molecule with the maximium at the $P(21)$ line. An output radiation pulse had a profile typical of N_2O and CO lasers pumped by VDA. We also observed

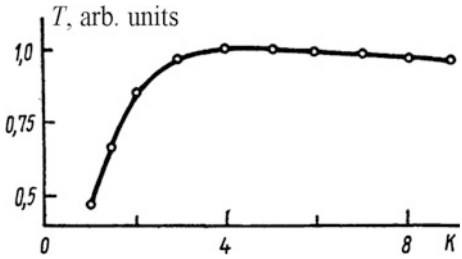

Fig. 20.1 Dependence T(K) for an N_2O-CO-N, mixture with a total pressure of p = 0.3 atm when the partial pressure of N_2O was 2 Torr

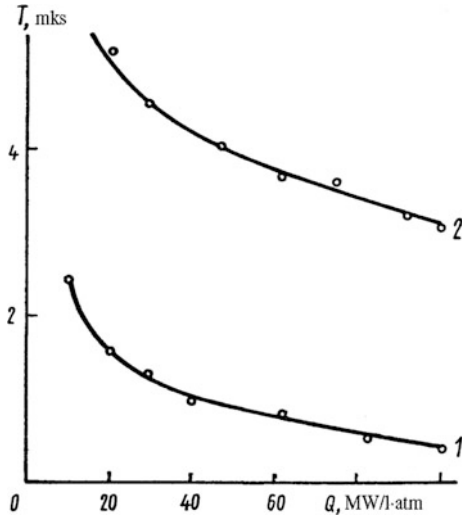

Fig. 20.2 Dependences T(Q) for pure N_2 (*1*) and for an N_2O-CO-N, mixture at p = 0.3 atm when the partial pressure of N_2O was 2 Torr and K = 4 (*2*)

Table 20.1 Typical dependence T(K) obtained for a constant value of b

Installation	N_2O:CO:N_2:He	p_M (atm)	p (atm)	W (J)	W_{ud} (J/l.atm)	Efficiency (%)
L_1	4:16:0:30	0.2	0.5	60	12.6	6.7
	4:16:0:50	0.2	0.7	72	10.8	5.5
	3:10:10:27	0.184	0.4	53	14	6
	3:10:10:47	0.184	0.6	66	11.6	6.7
L_2	5:20:0:35	0.25	0.6	432	16.4	5.6
	5:20:0:45	0.25	0.7	465	15.1	5.3

simultaneous lasing due to transitions in the CO_2 arid N_2O molecules when CO_2 was added to the working mixture in the N_2O laser.

At a constant specific input energy, the N_2O laser efficiency increased on increase in the proportion of the molecular gases in the mixture. Table 20.1 gives the parameters (efficiency and specific output energy: *W*) for mixtures characterized by the maximum output energy, *W*, of the N_2O laser (p_M is the pressure of the molecular gases in the mixture). Clearly, the values of *W*, W_{ud}, and the efficiency we obtained were much better than all the other published values of the same parameters that have previously been obtained for N_2O lasers with SSVD pumping [3] and *W* was more than one order of magnitude greater than the maximum energy achieved in an N_2O electron-beam-controlled laser. A comparison of the results obtained with those reported in [1, 2] and [3] also demonstrated that the low efficiency (compared with N_2O electron-beam-controlled lasers) of N_2O lasers with SSVD pumping was not due to high values of the parameter E/p, typical of the SSVD plasma, but due to an insufficiently homogeneous excitation of the active medium in [3].

Our results thus demonstrated that the methods of formation of an SSVD, ensuring a high homogeneity of the active medium in CO_2 lasers, could be applied successfully to N_2O lasers with an output radiation energy amounting to several hundreds of joules. It is clear that the values of the output energy we obtained were not the highest attainable.

References

1. A.F. Suchkov, K.K. Frolov, Kvantovaya Elektfon. (Moscow) **15**, 1967 (1988)
2. A.F. Suchkov, K.K. Frolov, Sov. J. Quantum Electron. **18**, 1228 (1988)
3. W.T. Whitney, H. Kara, IEEE J. Quantum Electron. QE-19, 1616 (1983)
4. V.V. Apollonov et al., Pis'ma Zh. Tekh. Fiz. **12**, 401
5. V.V. Apollonov et al., Sov. Phys. Tech. Phys. **12**, 163 (1986)
6. V.V. Apollonov, Yu.M. Vas'kovskii, M.I. Zhavoronkov, et al., Kvantovaya Elektron. (Moscow) **12**, 5 (1985)
7. V.V. Apollonov, Yu.M. Vas'kovskii, M.I. Zhavoronkov, et al., Sov. J. Quantum Electron. **15**, 1 (1985)
8. V.V. Apollonov et al., Kvantovaya Elektron. (Moscow) **13**, 2538 (1986)
9. V.V. Apollonov et al., Sov. J. Quantum Electron. **16**, 1680 (1986)
10. V.V. Apollonov et al., Kvantovaya Elektron. (Moscow) **15**, 553 (1988)
11. V.V. Apollonov et al., Sov. J. Quantum Electron. **18**, 351 (1988)
12. G. Bekefi (ed.), *Principles of Lasers Plasmas* (Wiley, New York, 1976)

Chapter 21
CO_2- and N_2O-Lasers with Preliminary Filling of the Gap by Electrons

Abstract One major advantage of the new technique over VUV irradiation is that it is able to efficiently preionize large-aperture devices that contain a high percentage of molecular gas. With the subsequent application of a tailored voltage pulse to the main transverse gap, space-charge screening effects reduce field enhancement at the cathode, thereby retarding or suppressing instabilities from developing within cathode spots associated with the boundary layer. Simple, easily machined electrodes can therefore be used without danger of arcing at the edges. Dynamic enhancement of the electric field at or near the anode during the preionization phase reduces the minimum voltage to $U_{\min} = (2/3)U_{sb}$, where U_{sb} is the static self-breakdown voltage. With these electrode geometries, U_{sb} is about half the value measured with profiled electrodes with a uniform field distribution. Recent advancement of this technology has led to impressive aperture ($g > 70$ cm) and volume ($V = 4001$) scaling.

Development of CO_2 lasers using VUV preionization has been impeded because of discharge instabilities that occur in devices with large transverse gaps and large volumes. Realization of volumetrically uniform preionization is extremely difficult when the gap dimension greatly exceeds the mean free path for VUV photons. Contoured electrodes with profiles of extreme accuracy are needed to minimize field distortions and ensure discharge stability. Furthermore, fast (low-inductance) circuitry is necessary to rapidly increase the electron concentration from photo-preionization levels ($n_{eO} \sim 10^6$–10^8 cm^{-3}) to lasing densities ($n_e \sim 10^{12}$–10^{14} cm^{-3}). The minimum voltage needed to initiate a stable, SSVD $U_{\min}$ is quite high when the transverse gap, g, is increased beyond a few centimeters, even for mixtures with a low molecular gas content K (e.g., $U_{\min} = 280$ kV for $g = 30$ cm and $K = 20$ %). $U_{\min}$ can be reduced by the addition of small concentrations of readily ionizable organic compounds that contribute electrons to the discharge via VUV photoionization and via Penning reactions with electronically excited N_2 molecules. The two most common additives are tri-*n*-propylamine (TPA, 7.23 eV ionization potential) and triethylamine (TEA, 7.59 eV ionization potential). For a constant specific input energy ξ_i, however, any reduction in the quasi-steady SSVD

© Springer International Publishing Switzerland 2016

V.V. Apollonov, *High-Energy Molecular Lasers*,
Springer Series in Optical Sciences 201, DOI 10.1007/978-3-319-33359-5_21

U_{qs} will require an *arc-free* increase in the quasi-steady-state duration t_{qs}. Furthermore, the optimum partial pressure for the Penning process (P_{ri} = 1 − 1.5 Torr) is greater than that required for enhanced VUV photoionization, thus reducing the density of photoelectrons at large distances from the radiation source to values less than in the pure gas.

Alternatively, an auxiliary discharge [1–15], placed adjacent to an unprofiled (i.e., flat) cathode with marginally radiused edges, acts as an electron beam capable of producing in-depth volume preionization levels, which are greater than the minimum required for discharge stability. The auxiliary discharge can be implemented as a volume discharge, a barrier discharge, a corona discharge, or a complete or incomplete surface discharge. One major advantage of this technique over VUV irradiation is that it is able to efficiently preionize large-aperture devices that contain a high percentage of molecular gas. With the subsequent application of a tailored voltage pulse to the main transverse gap, space-charge screening effects reduce field enhancement at the cathode, thereby retarding or suppressing instabilities from developing within cathode spots associated with the boundary layer. Simple, easily machined electrodes can therefore be used without danger of arcing at the edges. Dynamic enhancement of the electric field at or near the anode during the preionization phase reduces the minimum voltage to $U_{min} = (2/3)U_{sb}$, where U_{sb} is the static self-breakdown voltage. With these electrode geometries, U_{sb} is about half the value measured with profiled electrodes with a uniform field distribution. Recent advancement of this technology has led to impressive aperture (g > 70 cm) and volume (V = 4001) scaling [16, 17].

21.1 Necessary Conditions for Preionization and Field Enhancement

To provide complete, in-depth preionization of the transverse gap, it is necessary that the auxiliary discharge flux be maintained for a duration t_{aux} which approximates or exceeds the characteristic electron drift time across the main gap, i.e.,

$$t_{aux} \geq t_{dr} = \frac{g}{\mu_e E_0}, \tag{21.1}$$

where

$$E_0 = \frac{U_{bias}}{g} \approx \frac{U_{sb}}{3g} \tag{21.2}$$

is the quasi-dc field applied to the main transverse gap prior to discharge ignition. U_{bias} is the bias voltage and μ_e is the electron mobility. If, on the other hand, a slowly rising voltage pulse is used both for preliminary filling of the gap with preionization electrons and ignition of the discharge, then

$$E_0 \approx \frac{2U_{\mathrm{pk}}}{3g}, \tag{21.3}$$

where U_{pk} is the peak discharge voltage. The auxiliary discharge is electrically driven for a duration t_{ad} and, typically, $t_{\mathrm{ad}} \sim t_{\mathrm{aux}}$. Furthermore, it is necessary that the current density extracted from the auxiliary discharge J_{aux} exceeds a minimum value to effect space-charge screening of the cathode, i.e.,

$$J_{\mathrm{aux}} \geq J_{\mathrm{min}} = f\left(\text{gas composition}, P, \frac{dU_{\mathrm{d}}}{dt}\right), \tag{21.4}$$

where P is the total gas pressure and $dU_{\mathrm{d}}/\mathrm{d}t$ is the rate of rise of the voltage applied to the main transverse gap. The duration t_{aux}, effective electrode area A, and current density J_{aux} define the total charge q_{aux} transferred between the cathode and anode during the preionization phase.

21.2 Discharge Preionization and Ignition Model

Numerical modeling and simulation of discharge ignition have been performed by Beverly [18, 19]. The former model, which includes negative ions, is followed here. The conservation equations for charged particle densities $n(x, t)$ in one spatial dimension are

$$\frac{\partial n_e}{\partial t} = S_e - \frac{\partial J_e}{\partial x}, \tag{21.5}$$

$$\frac{\partial n_+}{\partial t} = S_+ - \frac{\partial J_+}{\partial x}, \tag{21.6}$$

$$\frac{\partial n_-}{\partial t} = S_- - \frac{\partial J_-}{\partial x}, \tag{21.7}$$

where n represents particle concentration (particles/cm^3), S collectively represents source and loss terms (particles/cm^3 s) associated with various kinetic processes, J represents scalar current density (particles/cm^2 s), and the subscripts e, +, and − denote electrons, positive ions, and negative ions, respectively. The relations between particle current density, J; drift velocity, W (cm/s); and mobility μ (cm^2/V s) are

$$J_e(x,t) = n_e W_e = -\mu_e n_e E, \tag{21.8}$$

$$J_+(x,t) = n_+ W_+ = \mu_+ n_+ E, \tag{21.9}$$

$$J_-(x,t) = n_- W_- = -\mu_- n_- E, \tag{21.10}$$

where the electric field vector points in a direction from anode ($x = g$) to cathode ($x = 0$) and, thus, $E = |\vec{E}| < 0$. With this sign convention, W_e and W_- are positive and W_+ is negative. The source terms are

$$S_e(x,t) = (\bar{k}_i - \bar{k}_a) n_e N - k_r^{ei} n_e n_+ + \bar{k}_d n_- N + S_{vuv} + S_p, \tag{21.11}$$

$$S_+(x,t) = \bar{k}_i n_e N - k_r^{ei} n_e n_+ - k_r^{ii} n_+ n_- + S_{vuv} + S_p, \tag{21.12}$$

$$S_-(x,t) = \bar{k}_a n_e N - \bar{k}_d n_- N - k_r^{ii} n + n_-, \tag{21.13}$$

where processes (and rate coefficients) include primary electron-impact ionization (k_i), electron attachment (k_a), electron detachment (k_d), electron-ion recombination (k_r^{ei}), and ion–ion recombination (k_r^{ii}). The bar notation indicates rate coefficients that are weighted for the particular gas mixture, and which are functions of the local value of the reduced field *E/N,* where N is the total particle concentration. S_p and S_{vuv} are additional source terms, described subsequently, for Penning ionization of a readily ionizable organic additive and for VUV preionization by an external illumination source. Equations (21.5–21.7) must be solved simultaneously with Poisson's equation relating the electric field $E(x,$ t) to the charge density $\sigma(x, t)$,

$$\frac{\partial E}{\partial x} = -\frac{\sigma}{\varepsilon}, \tag{21.14}$$

$$\sigma = e(n_+ - n_e - n_-), \tag{21.15}$$

where ε is the permittivity of free space and e is the electronic charge.

The charged particle conservation equations are subject to mixed Dirichlet and Neumann boundary conditions at the electrodes. At the cathode,

$$\phi_e(0,t) = 6.24 \times 10^{15} J_{aux}, \tag{21.16}$$

$$n_-(0,t) = 0, \tag{21.17}$$

where ϕ_e is the electron flux (electrons/cm^2 s) and J_{aux} is the beam current density from the auxiliary discharge (mA/cm^2). At the anode,

$$n_+(g,t) = 0. \tag{21.18}$$

The constant of integration is lost in solving (21.14) and thus the additional condition

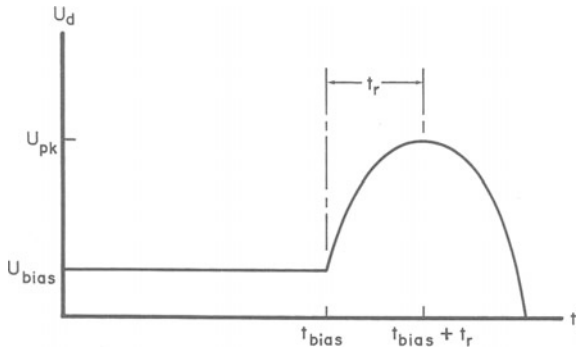

Fig. 21.1 Voltage waveform for the discharge ignition model

$$U_{\mathrm{d}}(t) = -\int_0^g E(x,t)dx \tag{21.19}$$

is imposed where U_{d} is the voltage between the electrodes. U_{d} can be incorporated into Kirchoff's equation, with appropriate RLC terms, to model the external capacitive-discharge circuit (a discussion of circuit response is given in [20]). For the present model, however, the discharge is simply connected to a voltage source whose temporal characteristics are (Fig. 21.1):

$$U_{\mathrm{d}}(t) = \begin{cases} U_{\mathrm{bias}}, & t \le t_{\mathrm{bias}} \\ U_{\mathrm{pk}} + \frac{(U_{\mathrm{pk}} - U_{\mathrm{bias}})}{2}\left\{1 - \cos\left[\frac{\pi(t - t_{\mathrm{bias}})}{tr}\right]\right\}, & t_{\mathrm{bias}} < t < t_{\mathrm{bias}} + 2tr \\ 0, & t \ge t_{\mathrm{bias}} + 2t_r. \end{cases} \tag{21.20}$$

A formula for the discharge current has been derived from first principles [21], from which we determine the current density:

$$Jd(t) = \frac{e}{g}\int_0^g (n_+ W_+ - n_- W_- - n_e W_e)dx. \tag{21.21}$$

The equation describing evolution of the combined $N_2 a'^1\Sigma_u$ ($\tau_{\mathrm{r}} \geq$ 23 ms) and $a^1\Pi_g$ ($\tau_{\mathrm{r}} = 80\ \mu s$) metastable state concentration $n_{\mathrm{m}}(x,\ t)$ is

$$\frac{\partial n_{\mathrm{m}}}{\partial t} = k_{\mathrm{m}} n_{\mathrm{e}}[N_2] - \frac{nm}{\bar{\tau}}, \tag{21.22}$$

where k_m is the rate coefficient for electronic excitation from the N_2 ground state to the metastable level, $\bar{\tau}$ is the characteristic time for collisional deactivation of the metastable level (weighted for the particular gas mixture), and N_2 is the nitrogen gas concentration (constant). Losses due to radiative decay (τ_{r}) are ignored. Although the N_2 $A^3\sum_u^+$ and $B^3\Pi_g$ states are produced in significant quantities in

CO_2-laser discharges, only the *a*-states have sufficient energy ($\sim$8.5 eV) and are produced in large enough concentrations to participate in Penning ionization of typical readily ionizable compounds. The source term for Penning ionization is therefore

$$S_{\mathrm{p}}(x,t) = \frac{n_{\mathrm{m}}}{\tau_{\mathrm{p}}}, \tag{21.23}$$

where τ_{p} is the characteristic time for Penning collisions ($1/\tau_{\mathrm{p}} = k_{\mathrm{p}} N_{\mathrm{ri}}$, where N_{ri} is the concentration of readily ionizable molecules).

Certain types of auxiliary discharges also emit VUV radiation. The source term for VUV preionization through a mesh cathode is

$$S_{\mathrm{vuv}}(x,t) = \begin{cases} \zeta\alpha\phi_{\mathrm{vuv}} \exp(-\alpha x)(t/t_1), & t \le t_1, \\ \zeta\alpha\phi_{\mathrm{vuv}} \exp(-\alpha x) \exp(-t/t_2), & t > t_1, \end{cases} \tag{21.24}$$

where $\alpha = \sigma_{\mathrm{a}} N_{\mathrm{ri}}$ is the photoabsorption coefficient (cm^{-1}), σ_{a} is the photoabsorption cross section (cm^2), ζ is the photoionization yield (dimensionless), and ϕ_{vuv} is the peak photon flux (photons/cm^2 s) incident upon the gas volume through the mesh cathode structure. The temporal dependence of the VUV irradiation is thus described by a linear rise over a duration t_1 followed by an exponential decay with time constant t_2. An analogous, optional source term is included for VUV preionization through the anode; firing of these sources can be delayed until $t' = t - t_{\mathrm{d}}$.

21.3 Method of Solution and Rate Data

Solution of the hyperbolic (21.5)–(21.7) is accomplished using the low-phase-error phoenical sharp and smooth transport algorithm (LPE SHASTA), as originally proposed by Zalesak [22] and implemented by Morrow et al. [23–26]. To impose the Neumann boundary condition (16), ϕ_e is simply added to the corrected antidiffusive flux at the cathode. Dirichlet boundary conditions are specified by (17) and (18). Source terms were integrated using a time-splitting technique [27]. Integration of (14) is performed separately and accuracy is greatly improved by subdividing each spatial interval into a finer mesh. The charge density distribution on the fine mesh is evaluated by a fourth-order (cubic) Lagrangian interpolator, using only the central interval for accuracy. Solution of (22) is effected by transforming the single parabolic partial differential equation (PDE) into a coupled set of ordinary differential equations (ODEs), one ODE for each spatial mesh point (*i.e., method of lines approach*). Since this set of ODEs is not stiff, solution is obtained using a straightforward, fourth-order Runge-Kutta algorithm. Two fictitious mesh points are introduced beyond the boundaries as a method for continuing the solution into

the electrodes. This technique avoids problems associated with reducing numerical order when approaching a boundary.

Rate coefficients for CO_2:N_2:He gas mixtures were computed by solution of Boltzmann's transport equation using the ELENDIF code [28] and included 39 inelastic processes. Computed rate coefficients are shown in Fig. 21.2 for a gas mixture with high molecular gas content ($K = 0.50$). Here, 1 Td = 1 Townsend = 10^{-17} V cm^2. The predicted self-sustained equilibrium can be estimated by finding the value of E/N at which $\bar{k}_i = \bar{k}_a$; for a 1:4:5 mixture, this occurs at E_{qs}/N = 49 Td without a readily ionizable additive, while for a 4:16:80 mixture, the corresponding value is lower (E_{qs}/N = 28 Td), which is consistent with a lower fractional content of molecular gases. The parameterized electron drift velocity is

$$|W_e| = c\left(\frac{|E|}{N}\right)^m, \tag{21.25}$$

where $c = 2.44 \times 10^{17}$, $m = 0.68$ (CO_2: N_2: He = 1:4:5) and $c = 6.11 \times 10^{18}$, $m = 0.77$ (CO_2:N_2:He = 4:16:80). Similarly, rate coefficients were also computed for a representative N_2O-laser gas mixture as shown in Fig. 21.3. The predicted quasi-steady reduced field is E_{qs}/N = 67 Td, which does not include the effects of electrondetachment that are discussed subsequently. The added electron production rate due to detachment reactions will reduce E_{qs}/N substantially. Electron drift velocity coefficients for the N_2O:CO:N_2:He = 3:10:10:47 gas mixture are $c = 4.80 \times 10^{17}$ and $m = 0.70$.

Sources of fundamental data are as follows: τ_p and τ [29, 30], σ_a and ζ [31, 32], $k_r^{ei}(E/N)$ [33], and k_r^{ii} and k_d [34]. Penning rate data are only available for TPA. Positive and negative ion mobilities in pure gases can be found in [35, 36]. Blanc's law is then used to calculate ionic mobility in the various gas mixtures [37].

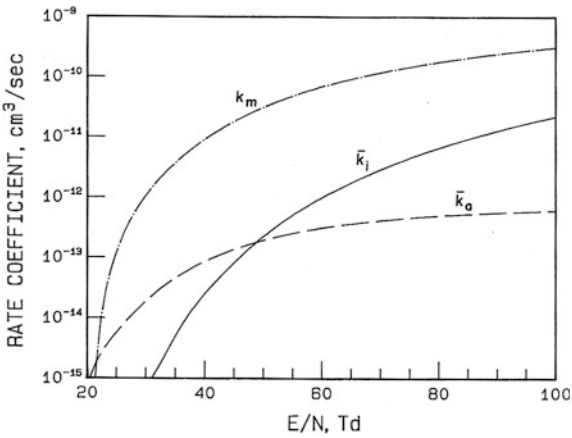

Fig. 21.2 Rate coefficients for a CO_2:N_2:He = 1:4:5 gas mixture at 300 K

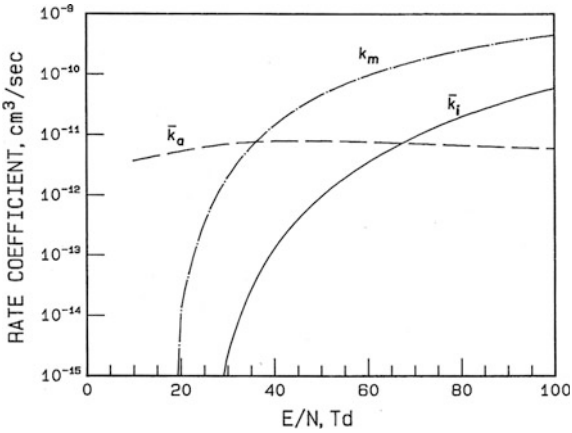

Fig. 21.3 Rate coefficients for an N_2O:CO:N_2: He = 3:10:10:47 gas mixture at 300 K

21.4 Discharge Ignition Phenomena

21.4.1 CO_2 Lasers

The computational run shown here is for a CO_2:N_2:He = 1:4:5 gas mixture (T = 293 K, P = 750 Torr) that contained an admixture of TPA (P_{ri} = 1.5 Torr). The interelectrode gap is g = 10 cm. Cathode and anode VUV preionization are absent. The discharge initiation scheme is described by auxiliary preionization in the presence of a quasi-DC field followed by application of a slow-ignition voltage pulse (t_{bias} = 1.8 μs, t_r = *2* μs, J_{aux} = *1* mA/cm^2, U_{bias} = 40 kV, and U_{pk} = 120 kV). During the *filling* phase ($t < t_{bias}$), the electron preionization front progresses in the absence of electron-impact ionization and no positive charge carriers are generated (Figs. 21.4 and 21.5). The electron flux reaches $x \sim 2.4$ cm

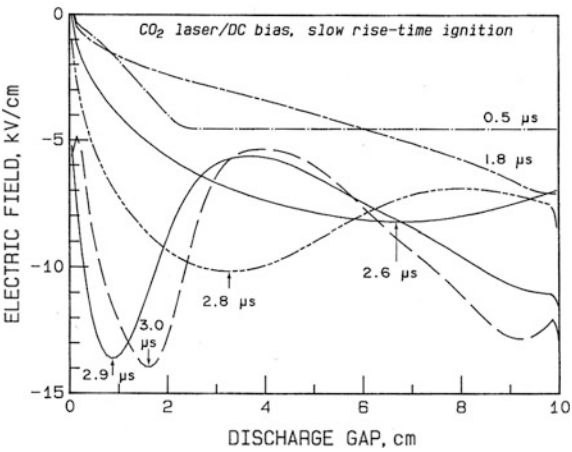

Fig. 21.4 Computed E-field during preionization and ignition of a CO_2-laser gas mixture; each arrow locates the crest of the cathode-directed ionization wave at a particular instant

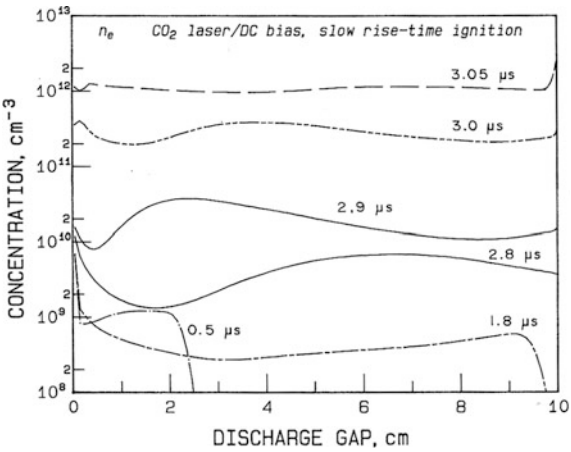

Fig. 21.5 n_e evolution corresponding to Fig. 21.4

at t = 0.5 μs and almost reaches the anode at t = 1.8 μs; the negative space charge present at the conclusion of the filling phase distorts the field so that it is largest at the anode (E = 7.1 kV/cm). In the absence of this space charge, the electric field would be uniform across the gap and equal to 4.0 kV/cm. As $U_d(t)$ increases, electron avalanche begins within the local region of highest field strength. A cathode-directed ionization wave with a velocity $\sim 10^7$cm/s develops near the anode at $t \sim$ 2.5 μs, accelerates, and reaches the cathode at $t \sim$ 2.95 μs. After passage of the first cathode-directed wave, the region of maximum plasma conductivity is adjacent to the cathode and the maximum electric field again occurs near the anode, launching a second ionization wave just prior to discharge ignition (curve labelled t = 3.0 μs). These waves then relax and establish a homogeneous SSVD at $E_{qs} = U_{qs}/g$, which is typically 20 % smaller than the value predicted in Sect. 21.3 by neglecting Penning ionization. In addition, the presence of these waves decreases the minimum ignition field E_{min} by $\sim$30–40 %.

Evolution of the N_2 metastable concentration with time is shown in Fig. 21.6. n_m is initially largest at the anode and the peak value follows the spatio-temporal evolution of the electric field more closely than n_e. Lastly, spatially dependent concentrations of all species at the time corresponding to imminent arrival of the first ionization wave at the cathode are shown in Fig. 21.7. It is important to note that for the present conditions, the concentration of negative ions has little influence upon discharge development. This situation is misleading, since gas impurities (e.g., O_2, H_2O) and secondary reaction by-products (CO, NO_x) typically found in recirculating-flow systems have not been included in this computation. Additional computational studies show that a high concentration of NO_x, for example, impedes transport of the electron beam and greatly alters the discharge ignition mechanism. Negative ions become the principal negative charge carrier and establishment of a stable SSVD is unlikely.

Identical computer runs have been performed with the addition of VUV preionization through a mesh anode structure, consisting of a fast rise time

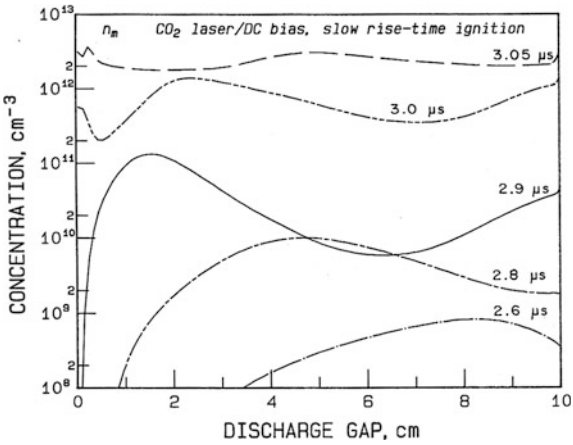

Fig. 21.6 n_m evolution corresponding to Fig. 21.4

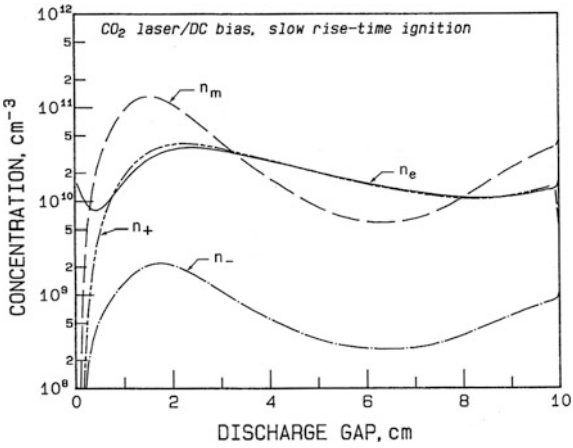

Fig. 21.7 Species concentrations at t = 2.9 μs for the CO_2-laser discharge

(t_1 = 100 ns), exponential decay (t_2 = 750 ns) source that produces an in-band (~160 nm) VUV photon energy density of 2 μ J/cm^2. If the VUV source is fired during the rise in discharge voltage ($t_d \sim t_{bias} + t_r/2$), then sufficient positive space charge is generated adjacent to the anode to shift the peak electric field and, hence, the origin for the cathode-directed ionization wave into the mid-gap region. Since the duration of the VUV source is characteristically less than the discharge voltage rise time, anode space-charge screening does not persist throughout the ignition period. Simultaneous cathode- and anode-directed waves form and dissipate prior to the realization of quasi-equilibrium conditions.

21.4.2 N_2O Lasers

Advancement of N_2O lasers has been frustrated by the highly electronegative nature of representative gas mixtures. The threshold energy for the dissociative attachment reaction

$$N_2O + e^- \rightarrow N_2 + O^- \tag{21.26}$$

is very low ($E_{thr} = 0.15$ eV) and the weighted rate coefficient is quite large ($k_a \sim 10^{-11}$ cm^3/s) over a wide range ($E/N = 10 - 100$ Td). This forces the discharge to operate at high E_{qs}/N values in self-sustained devices (cf. Fig. 21.3), which is non-optimal both for the excitation of the upper laser level and for retarding instabilities. These instabilities induce striations that degrade discharge homogeneity and severely limit the specific input and output energies. Furthermore, operation of an auxiliary discharge in this environment is not possible since the electron flux would be immediately depleted even for very small E_0.

Electron losses due to dissociative attachment can be offset by electron detachment involving the principal negative ion and added CO gas:

$$O^- + CO \rightarrow CO_2 + e^-, \tag{21.27}$$

where $k_d = 5.5 \times 10^{-10}$cm^3/s. The electron attachment and detachment frequencies approximately balance when the ratio of molecular gases $[CO]/[N_2O] \sim 4$. Significant improvements in laser output energy, specific input and output energies, and discharge efficiency have been reported using the auxiliary-discharge technique [38].

Numerical simulations were performed for an N_2O:CO:N_2:He = 3:10:10:47 gas mixture ($T = 293$ K, $P = 450$ Torr), which contained an admixture of TPA ($P_{ri} = 0.9$ Torr). The interelectrode gap is $g = 10$ cm. Cathode and anode YUY preionization are absent. The discharge initiation scheme is described by auxiliary preionization in the presence of a quasi-dc field followed by application of a slow-ignition voltage pulse ($t_{bias} = 2.2$ μs, $t_r = 2$ μs, $J_{aux} = 1$ mA/cm^2, $U_{bias} = 24$ kV, and $U_{pk} = 96$ kV). Progress of the auxiliary-discharge electron flux can be tracked in Fig. 21.8, which shows the computed electric-field distribution for selected times. The electron flux reaches $x \sim 2$ cm at $t = 0.5$ μs and the anode at $t = 2.2$ μs. Negative space charge present at the end of the filling phase distorts the field so that it is largest at the anode ($E = 4.2$ kV/cm). In the absence of this space charge, the electric field would be uniform across the gap and equal to 2.4 kV/cm. A cathode-directed ionization wave develops near the anode at $t \sim 3.2$ μs, accelerates, and reaches the cathode at $t \sim 3.5$ μs, i.e., before the peak discharge voltage is reached. This phenomenon is completely analogous to that observed experimentally and computationally with CO_2 lasers employing auxiliary-discharge preionization. However, the E-field amplitude of the ionization wave is typically not as large.

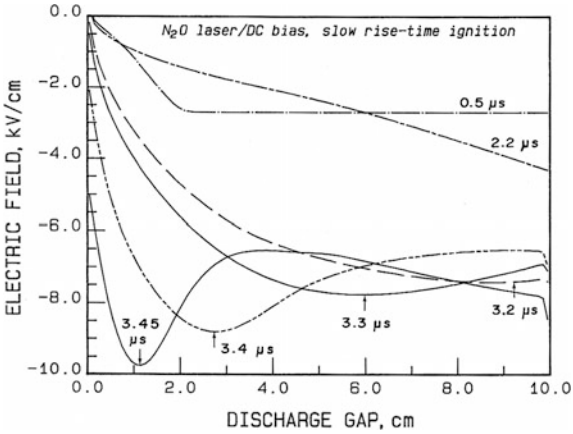

Fig. 21.8 Computed *E*-field during preionization and ignition of an N_2O-laser gas mixture

The spatially dependent concentrations of all species at the time corresponding to imminent arrival of the ionization wave at the cathode are shown in Fig. 21.9. The negative-ion concentration is larger than observed with typical CO_2-laser simulations, but still only about one-tenth of the electron concentration. Thus, the presence of CO largely compensates for the strongly attaching nature of the N_2O component. The metastable N_2 concentration, however, is greatly reduced. Ignition simulations in typical CO_2-laser discharges yield $n_m > 10^{11}$ cm^{-3} at the crest of the ionization wave while the peak value here is $n_m = 7 \times 10^9$ cm^{-3}. Hence, strong quenching by N_2O reduces the metastable concentration to levels that are insignificant and Penning ionization of the readily ionizable additive is ineffective. This is confirmed by experiments where these compounds had no effect on either U_{min} or U_{qs} in SSVD N_2O-laser gas mixtures [38].

The importance of electron detachment via reaction (27) is demonstrated by an additional simulation with $k_d = 0$. Negative ions immediately become the principal

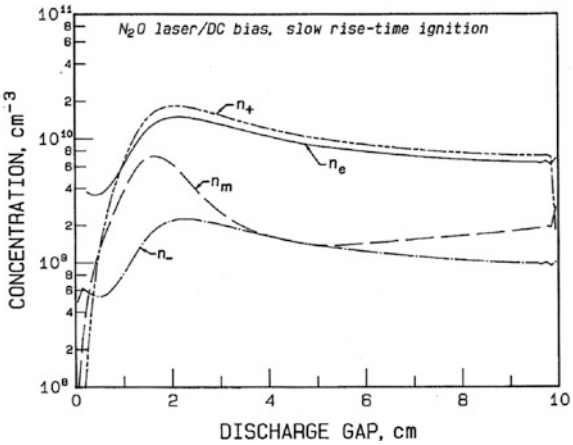

Fig. 21.9 Species concentrations at $t = 3.45$ μs for the N_2O-laser discharge

negative charge carrier and the preionization front stalls adjacent to the cathode. Even a dramatic increase in U_{bias} was unable to transport these negative ions across the gap in a reasonable time ($t \sim t_{bias}$) since $\mu_- < \mu_e$. Therefore, the processes of preliminary filling of the discharge gap with an electron flux from an auxiliary discharge, dynamic profiling of the E-field distribution, and ignition via ionization waves are only possible in N_2O lasers with optimized gas mixtures.

21.5 Discussion and Conclusions

The processes of preliminary filling of the discharge gap with electrons, dynamic profiling of the electric field, discharge ignition, and establishment of an SSVD occur under conditions of greatly reduced cathode field and absence of the usual cathode fall layer. Electrons are continuously supplied by the auxiliary discharge and an electron flux flows through the cathode boundary layer. To obtain the maximum benefit from the dynamic profiling process, it is important that the gap be completely filled with preionization electrons; the electron flux must reach the anode prior to electron avalanche and discharge ignition. However, the requirements for a minimum preionization concentration and for complete filling of the gap are necessary but insufficient conditions for the formation of ionization waves. Although the location of the field maximum will occur at the anode for any value of $E_0 < E_{sb}$, a cathode-directed ionization wave will not form if E_0 is too small, regardless of whether or not the gap is completely filled with preionization electrons. To ensure optimal efficacy of discharge ignition utilizing the dynamic profiling phenomenon, E_0 should be adjusted so that $E(g, t_{dr})$ is just below the threshold for ionization avalanche. ($E_0 \sim E_{sb}/3$ is usually satisfactory.) This requirement is also necessary to remain in a regime where losses due to dissociative attachment are negligible. The low-current, low-energy electron beam extracted from the auxiliary discharge can therefore progress across the discharge gap unimpeded.

Only cathode-directed waves are possible if the gap is completely filled with electrons during the preionizarion phase. If incomplete filling occurs, or if a VUV source at the anode is fired during the rise in applied voltage [5], both cathode- and anode-directed waves are formed. These model predictions are in good agreement with observations of ionization-wave behavior made using an image-converter camera [8, 10]. The combination of ionization waves and Penning ionization involving metastable species reduces the ignition voltage by 30–40 % compared with fast-pulse, VUV-preionized discharges. The presence of readily ionizable additives also decreases the quasi-steady discharge voltage and promotes discharge stability by reducing the growth rate for the multistep-ionization instability [12].

Complete depletion of electrons from the cathode region and accumulation of a large positive space charge in the cathode boundary layer are prevented by continued preionization during the ignition process. For auxiliary barrier discharge sources ($J_{aux} < 1$ mA/cm^2), maintenance of the negative space-charge screen

requires a rate of voltage rise of $dU_d/dt < 10$ kV/μs [10]. *Higher-productivity* auxiliary surface discharges [13] can relax this requirement ($dU_d/dt < 30$–40 кV/μs) and are especially significant in large-aperture systems. By shifting the region of ionization avalanche into the mid-gap, mid-electrode region, distortions and perturbations to the electric field within the boundary layers have minimal impact upon SSVD stability, which permits the use of unprofiled electrodes.

Acknowledgments This part of the book had been prepared together with Dr. R.E. Beverly III on the experimental basis created by our team from Prokhorov GPI RAS.

References

1. V.V. Apollonov et al., Sov. J. Quantum Electron. **15**, 1–3 (1985)
2. V.V. Apollonov, N. Akhunov, G.G. Baitsur, A.M. Prokhorov, in *Proceedings International Conference on LASERS'85* (Las Vegas, Nevada 1985), pp. 681–687
3. V.V. Apollonov et al., Sov. Tech. Phys. Lett. **11**, 521–523 (1985)
4. V.V. Apollonov et al., Sov. J. Quantum Electron. **16**, 1680–1682 (1986)
5. V.V. Apollonov et al., Sov. J. Quantum Electron. **16**, 1294–1295 (1986)
6. V.V. Apollonov et al., Sov. J. Quantum Electron. **17**, 76–82 (1987)
7. V.V. Apollonov et al., Sov. J. Quantum Electron. **17**, 134–135 (1987)
8. V.V. Apollonov et al., Sov. Tech. Phys. Lett. **13**, 230–231 (1987)
9. V.V. Apollonov et al., Sov. J. Quantum Electron. **17**, 1364–1365 (1987)
10. V.V. Apollonov et al, Small signal gain of CO_2-lasers pumped by SSVD, in *International Conference on Lasers-87*, Lake Tahoe, 495–501 (1987)
11. V.V. Apollonov et al., Sov. J. Quantum Electron. **18**, 321–325 (1988)
12. V.V. Apollonov et al., Sov. J. Quantum Electron. **18**, 351–354 (1988)
13. V.V. Apollonov et al., Sov. Tech. Phys. Lett. **14**, 241–242 (1988)
14. V.V. Apollonov et al., Instrum. Exp. Technol. **32**, 149–152 (1989)
15. V.V. Apollonov et al., Sov. Tech. Phys. Lett. **14**, 915–916 (1988)
16. V.V. Apollonov et al., Ultraviolet-preionized volume self-sustained discharge in a volume of 400 liters, paper scheduled for presentation at Pulse Power for Lasers III (Los Angeles 1991); in *Proceedings of the SPIE* **1411**
17. V.V. Apollonov et al., New principles and techniques of SSVD formation in high-power molecular lasers, paper scheduled for presentation at Pulse Power for Lasers III (Los Angeles 1991); in *Proceedings of the SPIE* **1411** (to be published)
18. R.E. Beverly III, Modeling of ignition phenomena in transverse discharges preionized by an auxiliary discharge, in *Proceedings of the XIII International Conference on Coherent and Nonlinear Optics* (Minsk, BSSR 1988), vol. IV, pp. 29–30
19. R.E. Beverly III, Enhanced transverse discharge stability using preionization from an auxiliary barrier discharge, in *Seventh International Symposium on Gas Flow and Chemical Lasers (Wien 1988); Proc SPIE* **1031,** 458–466 (1989)
20. R.E. Beverly III: Pulsed power modeling of very-large-aperture, transverse-discharge CO_2 Lasers. Appl. Phys. B 53 (1991)
21. N. Sato, J. Phys. **D13**, L3–L6 (1980)
22. S.T. Zalesak, J. Comput. Phys. **31**, 335–362 (1979)
23. R. Morrow, J. Comput. Phys. **43**, 1–15 (1981)
24. R. Morrow, L.E. Cram, J. Comput. Phys. **57**, 129–136 (1985)
25. P. Steinle, R. Morrow, J. Comput. Phys. **80**, 61–71 (1989)
26. P. Steinle, R. Morrow, A.I. Roberts, J. Comput. Phys. **85**, 493–499 (1989)

27. R. Morrow, J. Comput. Phys. **46**, 454–461 (1982)
28. W.L. Morgan, B.M. Penetrante, Comp. Phys. Commun. **58**, 127–152 (1990)
29. V.V. Apollonov et al., Sov. Tech. Phys. Lett. **6**, 450–452 (1980)
30. L.G. Piper, J. Chem. Phys. **87**, 1625–1629 (1987)
31. D.F. Grosjean, P. Bletzinger: IEEE J. QE-13, 898–904 (1977)
32. A. Goehlich, W. Terbeck, H.F. Dobele, Rev. Sci. Instrum. **58**, 701–703 (1987)
33. I.M. Littlewood, M.C. Cornell, K.J. Nygaard, J. Chem. Phys. **81**, 1264–1270 (1984)
34. R.E. Beverly III, Opt. Quantum Electron. **14**, 501–513 (1982)
35. H.W. Ellis, R.Y. Pai, E.W. McDaniel, E.A. Mason, L. Viehland, At. Data Nucl. Data Tables **17**, 177–210 (1976)
36. H.W. Ellis, E.W. McDaniel, D.L. Albritton, L.A. Viehland, S. Lin, E.A. Mason, At. Data Nucl. Data Tables **22**, 179–217 (1978)
37. E.W. McDaniel, E.A. Mason, *The Mobility and Diffusion of Ions in Gases* (Wiley, New York, 1973), p. 159
38. V.V. Apollonov et al., Sov. J. Quan-tum Electron. **19**, 839–840 (1989)

Chapter 22
Modeling of Large-Aperture CO_2-Lasers

Abstract Transverse-discharge excitation of large-aperture CO_2 lasers places demanding and unusual constraints on the pulsed power supply. Stable discharges with interelectrode gaps as large as g = 70 cm were achieved using pulsed power supplies that satisfy specific requirements imposed by volume preionization and discharge ignition. The supply must initially apply a quasi-DC or slow-rise voltage to in order to effect preliminary filling of the gap with electrons from an auxiliary discharge, followed by application of a controlled rise voltage to ignite an SSVD. A coupled particle kinetics-equivalent circuit model has been developed to simulate discharge behavior for the various pulsed power configurations. Computational results are compared with experiments involving very-large-aperture, large-volume devices.

An excitation of large-aperture CO_2 lasers places demanding and unusual constraints on the pulsed power supply. Stable discharges with interelectrode gaps as large as g = 70 cm were achieved [1, 2] using pulsed power supplies [3] that satisfy specific requirements imposed by volume preionization and discharge ignition. The supply must initially apply a quasi-DC or slow-rise voltage to effect preliminary filling of the gap with electrons from an auxiliary discharge, followed by application of a controlled rise voltage to ignite an SSVD. A coupled particle kinetics-equivalent circuit model has been developed to simulate discharge behavior for the various pulsed power configurations. Computational results are compared with experiments involving very-large-aperture, large-volume devices [1–4].

© Springer International Publishing Switzerland 2016

V.V. Apollonov, *High-Energy Molecular Lasers*,
Springer Series in Optical Sciences 201, DOI 10.1007/978-3-319-33359-5_22

22.1 Excitation Waveform Requirements

22.1.1 Single-Pulse Waveforms

Three types of voltage waveforms have been used to establish SSVDs in CO_2-laser gas mixtures that are preionized by auxiliary discharges. As illustrated by the waveform shown in Figure la, the first method uses a continuously increasing applied voltage (rise time t_r) to sweep electrons generated by the auxiliary discharge across the main transverse gap and to ignite the discharge. The induced electron drift velocity is zero when the auxiliary discharge is initially fired and then increases as the voltage applied across the main gap $U_d(t)$ rises. Preliminary filling should be complete before discharge ignition [5, 6], which requires that

$$t_r \geq (3/2)t_{dr} \cong \frac{9g^2}{4\mu_e U_{pk}}. \tag{22.1}$$

Here t_{dr} is the characteristic drift time, μ_e is the electron mobility, and U_{pk} is the peak discharge voltage.

The second method, as illustrated by the waveform in Fig. 22.1b, involves the application of a quasi-DC bias voltage U_{bias} for a duration that approximates or exceeds t_{dr}, i.e.,

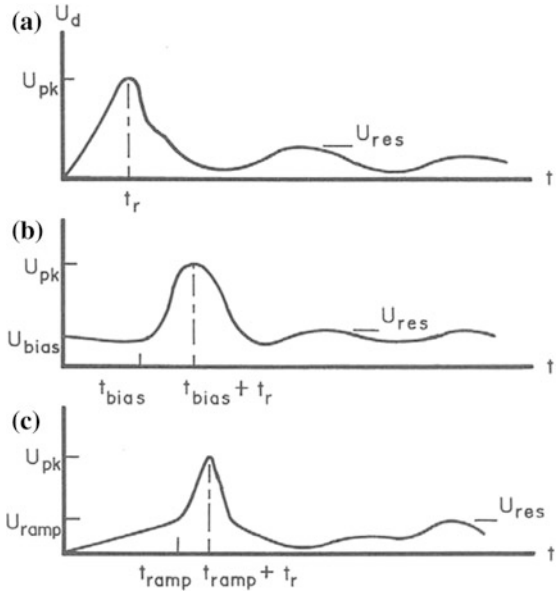

Fig. 22.1 **a–c** Voltage waveforms for single-pulse excitation: smoothly rising leading edge **a**; smoothly rising leading edge with preapplied quasi-DC bias, (**b**); an ramped bias voltage followed by smoothly rising leading edge (**c**) [3]

$$t_{\text{bias}} \geq t_{\text{dr}} = \frac{g^2}{\mu_{\text{e}} U_{\text{bias}}}. \tag{22.2}$$

The value chosen for the quasi-DC bias field, $E_{\text{bias}} = U_{\text{bias}}/g$, must be large enough to transport electrons across the gap in a reasonably short time but small enough to avoid operation in an *E/N* regime where losses due to dissociative attachment are a problem. The preionization phase is followed by a gradually rising voltage to ignite the discharge. Sensible current begins to flow across the main gap at or just prior to the time of maximum applied voltage. The voltage rise time is again defined as t_{r} and its value must be of sufficient duration to avoid premature depletion of the cathode space-charge layer during ignition; hence, there is a maximum rate of voltage rise,

$$\left.\frac{\mathrm{d}U_d}{\mathrm{d}t}\right|_{\max} = f(\text{gas composition}, P, J_{\text{aux}}), \tag{22.3}$$

that should not be exceeded. P is the total gas pressure, and J_{aux} is the current density produced by the auxiliary discharge for a duration t_{aux}. This method can lead to problems if the space-charge screen is suddenly depleted during commutation of the U_{bias} potential; this phenomenon occurs if the condition

$$E_{\text{cf}} \ll E_{\text{bias}} \tag{22.4}$$

is violated, where E_{cf} is the field associated with the cathode fall. Condition (4) can be satisfied if U_{bias} is sufficiently small (which may not be practical) or if the auxiliary discharge is fired prior to commutation of U_{bias}.

The third method uses a slowly increasing ramp voltage waveform to transport the preionizing electrons across the interelectrode gap, followed by a more steeply increasing voltage to ignite the discharge (Fig. 22.1c). The voltage initially increases from zero to U_{ramp} at $t = t_{\text{ramp}}$ and then increases more abruptly to U_{pk} over a duration t_{r}. This method avoids those problems associated with the sudden application of a quasi-DC bias at $t = 0$.

22.1.2 Double-Pulse Waveforms

With this method, any of the three waveform types described previously in Sect. 22.1.1 is used to establish a low-current, quiescent SSVD. This plasma acts as a prepared load for discharge of a second, fast-pulse power supply. The fast-pulse circuit is optimized for maximum electrical efficiency.

22.1.3 Minimum Ignition Voltage

A necessary but insufficient condition for discharge stability is

$$U_{pk} \geq \zeta U_{sb}, \tag{22.5}$$

where $U_{sb}(E_{sb})$ is the self-breakdown voltage (field) for unprofiled electrodes. U_{sb} is approximately half the selfbreakdown value measured for profiled electrodes having a uniform electric-field distribution. The factor ζ is stipulated differently depending upon the particular citation: $\zeta = 1.8$ for $g < 10$ cm [7] and $\zeta \sim 1.1$–1.3 for $g = 20$–60 cm [3]. Operation with $U_{pk} < \zeta\ U_{sb}$ causes arcs that occur shortly after the time of voltage maximum if the auxiliary discharge is on, and during the voltage rise if the auxiliary discharge is off or if $t_{aux} < t_r$.

22.2 Coupled-Particle Kinetics-Equivalent Circuit Model

The behavior of a pulse forming network (PFN) that provides the requisite voltage waveforms can be predicted by modeling the equivalent circuit shown in Fig. 22.2. The constitutive equations for circuit voltages and currents are

$$\frac{dU_1}{dt} = -\frac{I_1}{C_1}, \tag{22.6}$$

$$\frac{dU_2}{dt} = -\frac{I_1 - I_2}{C_2}, \tag{22.7}$$

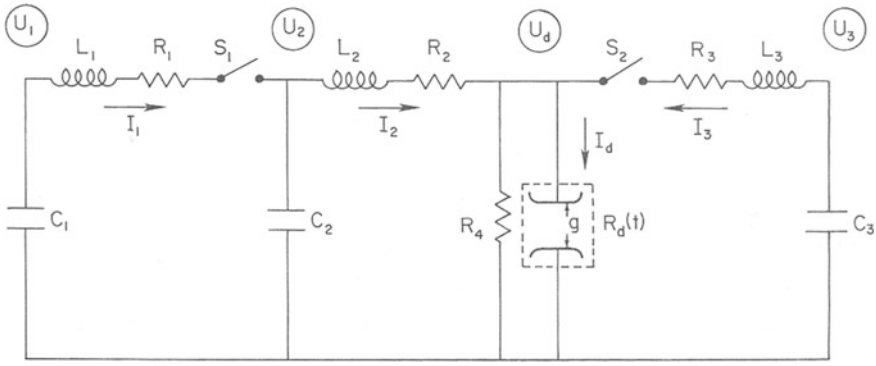

Fig. 22.2 Equivalent-circuit schematic diagram

$$\frac{\mathrm{d}U_3}{\mathrm{d}t} = -\frac{I_3}{C_3}, \tag{22.8}$$

$$\frac{\mathrm{d}I_1}{\mathrm{d}t} = \frac{U_1 - R_1 I_1 - U_2}{L_1}, \tag{22.9}$$

$$\frac{\mathrm{d}I_2}{\mathrm{d}t} = \frac{U_2 - R_2 I_2 - U_\mathrm{d}}{L_2}, \tag{22.10}$$

$$\frac{\mathrm{d}I_3}{\mathrm{d}t} = \frac{U_3 - R_3 I_3 - U_\mathrm{d}}{L_3}. \tag{22.11}$$

The prolonged voltage rise necessary for dynamic profiling of the electric field is produced by the PFN, which consists of capacitors C_1 and C_2 and inductors L_1 and L_2. R_1 and R_2 represent resistive losses associated with the transmission lines and switchgear. Switch S_1 is commuted at $t = 0$, which initiates discharge of energy-storage capacitor C_1. A second, fast rise-time voltage is superimposed upon the transverse gap at a later time by commuting switch S_2 at $t = t_\mathrm{f}$. This initiates discharge of energy-storage capacitor C_3. R_3 represents resistive line and switch losses and resistor R_4 is necessary to ensure reproducible switch closure and to partially reduce circuit ringing. These equations must be solved simultaneously with equations describing the electron, negative-ion, and N_2, metastable densities:

$$\frac{\mathrm{d}n_\mathrm{e}}{\mathrm{d}t} = (\bar{k}_\mathrm{i} - \bar{k}_\mathrm{a})n_\mathrm{e}N - k_\mathrm{r}^\mathrm{ei} n_\mathrm{e} n_+ + \bar{k}_\mathrm{d} n_- N + \frac{n_\mathrm{m}}{\tau_\mathrm{p}}, \tag{22.12}$$

$$\frac{\mathrm{d}n_-}{\mathrm{d}t} = \bar{k}_\mathrm{a} n_\mathrm{e} N - \bar{k}_\mathrm{d} n_- N - k_\mathrm{r}^\mathrm{ii} n_+ n_-, \tag{22.13}$$

$$\frac{\mathrm{d}n_m}{\mathrm{d}t} = k_\mathrm{m} n_\mathrm{e}[N_2] - \frac{n_\mathrm{m}}{\bar{\tau}}, \tag{22.14}$$

where n represents particle concentration (particles/cm^3) and the subscripts e, +, −, and m denote electrons, positive ions, negative ions, and metastable species, respectively. Processes (and rate coefficients) include primary electron-impact ionization (k_i), electron attach-ment (k_a), electron detachment (k_d), electron-ion recom-bination (k_r^ei), ion-ion recombination (k_r^ii), and N_2 *a*-state excitation (k_m). The bar notation indicates rate coefficients, which are weighted for the particular gas mixture and which are functions of the local value of the reduced electric field *E/N,* where N is the total particle concentration. N_2 is the nitrogen gas concentration (constant). $\bar{\tau}$ is the characteristic time for collisional deactivation of the metastable level (weighted for the particular gas mixture) and τ_p is the characteristic time for Penning collisions; $1/\tau_\mathrm{p} = k_\mathrm{p} N_\mathrm{ri}$, where N_ri is the concentration of readily ionizable molecules such as tri-*n*-propylamine (TPA). The positive-ion density is found by assuming charge neutrality in the positive column:

$$n_+ = n_e + n_-. \tag{22.15}$$

The initial conditions for the system of ordinary differential equations (ODEs) are

$$U_1(0) = U_c, \tag{22.16}$$

$$U_2(0) = U_d(0) = U_{bias}, \tag{22.17}$$

$$U_3(0) = U'_c, \tag{22.18}$$

$$I_1(0) = I_3(0) = I_d(0) = 0, \tag{22.19}$$

$$I_2(0) = U_{bias}/R_4, \tag{22.20}$$

$$n_e(0) = n_{e0}, \tag{22.21}$$

and

$$n_-(0) = n_m(0) = 0, \tag{22.22}$$

where U_e is the charging voltage on capacitor C_1, U'_e is the charging voltage on capacitor C_3, and n_{e0} is the initial electron density. U_{bias} is the quasi-DC bias voltage applied to the gap prior to closure of either switch or S_2. If $U_{bias} > 0$, then a quasi-DC field was used to sweep preionizing electrons across the interelectrode gap and the initial potentials on capacitor C_2 and the discharge gap were equal to U_{bias}. The duration of this preionization process ($\sim t_{dr}$) does not enter into the present model since we assume that the entire interelectrode gap is uniformly filled with electrons with density n_{e0} at $t = 0$. The discharge voltage and current are

$$U_d(t) = \frac{I_2 R_4 R_d}{R_4 + R_d} \tag{22.23}$$

and

$$I_d(t) = I_2 - \frac{U_d}{R_4}. \tag{22.24}$$

The discharge resistance is related to the electron density by

$$R_d(t) = \frac{g}{e\mu_e n_e A}, \tag{22.25}$$

where e is the electronic charge and A is the effective discharge area. The contribution to plasma conductivity by positive- and negative-ion species is small and is neglected in (22.25). Since $\mu_e = \mu_e(E/N)$, (22.25) must be solved iteratively and self-consistently along with (22.6–22.15). The bias voltage, if nonzero, is small

enough that the discharge gap is initially non-conductive, i.e., $R_d(0) \gg R_4$. The instantaneous power supplied to the discharge is

$$P_d(t) = U_d(t) I_d(t), \tag{22.26}$$

the energy dissipated in the discharge is

$$E_d = \int P_d(t) dt, \tag{22.27}$$

the electrical efficiency is

$$\eta_{e1} = 2E_d/(C_1 U_e^2 + C_2 U_{bias}^2 + C_3 U_e'^2, \tag{22.28}$$

and the specific input energy is

$$\xi_i = E_d/V, \tag{22.29}$$

where V is the disharge volume.

With this model, we have the option of simulating either double-pulse excitation using the entire circuit or single-pulse excitation using the reduced-form equivalent circuit (by setting $t_f = \infty$). The system of differential equations was coded for computer solution using a robust ODE solver (LSODE from the Lawrence Livermore ODEPACK collection [8]). Rate and transport coefficients were determined separately by solution of the Boltzmann equation at tabulated values of *E/N* and then determined within the code using a fourth-order (cubic) Lagrangian interpolator [5].

22.3 Pulsed Power Systems

Both Marx [3, 9] and Fitch-Howell [3, 10] pulse generators, with suitable modifications, have been used to produce the waveform types shown in Fig. 22.1. The equivalent circuit in the present model (Fig. 22.2) is applicable only to the former system. To produce the voltage waveform with a smoothly rising leading edge (Fig. 22.1a), the PFN parameters are adjusted so that

$$t_r \approx \pi \left(\frac{L_1 C_1}{4} \right)^{1/2}, \tag{22.30}$$

where $C_1 = C/N_s$ is the equivalent Marx bank capacitance, C is the capacitance of each stage, and N_s is the number of stages. The equivalent charging voltage is then

$U_c = N_s U_g$, where U_g is the actual generator charging voltage. Apollonov et al. [3] typically use $C_2 = C/N_s$, so the discharge current period is

$$T \approx 2\pi (L_2 C_2)^{1/2}. \tag{22.31}$$

The voltage waveform with a quasi-DC bias (Fig. 1b) is produced simply by charging capacitor C_2 to voltage U_{bias} and inserting the main switch between C_2 and the discharge. No isolation switch is necessary between the Marx bank and C_2 if $U_{bias} = U_g$. The voltage waveform with an initial ramp to U_{ramp} (Fig. 22.1c) is produced by substituting a two-stage *LC* circuit for the single capacitor C_2.

22.4 Computational Results

22.4.1 Single-Pulse Excitation Without Quasi-DC Bias

The rise time t_r (cf. Fig. 22.1a) is adjusted by varying the ratio of PFN inductances, here expressed by the dimensionless parameter

$$M = \frac{L_1}{L_2}. \tag{22.32}$$

To achieve a deliberately prolonged rise time for practical devices, however, it is often necessary to increase M to a value for which impedance matching between the PFN and load is poor. Typically, the PFN impedance is larger than the load (laser discharge) and the voltage waveform oscillates as shown by the example in Fig. 22.3. This computation was performed for a small (g = 10 cm, A = 400 cm^2), atmospheric-pressure (CO_2:N_2:He = 1:4:5) device with electrical parameters C_1 = 0.25 μF, C_2 = 0.1 μF, U_c = 120 kV, L_1 = 35 μH, L_2 = 1 μH, $R_1 = R_2$ = 10 m Ω, R_4 = 2 k Ω; also, n_{e0} = 10 cm^{-3} and P_{ri} = 0.75 Torr (TPA). If U_{res} is defined as the amplitude of the second or *residual* voltage peak that occurs at time t_{res} and if U_{qs} is defined as the discharge voltage at peak discharge current, then it is useful to find the electrical circuit parameters that minimize the dimensionless parameter

$$Q = \frac{U_{res}}{U_{qs}}. \tag{22.33}$$

I_{pk} is the peak current that occurs at time t_{pk} and t_{qs} is defined by the full width at half maximum (FWHM) current pulse width. In this example, Q = 0.61, E_{qs} = 10 kV/cm, I_{pk} = 13 kA, t_{qs} = 0.8 μs, η_{el} = 66%, and ξ_i = 297 J/l.

U_{res} can be reduced by decreasing the parallel resistance R_4, but this occurs at the expense of reduced electrical efficiency. For example, the device in [11] employed a CO_2:N_2:He = l:4:5 gas mixture at atmospheric pressure with g = 10 cm and A = 400 cm^2. Stated circuit parameters were C_1 = 0.25 μF, C_2 = 0.1 μF, U_c = 120

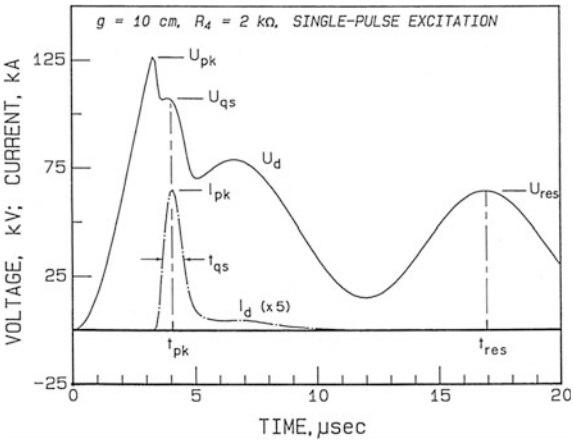

Fig. 22.3 Representative I_d — U_d waveforms for single-pulse excitation and definition of nomenclature

κV, $L_1 \sim$ 15–20 μH, $L_2 \sim$ 1 μH, and $R_4 = 75/N_r\ \Omega$, where N_R is an unspecified number of resistors in parallel. The small value of R_4 helps to prevent discharge voltage ringing and arc formation after the glow period. The choice of N_R strongly effects the computed value of I_{pk} and $N_R = 2$ gave the best agreement with experiment. Assumed parameters were $R_1 = R_2 = 10$ mQ, $n_{e0} = 10^7$ cm^{-3}, and $P_{ri} = 0.75$ Torr (TPA). Computations performed with these parameters gave values of t_r and t_{pk} that were too short, indicating that M was too small. By increasing to 35 μF (i.e., $M = 35$), voltage and current waveforms (Fig. 22.4) were obtained in approximate qualitative and quantitative agreement with measurements (the computations depicted in Figs. 22.3 and 22.4 are therefore identical, with the exception of R_4). The principal discrepancy is between the computed ($t_{qs} = 0.9$ μs) and experimental ($t_{qs} = 1.4$ μs) current pulse widths, which is probably related to two-dimensional effects, such as the current density distribution across the

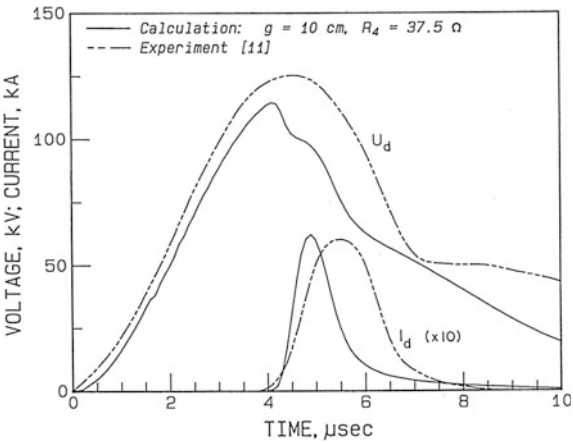

Fig. 22.4 Computed and measured $I_d - U_d$ waveforms for the device described in [11]

electrodes. This circuit is poorly designed, with η_{e1} = 34% and ξ_i = 153 J/l. The importance of Penning ionization of the readily ionizable additive is illustrated by a computational experiment with the N_2 metastable kinetics turned off. In this case, $I_{pk} < 2$ kA.

It is useful to examine parametric regions where Q can be maintained below a specified minimum, i.e., $Q < Q_{min}$. For each value of Q_{min} there exists an $M_{max} = M(Q_{min})$ at which it is still possible to obtain $Q < Q_{min}$. In the paper [9], it was found that M_{max} is only weakly dependent upon L_1, L_2, $C_1 = C_2$, g, A or n_{e0}. In addition, there exists a maximum value of t_r for each Q_{min}, $t_{r,max}$, given by

$$t_{r,max}(Q_{min}) = \pi\left(\frac{L_2 C_1 M_{max}}{4}\right)^{1/2}. \tag{22.34}$$

$t_{r,max}$ can be increased by increasing inductance L_2, but this also increases the discharge current pulse width. The duration of the SSVD can be crudely bounded by the duration of the discharge half-period [cf. (22.31)], i.e.,

$$t_{qs} \geq T_{1/2} = \pi(L_2 C_2)^{1/2}. \tag{22.35}$$

Combining (34) and (35) yields the condition

$$t_{r,max} \leq t_{qs}\left(\frac{M_{max}}{4}\right)^{1/2}. \tag{22.36}$$

Thus, the maximum voltage rise time is limited by the requirement to deposit energy into the VSD efficiently. The maximum permissible discharge gap can be estimated from the requirement for complete electron filling during the preionization phase as discussed previously, hence

$$g_{max} \cong (0.3 - 0.4)\mu_e t_{r,max} U_c/g, \tag{22.37}$$

where the numerical factor arises from the necessity to complete the preliminary filling process prior to discharge ignition. If we desire t_{qs} = 5 μs and Q_{min} = 0.3, then $t_{r,max} \sim 15$ μs. Using representative values of $\mu_e = 10^3$ cm^2/V-s and $U_c/g \sim 2U_{qs}/g$ = 10 kV/cm, we obtain g_{max} = 40–50 cm for atmospheric-pressure operation. The largest experimental values of g for this type of excitation are indeed comparable to this estimate [1–3]. Arc-free SSVDs in a 60 cm gap could only be obtained with a 50% probability by means of single-pulse excitation [1]. Note that (37) applies *only* for single-pulse excitation without quasi-DC bias.

22.4.2 Single-Pulse Excitation with Quasi-DC Bias

In this type of excitation, the processes of preionization and discharge ignition are separate (cf. Fig. 22.1b) and there is no maximum rise-time condition analogous to

(34). Instead, there exists a maximum rate of voltage rise $dU_d/dt|_{max}$, which produces consequential depletion of the negative space-charge layer covering the cathode. Operation with $dU_d/dt > dU_d/dt|_{max}$ spoils the dynamic profiling process [cf. (3)] and reduces the probability for establishing a stable, homogeneous VSD. For auxiliary barrier discharges, $dU_d/dt|_{max} \sim 10$ kV/μs [9]. By replacing the auxiliary barrier discharge with an auxiliary surface discharge, the maximum rate of voltage rise could be increased to $dU_d/dt|_{max} \sim 30$–40 kV/μs [2]. This attests to a higher productivity (larger J_{aux}) by the surface discharge and allows a decrease in t_r.

The current–voltage characteristics of a 50–1 device were numerically simulated to better understand the electrical design constraints that accompany this type of excitation. The parameters chosen for three cases are listed in Table 22.1 and would be typical of a 5-stage Marx bank. Case (a) is described by $E_s/V \equiv \xi_i/\eta_{el} = 200$ J/L (i.e., ideal operation of this circuit would produce a specific input energy of 200 J/l) and by a peak discharge voltage that is above the ignition threshold but below the value for impedance matching. By varying L_1 from 2 to 200 μH (M = 1 to 100), t_r can be adjusted over about one order of magnitude. Computational results clearly show that although the discharge efficiency η_{el} initially increases with increasing rise time (Fig. 22.5), circuit ringing is a persistent problem and no value of M produces $Q < 0.3$ (Fig. 22.6). t_{qs} increases gradually as a function of t_r and approaches the asymptote $T_{1/2} = 2.2$ μs. I_{pk} increases rapidly with t_r, reaches a maximum at $t_r \sim 3$ μs ($I_{pk} = 33$ kA), and then decreases gradually. The minimum degree of circuit ringing (Q = 0.34) and the maximum electrical efficiency ($\eta_{el} = 93\%$) occur simultaneously at $t_r = 4$ μs ($M = 13$). However, operation with such a short value of t_r yields a rate of voltage rise, $dU_d/dt \sim (U_{pk} - U_{bias})/t_r = 40$ kV/μs, which is probably too large. If M and thus t_r are adjusted to reduce

Table 22.1 Computational parameters for single-pulse excitation with DC bias

Circuit parameters	Case (a)	Case (b)	Case (c)
C_1; C_2 (μF)	0.25	0.50	0.15
L_1 (μH)	ML_2	ML_2	ML_2
L_2 (μH)	2.0	2.0	2.0
R_1; R_2 (Ω)	0.01	0.01	0.01
R_4 (Ω)	2000	2000	2000
U_c (kV)	280	280	360
U_{bias} (kV)	56	56	72
E_s/V (J/l)	200	400	200
Geometry and initial conditions gas mixture			
g [cm]	25	CO_2:N_2:He	1:4:5
A [cm^2]	2000	P_{ri} [Torr] (TPA)	0.75
V [l]	50	P [Torr]	750
n_{e0} [cm^{-3}]	10^7	T [K]	293

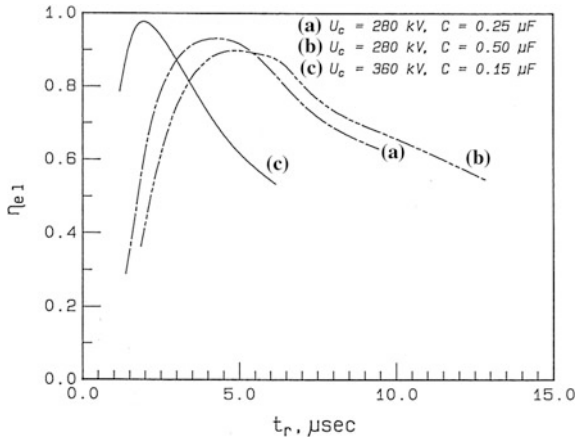

Fig. 22.5 Computed dependence of the electrical efficiency η_{e1} on the voltage rise time t_r

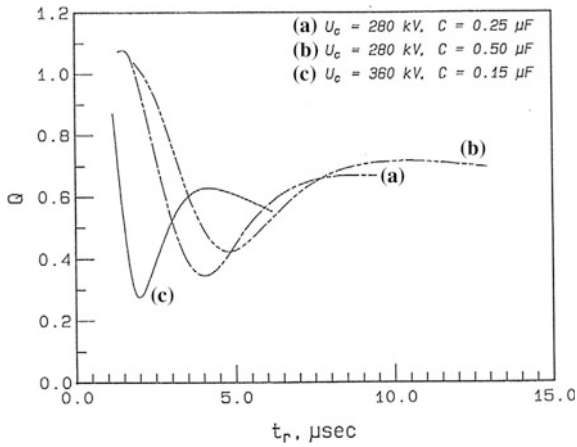

Fig. 22.6 Computed dependence of the dimensionless parameter Q on the voltage rise time t_r

the maximum rate of voltage rise to $dU_d/dt < 10$ kV/μs, then the large residual voltage amplitude ($Q > 0.6$) will invite arc formation at $t = t_{res}$.

Case (b) is identical to (a) with only a doubling in the capacitances C_1 and C_2 (i.e., $E_s/V \equiv \xi_i/\eta_{e1} = 400$ J/L, which may be above the maximum for this gas mixture and type of excitation). Since $I_{pk} \propto (C_2/L_2)^{1/2}$ and $t_{pk} \propto (C_1/L_1)^{1/2}$, both parameters are characteristically larger in the present case, but discharge ringing is not alleviated. The minimum degree of circuit ringing ($Q = 0.42$) and the maximum electrical efficiency ($\eta_{e1} = 89\%$) occur simultaneously at $t_r = 5$ μs ($M = 13$). Again, however, such a large rate of voltage rise ($dU_d/dt \sim 30$ kV/μs) may preclude satisfactory operation at this value of t_r.

All of the energy stored in the PFN is deposited into the laser discharge in the first cycle of operation if their impedances are matched. Since the laser discharge is effectively a constant voltage load, this occurs only if

$$U_c \cong 2U_{qs}. \tag{22.38}$$

Case (c) maintains $E_s/V \equiv \xi_i/\eta_{e1} = 200$ J/1 as in case (a) but increases the charging voltage to $U_c = 360$ kV in conformance with this condition. C_1 and C_2 are decreased accordingly. Optimization of the circuit is now possible with marked improvement in current–voltage characteristics. Minimum circuit ringing ($Q = 0.28$) and maximum electrical efficiency ($\eta_{e1} = 98\%$) occur concurrently at $t_r = 2.0$ μs. The glow duration ($t_{qs} = 1.3$ μs) is now approximately the same as in the previous cases and the peak current ($I_{pk} = 44$ kA) is approximately equal to the maximum encountered with case (b). Note that a value of $Q \sim 0$ is not obtained because (38) is valid only if $C_1 = C_2$ and $U_{bias} = 0$. While the optimization described here appears to have alleviated the impedance matching problem, the large rate of voltage rise ($dU_d/dt \sim 100$ kV/μs) will certainly destroy the cathode space-charge screen for even the highest productivity auxiliary discharges. Establishment of a stable SSVD under these conditions is highly unlikely.

22.4.3 Double-Pulse Excitation

This type of excitation is produced by firing the left-hand PFN (switch S_1) at decreased charging voltage and stored energy, which produces a slowly increasing discharge voltage waveform and establishes a low-current but stable SSVD, followed by commutation of switch S_2, which dumps the main energy store (capacitor C_3 charged to voltage U'_c) into the plasma. The advantage here is that the SSVD is established under *low*—dU_d/dt conditions and the negative space-charge layer adjacent to the cathode is not depleted. After establishment of the quiescent SSVD, additional energy can be rapidly loaded without disruption of plasma homogeneity or stability [1, 2].

Waveforms for single- and double-pulse excitation of a 60 cm aperture, device are given in [1]. The atmospheric-pressure gas mixture (CO_2:N_2:He = 4:16:80) was preionized by an auxiliary barrier discharge attached to the top surface of the cathode. Explicit PFN parameters are not given. For the double-pulse computation, therefore, numerical simulations were performed to find electrical parameters that would produce a quiescent plasma with an electron concentration $n_e \sim 10^{10}$ cm^{-3} at the conclusion of a slowly rising voltage pulse of duration

$$t_r \approx \frac{9g^2}{4\mu_e U_e (C_1/C_2)^{1/2}}. \tag{22.39}$$

Then at $t_f = t_r$, switch S_2 is closed, depositing $\sim$200 J/l into the plasma in accordance with impedance-matching condition 138). To yield these results, a

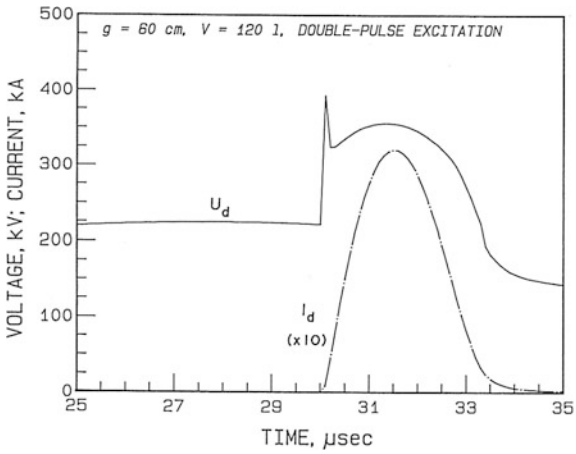

Fig. 22.7 Computed $I_d - U_d$ waveforms for double-pulse excitation of the device described in [1]

double-pulse PFN was designed with electrical parameters C_1 = 0.2 μF, C_2 = 0.1 μF, C_3 = 0.2 μF, L_1 = 1200 μH, L_2 = 100 μH, L_3 = 5 μH, $R_1 = R_2 = R_3$ = 10 m Ω, R_4 = 5 k Ω, U_c = 180 kV, U_{bias} = 45 kV, U'_c = 520 kV; also, $n_{e0} = 5 \times 10^6$ cm^{-3} and P_{ri} = 1.5 Torr. Closure of switch S_1 produces a gradual increase in U_d to 220 kV over a duration t_r = 30 μs, generating a current flow of only $I_d \sim$ 10 A. It is important to note that this PFN is designed as a voltage multiplier (i.e., $C_1 > C_2$) so that $U_d(t_r) > \zeta U_{sb}$ even though $U_c < \zeta U_{sb}$. The PFN that consists of capacitors C_1 and C_2 and inductors L_1 and L_2 is effectively isolated from the second discharge pulse produced by the $L_3 - C_3$ PFN provided that $L_2 \gg L_3$. Furthermore, the stored energy for the first pulse is only 12% of that for the second, main pulse. Computed $I_d - U_d$ waveforms for the time interval encompassing the second pulse are shown in Fig. 22.7.

Measured and computed discharge parameters are listed in Table 22.2. This type of excitation produces a shorter-duration, higher-current SSVD than is possible

Table 22.2 Comparison of computed and experimental discharge parameters for double-pulse excitation of a 120–1 device

Parameter	Experiment [1]	Computation
t_r [μs]	≈ 30 − 45	30
$U_d(t_r)$ [kV]	240	221
$n_e(t_r)$ [cm^{-3}]	–	9×10^{10}
U_{pk} [kV]	≈ 380	393
U_{qs} [kV]	≈ 290	355
t_{qs} [μs]	≈ 3	2.2
I_{pk} [kA]	42	32.1
ξ_i [J/l]	~80	188
η_{el}	~0.90	0.74

with single-pulse excitation in qualitative agreement with experiment. The computed values of U_{qs} and I_{pk} are respectively larger and smaller than the experimental measurements, but the agreement between ξ_i values is excellent. Furthermore, it is now possible to vary t_{qs} and therefore I_{pk} by adjusting L_3 without sacrificing electrical efficiency. The simulation here showed little circuit oscillation beyond the first cycle (i.e., $Q < 0.1$).

A 140–1 device with a 70 cm interelectrode gap is described in [2]. This device employed an auxiliary surface discharge that was placed beneath the mesh cathode. The cathode was operated at ground potential and the auxiliary discharge was fed by a separate pulsed-power system. Electrons were repelled from the surface-discharge plasma and through the grid by applying a negative bias voltage to the auxiliary discharge circuit. VUV radiation is only produced during the breakdown process for this type of auxiliary discharge, whereas electrons can be extracted during the entire duration t_{aux}. PFN parameters are not given and the $I_d - U_d$ waveforms are described as being qualitatively similar to those in [1]. For the present simulation, PFN parameters that initially establish a quiescent SSVD were again chosen by trial and error. The second, high-current discharge then operates according to impedance matching condition (38). The interelectrode gap is filled both by an initial burst of photoelectrons produced by surface-discharge VUV radiation and from electrons extracted from the surface-discharge plasma during the entire quiescent period. The computed specific input energy (ξ_i = 130 J/l) is in good agreement with experimental findings (ξ_i = 140 J/l) and the computed electrical efficiency is quite high (η_{el} = 80%).

22.5 Conclusions

Computational runs using a coupled-particle kinetics-equivalent circuit model were performed to simulate response of the various PFNs that are used with the auxiliary discharge excitation scheme. A single-pulse PFN, with or without quasi-DC bias, can only be employed with g < 40–50 cm, in excellent agreement with experimental findings. This limitation is imposed by design conflicts between the need for increasingly longer rise times as the gap is increased, and the requirement for impedance matching between the PFN and discharge plasma load. Larger discharge gaps require more complex circuitry to first establish a low-current, quiescent SSVD using a slow rise-time initial pulse, followed by a second high-current, fast rise-time pulse that deposits the bulk of the stored energy into the discharge plasma.

Acknowledgments This part of the book had been prepared as well together with Dr. R.E. Beverly III on the experimental basis created by our team from Prokhorov GPI RAS.

References

1. V.V. Apollonov, G.G. Baitsur, A.M. Prokhorov et al., Sov. Tech. Phys. Lett. **14**, 241–242 (1988)
2. V.V. Apollonov, G.G. Baitsur et al., Sov. Tech. Phys. Lett. **14**, 915–916 (1988)
3. V.V. Apollonov et al., Instrum. Exp. Technol. **32**, 149–152 (1989)
4. V.V. Apollonov, G.G. Baitsur et al., Ultraviolet-preionized SSVD in a volume of 400 liters, paper scheduled for presentation at Pulse Power for Lasers III (Los Angeles 1991), in *Proceedings of the SPIE*, vol. 1411 (1991)
5. V.V. Apollonov et al., J. Opt. Soc. Am. B **8**, N2 (1991)
6. R.E. Beverly III, Enhanced transverse discharge stability using preionization from an auxiliary barrier discharge, in *Proceedings of the Seventh International Symposium on Gas Flow and Chemical Lasers (Wien 1988), SPIE*, vol. **1031,** pp. 458–466 (1989)
7. V.V. Apollonov et al., Sov. J. Quantum Electron. **17**, 76–82 (1987)
8. A.C. Hindmarsh, in *Scientific Computing,* ed. by R.S. Stepleman (North-Holland, Amsterdam 1983), pp. 55–64. A.C. Hindmarsh: Lawrence Livermore National Laboratory, private communication (1990)
9. V.V. Apollonov, Small signal gain of CO_2-lasers pumped by SSVD, in International conference on Lasers-87, Lake Tahoe, pp. 495–501(1987)
10. R.A. Fitch, V.T.S. Howell, in *Proceedings of the IEE*, vol. 111, pp. 849–855 (1964)
11. V.V. Apollonov, YuM Vas'kovskii et al., Sov. J. Quantum Electron. **15**, 1–3 (1985)

Part II
High Energy HF/DF Lasers

For a long period of time, from 1971 until 1995, progress in the development of nonchain HF(DF) lasers on mixtures of SF_6 with hydrocarbons (deuterocarbons) with initiation of chemical reaction by SSVD was retarded by producing SSVD in SF_6 and SF_6-based mixtures. The conventional approach to the formation of SSVDs in nonchain lasers is based on the preionization of gas by VUV or soft X-ray radiation in the discharge gap with a uniform electric field followed by a high-voltage pulse applied across the gap. This method can hardly be used due to the strong electronegativity of SF_6 that is responsible for high losses of initial electrons regardless of the type of the ionizator used. In addition, most simple sources of VUV radiation cannot be used in non-chain lasers possessing high aperture parameter because the radiation is strongly absorbed in SF_6. Sources of soft X-ray radiation with the emitting area greater than a few decimeters squared are rather exotic devices even in the simplest variants. In enhancing the aperture and the volume of the active medium of nonchain HF(DF) lasers, there are also difficulties that arise from the particular profiling of electrodes needed in this case (Rogovskii profile, Chang profile, etc.) for making the electric field in the gap more uniform. This profiling is difficult and results in greater laser dimensions and higher inductance of the discharge gap with a short duration of stable burning of SSVD in SF_6. There is also an approach based on a preliminary filling of the discharge gap by electrons drifting in an electric field and a dynamic profiling of the electric field in the gap by volume charges. This method can not be used in nonchain lasers because of the strong electronegativity of SF_6. A new approach to scaling problem of nonchain HF(DF) lasers (for increasing the volume of active medium and the output laser energy) is presented in this Chap. 2. It was found that the characteristics of SSVD and the output power are independent of preionization if the cathode surface possesses small-scale (~ 50 μm) nonuniformities. In other words, if the cathode surface is rough, then no preionization is needed for obtaining an SSVD in working mixtures of nonchain HF(DF) lasers. We termed this form of SSVD the

SIVD. The task of this part of our book is to show the possibility of obtaining an SIVD with a uniform (with respect to volume) energy deposition in a system of plane electrodes with electric field strongly enhanced at edges, i.e., in the conditions $r << d$, h, where r is the radius of electrode rounding off over its perimeter, d is the interelectrode separation, and h is the transversal dimension of the electrode.

Chapter 23
Non-chain High Radiation Energy Electric-Discharge HF(DF) Lasers

Abstract We demonstrate in this chapter that an SSVD is possible in mixtures of SF_6 with hydrocarbons (or deuterated carbons) without special devices for the preionisation of the gas. We demonstrate in this chapter that an SSVD is possible in mixtures of SF_6 with hydrocarbons (or deuterated carbons) without special devices for the preionisation of the gas. This can be achieved with an extremely compact electrode system. Wide-aperture nonchain HF (DF) lasers with a high output radiation energy can be constructed on the basis of the discharge. It is reported in this chapter that output energies of 144 J for HF and 115 J for DF were achieved in a system with a 21 L active medium and an aperture of $\sim$15 cm. The electric efficiencies were 2.8 and 2.2%, respectively.

We have previously demonstrated [1, 2] that the active volume and the output radiation energy of nonchain HF (DF) lasers with initiation of the chemical reaction by an SSVD can be increased considerably if H_2 (D_2) in SF_6-H_2 (SF_6-D_2) mixtures is replaced with a hydrocarbon (deuterated carbon). If the SSVD is initiated by a barrier discharge distributed on the cathode surface, the output energy of an HF laser can reach 31 J when the volume of the active medium is 5 L and the inter-electrode spacing is d = 10 cm. We have also found [3] that if the cathode surface is very rough (as a result of scouring with a sand jet or cleaning of the surface with a coarse emery paper), the SSVD in mixtures of SF_6 with hydrocarbons (deuterated carbons) can be achieved without special preionization devices.

The SSVD reported in [3] was ignited in a homogeneous electric field between Chang-profile electrodes, and an increase in the volume of the active medium and in the laser aperture gave rise to familiar problems when such electrode profiles are used. These problems were associated primarily with an increase in the laser chamber dimensions and in the discharge-circuit inductance, which were particularly critical for an HF (DF) laser because of the very limited duration of a stable SSVD even in mixtures of SF_6 with hydrocarbons (deuterated carbons) [4].

© Springer International Publishing Switzerland 2016

V.V. Apollonov, *High-Energy Molecular Lasers*,
Springer Series in Optical Sciences 201, DOI 10.1007/978-3-319-33359-5_23

In the present study, we therefore considered the possibility of a further increase in the output characteristics of a nonchain HF (DF) laser by employing an SSVD with a homogeneous energy deposition throughout the discharge volume with a large value of d, but without preionization in an extremely compact electrode system, i.e. under conditions when the discharge was initiated over the whole surface of a flat cathode for h $\sim$ d and r $\ll$ d (r is the rounding radius of the cathode along the perimeter and h is the transverse size of the flat part of the cathode surface) [5]. Such electrode systems are characterized by a high degree of the edge inhomogeneity of the electric field and an SSVD usually contracts at the edge of the discharge gap [6], unless dynamic profiling of the field by the space charge is employed [5, 7].

We investigated a system of flat Al electrodes with d = 15 cm. The anode dimensions were 30 cm $\times$ 90 cm. The cathode with a flat surface area of 15 cm 75 cm was rounded at the perimeter to a radius r = 1 cm and its surface was subjected to sand-jet scouring. The electrodes were placed in a glass-epoxy tube that was 120 cm long with a diameter of 40 cm. A laser cavity was formed by an Al mirror with an 80 m radius of curvature and a plane-parallel CaF_2 plate, both attached directly to the ends of the discharge chamber.

The electric circuit is shown in Fig. 23.1. Energy was stored in capacitors C_1–C_{10} of a ten-stage Arkad'ev-Marx voltage pulse generator (VPG) with an impulse capacitance 40 nF and a maximum output voltage 550 kV. This VPG charged a capacitor C_{11} = 50 nF through an inductance (L) in $\sim$2 μs. The voltage was then applied, via parallel-fired spark gaps SG_{11} and SG_{12}, to a peaking capacitor C_{12} = 22.5 nF and to the main discharge gap. The moment of ignition of the gaps SG_{11} and SG_{12} was controlled by a special delay circuit triggered simultaneously with the VPG.

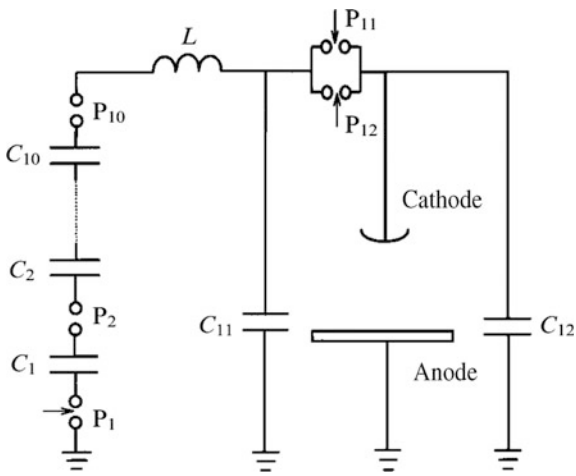

Fig. 23.1 Electric circuit of the investigated laser (C_{1-10} = 0.4 μF, C_{11} = 50 nF, C_{12} = 22.5 nF)

The donors of $H_2(D_2)$ were C_2H_6 and C_6D_{12}, respectively. Mixtures were prepared so that for every 10–20 atoms of F there was one atom of H(D). The pressure in the mixture was selected to satisfy the condition (U/p)d = 200 kV cm^{-1} bar^{-1} (U is the maximum voltage across the capacitor C_{11}, found taking account of the energy losses in the course of charging this capacitor by the VPG; p is the pressure in the mixture): when the VPG voltage was 500 kV, this pressure was 103 Torr. The energy and profile of the output radiation pulses were determined with, respectively, an array of TPI-2 M calorimeters and a pyroelectric detector with a time resolution $\sim$20 ns.

After tuning of the spark gaps SG_{11} and SG_{12}, an SSVD was ignited stably by voltages from the VPG up to 510 kV. Photographs and visual examination of the main discharge gap showed that the SSVD was in the form of diffuse channels widening towards the anode and attached to brighter and denser channels (of lengths not exceeding 3–5 mm at the maximum input energy), which grew out of the cathode spots. These spots covered the whole surface of the cathode, including its rounded edges. The surface density of the cathode spots was maximal ($\sim$30 cm^{-2}) at the centre of the cathode and it fell to $\sim$20 cm^{-2} at its edges (in a section perpendicular to the optic axis). The length of the bright parts of the channels in the narrow zone at the edge of the main discharge gap was somewhat greater than the length at the centre, as we recorded previously for CO_2 lasers when cathodes with sharp or slightly rounded edges were used.

In view of the high surface density of the cathode spots, the diffused channels overlapped at a distance of $\sim$2 cm from the cathode surface. The nature of the observed SSVD resembled a high-voltage diffuse discharge investigated earlier [8], but in the present case (in contrast to [7]), the diffuse channels overlapped and the discharge took place at the usual (for molecular lasers) overvoltages amounting to $\sim$2 (representing the ratio of the voltage from the VPG to the voltage during the quasi-steady phase of the discharge) and for a relatively low ($\sim 2 \times 10^{11}$ V s^{-1}) rate of rise of the voltage across the main discharge gap.

An imprint formed by the laser radiation on thermally sensitive paper was trapezium with the base 16 cm long near the cathode and 21 cm near the anode. The radiation energy density fell smoothly away from the centre to the edges of the main discharge gap. Consequently, in spite of the strong edge inhomogeneity of the electric field in this electrode system, there was no 'pinching' of the current density in the SSVD at the edge of this gap.

According to [5, 7], the distribution of the current density observed under these conditions could only result from the appearance of a space charge in the gap during formation of the SSVD (in the present case, this may have been the negative-ion charge) or of a plasma layer with an electron concentration $n_e > 10^{10}$ cm^{-3}. We could assume that this space charge or the cathode plasma layer [8] appeared as a result of flow of considerable prebreakdown currents in the main discharge gap [9] because of the high electric field at microprojections of the rough cathode surface, but this question would require a detailed investigation.

It should also be highlighted that the feasibility of igniting an SSVD without preionization in an electric field with a strong edge inhomogeneity was associated

with the specific nature of SF_6, namely its high electronegativity and/or the nature of the dependence of the electron attachment rate on E/p (E is the electric field intensity) [10]. Attempts to ignite an SSVD in gases with a lower electronegativity and an electron attachment rate increasing with increase in E/p (air, CO_2, N_2O, and also their mixtures with hydrocarbons and other substances characterized by low ionization potentials) showed that, even at low input energies, the current density became 'pinched' at the cathode edge. It would be of interest to investigate SSVDs in other gases with a high electronegativity and an electron attachment mechanism similar to that in SF_6.

The discharge volume was estimated from the laser imprint: it was $\sim$21 L, which corresponded to an average specific input energy of $\sim$240 J L^{-1} deposited in the plasma (deduced from the energy stored in the VPG capacitors). Oscillograms of a voltage pulse across the discharge gap and of an HF laser radiation pulse are given in Fig. 23.2. The pedestal of the voltage oscillogram resulted from charging the capacitor C_{12} by the VPG via inductances wound on the spark gaps SG_{11} and SG_{12} in order to equalize the distribution of the electric field on the surfaces of the electrodes forming these gaps. The maximum voltage across the main discharge gap and the duration of the SSVD current, estimated from the duration of the quasi-steady phase of the voltage, were 183 kV and 300 ns, respectively. The half-amplitude duration of the output radiation pulse was $\sim$180 ns. The output energy reached 144 J for HF and 115 J for DF, and the electric efficiencies were 2.8 and 2.2%, respectively. If account was taken of the energy losses ($\sim$50%) in the circuits charging the capacitors C_{11} and C_{12}, it was found that the physical efficiency should be at least twice the values quoted here.

We shall conclude by noting that stable simultaneous firing of the spark gaps SG_{11} and SG_{12} under automated conditions should make it possible to further increase the output radiation energy of an HF (DF) laser subjected to a given maximum voltage ($\sim$500 kV) by an increase (proportional to the active volume) in the capacitances C_{11} and C_{12}, in the impulse capacitance of the VPG, and in the number of spark gaps (such as SG_{11} and SG_{12}) connected in parallel.

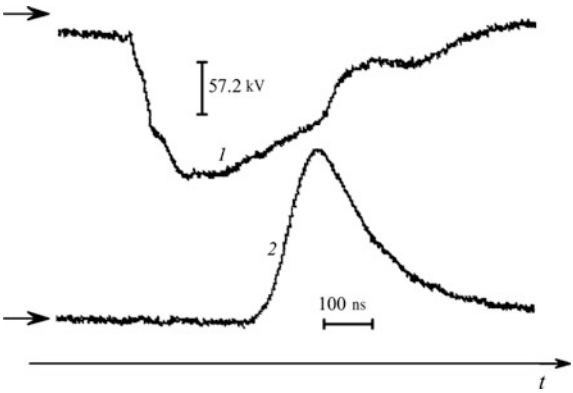

Fig. 23.2 Oscillograms of a voltage pulse across the main discharge gap (*1*) and of the output radiation pulse (*2*)

We thus demonstrated that an SSVD can take place without preionization under conditions of a strong edge inhomogeneity of the electric field in the main discharge gap and this can be used as the basis of wide-aperture nonchain HF (DF) lasers with a high output radiation energy.

References

1. V.V. Apollonov, et al., Conf. po Fizike Gazovogo Razryada, Ryazan, 1996 (Proceedings of the Seventh Conference on Gas Discharge Physics, Ryazan, 1996, p. 6
2. V.V. Apollonov et al., Kvantovaya Elektron. (Moscow) **24**, 213 (1997) [Quantum Electron. 27, 207 (1997)]
3. V.V. Apollonov et al., Pis'ma. Zh. Tekh. Fiz. **22**(23), 60 (1996) [Tech. Phys. Lett. *22*, 1026 (1996)]
4. V.V. Apollonov, et al., *II Mezhdunar. Konf. po Fizike Plazmy i Plazmennym Tekhnologiyam, Minsk, 1997* (Proceedings of the Second International Conference on Plasma Physics and Plasma Technologies, Minsk, 1996) (National Academy of Sciences of Belarus, Minsk, 1997) p. 154
5. V.V. Apollonov et al., Kvantovaya Elektron. (Moscow) **14**, 135 (1987) [Sov. J Quantum Electron. 17, 76 (1987)]
6. Robinson AM/ Appl. Phys. **47**, 608 (1976)
7. V.V. Apollonov et al., Kvantovaya Elektron. (Moscow) **11**, 1327 (1984) [Sov. J. Quantum Electron. 14, 898 (1984)]
8. A.I. Pavlovskil, M.A. Voinov, V.V. Gorokhov, V.I. Karelin, Repin P.B. Zh, Tekh. Fiz. **60**(1), 64 (1990) [Sov. Phys. Tech. Phys. 35, 37 (1990)]
9. I.M. Bortnik, *Fizicheskie SvoTstva i Elektricheskaya Prochnost' Elegaza* (Physical Properties and Electric Strength of SF_6) (Energoatomizdat, Moscow, 1988)
10. J.P. Novak, M.F. Frechette, J. Appl. Phys. **55**, 107 (1984)

Chapter 24
SIVD in Nonchain HF Lasers Based on SF_6-Hydrocarbon Mixtures

Abstract An SSVD without preionization, i.e. an SIVD, in nonchain HF lasers with SF_6-C_2H_6 mixtures was investigated. It was established that, after the primary local electrical breakdown of the discharge gap, the SIVD spreads along the gap in directions perpendicular to that of the electric field by means of the successive formation of overlapping diffuse channels under a discharge voltage close to its quasi-steady state value. It is shown that, as new channels appear, the current flowing through the channels formed earlier decreases. The volume occupied by the SIVD increases with increase in the energy deposited in the plasma and, when the discharge volume is confined by a dielectric surface, the discharge voltage increases simultaneously with increase in the current. The possible mechanisms to explain the observed phenomena, namely the dissociation of SF_6 molecules and electron attachment SF_6 molecules, are examined. A simple analytical model that makes it possible to describe these mechanisms at a qualitative level was developed.

24.1 Introduction

The main problem arising in the construction of powerful wide-aperture nonchain HF(DF) lasers in which a chemical reaction is initiated by an SSVD is the implementation of the SSVD itself in mixtures of SF_6 with hydrogen carriers (deuterium carriers). The possibility of applying the usual methods for this purpose—namely the preliminary ionization of the gas in a homogeneous electric field with the subsequent application of a high-voltage pulse to the discharge gap [1]—is limited by the high electronegativity of the SF_6 molecules.

A new approach to the solution of the problem of increasing the volume of the active medium and the energy of the radiation emitted by nonchain HF(DF) lasers was found in our earlier studies [2–4]. In a study [3] of a nonchain HF(DF) laser with preionization by soft X-rays, it was observed that the SSVD characteristics and the laser output characteristics are independent of the presence of preionization if the cathode surface has been subjected to a treatment involving the deposition on it of small-scale ($\sim$50 μm) inhomogeneities. In other words, if the cathode has a

© Springer International Publishing Switzerland 2016

V.V. Apollonov, *High-Energy Molecular Lasers*,
Springer Series in Optical Sciences 201, DOI 10.1007/978-3-319-33359-5_24

rough surface, preionization is not essential in order to obtain an SSVD in the mixtures of an HF(DF) laser.

The possibility of achieving an SSVD without preionization and with an energy input homogeneous throughout the volume under the conditions of a high edge inhomogeneity of the electric field in the discharge gap of an HF(DF) laser has also been demonstrated [4]. These investigations made it possible to increase the aperture of a nonchain HF(DF) laser based on SF_6—hydrocarbon (deuterocarbon) mixtures up to 27 cm and to obtain a radiation energy of ~400 J for an electric efficiency of approximately 4% [8].

An SSVD without preionization in SF_6 and in mixtures containing it, i.e. an SIVD [5], has a number of properties unusual for volume discharges. The observation of a discharge of this kind opens up unique opportunities for the development of simple and effective nonchain HF(DF) lasers operating in both pulsed and repetitively pulsed regimes. Further investigations of the SIVD in order to establish the principal mechanisms determining its development is therefore of undoubted interest. This was the subject of the present investigation.

24.2 Experimental Apparatus

The SIVD characteristics were investigated in discharge gaps with electrodes with different configurations (Fig. 24.1) with the ratio of the partial pressures of the mixture components SF_6:C_2H_6 = 10:1 − 10:3 and pd = 0.02 − 0.7 cm bar (p is the pressure of the mixture and d the interelectrode distance). The integral characteristics of the discharge and the dynamics of its development were studied by using a system of plane electrodes illustrated schematically in Fig. 24.1a. The SIVD was struck with d = 2–6 cm between an aluminium cathode 6 cm in diameter, rounded (1 cm radius) along the perimeter, and an aluminium anode 12 cm in diameter. The surface of the cathode, including the rounded parts, was sandblasted.

In order to investigate the SIVD dynamics, an artificial (transmission) line with a variable number of cells was discharged across this gap [6]. This made it possible to follow, by varying the duration of exposure to the voltage across the gap in the range 40–400 ns at a constant current, the development of the discharge in time and in space by photographing it at various exposures to the voltage. In the remaining SIVD studies in which the above and other electrode systems shown in Fig. 24.1 were used, the discharge of a capacitor was used to strike the volume discharge. The discharge gaps (Figs. 24.1a, b) were additionally illuminated from the side by a low-current (I < 3 A) spark enclosed in a quartz envelope. This spark could not ensure the volume photoionization of the gas, but, as a result of the initiation of electrons at the cathode, it was possible to stabilize the scatter of the gap-breakdown delay times. The discharge gaps in the configurations shown in Figs. 24.1c.

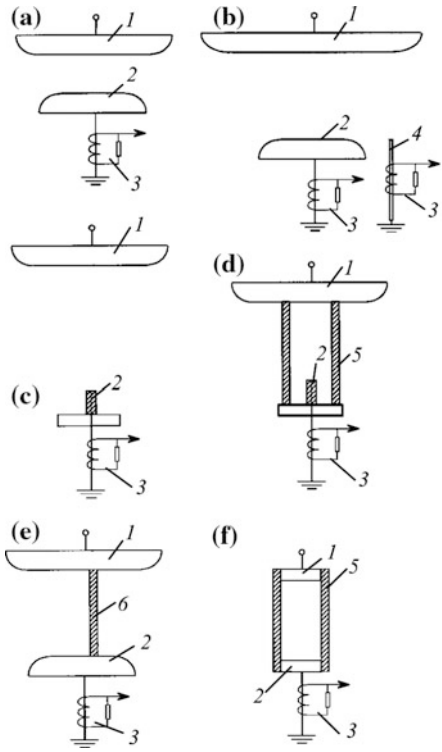

Fig. 24.1 Discharge gaps with electrodes with different configurations: anode (*1*); cathode (*2*); Rogowski loop (*3*); initiating electrode (*4*); glass tube (*5*); glass plate (*6*)

The dynamics of the development of the SIVD was also investigated in an electrode system with a sectioned cathode (Fig. 24.1b). Here, the main cathode and anode were the same as in Fig. 24.1a, but an earthed conductor 1.5 mm in diameter (the initiating electrode) was connected in parallel to the main cathode at a distance of 5 mm in a horizontal plane extending from its edge. The vertical distance between the cathode surface and the tip of the conductor was chosen in such a way that, during the initiation of the discharge by a low-current spark, the electrical breakdown of the gap extended initially to the conductor.

A conductor with polyethylene insulation and a core diameter of 1.5 mm served as the cathode in the electrode system in Figs. 24.1c, d (the discharge occurred between the rod and the plane). In these experiments, the SIVD was investigated under conditions such that not more than one cathode spot could be formed on the cathode. In the discharge gap shown in Fig. 24.1d, the discharge cross section on the anode was confined by a glass tube 6–8 mm in diameter (confined discharge), placed between the electrodes in such a way that its upper edge touched the surface of the anode.

In the configuration presented in Fig. 24.1e, the plane electrodes (the same as in Fig. 24.1a) were linked by a dielectric plate 2 mm thick with a transverse dimension of 5 cm. In the electrode system shown in Fig. 24.1f, the SIVD was struck for

an interelectrode distance (the distance between two aluminium disks 3.6 cm in diameter) of 5.5 cm; the disks were placed in a quartz tube with an internal diameter of 3.8 cm, the electrodes had sharp edges, and the cathode surface was sandblasted.

24.3 Experimental Results

A typical photograph of an SIVD in a plane-electrode system is presented in Fig. 24.2a. Figure 24.2b shows the corresponding current (I) and voltage (U) oscillograms. It can be seen from Fig. 24.2 that the SIVD does not outwardly differ from the usual SSVD with preionization. It consists of a set of diffuse channels, linked to bright cathode spots and expanding towards the anode. By overlapping, the diffuse channels generate an overall diffuse glow. Despite the appreciable strengthening of the electric field on the edge of the gap, this region is scarcely distinguishable and the cathode spots cover the entire surface of the cathode.

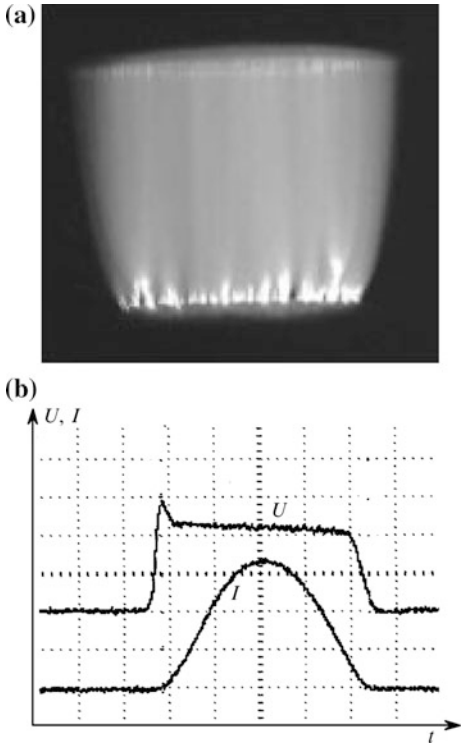

Fig. 24.2 Photograph of an SIVD in a system of plane electrodes (**a**) and typical current (*I*) and voltage (*U*) oscillograms for the SIVD; scan—100 ns division^{-1} (**b**)

The SIVD voltage and current oscillograms are also typical for an SSVD in electronegative gases. Energy is deposited in the SIVD plasma at a quasi-steady-state voltage U_{qs}. The voltage U_{qs} in mixtures of SF_6 with hydrocarbons, when the content of the latter is not greater than 17%, depends only slightly on their partial pressure. The dependence of U_{qs} on pd for $pd = 0.05 - 2.5$ cm bar and specific energy inputs in the discharge plasma up to 0.2 J cm^{-3} is described satisfactorily by the expression $U_{qs} = A + Bp_{SF_6}d$, where p_{SF_6} is the partial pressure of SF_6 in the mixture. For pure SF_6 and SF_6: C_2H_6 = 10:1, 10:2 mixtures, we have respectively A = 0.72, 0.79, and 1.1 kV and B = 92.7, 94.8, and 96.4 kV cm bar. The value of B obtained in the present experiments is close to the known [7] critical reduced electric field strength $(E/p)_{cr}$ = 89 kV cm^{-1} bar^{-1} (the difference is ~ 8 %).

The differences between SIVDs and SSVDs with preionization are manifested in the dynamics of their development. Figure 24.3 presents the results of studies on the dynamics of the development of an SIVD in a plane-electrode system

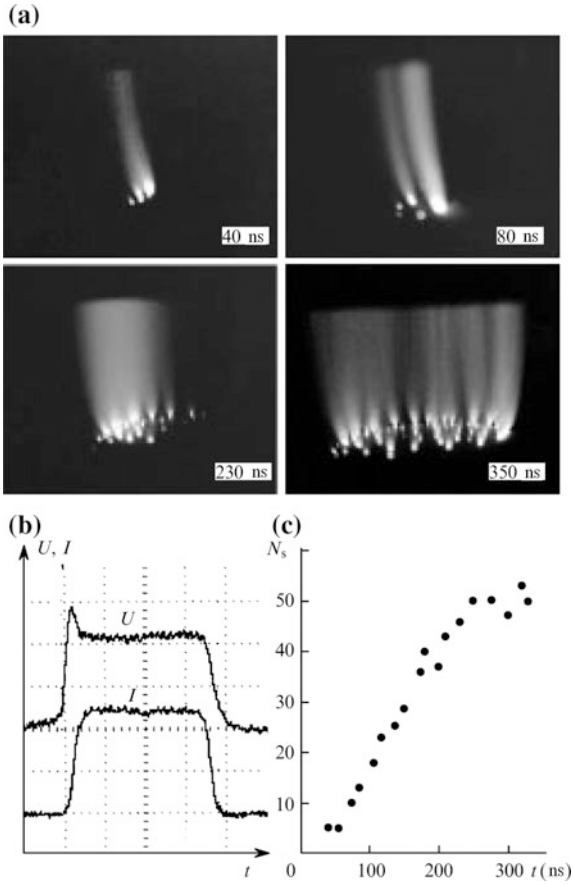

Fig. 24.3 Characteristics of an SIVD: photographs of an SIVD in a system of plane electrodes at different times (spark illumination from the *left*) (**a**); voltage (U) and current (I) oscillograms for the SIVD during the discharge across the gap of an artificial line consisting of 20 cells (scan—100 ns $division^{-1}$) (**b**); and time dependence of the number of spots on the cathode N_s (**c**)

(Fig. 24.1a) for the discharge across the gap of an artificial line with a variable number of cells. As can be seen from Fig. 24.3, in contrast to SVDs with preionization, an SIVD is struck initially in the zone of the maximum amplification of the electric field on the gap edge in the form of one or several diffuse channels linked to the cathode spots. The radiation from the discharge in the remainder of the gap is not detected at this instant. The channels formed first initiate the appearance of the subsequent channels and the SIVD spreads over the gap, perpendicular to the direction of the electric field at a constant voltage (equal to U_{qs}), gradually filling the entire gap. The total number of spots on the cathode increases from the instant of the electrical breakdown of the gap virtually in proportion to time, i.e. proportional to the energy injected into the discharge when experimental conditions are taken into account.

Since the SIVD develops at a constant current (with the exception of the leading and rear edges), under the experimental conditions described, the current flowing through channels formed earlier should diminish after the appearance of new ones. The characteristic features of the development of an SIVD listed above suggest the operation of current-limiting mechanisms in SF_6 and in mixtures based on it, which hinders the transfer of the entire energy through a single channel. It appears that it is precisely these mechanisms that are in fact responsible, to a large extent, for the existence of the unusual form of the discharge, such as the SIVD, including the possibility of achieving it in gaps with a strong edge inhomogeneity of the field.

The existence of such mechanisms is also indicated by the results of experiments in an electrode system with simulation of the first diffuse channel by the initiating electrode (Fig. 24.1b). Figure 24.4a, which presents characteristic oscillograms of the discharge current through the initiating (curve 1) and main (curve 2) cathodes, shows that the current through the initiating cathode does indeed appear appreciably earlier than the current through the main cathode and its maximum is attained at an instant when the main current still continues to grow.

Figure 24.4b illustrates the dependence of the fraction of the energy, Δ, transmitted by the initiating cathode, relative to the total energy, W, injected into the discharge. The quantity of Δ decreases monotonically with an increase in W, reaching saturation, which yet again constitutes evidence in favour of the existence of mechanisms preventing the transfer of the entire SIVD energy through one channel.

However, it can be noted that in the experiment under consideration, the simulation of the initial diffuse channel with the aid of a special electrode is not entirely equivalent to the real conditions, because, in order to guarantee that the discharge begins from the initiating cathode, it would be necessary to raise it by approximately 1 mm above the surface of the main cathode. For this reason, the brightness and transverse dimensions of the simulated initial diffuse channel differed appreciably from those of channels in the main gap, whereas under real conditions, this was not observed (Fig. 24.2).

Figure 24.5 presents a typical dependence of the total number of spots on the cathode N_s on the average specific energy injected into the plasma. It was recorded in a system of plane electrodes for different values of d and p. W_{sp} was varied

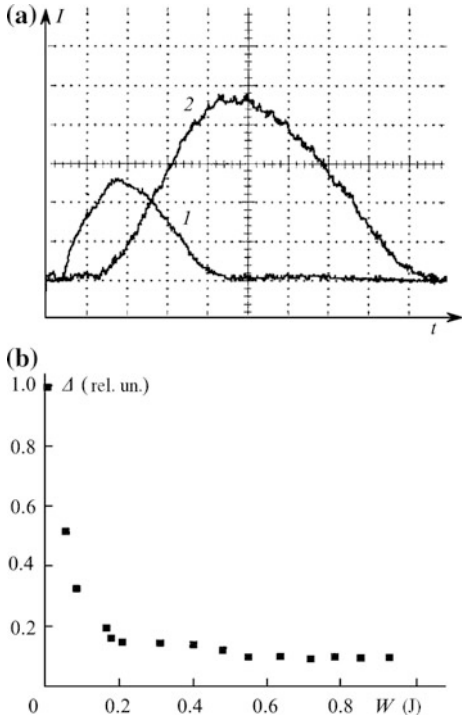

Fig. 24.4 Oscillograms of the current through the initiating (*1*) and main (*2*) cathodes (39.7 A division^{-1}, scan—50 ns division^{-1}) (**a**) and dependence of the fraction of energy Δ transmitted through the initiating electrode relative to the total energy W (**b**)

during the experiments by varying the charging voltage and charging capacitance. The duration of the discharge current was also varied. Evidently, for a fixed value of p, N_s depends only slightly on d. Within the limits of error, the points fit satisfactorily on a linear dependence of N_s on W_{sp}.

Consequently, for a fixed value of p, the number of spots on the cathode is determined by W_{sp} and not the density and duration of the current. For a short duration (less than 100–150 ns) of the current, the spots may not cover the entire surface of the cathode but only its section near the site of the primary electrical breakdown of the gap. In short discharges, the local density of spots may therefore be greater than in long discharges.

The dependence of N_s on p may be more complex: N_s increases with increase in p and the increase is nonlinear. A diminution of the transverse dimensions of the spots on the cathode and of the diffuse channels on the anode is also observed under these conditions, i.e. the volume occupied by each channel decreases simultaneously with increase in N_s. One may postulate that such influence of the growth of p on N_s is associated with the increase in the electric field strength (defined as $E_{qs} = U_{qs}/d$) for which an SIVD develops and which is known [1] to determine the probability of the formation of a cathode spot. The dependence of N_s on the

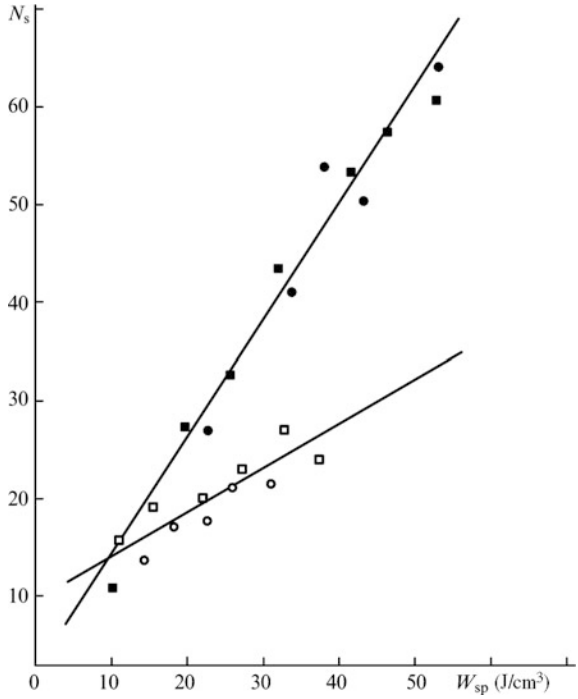

Fig. 24.5 Dependence of the number of cathode spots N_s on the specific input energy W_{sp} for the SF_6: C_2H_6 = 10:1 mixture with D = 6 cm and P = 33.6 Torr (■), D = 2 cm and P = 33.6 Torr (•), D = 6 cm and P = 16.8 Torr (□), and D = 2 cm and P = 16.8 Torr (o)

parameter $W_{sp}E_{qs}$, plotted for different values of p and d taking into account this hypothesis, is presented in Fig. 24.6. It is satisfactorily fitted by the linear function $N_s = a + bW_{sp}E_{qs}$, in which the constant b is in its turn a function of the state of the cathode surface and of the hydrocarbon content in the mixture [8].

A conclusion that isimportant for the further interpretation of the mechanisms of the development of an SIVD follows from Figs. 24.5 and 24.6: the volume occupied by the discharge increases with increase in the amount of energy injected into the plasma and almost in proportion to the energy.

Figures 24.7a, b present photographs of an SIVD in a rod-plane electrode system (Fig. 24.1c) for d = 5 cm and p = 34 Torr in the SF_6: C_2H_6 = 10:1 mixture recorded for two energies, W, deposited in the discharge plasma. In this geometry, the SIVD consists of a diffuse plume, expanding towards the anode, with formation of a bright plasma near the cathode. Under conditions such that new spots cannot be formed on the cathode, the volume, V, of the glowing part of the plume (an analogue of a diffuse channel) increases with increases in W.

The dependence of V on W obtained under the same conditions as in Fig. 24.7 is presented in Fig. 24.8. A linear growth of V with increase in W can be seen. For W = 5 J, the volume V is ~20 cm^3, whereas the size of the plume on the anode is ~3.6 cm. The high stability of the discharge in the gap geometry under

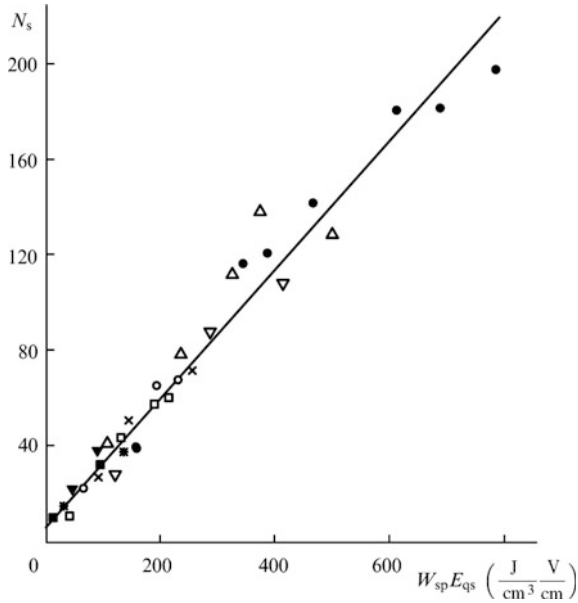

Fig. 24.6 Dependence of the number of cathode spots N_s on $W_{sp}E_{qs}$ for the SF_6: C_2H_6 = 10:1 mixture with D = 6 cm and P = 33.6 Torr (□), d = 6 cm and P = 16.8 Torr (■), D = 4 cm and P = 23.3 Torr (*), D = 3 cm and P = 23.3 Torr (y), D = 3 cm and P = 33.6 Torr (o), D = 3 cm and P = 50.4 Torr (Δ), D = 3 cm and P = 67.2 Torr (•), and D = 2 cm and p = 33.6 Torr (x)

consideration, despite the fact that the current density of the cathode is $j = 1.2 \times 10^5$ A cm^{-2}, is striking. It is noteworthy that the influence of the duration of the discharge current on V is also appreciable in this geometry. This accounts for the considerable scatter of the points in Fig. 24.8 because, in the experiments, the duration of the current varied from 50–300 ns.

Figures 24.9a, b present voltage (U) and current (I) oscillograms for an SIVD in the rod-plane electrode system (Fig. 24.1c) for current pulses of 100 and 200 ns duration with identical charging voltage and charging capacitance in the SF_6: C_2H_6 = 10:3 mixture (p = 40 Torr, d = 4.4 cm). Figures 24.9c, d show similar voltage and current oscillograms for an SIVD recorded under the same conditions but with confinement of the discharge on the anode by a tube 7 mm in diameter (Fig. 24.1d). As can be seen from Figs. 24.9a, b, the voltage and current oscillograms in the rod-plane system do not differ in any way from typical oscillograms obtained in a plane electrode system.

Confinement of the discharge leads to an appreciable change in the type of oscillograms. For a long duration of the current pulse (Fig. 24.9d), after the initial fall of the voltage, one observes its increase simultaneously with an increase in the current—the current maximum being attained sooner than in the case of an 'unconfined' discharge. The current amplitude also diminishes, whereas the voltage is appreciably higher at its maximum than in the case of an 'unconfined' discharge. Voltage oscillograms of a similar type are obtained when the discharge characteristics are calculated taking into account the attachment of electrons to vibrationally excited SF_6 molecules [9]. However, the calculated oscillograms in [9] do

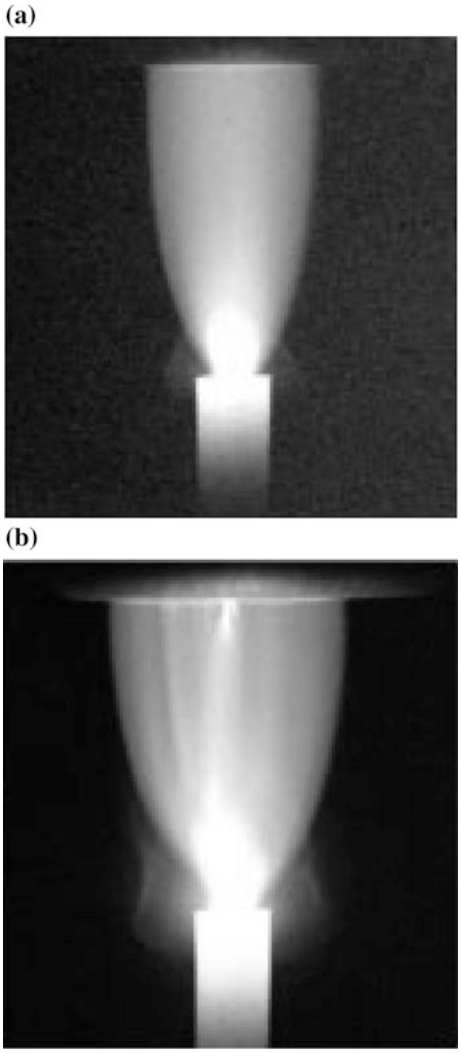

Fig. 24.7 Photographs of an SIVD in the rod-plane electrode system with W = 0.73 J (**a**) and 2.33 J (**b**)

not agree with the experimental oscillograms; we are not aware of other studies in which a similar form of the discharge voltage was observed in SF_6 and in mixtures based on it.

For τ = 200 ns, the confined SIVD contracts after the current has reached a maximum. A decrease in the duration of the current makes it possible to obtain an uncontracted confined SIVD (Fig. 24.9c). In this case, there is no break in the voltage oscillogram and, following a general increase in the discharge voltage, the 'tail' becomes less tilted. It may be noted that the modification of the voltage pulse observed in Figs. 24.9c, d following the confinement of the SIVD is associated precisely with the increase in the specific energy input in the plasma, because under

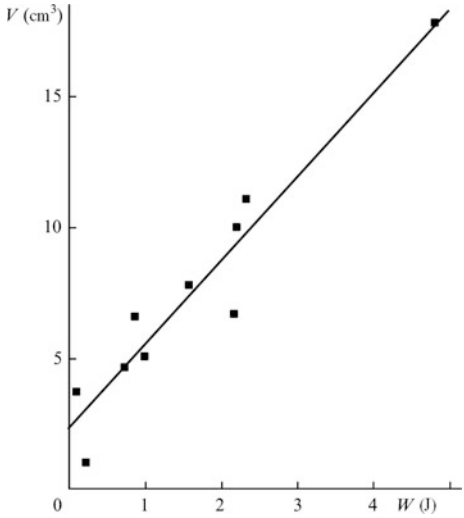

Fig. 24.8 Dependence of the volume, V, of an SIVD on the energy, W, in the rod-plane electrode system

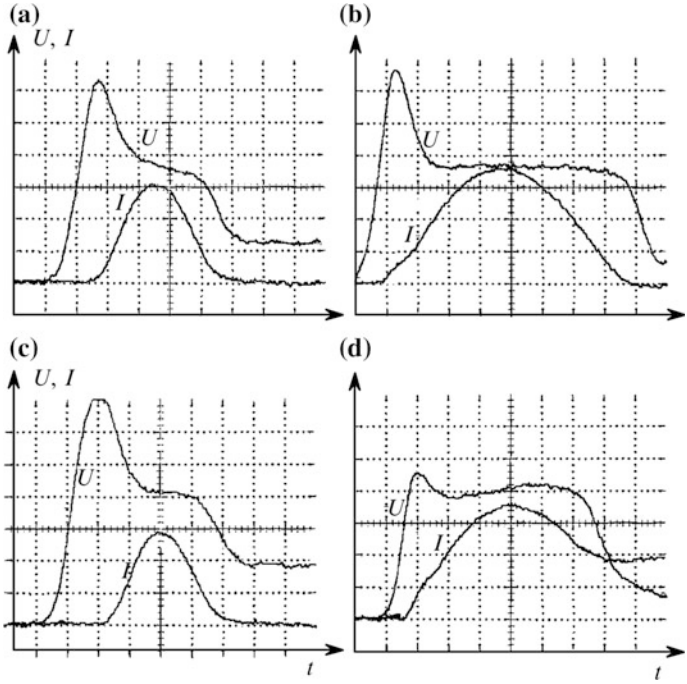

Fig. 24.9 Voltage (*U*) and current (*I*) oscillograms for an unconfined (**a**, **b**) and confined (**c**, **d**) SIVD in the rod-plane electrode system with τ = 100 ns (**a**, **c**) and 200 ns (**b**, **d**). Oscillogram scales: 5.1 kV division^{-1} (**a**–**d**), 79.4 A division^{-1} (**b**, **d**), 198.5 A division^{-1} (**a**, **c**); time scan – 25 ns division^{-1}

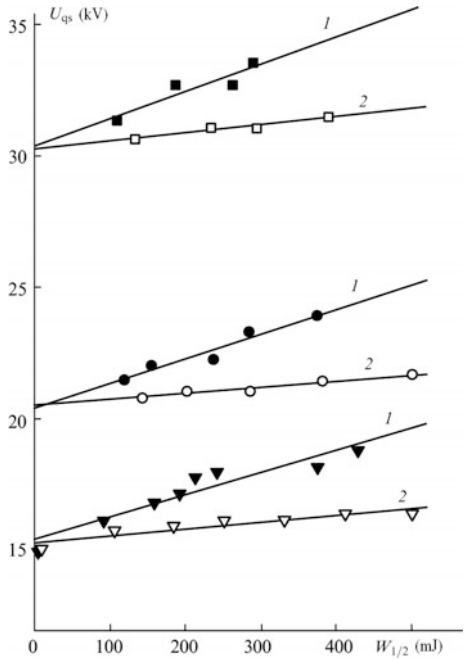

Fig. 24.10 Dependence of U_{qs} on the energy $W_{1/2}$ for a confined (*1*) and unconfined (*2*) SIVD with p = 33.6 Torr (*triangles*), 45.8 Torr (*circles*), and 67.2 Torr (*squares*); SF_6:C_2H_6 = 10:1 mixture, d = 4 cm

the conditions of the given experiment, the discharge cannot expand during the energy deposition process.

Figure 24.10 presents dependences of U_{qs} on the energy $W_{1/2}$, deposited in the discharge plasma before the attainment of the current maximum, in the rod-plane electrode system for confined (curve 1) and unconfined (curve 2) SIVDs; (U_{qs} was determined at the current maximum. Evidently, with increase in $W_{1/2}$ an appreciable growth of U_{qs} is observed in the confined SIVD, which is significantly more notable than in the unconfined SIVD. The relative increase in U_{qs} (compared with U_{qs} for the unconfined SIVD) for the same values of $W_{1/2}$ is greater, the smaller the value of p, i.e. the greater the energy deposited in the plasma per unit volume and per molecule.

The results presented in Figs. 24.9 and 24.10 indicate an increase in the electron attachment coefficient in SF_6-based mixtures with increase in the specific energy input in the discharge plasma.

The possibility of obtaining a volume discharge in the electrode systems illustrated in Figs. 24.1e, f is a consequence of the existence of mechanisms restricting the SIVD energy transmitted by an individual diffuse channel and leading to an increase in the volume occupied by the discharge with increase in the input energy. Figure 24.11 presents photographs of a discharge in air and in the SF_6; C_2H_6 = 10:1 mixture, respectively, at a pressure of 65 Torr obtained in the system comprising plane electrodes linked by a dielectric plate (Fig. 24.1e). As was to be expected, the discharge in air develops in the form of the electrical spark breakdown

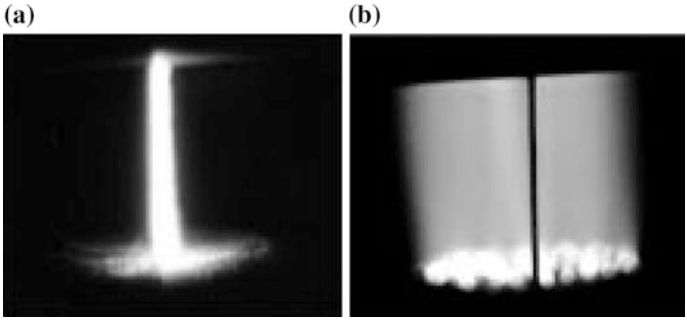

Fig. 24.11 Photographs of a discharge in a system of plane electrodes linked by a glass plate in air (**a**) and in the SF_6: C_2H_6 = 10:1 mixture (**b**)

of the gap along the surface of the dielectric plate, the bulk phase being entirely absent. In an SF_6–C_2H_6 mixture, the discharge is very much of the volume type, its external appearance and oscillograms being completely indistinguishable from an SIVD obtained in the same system in the absence of a plate (with the exception that the photograph shows a black band at the site where the plate is located).

In the system with transverse dimensions of the electrodes close to the internal diameter of the tube (Fig. 24.1f), the discharge is also very much of the volume type for the mixture SF_6:C_2H_6 = 10:1 and p = 15–65 Torr. When $W_{sp} > 0.05$ J cm^{-3}, the surface density of the cathode spots has a maximum in the central zone of the cathode, as in the usual gap with plane electrodes that are not linked by a dielectric surface.

In the subsequent ignitions of an SIVD without a change of mixture, an appreciable increase in U_{qs} and a decrease in the current are observed in the above electrode system. Since in the case under consideration, the SIVD occupies the entire volume of the discharge chamber (Fig. 24.1f), this fact indicates that, in the mixture of gases formed as a result of the dissociation of the starting materials, the effective ionization coefficient is smaller than in the initial mixture. It is worthy of note that a volume discharge in a tube with an internal diameter close to the diameter of the electrodes had been obtained earlier in an SF_6-H_2 mixture [10]; however, the authors did not interpret the result.

24.4 Discussion of the Results

The following processes are characteristic of SIVDs: consecutive formation of diffuse channels (with a simultaneous decrease in the current through the channels that had arisen earlier) during the development of the SIVD in a gap with planar geometry, the expansion of the diffuse-glow zone in the rod-plane gap, an increase in the discharge voltage with an increase in the specific energy. As previously

mentioned, these processes are apparently determined to a large extent by the mechanisms of the confinement of the current in the conducting channel, which depend on the specific energy input. We shall consider two possible mechanisms leading to this state of affairs, namely the dissociation of SF_6 by electron impact and the attachment of electrons to vibrationally excited SF_6 molecules.

Firstly, it is important to note that for the ratios *E/N* close to the critical value, virtually the entire energy deposited in SF_6 is consumed in dissociation [14]. According to [7, 11], the SF_6 $SF_6 \rightarrow SF_4 + 2F$ channel is dominant.

The ionization potential of F atoms (17.42 eV) exceeds that for SF_6 (15.7 eV) [12], so that an appreciable contribution by the F atoms produced to the overall ionization should not be expected even at their considerable concentrations. With regard to the attachment of electrons, the formation of F^- ions via any of the possible mechanisms is known to be incapable of competing, as shown by estimates [13], with the attachment of electrons to SF_6 molecules. The F excitation threshold is 12.7 eV [12] (the component of the main doublet with a threshold energy of ~ 0.05 eV may naturally be disregarded in the given instance), i.e. it is in the region of the intense excitation of the SF_6 terms by electron impact [14]. Furthermore, there are grounds for the postulate that inelastic processes with participation of SF_4 molecules also do not influence in any way that is significant the energy spectrum of the electrons in the discharge.

Bearing in mind the qualitative nature of the models considered and neglecting therefore the difference between the cross sections for the elastic scattering of electrons by SF_6 molecules and their decomposition products, one may postulate that the influence of the dissociation of SF_6 may only affect the decrease in the reduced field strength *E/N* with increase in the total concentration of neutral particles, N, as the specific energy input increases. The dependences of the main transport coefficients on *E/N* can be reasonably assumed to be the same as in pure SF_6. In particular, we shall assume that the effective ionization coefficient is $a_{\text{eff}} = AN[E/N - (E/N)_{\text{cr}}]$, where $(E/N)_{\text{a}}$ is the critical value of the parameter *E/N* [7]. Depending on the specific energy $\int_0^t Ej\,\mathrm{d}\tau$ deposited in the gas, the total concentration of neutral particles N can be expressed as follows:

$$N(t) = N_0\left(1 + \alpha\int_0^t Ej\,\mathrm{d}\tau\right).$$

Here, j is the current density; N_0 is the initial gas concentration; the coefficient, a, is expressed in terms of the dissociation constant, k_{d}, and is assumed to be subsequently constant. The condition for the admissibility of such formulation is $\alpha\int_0 Ej\,\mathrm{d}\tau \ll 1$.

Passing now to the 'energy' variable $q = \alpha \int_0^t Ej\,\mathrm{d}\tau$ [15], we have for the electron concentration $n_e(q)$ in the channel

$$\frac{\mathrm{d}n_e}{\mathrm{d}q} = \frac{A}{\alpha e}\left(1 - \frac{1+q}{K_n}\right), \tag{24.1}$$

where e is the electron charge; $K_n = E/E_{cr}$ is the overvoltage factor; E_{cr} is the critical field for $N = N_0$. It follows from (24.1) that the $n_e(g)$ relationship has a maximum at $q = q_{max} = K_n - 1$, so that the electron concentration in the channel begins to fall for $q > q_{max}$ as a result of the dissociation of SF_6.

If we employ the fit to the dependence of the drift velocity of the electrons in SF_6 on *E/N* recommended in [7], then the current density in the channel is $j(q) \sim n_e(q)(1 + q)^{-0.6}$. Evidently, the current density in the channel also passes through a maximum, but this time at $q = q' < q_{max}$. Under the experimental conditions, $K_n \sim 1$ and hence $q < 1$, therefore the use of an approximation linear in q is justified. The fact that, according to [14], the fraction of the energy deposited in the discharge and consumed on the decomposition of SF_6 increases with decrease in *E/N* in the $E/N > 200\tau d$ region of interest constitutes significant evidence in support of the important role of the dissociation of SF_6 in the SIVD.

At a qualitative level, it is not difficult to also follow the attachment of electrons to the vibrationally excited SF_6 molecules described by $N^*_{SF_6}$. Taking Eq. (24.1) into account, the corresponding system of equations assumes the form

$$\begin{aligned} \frac{\mathrm{d}n_e}{\mathrm{d}q} &= \frac{A}{\alpha e}\left(1 - \frac{1+q}{K_n}\right) - \frac{\eta^*_a(q)N^*_{SF_6}(q)}{\alpha e E}, \\ \frac{\mathrm{d}N^*_{SF_6}}{\mathrm{d}q} &= \frac{\eta^*(q)N(q)}{\alpha e E}. \end{aligned} \tag{24.2}$$

Here, $\eta * (q)$ and $\eta^*_a(q)$ are the vibrational excitation coefficient and the coefficient for electron attached to vibrationally excited SF_6 molecules, respectively. We then have

$$\begin{aligned} \frac{\mathrm{d}n_e}{\mathrm{d}q} &= \frac{A}{\alpha e}\left(1 - \frac{1+q}{K_n}\right) - Q(q), \\ Q(q) &= \frac{\eta^*_a(q)}{\alpha^2 e^2 E^2}\int_0^q N(s)\eta^*(s)\mathrm{d}s. \end{aligned} \tag{24.3}$$

It follows from formula (24.3) that the $n_e(g)$ relationship passes through a maximum at $q = q'' = g_{max} - ueK_nQ(q'')/A$. Since $Q(q)$^ 0 for any q, it follows that $q'' > g_{max}$. However, the lack of any detailed information concerning r* and > 7* makes it difficult to be more specific about the value of q''.

It is possible to show that allowance for additional factors will significantly complicate the mathematical description without fundamentally altering the result: the dissociation of SF_6 by electron impact and the attachment of electrons to vibrationally excited SF_6 molecules may indeed serve as the mechanisms of the limitation of the current in the conducting channel in the active media of an HF laser. At the same time, it is important to note that resorting to only the mechanisms of current limitation in the conducting channel is not by itself sufficient for the complete understanding of the processes observed in the experiment, in particular the propagation of the discharge into the interior of the gap in the direction perpendicular to the applied field.

24.5 Conclusions

The SIVD in SF_6-hydrocarbon mixtures, used as the active media for nonchain HF lasers, has been investigated. The following features of the development of the SIVD have been established:

1. After the primary electrical breakdown of the discharge gap, the SIVD spreads in the gap in the direction perpendicular to that of the electric field as a result of the cosecutive appearance of overlapping diffuse channels. As the new channels appear, the current flowing through the channels formed earlier diminishes.
2. The volume occupied by the SIVD increases $\ll$ hum linearly with increase in the energy deposited in the plasma ir.c. when the discharge volume is confined by a dickcuk surface, the discharge voltage increases simultaneously with increase in the current.

The hypothesis that mechanisms exist for the limitation of the current in the conducting channel has been put forward. They are associated with the specific energy released ir. The plasma and they prevent the transfer of all the deposited energy through a separate channel. It is shown that such mechanisms may include the dissociation of SF_6 and the attachment of electrons to vibrationally excited SF_6 molecules.

References

1. Y.D. Korolev, G.A. Mesyats, Fizika Impul'snogo Proboya Gazov (The Physics of the Pulsed Electrical Breakdown of Gases) (Nauka, Moscow, 1991)
2. V.V. Apollonov et al., Pis'ma. Zh. Tekh. Fiz. **22**(23), 60 (1996) [Tech. Phys. Lett. 22, 1026 (1996)]
3. V.V. Apollonov et al., Kvantovaya Elektron. (Moscow) **24**, 213 (1997) [Quantum Electron. 27, 207 (1997)]
4. V.V. Apollonov et al., Kvantovaya Elektron. (Moscow) **25**, 123 (1998) [Quantum Electron. 28, 116 (1998)]

5. V.V. Apollonov et al., Proc. SPIE Int. Soc. Opt. Eng. **3574**, 374 (1998)
6. V.V. Apollonov et al. II Mezhdunar. Konf. Po Fizike Plazmy i Plazmennym Tekhnologiyam, Minsk, 1997 (Proceedings of the Second International Conference on Plasma Physics and Plasma Technologies, Minsk, Belarus, 1997) (National Academy of Sciences of Belarus, Minsk, 1997), p. 154
7. I.M. Bortnik, Fizicheskie Svoistva i Elektricheskaya Prochnost' Hlegaza (The Physical Properties and the Electrical Strength of Sulfur Hexafluoride) (Energoatomizdat, Moscow, 1998)
8. V.V. Apollonov et al., IX Konf. Po Fizike Gazovogo Razryada, Ryazan, 1998 (Proceedings of the Ninth Conference on the Physics of Gas Discharges, Ryazan, 1998) (Ryazan: Ryazan Radio Engineering Academy, 1998) p. 58
9. L. Richeboeuf, S. Pasquiers, M. Legentil, V.J. Puech, Phys. D **31**, 373 (1998)
10. A.F. Zapol'skii, K.B. Yushko, Kvantovaya Elektron. (Moscow) **6,** 408 (1979) [Sov. J. Quantum Electron. 9, 248 (1979)]
11. E.B. Gordon, V.I. Matyushenko, P.B. Repin, Sizov V D. Khim. Fiz. **8**, 1212 (1989)
12. A.A. Radtsig, *Smirnov B M Spravochnik po Atomnoi i Molekulyarnoi Fizike (Handbook of Atomic and Molecular Physics)* (Atomizdat, Moscow, 1980)
13. H.S.W. Massey, Negative Ions (Cambridge University Press, Cambridge, 1976)
14. D.I. Slovetskii, A A. Deryugin, in Khimiya Plazmy (The Chemistry of Plasma) (Moscow, 1987), p. 240
15. A.A. Belevtsev, in *Proceedings of the Thirteenth International Conference on Dielectric Liquids (ICDL'99)*, Nara, Japan, 1999, p. 672

Chapter 25
Discharge Characteristics in a Nonchain HF(DF) Laser

Abstract It was found that for SF_6-hydrocarbon (deutero-carbon) mixtures with a composition typical for nonchain HF(DF) lasers, the electric field strength reduced to the partial pressure of SF_6 (p_{SF_6}) in the quasistationary phase of an SSVD $(E/p_{SF_6})_{st}$ = 92 V $m^{-1}Pa^{-1}$ is close to the known critical value $(E/p)_{cr}$ = 89 V m^{-1} Pa^{-1}, which is specified by the condition that the electron-impact ionization rate of SF_6 is equal to the rate of electron attachment to SF_6 molecules. This testifies to the decisive role of these two processes and allows the use of the known approximations of the effective ionization coefficient and the electron drift velocity for pure SF_6 when calculating the discharge characteristics. The oscilloscope traces of voltage and current calculated in this approximation for lasers with apertures ranging from 4 to 27 cm deviated from the experimental data by no more than 10%.

Initiating nonchain HF(DF) lasers on a basis of SF_6-hydrocarbon (deuterocarbon) mixtures by an SSVD makes it possible to obtain substantial output energies with a reasonably high efficiency [1–3]. Despite the fact that this initiation method has long been known, the processes occurring in an SSVD plasma in the working media of nonchain lasers have not been adequately studied until now. In particular, tens of elementary processes are taken into account in calculating SSVD characteristics, including the increase in electron losses owing to their attachment to vibrationally excited SF_6 molecules, the gas heating, and the parameters of the external circuit (see, e.g. [4, 5]). However, the calculated oscilloscope traces of voltage and current differ greatly from the experimental ones. This is supposedly related to the inexactness of the data on the rate coefficients for many elementary processes, which in turn does not permit selection of the principal processes that control the SSVD characteristics. The aim of this work is to determine the processes whose inclusion would make it possible to attain a good agreement between the calculated and experimental oscillograms.

© Springer International Publishing Switzerland 2016

V.V. Apollonov, *High-Energy Molecular Lasers*,
Springer Series in Optical Sciences 201, DOI 10.1007/978-3-319-33359-5_25

A clearly defined 'step' is observed in the oscilloscope traces of the SSVD voltage in SF_6 and its mixtures with hydrocarbons (deuterocarbons). This step corresponds to the quasi-stationary phase of the SSVD during which the voltage across the discharge gap was in fact constant. It is easy to show that, when the voltage varies in this way, the maxima of the SSVD current and of the electron concentration coincide in time with a good accuracy; i.e., the quasi-stationary voltage measured from the oscilloscope traces at the time the current reaches a maximum is close to the voltage for which the rates of the electron production and loss in a discharge plasma become equal. Therefore the quasi-stationary voltage is determined by the electron production and loss, and its changes caused by variations in the mixture composition reveal information on the nature of these processes.

We have measured the quasi-stationary voltages of the SSVD in SF_6 and its mixtures with hydrocarbons (deuterocarbons) over a wide range of parameters: the mixture pressure p = 10−60 Torr, the interelectrode gap d = 2−27 cm, and the energy deposition W = 20−200 J L^{-1}. The length of the discharge pulse was varied between 200 and 400 ns. These are operating conditions for nonchain HF(DF) lasers with large volumes of the active medium [1–3]. In experiments presented here, the SSVD was ignited between two disk electrodes: a cathode 6 cm in diameter and an anode 12 cm in diameter, which were perimetrically rounded off with a radius of curvature 1 cm. A capacitor discharged into the gap via a variable inductance. The SSVD current and voltage were recorded by using calibrated shunts or Rogowski loops and voltage dividers. The electric signals were recorded with a Tektronix TDS 220 oscilloscope.

Figure 25.1 shows the quasi-stationary voltage U_{st} as a function of the parameter $p_{SF_6}d$ for pure SF_6 and for its mixture with C_2H_6 for a ratio of partial component pressures of 10:1 (p_{SF_6} is the partial pressure of SF_6 in the mixture). One can see that U_{st} is hardly affected by the addition of C_2H_6 to SF_6; i.e., for mixture compositions typical of HF(DF) lasers, U_{st} is determined primarily by the partial pressure of SF_6. The U_{st} voltage depends linearly on $p_{SF_6}d$. The electric field strength in the quasi-stationary phase derived from Fig. 25.1 and reduced to the partial SF_6 pressure is (E/p_{SF_6}) = 92 V m^{-1} Pa^{-1} (where E is the electric field strength in the SSVD column). This value is close to the critical reduced electric field strength for pure SF_6 $(E/p)_{cr}$ = 89 V m^{-1} Pa^{-1} known from the literature [6], which is given by the condition that the coefficient of electron attachment to SF_6 molecules be equal to the electron-impact SF_6 ionization coefficient. For SF_6 mixtures with relatively small (below 20%) additions of hydrocarbons (deuterocarbons), U_{st} is approximated well by the expression $U_{st} = (E/p_{SF_6})_{st}\, p_{SF_6}d + U_c,\ U_c \approx 800$ V.

The results of measurements of U_{st} suggest that only the processes of SF_6 ionization by electron impact and of electron attachment to SF_6 molecules are significant for the SSVD under the conditions involved. At the same time, such processes as stepwise ionization, the Penning process, electron attachment to the

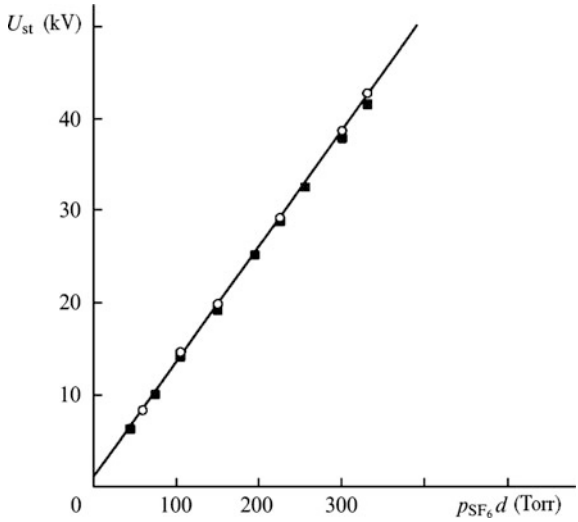

Fig. 25.1 Quasi-stationary voltage U_{ST} as a function of the parameter $p_{SF_6}d$ in pure SF_6 (■) and in a mixture of composition SF_6: C_2H_6 = 10:1 (o)

excited SF_6 molecules, and ionization of impurity molecules can be neglected, at least for an energy deposition not exceeding 200 J I^{-1} and for the SSVD current pulse length above 200 ns. In this approximation, the main characteristics of the SSVD in the working mixtures of nonchain HF(DF) lasers were calculated by using simple approximations for the effective ionization coefficient α_{ef} and the electron drift velocity u_e for pure SF_6 taken from [6]. The electron concentration n_e was determined from the combined solution of the continuity equation for the electron component of the current and the Kirchhoff equations for the electric circuit, as in [7]. The ion component of the current was disregarded. The initial electron concentration was assumed to be equal to the background value. In the equivalent electric circuit, the discharge gap was represented as a resistive element with resistance $R_d = U/I = U/(en_eu_eS)$, where U is the voltage across the gap, I is the discharge current, e is the electron charge, and S is the cathode surface area.

The validity of the above approximation was verified by the example of a simple discharge circuit whose equivalent electric circuit is shown in Fig. 25.2a. The capacitor capacitance was C = 3.9 nF; the inductance and the resistive losses in the circuit were determined experimentally. The oscilloscope traces of the voltage and the current were recorded for d = 4 cm, S = 12.6 cm^2, and a 33.5 Torr pressure of the mixture with the composition SF_6:C_2H_6 = 10:1. In the calculation, the fact that an ohmic divider measures the sum of potential drops across the gap and the inductance of the electrode current supplied was taken into account. Also shown in Fig. 25.2a are the experimental and calculated oscilloscope traces of the voltage and current. One can see that the calculated oscilloscope traces agree well with the experimental ones (within 6%).

This model was used for calculating the SSVD characteristics in two laser systems with d = 5 cm, p = 67 Torr and d = 26.6 cm, p = 58 Torr. The equivalent

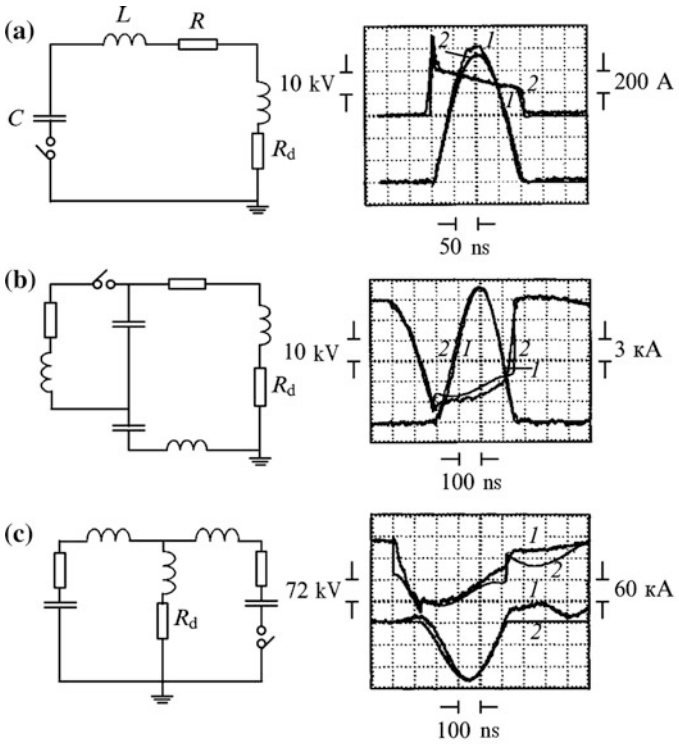

Fig. 25.2 Different equivalent electric circuits of discharge circuits and the corresponding experimental (*1*) and calculated (*2*) oscilloscope traces of the voltage (*the upper trace*) and the current (*the lower trace*)

electric circuits of the two laser systems are shown in Fig. 25.2b, c. In both cases, the discrepancy between the calculated and experimental oscilloscope traces was within 10%.

To obtain good agreement between experimental and calculated oscilloscope traces of the voltage and the current of the SSVD in SF_6 and its mixtures with hydrocarbons (deuterocarbons) under conditions typical of nonchain large-volume HF(DF) lasers (energy deposition below 200 J^{-1}, current pulses longer that 200 ns), one should take into account only the ionization of SF_6 by electron impact and the electron attachment to SF_6 molecules. Why, despite the existence of many processes in the discharge plasma, are only these two significant?

The reason for their significance is possibly related to the specific features of the SSVD development in SF_6 and its mixtures with hydrocarbons (deuterocarbons). Earlier we considered a mechanism of local current density limitation on reaching some limiting value, which resulted in the increase in the discharge volume during the discharge development with increasing energy introduced into the plasma [1]. As a result, at every instant of time, the discharge current flows primarily through

an unexcited gas, resulting in the independence of the voltage across the discharge gap of the accumulation of excited particles in the discharge volume. If the specific energy deposition is raised in some way, e.g. by limiting the discharge volume, it is possible that the dependence of the quasi-stationary voltage on the specific energy deposition would be observable in the oscilloscope traces.

References

1. V.V. Apollonov et al., Proc. SPIE Int. Soc. Opt. Eng. **3574**, 374 (1998)
2. V.V. Apollonov et al., Kvantovaya Elektron. (Moscow) **24**, 213 (1997) [Quantum Electron. 27, 207 (1997)]
3. V.V. Apollonov et al., Kvantovaya Elektron. (Moscow) **25**, 123 (1998) [Quantum Electron. 28, 116 (1998)]
4. L. Richeboeuf, S. Pasquiers, M. Legentil, V. Puech, J. Phys. D Appl. Phys. **31**, 373 (1998)
5. F. Doussiet, M. Legentil, S. Pasquiers, C. Postel, V. Puech, L. Richsboeuf, Proc. SPIE Int. Soc. Opt. Eng. **2702**, 179 (1996)
6. I.M. Bortnik, *Fizicheskie Svofstva i Elektricheskaya Prochnost' Elegaza (The Physical Properties and the Electric Strength of Hexafluoride of Sulfur)* (Energoatomizdat, Moscow, 1998)
7. Y.I. Bychkov, V.P. Kudryashov, V.V. Osipov, Savin V.V. Zh, Prikl. Mekh. Tekh. Fiz. **2**, 42 (1976)

Chapter 26
Ion–Ion Recombination in SF_6 and in SF_6–C_2H_6 Mixtures for High Values of E/N

Abstract Ion-ion recombination coefficients in a decaying SF_6 plasma and in SF_6–C_2H_6 mixtures were measured in the pressure range 15–90 Torr for reduced field strengths 100–250 Td. The charge composition was analyzed and dominating ion-ion recombination channels in such plasmas were determined. Relations for estimating the potential drop at the electrodes were obtained for decaying plasma in strongly electronegative gases. The results of measurements are extrapolated in order to estimate the ion-ion recombination coefficient in SF_6 for nearly critical field strengths. We conclude that the ion-ion recombination should be taken into account in calculations of the discharge characteristics in non-chain reaction HF lasers.

26.1 Introduction

The possibility of exciting an SSVD without preionization, i.e.,an SIVD [1] in SF_6 mixtures with hydrocarbons, was discovered in [2], and raised the problem of scaling nonchain reaction HF lasers to a qualitatively new level, increasing their power and energy by more than an order of magnitude (by a factor of 40). At present, the energy emitted by SSVD-initiated non-chain reaction HF lasers exceeds 400 J for an electrical efficiency of more than 4% [3].

In this connection, it is interesting to continue the investigation of SSVD in SF_6 and in mixtures of SF_6 with hydrocarbons. Because of its strongly electronegative nature, the SF_6 plasma of such a discharge possesses a number of specific features. For example, the concentration of positive and negative ions in such a plasma is much higher than the electron concentration (by almost two orders of magnitude) [1, 4]. For this reason, processes associated with the ionic component of plasma (destruction of negative ions by electron impact, dissociative electron-ion recombination and ion-ion recombination) may play a significant role in the discharge kinetics [4]. The latter process considerably affects the ion concentration in SSVDs and completely determines the charge kinetics in a decaying plasma.

The ion-ion recombination in SF_6 and its mixtures with hydrocarbons in an external electric field has not been adequately studied. Apparently, only two works

© Springer International Publishing Switzerland 2016

V.V. Apollonov, *High-Energy Molecular Lasers*,
Springer Series in Optical Sciences 201, DOI 10.1007/978-3-319-33359-5_26

[5, 6] reported the measurement of the ion-ion recombination coefficient β in SF_6, binary mixtures of SF_6 with the hydrocarbon CH_4 used rarely in HF lasers, and in ternary SF_6–CH_4–Ar/He mixtures at working pressures $p > 100$ Torr and relatively low reduced electric field strengths $E/N < 160$ Td (N is the concentration of neutral particles). The remaining experimental [7] and theoretical (simulation by the Monte Carlo method) [8] studies cover a much wider range of pressures ($\sim 10^2$–10^4 Torr), however, in the zero electric field approximation.

To calculate the SSVD characteristics in a non-chain reaction HF laser, of main interest is the coefficient β for mixtures of SF_6 with the hydrocarbon C_2H_6 [1–3] for p = 30–90 Torr (lasers with quite large apertures) and values of E/N close to the critical value $(E/N)_{cr}$ in SF_6. The aim of this paper is to measure the ion-ion recombination coefficient in pure SF_6 and its mixtures with C_2H_6 in the above-mentioned pressure range for values of E/N up to 250 Td. In particular, this makes it possible to obtain a reasonable value of the coefficient β for $E/N \sim (E/N)_{cr}$ characteristic of the SSVD.

26.2 Experimental

Ion plasma for measuring the coefficient β was induced by a pulsed SSVD. The scheme of the experimental setup is shown in Fig. 26.1. The SSVD was ignited between an anisotropically resistive cathode K of size 5 cm × 5 cm (similar to the one used in [9]) and a disc-shaped anode, A, with a diameter of 12 cm, rounded off at the edge to a radius of 1 cm, by commutating the voltage with a gap, PI. The interelectrode distance was varied from 2–8 cm. The anisotropically resistive cathode made it possible to obtain a discharge distributed uniformly over the cathode surface, which is necessary for the applicability of comparatively simpler relations that we will use below for determining ion concentration.

The resistance $R_c \sim 1\ \Omega$ of the anisotropically resistive cathode is much smaller than the resistance $R_p \sim 1\ k\Omega$ of the ion plasma, and hence does not introduce any noticeable distortions in the measured values of ion current. The capacitance 2–8 nF

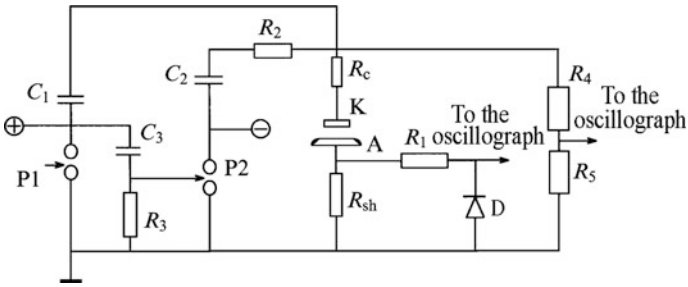

Fig. 26.1 Scheme of the setup for measuring the ion-ion recombination coefficient

of capacitor C_1 was determined from the conditions of the SSVD stability and homogeneity. The capacitor C_2 = 174 nF connected to the gap P2 was used to mantain a constant voltage across the discharge gap during the measurement of the ion current (up to 20 μs). The resistance R_2 = 50 Ω, connected in the discharge circuit of this capacitor, minimizes its influence on the energy released in the SSVD plasma. The gap P2 was triggered automatically upon activation of the gap PI and closure of the capacitor C_3 circuit through the resistor R_3. The current was detected by the shunt resistance R_{sh}.

Since the ion current of the decaying plasma was much weaker (by several orders of magnitude) than the maximum SSVD current, to improve the accuracy of measurements, the signal from the shunt was cut off at the level of 1 V by the R_1 – D diode limiter. Calibration of the ion current measuring circuit and verification of its linearity were performed by shunting a capacitor (through the gap) charged to a voltage ~4 kV through a resistance ~1 kΩ. Figure 26.2a shows typical oscillograms of the current and voltage across the discharge gap recorded in this way. The negative spikes on the oscillograms correspond to the SSVD current and voltage.

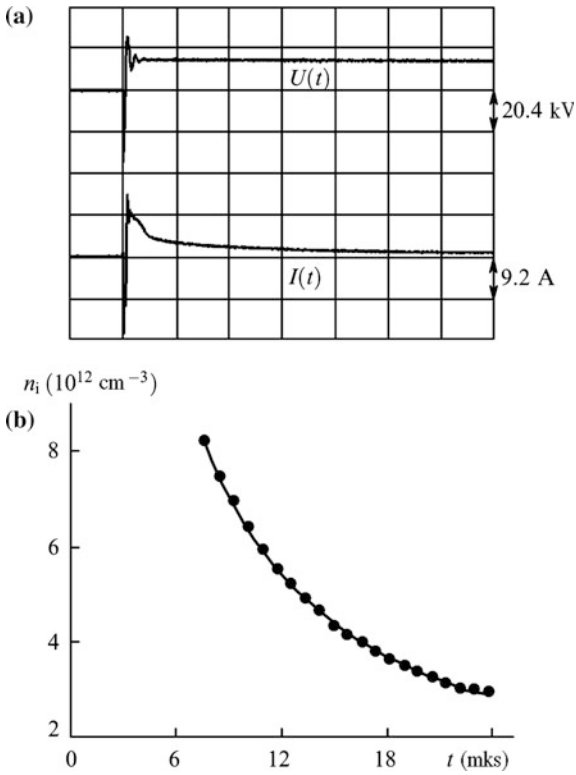

Fig. 26.2 **a** Oscillograms of voltage U across the discharge gap (*upper trace*) and the current I in a decaying plasma (*lower trace*), and **b** dependence of the ion concentration, n_i, on time t, calculated from the oscillograms of Fig. 26.2a (*dark circles*) and by the method of least squares (*solid curve*) for p = 30 Torr and E/N = 230 Td

The ion-ion recombination coefficient β was calculated from the current oscillogram $I(t)$ for a fixed voltage U across the discharge gap with the help of the relations

$$n_i(t) = \frac{I(t)}{Se(b_i^+ + b_i^-)E}, \tag{26.1}$$

$$n_i(t) = \frac{n_i(0)}{1 + n_i(0)\beta t}. \tag{26.2}$$

Here, $n_i(t)$ is the ion concentration; S is the cathode area; e is the electron charge; $E = U/d$; $n_i(0)$ is the initial ion concentration. Relations (26.1) and (26.2) are written under the assumption that there is only one type of positive and one type of negative ions with mobilities b_i^+ and b_i^-, respectively. The possibility of such an assumption is discussed below. The quantities $n_i(0)$ and β were determined from relation (26.2) from the values of $n_i(t)$ reconstructed from (26.1) by the method of least squares (Fig. 26.2b).

26.3 Results of Measurements

Figure 26.3 shows the dependences of the ion-ion recombination coefficient β on the parameter E/N in pure SF_6 under a pressure p = 15–90 Torr. It can be seen that β strongly decreases with increasing E/N over the entire pressure range. This result is consistent with the data presented in [5], where measurements were performed by the standard technique using an electron beam for producing the ion plasma. In the region of small E/N, the coefficient increases with pressure p almost linearly. In the

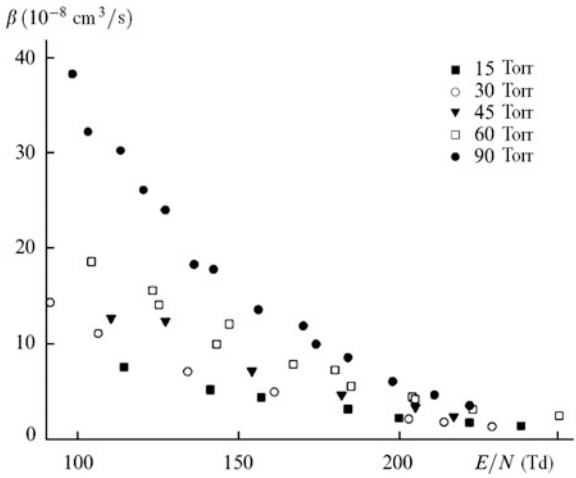

Fig. 26.3 Dependences of the ion-ion recombination coefficient β on the parameter E/N for SF_6 under different pressures

range $E/N > 200$ Td, this law is violated and the dependence of β on p becomes weaker. This fact does not contradict the results obtained in [10], where it was shown by calculations that the ion-ion recombination coefficient depends not only on the parameter E/N, but also on the absolute value of the electric field strength E, decreasing with increasing E.

Note also that in the region of low values of $E/N = 100$–160 Td, the values of the coefficient β measured in our experiments for $p = 90$ Torr are close to the corresponding values from [9]. In the SF_6:C_2H_6 = 10:1 mixture, the values of β obtained for $E/N = 250$ Td and $p = 60$ and 90 Torr are 4.3×10^{-8} and 6.5×10^{-8} $cm^3\ s^{-1}$, respectively. No changes β were observed upon variation of the SSVD parameters, such as the specific deposited energy and the discharge-current duration over a rather wide range.

26.4 Discussion of Results

Consider the ion composition and the nature of ion-ion recombination in SF_6 and its mixtures with C_2H_6. We are not aware of any experimental facts confirming the presence of positive SF_6^+ ions in the plasma of SSVD in SF_6. According to the results of direct mass-spectrometric measurements (see, for example, [10, 12]), the SF_5^+ ion dominates in the plasma. This is consistent with the results presented in paper [13], in which it was shown that the SF_6^+ ion formed in the plasma is in predissociative state and dissociates into the SF_5^+ ion during a time period much smaller than any characteristic discharge times. As for the negative ions, several kinds of such ions should be considered in general.

In the range of values of E/N close to $(E/N)_{cr}$ and below, in which we are interested, the dissociative attachment of electrons to SF_6 molecules results in the formation of predominantly negative SF_6^- ions [14]. The rates of generation of the SF_5^- and F^- ions are approximately half the rate of formation of SF_6^- ions [14]. The mobilities of the SF_6^- and SF_5^- ions are virtually identical and are close to those obtained in the Langevin (polarisation) approximation [13]. The mobility of the F^- ions can also be estimated quite accurately in the same approximation.

The dissociative charge exchange of the SF_6^- and SF_5^- ions with SF_6 molecules, resulting in the formation of negative ions of another kind (mainly F^- ions) does not have time to occur even under the maximum pressures $\sim$90 Torr used in our experiments. For example, according to the data presented in [15], the minimum time τ_{min} for the reaction $SF_6^- + SF_6 \rightarrow SF_6 + SF_5 + F^-$ at $p = 90$ Torr and for $E/N \sim (E/N)_{cr}$ corresponding to the SSVD stage exceeds 1 μs, while the duration of the SSVD itself in these experiments is $\sim$100–300 ns.

In a decaying plasma with much smaller values of the ratio E/N, the time τ_{min} increases by several orders of magnitude. Thus, the SF_6^- and SF_5^- ions vanish in the decaying SF_6 plasma only as a result of recombination with the SF_5^+ ions. The detachment of an electron from the F^- ion can occur only in the layers in the vicinity

of the electrode (see below). As a result, the decrease in the concentration of F^- ions in the plasma is also determined only by their recombination with $SF_5{}^+$ ions.

In the pressure range under investigation, a three-body mechanism of ion-ion recombination is realized. According to the preliminary estimates obtained by using the well-known three-body recombination models [16] and assuming the polarization nature of interaction of ions with gas molecules, it can be expected that the coefficients of recombination of SF_6^- and SF_5^- ions with SF_5^+ ions are close, while the coefficients of recombination of F^- and $SF_5{}^+$ ions are much higher. In this connection, we consider a decaying ion plasma with one type of positive ions with the concentration $n^+(t)$ and two types of negative ions with concentrations $n_1^-(t)$ and $n_2^-(t)$.

Suppose that the ion-ion recombination coefficients are equal to β_1 and β_2, respectively. For the sake of definiteness, we assume that $\beta_2 > \beta_1$. Taking into account the quasi-neutrality of the plasma, we obtain the following integro-differential equation for the density of positive ions:

$$\begin{aligned} &\frac{d\varphi}{d\tau} = q_1 \exp(-\varphi) + q_2 \exp(-\sigma\varphi), \\ &\varphi = \int_0^\tau y d\tau, \quad y = \frac{n^+(t)}{n^+(0)}, \\ &\tau = \beta_1 n_1^-(0)t, \quad \sigma = \frac{\beta_2}{\beta_1}, \quad q_1 = \frac{n_1^-(0)}{n^+(0)}, \quad q_2 = \frac{n_2^-(0)}{n^+(0)}. \end{aligned} \tag{26.3}$$

Here, $n^+(0)$, $n_1^-(0)$ and $n_1^-(0)$ are the initial concentrations of positive and negative ions.

Because $\sigma > 1$ and $\varphi(\tau) \to \infty$ for $\tau \to \infty$, the second term in (26.3) can be neglected starting from a certain instant of time. Taking into account that $n_1^-(t) = n_1^-(0)\exp(-\varphi)$, this equation is transformed into the recombination equation only for negative ions with the smaller recombination coefficient β_1. As applied to the SF_6 plasma, this means that within a certain time interval after the recombination onset, negative ions SF_6^- and SF_5^-, which have close values of the mobility and recombination coefficient (see above), start dominating in the plasma along with the positive $SF_5{}^+$ ions. This justifies the use of (26.1) and (26.2). This is clearly shown in Fig. 26.2b. One can see that for $t > 8$ μs, the time decay $n_i(t)$ of the ion concentration calculated from (26.1) strictly follows the recombination relation (26.2). The values of ion mobilities used in calculations were borrowed from [13].

The complex $SF_6^-(SF_6)$ ion was considered as the main negative ion in [5, 6, 8]; however, the gas pressures were 5–10 times higher in these works than in our experiments. Taking into account that the rate of clusterization of the SF_6^- ions quadratically depends on *p,* we can expect that the fraction of the complex $SF_6^-(SF_6)$ ions in the investigated plasma is insignificant. Moreover, according to [13], the mobilities of ions SF_6^- and $SF_6^-(SF_6)$ differ by just a few percent in the range $E/N \sim$ 100–250 Td, so that the formation of complex ions under the conditions of our experiments is insignificant at all.

In addition to the SF_5^+ ions, the SF_6:C_2H_6 = 10:1 mixture also contains positive ions formed upon the electron impact ionization of C_2H_6. According to [17, 18], the mechanism of dissociative ionization with the formation of $C_2H_4^+$ ions and H_2 molecules dominates in this case. Using the Langevin approximation and the Blank law [19], we find that the mobility of SF_5^+ and $C_2H_4^+$ ions in the SF_6:C_2H_6 = 10:1 mixture is determined by their interaction with the SF_6 molecules. Despite the fact that the mobility of $C_2H_4^+$ ions (estimated in the polarisation limit) is approximately 1.8 times higher than the mobility of SF_5^+ ions, the $C_2H_4^+$ ions do not make a significant contribution to the total current $I(t)$ for the above-mentioned ratio of the concentrations of SF_6 and C_2H_6. As a result, the set of negative ions remains unchanged. Taking into account that positive SF_5^+ ions dominate in the plasma under study, expression (26.2) describing the recombination kinetics remains applicable for the mixture as well.

While the formation of positive ions in the SF_6–C_2H_6 mixture is also possible upon the charge exchange of the SF_5^+ ions with the C_2H_6 molecules (although, in our opinion, the situation is not quite clear), estimates show that the charge exchange times are $\sim 10^{-8}$–10^{-7} s even for the lowest C_2H_6, concentrations of $\sim 10^{17}$ cm^{-3}. Therefore, only one positive ion will dominate on the time scale exceeding 1 μs of interest to us.

The polarisation approximation was used several times while estimating the ion mobility, although this cannot be always substantiated rigorously under the conditions of our analysis. However, it is known that, as a rule, the values of mobility obtained by using the Langevin formula do not differ significantly from the measured values. This is clearly demonstrated in [13] for the SF_6 molecules. Thus, the above arguments concerning the ion composition of the working medium and the nature of ion recombination under the investigated conditions are justified, at least in principle. The above-mentioned constancy of the ion-ion recombination coefficient upon a considerable variation of the discharge parameters is another indirect evidence in favour of this conclusion, since it follows from what has been stated above that the set of negative ions in the recombination plasma depends weakly on the initial discharge conditions.

The field strength E_p in the plasma was determined in our experiments by dividing the voltage across the discharge gap by the interelectrode distance. It is well known, however, that the voltage drop at the electrode may be very high in the case of strongly electronegative gases. Therefore, it should be interesting to estimate the error introduced in the value of E_p by this method.

To estimate the voltage drop U_c across the cathode, we will use the one-dimensional approximation and assume as in [20], that the field $E_c(x)$ in the cathode layer is independent of the longitudinal coordinate x, i.e., $E_c(x) = E_c$. The estimates made below show that under the conditions under study, this quantity greatly exceeds not only E_p, but also the critical field strength E_{cr}, so that the formation of negative ions in the layer can be neglected. In this case, the distributions of the current density $j_e(x)$ of electrons and $j_+(x)$ of positive ions in the cathode region are described by the same equations as in the case of an

electropositive gas. Beyond the cathode layer ($x > d_c$), the electron component of the total current density J_t in a decaying plasma rapidly vanishes because of an intense attachment of electrons. As a result, the boundary conditions are somewhat different from those considered normally for the electropositive gas:

$$j_e(0) = \gamma j_+(0), \quad j_e(d_c) + j_+(d_c) = J_t, \tag{26.4}$$

where γ is the secondary electron emission coefficient. The second condition in (26.4) can also be formulated as $j_\varepsilon(d_c) + j_-(d_c)$, where $j_(x)$ is the current density of negative ions. Using the standard technique (see, for example, [20]), the continuity equations for $j_e(x)$ и $j_+(x)$ taking into account (26.4) and the fact that $\gamma \ll 1$, we can easily obtain the following expression in the reduced variables accepted in the theory of near-electrode layers [21]:

$$\frac{\alpha(E_c/p)}{p} p d_c = B_1, \quad B_1 = \ln\left(\frac{1+\gamma}{\gamma}\frac{b_i^-}{b_i^+ + b_i^-}\right), \tag{26.5}$$

where α is the Townsend coefficient.

Proceeding from the Poisson equation, we obtain a relation between parameters E_c and d_c [20]:

$$\left(\frac{E_c}{p}\right)^2 = \frac{(J_t p^2) p d_c}{\varepsilon_0 b_i^+ p}, \tag{26.6}$$

where ε_0 is the dielectric constant of vacuum. Then, we obtain from (26.5) and (26.6) the following relations for determining U_c:

$$\frac{(E_c/p)^2[\alpha(E_c/p)/p]\varepsilon_0 b_i^+ p}{J_t/p^2} = B_1, \quad U_c = \frac{E_c}{p} p d_c. \tag{26.7}$$

To estimate the potential drop in the anode region, we should consider impact ionization as well as the formation and neutralization of negative ions The latter process leads to the emergence of seed electrons in the anode region because the electron current coming to this region from the decaying plasma is vanishingly small. In analogy with the above conclusion, we assume that the field E_a in the anode layer is constant.

In the approximation of a planar layer, the system of corresponding continuity equations can be written in the form

$$\begin{aligned} &\frac{dj_\varepsilon(x)}{dx} = -\alpha j_\varepsilon(x) - \delta j_-(x), \quad \frac{dj_-(x)}{dx} = -\eta j_\varepsilon(x) + \delta j_-(x), \\ &\frac{dj_+(x)}{dx} = \alpha j_\varepsilon(x). \end{aligned} \tag{26.8}$$

Here, η is the electron attachment coefficient; δ is the coefficient of detachment of electrons from negative ions in collisions with gas molecules. The coordinate x is measured from the anode ($x = 0$) into the depth of the discharge gap.

The decrease in the electron current caused by the attachment to the SF_6 molecules can be neglected for the same reason as in the case of the cathode layer ($E_a \gg E_{cr}$). Taking this into account, the boundary conditions at the anode and at the boundary between the anode layer and the plasma ($x = d_a$) have the form

$$j_+(0) = 0, \quad j_\varepsilon(d_a) = 0, \quad j_-(d_a) + j_+(d_a) = J_t. \tag{26.9}$$

As a result, we arrive at the relation

$$\begin{aligned} &(\lambda_1 + \lambda_2)d_a = B_2, \\ &B_2 = \ln\left\{\frac{b_i^+}{b_i^-}\frac{\lambda_2}{\lambda_1}[1 + (\lambda_1 + \lambda_2)d_a]\frac{b_i^+ + b_i^-}{b_i^-}\right\}, \end{aligned} \tag{26.10}$$

where $\lambda_{1,2} = \{\pm(\delta - \alpha) + [(\alpha - \delta)^2 + 4\alpha\delta]^{1/2}\}/2$. Since $E_a \gg E_{cr}$, we have, $\lambda_1 \cong \delta, \lambda_2 \cong \alpha$ and expression (26.10) is considerably simplified:

$$\frac{\alpha(E_a/p)}{p}pd_a \approx \ln\left[\frac{\alpha(E_a/p)}{\delta(E_c/p)}\right]. \tag{26.11}$$

Using a relation between E_a and d_a analogous to (26.6), and neglecting the difference in the mobilities of positive and negative ions ($b_i^+ \approx b_i^- \approx b_i$), we obtain in the approximation $\alpha \gg \delta$ the following expression for E_a:

$$\left(\frac{E_a}{p}\right)^2 \frac{[\alpha(E_a/p)/p]\varepsilon_0 b_i p}{J_t/p^2} \approx \ln\left[\frac{\alpha(E_a/p)}{\delta(E_a/p)}\right], \tag{26.12}$$

which is used, together with (26.11), for finding d_a and, hence, the potential drop U_a across the anode.

Using the results obtained, we can now easily estimate the relative error $\xi = (E - E_p)/E$ in determining the field E_p in a decaying plasma:

$$\xi = \frac{B_1/\eta_c + B_2/\eta_a}{U}, \quad \eta_{c,a}(E_{c,a}/N) = \frac{k_i(E_{c,a}/N)}{u_\varepsilon(E_{c,a}/N)(E_{c,a}/N)}, \tag{26.13}$$

where $k_i(E_{c,a}/N)$ and $u_e(E_{c,a}/N)$ are the impact ionization constant and the drift velocity of electrons, respectively.

As an example, consider the SF_6 plasma under a pressure $p = 30$ Torr with a characteristic current density $J_t \sim 1$ A cm^{-2}. Using the data of [14, 15, 22] for k_i and u_e and expressions (26.7), (26.11), (26.12) and (26.13), we obtain $\xi \sim 0.1$. The same relative error is typical for all other plasma decay regimes considered in this work.

We have made a number of assumptions while estimating the quantities U_c and U_a (for example, the possibility of formation of double layers in the electrode region was also not considered). Nevertheless, the estimates obtained approximate well the real values. An indirect confirmation of this is provided, for example, by the fact that the estimates of the quantities $\Delta U = U_c + U_a$ are in satisfactory agreement with the corresponding values obtained by us by extrapolating the experimental dependence $U_{st}(pd)$ [1] for SF_6 and mixtures of SF_6 with C_2H_6 in the region $pd \to 0$ (U_{st} is the voltage in the quasi-stationary phase of the SSVD).

The order of magnitude of the electrode layer relaxation time coincides with the drift time $\tau_{c,a} = \varepsilon_0(E_{c,a}/p)[(J_t/p^2)p]$ of ions through this layer. For example, we obtain $\tau_{c,a} \sim 10^{-8}$ s for $p = 30$ Torr and $J_t \sim 1$ A cm^{-2}. Values of $\tau_{c,a}$ of the same order of magnitude are also obtained under other conditions. Because we are interested only in the microsecond region in this work, the quasi-stationary approximation used above is fully justified.

For the characteristic values of E_c and E_a in the investigated gases under the conditions described above, the relation $l_e \sim l$ is satisfied in the electrode regions, where l and l_e are the mean free path and the energy relaxation length of electrons, respectively. It also follows from relations (26.5), (26.6), (26.11) and (26.12) that $d_{c,a} \gg l_i$, where l_i is the ionization lepgth in the cathode or anode region. Taking into account that $l/l_i < 1$, we obtain $l_e/d_{c,a} \ll 1$. Therefore, local dependences of transport coefficients on the field strength can be used in the above description.

26.5 Conclusions

We have measured the ion-ion recombination coefficients in SF_6 and in SF_6:C_2H_6 = 10:1 mixtures in the pressure range 15–90 Torr for reduced electric field strengths E/N =100–250 Td. The error in the estimates of fields in the plasma does not exceed 10% for an overall measuring error below 20%. The extrapolation of the results of measurements to the region of higher values of E/N provides an estimate 10^{-8} cm^3 s^{-1} for the coefficient of recombination β of the SF_6^- and SF_5^- ions with the SF_5^+ in SF_6 for $E/N \sim (E/N)_{cr}$. The values of β for SF_6 at $p = 90$ Torr and for $E/N < 160$ Td are close to those obtained in [5] by a different technique. For pressures $p = 60$ Torr typical of HF lasers, the recombination coefficient in a decaying plasma is $\beta = 4.3 \times 10^{-8}$ cm^3 s^{-1} in the SF_6:C_2H_6 = 10:1 mixtures. Calculations [4] show that a decrease in the ion concentration by an order of magnitude occurs over a time $\sim$200 ns comparable with the duration $\sim$300 ns of the entire discharge. This leads to the assumption that ion-ion recombination in SF_6–C_2H_6 mixtures may considerably limit the ion concentration at the stage of self-sustained discharge, and should be taken into account in the calculations of the HF-laser characteristics. The simulation of the SSVD in SF_6 using the value $\beta = 10$ cm^3 s^{-1} for the recombination coefficient shows that in, this case, the ion-ion recombination also may considerably affect the ion density balance at all stages of the discharge.

References

1. V.V. Apollonov, A.A. Belevtsev et al., Kvantovaya Elektron. **30**, 207 (2000) [Quantum Electron. 30, 207 (2000)]
2. V.V. Apollonov et al., Kvantovaya Elektron. **24**, 213 (1997) [Quantum Electron. 27, 207 (1997)]
3. V.V. Apollonov et al., Proc. SPIE Int. Soc Opt. Eng. **3886**, 370 (2000)
4. V.V. Apollonov et al, in *Proceedings of the XIII Internatinal Conference on Gas Discharges and Their Applications*, vol. 1 (Glasgow, 2000), p. 409
5. M.C. Cornell, I.M.J. Littlewood, Phys. D **20**, 616 (1987)
6. I.M.J. Littlewood, Phys. D **23**, 308 (1990)
7. W.F. Schmidt, H. Jungblut, D. Hansen, H. Tagashira, in *Proceedings of the II International Symposium on Gaseous Dielectrics* (New York, Pergamon Press, 1980)
8. I.M. Littlewood, R.E. Pyle, Phys. D **23**, 312 (1990)
9. V.V. Apollonov et al, Pis'ma Zh. Tekh. Fiz. **22**(24), 60 (1996)
10. W.L. Morgan, J.N. Bardsley, J. Lin, B.L. Whitten, Phys. Rev. A **26**, 1696 (1982)
11. I. Sauers, G.J. Harman, Phys. D **25**, 761 (1992)
12. J.J. Wagner, W.W. Brandt, Plasma Chem. Plasma Processing **1**, 201 (1981)
13. K.P. Brandt, H. Jungblut, J. Chem. Phys. **78**, 1999 (1983)
14. N. Nakano, N. Shimura, Z.L. Petrovic, T. Makabe, Phys. Rev. E **49**, 4455 (1994)
15. J.K. Olthoff, R.J. Van Brunt, J. Chem. Phys. **91**, 2261 (1989)
16. B.M. Smirnov, lony i Vozhuzhdennye Atomy v Plazme (Ions and Excited Atoms in Plasma), (Atomizdat, Moscow, 1974)
17. J. Flesch, R.E. Utecht, Svec H. J. Int. J. Mass Spectrom. Ion Processes **58**, 151 (1984)
18. H. Chatham, D. Hill, R. Robertson, A. Gallagher, J. Chem. Phys. **81**, 1770 (1984)
19. E. McDaniel, E. Mason, *The Mobility and Diffusion of Ions in Gases* (Wiley, New York, 1973)
20. Y.P. Raizer, *Fizika Gazovogo Razryada* (Physics of Gas Dis-charge) (Nauka, Moscow, 1987)
21. V.L. Granovskii, *Elektricheskii Tok v Gaze. Ustanovivshiisya Tok* (Electric Current in a Gas. Steady-State Current) (Nauka, Moscow, 1971)
22. V.A. Lisovskiy, V.D. Yegorenkov, in *Proceedings of the International Symposium on Electron-Molecule Coll. Swarms* (Tokyo, Japan, 1999), p. 156

Chapter 27
SSVD Instability of Nonchain HF(DF) Laser Mixture

Abstract The development of detachment instability in active media of electric-discharge non-chain HF(DF) lasers due to the electron-impact detachment of electrons from negative ions is considered in this chapter. This instability is initiated in large volumes of SF-based gas mixtures, spatially separated from electrodes and heated by a pulsed CO_2 laser. The self-organization of SSVD upon laser heating, which results in the formation of quasi-periodic plasma structures within the discharge gap, was experimentally investigated. The evolution of these structures, depending on the gas temperature and specific contribution of electric energy, is analyzed in this chapter. The possible relationship between the self-organization and detachment instability is discussed here. In addition, a mechanism of development of single plasma channels in the working media of HF(DF) lasers, based on electron-impact destruction of negative ions is proposed.

27.1 Introduction

SSVD ionization instability in SF_6 and its mixtures is of great interest in view of the development of nonchain chemical HF(DF) lasers [1].

Several mechanisms of ionization instability in electronegative gases are known. A general theoretical approach to their analysis was formulated in [2]. The development of instabilities in working media of CO_2 lasers as a result of detachment of electrons from negative ions by neutral and electron-excited gas components was considered in [3–5]. The mechanism of instability caused by electron-impact dissociation of a small amount of electronegative impurity ('burning out' of halogen additive) was analyzed in detail for excimer lasers [6–9]. The instability in SF_6, according to [10], should be related to the step ionization of SF_6 molecules.

The instability caused by electron-impact detachment of electrons from negative ions in highly electronegative polyatomic gases at intermediate pressures and for times of few tens of nanoseconds may develop according to a qualitatively different scenario. This issue was considered for the first time in [11] for SSVD in SF_6 and its mixtures. In this context, the following circumstance is of fundamental importance.

© Springer International Publishing Switzerland 2016

V.V. Apollonov, *High-Energy Molecular Lasers*,
Springer Series in Optical Sciences 201, DOI 10.1007/978-3-319-33359-5_27

At intermediate pressures of SF_6-based gas mixtures at room temperatures the best agreement between the calculated time dependences and experimental SSVD current and voltage oscillograms, including those recorded in the quasi-stationary SSVD phase (at $E/N \approx (E/N)_{cr}$), is observed (see below) at the approximate equality $\beta_{ei} \approx k_d$. Here, E is the electric field strength; N is the gas concentration; β_{ei} and k_d are the rate constants of electron-ion recombination and electron-impact detachment of electrons from negative ions, respectively; and $(E/N)_{cr}$ is the critical reduced electric field strength. In this case, the increase in the electron concentration due to the electron-impact destruction of negative ions is almost completely compensated for by their loss as a result of dissociative electron-ion recombination. The above-mentioned nonlinear mechanism of electron multiplication manifests itself only at a significant unbalance between the constants k_d and β_{ei}, which may occur either upon strong gas heating or at $E/N \gg (E/N)_{cr}$. Indeed, the constant $\beta_{ei} \sim T_g^{-1} T_e^{-\chi}$ ($\chi > 0$, T_g is the gas temperature, $T_e = 2\langle\varepsilon\rangle/3$, $\langle\varepsilon\rangle$ is the mean electron energy [12]) decreases under these conditions, whereas the constant k_d can only increase.

The conditions under which $E/N \gg (E/N)_{cr}$ are implemented, for example, near the tip of incomplete channel, developing from the cathode side. However, in this case ionization processes develop at distances of the same order of magnitude as the channel radius; hence, they are fairly difficult to experimentally study. At the same time, one can implement a significant unbalance between the constants k_d and β_{ei} and initiate the mechanism of detachment instability under consideration even in large gas volumes. An efficient way to do this is to heat SF_6-based gas mixtures by a pulsed CO_2 laser [13]. Here, we used this approach to study the SSVD instability caused by electron-impact detachment of electrons from negative ions in SF_6 and SF_6-based gas mixtures, including working media of HF(DF) lasers.

27.2 Experimental Setup

The experimental setup (see schematic in Fig. 27.1) and analytical technique did not differ much from those used by us previously [11]. We investigated SSVD in SF_6 and its mixtures with C_2H_6, H_2, and Ne at a partial SF_6 pressure of 15 Torr and a total mixture pressure up to 50 Torr. A discharge was ignited in the needle (cathode)–cylinder (anode) geometry at an interelectrode distance of 43 mm. The needle was imitated by a segment of polyethylene-insulated copper wire. The cathode was placed in a segment of a dielectric tube with an inner diameter of 15 mm, protruding above the needle tip by 12 mm. The specific electric energy contribution W_{el} to the plasma discharge was varied from 0.02–0.2 J cm^{-3}.

The gas was preliminarily heated only in a narrow region of the discharge gap due to the gap irradiation by a pulsed CO_2 laser through a 10 mm-wide slit diaphragm, oriented perpendicularly to the applied electric field (Fig. 27.1). As will be shown subsequently, this irradiation scheme makes it possible to observe SSVD contraction directly in the heated-gas volume (similarly to the glow discharge

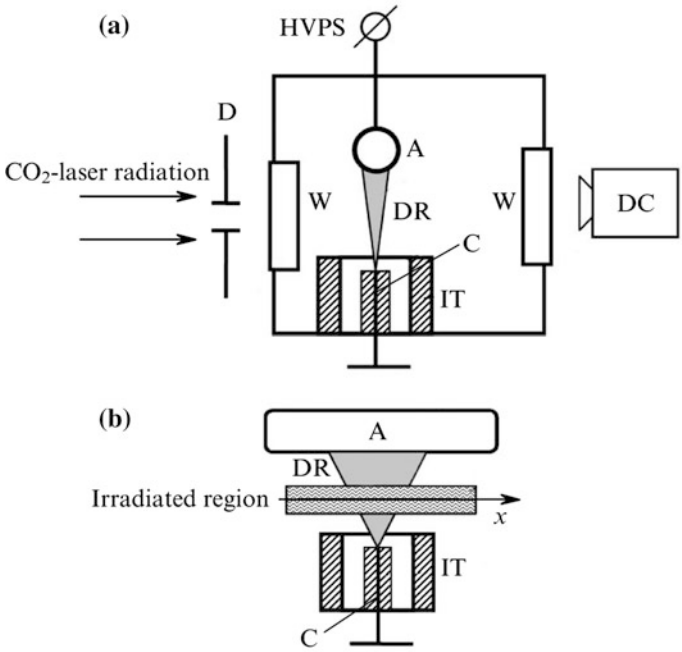

Fig. 27.1 Experimental setup, viewed (**a**) form aside and (**b**) from the side of the camera: (*A*) anode, (*C*) cathode, (*D*) slit diaphragm, (*HVPS*) high-voltage power supply, (*W*) BaF_2 windows, (*IT*) insulating tube, (*DC*) digital camera, and (*DR*) discharge region

contraction [12, 14]) rather than in the form of a channel, evolving from the cathode spot and finally closing the discharge gap [15]. The gas temperature T_g, which is set in the SSVD burning region, was determined from the amount of laser energy absorbed by SF_6 molecules [13] and from the propagation velocity of the shock wave formed at the boundaries between the cold and heated gas regions [16]. The temperature T_g was varied in the range of 800–2100 K (the specific energy W_a of the laser radiation absorbed by SF_6 in the SSVD region was 0.05–0.23 J cm^{-3}). A voltage pulse was applied to the discharge gap with a delay of 4 μs with respect to the μs laser pulse (the delay was counted with respect to the leading edges of the pulses [17]) at a level of 0.1, which ensured a thermal equilibrium between the translatory and internal degrees of freedom of the irradiated-gas components by the instant of discharge ignition in the pressure range under study [18].

During the experiments we monitored the voltage across the discharge gap and the VSSD current using a resistive voltage divider and low-resistivity shunt, respectively, and recorded VSSD by a digital camera, synchronized with the laser pulse. To identify the main processes determining the VSSD current–voltage *(I–U)* characteristics, we also recorded voltage and current oscillograms for a limited discharge, which is known to exclude the influence of the factors caused by the increase in the discharge volume with an increase in the amount of energy

introduced into the plasma on the discharge current and voltage [19]. To this end, SSVD was ignited in a quartz tube 8.5 mm in diameter at an interelectrode distance of 43 mm (in the needle-plane geometry). The experimental oscillograms were compared with the calculation results (the calculation technique was described in detail in [20]).

27.3 Experimental Results

Figures 27.2a, b show photographs of an SSVD in an SF_6–Ne–C_2H_6 mixture, obtained at W_{el} = 0.2 J cm^{-3}, discharge current pulse width τ_{dis} = 150 ns, and different T_g values. The distributions of discharge glow intensity along the x axis (which is parallel to the boundaries of the heated region and passes through its middle; see Fig. 27.1), corresponding to the aforementioned photographs, are shown in Fig. 27.2c, d. It can be seen that SSVD in the heated region becomes stratified, acquiring a quasi-periodic plasma (current) structure. Its spatial period decreases with an increase in T_g. It is noteworthy that the large plasma (current)

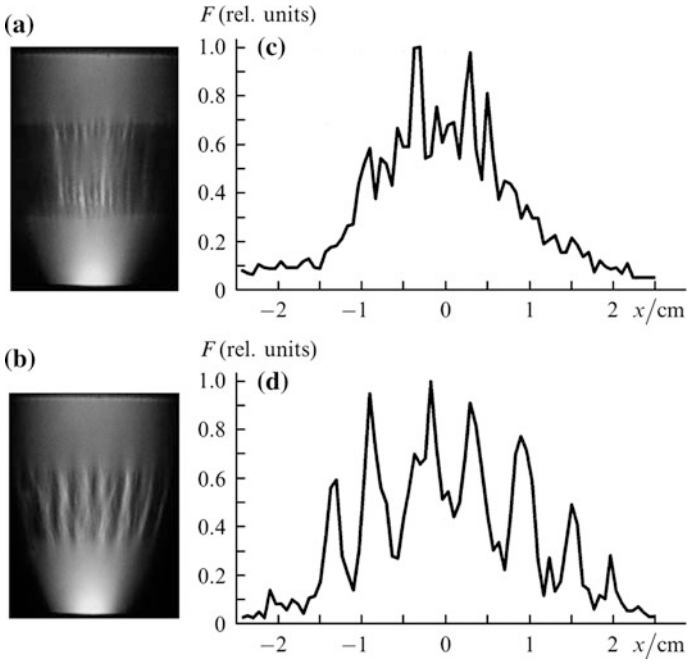

Fig. 27.2 SSVD photographs at T_g = 1550 an 800 K (**a** and **b**, respectively); distributions of VSSD radiation intensity F along the coordinate x in the heated region at T_g = 1550 and 800 K (**c** and **d**, respectively); SF_6:Ne:C_2H_6 = 5:5:1 mixture, p = 33 Torr; W_d = 0.2 J cm^{-3}, and τ_{dis} = 150 ns

channels in Fig. 27.2b consist of thinner filaments. Despite the SSVD stratification, the plasma channels in the heated region are diffuse at not very large W_{el} and τ_{dis} values. An increase in W_{el} or τ_{dis} leads to dominance of one of the channels (lying generally near the central electric field line) and its contraction. It is noteworthy that both in the case of cold gas [19] and, upon heating, the SSVD contraction threshold with respect to W_{el} and τ_{dis} in pure SF_6 is lower than in SF_6–C_2–H_6 mixtures. This is illustrated in Fig. 27.3 by a photograph of SSVD in pure SF_6, recorded at τ_{dis} = 160 ns and W_{el} = 0.12 J cm^{-3}. One can see that an instability develops directly in the irradiated region of the discharge gap. Apparently, a pertinent analogy for this situation is the contraction of low-pressure glow discharge [12, 14]. With a further increase in W_{el} or τ_{dis} the spark channel covers the entire gap. For constant W_{el} and τ_{dis} values the probability of SSVD contraction also increases with an increase in T_g in the irradiated part of the gap.

Figure 27.4a shows a voltage oscillogram for a limited SSVD in SF_6 at a pressure p = 15 Torr and W_{el} = 0.12 J cm^{-3}. Figure 27.4b presents the time dependences of voltage, calculated taking into account the following processes: electron-impact ionization and attachment of electrons (IA), ion–ion recombination (HR, rate constant $\beta_{ii} = 2 \times 10^{-8}$ cm^{3}s^{-1} [21), dissociative electron-ion recombination (EIR, rate constant β_{ei} varied in the range of (0.5–3) $\times$ 10^{-7} cm^3 s^{-1} in the calculation), electron-impact detachment of electrons from negative ions (ED, k_d = 3 $\times$ 10^{-7} cm^3 s^{-1} [22]), and electron-impact dissociation of SF_6 (EID, the dissociation energy per fluorine atom, according to different researchers, was 4–6 eV (see [23, 24] and references therein). The time dependence of current in Fig. 27.4b is given for the case where all these processes are taken into account. The attachment of electrons to vibrationally excited SF_6 molecules was disregarded, because in our previous experiments we found the contribution of this process to the total balance of charged particles in SSVD plasma in SF_6 to be small [18].

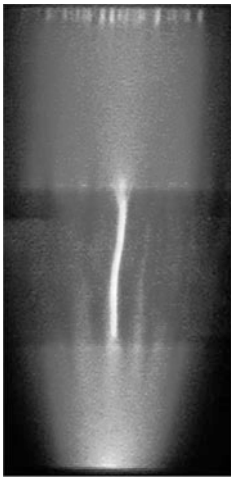

Fig. 27.3 Photograph of SSVD in SF_6 at W_{el} = 0.12 J cm^{-3}, T_g = 1150 K, τ_{dis} = 50 ns, and p = 15 Torr

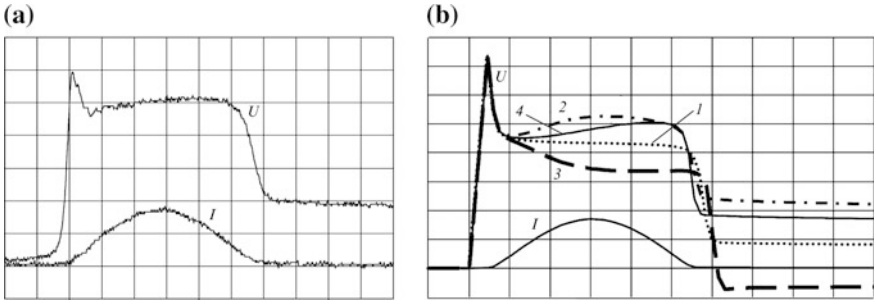

Fig. 27.4 Experimental oscillograms (**a**) and calculated time dependences (**b**) (disregarding the cathode drop) of the SSVD voltage U and current I in SF_6 at p = 15 Torr and interelectrode distance of 43 mm (limited discharge). The calculation was performed taking into account the following processes: (*1*) IA, (*2*) IA and EIR, (*3*) IA and ED, and (*4*) IA and EID; $k_d = \beta_{ei}$. The scale-division values are 2 kV *(U),* 80 A (*I*), and 50 ns (*sweep*)

A comparison of the calculated time dependences with the experimental SSVD voltage oscillogram shows their best agreement at $k_d \approx \beta_{ei}$.

Thus, we can note three results that are most important for further analysis of the mechanisms of SSVD instability development in Sfe-based gas mixtures, including working media of HF lasers: (i) SSVD in the heated region is stratified with the formation of quasi-periodic plasma channels, whose spatial period depends on T_g; (ii) the development of SSVD instability begins with the discharge contraction directly in the irradiated region of the discharge gap; and (iii) the increase in the concentration of electrons due to their electron-impact detachment from negative ions in the gas at room temperature is compensated for by their loss during electron-ion recombination $(k_d \approx \beta_{ei})$.

27.4 Results and Discussion

27.4.1 Nonlinear Mechanism of Ionization Development in Active Media of HF/DF Lasers 4.1

SF_6^- and SF_5^- ions, which are formed as a result of electron attachment to SF_6 molecules [25], are dominant in SSVD plasma. The nonlinear mechanism of electron generation in SF_6 due to the electron-impact destruction of negative ions was considered for the first time in [22], where the electron-impact detachment rate of electrons from negative SF_6^- ions was estimated to be $k_d\,(SF_6^-) = 3 \times 10^{-7}$ cm^3 s^{-1}. This estimation was obtained on the assumption that the detachment cross section is no less than the elastic electron scattering cross section from the SF_6 molecule. The latter parameter is known to exceed 10^{-15} cm^2 [25]. It was also taken into account that at $E/N \sim (E/N)_{cr}$ the mean electron energy $\langle\varepsilon\rangle \sim$ 8–10 eV is much higher than

the electron binding energy in negative SF_6^- ions (0.65–1 eV [25]), due to which the electron-impact destruction of SF_6^- ions can be considered as thresholdless.

Concerning SF_5^- ions, which have a binding energy $E_b \sim 2.8$ eV [25], the corresponding value k_d (SF_5^-), with allowance for the Boltzmann factor $\exp(-E_b/T^*)$ ($T^* < 2\langle\varepsilon\rangle/3$), is smaller than k_d (SF_6^-) but by no more than 40%. Hence, when quantitatively describing the electron-impact detachment of electrons from SF_6^- and SF_5^- ions, one can use the approximation of negative ions of the same type and introduce a unified detachment rate constant k_d.

A fact of fundamental importance is that no other processes of electron detachment can compete with the electron-impact destruction of negative ions in the above-mentioned ranges of pressures and times. Indeed, at $E/N \approx (E/N)_{cr}$ almost all heavy polyatomic negative ions, except for their negligible fraction in the energy tail have energies insufficient for electron detachment in collisions with neutral molecules [25], and the relatively low gas density practically excludes the effect of electron-excited components on the negative ion destruction.

The expressions for the electron concentration $n_e(t)$ were obtained in [11] based on the exact analytical solutions to the nonlinear integro-differential equation. The character of increase in $n_e(t)$ depends decisively on the parameter ξ [11]:

$$\xi = \frac{a^2/\lambda - 2}{\lambda}, \quad a = \frac{\alpha}{\eta} - 1, \quad \lambda = \frac{n_e(0)(k_d - \beta_{ei})}{\eta u_e}, \tag{27.1}$$

where $n_e(0)$ is the electron concentration established by the onset of quasi-stationary phase; α and η are the impact ionization and attachment rates, respectively; and u_e is the electron drift velocity.

If $\xi > 0$,

$$n_e(t) = \frac{2n_e(0)b^2\lambda A}{(1-A)^2}, \quad A = \frac{a/\lambda - b}{a/\lambda + b}\exp(b\lambda\eta u_e t), \quad b = \sqrt{\xi}. \tag{27.2}$$

In this case, nonlinear electron multiplication occurs against the background of significant contribution of linear processes of impact ionization and attachment. Therefore, it is no wonder that solution (27.2) remains valid at arbitrarily small values of $n_e(0)$ and/or difference $k_d - \beta_{ei}$. In the limit $\lambda \to 0$ it passes, as one would expect, to the well-known 'classical' expression for electronegative gases [15]:

$$n_e(t) \approx n_e(0)\exp[(\alpha - \eta)u_e t]. \tag{27.3}$$

At $\xi < 0$ the electron-impact detachment of electrons from negative ions plays a key role, and the expression for the electron concentration,

$$n_e(t) = n_e(0)\left\{\cos^2(b_1\lambda\eta u_e t)\left[1 - \frac{a}{b_1\lambda}\tan\left(\frac{b_1\lambda\eta u_e t}{2}\right)\right]\right\}^{-1}, \tag{27.4}$$

$$b_1 = \sqrt{-\xi}.$$

Is not transformed into (27.3) at any values of $n_e(0)$ and difference $k_d - \beta_{ei}$.

It follows from relations (27.1), (27.2), and (27.4) that, when the detachment and recombination constants are unbalanced $(k_d - \beta_{ei} > 0)$, in the stage of increasing discharge current $(\alpha > \eta)$, both solutions, (27.2) and (27.4), have a pronounced 'explosive' character; i.e., some finite time after the ionisation onset the electron concentration formally becomes arbitrarily high. One can easily find the corresponding characteristic 'explosion' times τ^i_{exp} from (27.2) and (27.4). If $\xi > 0$,

$$\tau^i_{exp} = \ln\left(\frac{a/\lambda + b}{a/\lambda - b}\right)\frac{1}{b\lambda\eta u_e}. \tag{27.5}$$

At $\xi < 0$

$$\tau^i_{exp} = 2\arctan\left(\frac{\lambda b_1}{a}\right)\frac{1}{b_1\lambda\eta u_e}. \tag{27.6}$$

In fact, this result means only that after some time $(\tau^i_d \sim \tau^i_{exp})$ the attachment of electrons is partially compensated for by their detachment from negative ions, as a result of which the electron multiplication rate sharply increases. By analogy with the terminology used in the theory of excimer lasers, this process could be referred to as the electronegativity 'burning out', because in this case we deal with not destruction of electronegative molecules but with the loss of gas electronegativity as a result of electron detachment.

When deriving relations (27.2) and (27.4), we did not take into account the small change in the time of the difference $\alpha - \eta$; however, the 'explosive' character of these solutions, which in a sense tend (in the limit) to the exact dependence $n_e(t)$, indicates that the dependence $n_e(t)$ has the same specific feature.

In the stage where the discharge current decreases, in the quasi-stationary SSVD phase $\alpha < \eta$ and, correspondingly, $a < 0$. It follows from relations (27.2) and (27.4) that in this case the electron concentration always tends to zero with time. In other words, the volume multiplication of electrons as a result of their electron-impact detachment from negative ions cannot compete with the attachment-caused electron loss if the electron capture efficiency exceeds that of impact ionization. Thus, in the quasi-stationary SSVD phase the ionization instability in the plasma volume, which is related to the 'explosive' character of electron multiplication, may develop only when the discharge current increases.

27.4.2 Self-Organization of SSVD Plasma upon Laser Heating of SF_6-Based Mixtures

The nature of self-organization of SSVD plasma in heated SF_6-based gas mixtures remains unclear. However, there are some indications that this phenomenon can be due to a great extent to the development of ionization instability in SSVD plasma, caused by the above-considered electron-impact detachment of electrons from negative ions. Here are some qualitative considerations on this subject.

At high gas temperatures $k_d - \beta_{ei} > 0$; when the discharge current increases ($\alpha > \eta$), this relation leads to an 'explosive' increase in $n_e(t)$. The characteristic time τ_c of current change in the quasi-stationary SSVD phase is controlled by the LC chain ($\tau_c \sim \sqrt{LC}$); in our experiments it was approximately several hundreds of nanoseconds, whereas $\tau_d^i \sim 20 - 30$ ns. Since $\tau_c \gg \tau_d^i$, in the quasi-stationary SSVD phase (at $E/N \approx (E/N)_{cr}$), the current should inevitably be redistributed in the discharge gap volume with the formation of current channels in the form of individual filaments (thin at large T_g values) with a higher electron concentration. Indeed, a standard linear analysis shows that under the conditions considered here specifically, spatially inhomogeneous perturbations oriented perpendicularly to the current are characterized by the largest increment. Quasi-periodic structures can be formed in the nonlinear stage of perturbation development and experimentally observed.

According to [26], it is possible to show that such channels in the form of individual current filaments are stable. The difference $k_d - \beta_{ei}$ also increases with an increase in the gas temperature, causing a more rapid increase in $n_e(t)$. One might suggest that, specifically for this reason, an increase in T_g is accompanied by an increase in the number of conducting channels and, correspondingly, a decrease in the spatial period of the current structure. The experimental data in Fig. 27.2 do not contradict this suggestion. An additional argument in favour of the above considerations is that quasi-periodic current structures did not arise at very small T_g values implemented in the experiment. Indeed, in this case $\tau_d^i \gg \tau_c$.

When the discharge current decreases, the above-considered 'explosive' mechanism does not work, because $E/N < (E/N)_{cr}$ and $\alpha < \eta$ (see Sect. 4.1). In this case, an instability may develop on the descending portion of the quasi-static *I–V* discharge characteristic (the *I–U* characteristic settling time $\tau_{UI} \ll \tau_c$), which is controlled by the effective ionization coefficient $\alpha_{eff}(n_e) = \alpha - \eta + (k_d - \beta_{ei})N_n(n_e)/u_e$, where $N_n(n_e)$ is the concentration of negative ions. In this case, the excess of the electron attachment rate above the impact ionization rate is compensated for by the electron-impact detachment of electrons from negative ions. On this portion of the *I–U* characteristic, the SSVD is unstable with respect to spatially homogeneous fluctuations of plasma parameters. However, inhomogeneous fluctuations, leading to the formation of spatial stures in the form of individual current filaments with elevated electron concentration may also increase in SSVD plasma. The corresponding scenarios of self-organization and problem of stability of the structures

formed in this plasma have been considered in detail (see, for example, [26, 27]). It is likely that the instability developing on the descending portion of the *I–U* characteristic leads to SSVD contraction at wide discharge pulses (Fig. 27.3).

27.4.3 Mechanism of Evolution of Conducting Channels in SF_6 and Its Mixtures

The nonlinear mechanism of electron multiplication due to the unbalance between k_d and β_{ei} may lead to the development of ionization instability in SF_6-based gas mixtures even at room temperatures if, as was noted above, $E/N \gg (E/N)_{cr}$. Specifically, this situation is implemented near the tip of a single conducting channel, developing from the side of the cathode.

The reduced electric field strength at the tip of this channel significantly exceeds the $(E/N)_{cr}$ value [15]. This leads to a significant increase in T_e and, accordingly, to a dramatic decrease in β_{ei} (see Introduction). A situation arises, where, as in the case of high gas temperature, the difference $k_d–\beta_{ei} > 0$. As a result, the above-considered mechanism of the 'explosive' increase in the electron concentration is initiated and a new, plasma-filled portion of the channel is formed, which promotes the channel evolution into the discharge gap bulk. In this case, it is not necessary to apply the mechanism of step ionization of SF_6 molecules [10] to explain the development of conducting channels in SF_6 and its mixtures.

27.5 Conclusions

We investigated a radically new mechanism of detachment instability, which develops in active media of HF(DF) lasers due to the electron-impact detachment of electrons from negative SF_6^- and SF_5^- ions. The analysis of the main mechanisms of the formation and destruction of negative ions in SF_6 and its mixtures showed that the instability is caused by the unbalance between the rate constants of electron-impact detachment of electrons from negative ions and dissociative electron-ion recombination. Analytical expressions were obtained for the time dependence of electron concentration. It was shown that an increase in the discharge current resulted in 'explosive' instability development; the characteristic 'explosion' time was estimated. The development of detachment instability in large volumes was initiated by heating SF_6-based gas mixtures with a pulsed CO_2 laser for experimental study. The possible relationship of this process with the spatial self-organization (formation of current filaments) in the SSVD plasma in previously irradiated SF_6 and its mixtures was discussed. The mechanism of development of a single incomplete channel due to the electron-impact detachment of electrons from negative ions was considered.

References

1. V.V. Apollonov et al., *High Power P-P lasers* (NOVA, New York, 2014)
2. R.A. Haas, Phys. Rev. A **8**, 1017 (1973)
3. W.L. Nighan, W.J. Wiegand, Phys. Rev. A **10**, 922 (1974)
4. Nighan W.L., in: *Principles of Laser Plasmas*, Chap. 7 (New York, 1976)
5. A.P. Napartovich, A.N. Starostin, *Khimiya plazmy* (Chemistry of Plasma), vol. 6 (Atomizdat, Moscow, 1979), p. 153
6. J. Coutts, J. Phys. D Appl. Phys. **21**, 255 (1988)
7. M.R. Osborne, M.R. Hutchinson, J. Appl. Phys. **59**, 711 (1986)
8. M.R. Osborne, Appl. Phys. B **45**, 285 (1988)
9. A. Garscaden, M.J. Kushner, IEEE Trans. Plasma Sci. **19**, 1015 (1991)
10. Yu. Bychkov, S. Gortchakov, B. Lacour, S. Pasquiers, V. Puech, J. Phys. D Appl. Phys. **36**, 380 (2003)
11. A.A. Belevtsev et al., J. Phys. D Appl. Phys. **42**, 215205 (2009)
12. A.V. Eletskii, *Khimiya plazmy* (Chemistry of Plasma), vol. 9 (Atomizdat, Moscow, 1982), p. 151
13. A.A. Belevtsev et al., Kvantovaya Elektron. **36**, 646 (2006) [Quantum Electron. 36, 646 (2006)]
14. E.P. Velikhov, A.S. Kovalev, A.T. Rakhimov, *Fizicheskie yavleniya v gazorazryadnoi plazme (Physical Phenomena in Gas-Discharge Plasma* (Nauka, Moscow, 1987)
15. YuD Korolev, G.A. Mesyats, *Fizika impul'snogo proboya v gazakh (Physics of Pulsed Breakdown in Gases)* (Nauka, Moscow, 1991)
16. A.A. Belevtsev et al., J. Phys. D Appl. Phys. **41**, 045201 (2008)
17. A.A. Belevtsev et al., J. Phys. D Appl. Phys. **37**, 1759 (2004)
18. A.A. Belevtsev et al., Appl. Phys. B **82**, 455 (2006)
19. V.V. Apollonov et al., Kvantovaya Elektron. **30**, 646 (2000) [Quantum Electron. 30, 646 (2000)]
20. V.V. Apollonov et al., Kvantovaya Elektron. **32**, 95 (2002) [Quantum Electron. 32, 95 (2002)]
21. V.V. Apollonov et al., Kvantovaya Elektron. **31**, 629 (2001) [Quantum Electron. 31, 629 (2001)]
22. A.A. Belevtsev, L.M. Biberman, Izv. Akad. Nauk SSSR, Ser. Energetika Transport **3**, 74 (1976)
23. V.V. Apollonov et al., in *Proceedings 14th International Conference on Gas Discharges and their Applications* (Glasgow, UK, 2000), p. 409
24. E.B. Gordon, V.I. Matyushenko, P.B. Repin, V.D. Sizov, Khim. Fiz. **8**, 1212 (1989)
25. L.G. Christophorou, I.K. Olthoff, J. Phys. Chem. Ref. Data **29**, 267 (2000)
26. E. Scholl, Nonequilibrium Phase Transitions in Semiconductors: Self-Organization Induced by Generation and Recombination Processes(Springer, HcvHn, 1987; Mir, Moscow, 1991)
27. A.F. Volkov, ShM Kogan, Usp. Fiz. Nauk **96**, 633 (1968)

Chapter 28
Dynamics of a SIVD in Mixtures of Sulfur Hexafluoride with Hydrocarbons

Abstract In the present chapter, the SIVD dynamics are discussed. These were studied with a high-speed electron-optic camera (EOC). Computer modelling of the process was also performed, allowing for most probable mechanisms of restricting the current density in a diffuse channel.

28.1 Introduction

An interest in investigating an SSVD without preionization in mixtures of SF_6 with hydrocarbons—SIVD is mainly caused by its successful employment in nonchain HF lasers. The use of this discharge allows development of wide-aperture nonchain powerful HF lasers of a reasonable efficiency [1–3]. A remarkable feature of SIVD is its ability to advance normally to the electric field applied starting from the point of the initial breakdown and then gradually filling up the whole gap through successively forming overlapping diffuse channels at practically constant voltage [1, 3, 4]. The possibility of obtaining an SIVD is closely associated with the existence of the mechanisms limiting a current density in SF_6 and SF_6-based mixtures, hampering the passage of the total energy stored in the capacitor through a single diffuse channel and leading to an increase in the volume occupied by the discharge with growing the energy put into the discharge plasma [4]. In papers [1, 4], the SIVD dynamics was studied with a technique similar to that of the interrupted discharge with recording the plasma glow on a film. This permitted the process of forming diffuse channels and their filling up the gap to be followed, but gave no information on changing the channel glow intensities beginning with instant of their formation and ending with that of the discharge termination, i.e, this did not enable direct confirmation of the fact that with developing new channels the current flowing through those previously formed decreases.

© Springer International Publishing Switzerland 2016

V.V. Apollonov, *High-Energy Molecular Lasers*,
Springer Series in Optical Sciences 201, DOI 10.1007/978-3-319-33359-5_28

28.2 Experimental Investigation

In this part of our investigation, the SIVD dynamics were studied with a high-speed electron-optic camera (EOC). Computer modelling of the process was also performed, allowing for most probable mechanisms of restricting the current density in a diffuse channel.

The setup used is schematically drawn in Fig. 28.1. SIVD of a total duration of ~500 ns was initiated in mixtures SF_6:C_2H_6 = 10:1 at a total pressure of 33 Torr and interelectrode distance of 4 cm. As electrodes taken were a metal-covered strip of 16 cm in length and of 0.5 mm in thickness (cathode) standing edgewise and a disk anode of 6 cm in diameter rounded off over its perimeter with a radius of 1 cm. A breakdown was initiated at the discharge gap end by a spark restricted with a resistor of 900 Ω. The SIVD glow was recorded by electron-optic camera with an exposure time of 20 ns triggered with a varying delay T relative the discharge initiation moment.

The SIVD frames for different T-values are presented in Fig. 28.2. SIVD starts as an isolated diffuse channel close to the point of spark illumination. Then, near the first channel, new channels of much less luminosity appear the number of which increases in time while their brightness gradually compare with that of the first channel, the most bright channels being those located closer to the initial one. In time, the glow intensity of the first channel noticeably diminishes while all other channels become equally bright. On further development of SIVD, a gradual increase in its glow intensity is observed at the gap end removed from the point of illumination; however, at T > 250 ns the glow becomes again uniform lengthwise of the cathode, with the glow in the vicinity of the initial channel also resuming. Against the background of this common diffuse glow, the instability of SIVD then develops. A small-sized spot in all the frames is due to the camera imperfection.

The results presented are in good agreement with the proposals previously made that, in these mixtures, there exist certain mechanisms of limiting the current

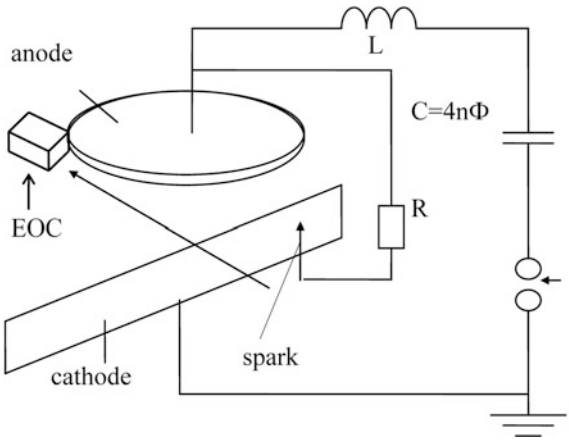

Fig. 28.1 Scheme of setup

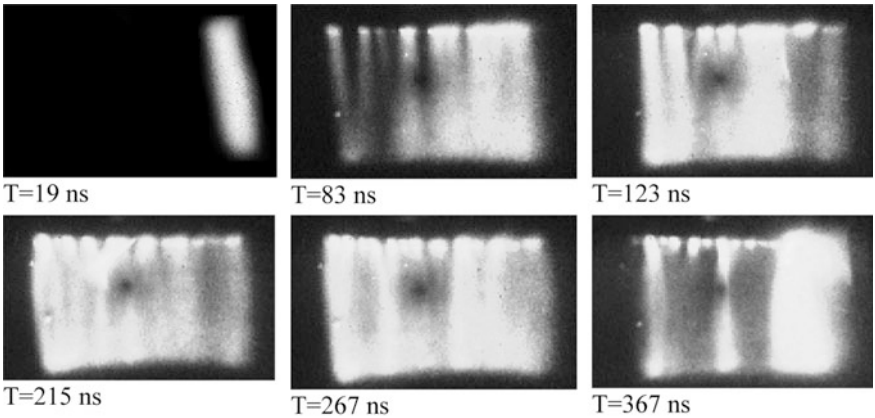

Fig. 28.2 SIVD frames for different T-values

through an individual channel [4]. The mechanisms are can be assumed to be as follows: (a) dissociation of SF_6 molecules by electron impact, which leads to increasing the total particle number density in a diffuse channel, locally decreasing parameter E/N and, consequently, lowering the ionization rate and growing the attachment rate in the channel; (b) dissociative electron–ion recombination, which causes growth in electron losses with increasing the current density in the channel. To verify the adequacy of the mechanisms assumed, computer modelling of SIVD has been performed. The channel SIVD structure was modelled by a set of pure resistances placed in parallel, each having value RHJ/[S-e-(n_i''-V_i'' + n_i^+-V_i^++n_e-V_e)] where U is the voltage across the discharge gap, S is the cathode area, e is the charge of the electron, nf, п;$^+$,-п$_e$, v', v;$^+$, v_e are the number densities and drift velocities of negative and positive ions and of electrons, respectively. The particle number densities were derived from the equations of continuity for each the kind of particles combined with the Kirchhoff s equations for the discharge circuit by analogy with paper [1]. In addition to SF_6 ionization by electron impact and electron attachment to SF_6 molecules, account is also taken of SF_6 dissociation by electron impact (the energy spent for F-atom production is chosen in accordance with recommendations of 151) [5], dissociative electron–ion recombination and ion–ion recombination (the relevant rate coefficients are (β_{ei} = 10^{-7} cm^{-3}/s) and (β_{ii} = 2 × 10^{-7} cm^{-3}/s, respectively), detachment of electrons from SF_6 negative ions by electron impact (k_d = 10^{-7} cm^{-3}/s) [6]. The differences in the initial conditions in developing the channels lengthwise of the cathode were taken into account by putting some initial electron number density n_0 for each the channel. Let there be four such channels to be further considered with n_{0i} = 10 cm^{-3}, n_{02} = 10 cm^{-3}, n_{03} = 10 cm^{-3}, n_{04} = 10 cm^{-3}. Figure 28.3 presents the calculated oscillograms of the discharge voltage, U, the total discharge current, I, and, as an example, the current through one of the channels, I_1. It can be seen that the current

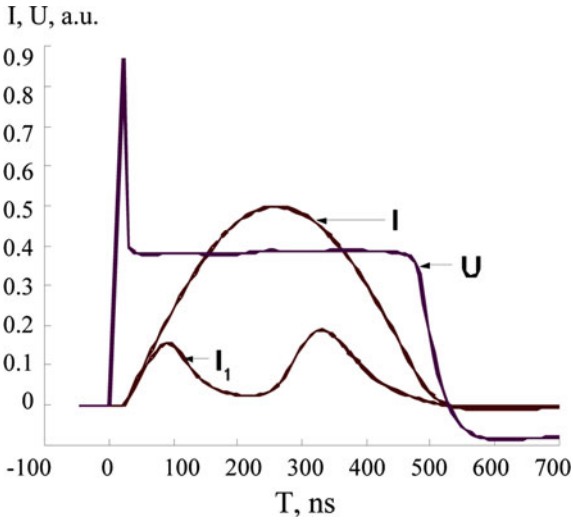

Fig. 28.3 Calculated oscillograms of the discharge voltage, U, the total discharge current, I and, the current through one channel, I_1

through an individual channel exhibits several maximums that are in qualitative agreement with the experimentally observed redistribution of the channel glow intensities in the course of developing an SIVD.

28.3 Conclusion

The studies performed in the present work lend support to the phenomenon of limiting the current density in a volume discharge in SF_6 and mixtures of SF_6 with hydrocarbons. Allowance for such limitation mechanisms as dissociation by electron impact and dissociative electron–ion recombination in modelling SIVD permits a qualitative agreement between a theoretical description and the experimental data available to be attained.

References

1. V.V. Apollonov et al., Proc. SPIE **3886**, 370–381 (1999)
2. V.V. Apollonov et al., Quantum Electron. **27**, 207–209 (1999)
3. V.V. Apollonov et al., Proc. SPIE **3574**, 374–384 (1998)
4. V.V. Apollonov et al., Quantum Electron. **30**, 207–214 (2000)
5. E.B. Gordon, V.I. Matyushenko, P.B. Repnin, V.D. Sizov, Khemicheskaya Fizika **8**, 1212–1218 (1989)
6. A.A. Belevtsev, L.M. Biberman, Izvestiya Akademii Nauk SSSR. Energetika i Transport **3**, 74–78 (1976)

Chapter 29
High-Energy Nonchain HF(DF) Lasers Initiated by SSVD

Abstract We have previously demonstrates the possibility of creating high-efficiency nonchain HF(DF) lasers on mixtures of SF_6 with hydrocarbons (deuterocarbons) initiated by SSVD. With the laser aperture of 15 cm, we obtained the radiation energy $W = 150$ J and the efficiency $\sim 3\%$. The present chapter is devoted to further possible enhancement of output energy of nonchain HF(DF) lasers and approaches to their scaling. Apparently, the scaling characteristics of the lasers imply obtaining SSVD at longer separation between electrodes d and greater area of the cathode. Thus, we first focus our attention on certain specific features of SSVD in SF_6 and in mixtures of SF_6 with hydrocarbons (deuterocarbons) that are distinct from the discharge in other gases. It is these effects that made it possible to increase the active volume and the generation energy of nonchain HF(DF) lasers with unexpected ease.

29.1 Introduction

We have previously demonstrated [1–5] the possibility of creating high-efficiency nonchain HF(DF) lasers on mixtures of SF_6 with hydrocarbons (deuterocarbons) initiated by SSVD. With the laser aperture of 15 cm, we obtained the radiation energy $W = 150$ J and the efficiency $\sim 3\%$ [5]. The present section is devoted to further possible enhancement of output energy of nonchain HF(DF) lasers and approaches to their scaling.

Apparently, the scaling characteristics of the lasers imply obtaining SSVD at longer separation between electrodes d and greater area of the cathode. Thus, we first focus our attention on certain specific features of SSVD in SF_6 and in mixtures of SF_6 with hydrocarbons (deuterocarbons) that are distinct from the discharge in other gases. It is these effects that made it possible to increase the active volume and the generation energy of nonchain HF(DF) lasers with unexpected ease.

© Springer International Publishing Switzerland 2016

V.V. Apollonov, *High-Energy Molecular Lasers*,
Springer Series in Optical Sciences 201, DOI 10.1007/978-3-319-33359-5_29

29.2 Features of SSVD in the Mixtures of SF_6 with Hydrocarbons or with Deuterocarbons

29.2.1 Possibility of Obtaining an SSVD Without Preionization

It is known [6, 7] that a preliminary gas ionization that provides a minimum initial concentration of electrons is a necessary condition for obtaining an SSVD. We have found [1–3] lasers with a rough cathode surface (subjected to sandblasting or emery treatment), the SSVD and output laser characteristics are independent of preionization. In other words, no preionization is necessary in this case.

The spatial-temporal evolution of SSVD without preionization was studied on the installation schematically shown in Fig. 29.1, in order to clear the formation mechanism of the discharge. SSVD was observed in a system of plane electrodes with polished anode with a the diameter of 12 cm and the cathode with a the diameter of 6 cm, rounded off to a radius of 1 cm along its perimeter. The separation between electrodes was 4 cm. The cathode surface was subjected to sandblasting. From one side, the gap was illuminated by a low-current ($\sim$1 A) spark, enclosed in quartz bulb. The spark could not produce a volume photoionization of gas (the mixture SF_6-C_2H_6 with the ratio of partial component pressure 10:1 at the total pressure 33 Torr); however, it provided a stable time delay of gap breakdown due to electron initiation at the cathode. An artificial delay line with variable number of cells was discharged through the gap, which made it possible to vary the pulse duration of the voltage across the gap within the limits 40 ÷ 400 ns at approximately constant SSVD current. Typical oscillograms of SSVD voltage and current at two different voltage expositions across the electrodes are shown in Fig. 29.2. Spatial-temporal evolution of SSVD was studied by photographs taken at various voltage expositions across the discharge gap.

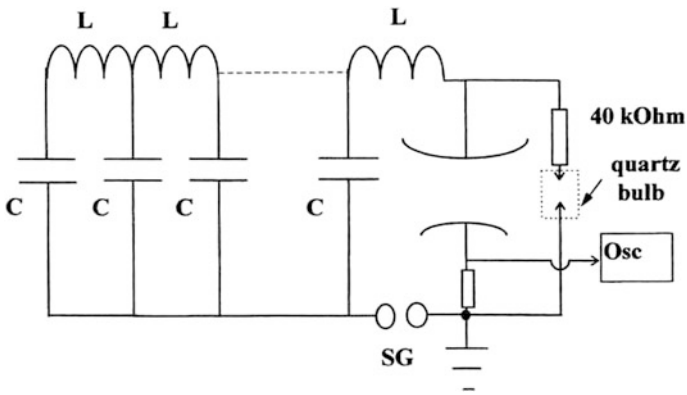

Fig. 29.1 Electric diagram of the setup for investigating the spatial-temporal evolution of an SSVD

Fig. 29.2 Typical oscillograms of voltage (*upper trace*) and current (*bottom trace*) for two different voltage pulse durations (see Fig. 29.1). The time scale is 100 ns/div

The development of an SSVD was also controlled by a sectioned cathode according to the diagram on Fig. 29.3. Holes with a diameter of 2 mm were drilled through the plane part of the cathode with the maximum distance ($\sim$4 cm) between them. Then, insulated wires with a 1 mm diameter were fixed in the holes. The current in each wire was measured by Rogovski coils. One of the wires was 1 mm higher than the cathode surface, which provided guaranteed initiation of the discharge exactly at this particular point. Oscillograms of currents through the initiating and the control wires make it possible to study the dynamics of SSVD development in the gap.

It worth noting that a corona on the rough cathode surface cannot provide initial concentration of electrons needed for SSVD initiation in the discharge gap, because without spark illumination (see Fig. 29.1) the delay of the gap breakdown is $\sim$1 μs even at three-fold overvoltage level (with respect to the voltage of the quasi-steady SSVD phase). Thus, the volume character of the discharge without preionizalion should be explained by other reasons.

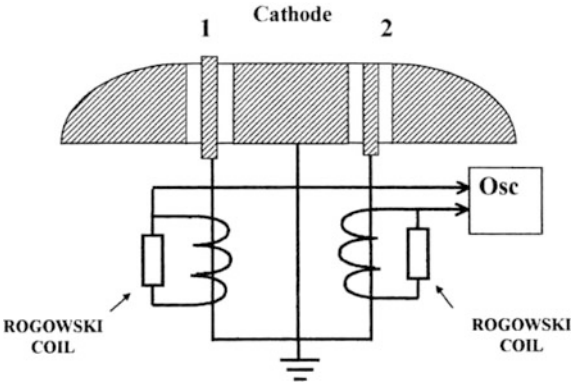

Fig. 29.3 Sectioned cathode: the initiating wire (*1*); the control wire (*2*)

Photographs of the discharge gap taken according to Fig. 29.1 show that SSVD starts at the gap edge in a rопе closest to the spark source in the form of one or several diffuse channels attached to the bright cathode spots, No glow is detected in the rest of the gap even with the sensitivity 1600 ASA of a photographic film. Then, the cathode spots that *were* formed first initiate in the neighboring zone additional cathode spots with diffuse channels and soon. Cathode spots with the attached diffuse channels propagate from the initiation point over the gap and finally cover all the surface of the cathode. This process is illustrated in Fig. 29.4, where the number of cathode spots, *N*, is shown versus time for the scheme given in Fig. 29.1, Time is counted up from the instant of gap breakdown and current appearance (see Fig. 29.2). As can be seen from Figs. 29.2 and 29.4, the spots spread over the cathode surface at virtually constant discharge current and quasi-stationary voltage across the gap that is determined by the equilibrium of burning and loss rates of electrons in the processes of ionization and attachment, respectively. Hence, as new cathode spots arise, the current through the previous spots should fall. Indeed, this effect is confirmed by Fig. 29.5, where the oscillograms of the currents through the initiating and control wires are shown according to the scheme given in Fig. 29.3. It is seen in Fig. 29.5, that the current through the control wire corresponding to the origin of a cathode spot on it starts at the moment when the corresponding current through the initiating wire reduces more than twice due to origin of new spots and their spread over the cathode surface from the initiating point. Because the control and the initiating wires are disposed at maximum possible distance in the considered geometry, then the cathode spot at the control wire has a considerable delay with respect to the instant of the spot origin at the initiating wire.

Thus, in the considered conditions, there is a mechanism of SSVD stabilization related to a limitation of the current through the cathode spot. The fact that the cathode spots arise at early stages of the discharge, the following cathode spots are

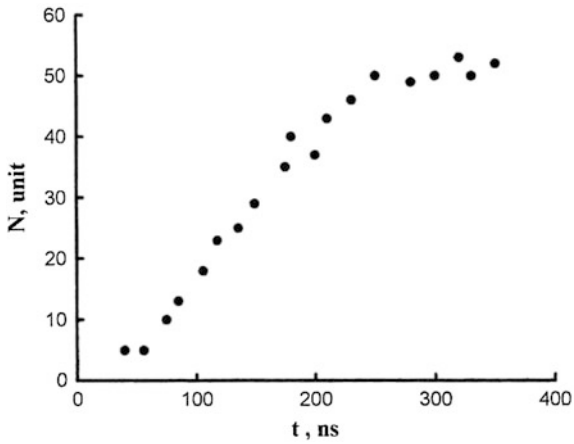

Fig. 29.4 Number of cathode spots *N* as a function of time

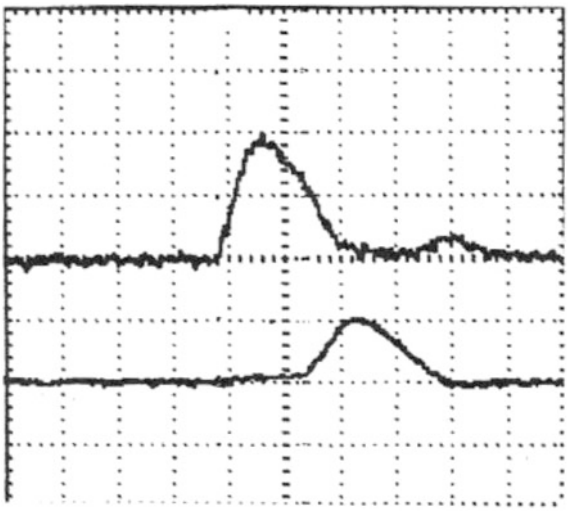

Fig. 29.5 Oscillograms of current through the initiating (*upper trace*) and the control (*bottom trace*) wires. The time scale is 50 ns/div

initiated by the preceding one and the discharge is stabilized by current limitation in the cathode spot results in a negligible part of preionization in the considered case. This kind of discharge can be termed the SIVD. It can conditionally be ascribed to conventional SSVD because it is presented by a number of diffuse channels originated from cathode spots, i.e., this type of discharge has principally filament structure. Thus, the stability of the considered type of the discharge depends mainly on the surface density of cathode spots (determined by the surface conditions) rather than on the initial concentration of electrons. This is the reason for higher SSVD stability in working mixtures of HP (DF) lasers with rough cathode surface as compared to systems with polished cathodes. We may assume that these surface effects are responsible for higher SSVD stability in systems with hydrocarbons (deuterocarbons) added to SF_6 [1, 2]. In Fig. 29.6, the surface density of cathode spots N_s is shown versus partial pressure of ethane $P_{C_2H_6}$ in the mixture SF_6-C_2H_6, the partial pressure of SF_6 being constant. It is seen, that the surface density of cathode spots increases with the partial pressure $P_{C_2H_6}$, which, naturally, entails higher SSVD stability due to the reduction of current through a singe spot. Apparently, this effect is caused by adsorption of C_2H_6 on the cathode surface, which, on one hand, changes the work function of electron from the surface and, on the other hand, the initiation of additional cathode spots by a radiation of the preceding spots is easier due to lower potential of ionization of hydrocarbons as compared with SF_6.

The rate of the cathode spot spread from the initiation zone over the cathode surface and the final surface density of cathode spots increase with the discharge current. The dependence of N_s on maximum discharge current, I, is shown in Fig. 29.7 (see the diagram on Fig. 29.1), where an artificial delay line was substituted by a capacitor. It can be seen from Fig. 29.7 that the maximum value of N_s exceeds 15 cm^{-2}.

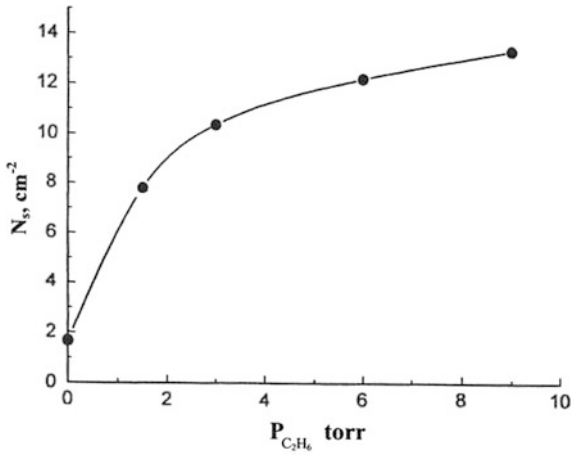

Fig. 29.6 Surface density of cathode spots N_s as a function of partial pressure of C_2H_6 $P_{C_2H_6}$. The pressure of SF_6 is P_{SF6} = 30 Torr

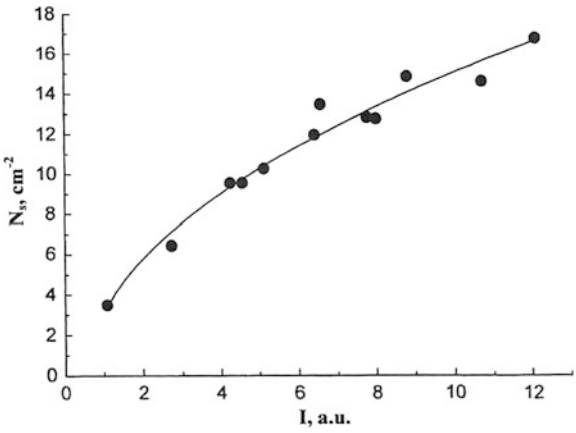

Fig. 29.7 Surface density of cathode spots as a function of the total current I of SSVD

In practical laser geometry at considerably high cathode area (150 cm^2 and greater), no particular initiation of the discharge is needed, the delay of the gap breakdown is negligible. The discharge starts in zones of enhanced field at the cathode edges and spreads from edges to the center of the cathode. The surface density of the cathode spots at the energy deposition $\sim$200 J/l is considerably high at the cathode edges $\sim$20 cm^{-2} and in the center $\sim$30 cm^{-3} [5]. The diffuse channels expand from the cathode to anode and overlap (at the distance $\sim 1 \div 2$ cm from the cathode surface with the separation between electrodes d = 15 cm), hence, the filament structure of the considered discharge does not affect the optical quality of the laser.

29.2.2 Obtaining an SSVD in a System of Electrodes with High Edge Nonuniformity

It is known [8] that in the system of electrodes schematically shown on Fig. 29.8 at $r \ll d,\ h$ (where d is the separation between electrodes, h is the transversal dimension of the cathode, r is the rounding radius of cathode edges along its perimeter, and the x-axis is normal to the laser optical axis) in working mixtures of CO_2. N_2O and excimer lasers, the SSVD current is concentrated at edges of the discharge gap so that the distribution of output laser energy over the aperture has maximums corresponding to gap edges (see Fig. 29.9). Distribution of the output characteristics with the maximum at the optical axis in such systems of electrodes and the considered mixtures can only be obtained using special dynamic profiling of electric field in the discharge gap by volume charges [9]. Quite a different picture is obtained in a similar system of electrodes in working mixtures of nonchain HF (DF) lasers. In Fig. 29.10, the output energy distribution of HF(DF) laser over its aperture is shown in a direction parallel to the surface of electrodes The separation

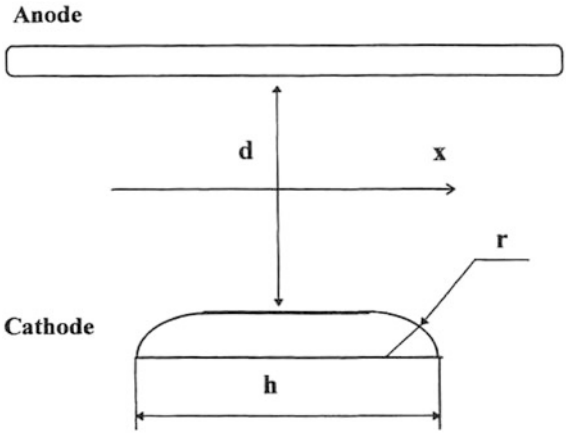

Fig. 29.8 Schematic diagram of the discharge gap

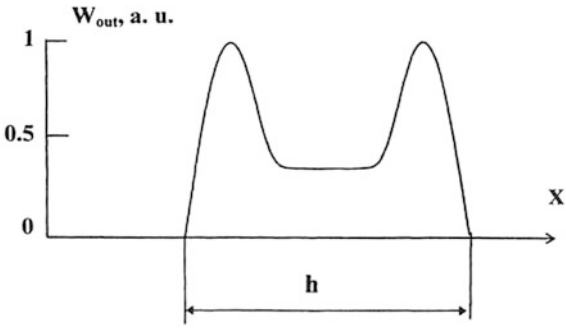

Fig. 29.9 Typical laser radiation energy distribution W_{out} over the aperture in a system with high edge nonuniformity of electric field

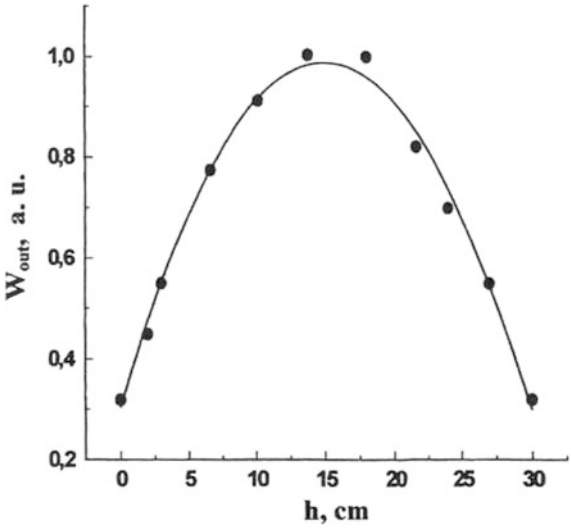

Fig. 29.10 Radiation energy distribution W_{out} of nonchain HF(DF) lasers over the aperture in a system with high edge nonuniformity of electric field

between electrodes was 27 cm and the cathode rounding radius was r = 1 cm. The pressure of tin mixture SF_6-C_2H_6 was 60 Torr and the ratio of partial pressures of the components was 20:1. We used a stable cavity configuration for the laser. As can be seen in Fig. 29.10, the obtained distribution is typical for gaps with a uniform electric field [8]; however, we used no special methods for the dynamic profiling of electric field and the SSVD was realized in a system of simple plane electrodes without preionization. As was noted, the discharge starts burning in a zone of enhanced field near the gap boundaries and the cathode spots spread from the boundaries to the cathode center This is illustrated by Fig. 29.11, where the oscillograms are shown of generation pulses taken at the optical axis (1) and near

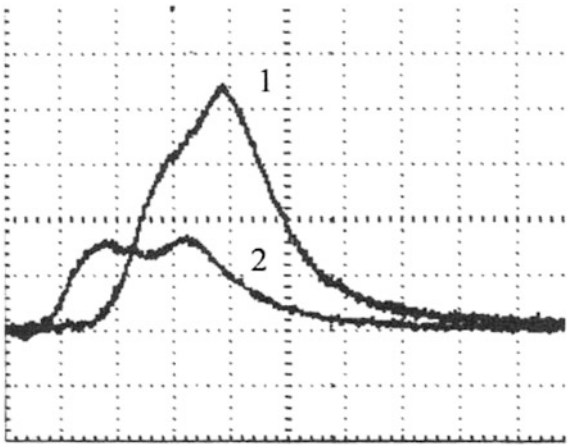

Fig. 29.11 Oscillograms of radiation pulses of HF(DF) laser obtained at the optical axis (*1*) and at the aperture edge (*2*). The time scale is 100 ns/div

the gap boundary (2). The detectors were placed along the *x*-axis shown in Fig. 29.8. From Fig. 29.11, it is possible to see that despite the higher density of radiation energy at the edge of aperture (as compared with that at the optical axis) the generation starts here 100 ns earlier in accordance with the described dynamics of the discharge development. It should be noted that this time lapse will cease in an unstable cavity that provides generation in single transversal mode. Photographs of the discharge gap (d = 27 cm) of the considered laser show that the surface density of cathode spots has a maximum at a central zone of the cathode (in the coordinates of Fig. 29.8) and reduces towards the. electrode edges. It is in agreement with the energy distribution over laser aperture, because the surface density of cathode spots echoes the current density distribution and, hence, the energy deposition to active, medium.

What is the reason for obtaining an SSVD in nonchain HF(DF) lasers under high edge nonuniformity of electric field in the discharge gap? We can assume it may be limitation of the current through the cathode spot described above, which deteriorates the flow of the total discharge current through the channels produced in the region of edge nonuniformity of electric field. However, the mechanism of this phenomenon is not clear yet. Further investigations of the discharge in both strongly electronegative gases (that are simitar to SF_6 in terms of the rate-of-attachment dependence on the parameter *E/p; E* is the electric field intensity and p is the gas pressure) and less electronegative gases, e.g., in CO_2 and N_2O.

29.2.3 SSVD Stability in Mixtures of SF_6 with Hydrocarbons or Deuterocarbons

We have already discussed factors affecting the SSVD stability in working mixtures of nonchain HF(DF) laser. The next focus is the particular characteristics of SSVD stability in the following coordinates: the upper limit of specific energy deposition (W_{sp}), the duration of SSVD stable burning (T). This dependence was studied according to the scheme shown on Fig. 29.1, where a capacitor connected in series with an inductance was discharged across the gap instead of the artificial delay line. The time parameter, T, was defined as the half-period of the short-circuit connection, $T = \pi\sqrt{LC}$, where L is the inductance and C is the capacitance. By varying C, L, and the discharge current, we may study the stability of SSVD in a wide range of T and W_{sp} variations. The dependence of W_{sp} on T^{-1} is shown on Fig. 29.12. It can be seen, that at a characteristic value W_{sp} = 200 J/l, the duration of stable SSVD burning is $\sim$500 ns. It is not a strong restriction as compared, for example, with excimer lasers used for obtaining SSVD in large active volumes.

Presently, we have no clear understanding of all the details of the processes responsible for the considered effects. However, it is these effects (obtaining an SSVD without preionization, initiation of uniform SSVD burning under the conditions of high edge nonuniformity of electric field, and considerably high SSVD

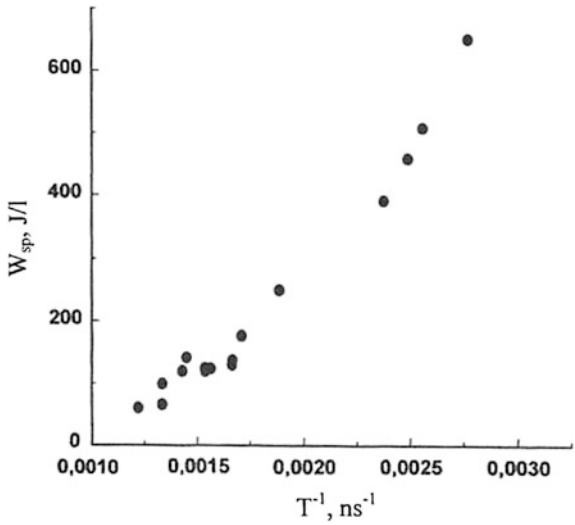

Fig. 29.12 Maximum specific energy deposition W_{sp} into SSVD plasma versus inverse time

stability in the mixtures of SF_6 with hydrocarbons (deuterocarbons)) that made it possible to carry out experiments on scaling characteristics of nonchain HF (DF) laser.

29.3 Scaling of Nonchain HF/DF Laser

In experiments on scaling nonchain HF(DF) lasers, we used cathodes of the size $h \times l = 10 \times 50$ cm, 15×75 cm and 20×100 cm, rounded off to the radius $r = 1$ cm along the perimeter. The cathode surfaces were subjected to sandblasting. A plate of the size 40×120 cm was taken for anode. The separation between electrodes varied within the limits $d = 10 \div 27$ cm. The electrodes were placed inside a glass-epoxide tube with a the diameter of 50 cm and a length of 140 cm. Laser cavity was formed by a plane-parallel plate made of CaF_2 and a concave *Al* mirror with a radius of curvature 20 m, placed directly on the faces of the discharge chamber.

The electric diagram of the experimental setup is given on Fig. 29.13. The energy was stored in 10-step Marks generator with the effective capacitor C_1, the maximum output voltage was $U_{max} = 500$ kV, and the maximum stored energy was $W_{max} = 12$ kJ. Marks generator through the inductance, L, charges the capacitor, C_2, in a time lapse $2 \div 4$ μs. Then, through the simultaneously initiated spark gaps, $SG_1 \div SG_n$, the voltage is applied to the peaking capacitor, C_3, and to the discharge gap. The values of the capacitors were taken from the condition $C_1 = (0.8 \div 0.9)\ C_2$; $C_3 = (0.35 \div 0.45)C_2$.

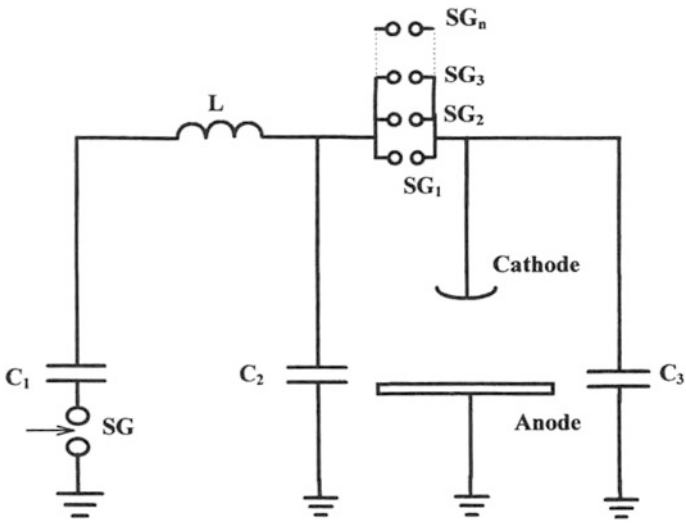

Fig. 29.13 Diagram of experimental setup of a nonchain HF(DF) laser

Under conditions in which we are limited by certain reasonable maximum voltage in the system determined by the insulation breakdown voltage (in our case the air insulation threshold U_{max} = 500 кV), the stored energy and the laser generation energy can only be increased by increasing the capacitance *(C),* i.e., by a proportional increase of all the capacitors of the diagram on Fig. 29.13 with the corresponding enlargement of the active medium volume, V_a, in order to maintain the SSVD stability. The most simple way to scale the output characteristics of a laser is to enlarge active volume by making its length, *I*, longer. In this case, all laser parameters vary proportionally to *l*: $V \sim l$, $C \sim l$, $W_{\text{out}} \sim l$ and the number of spark gaps initiated simultaneously ($SG_1 \div SG_n$) is $n \sim l$. The discharge duration is T = const, so that SSVD stability is not disturbed. Nevertheless, this approach to scaling problem is of low interest for a variety of reasons.

The more attractive approach to scaling is to increase the aperture, i.e., the separation *d* between electrodes and the transversal dimension *h* of the cathode. In this case, the mixture pressure is $P \sim l/d$ and, since the inductance of the discharge contour does not noticeably vary when *d* and *h* are increased, hence, the discharge duration increases as $T \sim \sqrt{C}$, which leads to a lower SSVD stability. Thus, while increasing *C,* we should reduce the specific energy deposition to plasma at the expense of corresponding variation of V_a. As can be seen from Fig. 29.12, within the limits of $W_{sp} = 100 \div 300$ J/1 we may approximately ($\sim$30%) assume $W \times T \sim$ constant, hence, if the capacitance is increased, then for maintaining the SSVD stability the parameter V_a should also be increased as $\sim C^{3/2}$ regardless of which the parameter *d* or *h* is considered.

Indeed, this simple and obvious relationship was found in our experiments. The maximum generation energy was obtained at $d = 27$ cm and the cathode dimensions 20×100 cm and was equal to 397 J for HF laser and 312 J for DF laser with the electric efficiency 3.8 and 3%, respectively.

29.4 Conclusion

In the present part of this book, we analyze the mechanisms of SSVD initiation in mixtures of SF_6 with hydrocarbons (deuterocarbons). The possibility is shown of obtaining SSVD in large volumes of mixtures SF_6 with hydrocarbons (deuterocarbons) without preionization in a discharge gap with high edge nonuniformity of electric field. The scaling features of nonchain HF(DF) lasers were studied. The record values of generation energy have been obtained, namely, 397 J for a HF laser and 312 J for a DF laser with the efficiency 3.8 and 3%, respectively. The investigations that were carried out show the possibility for further increase of the generation energy of HF(DF) nonchain lasers on the basis of the considered approaches to, at least, 1 kJ.

References

1. V.V. Apollonov et al., *Proceedings of the Seventh Conference on Gas Discharge Physics, Ryazan*, pp. 6–7 (1996)
2. V.V. Apollonov et al., Quantum Electron. **27**, 207–209 (1997)
3. V.V. Apollonov et al., Tech. Phys. Lett. **22**, 1026 (1996)
4. V.V. Apollonov et al., *Proceedings of the Second International Conference on Plasma Physics and Plasma Technologies (FPPT-2)* [in Russian], Minsk, p. 154 (1997)
5. V.V. Apollonov et al., Quantum Electron **28**(2), 116 (1998)
6. A.J. Palmer, Appl. Phys. Lett. **25**, 138 (1974)
7. J.I. Levatter, S.C. Lin, J. Appl. Phys. **51**, 210 (1980)
8. A.M. Robinson, J. Appl. Phis. **47**, 608 (1976)
9. V.V. Apollonov et al., Sov. J. Quant. Electron. **17**, 76 (1987)

Chapter 30
SSVDs in Strongly Electronegative Gases

Abstract In strongly electronegative gases, the lifetime of an electron with respect to being captured by a neutral molecule to form a stable negative ion $t \sim 1/(\eta \cdot v_e)$, ($\eta$ is the attachment rate, v_e is the electron drift velocity) is extremely restricted, so that a preionization source should be more powerful than in gas mixtures characterized by negligible losses of electrons due to attachment. This brings up certain difficulties in realizing SSVDs in large volumes of strongly electronegative gas mixtures.

30.1 Introduction

Traditional methods of obtaining an SSVD, applied, for example in different TEA-lasers, suggest a preliminary gas ionization (e.g., by electron beam, VUV irradiation or by soft X-ray radiation) followed by impressing a high-voltage impulse on a discharge gap with a uniform electric field [1]. However, in strongly electronegative gases, the lifetime of an electron with respect to being captured by a neutral molecule to form a stable negative ion, $t \sim 1/(\eta \cdot v_e)$, ($\eta$ is the attachment rate, v_e is the electron drift velocity) is extremely restricted, so that a preionization source should be more powerful than in gas mixtures characterized by negligible losses of electrons due to attachment. This brings up certain difficulties in realizing an SSVD in large volumes of strongly electronegative gas mixtures. Another problem arising from the attempts to increase the discharge volume in strongly electronegative gases, including, e.g., mixtures of SF_6 with hydrocarbons employed in nonchain HF(DF) lasers, is the necessity to provide the electric field uniformity by specially profiling the electrodes (Rogowsky profile, Chang profile, etc.). Apart from pure technical problems, this leads to growing the setup in size and, correspondingly, increasing the inductance of discharge circuits, whereas the time of stable burning of SSVD is extremely restricted in strongly electronegative gases.

© Springer International Publishing Switzerland 2016

V.V. Apollonov, *High-Energy Molecular Lasers*,
Springer Series in Optical Sciences 201, DOI 10.1007/978-3-319-33359-5_30

30.2 Experimental Investigation

With the above in mind, it is surprising therefore that in SF_6 and mixtures of SF_6 with hydrocarbons in the special case that the cathode surface possesses a small-scale ($\sim$50 μm) roughness, a stable SSVD without preionization (an SIVD) can nevertheless be observed [2]. SIVD shows up as a number of overlapping diffuse channels attached to cathode spots and in its integral characteristics (e.g., visual appearance, voltage and current oscillograms and also in the stability parameters), it does not differ at all from an ordinary SSVD with preionization [2]. SIVD in SF_6 and mixtures of SF_6 with hydrocarbons is also distinguished by the possibility of being realized in the discharge gaps, displaying an appreciable edge enhancement of the electric field; in so doing, the energy is put into the discharge gap almost spatially uniformly [3]. Studies investigating SIVD dynamics point to the existence of mechanisms in SF_6 and SF_6-based mixtures that limit current density in a diffuse channel, which cause expanding of the discharge volume as the energy putted into the plasma increases, displacing SIVD into the interior of the discharge gap, even though it was first initiated in the zone of the enhanced edge electric field [4]. The finding of SIVD has brought the problem of scaling of nonchain lasers to a qualitatively new level and allowed their output characteristics to increase considerably along with an extremely simple setup design. Therefore, it is of interest to examine the possibilities of obtaining an SIVD in other strongly negative gases, which could be employed not only as working mixtures for non-chain chemical lasers, but in various modem technologies too.

The present chapter investigates the possibility of obtaining an SIVD in CF_4, C_3F_8, CCl_4, C_2HCl_3 and in their mixtures with hydrocarbons.

The experiments were carried out in the system of plane electrodes comprising a polished Ø12 cm A1 anode and Ø6 cm cathode rounded off over its perimeter with a radius of 1 cm. The cathode surface was sandblasted similarly to that in papers [2, 4]. The interelectrode distance was d = 2–4 cm at total pressures of the gases studied (CF_4, C_3P_8, CCl_4, C_2HCl_3 and their mixtures with C_2H_6) equaled p = 10–75 Torr. The gap was stressed by discharging a capacitor.

The presence of the mechanisms restricting a current density, precluding the passage of all the energy stored in the capacitors through a single channel and, thus, determining the existence of such a kind of SSVD as SIVD can be inferred from the voltage oscillograms only at high specific energy depositions [4]. Therefore, for detecting this effect, special experiments in the rod (cathode)–plane (anode) gap were carried out, where the transverse size of SIVD was restricted with a Ø6–8 cm glass tube (bounded SIVD) by analogy with reference [4]. The discharge limitation avoided growing the volume it occupies with increasing the energy putted into the plasma and enabled attaining high specific energy depositions (up to 1 J/cm^3), such that the influence of the restriction mechanisms became noticeable on the oscillograms.

The studies into the discharge between plane electrodes have shown that, in the presence of strong edge nonuniformity of the electric field in SSVD in CF_4 and its mixtures with C_2H_6, the discharge confines itself at the cathode edge in the region of a maximum electric field enhancement. With an increase in the energy deposition in SSVD plasma, spark channels begin to grow from the cathode edge bridging the gap. Thus, in contrast to SSVD, in mixtures of SF_6 with hydrocarbons, discharge in CF_4 does not extend over the entire gap, i.e., in this gas, the peculiarities typical of SIVD do not manifest themselves despite a strong electronegativity of CF_4. A qualitatively similar situation is observed in developing SSVD in C_3F_8, mixtures of C_2HCl_3 with C_2H_6 and mixtures of CCl_4 with C_2H_6. In these gases, although an initial breakdown also occurs at the edge of the discharge gap in the region of a maximum electric field enhancement, SSVD further advances in the direction from the cathode edge to the gap center wholly occupying the flat cathode surface similar to the discharge in mixtures of SF_6 with hydrocarbons. Hence, in the gases in question, SIVD is also observed. However, SIVD stability in CCl_4, C_2HCl_3 and in their mixtures with C_2H_6 is appreciably lower than even in pure SF_6 [5]. Conversely, the discharge stability in C_3F_8 is considerably higher than in SF_6 and mixtures of SF_6 with hydrocarbons (at the same total pressures) (Fig. 30.1).

In Fig. 30.2, the voltage oscillograms of SIVD in C_3F_8 and mixtures of C_2HCl_3 with C_2H_6, respectively, are shown. It can be seen from the figures that restricting SIVD sizes leads, as in SF_6 and its mixtures with hydrocarbons, to increasing the operating discharge voltage [4], with this phenomenon manifesting itself most pronounced in C_3F_8. It seems plausible that this fact causes SIVD in C_3F_8 to exhibit a higher stability than in other gases [5]. However, this question calls for further examination.

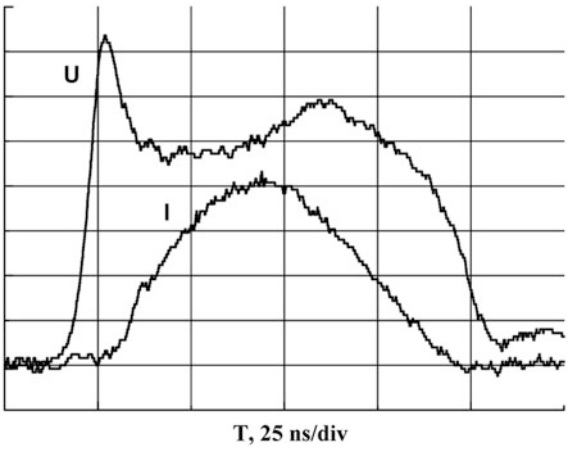

Fig. 30.1 Current (*I*) and voltage (*U*) oscillograms for bounded SIVD in C_3F_8

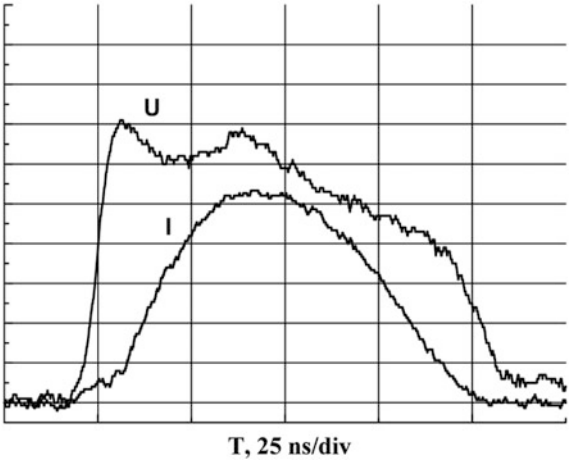

Fig. 30.2 Current (*I*) and voltage (*U*) oscillograms for bounded SIVD in mixture of C_2HCl_3 with C_2H_6

30.3 Conclusions

Parametric investigations of SIVD in C_3F_8, SF_6 and mixtures of SF_6 and C_2HCl_3 with hydrocarbons have revealed the distinguishing features as follows: (1) the discharge with a uniform energy deposition is formed in a gap with a high edge nonuniformity of the electric field; (2) increasing the energy putted into the discharge leads to growing the volume it occupies; (3) on limitation on the transverse discharge sizes, the voltage oscillograms show a characteristic rise just after the gap breakdown.

By these means, in the course of the studies performed, it was established that SIVD is observed not only in SF_6 and SF_6-based mixtures, but in other strongly electronegative gases: C_3F_S and mixtures of CCl_4 and C_2HCl_3 with C_2H_6. Data on the SIVD basic parameters in these gases were obtained. Further studies into the mechanisms of development of this type of discharge, as well as seeking new gas mixtures that allow SIVD to be obtained, are required.

References

1. Y.D. Korolev, G.A. Mesyats, in *Physics of Pulse Discharge in Gases* (Moscow, 1991)
2. V.V. Apollonov et al., Proc. SPIE **3574**, 374 (1998)
3. V.V. Apollonov et al., Quantum Electron. **25**, 123 (1998)
4. V.V. Apollonov et al., Quantum Electron. **30**, 207 (2000)
5. V.V. Apollonov et al., in *Proceedings of the 10th Conference on Gas Discharge Physics*, Russia, 28, (2000)

Chapter 31
High-Energy Pulse and Pulse-Periodic Nonchain HF/DF Lasers

Abstract In this chapter, the attempt has been made to gain an insight into the physics of SIVD starting from the results of our investigations into nonchain HF (DF) lasers performed in our laboratory and to analyze the potentialities for increasing energy parameters of nonchain lasers.

31.1 Introduction

Nonchain HF(DF) chemical reaction-based lasers are the most suitable sources of powerful coherent radiation in the 2.6 ÷ 3.1 μm (HF laser) and 3.5 ÷ 4.1 μm (DF laser) spectral regions. Among different methods of initiating a nonchain reaction in HF(DF) lasers, that of initiation by an SSVD seems to be one of the most attractive [1]. The basic advantages of nonchain electric discharge HF(DF) lasers are high radiation pulse power, possibility to operate at high pulse repetition frequencies, simple design and convenience in use. However, for an appreciable length of time (until 1996) these lasers were of limited usage because of their relatively low maximum radiation energy (~10 J). Evidently, the problem of improving the energy characteristics of similar lasers, as of most of other electric discharge lasers operating at intermediate and high gas pressures, is readily connected to the challenge of performing SSVD itself. We have carried out special-purpose investigations of SSVD in the working mixtures of nonchain HF(DF) lasers aimed at increasing their radiation energy, at least, to a level of several hundreds Joules [2–12]. As a result of this study a number of special features of nonchain HF(DF) lasers were found [3–12], which not only follow the traditional principles of forming a volume discharge at intermediate and high gas pressures [13, 14], but are largely contradictory to them. Specifically, ignition of SSVD without any preliminary ionization in SF_6 and mixtures of SF_6 with hydrocarbons (deuterocarbons) was found to be possible [2, 3]. We called this form of discharge SIVD [5]. Realization of SIVD in large volumes allowed an increase in the radiation energy of nonchain HF(DF) lasers of up to ~400 J at electric efficiency of ~4% [7–11].

© Springer International Publishing Switzerland 2016

V.V. Apollonov, *High-Energy Molecular Lasers*,
Springer Series in Optical Sciences 201, DOI 10.1007/978-3-319-33359-5_31

In this chapter, the attempt has been made to gain an insight into the physics of SIVD starting from the results of our investigations into nonchain HF(DF) lasers performed in our laboratory and to analyze the potentialities for increasing energy parameters of nonchain lasers.

31.2 SIVD—a New Form of an SSVD

31.2.1 What Is an SIVD?

Following a common practice, now already classical, certain conditions should be met for the realization of SIVD in dense gases, the most basic of which are as follows: (1) primary electrons of the number densities of no less than 10^6–10^9 cm^3 must be created within a gas volume through its preliminary ionization; (2) in the special case that SSVD is employed for laser excitation, which imposes tight constraints on uniformity of the active medium characteristics over the working volume, the primary electron multiplication should occur in a uniform electric field, which is usually provided by specially profiling the electrode surfaces. (Regardless of lasers, SSVD can in principle be obtained in a highly nonuniform field, for instance, in the rod–plane gap.) Clearly, the first condition cannot practically be met in such strongly electronegative gas as SF_6 [5, 7] because of great losses of primary electrons, due to electron attachment, except for the special "photo triggered discharge" mode [15], which, however, is ineffective for energy input into molecular gases owing to low over-voltages at the gap and, in the case of large discharge gaps and active medium volumes (large-sized electrodes), is not realized at all. On increase of the laser aperture and discharge volume, the problem also arises of to how to meet the second condition, owing to both technical difficulties in the fabrication of large-sized intricate shape electrodes and in connection with rise of the discharge circuit inductance caused by a useless growth in the transverse sizes of the electrodes [3, 4].

Thus, it clearly follows from the simplified analysis presented here that the possibilities for the creation of powerful electric discharge nonchain HF(DF) lasers coming from the known physical principles of forming an SSVD in dense gases are very limited. Moreover, when starting from these principles, all attempts to create nonchain HF(DF) lasers with the radiation energy 1 kJ and above seem to hold no promise. This evidence appeared to restrain the researcher's efforts in the direction of increasing energy parameters of nonchain HF(DF) lasers. Although there have been numerous works concerned with nonchain HF(DF), their radiation energy attained by 1996 was only slightly in excess of 10 J [16–18].

Incompleteness of the traditional notions of the physics of forming volume discharges in dense gases came to be understood after we found the possibility of obtaining an SSVD in SF_6 and mixtures of SF_6 with hydrocarbons (deuterocarbons) in the systems of plane electrodes with high electric field enhancement at the edge

without any preionization in a gas [2, 3]. The sufficient condition for realization of SSVD in this case was the presence of small-scale (~50 μm) roughness on the cathode. We called this form of SSVD an SIVD [5]. SIVD is not dissimilar in aspect to an ordinary SSVD with preionization. It comprises a set of diffuse channels diverging in the direction of the anode and attached to bright cathode spots. When overlapped, these diffuse channels show common diffuse glow [3, 5]. The SIVD current and voltage oscillograms are also typical of SSVD in electronegative gases [5].

It is worthy of note that in nonchain HF(DF) lasers with a rough cathode surface, preionization does not influence only the discharge characteristics (i.e., glow homogeneity, the presence of cathode spots, and the limiting energy deposited in the discharge plasma), but also the output laser energy [3, 5].

It should also be mentioned that analysis of literature data is indicative of a negligible role of preionization in forming SSVDs in nonchain lasers. For example, in papers [16, 18], approximately the same output energies and efficiencies were obtained. However in [16], where a set of metal rods connected to a common busbar through a resistance (resistance uncoupling) served as the discharge gap cathode, preionization was absent, whilst in [18] it was performed by a high-current dielectric surface discharge whose spectrum displayed not only UV radiation, but soft X-ray radiation as well.

By these means, we define SIVD as a form of SSVD obtained without preionization in SF_6 and SF_6-based mixtures under SF_6 pressures of 30–150 Torr typical of HF(DF) lasers. Based on analysis of the experimental results, the following questions are considered below: (1) the key features of the development of SIVD; (2) the physical mechanisms determining the possibility of the existence of SIVD; (3) is SF_6 a unique gas or SIVD can be observed in other gases?; (4) the active medium characteristics and output characteristics of nonchain HF(DF) lasers based on SIVD; and (5) the prospect for further increase of radiation energy of nonchain lasers.

a. Dynamics of SIVD formation

The key features of SIVD can most clearly be inferred from its dynamics.

i. Experimental setup

The setup used for investigations of the dynamics of forming SIVD is represented schematically in Fig. 31.1a. An SIVD of ~500 ns duration was initiated in mixture SF_6:C_2H_6 = 10:1 at the pressure of 33 Torr and interelectrode distance of 4 cm. As the electrodes there were a copper stripe of 0.5 mm thick and 16 cm long (cathode) stood edgewise and a disk anode of diameter 6 cm rounded off along its perimeter to a radius of 1 cm. The breakdown was force initiated at the gap edge by a low-current spark restricted by resistance R = 900 Ohm. This spark could not in principle provide a sufficient number of primary electrons in the gas volume;

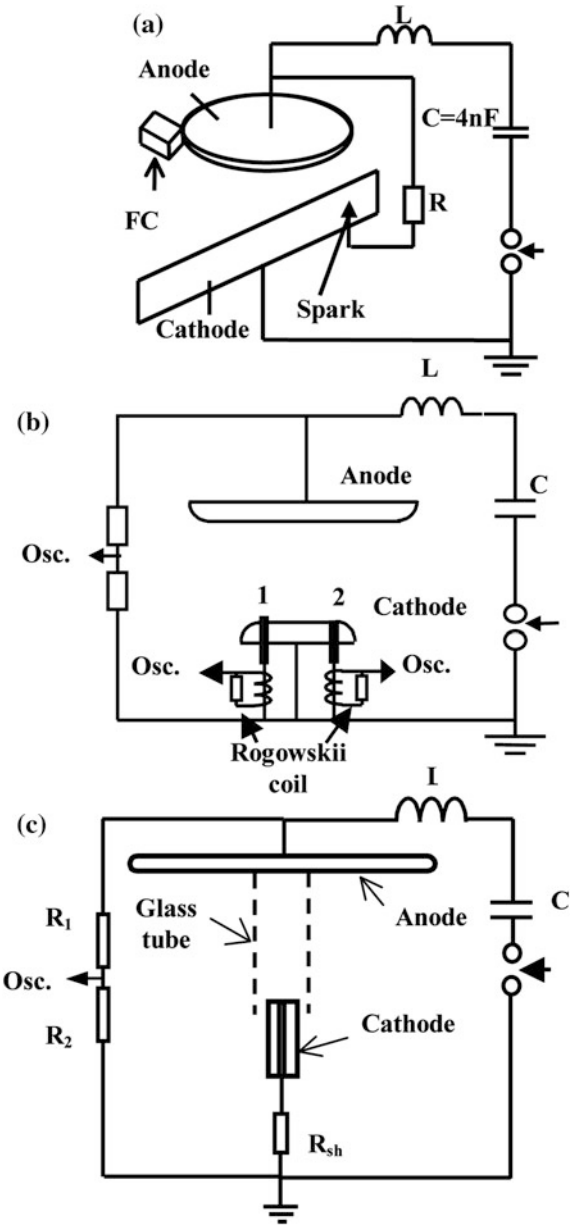

Fig. 31.1 Scheme of the experimental set-up for SIVD dynamics investigation

however, it allowed the site of the primary gap breakdown to be spatially stabilized. Luminosity of SIVD was recorded by a single frame camera with an exposure time of 20 ns run with varying delay, T, relative to the instant of the gap breakdown.

The SIVD dynamics was also studied in the plane–plane gap geometry in experiments with a sectioned cathode diagrammatically depicted in Fig. 31.1b. In this case, the interelectrode distance, working medium pressure and setup electrical scheme were the same as in the former experiment; however, as a cathode there was a 0.2 mm flat disk rounded off along its perimeter to a radius of 1 cm. Isolated conductors of 1 mm in diameter were inserted into holes 2 mm in diameter drilled within the flat part of the cathode and spaced by a distance of $\sim$4 cm. The basic cathode and these conductors were connected to a common bus. The current through each the conductor was recorded by Rogowskii coils. One of the conductors (1) extended $\sim$1 mm above the cathode surface, which ensured a primary gap breakdown just at this point whilst comparison of oscillograms of currents through the initial (1) and control (2) conductors allowed the SIVD extension over the gap to be followed.

Dynamics of a single diffuse channel were investigated with use of a setup represented schematically in Fig. 31.1c. Diffuse channel was initiated by discharge in the rod (cathode)–plane geometry in mixture SF_6:C_2H_6 = 10:1 at pressures p = 16.5 + 49.5 Torr and interelectrode distance d = 4 cm. The end of a 1.5 mm diameter rod dressed with polyethylene insulation was used as a cathode and the anode was a disk of diameter 10 cm. Limitation of the cathode surface ensured development of no more than one cathode spot. The SIVD dynamics was followed by a single frame camera as in the experiments performed by the scheme of Fig. 31.1a. SIVD was also filmed with a video camera, which allowed the volume occupied by the discharge to be exactly calculated as a function of the energy putted into the plasma, the latter being calculated by the current and voltage oscillograms. With the aim to increase a specific power input into the discharge plasma, SIVD in the given gap geometry was bounded, in a number of experiments, by a glass tube of diameter 6–8 mm (bounded SIVD [6, 11]) shown in Fig. 31.1c with dashed line. This made possible to bring up specific energy depositions to $\sim$1 J/cm^3.

ii. Experimental results

The frames of SIVD obtained by a single frame camera at different instants of time relative to the instant of the gap breakdown are shown in Fig. 31.2. In Fig. 31.3 the discharge voltage and current oscillograms corresponding to the process described are shown. As is seen from Fig. 31.2, the gap is broken down at the edge in the vicinity of an auxiliary electrode. At this instant in time, the SIVD constitutes a single diffuse channel with an already developed cathode spot. Then, near the first channel much less bright new channels appear, which temporally grow in number while their brightness becomes gradually comparable to that of the first channel, with the brightest channel being that located closer to the primary channel. In time, all the channels become equally bright whilst the glow intensity of the first channel noticeably decreases. On further development of the SIVD, increase in glow intensity of diffuse channels at the gap edge removed from the region of the first breakdown is observed. However, at T > 250 ns, the glow again becomes homogeneous throughout the length of the cathode, and the glow within the region

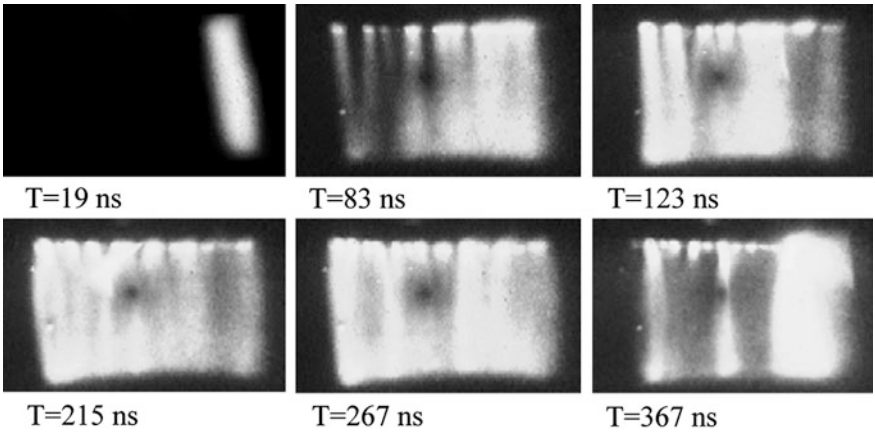

Fig. 31.2 SIVD frames for different T-values

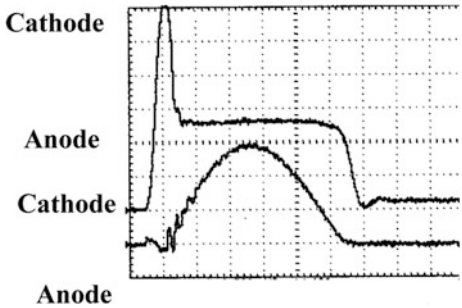

Fig. 31.3 Typical oscillograms of voltage (*upper trace*) and current (*bottom trace*). Time scale 100 ns/div

of the first channel is recovered. Furthermore, discharge instability begins to develop against the background of the total glow.

Thus, a very strange picture of the development of an SSVD is observed. Despite a local gap breakdown and the drop of the voltage across the gap to its quasi-stationary value (see Fig. 31.3) close to that of the static breakdown voltage in SF_6 [19], the initially formed channel is no more capable of passing all energy restored in the capacitor through itself, as it takes place, for example, in air or nitrogen [7] where a local gap breakdown, even in the form of a diffuse channel, must be followed by discharge instability and, at a sufficiently high restored energy, transition of the discharge from its diffuse to a constricted state. Instead, we see the formation of new diffuse channels after appearance of the first one and extension of an SIVD to the whole gap at the voltage close to the static breakdown value (see Fig. 31.3); in so doing, judging from decrease of the brightness of the first channel in time, the current through it not only rises, but, conversely, falls with appearing new channels, i.e., an initially formed channel progressively quenches. 'It should be noted that the effect of current recovery, demonstrated by Fig. 31.2, which

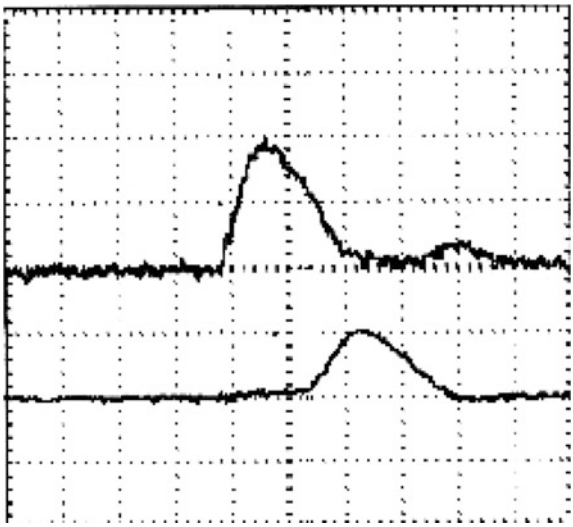

Fig. 31.4 Oscillograms of current through the initiating (*upper trace*) and the control (*bottom trace*) wires. The time scale is 50 ns/div

manifests itself in equalizing the 'brightness' of all channels after their initial drop is observed only under sufficiently high deposited energies'. On decrease in energy or growth of the cathode in size (accompanied, naturally, by increase the anode size), this effect is absent. However, at high energies deposited in the discharge plasma (150–200 J/1), typical of HF(DF) lasers, the SIVD extends to the whole gap so quickly, that the single frame camera we used does not allow the process to be resolved.

A similar picture of developing SIVD is observed in the discharge gaps with plane–plane geometry too. In Fig. 31.4 are shown oscillograms of the currents through initiating and control conductors (see Fig. 31.1b) obtained in the experiment with a sectioned cathode. It is seen from this figure that the current through a control conductor begins to flow with a noticeable delay relative to the current through the initiating conductor. Also seen is that the amplitude of the current through the initiating conductor reduces, by the instant of appearance of the current through a control conductor, by half, i.e., in the given experiment the effect of quenching the first channel with appearing the next channels successively filling the discharge gap is observed. The number of diffuse channels formed during the discharge current pulse duration, as shown in [5, 7], is proportional to the specific energy input into the discharge plasma. It is seen from the oscillograms in Fig. 31.4 that in the plane–plane discharge gap geometry, too, the effect of current recovery in the first channel after its almost complete quenching takes place.

As in the experiments described above, increase of the volume occupied by SIVD in the course of the energy input into plasma was observed in the rod–plane geometry, i.e., the discharge volume immediately depended on the energy deposited in this volume. In Fig. 31.5, the dependence of volume, V, occupied by an SIVD on parameter W/p where W is the energy put into the discharge and p is the gas mixture

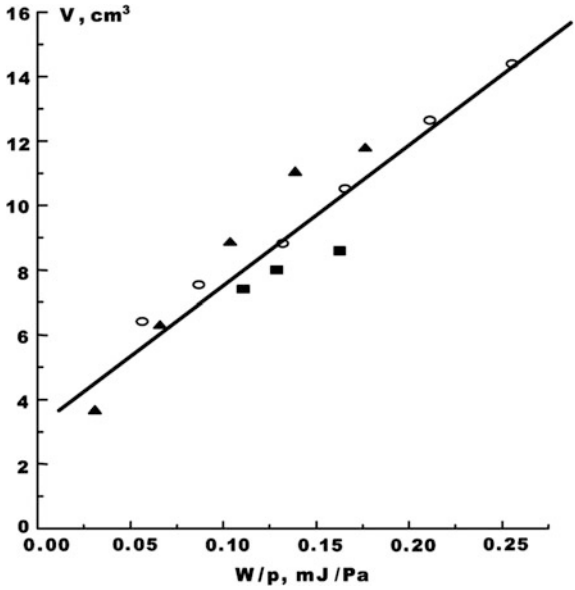

Fig. 31.5 Dependence of volume, V, occupied by SIVD on W/p, mixture SF_6: C_2H_6 = 10:1; p = 5 Torr (I); p = 30 Torr (A): p = 45 Torr (O)

pressure is given. It can be seen from Fig. 31.5 that the volume the discharge occupies grows linearly with parameter *W/p*.

After the size of SIVD in the rod–plane geometry was restricted by a glass tube, the discharge voltage and current oscillograms at energy depositions of up to W_{in} = *200 J/l* showed no changes; however, at energy depositions in excess of 400 J/1, oscillograms of a bounded SIVD displayed appreciable characteristic changes. Figure 31.6 depicts voltage and current oscillograms of bounded (U_b, *h*) and unbounded (*U, I*) SIVDs in mixture SF_6:C_2H_6 = 10:2 at pressure p = 33 Torr and d = 4 cm. As may be inferred from this figure, on restriction of the SIVD volume (equivalent to increasing a specific energy deposition), the voltage, just after its initial drop under breakdown, rises simultaneously with the current even during a certain period of time after the current passes its maximum. As a whole,

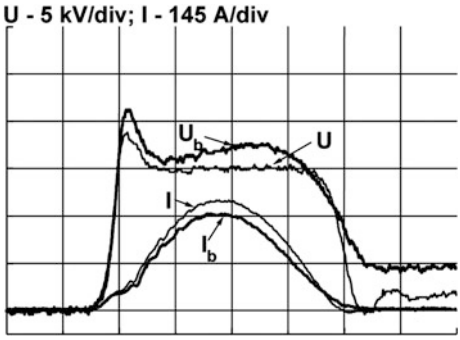

Fig. 31.6 Experimental voltage and current oscillograms for bounded (U_b, I_b) and free (U, I) discharges, time scale 50 ns/div

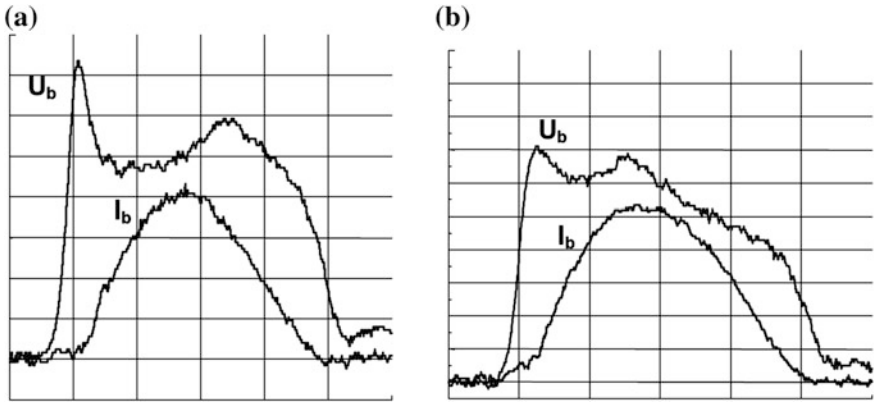

Fig. 31.7 Current (I_b) and voltage (U_b) oscillograms for a bounded SIVD; time scale 50 ns/div. **a** −30 Torr C_3F_8; **b** mixture: 15 Torr C_2HC1_3 + 3 Torr C_2H_6

$U_b > U$ whilst $I_b < I$, i.e., an unusual situation is observed here—the gap conductivity decreases with increasing specific energy deposition. It should be highlighted that SF_6 and SF_6-based mixtures are not unique in this respect. Electric discharges in other strongly electronegative gases and their mixtures exhibit similar features. In Fig. 31.7a, b the current and voltage oscillograms of a bounded SIVD in C_3F_8 and mixture C_2HC1_3:C_2H_6, respectively, are shown. It can be seen from Fig. 31.7a that oscillogram U_b shows in C_3F_8 a more pronounced bend than in SF_6.

The above-listed features of the development of SIVD allow for the assumption that mechanisms of current restriction in SF_6 and SF_6-based mixtures exist, which make difficult the passage of all the stored energy through a single channel.

It seems that it is these mechanisms that, to a large extent, cause the existence of such an unusual form of discharge as SIVD, as well as the possibility of its generation in the gaps with a high edge nonuniformity of the electric field.

31.2.2 The Mechanisms of Restriction of a Current Density in Diffuse Channels of SIVD in SF_6 and Mixtures of SF_6 with Hydrocarbons and Deuterocarbons

The results presented here are indicative of the presence of certain restriction mechanisms of the current density in diffuse channels in SF_6 and SF_6-based mixtures. (The same effect can be found in some other strongly electronegative gases; however, data for most of them on the rate of coefficients necessary for interpreting these effects even at a qualitative level are absent.) It is natural to link the presence of these mechanisms to such a distinguishing feature as SF_6 owing to its high electronegativity.

Relative to other gases capable of attaching electrons to their molecules to form stable negative ions, strongly electronegative gases, such as SF_6, are distinguished by (i) high values of their operating reduced electric fields E/N and (ii) high magnitudes of electronegativity χ_a defined as the negative ion to electron concentration ratio. This gives rise to some special features the discharge displays. To briefly summarize, they are as follows.

First, SF_6 molecule dissociation by electron impact becomes important. Indeed, at E/N-values such that electron impact ionization coefficient α is no less than electron attachment rate η, high mean electron energies approaching the SF_6 dissociation thresholds are attained. As a result, more than 80% of the energy deposited goes into dissociation [20]. It is worthy of note that dissociative ionization and electron attachment processes characteristic of SF_6 can significantly contribute to the gas decomposition, specifically to F-atom production [21]. On the submicrosecond time scale, the by-products formed have no time to leave the discharge channel, thus leading to a local increase in the total gas number density, N, and, consequently, diminishing electric conductivity.

Secondly, because χ_a is normally well over unity, large negative ion concentrations are achieved in SIVDs, resulting in electron generation processes by electron detachment from negative ions that may come into play. Traditionally, the detachment processes via negative ion-neutral molecule collisions or/and associative ionization are invoked. However, at intermediate gas pressures (10–100 Torr) on a microsecond time scale, the mechanisms mentioned do not contribute at all to electron multiplication as it follows from experiments and theoretical considerations [22]. On the other hand, there are strong grounds to believe that electron detachment by electron impact may be very efficient in producing secondary electrons in SF_6. Applied to development of electron avalanches in SF_6, this ionization mechanism was first proposed and quantitatively assessed in [23]. Later it was also considered for plasmas formed in other fluorine-containing gases (see, e.g., [24] and references cited therein).

Thirdly, high positive ion concentrations attained in SIVDs along with that the relation $\alpha \approx \eta$ holds under the working conditions lead to the dissociative electron-ion recombination which can strongly influence the SF_6 discharge plasma parameters, both qualitatively and quantitatively. At the stage of SF_6 plasma decay (the trailing edge of the voltage impulse), the ion-ion recombination considerably affects the discharge characteristics too. It should, however, be stressed that both the recombination processes in SF_6 are poorly known, so that no firm data on the corresponding rate constants at elevated reduced electric fields close to $(E/N)_{cr}$ are available in the current literature.

To understand how the above-mentioned processes can influence the SIVD characteristics, the discharge voltage oscillograms have been numerically simulated for conditions of Fig. 31.6. The equivalent electric circuit including spark and discharge gaps as well as the calculation procedure are described elsewhere [10, 19]. Figure 31.8 shows typical voltage oscillograms thus obtained, each curve accounting for only one of the listed mechanisms, except for curve 3 which also depicts the ion-ion recombination.

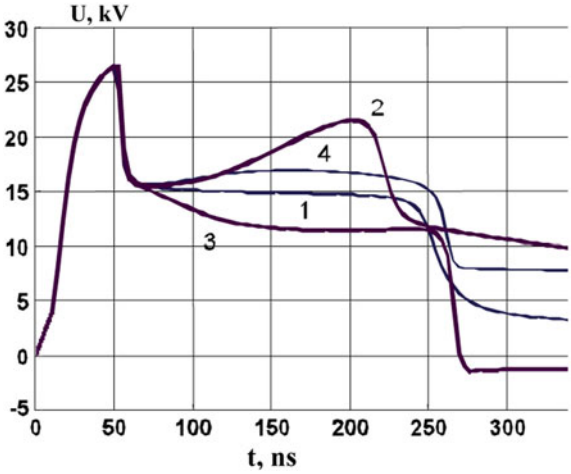

Fig. 31.8 Numerically simulated discharge voltage oscillograms. Electron impact ionization and electron attachment (EIIEA) only (*1*); EIIEA + SF_6 dissociation (*2*); EIIEA + electron impact detachment (Keid recombination ($b_{ii} = 10^{-8}$ cm^3/s) (*3*); EIIEA + electron-ion recombination cm^3/s (*4*)

To describe SF_6 dissociation, the energy spent for F-atom production is taken to be equal to 4.5 eV. Furthermore, it is suggested that negative ions SF_6^- dominates under the conditions of interest because charge transfer reactions have no time to be accomplished [22] and cross sections for directly producing other negative ions by electron impact are too small [21]. The rate constant for electron impact detachment from negative ions is assessed as $k_d = 10^{-7}$ cm^{-3}/s on the assumption that this quantity is no less than that of elastic electron scattering in SF_6 [23]. The rate constant b_{ei} for dissociative electron-ion recombination is derived with regard to that positive ion SF_5^+ predominates in SF_6 electric discharge plasma [21]. In addition, it was assumed that $b_{ej} \sim T_e^{-1/2}$ where T_e is the electron temperature. As a result, $b_{ei} = 10^{-7}$ cm^{-3}/s is taken. To determine ion-ion recombination rate constant b_{ii} special experiments were carried out [25, 26]. Without going into detail we give here = 10^{-8} cm^{-3}/s as an adequate value for the conditions in question.

It has been speculated in literature that electron attachment to vibrationally excited SF_6 molecules is capable of appreciably contributing to electron disappearance [27]. Meanwhile, there is no information regarding which SF_6 vibrational modes are be taken into account in this context. What are the corresponding cross sections or rate constants? However, a simple mathematical model has been proposed in [7, 9] with an eye to qualitatively examining this mechanism.

It is seen from Fig. 31.8 that all the processes considered, when taken into account with their actual rate constants, may considerably influence the SIVD voltage ocsillograms. Moreover, comparing Figs. 31.6 and 31.8, it is possible to establish that SF_6 decomposition plays a decisive role. The dissociative electron-ion recombination and electron detachment by electron impact affect the SIVD in opposite directions. It can be inferred from Figs. 31.6 and 31.8 that both these processes appear to equilibrate each other, at least within the accuracy to which the corresponding rate constants are presently known. This seems to lend an additional support to the estimates for rate constants k_d and b_{ei} presented in the book.

Advanced studies on a submicrosecond intermediate pressure SIVD in SF_6 and SF_6–C_2H_6 mixtures are presented. It was found that SF_6 molecules decomposition, ether through electron impact immediately or by the dissociative ionization and electron attachment greatly influence the discharge characteristics, specifically its voltage and current oscillograms. Breakup of C_2H_6 molecules may also be thought of as a noticeable dissociation mechanism. The electron-ion dissociative recombination and electron impact detachment from negative ions are felt to balance each other in pure SF_6 and in SF_6 with small C_2H_6 additives under conditions of interest. The considered processes enable one to qualitatively explain such a unique phenomenon as an SIVD.

It should also be noted that electron detachment from negative ions owing to electron impact can be thought of as one of the most probable mechanisms of developing instability of SSVDs in SF_6 and SF_6-based mixtures. Taking into account the influence of the listed processes enables the dynamics of SIVD formation to be qualitatively described. In our calculations, the channel structure of SIVD was modeled by a set of paralleled pure resistances whose conductivity was determined in accordance with [10, 19]. The differences in the initial conditions in developing the channels lengthwise of the cathode were specified by different initial electron number densities, n_0, for each channel. A total of 9 channels were taken into account, which corresponds to using a knife cathode in the experiment (see Fig. 31.2). In Fig. 31.9, the calculated oscillograms of voltage, *U;* total current, *I;* and the current through the first channel (with a maximum initial value of n_0) *are given*. The time scale was l00 ns/div. It can be seen that a current through an individual channel displays two maxima, which qualitatively correlates with the results of the experiments investigating the SIVD dynamics wherein the effect of current recovery was observed.

By these means, it is the presence of the mechanisms restricting a current through a conducting channel that makes possible the formation of an SSVD without preionization, an SIVD. However, a sufficiently high uniformity and stability should also be ensured for SIVD to be used in nonchain HF(DF) lasers.

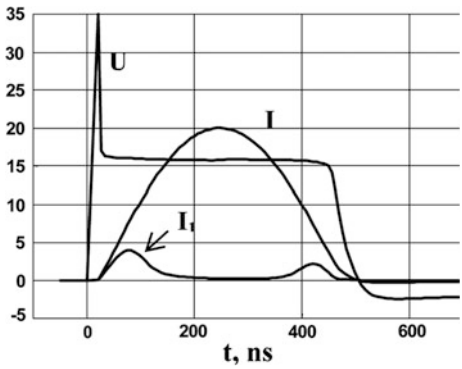

Fig. 31.9 Calculated oscillograms of voltage, U, and general current, I, and the current through the first channel, I_b. Scales: current: 25A/div.; voltage: 5 kV/div.; time: 200 ns/div

31.2.3 Stability and Uniformity of SIVD

SIVD can only conventionally be assigned to ordinary volume discharges. A volume nature of SIVD is attained through overlapping individual diffuse channels attached to cathode spots, i.e., SIVD has, in principle, a jet structure. Of importance for uniformity and stability of such discharges is, therefore, not an initial electron number density as such, but a surface density of cathode spots determined to a large extent by the surface state as well as a number of other factors. The results of experiments performed with the aim to reveal these factors are discussed subsequently.

31.2.3.1 Experimental Setup

Experiments were carried out in a dielectric discharge camera filled with mixture of SF_6 with hydrocarbons (C_2H_6 or C_3H_8) at a total pressure of p = 5 +15 Torr. A volume discharge burnt between A1 Ø6 cm cathode rounded off to a radius 1 cm along its perimeter and Al Ø12 cm anode at values pd = 0.02 ÷ 0.7 cm/atm. In the experiments, both cathodes that were polished and that were subjected to sand-blasting were used. A capacitor discharged through the gap. Changing the capacitance and capacitor's discharge voltage varied the energy inserted into the SIVD plasma.

31.2.3.2 Experimental Results

Figure 31.10 shows the number of spots, $N_{s,}$ on the cathode subjected to sand-blasting as a function of parameter $W_{sp}E_{qs}$ where W_{sp} is the deposited energy per unit gas volume and E_{qs} is the electric field strength in the quasi-stationary phase of SIVD. As is seen from Fig. 31.10, this relationship is satisfactorily approximated by a linear function.

$$\mathrm{N_s = a + b\ W_{sp} - E_{qs}} \tag{31.1}$$

Rise of quantity $\boldsymbol{N_s}$ and, consequently, of the cathode spots surface density, observed not only in increasing a specific energy deposition, but the electric field strength, reflects the fact that the electric field strength magnitude considerably determines the probability of formation of a cathode spot [14]. Constant $\boldsymbol{b}$ in expression (1) is, in turn, a function of the cathode surface state and the hydrocarbon content in the mixture.

Indeed, Fig. 31.11 shows the dependences of N_s on a partial pressure of C_2H_6 in the mixture at SF_6 pressure of 30 Torr and d = 4 cm obtained using a polished

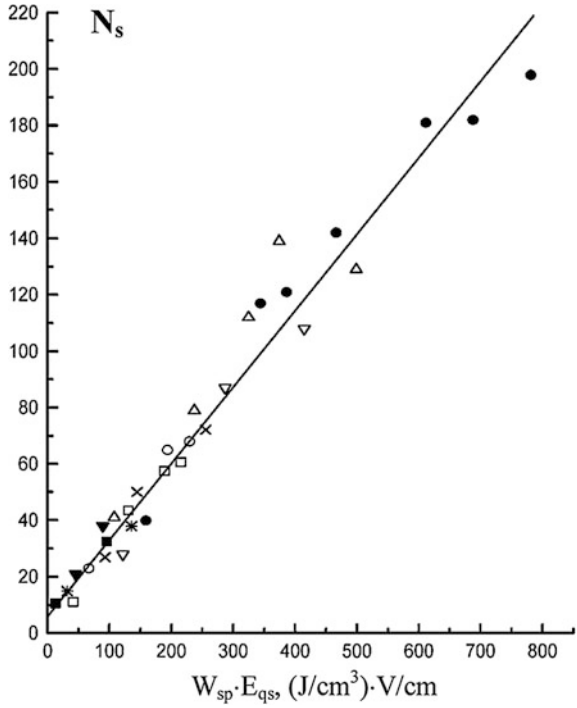

Fig. 31.10 Cathode spots number N_s versus parameter $W_{sp}E_{qs}$. Mixture SF_6: C_2H6 = 10:1: ϒ – *d* = 6 cm, p = 33.6 Torr; B – *d* = 6 cm, p = 16.8 Torr; * −*d* = *4* cm, *p* = 23.3 Torr; ▼ −*d* = *3* cm, *p* = 23.3 Torr; *o* – *d* = *3* cm, p = 33.6 Torr; Δ − *d* = *3* cm, p = 50.4 Torr; −*d* = 3 cm, *p* = 67.2 Torr.; x – *d* = 2 cm, *p* = 33.6 Torr

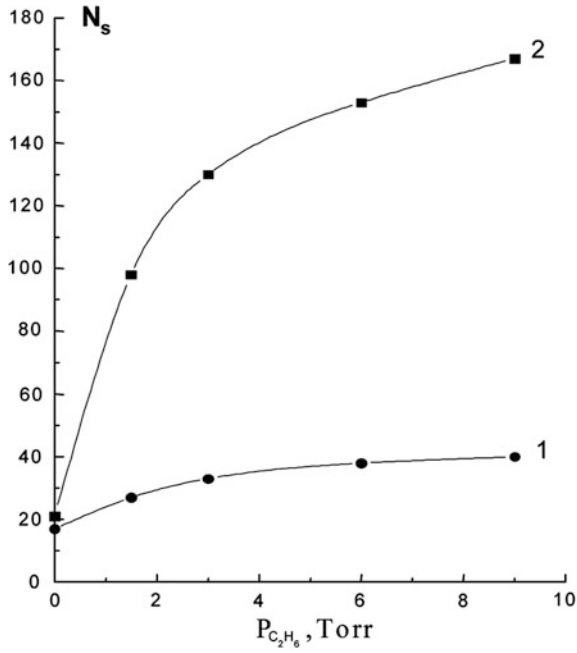

Fig. 31.11 Dependences of the cathode spots number, N_s, on a partial pressure of C_2H_6 in mixture SF_6:C_2H_6. SF_6 pressure p = 30 Torr. Polished cathode (*1*); cathode subjected to sandblasting (*2*)

cathode (curve 1) (mechanical polish of the surface followed by aging it by approximately 100 discharges) and a cathode subjected to sandblasting (curve 2). These dependences were obtained at a constant energy depositions in the SIVD plasma. As is seen in Fig. 31.11, quantity of N_s appreciably increases with increasing the hydrocarbon partial pressure. From this figure, it is also evident that roughness of a cathode surface plays a role in increasing the density of cathode spots and, correspondingly, in increasing the effective volume occupied by the SIVD.

In accord with expression (1), the density of cathode spots in mixture SF_6–C_2H_6 can also be increased through stepping up the discharge burning voltage by adding small quantities of gases that are more electronegative than SF_6; for example, $CC1_4$ or C_2HC1_3. It is worthy of note that 2 Torr C_2HC1_3 addition to mixture SF_6–C_2H_6 does not lead to a noticeable decrease in stability of SIVD.

The problem of increasing the stability of SIVD in SF_6-based mixtures is adequately covered in works [5–10]; therefore, it is not especially touched on in this paper. We only report here on the basic results in this area. In paper [5], it was shown that the addition of hydrocarbons and deuterocarbons to SF_6 allows the specific energy depositions to be increased by a factor of $5 \div 6$ at a given discharge duration, for which reason employment of these hydrogen (deuterium) donors is preferable to H_2 and D_2 for being used in a nonchain HF(DF) laser. In addition, it has been shown in [8, 10] that stability of SSVD in mixture of SF_6 with hydrocarbons (deuterocarbons) does not practically depend on whether there are the sites of a local electric field enhancement at the discharge gap, which enables us to use in nonchain HF(DF) lasers as anode and cathode identical flat electrodes rounded off to small radii $r \ll d$ along their perimeters, i.e., to employ essentially compact electrodes. This makes it possible to substantially decrease the sizes of the discharge camera and, correspondingly, the discharge circuit inductance, which is of considerable importance in scaling the characteristics of nonchain HF(DF) lasers.

In conclusion, we highlight in this section that the detachment of electrons from negative ions taken into account by ourselves, when considering the mechanisms of electric current density restriction, may be thought of as one of the possible mechanisms leading to the development of instability in SF_6 and SF_6-based mixtures. However, such an analysis faces great difficulties owing to the severity of exactly accounting for the plasma composition within the channel growing from a cathode spot wherein the initial components of the working mixture are strongly dissociated owing to great current densities (up to 10^4 A/cm^2).

31.3 Nonchain HF(DF) Lasers Excited by an SIVD

31.3.1 The Operation Features of Pulse and Pulse-Periodic Nonchain HF(DF) Lasers with Small Apertures and Active Medium Volumes

Because of being easy to obtain, SIVD opens great potentialities for creation of extremely simple and compact nonchain HF(DF) lasers. However, the setups with the working medium volumes of less than 2 L at a relatively small cathode surface exhibit, in the absence of preionization, an appreciable scatter in the pulse breakdown voltage amplitudes that is especially undesirable under the pulse-periodic working mode. Therefore, in the given case, it is expedient to initiate SIVD, for example, by a low-current spark located either outside the discharge gap or in a hole on the cathode [5]. In principle, this regime is similar to a "photo triggered discharge" mode [15, 17, 28]. However in classical "photo triggered discharge" schemes applied to excimer lasers, a powerful illumination of the gap is necessary since this illumination serves the dual function of initiating breakdown and producing the necessary primary electron number density in a gas medium. In mixtures of SF_6 with hydrocarbons, a powerful illumination is not needed because the distinguishing feature of an SIVD is that a discharge, after a local gap breakdown wherever this may occur, spreads, as shown previously, over the whole surface of the cathode [5]. This means that a local illumination of the cathode by a low-current spark is quite sufficient for stabilizing electric and output characteristics of HF(DF) lasers. With reference to an unusual operating mode we suggest, some special features of the HF(DF) laser with an aperture of 5 cm will be considered in this section in detail.

31.3.1.1 Experimental Setup

In the laser, flat A1 electrodes with dimensions of 20 × 80 cm (anode) and 7 × 60 cm (cathode), rounded off to a radius of l cm in their perimeters and separated by a distance of d = 5 cm were used. The cathode surface was subjected to sandblasting. To obtain an SIVD, the Fitch scheme, standard for small aperture lasers, was used (see Fig. 31.12) with capacitors C_1 and C_2 of 0.1 μF and a maximum discharge voltage of 50 kV. The discharge gap was laterally illuminated with a spark limited by two resistances of r = 5 kOhm connected directly to the electrodes. The spark was located symmetrically relative to the electrodes at a distance of ~5 cm from the cathode edge. Ten blowers ensured operation of the laser in a pulse-periodic regime with a frequency of up to 10 Hz. The laser worked with mixtures SF_6–C_2H_6 and C_6D_{12} at pressures of 45 ÷ 70 Torr. In the majority of the experiments, a resonator formed by A1 mirror with a radius of curvature of 20 m and a plane-parallel plate of BaF_2 was employed. The laser radiation divergence was measured using unstable telescopic resonator with the amplification

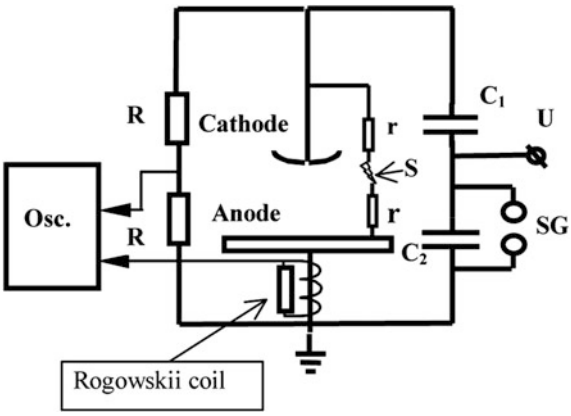

Fig. 31.12 Electrical scheme of the nonchain HF(DF) laser

coefficient M = 3. To rule out the influence of the near-electrode regions on the results, the laser aperture in these measurements was limited to a diameter of 4 cm. The radiation divergence measurements were carried out by the focal spot method using a mirror wedge [29].

It is important to note that in contrast to a typical "photo triggered discharge" system, breakdown initiation in our case occurs spontaneously, as soon as the voltage across the gap exceeds a certain critical magnitude. With separation of the illumination scheme from the laser-pumping scheme, it was possible to initiate breakdown at an arbitrary instant of time.

31.3.1.2 Experimental Results

Typical oscillograms of pulses of the laser generation, current and voltage across the gap are presented in Fig. 31.13 (curves 1, 2 and 3, respectively). As can be seen from this figure, the discharge gap breakdown occurs due to photo initiation at the

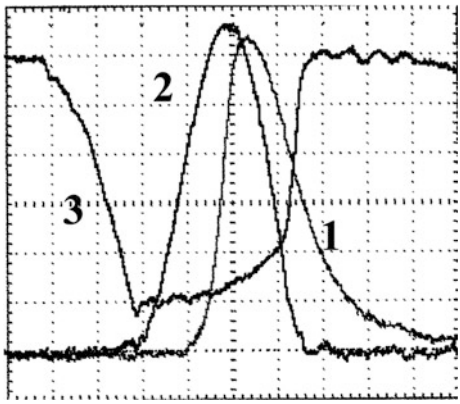

Fig. 31.13 Typical oscillograms of laser pulse (*1*); current pulse (*2*); and voltage across the discharge gap (*3*) for mixture: 66 Torr SF_6 + 6 Torr C_2H_6. Scales current: 3 kA/div.; voltage: 10 kV/div.; time: l00 ns/div

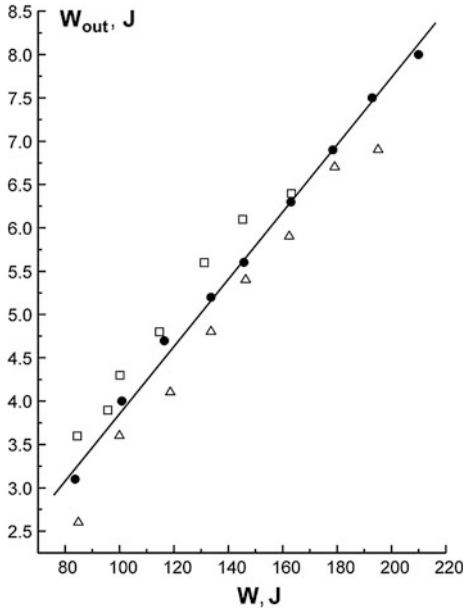

Fig. 31.14 Dependences of the output laser energy (W_{out}) (generation on HF) on energy W deposited in the discharge plasma obtained for mixtures C_2H_6:SF_6 with different ratios of the components: ϒ − 1:22; ● −1.5:22; Δ − 2:22

leading edge of the voltage pulse, with a laser pulse maximum slightly delaying relative to the current maximum. Without the initiating spark, the scatter in the gap breakdown voltages amplitudes was as high as 20%, which, correspondingly, caused the spread of 15% in the magnitudes of the output laser radiation energies.

Figure 31.14 shows the dependence of the output laser energy ($\boldsymbol{W}_{out}$) (generation on HF) on the energy, $\boldsymbol{W}$, deposited in the discharge plasma for mixtures with different content of C_2H_6. It can be seen that in the mixtures with the component's ratios C_2H_6:SF_6 = 1.5:22 and 2:22, the output energy rises with increasing the deposited energy practically linearly. In the experiment conditions, mixture C_2H_6: SF_6 = 1.5:22 turned out optimal, on which a maximum value of the generation energy $\boldsymbol{W}_{out}$ = 8 J at electrical efficiency of 3.2% was obtained. The discharge volume assessed by the laser radiation print on thermal paper was −1.51 which corresponds a specific energy deposition in the plasma ~220 J/L (Fig. 31.14). Decrease of $\boldsymbol{W}_{out}$ with increasing $\boldsymbol{W}$ in mixtures with a lower content of C_2H_6 (mixture C_2H_6:SF_6 = 1:22) arises from the discharge instability at high energy depositions. Indeed, in this mixture, when operating at energy depositions of ~200 J/l, there could bright plasma stems growing from the cathode edge, which sometimes bridged the gap, could be visually observd. For the mixtures with a higher C_2H_6 content, there was no decrease in laser efficiency with increasing $\boldsymbol{W}$ until the discharge remained stable and the lengths of plasma channels was not in excess of d/2. This causes us to anticipate that rise of the electric efficiency with increasing interelectrode distance takes place since SIVD becomes more uniform due to a greater overlapping of diffuse channels [5, 7].

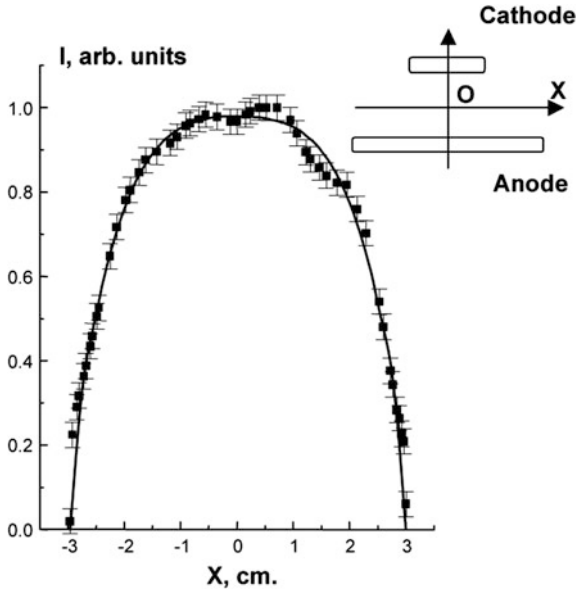

Fig. 31.15 SIVD plasma intensity distribution over the optic axis-contained plane placed in parallel to the electrode surfaces

In the investigated electrode system, a great enhancement of the electric field at the gap edge takes place. In such gases as CO_2, air, N_2, this results in the discharge concentrating at the gap edge [4]. In mixtures of SF_6 with hydrocarbons, this is not so because of the distinguishing feature of SIVD—even though SIVD originates at the edge, it then displaces into the interior of the gap because of the existence of the mechanisms that limit the current density in a diffuse channel. In Fig. 31.15, the SIVD plasma intensity distribution over the optic axis-contained plane placed in parallel to the electrode surfaces is given. It can be seen from this figure that the maximum of the SIVD luminosity intensity attains at the axis. In a similar manner, also distributed over the laser aperture is the radiation energy, i.e., the edge electric field enhancement does not appreciably influence the distribution of the output laser radiation.

By these means, a local illumination of the cathode is quite sufficient for obtaining a uniform SSVD in mixtures of SF_6 with hydrocarbons and the presence of the regions displaying high edge nonuniformity does not worsen stability of SIVD and only slightly influences the distribution of the laser radiation energy over the aperture. Therefore, it is possible to use plane electrodes rounded off to small radii along their perimeters. Under investigation of a pulse-periodic operating mode, we found no appreciable features that have not been previously mentioned by other authors (see, e.g., [28, 30]).

The radiation divergence was measured in the special case that the laser operated on DF molecules. The results of measuring the divergence are represented in Fig. 31.16 where the angular radiation energy distribution is shown. As can be seen from this figure, the radiation divergence at a level of 0.5 is $\theta_{0.5} = 2.9.10^{-4}$ rad,

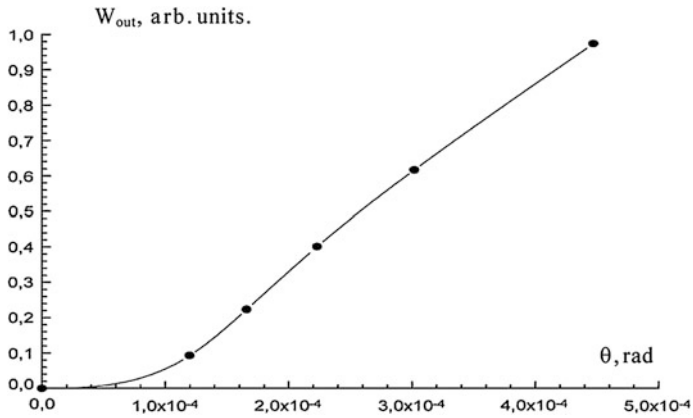

Fig. 31.16 Angular distribution of the radiation energy in the far zone

which corresponds to 4 diffraction limits. Further improvement of the given parameter can be expected in increasing the laser aperture because lengthening the interelectrode distance should improve the discharge uniformity owing to a greater overlapping of diffuse channels.

31.3.2 Wide Aperture Nonchain HF(DF) Lasers Excited by SIVD

On increase of the cathode surface and active medium volume, the necessity of initiating gap breakdown disappears. Delay in breakdown becomes, in this case, so negligible that it cannot be inferred from the oscillogram; the breakdown, in fact, occurs at the voltage leading edge. Therefore, when dealing with the setups of great volumes of active medium, there is no necessity for additional units for initiating the gap breakdown since a sufficiently uniform discharge forms spontaneously.

31.4 Conclusions

We considered the problems of scaling of nonchain HF(DF) lasers in our previous works [6, 8, 10] in detail. Therefore, in this chapter which is, to a large extent, a survey, we simply touch on the necessary conditions for obtaining an SIVD in large volumes:

(1) a cathode should posses a small-scale ($\sim$50 μm) surface roughness;
(2) to match a circuit wave impedance to the discharge plasma resistance at a given interelectrode distance, a mixture pressure should be chosen in such a

way that the discharge burning voltage determined by the conditions of the gap breakdown in SF_6 [19] be two times less than the voltage fed to the gap;

(3) increasing electric energy through increase in the generator's capacitance at a given maximum generator voltage should followed by growth of the discharge volume V as $V \sim C^{3/2}$ where C is the generator's capacitance [8, 10]. On fulfillment of all these conditions, one should also try to maximally decrease the period of time during which the energy is deposited in the discharge plasma.

Maximum generation energy of nonchain HF/DF laser obtained in our experiments was 407 J on HF and 325 J on DF at electric efficiencies of 4.3 and 3.4%, respectively. The active medium volume was ~60 L at an aperture of 27 cm.

Of natural interest is the problem of increasing laser radiation energy. Figure 31.17 depicts the dependence of the output HF laser energy, W_{out}, on the energy, W_p, stored in the capacitors of a high-voltage generator. In this figure, the data we obtained during the most recent 5 years at the setups with different volumes of active medium are plotted. It can be seen that all the points are in good agreement to the directly proportional relationship at electric efficiency of ≈4%. This allows one to predict the possibility of further increase in the output energy of nonchain HF/DF lasers through creating the setups operating at energy depositions of ~1 kJ and above using the methods we developed.

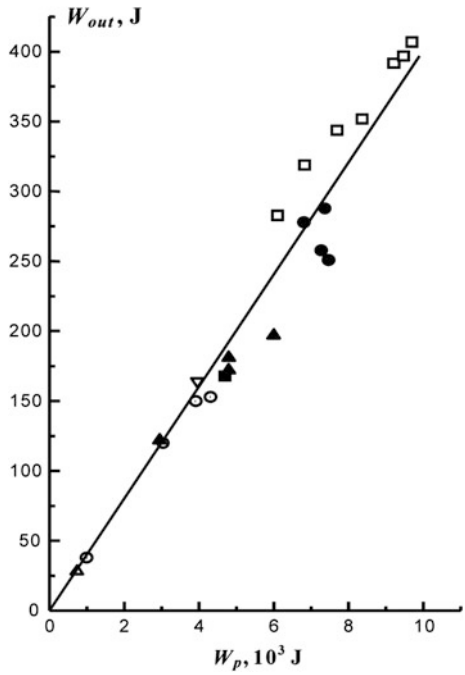

Fig. 31.17 Dependence of the output HF laser energy W_{out} on the energy stored in the generator's capacitors

References

1. V.K. Ablekov, Y.N. Denisov, V.V. Proshkin, *Chemical Lasers* (Atomizdat, Moscow, 1980)
2. V.V Apollonov et al., Effective non-chain HF(DF) lasers with high output characteristics. Pis'ma v Zhumal Tekhnicheskoi Fiziki **22**(22), 60 (1996)
3. V.V. Apollonov et al., Feasibility of increasing the output energy of a non-chain HF(DF) laser. Quantum Electron. **24**, 213 (1997)
4. V.V. Apollonov et al., Non-chain electric-discharge HF (DF) laser with a high radiation energy. Quantum Electron. **25**, 123 (1998)
5. V.V. Apollonov et al., High-power nonchain FIF (DF) lasers initiated by selfsustained volume discharge, in *Proceedings of SPIE, XII International Symposium on Gas Flow and Chemical Lasers and High-Power Laser Conference*, 31 August–5 September 1998, St. Petersburg, Russia, vol. 3574, p. 374
6. V.V. Apollonov et al., High-power SSD-based pulse nonchain HF(DF) laser. Proceedings of SPIE, High-Power Laser Ablation **3343**, 783 (1998)
7. V.V. Apollonov, A.A. Belevtsev et al., SIVD in non-chain HF lasers based on SF_6-hydrocarbon mixtures. Quantum Electron. **30**, 207–214 (2000)
8. V.V. Apollonov et al., SSVD for initiated wide aperture nonchain HF(DF) lasers. Izvestiy RAN Ser. Fizicheskai, [in Russian], **64**(7), 1439 (2000)
9. V.V. Apollonov et al, SIVD in mixtures of SF_6 with hydrocarbons to excite nonchain HF lasers, in *Proceedings of SPIE, International Conference on Atomic and Molecular Pulsed Lasers III*, vol. 4071 (2000), p. 31
10. V.V. Apollonov et al, Scaling up of nonchain HF(DF) laser initiated by SSVD, in *Proceedings of SPIE, High-Power Lasers in Energy Engineering*, vol. 3886, (2000), p 370
11. V.V. Apollonov et al, Generation and Properties of SSVD in Strongly Electronegative Gases, in *Proceedings of XXV International Conference on Phenomena in Ionized Gases, ICPIG-2001*, vol 1 (Nagoya, Japan, 17–22 July, 2001) p. 255
12. V.V. Apollonov et al, Volume discharge in SF_6 mixtures of SF_6 with gydrocarbons, in *Proceedings of XIII International Conference on Gas Discharge and their Applications, GD-2000*, vol 1 (Glagow, UK, 3–5 September, 2000), p. 409
13. E.W. McDaniel, L. Nighan William, Gas Lasers, in *Applied Atomic Collision Physics*, vol. 3 (Academic press, New York, 1982)
14. YuD Korolev, G.A. Mesyats, *Physics of Pulse Discharge in Gases* (Nauka, Moscow, 1991). (in Russian)
15. H. Brunet, M. Mabru, J. Rocca Serra, C. Vannier, Pulsed HF chemical laser using a VUV phototriggered discharge, in *VIII International Symposium on Gas Flow and Chemical Lasers, SPIE*, vol. 1397 (1990), pp 273–276
16. H. Pummer, W. Breitfeld, H. Welder, G. Klement, K.L. Kompa, Parameter study of 10-J hydrogen fluoride laser. Appl. Phys. Lett. **22**(7), 319 (1973)
17. V. Puech, P. Prigent, H. Brunet, High-efficiency, high-energy performance of a pulsed HF laser pumped by phototriggered discharge. Appl. Phys. B. **55**, 183 (1992)
18. V.A. Burtsev, V.M. Vodovozov, P.N. Dashuk, S.L. Kulakov, V.F. Prokopenko, V.M. Fomin, L.L. Chelnokov, On simultaneous formation of volume and sliding discharges of millimicrosecond duration for gas lasers pumping, in *Proceedings of VII All-Union Conference on Physics Low-temperature Plasma*. Tartu (1984), [in Russian]
19. V.V. Apollonov et al., Discharge characteristics of a nonchain HF (DF) laser. Quantum Electron. **30**(6), 483 (2000)
20. D.I. Slovetskii, A.A. Deryugin, Electron energy distribution functions and interaction of electrons with polyatomic molecules of fluorine-containing gases, Plasma Chemistry/Ed. B.M. Smirnov, Energoizdat (Moscow), vol. 13 (1987), p. 240 (In Russian)
21. N. Nakano, N. Shimura, Z.Lj. Petrovic, T. Makabe, Simulation of RF glow discharges in SF_6 by the relaxation continuum model: Physical structure and function of the nairow-gap reactive-ion etcher. Phys. Rev.E, **49**, 4455 (1994)

22. H. Hilmert, W.F. Schmidt, Electron detachment from negative ions of sulfur hexafluoride-swarm experiments. J. Phys. D Appl. Phys. **24**, 915 (1991)
23. A.A. Belevtsev, L.M. Biberman, About some nonlinear effect in development of electron avalanches in electronegative gases. Izvestiya Akademii Nauk SSSR, Energetika i Transport **3**, 74–78 (1976) (In Russian)
24. D. Hayashi, M. Nakamoto, N. Takada, K. Sasaki, K. Kodata, Role of reaction products in F″ production in low-pressure, high-density CF_4 plasmas. Jpn. J. Appl. Phys. **38**, 6084 (1999)
25. V.V. Apollonov et al., lon-Ion Recombination in SF_6 and SF_6–C_2H_6 Mixtures at High Values of E/N. Quantum Electron. **31**, 629 (2001)
26. V.V. Apollonov et al, lon-Ion Recombination in SF_6 and SF_6–C_2H_6 Mixtures at High Values of E/N, in *Proceedings of XXV International Conference on Phenomena in Ionized Gases, ICPIG-2001*, vol 3 (Nagoya, Japan, 17–22 July, 2001), p. 277
27. L. Richeboeuf, S. Pasquiers, M. Legentil, V. Puech, The influence of H_2 and C_2H_6 molecules on discharge equilibrium and F-atom production in a phototriggered HF lasers using SF_6. J. Phys. D Appl. Phys. **31**, 373 (1998)
28. B. Lacour, High average power HF/DF lasers. Proceedings of SPIE, III International Conference on Atomic and Molecular Pulsed Lasers **4071**, p9 (1999)
29. Yu.M. Abrosimov, Yu.A. Drozhbin, Yu.B. Morozov, V.E. Prokopenko, A.K. Semenov, V.B. Semenov, L.N. Favorov, Measuring of a divergence of a pulsing laser radiation by a method of a focal spot with application of a reflecting wedge. Izmeritel'nai texnika, [in Russian], No. 1 (1982), p. 30
30. S.D. Velikanov, A.F. Zapol'skii, Yu.N. Frolov, Physical aspects of the operation of HF and DF lasers with a closed active-medium replacement cycle. Quantum Electron. **24**(1), 11 (1997)

Chapter 32
UV-Preionization in Nonchain HF Lasers with a SSVD to Initiate Chemical Reaction

Abstract In this chapter, we investigate the problem of UV illumination in nonchain electric discharge HF lasers. For this purpose, we studied the influence of UV illumination on stability and uniformity of SSVD in working mixtures of HF lasers for the values of the discharge current duration and energy deposition varying over a wide range.

32.1 Introduction

The fundamental challenge in the creation of high power nonchain HF(DF) lasers with a nSSVD initiation of chemical reactions, as well as of most other gas lasers (e.g., CO_2, N_2O lasers, excimer lasers), is obtaining an SSVD in large volumes of working gases. Currently, the solution of this problem implies (i) preliminary gas ionization (by UV radiation, soft X-rays or e-beam) to ensure volume ionization in terms of overlapping avalanche heads and (ii) electric field uniformity throughout the discharge gap by specially profiling electrode surfaces (Rogowskii, Bruce, and Chang profiles, etc.) [1]. Preionization determines both SSVD stability and the laser radiation energy and efficiency.

Meanwhile, analysis of publications dealing with nonchain electric discharge HF (DF) lasers has brought to light a fairly strange fact—although experimental conditions greatly differed from paper to paper—for instance, in some setups, a powerful X-ray preionization [2] was applied, whereas in the others preionization was extremely weak or totally absent [3]—the output energy, efficiency and other laser parameters turned out to be close. Moreover, the assessments of initial electron number densities characteristic of these devices show they are quite insufficient for the discharge to develop in a volume form that would follow from traditional notions of the mechanisms of SSVD formation. The studies performed in our former works [4–6] have allowed us to establish that in working mixtures of nonchain HF(DF) lasers (mixtures of SF_6 with hydrogen and deuterium donors) an

© Springer International Publishing Switzerland 2016

V.V. Apollonov, *High-Energy Molecular Lasers*,
Springer Series in Optical Sciences 201, DOI 10.1007/978-3-319-33359-5_32

SSVD fundamentally differs from those in the less electronegative gases—it is capable of developing in the form of an SSVD even in the absence of gas preionization. The experiments involved laser setups with a volume of active medium: V = 1.5 ÷ 60 L, the cathode surface S = 240 ÷ 2000 cm^2; and a partial pressure of SF_6 in the mixture $P_{SF_6} < 120$ Torr using sources of soft X-ray and UV radiation and a barrier discharge plasma. A necessary and sufficient condition for running SSVD without preionization both in uniform electric fields and in gaps with high edge field enhancement turned out to be the presence of small-scale (~ 50 μm) inhomogeneities at the cathode surface. In this case, preionization did not considerably influence SSVD stability and uniformity, nor output laser characteristics. Currently, however, there are still publications whose authors continue to advocate that, for example, UV preionization considerably improves HF laser characteristics [7].

In this regard, we have decided to return to the problem of UV illumination in nonchain electric discharge HF lasers. For this purpose, we have performed special investigations into the influence of UV illumination on stability and uniformity of SSVD in working mixtures of HF laser for the values of the discharge current duration and energy deposition varying over a wide range.

32.2 Experimental Setup

In Fig. 32.1 the setup for SSVD investigations is schematically represented. As a working medium mixture SF_6:C_2H_6 = 10:1 at a total pressure P = 33 Torr was used. The discharge gap was comprised of a disk Ø6 cm cathode rounded off along its perimeter with a radius of 1 cm and subjected to sandblasting and a mesh anode with 4 parallel spark gaps placed behind it. The interelectrode distance was 4 cm. The capacitance magnitudes were C_1 = 4 ÷ 15 nF and C_2 = 680 pF (capacitor C_2 comprised 4 capacitors of 170 pF, each discharging through its own spark gap).

In experiments with initiation of SSVD without UV illumination, capacitor C_2 was withdrawn from the scheme and high-voltage leads of spark gaps were grounded. During this study, monitoring of the SSVD current and voltage was performed, and the discharge uniformity (the number of cathode spots and the attached diffuse channels) was assessed by the discharge gap photographs obtained with digital camera Olympus C3030. An SSVD stability in operating conditions with and without UV illumination was numerically estimated by the limiting energy deposition in the discharge plasma $C_1U^2/2$ yet allowing SSVD to burn without transforming into spark, as a function of parameter $T = \pi(LC_1)^{1/2}$, which was a measure of the discharge current duration (U, the voltage across C_1 and L, the discharge inductance).

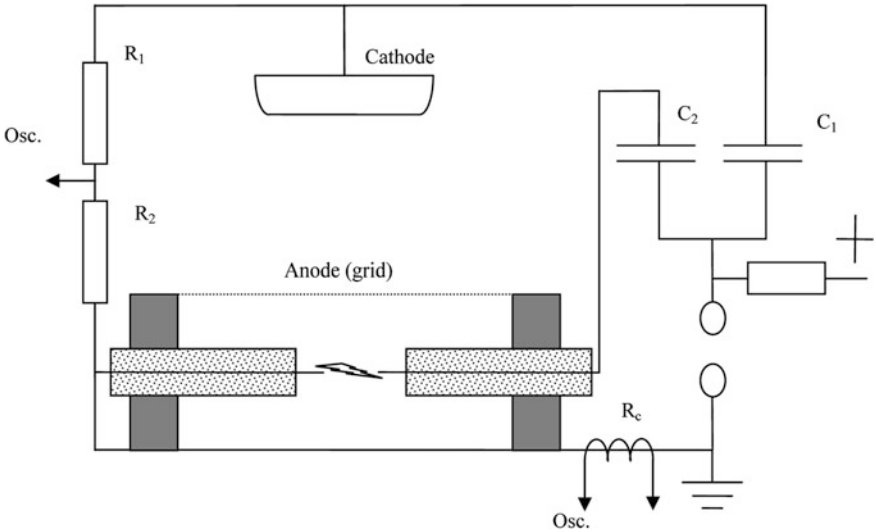

Fig. 32.1 Schematic diagram of setup for investigation of SSVD

32.3 Experimental Results

In Fig. 32.2 ,the dependences of the limiting value of parameter $C_1U^2/2$ on parameter T obtained with and without UV illumination are given. As seen from this figure, illumination has only a weak influence on the limiting energy deposited

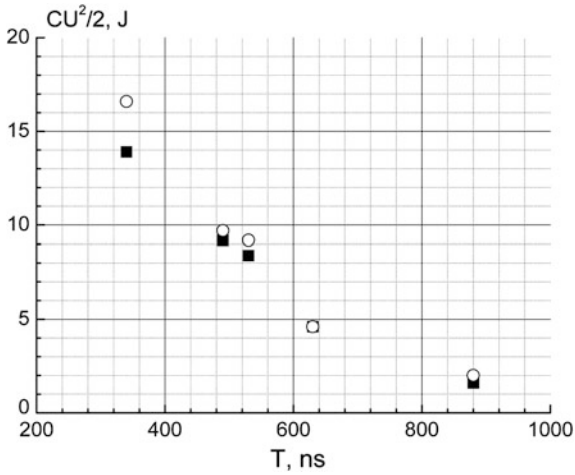

Fig. 32.2 Dependence of the limiting value of energy deposition $CU^2/2$ on parameter $T = \pi\sqrt{LC_1}$: ■—UV illumination; O—without illumination

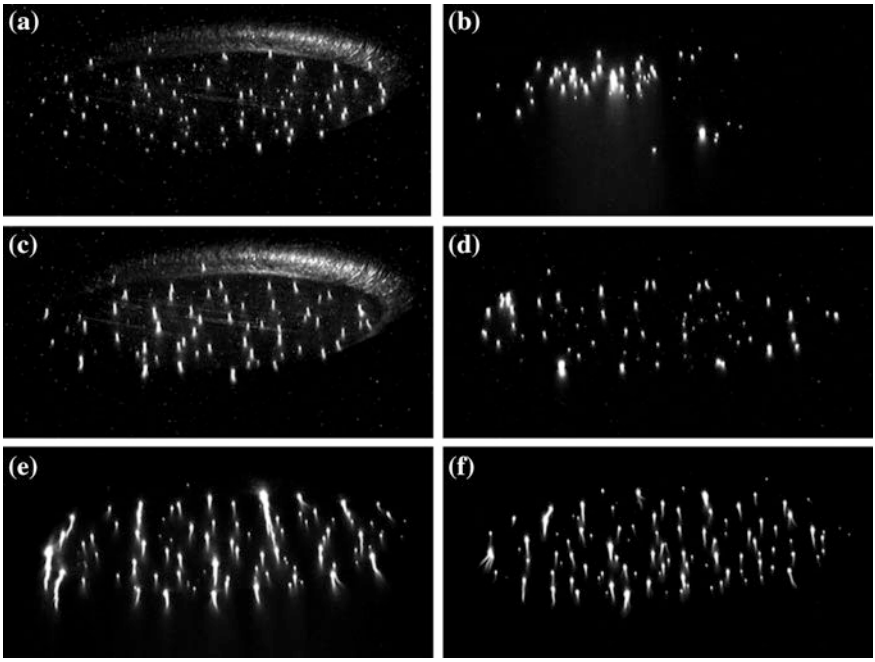

Fig. 32.3 Integrated photographs of discharge with UV illumination (**a**, **c**, **e**) and without UV illumination (**b**, **d**, **f**): **a**, **b**: energy deposition W_{in} = 1.4 J, T = 130 ns; **c**, **d**: W_{in} = 1.4 J, T = 270 ns; **e**, **f**: W_{in} = 10 J, T = 260 ns

in the plasma throughout the investigated range of the magnitudes of SSVD current duration. In Fig. 32.3 depicts photographs of the near-cathode region made for different SSVD current durations and energy depositions in the plasma involving UV illumination and in its absence. The photographs were taken such that the less bright diffuse channels attached to cathode spots were not seen. The surface density of cathode spots characterizes the degree of overlapping the channels attached to these spots and, ultimately, SSVD uniformity. As can be seen in Fig. 32.3, at a sufficient discharge current duration, T = 260–270 ns, cathode spots density and uniformity of their spreading over the cathode surface do not practically depend on the presence of UV illumination. Both in the presence of illumination and in its absence, the total number of spots and their density increases with increasing the energy deposited in the plasma, which is in agreement with our previous results [5, 6]. In the case of short discharge, T = 130 ns, (Fig. 32.3a, b) in the absence of illumination, spots cover only a part of the overall surface. This, too, is in accordance with our previous result [5] and is explained by the fact the discharge, after initial gap breakdown in the region of edge field enhancement, extends normally to the electric field at a finite rate.

In Fig. 32.4 are shown the dependences of a total number of spots on the cathode, N, on the energy deposited in the plasma at SSVD current duration

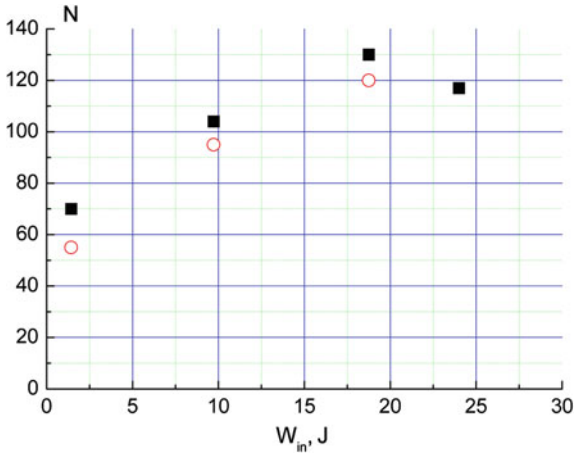

Fig. 32.4 Dependence of number of cathode spots N on the energy deposition in the discharge plasma W_{in}: ■: UV illumination is present; O: UV illumination is absent

T = 206 ÷ 350 ns obtained with and without UV illumination. Figure 32.4 demonstrates growth of spot number with increasing energy deposition, the value of N being even greater in the absence of illumination than in its presence. Decrease in the magnitudes of N at high energies is caused by the beginning of transforming SSVD into spark.

Figure 32.5 demonstrates the dependence of a total number of cathode spots N (without illumination) on the discharge current duration, T, at a fixed energy deposition. It can be seen that a magnitude of N depends only slightly on T. A lower N-value at great T, as well as at great energy depositions, is caused by transforming SSVD into spark.

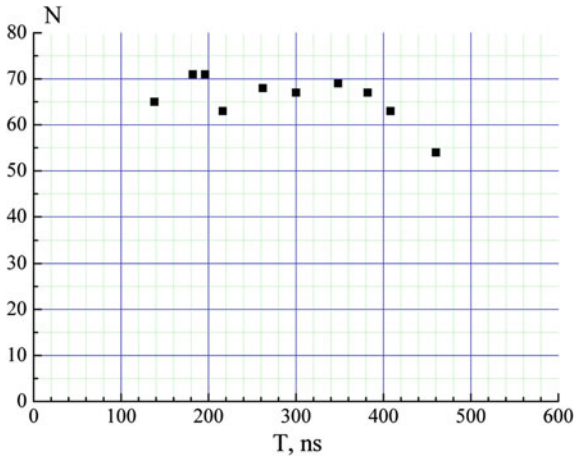

Fig. 32.5 Dependence of number of cathode spots N on SSVD current duration T at a fixed energy deposited in the discharge plasma (without UV illumination)

32.4 Discussion

It follows from the material presented that UV illumination does not considerably influence SSVD stability and uniformity in working mixtures of electric discharge nonchain HF lasers. What then is the reason for the dependence of the output energy of HF laser on UV illumination observed in some investigations?

It should be noted from the outset that in working mixtures of wide-aperture nonchain HF(DF) lasers, UV illumination in principle is not capable of providing volume gas ionization because this radiation is strongly absorbed by SF_6, i.e., in this case term "preionization" in the ordinary sense may not be applied. Using data on SF_6 photoabsorption cross section [8], it can easily be shown that at partial pressures typical of HF lasers, such as $P_{SF_6} \gg 60$ Torr, the mean free path of photons of energy, E = 10 eV (close to the ionization potentials of "heavy" hydrocarbons being hydrogen donors), is only $l_{Ph} = 5$ mm. This is evidently insufficient, for it would be possible to say of medium "preionization" by UV radiation even in small-size HF lasers.

What can then give UV illumination in HF(DF) lasers? At quantum energies E < 5 eV absorption of UV radiation in SF_6 is negligible [8], and UV illumination of the discharge gap by even low-current, ~1 A, spark allows, owing to the photoelectric effect at cathode, stabilization of electric discharge characteristics of the discharge gap. As an illustration, Fig. 6 shows the voltage and current oscillograms recorded in the absence of UV illumination.

In Fig. 32.6a shows the discharge gap voltage oscillograms for two different impulses for an SSVD in the setup shown in Fig. 32.1. It can be seen that even at more than twice the SSVD quasi-stationary phase voltage across the gap, the difference between breakdown delays for two impulses in the absence of UV

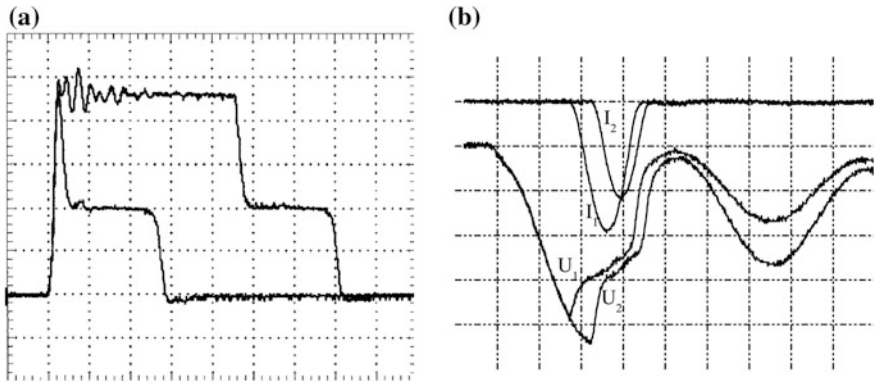

Fig. 32.6 SSVD voltage oscillograms (**a**) and SSVD voltage U_1, U_2 and current I_1, I_2 oscillograms (**b**) for two discharge impulses without UV illumination (time scale 100 ns/div): **a** capacitor was discharged through the gap, P = 33 Torr; **b** Fitch generator was discharged through the gap, P = 46 Torr

illumination reaches ~450 ns. In Fig. 32.6b shows voltage U_1, U_2 and current I_1, I_2 oscillograms of SSVD recorded in the absence of UV illumination using the same setup and the Fitch generator scheme (two discharge impulses) for triggering an SSVD. It is seen that increasing the gap voltage risetime in the absence of UV illumination results in not only in delay of spread but also in breakdown voltage amplitude scatter. This in turn, contrary to electric schemes using discharge of a capacitor or Arkadiev-Marks generator through the gap, is followed by great scatter in SSVD current amplitudes and, correspondingly, in energy depositions in the plasma from impulse to impulse. A similar situation is observed for discharge gaps with the cathode surface area S < 300 cm^2 and interelectrode distance d < 5 cm, especially in lasers with electrode systems with special profiles for ensuring electric field uniformity over the gap and polished surfaces (recall that in the experiments described here the cathode surface was sandblasted to produce small-scale, ~50 μm, inhomogeneities). Naturally, instability of SSVD current and voltage results in HF laser output energy to be not reproducible from impulse to impulse. In order to stabilize delay and breakdown voltage amplitudes in such systems, it is usually sufficient to illuminate a cathode with spark [9], which may even be located outside the laser discharge gap (illumination through a quartz window). When increasing interelectrode distance and cathode surface area and/or using electrodes with high electric field enhancement at their edges, the problem of stabilizing electric breakdown no longer arises [6].

The studies performed give firm evidence that the role of UV illumination in nonchain HF(DF) lasers can be reduced to stabilization of the delay and amplitudes of the discharge gap breakdown voltages owing to a photoelectric effect at the cathode. Volume photo ionization by UV radiation of working medium of nonchain lasers with apertures d > 5 mm cannot in principle be effective because of strong absorption of UV radiation in SF_6 (another reason hindering "preionization"; great losses of photoelectrons owing to attachment is not discussed here).

It should also be noted that, as follows from Fig. 32.3b, at short discharge currents (T < 150 ns) typical of setups with small volumes of active medium (~100–200 cm^3) [7] in the absence of UV illumination, apart from the breakdown instability, a nonuniform discharge current distribution over the cathode is possible because of a finite rate of extending discharge perpendicularly to the electric field after a local gap breakdown [5]. This naturally results in decreasing output HF laser characteristics, and equalization of the current density distribution in the presence of UV illumination (in this case it is expedient to arrange UV radiation sources along the cathode), followed by growth of output energy, perceived as the result of "preionization".

32.5 Conclusion

The results of this work confirm once again that the role of UV illumination in HF lasers with the cathode surface area not exceeding 300 cm^2, as well as in lasers with current impulse duration T < 150 ns, can be reduced to, correspondingly, stabilization of the delay and electric breakdown voltage amplitude and to equalization of the discharge current density over the cathode surface because of the photoelectric effect at the cathode. In lasers with larger apertures and active medium volumes there is no need for illumination.

References

1. E.W. McDaniel, W.L. Nighan, *Applied atomic collision physics*, in *Gas Lasers,* vol. 3 (Academic Press, New York, 1982)
2. V.A. Burtsev, V.M. Vodovozov, P.N. Dashuk, S.L. Kulakov, V.F. Prokopenko, L.L. Chelnokov, Simultaneous formation of volume and sliding nanosecond discharges, as applied to pumping gas lasers, *Abs. VII All—Union Conference on Physics of Low-temperature Plasma,* pp. 414–416, Tarty, 1984, (in Russian)
3. H. Pummer, W. Breitfeld, H. Welder, G. Klement, K.L. Kompa, Parameter study of 10-J hydrogen fluoride laser. Appl. Phys. Lett. **22**(7) (1973)
4. V.V. Apollonov et al., High-power nonchain HF (DF) lasers initiated by SSVD. Proc. SPIE **3574**, 374 (1998)
5. V.V. Apollonov, et al., SIVD in mixtures of SF_6 with hydrocarbons to excite nonchain HF lasers. in *Proceedings SPIE,* vol. 4071 (Tomsk, 2000), p. 31
6. V.V. Apollonov, et al., High-power pulse and pulse-periodic nonchain HF(DF) lasers. in *Proceedings of the SPIE,* vol. 4747 (Tomsk, 2001), p. 31–43
7. V.F. Tarasenko, V.M. Orlovskii, A.N. Panchenko, Energy parameters and stability of the discharge in a nonchain, SSVD pumped HF laser. Quantum Electron. **31**, 1035–1037 (2001)
8. A.S. Vinogradov, T.M. Zimkina, Photoarbsoption cross sections of hexafluoride sulfur in the region of soft and ultra-soft X ray radiation. Optika i spectr. **32**, 33–37 (1972)
9. V.V. Apollonov et al., Scaling up of nonchain HF(DF) laser initiated by SSVD. Proc. SPIE **3886**, 370 (2000)

Part III
Short Pulse Laser Systems

Regenerative amplification of a nanosecond pulse train in a large active volume of CO_2-based mixtures has been investigated both numerically and experimentally. The area in which regenerative amplification takes place was determined when varying the injected radiation parameters. The nanosecond pulse train utilization as an injected radiation instead of monopulse was shown to significantly broaden the injection time "window" and to enable variation of an individual pulse time structure in the output train. Recent advances in injection mode locking and high-power 10 μm pulse selection have been incorporated into a high-power CO_2 laser system built around a TEA CO_2 gain module. A pulse selected from a line-tuned [to $P(20)$] injection-mode-locked oscillator was amplified to produce a 20-J, 3-ns pulse with a main-pulse-to-prepulse contrast ratio of $>10^7$:1. The regenerative amplification enables the transformation of free running mode laser pulse into the train of nanosecond ones with varied duration of the individual pulse and time interval between the pulses. For this reason, we have used regenerative amplification for carrying out the experiments presented in this book. The numerical calculations made it possible to predict the influence of regenerative amplification scheme parameters upon the temporal structure of the nanosecond pulse train, and thus facilitate realization of the experimental set up.

Another short pulse laser system is also presented in the Chap. 3. Electric-discharge lasers based on transitions in the nitrogen molecule are promising sources of near-UV radiation. Such lasers are used widely in the microelectronics industry, medicine and laser chemistry, as pump sources of organic lasers, as well as in spectroscopy, laser diagnostics of plasmas, etc. The design of these lasers is relatively simple and the active medium is chemically inert. Moreover, in some applications the nitrogen laser wavelength is the most effective.

Chapter 33
Selection of High-Power Nanosecond Pulses from Large-Aperture CO_2 Oscillators

Abstract A high-contrast 6 J, 3 ns pulse has been obtained from an injection mode-locked TEA CO_2 oscillator using an extracavity SF_6-He saturable absorber to suppress the prepulse energy to <1 μJ and an intracavity semiconductor transmission switch to suppress postpulses. The techniques described in this chapter will allow the frequency and transverse-mode control of an oscillator to be maintained to much higher powers than are presently possible.

A simple reliable source of high-energy nanosecond pulses in near-diffraction-limited beams is useful for many experiments, including those related to quantum optics [1, 2], photochemistry, and laser fusion. The design of all nanosecond-pulse systems has been fundamentally the same [3–6]. A low-energy pulse is selected from a small oscillator and subsequently amplified to high powers. For CO_2 lasers, this has implied a large small-signal gain in the amplifier chain. The high small-signal gain adds considerable complexity to the system, for not only are many amplifier modules required but amplified spontaneous emission must be controlled. This is particularly difficult when a spherical or near-normal incidence target is placed at the output of the laser. Broadband saturable absorbers offer a partial solution to this problem [7, 8].

A different approach to the design of high-power CO_2 lasers has been proposed [9]. It is now possible to scale the size of mode-locked oscillators. [9–11] With suitable pulse selection, their integration into large laser systems should be possible. Large oscillators permit the use of amplifier gains that can be more easily controlled with standard isolation techniques while at the same time maintaining the transverse mode [12] and frequency control [13] of an oscillator to high-power levels. For this reason, it is important to explore techniques for obtaining single pulses from high-power mode-locked oscillators [9, 14].

This chapter describes a nanosecond-pulse selection technique that is both simple and scalable. It involves the independent suppression of all pulses prior to and following the largest pulse in the mode-locked train. Because the requirements are so much more stringent for the suppression of prepulses, this will be emphasized. However, we also report on the first application of a semiconductor

© Springer International Publishing Switzerland 2016

V.V. Apollonov, *High-Energy Molecular Lasers*,
Springer Series in Optical Sciences 201, DOI 10.1007/978-3-319-33359-5_33

transmission switch [14–16] as an intracavity, Q, switch for the suppression of postpulses.

High-power injection mode-locked CO_2 oscillators have been extensively developed. By appropriately matching the resonator length and therefore the resonator round-trip time to the rise time of the gain, it is possible to construct an oscillator with the peak pulse energy as high as that obtained from a saturated amplifier [11]. However, it has not been recognized that with injection mode locking it is possible to accurately control the prepulse energy and the main-pulse-to-prepulse contrast ratio. By controlling the time of injection, contrasts as high as 30:1 can be obtained reliably. Such control allows the use of saturable absorbers for the suppression of prepulses in a mode-locked train.

The experiment (Fig. 33.1) was carried out on a UV preionized TEA CO_2 discharge module that was situated inside a positive branch confocal unstable resonator consisting of a 1.9 cm diameter R = 23 m convex mirror and a 15 cm diameter R = 70 m concave mirror. The 1 m long gain medium had a cross section of 7.5 × 7.5 cm^2, a peak small-signal gain of 5% cm, and a gain rise time of ~1 μs [17]. The laser was mode locked by injecting a 4 ns pulse of P (20) 10.6 μm radiation through a small hole in the concave mirror. The time of injection was measured relative to the optical signal obtained from the output spark gap of the oscillator. The jitter of this timing system was ≤ 10 ns.

A typical mode-locked train (Fig. 33.3a) had an energy of approximately 50 J of which ~15 J was in a 3.7 ns duration peak pulse. By varying the time of injection, the main-pulse-to-prepulse contrast could be changed from 40:1 to 1:1 without significantly altering the energy of the main pulse.

As illustrated in Fig. 33.1, the laser output was monitored before and after passage through a 2.5 cm thick saturable absorber cell with calibrated photon drag detectors. The transmitted beam was then focused through a pinhole for either prepulse monitoring or to confirm that there was no deterioration of the focal spot distribution as a result of the saturable absorber.

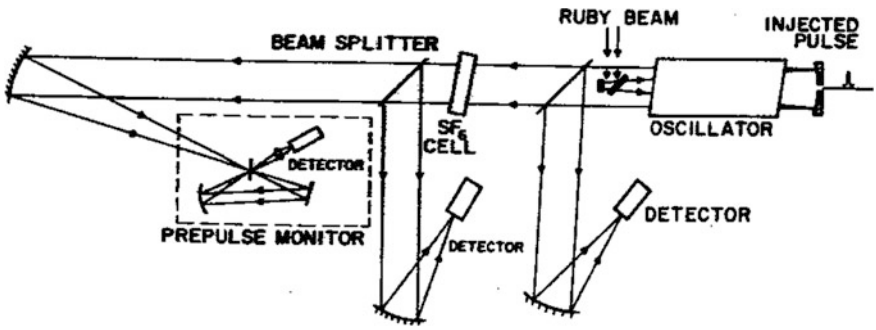

Fig. 33.1 Experimental configuration used to investigate the high-contrast selection of the peak pulse from a mode-locked train

The suppression of prepulses with SF_6, while still maintaining high transmission on the main pulse, has been demonstrated previously [18] for main-pulse-to-prepulse ratios of 500:1 and is widely used on high-power nanosecond pulse lasers. For ratios between 10:1 and 40:1, which are typical of the laser described above, a detailed knowledge of the SF_6 transmission curves is important. Therefore, the *P* (20) 10.6 μm ns-pulse transmission characteristics of SF_6 were measured over a wide range of pressures and with a number of different buffer gases [19]. The pulse selection experiment was performed with 15 Torr of SF_6 buffered to 1 atm with helium. The addition of a buffer gas increases the absorption at low energy densities and produces a region where a large change in transmission is observed for a relatively small change in pulse energy The transmission curves for 15 Torr of pure SF_6 with and without a helium buffer gas are shown in Fig. 33.2 (See [20]). The main-pulse energy density of $\sim$300 mJ/cm^2 ensured high transmission for this pulse while significantly attenuating the prepulse.

A prepulse monitor [17] capable of detecting pulse energies as small as 300 nJ, was used. The unattenuated output of the oscillator was focused in air with a $R = 6$ m concave mirror through a 1 mm diameter hole in a brass plate. The beam was then optically delayed for $\sim$3 ns and focused a second time through the same hole before being monitored by an Au: Ge detector. Low-intensity prepulses pass through the system unattenuated while high-intensity pulses cause optical breakdown on their first transit through the hole, and are further attenuated on the second transit, thereby preventing damage to the detector. With an initial contrast ratio of $\sim$25 : 1 the prepulse energy was suppressed to less than 1 μJ while the energy transmission for the main pulse was measured to be $\sim$40%. In excess of 6 J was present in the main pulse after transmission through the SF_6 cell.

Althrough prepulses could easily be suppressed, some 9 μm interpulse radiation ($\sim$1 μJ) was observed with the prepulse monitor. This radiation was removed by placing a selective absorber in the cavity.

The near-field beam distribution exhibited high spatial frequency intensity variations that are characteristic of the output of unstable resonators. To ensure that no phase distortion was introduced across the beam owing to the presence of the saturable absorber, the focal properties of the beam were monitored with and

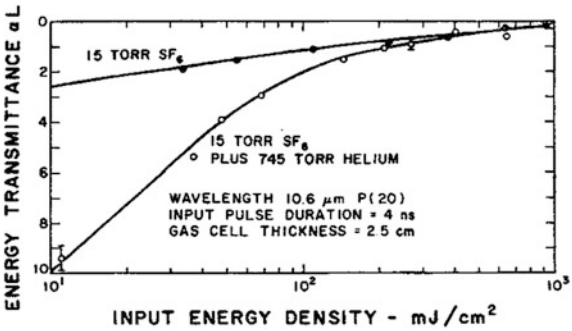

Fig. 33.2 Transmission curves for 15 Torr of SF_6 in a 2.5 cm thick absorption cell with and without a helium buffer gas [20]

without SF_6. The strong nonlinearity of buffered SF_6 (Fig. 33.2) makes phase distortion a possibility that should not be ignored.

Both the transmitted pulse shapes and the focal properties of the beam were monitored over a wide range of pulse energies incident on the SF_6 cell. The peak pulse duration was decreased by $\sim 10\%$ on transit through the SF_6 cell while the transmission through a pinhole placed after the SF_6 cell and having a diameter less than twice the diffraction limit was unchanged by the presence of the SF_6 for both low- and high-intensity pulses.

A number of techniques appear feasible for postpulse suppression. These include controlled optical breakdown at a vacuum aperture, intracavity breakdown in an appropriately designed resonator (e.g., a negative branch unstable resonator), and the use of a semiconductor transmission switch as a Q switch. We have chosen to demonstrate the latter.

Semiconductor transmission switching has been reported for a number of different semiconductors using both lasers [14, 18] and e-beams [15] as control sources. The combination of different semiconductors and switching methods makes transmission switching a versatile method for Q control in 10 μm laser systems. In this experiment, we report the first such application of transmission switching. Germanium was chosen as the semiconductor because of its long recombination time, which ensures that the switch remains absorbing for the duration of the CO_2 inversion. A Q-switched ruby laser was used as a control beam although any sufficiently powerful source of radiation capable of creating free carriers in the semiconductor could be used.

The 30 ns duration control beam illuminated the germanium (etched 10 μm window material) slab, which was placed inside the resonator near the convex mirror. The absorption of a few mJ/cm^2 of the 0.7 μm radiation produces a sufficient quantity of free carriers to absorb most of the 10 μm photons [14]. The timing between the ruby and CO_2 lasers was adjusted to terminate the germanium transmission after allowing transmission of the main pulse. This required that the ruby Q switch be synchronized to the CO_2 discharge to within one CO_2 cavity round-trip time (~ 130 ns). Better synchronization is not required since free-carrier absorption in the germanium slab is determined only by the total number of 0.7 μm photons absorbed within the 130 ns time interval subsequent to the last transmitted pulse.

Although it is possible to suppress the postpulses to any arbitrary level with the germanium $\boldsymbol{Q}$ switch alone, the presence of the saturable absorber cell outside the cavity makes this unnecessary. Even with a postpulse intensity $\sim 5\%$ of the main pulse (Fig. 33.3b), the SF_6-helium mixture could be used to further suppress such pulses to a point where they could not be measured (Fig. 33.3c) on a photon drag detector.

This paper has described a simple scalable technique for switching a single nanosecond pulse from a large-aperture mode-locked oscillator and a high-contrast 6 J pulse has been obtained. The use of buffer gases other than He, various lens arrangements, and/or a heating pulse may permit further improvement of the main-pulse transmission for a fixed discrimination.

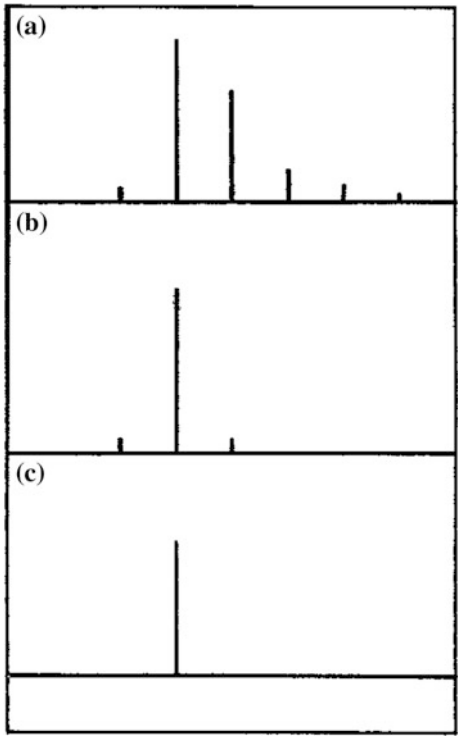

Fig. 33.3 Oscilloscope traces illustrating injection mode locking and single-pulse selection. A typical mode-locked train, poise separation is 130 nm (**a**); mode-locked train showing partial suppression of postpulses with an intracavity semiconductor transmission switch (**b**), horizontal scale same as (**a**); single 6 J, 3 ns pulse selected from the mode-locked train (**c**), horizontal scale same as (**a**)

It is of considerable interest to use such an oscillator as a source of single high-power nanosecond pulses for further amplification in a large-aperture amplifier. Experiments are presently in progress to investigate the operation of an oscillator-amplifier system using an appropriately scaled singlepulse oscillator (occupying a portion of our 5–1 gain module) to efficiently extract energy from the remaining portion of the module operated as a double-pass amplifier.

References

1. F.U. Bunkin, A.M. Prokhorov, *Polarization Matiere et Rayounement,* Vol. Jubilaire en L'Honneur d'Alfred Kastler, (Presses Universitaires de France, Paris, 1969), p. 157ff
2. H. Hora, *Laser Interaction and Related Plasma Phenomena,* ed. by H.J. Schwarz, H. Hora (Plenum, New York, 1975), p. 819ff
3. Lawrence Livermore Laboratory, Laser Program Annual Report, 1976
4. S. Singer, *Laser Interaction and Related Plasma Phenomena,* ed. by H.J. Schwarz, H. Hora (Plenum, New Vork, 1977), p. 121ff
5. K. Witte, G. Brederlow, E. Fill, K. Hohla, R. Volk, Ref. 4, p. 115ff
6. N.G. Basov, O.N. Krokhin, Y.A. Mikhailov, G.V. Sklizkov and S.I. Fedotov, Ref. 4, p. 15ff
7. S.J. Czuchlewski, A.V. Nowak, E. Foley, J.F. Figueira, Opt. Lett. **2**, 39 (1978)

8. M.D. Montgomery, R.L. Carlson, D.E. Casperson, S.J. Czuchlewski, J.F. Figueira, R.F. Haglund Jr., J.S. Ladish, A.V. Nowak, S. Singer, Appl. Phys. Lett. **32**, 324 (1978)
9. P.B. Corkum, A.J. Alcock, D.J. James, K.J. Andrews, K.E. Leopold, D.F. Rollin, J.C. Samson, Ref. 4, p. 143ff
10. P.B. Corkum, A.J. Alcock, Opt. Corrimun. **26**, 103 (1978)
11. P.A. Belanger, R. Tremblay, P. Lapierre, Opt. Commun. **26**, 256 (1978)
12. A.E. Siegman, Appl. Opt. **13**, 353 (1974)
13. P.E. Dyer, D.J. James, Appl. Phys. Lett. **26**, 331 (1975)
14. A.J. Alcock, P.B. Corkum, D.J. James, Appl. Phys. Lett. **27**, 680 (1975)
15. P.B. Corkum, A.J. Alcock, K.E. Leopold, J. Appl. Phys. **50**, 3079 (1978)
16. P.B. Corkum, A.J. Alcock, N.H. Burnett, J. Appl. Phys. (to be published)
17. M.C. Richardson, N.H. Burnett, H.A. Baldis, G.D. Enright, R. Fedosejevs, N.R. Isenor, I.V. Tomov, Ref. 4, p. 16Iff
18. I. Liberman, J.J. Hayden, S. Singer, *IEEE Conference on Laser and Electro-optical Systems,* San Diego, Calif., 1976 (IEEE, New York, 1976), p. 54
19. R.S. Taylor, V.V. Apollonov, P.B. Corkum, IEEE J. Quantum Electron. **16**, 314 (1980)
20. Absolute energy density measurements have an estimated experimental error of ±50%. Relative measurements are accurate to ±10%

Chapter 34
Nanosecond Pulse Transmission of Buffered SF_6 at 10.6 μm

Abstract The 10.6 μm transmission properties of SF_6 were measured using nanosecond-duration pulses for various buffer gases and buffer gas pressures up to 3 atm. The addition of a buffer gas strongly increased the SF_6 absorption at moderate energy fluences without significantly altering the high fluence pulse transmission. For pressures above 1 atm, the transmission behavior appeared independent of the pulse duration over the range of parameters investigated in this experimental chapter. The implication of these results for CO_2 laser applications is under discussion.

34.1 Introduction

In the last few years, considerable effort has been devoted towards understanding the infrared absorption properties of SF_6, in part because it should be possible to extend the conclusions concerning SF_6 to many other polyatomic molecules. Most of the work on SF_6 has been performed at low pressures (<1 Torr) and directed at understanding the absorption mechanisms that are important in laser-induced isotope separation [1]. Several experiments using long duration pulses (typically $\geq$ 100 ns) have been carried out at high SF_6 pressures [2, 3] or at low partial pressures of SF_6 with the addition of buffer gases [4, 5]. The primary motivation for nanosecond pulse transmission experiments has been the use of SF_6-based saturable absorbers for CO_2 laser applications. Published results on this topic have emphasized low total gas pressures (i.e. 100 Torr) with and without a helium buffer [6, 7]. However, in a recent experiment it has been shown that SF_6 buffered to high pressures can operate as a much more effective saturable absorber for many laser applications [8]. Furthermore, it has recently been demonstrated on a polyatomic molecule (CF_3 Br) that isotopic selectivity can be maintained at high pressures if short duration infrared pulses are used [9].

With the present uncertainties in the absorption mechanisms of SF_6, it is not possible to predict the high pressure short pulse behavior from low pressure long pulse data. Therefore, in this chapter, measurements are presented on the nanosecond

© Springer International Publishing Switzerland 2016

V.V. Apollonov, *High-Energy Molecular Lasers*,
Springer Series in Optical Sciences 201, DOI 10.1007/978-3-319-33359-5_34

transmission of SF_6 as a function of buffer gas pressure for several buffer gases. In particular, the paper will discuss the following points:

(1) The manner in which the high energy density transmission behavior is affected by the SF_6 partial pressure, the addition of different buffer gases, and high buffer gas pressures;
(2) The steepness of the nanosecond pulse transmission curve at moderate energy densities as a function of the small-signal absorption, the type of buffer gas, and the buffer gas pressure; and
(3) The manner in which the transmission behavior of buffered SF_6 depends on the pulse duration.

The implications of the above results for CO_2 laser applications will be emphasized.

34.2 Experimental Procedure

The experimental layout is shown in Fig. 34.1. An injection mode-locked TEA CO_2 oscillator [10] operating at 10.6 μm with either a stable or unstable resonator cavity configuration was used as the nanosecond source. Results with the two configurations were consistent and most of the data were obtained with the stable (TEM_{00}) oscillator arrangement. Without injection, the oscillator produced an ~130 ns nonmode-locked pulse (NML) with unpredictable temporal structure due to the beating of many longitudinal modes. With injection, the output consisted of a train of pulses separated by the cavity roundtrip time of ~80 ns with most of the energy contained in one or two main pulses [11]. For the mode-locked case, the output

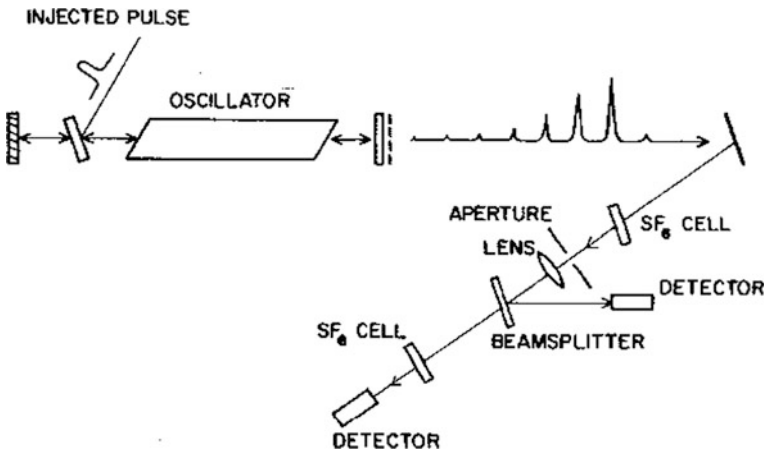

Fig. 34.1 Experimental layout for nanosecond pulse transmission measurements

beam was passed through a 2.5 cm thick cell containing 10 Torr of SF_6 buffered with 1 atm He in order to suppress all pulses prior to the first large pulse. This pulse was then used to probe a second, $I = 2.5$ cm thick, cell. A known fraction of the intensity incident on this cell was monitored using a NaCl beam splitter together with either a calibrated photon drag detector or an energy detector. A salt lens ($f = 1$ m) focused the beam through the second cell and then onto either a second photon drag or a Au:Ge detector. The long focal length lens ensured that the input and output beam areas were nearly equal. Mylar attenuators calibrated at 10.6 μm, together with the lens, were used to vary the input energy density. All energy measurements were made with Gen-Tec Inc. ED-200 energy meters (± 10%).

The first transmission measurement on each gas fill was repeated every 10–20 shots in order to confirm that dissociation, if it occured at the high energy densities, did not affect the transmission measurements.

34.3 Results and Discussion

Figure 34.2 shows the energy transmittance (αl) for a 3 ns (FWHM) pulse measured as a function of the input energy density for 5, 10, and 15 Torr of SF_6 buffered with 1 atm of He. The value of a can be reduced by a factor of ~ 50 from its small-signal value ($\alpha_0 = 0.54\,\mathrm{cm}^{-1} \cdot \mathrm{Torr}^{-1}$ at $P(20)$, 10.6 μm [12]). An effective absorption cross section can be defined as

$$\sigma = \frac{1}{nl}\ln(E_i/E_0) \equiv \frac{\alpha}{n} \tag{1}$$

where n is the number density of SF_6 molecules and E_i and E_0 are the respective energy densities at the input and output of the saturable absorber cell. The data in

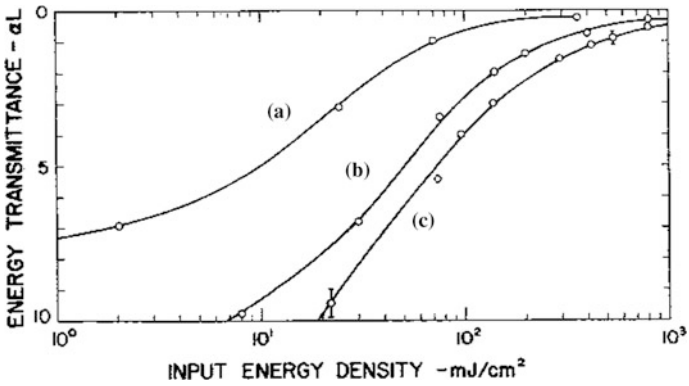

Fig. 34.2 Energy transmittance for a 3 ns pulse as a function of input energy density to the 2.5 cm thick cell containing 5 Torr SF_6 (**a**); 10 Torr SF_6 (**b**); and 15 Torr SF_6, buffered with 1 atm He (**c**)

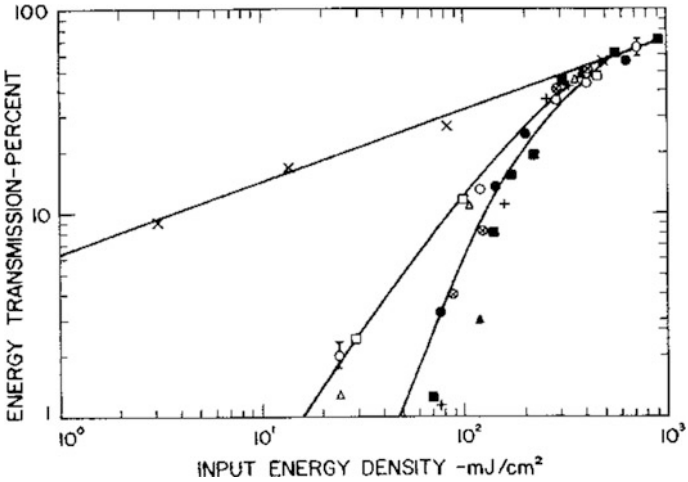

Fig. 34.3 Energy transmission for a 3 ns pulse as a function of the input energy density to the 2.5 cm thick gas cell containing 10 Torr of SF_6 plus no buffer gas (X); 140 Torr He (O); 140 Torr N_2 (Δ); 140 Torr Kr (□); 1 atm He (•); 1 atm N_2 (Δ); 1 atm Kr (□); 2 atm He (⊗), 200 Torr pure SF_6 at a cell thickness = 0.12 cm (+)

Fig. 34.2 imply that σ continually decreases with increased fluence. For example, the absorption cross section of $\sigma_0 = 1.7 \times 10^{-17}$ cm^2 valid for low energy densities becomes $\sigma = 3.4 \times 10^{-19}$ cm^2 at a fluence of 1 J/cm^2. Figure 34.2 also demonstrates that the absorption in the 20–200 mJ/cm^2 fluence range increases substantially as $\alpha_0 l$ is increased. (The steepening of the absorption curve as a function of fluence at high total gas pressure is useful for passive contrast enhancement of CO_2 laser pulses and will be discussed later in this chapter.)

Figure 34.3 shows the pressure dependent 3 ns pulse energy transmission behavior of 10 Torr SF_6 for several buffer gases. At low input energy densities, the addition of as little as ~100 Torr of buffer gas produces a strong increase in the absorption. At high energy densities, the absorption is nearly independent of the buffer gas pressure and over the range of parameters investigated in this experiment, nearly identical transmission curves are observed for He, Kr, and N_2 buffer gases. Furthermore, the transmission curve for 200 Torr of pure SF_6 (in an ~1.2 mm thick cell) with a similar small-signal absorption to the 10 Torr data is in reasonable agreement with the 1 atm buffer gas results. It is possible to conclude that the three buffer gases are equally effective in changing the SF_6 absorption.

The explanation of the observed collision-induced absorption behavior is not clear. Simple pressure broadening of the absorption lines cannot account for the increased absorption at the $P(20)$ wavelength observed in this experiment [13]. In order to estimate the importance of various mechanisms, relevant collision-dependent relaxation times for pure SF_6 and SF_6-buffer gas mixes are presented in Table 34.1. Clearly, for even the highest buffer gas pressures used, vibration to

Table 34.1 Relaxation times for SF_6-buffer gases

	V–V[a]	R–T[b]	V–T[c]
	μs-Torr	ns-Torr	μs-Torr
SF_6-SF_6	1.1	$36 \pm 3^{(*)}$	122
SF_6-He	1.9	–	41
SF_6-Kr	4	–	3040
SF_6-N_2	–	–	103

[a]Obtained from Reference [13]
[b]Obtained from Reference [23]
[c]Obtained from Reference [20]
[*]Appropriate to the ground state

translation (V–T) energy transfer can be neglected on the nanosecond time scale. Vibration to rotation (V–R) energy transfer is likely to be less important than V–T processes [14] and can also be neglected. However, rotational relaxation induced by the buffer gas is sufficiently fast to contribute to nanosecond pulse absorption. In addition, rotational relaxation processes are not expected to be sensitive to the type of buffer gas used in agreement with the results of Fig. 34.3. However, some doubt has been cast on the importance of rotational relaxation and the extent of its role in collision induced absorption is not clear [15]. Although V–V processes are apparently ruled out for low buffer gas pressures, at very high pressures (≥ 1 atm) collision-dependent intramolecular V–V energy transfer may be sufficiently rapid to be important on a nanosecond time scale. This is certainly true if the V–V time of a few μs Torr (see Table 34.1) measured for SF_6 molecules with a low degree of vibrational excitation, represents only a limiting relaxation time. If sufficient energy is absorbed from the laser pulse to populate higher, and therefore, more closely spaced vibrational levels, then the effective V–V relaxation rates may be dramatically increased. Furthermore, even though many more possibilities for V–V energy transfer exist for SF_6-SF_6 collisions than for SF_6-buffer gas collisions, fluorescence measurements have demonstrated that SF_6-SF_6 vibrational energy transfer is only 2–4 times more probable (see Table 34.1) than that involving SF_6-buffer gases. Thus, at present, it is not possible to assess the relative contributions of rotational relaxation and vibrational energy transfer in collision induced absorption. Definitive experiments are needed to measure V–V rates as a function of the energy absorbed into the vibrational manifold.

The importance of the pulse duration and, therefore, intensity on SF_6 absorption was investigated using (1) a 130 ns duration (FWHM) nonmode-locked (NML) pulse, (2) a train of 3 ns mode-locked (ML) pulses separated by a cavity transit time of 80 ns and contained in an envelope of $\sim$130 ns duration, and (3) a single 3 ns duration pulse. Krypton was used as the buffer gas since its long V–T time insured that this process was unimportant even for high buffer gas pressures and long pulse durations. This permits easier interpretation of the data. The data (see Fig. 34.4) taken for various Kr pressures added to 25 Torrcm of SF_6 indicate that the transmission characteristics above and below 300 mJ/cm^2 are distinctly

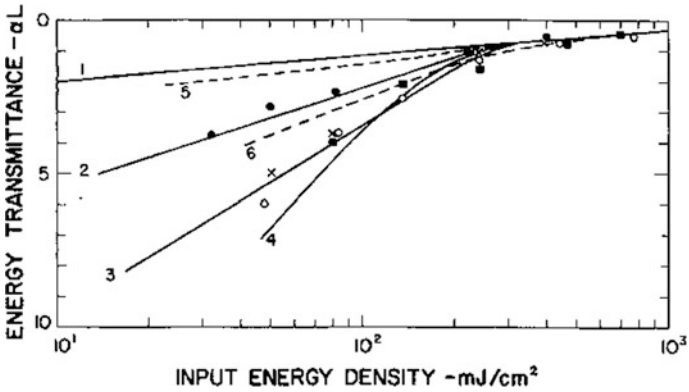

Fig. 34.4 Energy transmittance as a function of input energy density to a 2.5 cm thick *gas* cell containing 10 Torr of SF_6 probed with a 3 ns pulse (*solid curves*), a mode-locked train (*dashed curves*) and a 130 ns (FWHM) nonmode-locked pulse (*data points*) with (1), (5), (•) no buffer gas; (2), (6), (*X*) 140 Torr Kr; (3), (*O*) 1 atm Kr; (4) (■) 3 atm Kr

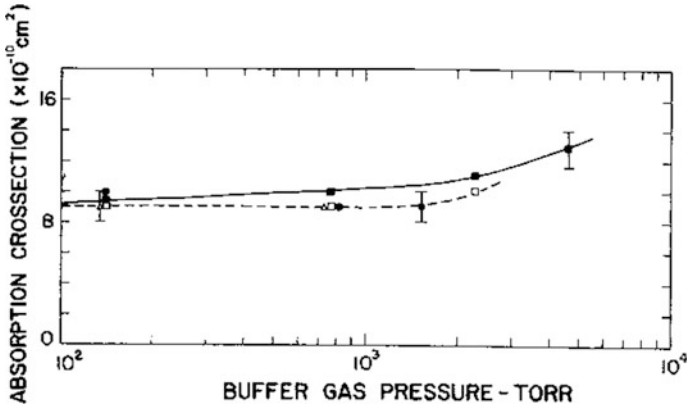

Fig. 34.5 Absorption cross section for a fluence of 400 mJ/cm^2 as a function of buffer gas pressure added to 10 Torr of SF_6, plotted for various buffer gases and two different pulse durations: a 130 ns (FWHM) pulse and a Kr buffer (■); 3 ns pulse and a Kr buffer (□); 3 ns pulse and N_2 buffer (•); and a 3 ns pulse and a He buffer (Δ)

different. At high fluences, the transmission is relatively independent of pulse duration and buffer gas pressure. Figure 34.5 shows the value of the effective cross section σ defined in (34.1) as a function of buffer gas pressure for the 3 ns as well as the NML pulse. The results are plotted for a fluence of 400 mJ/cm^2. These curves demonstrate that the cross section is largely independent (<15%) of the type of buffer gas, buffer gas pressure, and probe pulse duration. Furthermore, the absorption cross section appears to be independent of the type of buffer gas used while high fluence data (not plotted) using unbuffered SF_6 in the 1–200 Torr

pressure range indicate that σ is pressure independent (to within 20%) in this region also. This behavior is in general agreement with that found in a previous low pressure gain-switched pulse experiment [5] and is consistent with the absorption behavior believed to occur among the high density of levels belonging to the vibrational quasi-continuum.

For fluences between 10 and 300 mJ/cm^2 and for moderate buffer gas pressures, the SF_6 transmission is strongly dependent on pulse duration and on buffer gas pressures (see Fig. 34.4). The ML transmission curves[1] lie between the 3 ns and NML curves[2] and all three curves converge as the pressure increases to ~ 1 atm. Above 1 atm, the transmission curves are largely independent of the total gas pressure in the fluence range investigated (>50 mJ/cm^2).

The weak dependence of the transmission curves on rather large changes in buffer gas pressure above 1 atm together with the overlap of the 3 ns, ML, and NML curves at this pressure suggests that, at high buffer pressures, the transmission behavior is dominated by energy dependent processes, at least for fluences >50 mJ/cm^2. Such a limiting energy-dependent curve has been previously observed in high pressure SF_6 experiments using 200 ns, 10.6 μm pulses and was successfully explained by means of a vibrational bath model [17]. The model is based on the assumption that all vibration and rotation levels reach equilibrium in a time that is short compared to the pulse duration. The differences observed in the pressure dependence of the ns and NML transmission curves at low buffer gas pressures can, therefore, be qualitatively understood by assuming that equilibrium is not established within the duration of the nanosecond pulse until a pressure of ~ 1 atm is achieved.[3] At pressures above 1 atm, the observed similarity between the nanosecond and NML transmission curves indicates that, for fluences >50 mJ/cm^2, the vibrational bath model should adequately describe the transmission properties. However, if the relaxation rates are excitation dependent, as discussed earlier, the conditions for equilibrium at 1 atm may only be reached at these moderate to high fluences. Indeed, results obtained in a different experiment, where SF_6 was used as a saturable absorber in a CO_2 oscillator-amplifier system [19], suggest that even in the 1–3 atm range, the nanosecond pulse transmission curve is pressure dependent at low fluences (≤ 50 mJ/cm^2). Further experiments at low fluences are required before a detailed comparison with the vibrational bath model is attempted.

[1]The increase in absorption of the ML train with fluence that was reported in [16] for low SF_6 and low buffer gas pressures was not observed in this experiment.

[2]Data obtained for a limited number of energy densities using a smooth (single longitudinal mode) 130 ns (FWHM) pulse agreed within experimental error (10%) with the NML data at both low and high fluences and over the 10 Torr to 3 atm pressure range studied.

[3]For a given fluence, power broadening can result in greater absorption for the shorter duration more intense pulses [18]. Experimentally, the contribution at high energy densities appears to be small; however, it may be more important in determining the relative transmission of the 3 ns and NML pulses at moderate energy densities.

34.4 Laser Applications

SF_6 is most commonly used in nanosecond CO_2 laser systems for: (1) passive mode locking, and (2) contrast enhancement and gain isolation. The observations of this experiment are important for both applications not only because the nanosecond transmission of SF_6 has not been investigated at high buffer gas pressures, but also because they suggest a means of improving the performance of SF_6-based saturable absorbers, particularly for contrast enhancement.

The results described in this paper demonstrate that the nanosecond saturable absorber properties of SF_6 cannot be considered simply as the intensity saturation of 2, or 4, etc. levels but must involve energy dependent processes. For mode-locking, intensity saturation should occur. That is, there must be a significant difference between the transmission behavior for the ML and NML pulse. Experimentally, this difference is only found at low buffer gas pressures and is most pronounced at the lowest pressures. However, pulse narrowing in the SF_6 is most effective if the absorber relaxation time is somewhat less than the duration of a single mode-locked pulse. Thus, passive mode locking of CO_2 lasers with SF_6 requires a compromise between high pressure operation necessary for pulse shortening and low pressure operation necessary for intensity saturation.[4] This may explain why sub nanosecond pulses have not been obtained with TEA CO_2 lasers using polyatomic molecules as passive mode lockers [21, 22]. However, it is evident from the high-signal data obtained in this paper that residual absorption effects should pose no practical limitation to the mode locking or Q-switching behavior of SF_6.

At high buffer gas pressures, the rapid increase in SF_6 transmission for a small increase in fluence is important for passive systems to suppress unwanted pulses prior to and perhaps even following the peak pulse in a mode-locked train, or to improve the contrast of short pulses obtained using active switching techniques. Since the transmission at these pressures depends primarily on the amount of energy absorbed by the SF_6, prepulse suppression is favored. However, significant postpulse suppression can be obtained by using a buffer gas, such as He, which possesses a V–T time (See Table 34.1) that can be made smaller than a cavity roundtrip time at a manageable gas pressure (a few atm). This permits the absorption to recover between pulses. We have recently demonstrated a particularly striking example of passive contrast enhancement [8]. An injection mode-locked oscillator, which produced a peak pulse ($\sim$400 mJ/cm^2) to prepulse ratio of 25:1, was improved to $\sim 10^6$:1 while still maintaining high main pulse energy transmission ($\sim$40%) by simply passing the output beam through 38 Torr cm of SF_6 buffered to 1 atm with helium.

In the design of nanosecond CO_2 laser systems, it is useful to know the pulse shaping effects of buffered SF_6. In the experiments described in this paper, some pulse narrowing (10–30%, FWHM) was observed at moderate fluences. A detailed

[4]Another potential mode-locking regime is possible. If SF_6 is buffered to high pressures (>10 atm) with a gas with a large V–T energy relaxation rate (e.g., H_2 [20]), the saturation curves could again become intensity dependent and mode locking could occur.

study of pulse shaping, however, was not attempted. An even more important consideration in view of the highly nonlinear nature of SF_6 is the potential problem of phase distortion across the laser beam. This was thoroughly investigated in [8] and no modification was observed in the focal properties of the transmitted beam, even at high buffer gas pressures and large values of $\alpha_0 l$.

Although the present results were obtained with $P(20)$ 10.6 μm radiation, SF_6-based saturable absorbers should be effective anywhere between $P(12)$ and $P(26)$, and it is believed, based on the similarity of the nanosecond, ML, and NML results, that the general observations of this paper should remain valid at these other wavelengths [17].

34.5 Conclusions

Collision-induced absorption has been demonstrated with 3 ns duration, 10.6 μm pulses for SF_6-buffer gas pressures up to 3 atm. An understanding of the absorption properties of buffered SF_6 is important for laser isotope separation experiments performed at high-pressure, passive mode locking of TE-CO_2 oscillators, single pulse selection from mode-locked CO_2 oscillators, and contrast enhancement in nanosecond pulse laser systems. The following conclusions can be made concerning the high-pressure absorption characteristics in SF_6.

(1) The SF_6 absorption behavior is considerably different above and below fluences of 300 mJ/cm^2. For high fluences (but fluences well below the dissociation threshold), the absorption coefficient can be significantly reduced (by a factor of ~ 50) from the small-signal level. Furthermore, the absorption is only weakly dependent on buffer gas type, pressure, and pulse duration. In this region, the absorption is strongly energy dependent.
(2) For fluences below 300 mJ/cm^2 and for low buffer gas pressures, the addition of a buffer gas increases the SF_6 absorption. For the examples studied, the absorption does not depend on the type of buffer gas used but only on the buffer pressure. In this region, the pulse duration and, therefore, the pulse intensity is important.
(3) For buffer gas pressures above 1 atm and for fluences >50 mJ/cm^2, the pulse transmission is nearly independent of the pulse duration in the 1–100 ns range. The bleaching behavior in this region is energy dependent.

Taken together, these observations indicate that the pressure dependent absorption behavior of SF_6 for nanosecond pulses is very complex, involving both intensity and energy-dependent processes. However, at the highest gas pressures, only energy-dependent processes appear to remain important. Although no experiments were performed on other molecular gases, the same general pressure dependent behavior found for SF_6 may be expected in other polyatomic molecular gases.

References

1. R.V. Ambartzumian, V.S. Letokhov, Multiple photon infrared laser photochemistry, in *Chemical and Biochemical Applications of Lasers,* ed. by C.B. Moore, vol. 3 (Academic, New York, 1977), pp. 167–308
2. J.J. Armstrong, O.L. Gaddy, Saturation behavior of SF_6 at high pressure and laser intensity. IEEE J. Quantum Electron. **QE-8**, 797–802 (1972)
3. B.K. Garside, R.S. Taylor, E.A. Baffik, Saturation characteristics of SF_6 absorption at the 10.4 μm band of CO_2. Can. J. Phys. **55**, 849–854 (1977)
4. T.F. Deutsch, S.R.J. Brueck, 03 mode absorption behaviour of CO_2 laser excited SF_6. J. Chem. Phys. **70**, 2063–2073 (1979)
5. G.P. Quigley, Collisional effects in the multiple infrared photon absorption in SF_6. Opt. Lett. **3**, 106–108 (1978)
6. Laser Fusion Program at LASL, High-intensity absorption saturation in gases, in Progress Rep. for the period July 1-Dec. 31, Los Alamos Scientific Laboratory, July 1976, pp. 35–36, LA-6245-PR
7. Laser Fusion Program at LASL, Bleachable absorption in SF_6, in Progress Rep. for the period Oct. 1-Dec. 31, Los Alamos Scientific Laboratory, Los Alamos, NM, Oct. 1977, Rep. LA-6834-PR, pp. 35–37
8. V.V. Apollonov, P.B. Corkum, R.S. Taylor, Section of high-power nanosecond pulses from large-aperture CO_2 oscillators. Appl. Phys. Lett. **35**, 147–149 (1979)
9. J.B. Marling, I.P. Herman, Separation of deuterium and other isotopes by CO_2 laser multiple-photon absorption and subsequent reaction, in *Digestive Techniques Papers Conference Laser Engineering and Applications* (Washington, DC, May 30-June 1, 1979), p. 22
10. P.B. Corkum, A.J. Alcock, D.J. James, K.J. Andrews, K.E. Leopold, D.F. Rollin, J.C. Samson, Recent developments in high power $C0_2$ laser mode-locking and pulse selection, in *Laser Interaction and Related Plasma Phenomena*, ed. by H.J. Schwarz, H. Hora (Plenum, New York, 1977), pp. 143–160
11. P.B. Corkum, A.J. Alcock, Mode-locked operation of TEA CO_2 lasers with long optical resonators. Opt. Commun. **26**, 103–107 (1978)
12. R.S. Taylor, T.A. Znotins, E.A. Ballik, B.K. Garside, A vibrational-bath model for the dynamics of SF_6 absorption near 10.4 jim as a function of wavelength and absorbed energy. J. Appl. Phys. **48**, 4435–4443 (1977)
13. A.V. Nowak, J.L. Lyman, The temperature-dependent absorption spectrum of the ν_3 band of SF_6 at 10.6 μm. J. Quantum Spectrosc. Radiat. Transf. **15**, 945–961 (1975)
14. C. Bradley Moore, Vibration-rotation energy transfer. J. Chem. Phys. **43**, 2979–2986 (1965)
15. A.S. Akhmanov, V.Y. Baranov, V.D. Pismenny, V.N. Bagra- tashvili, Y.R. Kolomiisky, V.S. Letokhov, E.A. Ryabov, Multiple photon excitation of polyatomic molecules from the many rotational states by an intense pulse of IR radiation. Opt. Commun. **23**, 357–361 (1977)
16. H. Stafast, W.E. Schmid, K.L. Kompa, Absorption of CO_2 laser pulses at different wavelengths by ground-state and vibra- tionally heated SF_6. Opt. Commun. **21**, 121–126 (1977)
17. E.A. Ballik, B.K. Garside, R.S. Taylor, T.A. Znotins, High pressure SF_6 pulse transmission near 10.4 μm. Can. J. Phys. **55**, 1956–1961 (1977)
18. R.V. Ambartsumyan, Y.A. Gorokhov, V.S. Letokhov, G.N. Makarov, A.A. Puretskii, Mechanism of isotopically selective dissociation of SF_6 molecules by CO_2 laser radiation. Sov. Phys. JETP **44**, 231–238 (1976)
19. V.V. Apollonov, P.B. Corkum, R.S. Taylor, A novel approach to the generation of single nanosecond CO_2 laser pulses, in *Digestive Techniques Papers Conference Laser Engineering Applications*, Washington, DC, May 30-June 1, 1979, pp. 91–92
20. J.I. Steinfeld, I. Burak, D.G. Sutton, A.V. Nowak, Infrared double resonance in sulfur hexafluoride. J. Chem. Phys. **52**, 5421–5434 (1970)

21. R. Fortin, F. Rheault, J. Gilbert, M. Blanchard, J.L. Lachambre, Powerful nanosecond pulses by stable passive mode-locking of TEA CO_2 lasers. Can. J. Phys. **51**, 414–417 (1973)
22. P. Lavigne, J. Gilbert, J.L. Lachambre, Passive mode-locking of a large volume TEA-CO_2 laser using an unstable resonator configuration. Opt. Commun. **14**, 194–199 (1975)
23. P.F. Moulton, D.M. Larsen, J.N. Walpole, A. Mooradian, High-resolution transient-double-resonance spectroscopy in SF_6. Opt. Lett. **1**, 51–53 (1977)

Chapter 35
20-J Nanosecond-Pulse CO_2 Laser System Based on an Injection-Mode-Locked Oscillator

Abstract Recent advances in injection mode locking and high-power 10 μm pulse selection have been incorporated into a high-power CO_2 laser system built around a single 5 l TEA CO_2 gain module. A pulse selected from a line-tuned [to *P*(20)] injection-mode-locked oscillator was amplified to produce a 20 J, 3 ns pulse with a main-pulse-to-prepulse contrast ratio of $>10^7$:1.

Injection mode locking now provides a simple and versatile scheme for mode locking high-energy TEA CO_2 oscillators [1]. The technique is applicable to both large- [2, 3] and small-aperture oscillators [4], and it is capable of producing highly reproducible pulse trains [5], which contain approximately as much energy in the peak pulse as would be available if the same gain volume were operated as a saturated amplifier [6]. Moreover, any pulse in the mode-locked train can be synchronized to a high-voltage electrical pulse [6] and/or to an optical pulse from another laser [1, 4].

To fully exploit the benefits of injection mode locking, a simple pulse-selection scheme is needed. Recently, a technique was demonstrated that is simple, capable of high-contrast operation, and can be applied with nearly equal facility to systems of arbitrary aperture [5]. It uses a SF_6-based saturable absorber, buffered with helium, to passively suppress all pulses before the main pulse in the mode-locked train and an optical semiconductor transmission switch for active postpulse suppression [5, 7].

This can be investigated and concluded:

1. The application of these recent developments in mode locking and pulse selection to a nanosecond-pulse CO_2 laser system;
2. Progress toward completely passive pulse selection;
3. Contrast enhancement superior to that previously reported [8], using an SF_6-based saturable absorber;
4. The strong suppression of non-*P*(20) radiation by the use of a grating-tuned [to *P*(20)] injection-mode-locked TEA CO_2 oscillator.

© Springer International Publishing Switzerland 2016

V.V. Apollonov, *High-Energy Molecular Lasers*,
Springer Series in Optical Sciences 201, DOI 10.1007/978-3-319-33359-5_35

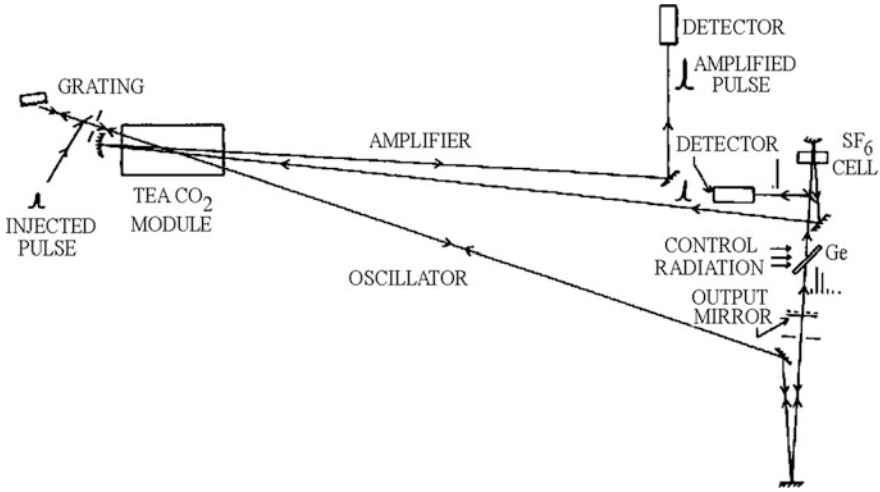

Fig. 35.1 Schematic of the oscillator-amplifier configuration. A single pulse is injected into the slave cavity, giving rise to an output train. Postpulses are suppressed by an optical semiconductor transmission switch and prepulses in a saturable absorber cell containing SF_6 buffered with helium. The selected pulse is double-pass amplified to the ~20 J level

The experiment was performed using a single 5 l TEA CO_2 gain module with a 1 m gain length, a small-signal gain of ~5%/cm, and a gain rise time of ~1 μs [9]. A schematic of the experimental arrangement is presented in Fig. 35.1. The resonator consisted of a 135 line/mm blazed grating and a 36% reflectivity germanium output coupler. The 20 m long cavity was folded several times (not shown) because of the physical constraints of the laboratory. The two turning mirrors included on the diagram were added to ensure that the distance from the output mirror to the gain medium was less for a pulse transmitted through than for a pulse reflected from the output coupler.

A grating-tuned ~1-W cw CO_2 laser served as a master oscillator from which a 4 ns segment was selected by using a pair of electro-optic switches. This pulse was injected into the slave cavity by reflection from a single surface of a wedged NaCl plate placed in the cavity at ~40° with respect to a resonator axis. The injected pulse entered the cavity at a reproducible (~±5 ns) but variable time with respect to the time at which threshold conditions (gain = loss) were achieved [6].

By tuning both the master and the slave oscillator, we obtained mode-locked trains on many CO_2 laser lines. However, for this experiment, the laser was operated only on the 10.6 μm $P(20)$ transition, and the grating ensured that no radiation was present at other frequencies. The TEM_{00} output of the oscillator contained ~1.5 J, of which ~400 mJ were available in the main pulse. The main pulse-to-prepulse contrast ratio could be reliably varied from 1:1 to 25:1 by varying the time of injection. As illustrated in Fig. 35.1, the laser output passed through an optically polished and etched germanium slab used as an optically controlled

semiconductor transmission switch [7] and then through a NaCl beam splitter for monitoring. This completed the active portion of postpulse suppression. Prepulse suppression and additional postpulse attenuation were achieved by double passing the beam through a 2.54 cm thick multiatmosphere saturable absorber cell with the beam reflecting off a 24 m radius-of-curvature convex mirror between passes. The selected pulse was then amplified and recollimated by a 70 m radius-of-curvature concave mirror located ~1.5 m from the gain module before making a second and final pass through the amplifier. The amplifier and the oscillator were arranged so that the active medium used by the oscillator was completely contained inside that used for the amplifier.

The amplifier optics were those used previously to form a confocal unstable resonator [6]. However, in the present case, the resonator was sufficiently misaligned to ensure that no significant output appeared. Even if this condition were not satisfied, the characteristics of this resonator ensure that a gain-switched output could not appear until ~1 μs after threshold gain has been achieved (thus after the main pulse has been amplified). In addition, this radiation would be in a near-diffraction-limited beam [10] not aligned with the amplifier pulse.

The amplified pulse was monitored simultaneously on a photon drag detector and a prepulse monitor [5, 9] capable of resolving pulses with energies as small as 10 nJ. In an alternate configuration, simultaneous monitoring using a photon drag detector and a pyroelectric energy meter was also possible.

The oscillator output was also monitored after the optical semiconductor transmission switch. Figure 35.2a shows a typical output with the input to the amplifier blocked. [Note: the small prepulse and postpulse visible on Fig. 35.2a are further suppressed in the SF_6 cell.]

Typical amplified pulses were of ~3 ns duration and contained ~20 J. Measured main-pulse-to-prepulse discrimination ratios after amplification are plotted in Fig. 35.3 as a function of the discrimination at the output of the oscillator. It should be noted

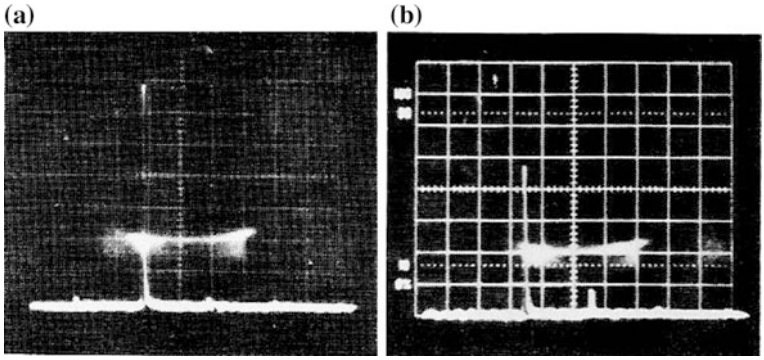

Fig. 35.2 Oscilloscope traces illustrating the mode-locked train after postpulse suppression (**a**) (horizontal scale, 50 ns/div); the output of the amplifier with no active postpulse suppression (**b**) (horizontal scale, 50 ns/div)

that the main pulse from both the oscillator and the amplifier saturates the gain medium; therefore, the energy contained in these pulses is largely independent of their associated discrimination ratio. Thus, Fig. 35.3 is essentially a plot of the reciprocal of the prepulse amplitudes plotted in relative units.

The transmission properties of SF_6 have been investigated previously for nanosecond pulses and buffer-gas pressures up to 1 atm over a wide range of fluences [5, 8] and up to 6 atm for higher fluences [8] (>50 mJ/cm^2). In the latter case, the transmission was almost independent of the buffer-gas pressure for pressures greater than 1 atm. The present experiment clearly indicates that the small-to-moderate signal-transmission properties are pressure dependent even at pressures in excess of 1 atm. At high pressures, the saturation behavior of SF_6 makes it ideal for contrast enhancement. In fact, the curve may be steeper than that

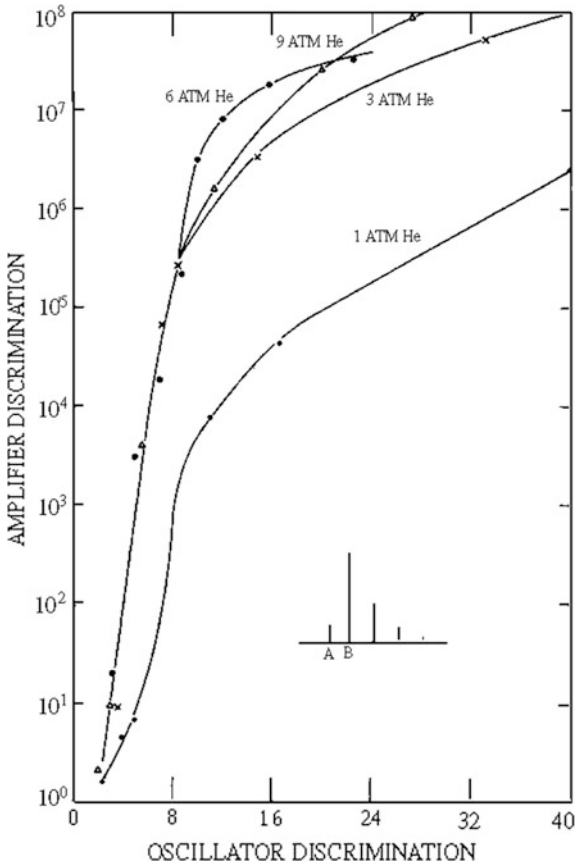

Fig. 35.3 Experimental values of the amplifier discrimination plotted as a function of the main-pulse-to-prepulse contrast ratio from the oscillator

indicated by Fig. 35.3 since the Gaussian spatial profile of our input pulse limits the maximum slope that can be experimentally resolved.

It should be emphasized that the transmission behavior of SF_6 illustrated in Fig. 35.3 assures reproducible operation of the system even in the presence of poor discharges or other effects that may result in shot-to-shot variation of the gain. The main pulse from the oscillator experiences saturated gain and therefore its intensity is insensitive to small variations in the laser parameters, whereas the prepulse need only contain less than one tenth of the main pulse energy to be highly attenuated. This prepulse requirement can be easily achieved. Furthermore, the SF_6 pressure in Fig. 35.3 was selected so that the small-signal transmission $e^{-\alpha}o^{l}$ could be resolved on the prepulse monitor. Had the cell contained 9 Torr of SF_6 buffered to 6 atm, the amplifier discrimination would have leveled off not at $\sim 10^7$ but at $\sim 10^{10}$. Thus, much higher discriminations are feasible with little or no effect on the amplifier output.

The only active element in the pulse-selection system just described is the optical semiconductor transmission switch. At present, it requires a few millijoules per square centimeter of 0.7 μm radiation any time within the appropriate 130 ns cavity transit time of the TEA oscillator. To obtain the results shown in Fig. 35.2a, only ~ 20 mJ of 0.7 μm light were required. However, there are preliminary indications that the optical semiconductor switch could be completely eliminated from an appropriately designed system. The postpulses in the mode-locked train are now about a factor of 2–3 too large to be strongly attenuated by the SF_6. (On this time scale, the behavior of SF_6 buffered with high-pressure helium is independent of all previous pulses.) Thus, completely passive suppression depends only on a mechanism to decrease the postpulses by a relatively small factor. It appears likely that this passive suppression can be achieved by using the saturation properties of the gain medium as itself. In particular, if the amplifier pulse enters the gain medium slightly in advance of the regeneratively amplified oscillator pulse in question, the oscillator pulse will see depleted gain and experience less amplification.

In this experiment, little effort was made to optimize passive postpulse suppression, yet significant suppression was observed (Fig. 35.2b).

This experiment has illustrated the generation of a single, high-contrast nanosecond pulse using a technique that is both simple and inherently scalable. Since the output was ultimately controlled by the 10^{-12} J injected pulse, we have also demonstrated that very-low-power laser pulses can be amplified through very high gains ($\sim 10^{14}$) in systems that strongly limit the amplification of spontaneous emission. This characteristic may be of particular significance for high-power fusion lasers in which automatic target alignment may be simplified by employing phase-conjugation techniques [11] in a system that amplifies low-level radiation scattered from an isolated target.

References

1. P.B. Corkum, Laser Focus **15**(6), 81 (1979)
2. P.A. Belanger, R. Tremblay, P. LaPierre, Opt. Commun. **26**, 256 (1978)
3. P.B. Corkum, A.J. Alcock, D.J. James, K.J. Andrews, K.E. Leopold, D.F. Rollin, J.C. Samson, in *Laser Interaction and Related Plasma Phenomena*, ed. by H.J. Schwarz, H. Hora (Plenum, New York, 1977), pp. 144 ff
4. P.B. Corkum, A.J. Alcock, D.F. Rollin, H.D. Mor-rison, Appl. Phys. Lett. **32**, 147 (1979)
5. V.V. Apollonov, P.B. Corkum, R.S. Taylor, Appl. Phys. Lett. **35**, 147 (1979)
6. P.B. Corkum, A.J. Alcock, Opt. Commun. **26**, 103 (1978)
7. A.J. Alcock, D.J. James, P.B. Corkum, Appl. Phys. Lett. **27**, 680 (1975)
8. R.S. Taylor, V.V. Apollonov, P.B. Corkum, IEEE J. Quantum Electron. **16**, 314 (1980)
9. M.C. Richardson, N.H. Burnett, H.A. Baldis, G.D. Enright, R. Fedosejevs, N.R. Isenor, I.V. Tomov, in *Laser Interaction and Related Plasma Phenomena,* ed. by H.J. Schwarz, H. Hora (Plenum, New York, 1977), pp. 161 ff
10. P.B. Corkum, H.A. Baldis, Unpublished results
11. E.E. Bergman, I.J. Bigio, B.J. Feldman, R.A. Fisher, Opt. Lett. **3**, 82 (1978)

Chapter 36
Numerical Simulation of Regenerative Amplification of Nanosecond Pulses in a CO_2 Laser

Abstract The results of a numerical simulation of regenerative amplification of nanosecond pulses in a high-power electric-discharge CO_2 laser are given in this chapter. The finite contrast of the injected pulse is allowed for in a determination of the ranges of the injection energy and time in which regenerative amplification can be expected. It is shown that the shape of a small-signal pulse has a considerable influence on the energy and contrast of the output pulse. The optimal combinations of the parameters of a regenerative amplification system are determined so as to maximize the energy and contrast of nanosecond pulses.

The results a of a numerical simulation of regenerative amplification of nanosecond pulses in a high-power electric-discharge CO_2 laser are given in this chapter. The finite contrast of the injected pulse is allowed for in a determination of the ranges of the injection energy and time in which regenerative amplification can be expected. It is shown that the shape of a small-signal pulse has a considerable influence on the energy and contrast of the output pulse. The optimal combinations of the parameters of a regenerative amplification system are determined so as to maximize the energy and contrast of nanosecond pulses.

One of the ways of generating high-power nanosecond CO_2 laser pulses is regenerative amplification [1–4]. In the process of such amplification, a small-signal pulse injected into a laser resonator near the lasing threshold makes it possible to control the nature of the output radiation, which is a train of pulses of total energy equal to the free oscillation energy of the laser. Regenerative amplification makes it possible to concentrate, in a single nanosecond pulse, a considerable proportion of the free-lasing energy of the laser for any aperture of the beam. Therefore, high-power pulses can be generated in active media. These are considerably shorter than in the traditional system comprising a master oscillator and a multistage amplifier. Inclusion in the regenerative amplification system, first applied to CO_2 laser in [1], of a saturable absorber made of SF_6 and of a GE plate with modulated transmission [3, 4] has made it possible to generate single pulses of energy representing 12% of the free-lasing energy (in the case of additional double-pass amplification the output pulse contained 40% of the free-lasing energy).

© Springer International Publishing Switzerland 2016

V.V. Apollonov, *High-Energy Molecular Lasers*,
Springer Series in Optical Sciences 201, DOI 10.1007/978-3-319-33359-5_36

Numerical optimization of the parameters of the regenerative amplification system similar to that in [4] is needed to achieve the maximum output energy and contrast of nanosecond pulses. The influence of various parameters on the regenerative amplification process was considered in [5, 6]. However, the results could not be used to optimize the system producing a single pulse. Moreover, the range of injection times in which regenerative amplification is possible (this range is governed by the ratio of the powers of the injected pulse and of the intrinsic radiation of the laser) was found only on the basis of a greatly simplified point model inapplicable to real conditions, and a fuller model of cells ignored the growth of intrinsic laser radiation.

We carried out calculations using the model of cells in which, in contrast to [5, 6], we allowed for intrinsic laser radiation. Our aim was to carry out several tasks: (1) to find the ranges of energy of the injected pulses E_{inj} and of the times of injection T in which regenerative amplification is possible (time was measured from the beginning of a pump pulse); (2) to study the influence of the contrast of the injected pulse on the regenerative amplification process; (3) to optimize the parameters of the system in order to obtain the maximum energy in a selected pulse when the ratio of this energy to that of a preceding pulse in a train was at least 20–30 (which should ensure a contrast of 10^6–10^8:1 at the output of a saturable absorber [4]).

We solved numerically a system of equations for the populations of the active levels and for the photon density in the resonator (i.e., for the intrinsic laser radiation) [7] by dividing the active medium and the resonator into cells. We used the following parameters of the system: the resonator length, L = 20 m; the reflection coefficient of the exit mirror, 0.6; the length of the active medium, l = 50, 100, or 150 cm; the energy of the injected pulses, 10^{-15}–10^{-10} J; the duration of the injected pulses τ = 5 ns; the working mixture composition, CO_2:N_2:He = 1:1:3 at atmospheric pressure. In these calculations, we used the experimental dependence of the electron density, n_e, on the time, t. The constants in the equations were selected so as to achieve the maximum agreement between the experimental and calculated shapes of the edge of the small-signal amplification pulse $\alpha_0(t)$. For simplicity, we assumed that the beam aperture was constant throughout the resonator and that it amounted to 6 cm. The following notation was employed: $\alpha_{0\max}$ is the maximum value of $\alpha_0(t)$; $\alpha(t)$ is the time dependence of the gain obtained by calculations relating to the regenerative amplification process; T_{th} is the moment at which the gain becomes equal to the losses in the resonator; δT_L is the interval between the pulses in a train; N is the number of a pulse in a train with a maximum energy; E_n is the energy of the nth pulse in a train; is the contrast of the injected pulse (in the task 1 it was assumed that $K_{\text{inj}} = \infty$).

Our calculations showed that there are three ranges of T and E_{inj} corresponding to three operating regimes of the laser (Fig. 36.la): (1) region A, where regenerative amplification takes place and there is practically no intrinsic laser radiation; (2) region B, where an injected pulse is being amplified and intrinsic laser radiation is observed it is assumed that in region B the energy of the intrinsic laser radiation during an interval δT_L exceeds by 10% the energy of the adjoining pulse in a train;

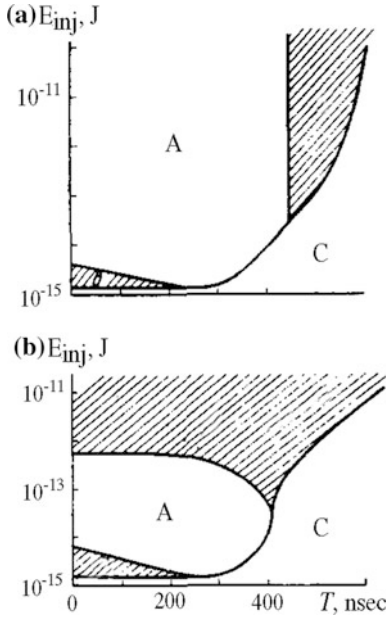

Fig. 36.1 Positions of regions representing various regimes of laser operation plotted in terms of the coordinates T and E_{inj} for l = 100 cm, $K_{inj} = \infty$ (**a**) and $K_{inj} = 10^3$ (**b**)

Table 36.1 The results of calculations of the value of DT for a fixed value of E_{inj} (10–10 J) but different values of l. See in the text

l, cm	ΔT, ns
50	550
100	450
150	400

(3) region C, where free lasing takes place. The existence of all these regions was established also in [6]. However, in contrast to the results of [6], where in the interval $0 < T < T_{th}$ there is a successive change from C, to B and A, our results indicated that in the range $E_{inj} > 5 \times 10^{-15}$ J, region A begins from the acoment $T = 0$. This difference is due to the fact that we considered a longer resonator (L = 20 m in the present case and 1.2 m in [5, 6]), which is desirable for the attainment of the maximum energy of the selected pulse [8]. In [6], it was assumed that $\delta T_L \ll \mathrm{T_{th}}$ and that if $T < T_{th}$, a pulse passes $\sim$ 100 times through the resonator during the interval $T < t < T_{th}$, when the losses exceed the gain. A considerable weakening of the pulse gives rise to regions B and C at times $T < T_{th}$. In our calculations, the number of passes in the interval $T < t < \mathrm{T_{th}}$ was assumed to be 3–4 so that there should be no significant weakening of the injected pulse. Therefore, region A begins from $T = 0$. Table 36.1 gives the results of calculations of the value of ΔT (measure of region A along the time axis) for a fixed value of E_{inj} $(10^{-10}\mathrm{J})$ but different values of l. We can see that ΔT decreases slowly on increase in l because of acceleration of the growth of intrinsic laser radiation.

The influence of the finite contrast of the injected pulse K_{inj} on the regenerative amplification process is of interest. Therefore, we introduced a constant external flux into the equation for the photon density in the resonator; this flux is

proportional to $I = E_{\text{inj}}/K_{\text{inj}}$. Calculations carried out for different values of E_{inj} in the range $10^{-10} - 2 \times 10^{-15}$ J assuming that I = 100 cm, demonstrated that ΔT decreases on reduction in K_{inj} because of an increase in the photon flux reaching the resonator before the arrival of the injected pulse and favoring the growth of intrinsic laser radiation. There is a limiting value $I_{\text{lim}} = 5 \times 10^{-16}$ J (practically independent of E_{inj}) such that $I > I_{\text{lim}}$, then there is no regenerative amplification. Hence, it follows that contrary to the $K_{\text{inj}} = \infty$ case, when region A is bounded in respect of the energy only from below by $E_{\text{inj}}^{\text{min}} = 2 \times 10^{-15}$J (Fig. 36.1a), if the contrast K_{inj} is finite, then this region is bounded also from above by the value of $I_{\text{lim}}\ K_{\text{inj}}$. In the range $2 \cdot 10^{-15} J < E_{\text{inj}} < l_{\text{lim}} K_{\text{inj}}$ there is an optimal value of $E_{\text{inj}}^{\text{opt}}$ corresponding to the maximum value of ΔT. Figure 36.1b shows the distribution of regions A, B, and C for a value of the contrast $K_{\text{inj}} = 10^3$ encountered in practice. It should be highlighted that if $E_{\text{inj}}^{\text{opt}} = 5 \times 10^{-14}$ J, the value of ΔT is close to that for the same K_{inj} and $K_{\text{inj}} = \infty$ (Fig. 36.1a).

For the working mixture and pump conditions assumed in our calculations the n-th pulse crosses the active medium during the falling part of $\alpha(t)$, when the medium is already saturated. In this case, we have $E_N/E_{N-1} \sim 1$. However, the quantity $K_{n,m} = E_{N-m}/E_{N-m-1}$ (m = 1, 2,…) may be considerably greater if the (N-m-l)-th pulse crosses the active medium under linear amplification conditions, whereas the (N-m)-th pulse already causes saturation. Since the dependences $E_n(t)$ are periodic in the period δT_L (as shown in [5]), it follows that $K_{N,m}$ is also periodic. Figure 36.2 shows the dependences of the maximum values of $E_{n\text{-}m}$ obtained for a fixed contrast in the range $K_{N,m} > 20$ but different values of T, on $K_{N,m}$ when l = 100 or 150 cm. It is clear from this figure that $E_{N\text{-}m}$ decreases on increase in $K_{N,m}$, whereas for fixed $K_{N,m}$ it rises on increase in l. If l = 150 cm and $K_{N,m}$ = 20, the value of $E_{N\text{-}m}$ reaches 5.7 J, which represents ~5% of the free-oscillation energy. In order to increase $E_{N\text{-}m}$ and the ratio $E_{N\text{-}m}/E_{out}$, where E_{out} is the total energy of pulses in a train, in the case of constant l, it is necessary to optimize the form of the amplification front (steepness, duration) governed by the composition of the mixture and the input energy in such a way that the (N-m)-th pulse passes through the active medium during the leading edge $\alpha(t)$ and near its maximum. With this in mind, we wrote an auxiliary program that made it possible to calculate the values of E_n for

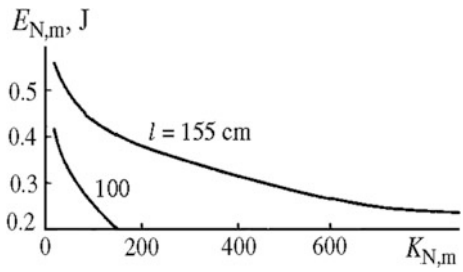

Fig. 36.2 Dependences of the energy of the selected pulse $E_{N,m}$ on the ratio $K_{n,m} = E_{N-m}/E_{N-m-1}$

Table 36.2 The results of calculations for the optimal combinations of the parameters L_{opt} = 20 m for all the mixtures under investigation

CO_2:N_2:He	α_{0max}, m^{-1}	Front duration, μs	l, cm	K_N, m	$E_{N\text{-}m}$, J	E_{inj}, 10^{-15}, J	T, ns
16.7:33.4:50	3.16	2.5	100	25.6	0.92	16	150
			150	21.2	2.12	16	250
20:40:40	3.75	2.5	100	31.2	1.47	5	50
			150	59	3.13	5	300
25:25:50	4.12	2.0	100	21.4	2.08	16	350
			150	135	4.08	16	350
30:30:40	4.38	2.0	100	40.9	2.97	5	350
			150	255	5.69	16	350
36:24:40	4.5	1.5	100	78.6	3.96	16	200
			150	417	8.15	5	300

n = 1, 2, 3,…, N-m from the experimental $\alpha_0(t)$ curve. We used the dependences $\alpha_0(t)$ for five different mixtures with a constant input energy 180 J/l. In these calculations we varied the parameters T and E_{inj} within region A assuming that $K_{inj} = 10^3$ (Fig. 36.1b), L = 8–20 m, and l = 100 or 150 cm.

Table 36.2 gives the results of calculations for the optimal combinations of the parameters (L_{opt} = 20 m for all the mixtures). They showed that the values of $K_{N,m}$ and $E_{N\text{-}m}$ increase on reduction in the front duration (governed mainly by the ratio CO_2:N_2) and on increase in α_{0max} assuming maximum values for the CO_2:N_2:He = 36:24:40 mixture. For this mixture and l = 150 cm, we found that $E_{N\text{-}m}$ = 8.15 J, which amounts to ~9% of the free-lasing energy.

In the present paper, we considered a long resonator (L = 20 m), allowed for the finite contrast of the injected pulses, and determined the ranges of the injection energy and time of such pulses in which regenerative amplification can be expected. We demonstrated that the energy and contrast of the output pulses depend strongly on the steepness of the leading edge and on the maximum value of the gain experienced by an injected small signal.

References

1. P.A. Belanger, J. Boivin, Can. J. Phys. **54**, 720 (1976)
2. V.V. Apollonov, P.B. Corkum, R.S. Taylor, Appl. Phys. Lett. **35**, 147 (1979)
3. V.V. Apollonov, P.B. Corkum et al., Opt. Lett. **5**, 333 (1980)
4. A.J. Alcock, V.V. Apollonov, P.B. Corkum, R.S. Taylor, Izv. Akad. Nauk SSSR Ser. Fiz. **44**, 1677 (1980)
5. K.J. Andrews, Analysis of injection mode locking of high power COj laser systems, Internal Report LPI/77/3 (May 1977)

6. P.B. Corkum, A.J. Alcock, D.J. James, K.J. Andrews, K.E. Leopole, D.F. Rollin, J.C. Samson, in *Laser Interaction and Related Plasma Phenomena* (Proceedings of Fourth Workshop, Rensselaer Polytechnic Institute, Troy, N.Y., 1976, ed. by H.J. Schwarz, H. Hora), vol. 4A (Plenum Press, New York, 1977), p. 143
7. K.J. Andrews, P.E. Dyer, D.J. James, J. Phys. E **8**, 493 (1975)
8. P.B. Corkum, A.J. Alcock, Opt. Commun. **26**, 103 (1978)

Chapter 37
Regenerative CO_2 Amplifier of a Nanosecond Pulse Train

Abstract Regenerative amplification of a nanosecond pulse train in the 50 L active volume CO_2 laser has been investigated both numerically and experimentally. The area in which RA takes place was determined when varying the injected radiation parameters. The nanosecond pulse train utilization as an injected radiation instead of a monopulse was shown to significantly broaden the injection time "window" and to enable variation of an individual pulse time structure in the output train.

37.1 Introduction

Nanosecond pulse regenerative amplifiers have been developed by many researchers [1–3]. The absence of any switches or modulators in the resonator, which limits both beam aperture and intensity, enables the construction of CO_2 regenerative amplifiers with large volumes or apertures of the active medium. A 200 J train of nanosecond pulses generated in a 30 L active volume CO_2 laser was reported in [2]. In order to carry out a number of physical experiments, it is of interest to obtain a nanosecond pulse train with a higher energy and wide range of time structure variation. For example, successive interaction of the electron beam with the laser train of pulses in the same focal volume (s.c. cyclic acceleration) should permit a significant increase in the efficiency of laser acceleration of particles [4]. It is effective to use numerical calculation of the regenerative amplification (RA) process in order to estimate the borders in which RA takes place at the varied injected radiation parameters [5, 6].

The present paragraph reports the numerical calculation results and experimental research of RA in the CO_2 laser with a 50 l volume active medium (L_1), moreover the injected radiation was a nanosecond pulse train with an interpulse time interval $\Delta T = 2l_1/c$ (where l_1 is the L_1 resonator length), obtained in a separate regenerative amplifier (L_2). The aim of the research was the determination of the RA area borders, as well as the study of the changes in the pulse train envelope and amplified spontaneous radiation (ASR) level by the variation of injected radiation parameters.

© Springer International Publishing Switzerland 2016

V.V. Apollonov, *High-Energy Molecular Lasers*,
Springer Series in Optical Sciences 201, DOI 10.1007/978-3-319-33359-5_37

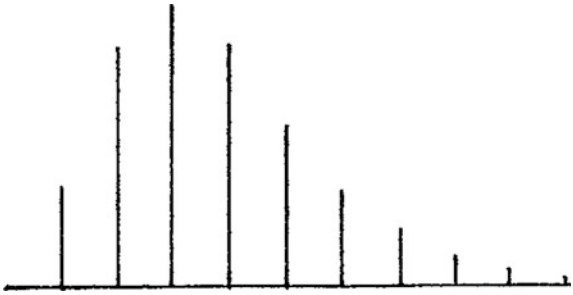

Fig. 37.1 Nanosecond pulse train injected into L_1

In [6] we reported the results of numerical calculations of nanosecond pulse RA in the 1.8 L active volume TEA-CO_2 laser with a stable resonator. In the present paper, the same numerical calculation algorithm was used [6], but some changes caused by a significant difference between the active medium cross section size and injected beam diameter and also the type of injected radiation (pulse train).

Specifically, the following items have been taken into consideration:

1. The injected radiation gradually fills in the fundamental transverse mode of an unstable telescopic resonator.
2. The resonator is divided into 2 zones in which only one or two oppositely directed radiation fluences propagate.
3. The injected radiation is a nanosecond pulse train with the envelope close to the experimental data (Fig. 37.1).

Let us introduce the following designations: T_i is the instant of injection of the first pulse in the train into L_1, the resonator in respect to the pump pulse starting; T_{thr} is the instant of the threshold gain in L_1; and E_i is the injected radiation energy. Note that the parameters of the resonator and active volume used in the calculations correspond to the experimental set up.

One of the main parameters of the RA scheme is the injection "window", that is the region of T_i variation at a fixed E_i, inside which ASR level does not exceed a given value In the present paper, we assume' that inside the injection "window" the ratio of the pulse train maximum pulse peak power P_N (N is the number of the maximum pulse in the train) to the ASR power P_{ASR} exceeds 10. According to [3], in this case the following propagation of the radiation through the saturable absorber (8 + 10 Torr SF_6 + 6 atm He) allows the ratio $K = P_N/P_{\text{ASR}} \geq 10^4$ to be obtained in the output. This value is sufficient for the majority of physical experiments.

The calculation results for the case $T_i = T_{\text{thr}}$ are shown in Fig. 37.2. The P_{N} value grows up with a decreasing injected train peak power Pi (Fig. 37.2a), because the maximum output train pulse is formed at a higher amplification of the active medium. P_N reaches a maximum value simultaneously with K parameter $P_i = 10^{-3}$W (Fig. 37.2b). Note that with P_i decreasing from 1 to 10^{-3}W (Fig. 37.2a), the peak power P_{ASR} also decreases, but the total ASR energy, E_{ASR}, in the L_1 pulse grows up. Figure 37.2c presenting the dependence of $A = E_{\text{tr}}/E_{\text{tr}} + E_{\text{ASR}}$ on P_i, where E_{tr} is

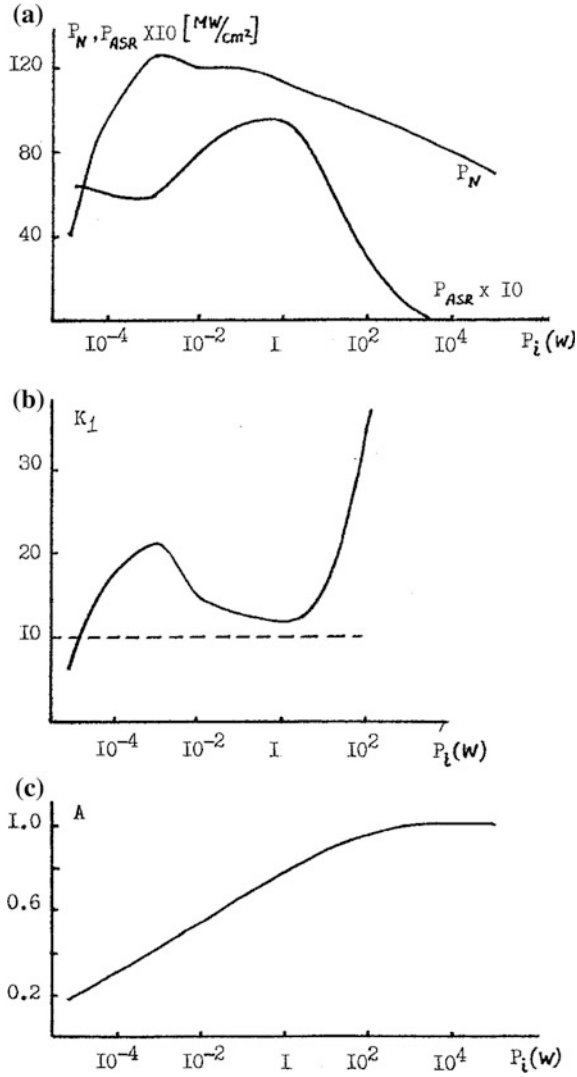

Fig. 37.2 Dependence of P_N, P_{ASR} (**a**); $K = P_N/P_{ASR}$ (**b**); and $A = E_{tr}/E_{tr} + E_{ASR}$ (**c**); on P_i—peak power of the injected train

the total energy of the L_1 pulse train). This is due to a more intensive saturation of the active medium.

It follows from Fig. 37.2b that $K \geq 10$ if $P_i \geq 2 \times 10^{-5} W$, then the minimum injected energy is $E_i^* = 3 \times 10^{-13} J$.

The train envelope form depends significantly on the E_i value. For $E_i = 1.5 \times 10^{-3} J$ (experi-mental data) the front peak of the envelope is insignificantly higher than the main part of the envelope due to the shift of the generation start into the time interval with a smaller amplification (similarly to the generation of a smooth long pulse at one longitudinal mode performance of the injection locked

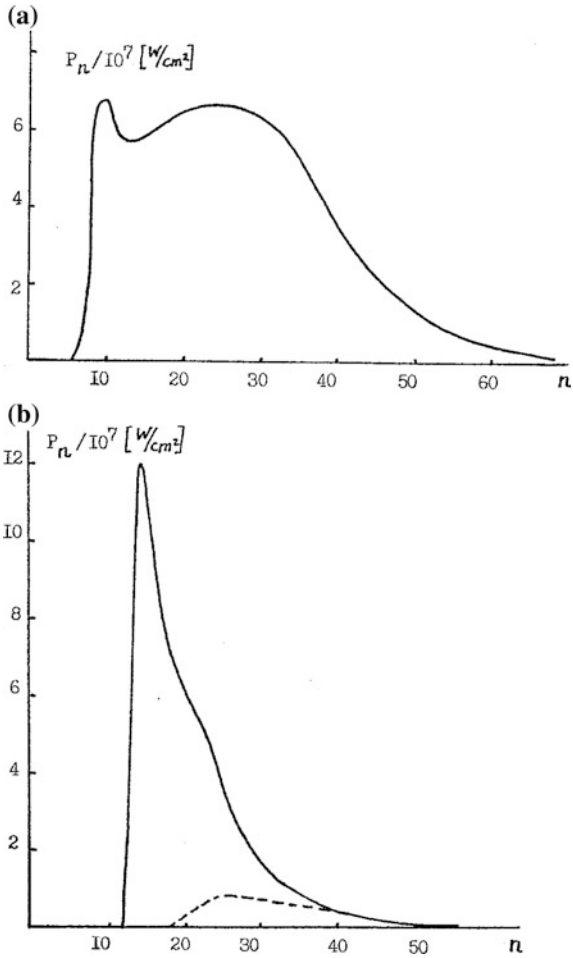

Fig. 37.3 Calculated envelopes of nanosecond pulse train (*solid line*) and amplified spontaneous radiation (ASR) (*dashed line*) for two values of E_i: **a** $E_i = 1.5 \times 10^{-3} J$, **b** $E_i = 1.5 \times 10^{-9} J$ (n—number of a pulse in the train, P_n—power density of the train pulse with the nth number)

laser Fig. 37.3a). When E_i is attenuated up to 1.5×10^{-9} J the first peak power is much higher than the "tail", but the ASR level increases ($K \approx 15$) (Fig. 37.3b).

Thus, in order to obtain maximum output peak power, the injected power must be far lower than that needed for a complete suppression of ASR ($A_1 \approx 1$). If the output peak power has a maximum, A_1, it is only about 0.4 (Fig. 37.2c).

The numerical calculations have shown that, unlike in previous studies [5, 6], the injection window is not symmetric relative to T_{thr}, i.e. for $E_i = 1.5\,\text{mJ}$: $T_{\text{thr}} - 1.5\ \ \mu\text{s} < T_i < T_{\text{thr}} + 0.75\,\mu\text{s}$. This difference is caused by the use of the pulse train as injected radiation, instead of monopulse [5, 6]. If the value $T_i M = T_i + \Delta T(M-1) < T_{\text{thr}}$ (M is the number of pulses in the train), than the train pulse with j number will be attenuated by the resonator losses proportionally to the number of passes through the resonator in the time interval from $T_i J = T_i + \Delta T(j-1)$ to T_{thr}. Therefore, the last pulse in the train has the

minimum losses and in numerical calculations the injection of the last train pulse with the addition of all previous pulses with different attenuation in the resonator has been considered. An equivalent power of the pulse injected at a T_i^M instant depends not only on the train maximum pulse peak power, P_i, but also on the resonator parameters, T_i, and the train envelope form. At the other parameters fixed the left border of the "injection window" moves further from T_{thr} with an increase in the full duration of the injected train. If $T_i > T_{\text{thr}}$ only 2–3 first pulses in the train influence the RA process due to a rapid increase of the light intensity in the resonator after the threshold.

Note that in the vicinity of the "injection window" borders, the dependence of K upon T_i is similar to that shown in Fig. 5.2b. When T_i appproaches the border, K increases from ~ 12 up to the maximum value of ~ 20 and then rapidly drops down.

Thus, when nanosecond pulse train is used as injected radiation instead of monopulse (with the same peak power P_i), the "injection window" broadens by the value close to the full duration of the injected train (~ 1.0 μs in the present case).

37.2 Experimental Set up

The CO_2 laser (L_1) with a $20 \times 20 \times 125$ cm^3 active medium has operated in an SSVD regime initiated by an electron beam, with a low-ionization additive(triethylamine) in a gas mixture [7]. The telescopic resonator mirrors were disposed at the edges of a 2 m^3 volume gas chamber. The resonator had a length of $l_1 = 8.6$ m; magnification was $M = 2.1$; and mirror apertures were 20 and 9 cm. The injected radiation was introduced into a resonator through a 4 mm diameter hole in the concave mirror center (Fig. 37.4). The L_1 worked on the CO_2:N_2:He = 1:1:3 (1 atm) gas mixtures with triethylamine (TEA) additive (1 Torr), CO_2:N_2 = 1:2 and CO_2:N_2 = 1:4 (0.5 atm) with TEA (1 Torr) and H_2O (2 Torr) [7, 8]. Pump energy of the active volume was up to 10 kJ, and electron beam energy did not exceed 200 keV. Maximum out put energy of L_1 was ~ 1200 J for CO_2:N_2 = 1:4 mixture.

The radiation injected into L_1 was the nanosecond pulse train generated in TEA CO_2 laser (L_2) with a 1.8 L active volume similar to [9]. The L_2 active length was 50 cm, the resonator length was $l_2 = l_1$ with 1 cm accuracy. When operated on the CO_2:N_2:He = 1:1:3 (1 atm) mixture and 160 J/l pump L_2 output energy was ~ 0.2 J at the fundamental transverse mode. Nanosecond pulse train (Fig. 37.1) was formed on injecting into the L_2 resonator a 3 ns duration and approximately a 10^{-12} J pulse cut off by electrooptical switch (S_1) from the 1 W CW CO_2 laser (L_3). The L_3 generated at a 10 $P(20)$ line. Pulse duration in the train was close to 2 ns due to the saturation effect.

The contrast ratio of the tain peak power to the L_2 ASR level exceeded 300:1 (measured by Tektronix 7104 oscilloscope). High peak power on the L_2 train ($\sim 10^6$–10^7 W) was much higher than the L_1 spontaneous emission power at the

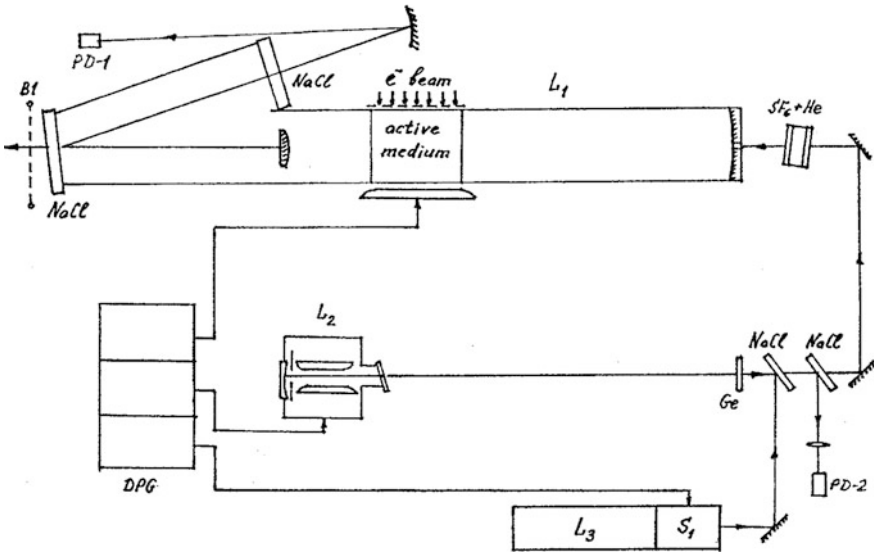

Fig. 37.4 Experimental set up

injection instant. This explains why the experimental set up exhibited a very reliable performance and the "injection window" was rather wide.

Photon drag detectors PD-1 and PD-2 have been used to control the L_1 and L_2 radiation. The L_1 energy was measured by a communicating B_1 bolometer connected with a resistance bridge. B_1 was calibrated by the calorimeters matrix. The energy measurement accuracywas 15%. L_1, L_2 and S_1, as well as the oscilloscopes to control the set up parameters were synchronized by a many channel delayed pulse DPG generator.

When L_1 worked on the CO_2:N_2:He = 1:1:3 p = 1 atm mixture, RA "window" was T_{thr}–1.6 μs < T_i < T_{thr} + 0.6 μs for $E_i = 1.5 \times 10^{-3} J$. Figure 37.5a presents the L_1 radiation oscillogram for this value of E_i and $T_i = T_{thr}$.

For $T_i = T_{thr}$ = 0.6–0.7 μs RA took place in L_1 (that is $K_1 \geq 10$) when E_i was attenuated up to 1.5×10^{-11} J. With smaller values of E_i the "injection window" width was close to the experimental jitter of $T_i = \pm 100$ ns, that is why it was difficult to determine an exact value of E_i^*. With an optimum value of $E_i = 1.5 \times 10^{-10}$ J. P_N had the maximum approximately 1.5 times higher than its value at $E_i = 1.5 \times 10^{-3}$ J. Figure 37.5b shows the train of pulses at $E_i = 1.5 \times 10^{-9}$ J.

Thus, the experimental values of the "injection window" and minimum E_i^*, as well as the train envelopes for two values of E_i are close to the calculated values.

When the L_2 resonator length is varied relative to l_1, the output train pulses are broadened at the base due to the delay of each successive pulse in the input train to the previous one having completed its cavity round trip (Fig. 37.6a). At a significant difference in the resonators lengths $\Delta t = 2l_2/c - 2l_1/c > \tau_i$ (τ_i– is an

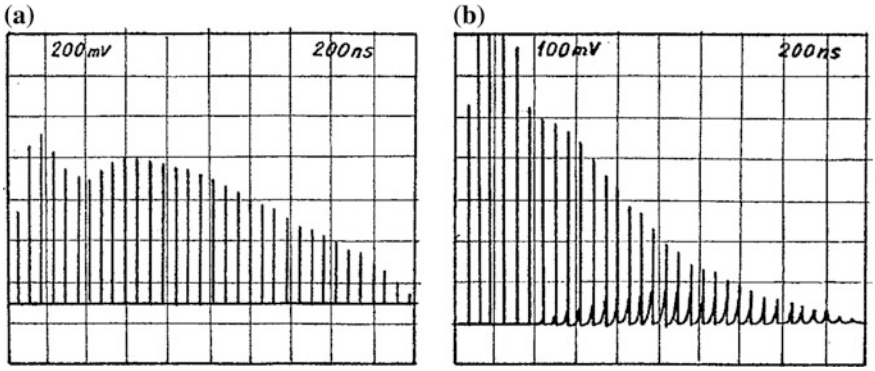

Fig. 37.5 L_1 radiation oscillograms for the case $T_i = T_{\text{thr}}$. **a** $E_i = 1.5 \times 10^{-3}$ J, **b** $E_i = 1.5 \times 10^{-9}$ J

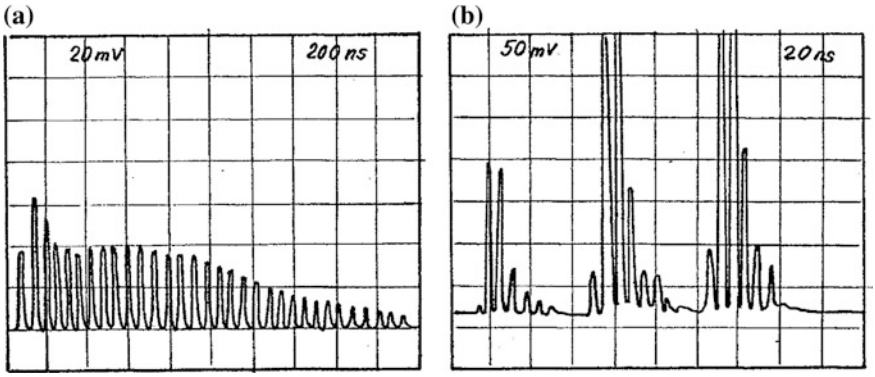

Fig. 37.6 L_1 radiation oscillograms for the case $l_2 \neq l_1$. **a** $2l_2/c - 2l_1/c < T_i$. **b** $2l_2/c - 2l_1/c < T_i$

individual pulse duration), each pulse in the output train is also a train of pulses separated by a Δt interval (Fig. 37.6b). The train of such a type may be of interest for different experiments of radiation interaction with matter.

37.3 Conclusion

1. The borders of regenerative amplification regime in the 50 l active volume CO_2 laser are determined both numerically and experimentally at varied parameters of the injected radiation (which is a train of nanosecond pulses).
2. The nanosecond pulse train utilization as injection radiation instead of mono-pulse was shown to significantly broaden the "injection window" and to enable the individual pulse time structure to change in the output train.

3. The possibility of controlling the peak power and envelope form in the train, as well as the amplified spontaneous emission level by varying the injected power was demonstrated both numerically and experimentally.
4. The numerical calculation results correspond satisfactorily to the experimental data.

References

1. P.A. Belanger, J. Boivin. Can. J. of Phys. **54**, 720 (1976)
2. P.A. Belanger, R. Trembley, P. Lapierre, Opt.-Commun. **26**, 256 (1978)
3. V.V. Apollonov, P.B. Corcum, R.S. Taylor, A.J. Alcock, H.A. Baldis, Opt. Lett. **5**(N08), 333 (1980)
4. V.V. Apollonov, A.J. Artemiev, YuL Kalachov, A.M. Prokhorov, Appl. Phys. Lett. **35**, 147 (1979)
5. K.J Andrews, Analysis of injection mode locking of high power CO_2 laser system (Internal report, LPI/77/3, May 1977)
6. V.V. Apollonov, A.M. Prokhorov, V.R. Sorochenko, Modelling. Simul. Control. A **11**(3), 29–38 (1987)
7. V.V. Apollonov et al., Letters, to Sov. J. Techn. Phys. **2**(7) (1986)
8. V.V. Apollonov et al., Preprint of General Physics Institute (1987)
9. V.V. Apollonov et al., Letters, to Sov. J. Techn. Phys. **10**(19), 1192 (1984)

Chapter 38
Regenerative CO_2 Amplifier with Controlled Pulse Duration

Abstract This chapter reports on the construction of a regenerative TEA CO_2 amplifier emitting a pulse train with the duration of individual pulses controlled in the range 10–40 ns, the time interval between them $\sim$110 ns, and their total energy $\sim$4 J. An injected pulse was formed by screening laser radiation by an optical breakdown plasma in air at the focus of a lens telescope. Good reproducibility of the temporal parameters of the injected pulse was ensured by injecting radiation from a cw frequency-stabilized CO_2 laser into a master oscillator.

This part of the book is given to reporting on the construction of a regenerative TEA CO_2 amplifier emitting a pulse train with the duration of individual pulses controlled in the range 10–40 ns, the time interval between them $\sim$110 ns, and their total energy $\sim$4 J. An injected pulse was formed by screening laser radiation by an optical breakdown plasma in air at the focus of a lens telescope. Good reproducibility of the temporal parameters of the injected pulse was ensured by injecting radiation from a cw frequency-stabilized CO_2 laser into a master oscillator. The regenerative amplification regime is widely used in CO_2 lasers in order to form regular sequences (trains) of nanosecond pulses with a radiation energy up to 1 kJ [1–4]. In the majority of cases, a pulse of the required duration, injected into an amplifier, is first selected from the radiation of a master oscillator by an electrooptic switch which provides the necessary reliability and stability, but requires the use of high-quality electrooptic crystals and also of a high-voltage nanosecond pulse generator. In some experiments, a high contrast ration ($>10^3$) of the pulses in the train, relative to the amplified spontaneous radiation, is needed and this requires not only at least as high a contrast ratio of the injected pulse, but also a two-stage electrooptic system [3]. It is a technical problem in itself to construct a high-voltage generator for such a system. There is therefore an urgent need for simpler methods of generating nanosecond pulses in order to control regenerative CO_2 amplifiers, including those with a large active medium volume [4]. We shall describe how such pulses were formed by screening laser radiation by an optical breakdown plasma in air at the focus of a lens telescope. A train of pulses with a total energy of E = 4 J, with an interpulse time interval of ΔT = 110 ns and a pulse duration that could be

© Springer International Publishing Switzerland 2016

V.V. Apollonov, *High-Energy Molecular Lasers*,
Springer Series in Optical Sciences 201, DOI 10.1007/978-3-319-33359-5_38

controlled in the range 10–40 ns was formed by injecting a master oscillator pulse into a regenerative amplifier.

Figure 38.1 is a schematic diagram of the apparatus. Ultraviolet-preionized TEA CO_2 modules of the Lamberton and Pearson type [3] were used in the master oscillator and regenerative amplifier. The active medium dimensions were $6 \times 6 \times 50$ cm and the pump source was based on a pulse autotransformer 2. Both modules operated using a CO_2:N_2:He = 1:1:3 mixture at an input energy of $\sim$200 J/l. Aperture stops 5 in the master oscillator and regenerative amplifier resonators served in the case of the master oscillator to select the central part of the active region for lasing in a single-mode regime and, in the case of the regenerative amplifier, ensured lasing in the fundamental TEM_{00} transverse mode. Stable shot to shot reproducibility of the radiation pulse shape was achieved by injecting into the master oscillator resonator radiation of power $\sim$1 W from an LGN-901 cw stabilized CO_2 laser, tunable in the range $\pm$40 MHz relative to the center of the 1 OP (20) line, using a Ge plate 6. The frequency detuning range in which a smooth single-frequency pulse was observed from the master oscillator (Fig. 38.2a) was quite large (20–30 MHz), and this made it possible to compensate thermal fluctuations of the master oscillator resonator length and to obtain a stably reproducible radiation pulse shape over several tens of shots.

The master oscillator output radiation passed through a telescope 7 formed by two f = 50 mm planoconvex germanium lenses with a 25 mm aperture. In order to check that the injected radiation reached the regenerative amplifier, the telescope was evacuated to prevent optical breakdown at the common focus of the lenses. Air pressure up to 1 atm was permitted in telescope in the short-pulse regime. This caused optical breakdown during the leading edge of the master oscillator radiation pulse. The optical breakdown plasma screened the remaining part of the radiation

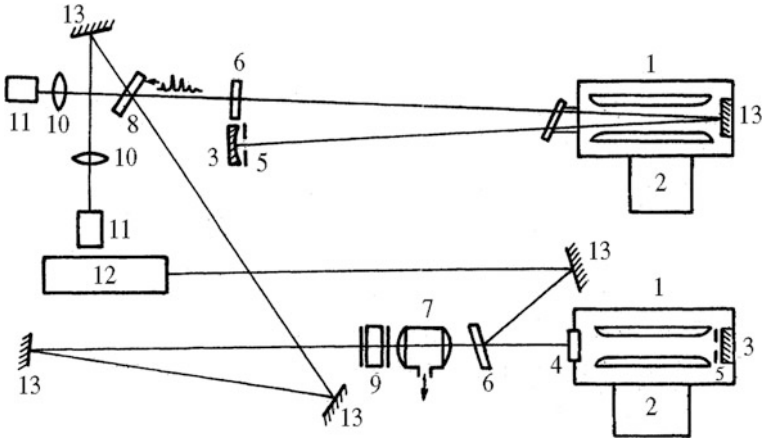

Fig. 38.1 Schematic diagram of the apparatus: *1* TEA CO_2 module with $6 \times 6 \times 50$ cm active volume *2* pulse autotransformers; *3* R = 70 m spherical mirrors; *4* plane-parallel germanium plate; *5* aperture stop; *6* plane-parallel germanium plates with one antireflection-coated fact; *7* lens telescope; *8* NaCl plate; *9* cell containing SF_6 + He nonlinear absorber; *10* lenses; *11* FP-0.5 photodetectors; *12* single-frequency cw CO_2 laser; *13* plane mirrors

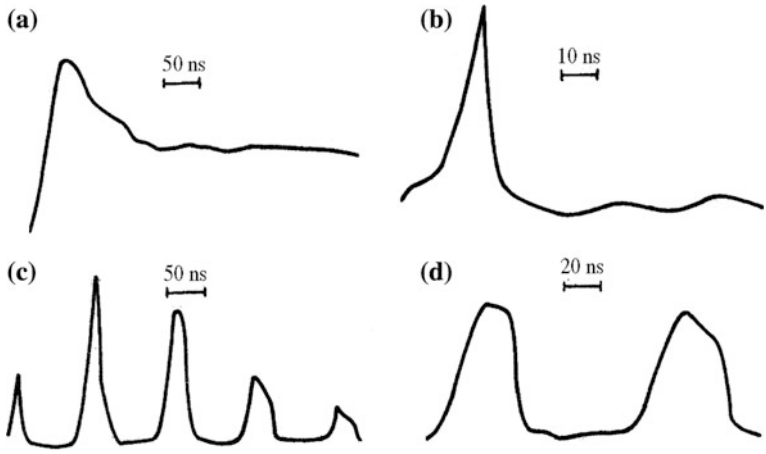

Fig. 38.2 Oscillogram of the master oscillator and regenerative amplifier radiation obtained when cw single-frequency radiation was injected into the master oscillator: **a** master oscillator output pulse; **b** short pulse after the "gating" telescope; **c** train of regenerative amplifier pulses for τ_p = 10 ns; **d** first two pulses of a regenerative-amplifier pulse train for τ_p = 30 ns

and a short pulse ws formed at the exit of the telescope. The injected pulse and the regenerative amplifier output radiation were recorded with a time resolution of 0.5 ns using an FP-0.5 photodetector 11 and a Tektronix 7104 oscilloscope (with a 1.1-GHz band width). The radiation energy was measured with a TPI-2 M calorimeter.

Figure 38.2b shows an oscillogram of a pulse, of τ_p = 10 ns duration injected into the regenerative amplifier. The pulse duration was varied in the range 10–30 ns by an attenuator that altered the moment (during the leading edge of the master oscillator radiation pulse) when optical breakdown was initiated. When the master oscillator contained a CO_2:N_2 = 1:1 mixture (p = 0.5 atm), a minimum duration of 6 ns was achieved owing to the shortening of the leading edge of the radiation pulse. The energy, E_p, of a short pulse of τ_p = 10 ns duration was 200 mJ at the exit of the telescope. Taking into account the losses in the optical path, this corresponded to a power of P_p = 400 kW injected into the regenerative amplifier. The relative spreads in the amplitude and duration of the injected pulses in a series of 10 shots were 12 and 5 %, respectively. This was considered to be satisfactory in view of the statistical nature of the optical breakdown. A saturable absorber (4 Torr of SF_6 with 6 atm of He) at the telescope exit aperture suppressed the pedestal that followed the main pulse. The latter was due to the radiation scattered by the plasma reaching the exit aperture of the telescope. In the absence of this saturable absorber, secondary pulses associated with amplification of the pedestal appeared in the regenerative amplifier pulse train.

For τ_p = 10 ns, the duration, τ_n, of the pulses in the train increased with n from $\tau_1 \approx \tau_p$ to roughly 30 ns in the tail of the pulse train (Fig. 38.2c). This was due to saturation of the gain of the regenerative amplifier active medium, leading to a displacement of the maximum intensity in the amplified pulse nearer to the leading edge after each pass through the amplifying medium. The value τ_1 did not become appreciably shorter than τ_p, which could be explained by the summed amplification of an injected pulse in the regenerative amplifier being compensated for, after a large number of resonator passes, by the nonlinear shortening of its leading edge after passing once through the absorber. When the absorber was placed ahead of the lens telescope, there was a shortening of τ_n and, in particular, the value of τ_1 could be varied in the range 10–30 ns, that of τ_2 in the range 20–40 ns, etc. Figure 38.2d gives an oscillogram of the first few pulses in a train for τ_p = 30 ns.

Owing to the high power of the injected pulse, the range T_p of the delays of the moment of its arrival at the regenerative amplifier resonator, within which a train of pulses was formed at the regenerative amplifier output, amounted to 0–2 μs (T_p was measured relative to the start of the regenerative amplifier pump pulse). When no cw radiation was injected into the master oscillator, a short pulse was formed at the telescope exit aperture (Fig. 38.3b), which had the spiky structure typical of the spontaneous mode selflocking of the longitudinal modes in the master oscillator (Fig. 38.3a) and an unstable overall duration. In this case (Fig. 38.3c), on account of the separate spikes of ~1 ns duration, the peak power in the regenerative amplifier pulse train rose by a factor of 2–3 relative to that in a train of smooth pulses.

Thanks to the high value of P_p, the train of pulses at the regenerative amplifier output was formed stably when the spark gaps in the master oscillator and regenerative amplifier autotransformers operated with a relative spread of less than 100 ns (in this case, we found that T_p = 0.8 + 0.1 μs). This made it possible to utilize the active medium of one TEA CO_2 module both to form a short pulse and to amplify it regeneratively, and ultimately to construct an experimental scheme. The high peak power of a pulse (P_p ~ 20 MW at the exit aperture of the telescope)

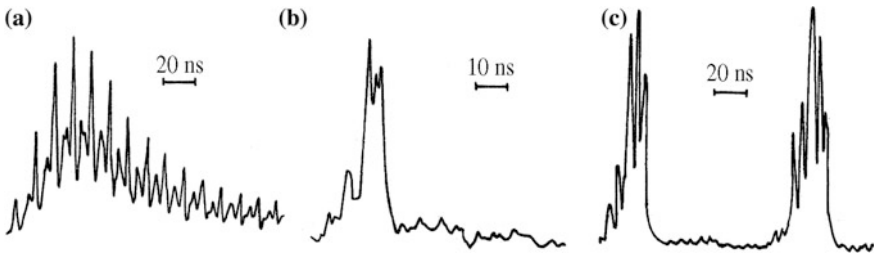

Fig. 38.3 Oscillograms of the master oscillator and regenerative amplifier radiation obtained in the absence of injection of cw single-frequency radiation into the master oscillator: **a** master oscillator output radiation with spontaneous mode locking of the longitudinal modes; **b** short pulse at the telescope exit aperture; **c** first two pulses of the regenerative-amplifier pulse train

made it possible to generate a pulse train having a total energy of up to 1 kJ in a regenerative amplifier with a 50 l active volume [4, 5].

In conclusion, it is worth noting that the high electron density at the focus of the telescope in the prebreakdown state must lead to a considerable distortion of the wavefront of radiation passing through the focus, and to a degradation of its divergence [6]. However, this is not of decisive importance in regenerative amplification since, in contrast to the case of single-pass or multipass amplifiers, the spatial characteristics of a regenerative amplifier are determined solely by its resonator.

References

1. P.-A. Belanger, J. Boivin, Can. J. Phys. **54**, 720 (1976)
2. A.J. Alcock, P.B. Corkum, D.J. James, Appl. Phys. Lett. **30**, 148 (1977)
3. V.V. Apollonov, G.G. Baitsur, V.V. Brytkov, S.I. Zienko, S.V. Murav'ev, V.R. Sorochenko et al., Pis'ma Zh. Tekh. Fiz. **10**, 1192 (1984) [Sov. Tech. Phys. Lett. **10**, 504 (1984)]
4. V.V. Apollonov, A.M. Prokhorov, V.R. Sorochenko, Yu. A. Shakir, Kvantovaya Elektron. (Moscow) **15**, 1766 (1988) [Sov. J. Q. Electron. **18**, 1102 (1988)]
5. V.V. Apollonov, F.V. Bunkin, S.I. Derzhavin, I.G. Kononov, K.N. Firsov, YuA Shakir, V.A. Yamshchikov, Izv. Akad. Nauk SSSR Ser. Fiz. **42**, 2488 (1978)
6. E. Yablonovitch, Phys. Rev. A **10**, 1888 (1974)

Chapter 39
Efficiency of an Electric-Discharge N_2 Laser

Abstract Electric-discharge lasers based on transitions in the nitrogen molecule are promising sources of near-UV radiation. Such lasers are used widely in the microelectronics industry, medicine, and laser chemistry, as pump sources of organic lasers, as well as in spectroscopy, laser diagnostics of plasmas, etc. The design of these lasers is relatively simple and the active medium is chemically inert. Moreover, in some applications the nitrogen laser wavelength is most effective [1].

A shortcoming of nitrogen lasers is their low efficiency. The scatter of the efficiencies reported in various papers is very wide, from 0.02% [2] to 0.8–1% [3, 4], in spite of the fact that there are no basic differences between the various designs. No acceptable explanation of the reason for this scatter has been put forward to date. Attempts to mathematically simulate the processes occurring in a nitrogen laser are usually confined to special cases [5, 6] or fail to ensure a satisfactory agreement with experiments. This hinders the search for the conditions that would increase the efficiency and would help to construct lasers with specified characteristics. We have therefore directly investigated the dependence of the efficiency of nitrogen lasers on the basic characteristics of the discharge, on the parameters of the pump circuit, and on the pressure and composition of the gas mixture.

The electric circuit of our laser was similar to that described in [7] and it is shown in Fig. 39.1a. It consisted of an *LC* Fitch pulse generator, a saturable choke L_2, and a peaking capacitor with its capacitance C_0 distributed along the discharge gap. The capacitances C_1 and C_2 were 20 nF each. The peaking capacitance was equal to the impulse capacitance of the Fitch generator: $C_0 = C_l/2 = 10$ nF. The winding of L_2 was in the form of a double metal tube with the space between the walls filled by ferrite rings with a total cross-sectional area $S = 67$ cm^2. This circuit was capable of generating voltage pulses up to 40 kV with a rise time of 80 ns. A discharge gap (DG in Fig. 39.1) of 20 × 20 × 500 mm dimensions was formed by two profiled electrodes. The distance between the electrodes was $d = 20$ mm. The discharge gap was illuminated with UV radiation from 50 spark gaps. The laser cavity was formed by a quartz plate and a nontransmitting plane-parallel mirror.

© Springer International Publishing Switzerland 2016

V.V. Apollonov, *High-Energy Molecular Lasers*,
Springer Series in Optical Sciences 201, DOI 10.1007/978-3-319-33359-5_39

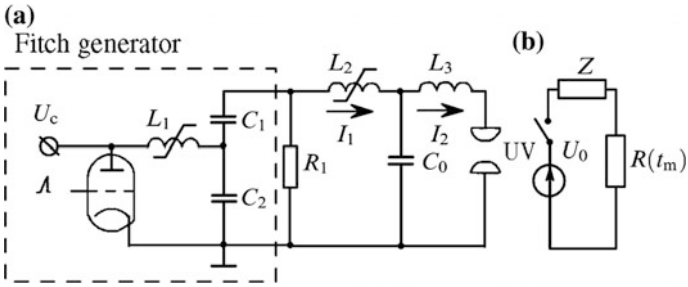

Fig. 39.1 Electric (**a**) and equivalent (**b**) circuits of the investigated laser

The experiments were carried out at a constant charging voltage of U_c = 20 kV. Figure 39.2 shows typical oscillograms of the pulses of the voltage $U(t)$ across the discharge gap, of the current, $I(t)$, through the peaking capacitor, and of the N_2 laser output radiation, $J(t)$. Figures 39.3 and 39.4 give the experimental dependences of the maximum voltage U_m across the discharge gap and of the output radiation energy W *of* a nitrogen laser and of a laser with a mixture of nitrogen and SF_6 (20 Torr) on the nitrogen pressure p_{N2}. The dependence of the ratio $E_m/p = U_m/pd$, representing the electron temperature in the discharge (E_m is the maximum electric field intensity and $p = p_{N_2} + p_{SF_6}$ is the total pressure in the gas mixture) on p_{N2} is plotted in Fig. 39.5. There is a widely held view [4, 8, 9] that the characteristics of the N_2 laser radiation depend primarily on the ratio E_m/p. However, it is evident from Figs. 39.4 and 39.5 that in the range of working pressures in the laser, a change in the parameter E_m/p has no significant influence on the behaviour of *W*.

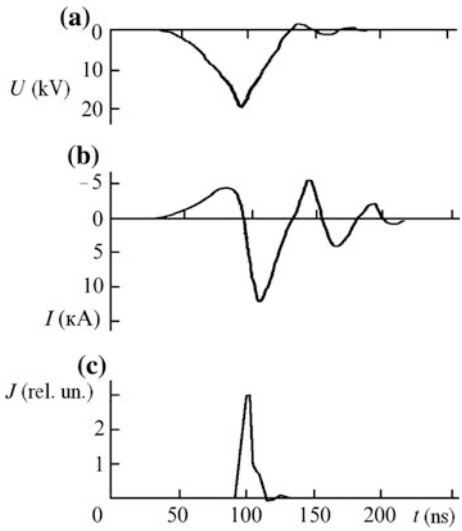

Fig. 39.2 Oscillograms of pulses of the voltage (**a**); of the current through the capacitance C_0 (**b**); and of the output radiation (**c**) obtained for an N_2 laser (p_{N2} = 120 Torr, U_c = 20 kV)

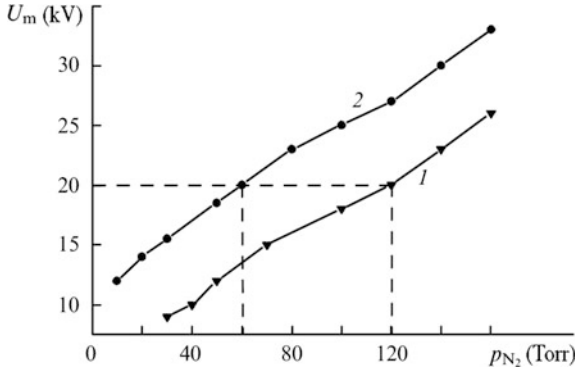

Fig. 39.3 Dependences of the maximum voltage, U_m, across the discharge gap on p_{N2} for N_2 (*1*) and $N_2 - SF_6$ (*2*) lasers

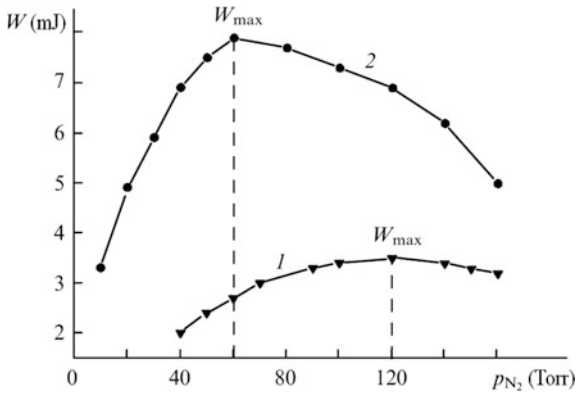

Fig. 39.4 Dependences of the output radiation energy W of N_2 (*1*) and $N_2 - SF_6$ (*2*) lasers on p_{N2} (p_{SF6} = 20 Torr)

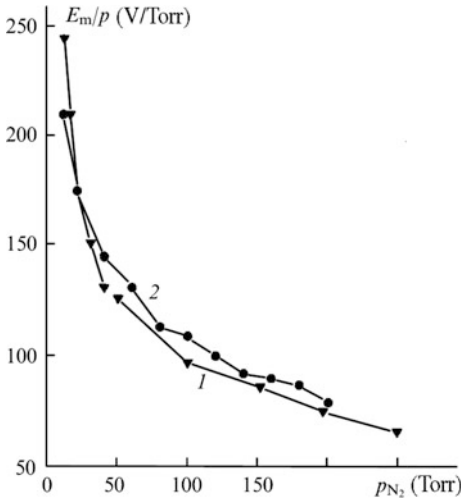

Fig. 39.5 Dependences of the ratio of the maximum electric field in the discharge to the total pressure in the gas mixture, E_m/p, on p_{N2} for N_2 (*1*) and $N_2 - SF_6$ (*2*) lasers (p_{SF6} = 20 Torr)

Special features of pumping of the N_2 laser are, as demonstrated in Figs. 39.3 and 39.5, low values of U_m (compared with the maximum voltage supplied by the Fitch generator, which is $2U_C = 40$ kV) as well as high values of E_m/p in the discharge. The latter is considerably greater than the ionization threshold of nitrogen $E_i/p = 40$ V cm^{-1} Torr^{-1}. This means that the ionization in the discharge gap and pumping of the active medium begin before the maximum voltage across the plasma is reached. The charging current I_1 and the discharge current I_2 then flow simultaneously through the capacitance C_0 (Fig. 39.1a). The breakdown condition (i.e., the maximum voltage, U_m, across the discharge gap) can be described by C_0 $dU(t)/dt = I(t) = I_1 - I_2 = 0$, i.e. $I_1 = I_2$. It is clear from Fig. 39.2b that at $p_{N2} = 120$ Torr, the discharge current is approximately 4 kA when the maximum voltage across the plasma is 20 kV.

The circuit in Fig. 39.1a can be reduced to an even simpler equivalent circuit [10] (see Fig. 39.1b). Here, $R(t_m)$ is the resistance of the self-sustained-discharge plasma at the moment t_m corresponding to the voltage maximum across the discharge gap, Z is the equivalent impedance of the electric circuit, equal to the impedance when the gap is short-circuited (in general, it is a complex quantity with active and reactive components), and U_0 is the voltage of the equivalent pulse generator in the idle mode. The peak pump power at the moment t_m can then be found from

$$P_m = I_m U_m = \frac{1}{Z}(U_0 - U_m)U_m. \tag{39.1}$$

An increase in the nitrogen pressure increases U_m (Fig. 39.3). Therefore, according to the above formula, the power, P_m, first increases and then falls, reaching its maximum at $U_m = U_0/2$ (on condition that $dP_m/dU_m = 0$):

$$P_{max} = \frac{U_0^2}{4Z}. \tag{39.2}$$

Since the pump pulses are generated by the Fitch generator, U_0 is understood to be double the charging voltage: $U_0 = 2U_C$.

It is evident from Figs. 39.3 and 39.4 that there is a single-valued relationship between U_m and W. If we use this relationship and formula (39.1), we can plot the dependences of W on P_m, given in Fig. 39.6 for the conditions in our experiments: $Z \approx [2(L_{2s} + L_3)/C_0]^{1/2} = 5\Omega$, $L_{2s} = 113$ nH (L_{2s} is the inductance of the first circuit when L_2 is saturated), $L_3 = 6$ nH, $U_0 = 40$ kV. It is quite obvious from Fig. 39.6 that W is proportional to P_m. The arrows identify the regions of rise (from left to right) and fall (from right to left) of P_m and W. The physical meaning of P_{max} is the value of P_m corresponding to $U_m = U_0/2$, which implies a matched pumping regime when the condition $R(t_m) = Z$ is satisfied (Fig. 39.1b).

Consequently, matched pumping should ensure that the output radiation energy is maximal (W_{max}). For the investigated mixtures, the maximum value of W was indeed observed at such gas pressures that the maximum of the discharge voltage

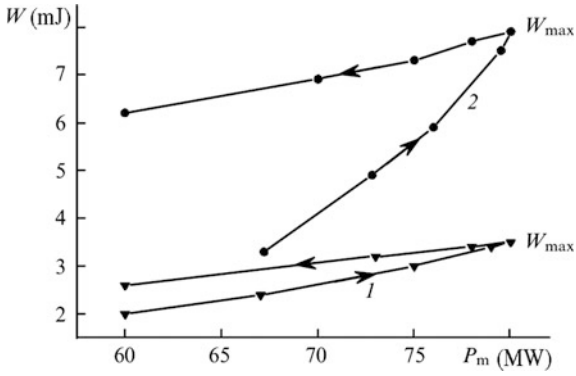

Fig. 39.6 Dependences of the output radiation energy W of N_2 (*1*) and N_2-SF_6 (*2*) lasers on the power, P_m, released at the moment of attaining the maximum voltage across the discharge gap (p_{SF6} = 20 Torr)

was 20 kV, i.e. when $U_m = U_0/2$ (Figs. 39.3 and 39.4). In this case, the maximum peak pump power and the maximum electron temperature in the discharge were reached simultaneously.

The different slopes of the curves in Fig. 39.6 before and after the maximum of W result from inequality of the fractions of the energy deposited in the discharge before and after the voltage maximum. This inequality increases with increase in p_{N2}. The considerable increase in the output energy obtained for a mixture containing SF_6 can be explained by an equivalent increase in the decay time of the voltage across the plasma, which again increases the pump energy deposited in the discharge after the voltage maximum.

If we assume that $W_{max} = K(P_{max} - P_{min})$, where K is the slope of curves in Fig. 39.6 in the region of rising W, and that P_{min} is the minimum power at which lasing is observed, we obtain the following parameters: $K_1 = 7 \times 10^{-11}$ s, $P_{1min} = 33$ MW for nitrogen, and $K_2 = 4 \times 10^{-10}$ s, $P_{2min} = 60$ MW for the investigated N_2-SF_6 mixture. The results of our experiments readily yield the nitrogen laser efficiency:

$$\eta = \frac{W_{max}}{W_0} 100\% = K\left(\frac{1}{2ZC} - \frac{P_{min}}{W_0}\right) 100\%, \tag{39.3}$$

where $W_{max} = K(P_{max} - P_{min})$; $P_{max} = U_0^2/4Z$; $W_0 = CU_0^2/2$ is the energy stored in the equivalent capacitance C of the high-voltage generator. Substitution in the above expression of the numerical values $U_0 = 40$ kV, $C = C_1/2 = 10$ nF, $Z = 5\ \Omega$, and also of K and P_{min}, gives $\eta_1 = 0.04\%$ for N_2 and $\eta_2 = 0.1\%$ for the N_2-SF_6 mixture.

In some of the cases that are most interesting in practice, when $\eta_1 \geq 0.1\%$ and $W_0 \geq 10$ mJ, the second term in expression (39.3) can be ignored. We then have $\eta \approx K/2ZC$. The parameter ZC represents the duration of discharge from the pump pulse generator.

It had been previously assumed [5] that pumping of an N_2 laser occurs only during the stage of the rapid fall of the voltage across the plasma. Therefore,

attempts were made to minimise only the inductance, L_d, in the circuit for discharging the peaking capacitor through the discharge gap (this inductance includes the contribution of the leads). It follows from our results that, in reality, the bulk of the pump energy is deposited near the maximum of the voltage across the plasma. According to expression (39.3), the efficiency η depends on the parameter, ZC. The pulse generators used to pump N_2 lasers are usually Blumlein lines, Fitch generators, or equivalent circuits with two oscillatory subcircuits of the type shown in Fig. 39.1a. Transfer of the maximum power and energy to the load requires that the capacitances in both cases are the same [11].

Under these conditions, we have $ZC \approx [2(L_\Sigma/C)]^{1/2}C = [2L_\Sigma C]^{1/2}$, where $L_\Sigma = L_g + L_d$ is the total inductance of the excitation circuit, L_g is the inductance of the pump-pulse generator, including the inductance of the discharge gap. It follows from expression (39.3) that, when C is reduced considerably, it is necessary to increase U_0. However, in the majority of cases this is not permissible, so that minimization of the total inductance, L_Σ, is of fundamental importance for a significant increase in η. Estimates based on expression (39.3) show that, for example, for an N_2 laser without SF_6, if the efficiency is to be $\eta \geq 0.5\%$, then for typical parameters W_{max} = 10 mJ and U_0 = 20 kV, it is necessary to ensure that $L_\Sigma \leq 1.5$ nH.

These conditions can be achieved in a Blumlein pulse generator with a multichannel pseudo-spark gap (charging voltage 10 kV, discharge current 15 kA, inductance 0.5 nH), similar to that described in [12]. If the active medium is then excited by a sliding discharge on the surface of an insulator [13] and if distilled water is used in the Blumlein line, it should be possible to achieve $L_\Sigma \approx 1.5$ nH. A further increase in the output radiation energy is possible only by increasing the charging voltage switched on by a discharge gap. In the majority of the traditional N_2 laser designs, the total inductance is $L_\Sigma \gg 1.5$ nH, which accounts for their low efficiency (e.g., for the circuit shown in Fig. 39.1a, we have $L_\Sigma = L_{2s} + L_3 = 113$ nH + 6 nH).

We shall conclude by considering the results reported in [14], where a description is given of an N_2 laser with a magnetic pump-pulse compression circuit and which (as stated by the authors of this investigation) delivered a UV radiation energy of 20 mJ with $\eta = 0.43\%$. If we use the data taken from [14] and expression (39.2), we can readily estimate the real efficiency to be less than 0.12%. The authors [14] attribute their very high radiation characteristics to reaching E/p = 170–200 V cm^{-1} Torr^{-1} (p_{N2} = 170–100 Torr) for an excitation circuit generating pulses with an ultrashort rise time ($\sim$10 ns). This was checked by us in an experiment in which the system used to pump the N_2 laser had two circuits performing magnetic compression of the pump pulses, similar to that described in [14]. This was achieved by supplementing the system in Fig. 39.1 with a C_3L_3 chain connected in series with the L_2 choke. The electric circuit is shown in Fig. 39.7. The saturable choke contained three ferrite cores, connected in parallel, with a total cross-sectional area S = 29 cm^2. The capacitances in this circuit were $C_1 = C_2$ = 20 nF, C_3 = 5 nF, and C_0 = 5 nF.

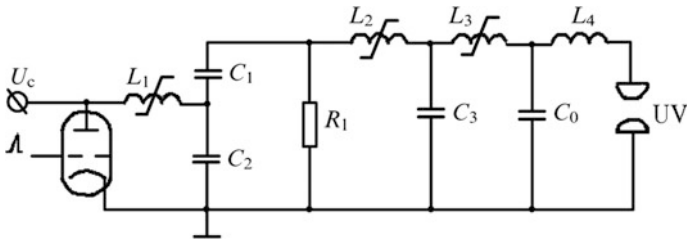

Fig. 39.7 Electric circuit of a laser with two magnetic loops for compression of voltage pulses

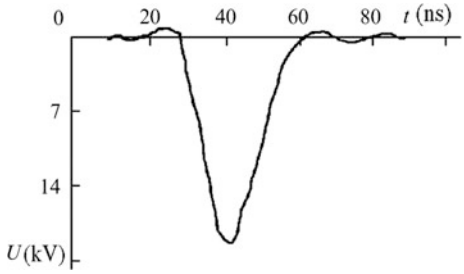

Fig. 39.8 Oscillogram of a voltage pulse across the gap for a discharge in N_2 (circuit in Fig. 39.7); p_{N2} = 50 Torr, U_c = 27 kV

Figure 39.8 shows a typical voltage pulse across the discharge gap. The rise time of this pulse did not exceed 20 ns, and the ratio E/p for the discharge was 170 V cm^{-1} Torr^{-1} (p_{N2} = 50 Torr). However, the need to use ferrite cores with a large cross-sectional area meant that we could not make L_{3s} (which was the inductance of the third circuit when L_3 was saturated) much less than L_{2s}. Moreover, the losses due to magnetic reversal in L_3 and the difference between the impulse capacitance, $C_1/2$, and the capacitance C_3 reduced the efficiency of energy transfer between them [11]. As a result, there was no significant increase in the pump power and in the output radiation energy when the circuit shown in Fig. 39.7 was used, instead of that given in Fig. 39.1a. The results obtained indicated that systems for magnetic compression of energy are not optimal for N_2 lasers because the chokes used in them have a fairly large winding inductance. In our opinion, the results given in [14] are overestimated and they require additional analysis.

It thus follows from our investigation that the ratio E_m/p for the discharge does not directly influence the N_2 laser characteristics. The laser efficiency depends on the parameters ZC, W_0, and P_{min}, where Z is the equivalent impedance of the excitation circuit, C is the equivalent capacitance of the high-voltage pulse generator, W_0 is the energy stored in this capacitance, and P_{min} is the threshold excitation power. The output radiation energy is proportional to the pump power released at the moment when the voltage across the plasma reaches its maximum value. The highest output energy is obtained at a gas pressure that ensures that pumping is matched and the voltage across the plasma is maximal.

References

1. J.P. Singh, S.N. Thakur, J. Sci. Ind. Res. **39**, 613 (1980)
2. A. Hariri, M. Tarkashvand, A. Karami, Meas. Sci. Technol. **1**, 659 (1990)
3. A.V. Martinez, V.I.E.E.E.J. Aboites, Quantum. Electron. **29**, 2364 (1993)
4. B. Godard, IEEE J. Quantum Electron. QE-10, **147** (1974)
5. G.A. Mesyats, V.V. Osipov et al., *Pulsed Gas Lasers* (Nauka, Moscow, 1991)
6. W.A. Fitzsimmons, L.W. Anderson, C.E. Riedhauser, J.M. Vrtilek, IEEE J. Quantum Electron. QE-12 624 (1976)
7. V.P. Ageev, V.V. Atezhev, V.S. Bukreev, S.K. Vartapetov, A.N. Zhukov, V.I. Konov, A.D. Savel'ev Zh. Tekh. Fiz. **56** 1387 (1986) [Sov. Phys. Tech. Phys. **31** 816 (1986)]
8. M.L. Lomaev, V.F. Tarasenko, V.S. VerkhovskiT, Elektron. Tekh Ser. **11**(1) 58 (1991)
9. S.N. Buranov, V.V. Gorokhov, V.I. Karelin, P.B. Repin, Kvantovaya Elektron. (Moscow) **17,** 161 (1990) [Sov. J. Quantum Electron. **20,** 120 (1990)]
10. B.P. Afanas'ev, O.E. Gol'din, I.G. Kolyatskin, G.Y. Pines, *Theory of Linear Electric Circuits* (Vysshaya Shkola, Moscow, 1973)
11. P. Persephonis, B. Giannetas, J. Parthenios et al., IEEE J. Quantum Electron. **29**, 2371 (1993)
12. G. Mechtersheimer, R.J. Kohler, Phys. E **20**, 270 (1987)
13. P.P. Bryzgalov, B.O. Zirkin, N.V. Karlov, I.O. Kovalev, A.V. Korablev, G.P. Kuz'min, Kvantovaya Elektron. Moscow **15**, 1971 (1988) [Sov. J. Quantum Electron. **18**, 1232 (1988)]
14. H. Seki, S. Takemori, T. Sato, IEEE J. Sel. Top. Quantum Electron. **1**, 825 (1995)

Part IV
Applications

Investigations of currents in close-to surface plasma, produced by CO_2-laser radiation of different temporal structure have been described in the chapter. The character of evolution of registered currents temporal structure at growing energy density was different when the target was irradiated in air and in vacuum by the train of short (τ = 2.5 ns) pulses. Experiments in vacuum have revealed that the transit from smooth single mode pulse to the nanosecond pulse train of the same total energy was followed by a considerable decrease in plasma formation energy thresholds and by the increase of amplitudes of currents induced by plasma. The current pulses from the target were registered after finishing the laser irradiation; their appearance was probably connected with cumulation effects, caused by the ring form of the irradiated area. Many phenomena accompaning the air optical breakdown (in particular the electric fields and currents arising in breakdown plasma) sufficiently depend on the temporal parameters of laser radiation. For example, utilization of two successive laser pulses results in considerable increase of the magnetic fields and currents.

The investigations of electric fields and currents in the air breakdown plasma produced by a train of CO_2 laser nanosecond pulses near the surface of uncharged metallic targets are presented. The breakdown thresholds as well as efficiency of plasma-target heat transmission for different temporal parameters of CO_2 laser radiation are measured and observed.

A technique for obtaining the repetitively pulsed operating regime in high-power wide-aperture lasers is proposed and was experimentally realized. In this regime, the laser emited a train of pulses with a duration of 100–150 ns and a pulse repetition rate of several tens of kilohertz. The main properties of the pulsed regime are theoretically analyzed and the proposed technique was tested in detail employing a test-bench gas-dynamic laser. The results of the test confirmed the conclusions of the theoretical analysis. The possibility of a repetitively pulsed regime in high-power wide-aperture lasers realization without significant reduction in the average output power was experimentally demonstrated.

Some very interesting applications of high energy molecular lasers with variable temporal structure of radiation are presented in this part. They include stimulation of a heterogeneous reactions; lasing of an He-Xe optical breakdown plasma; low-threshold generation of harmonics and X-ray radiation in the laser plasma; generation of submillimeter half-cycle radiation pulse; and subtraction of the CO_2 laser radiation frequencies in a $ZnGeP_2$ crystal.

Chapter 40
Stimulation of a Heterogeneous Reaction of Decomposition of Ammonia on the Surface of Platinum by CO_2 Laser Radiation

Abstract Stimulation of heterogeneous catalytic reactions involving decomposition of vibrationally excited ammonia molecules on the surface of platinum was observed after absorption of a CO_2 laser photon. This stimulated dissociation of $^{14}HN_3$ on Pt was attributed to the radiative excitation of the vibrational levels of the ammonia molecule.

The process of stimulation of heterogeneous processes by laser radiation has been reported in several recent papers [1–7]. Baklanov et al. [1] discovered acceleration of the reaction of chemical precipitation of bromine on the surface of germanium under the action of laser radiation. Other investigators [2, 3, 5, 6] studied the influence of the vibrational excitation of molecules on the physical adsorption and condensation at low temperatures. Isotope separation by physical adsorption and condensation of selectively excited molecules was studied in [2, 3, 6]. Stimulation of desorption and heterogeneous reactions by interaction of laser radiation with adsorbed molecules was discussed in [7]. The possibility of isotope separation by selective interaction of laser radiation with gas molecules participating in the heterogeneous catalytic reaction was highlighted by Borman et al. [4] According to these authors, the probability of overcoming a reaction barrier by a vibrationally excited molecule that reaches a catalyst surface after the adsorption of a photon may be greater than that of an unexcited molecule. Therefore, even at fairly low catalyst temperatures, laser irradiation may stimulate a heterogeneous catalytic reaction on the surface.

The present chapter describes experiments that resulted in our first observations of, stimulation of heterogeneous catalytic reactions by CO_2 laser radiation in the specific case of decomposition of ammonia on platinum.

The apparatus shown schematically in Fig. 40.1 was used. Ammonia in a cell was excited by a CO_2 laser pulse emitted as a result of the P(16) − P(24) transitions in the 00°1 − 10°0 band at the wavelength of 10.6 μ. The output energy of the laser (as supplied) was 0.5 J and the pulse duration at midamplitude was 150 ns. The energy was measured with a KDM calorimeter. The time characteristics of the radiation pulses were recorded using a Ge-Au detector (T = 77 °K) with a time

© Springer International Publishing Switzerland 2016

V.V. Apollonov, *High-Energy Molecular Lasers*,
Springer Series in Optical Sciences 201, DOI 10.1007/978-3-319-33359-5_40

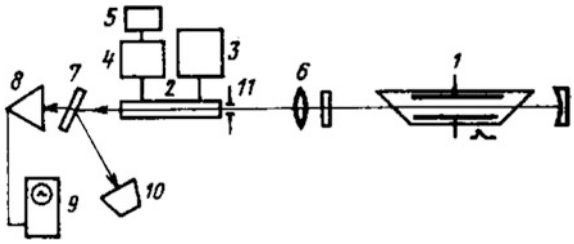

Fig. 40.1 Schematic diagram of the apparatus: transverse-discharge pulsed CO_2 laser (*1*); cell with a catalyst and investigated gas (*2*); vacuum system (*3*); IPDO-2A mass spectrometer (*4*); KSP-4 chart recorder (*5*); long-focus lens (*6*); BaF_2 plane-parallel plate (*7*); Ge-Au infrared radiation detector (*8*); S8-2 oscillograph (*9*); KDM calorimeter (*10*); stop (*11*)

resolution of $\sim 10^{-9}$ s and a S8-2 oscillograph with a pass band of 7 MHz. The laser radiation was directed to the ammonia cell by a long-focus lens (f = 55 cm). The cell was a glass tube whose internal diameter was d = 0.6 cm and whose length was 27 cm; the ends of the tube were closed by NaCl windows. The length and radius of the cell were selected to ensure sufficiently strong absorption at a given pressure and also that the inequalities $r \ll \tau_{VV}\bar{v}$ and $r \ll \tau_{VT}\bar{v}$ were satisfied (here, τ_{VV} and τ_{VT} are the VV and VT relaxation times, and $\bar{v}$ is the average velocity of a molecule). In fact, for a gas pressure in the cell p = 0.1 Torr and a temperature T = 250 °C, the results reported in [8, 9] indicated that $\tau_{VT} = 3 \times 10^{-5}$ s, $\tau_{VV} = 10^{-5}$ s, and $r/\tau_{VV}\bar{v} \approx 10^{-1}$ ($r = 3 \times 10^{-1}$ cm, $\bar{v} = 3 \times 10^{4}$ cm/s).

A catalyst was prepared by evaporating platinum on a thin (0.1 mm) copper foil, which fitted closely against the inner wall of the cell. The catalyst was heated by a Nichrome helix would on the cell surface.

We used an oil-free vacuum system to evacuate the cell and detector head of a mass spectrometer to 10^{-6} Torr. We used ammonia of natural isotopic composition. This ammonia was purified by repeated freezing in liquid-nitrogen traps.

An analysis of the composition of the gas mixture in the mass range from 1–50 was carried out using an IPDO-2A spectrometer. The detector of this spectrometer was additionally evacuated by an ion-sorption pump to 10^{-6} Torr. The investigated mixture of gases was admitted from the cell to the gas spectrometer at a pressure of 5×10^{-5} Torr. The spectra were recorded by means of an oscillograph and a KSP-4 recorder.

The absorption of the P(16) laser radiation of ν = 947.74 cm^{-1} frequency, corresponding to the P1* transition in NH_3, was measured with a KDM calorimeter. The initial ammonia pressure in the cell was within the range (8–15) $\times 10^{-2}$ Torr. At this pressure, the absorption was $\sim$0.2%. The absorption was low because the laser radiation frequency did not coincide exactly with the PI* transition of the ν_2 vibration of NH_3 and, moreover, the ammonia line itself was of low intensity. The alignment of the laser beam was such that the catalyst surface was not affected and it was assumed to be satisfactory if the irradiation of the cell, initially pumped to $p = 10^{-3}$ Torr, did not increase the pressure in 1 h.

A mass spectrum of the ammonia admitted to the cell is shown in Fig. 40.2a. The mass lines 2 and 15–17 represent the spectrum of the NH_3 molecule. The figure shows also the lines corresponding to H_2O and N_2, present in the residual gas ($p = 10^{-6}$ Torr) in the ion-source chamber of the IPDO-2A mass spectrometer. The spectrum of the reaction products of the decomposition of ammonia on platinum, whose temperature was kept at 400 °C for 2 h, is shown in Fig. 40.2b. The reduction of the ion-current peaks corresponding to the masses 15–17 demonstrates

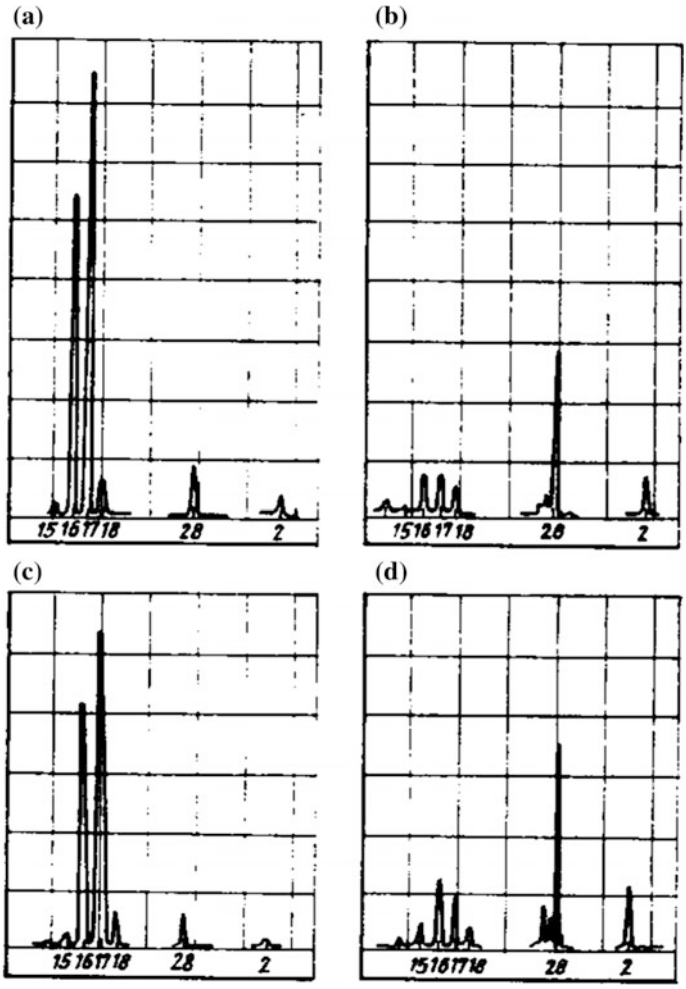

Fig. 40.2 Mass spectra of gases contained in a cell: **a** original ammonia, pressure in the ion-source chamber of the IPDO-2A mass spectrometer $p = 5.5 \times 10^{-5}$ Torr, catalyst temperature $T = 20$ °C; **b** $p = 3.8 \times 10^{-5}$ Torr, T = 400 °C; **c** $p = 4 \times 10^{-5}$ Torr; $T = 250$ °C; **d** $p = 4.2 \times 10^{-5}$ Torr, T = 250 °C

that ammonia is decomposed. It is clear from Fig. 40.2c that, within the limits of the experimental error (10%), the decomposition of NH_3 does not occur at 250 °C.

The mass spectrum of the products of the reactions stimulated by CO_2 laser radiation at the catalyst temperature of 250 °C is shown in Fig. 40.2d. The ammonia in the cell was subjected to CO_2 laser radiation for 20 min. The pulse repetition frequency was 0.4 Hz.

There was an increase in the pressure because of the reaction

$$2NH_3 \Leftrightarrow 3H_2 + N_2.$$

The occurrence of laser-radiation-stimulated decomposition of NH_3 on Pt was confirmed by the results of measurements of the pressure of the products determined after freezing with liquid nitrogen. Additional experiments indicated that the stimulated reaction occurred on the surface of platinum. In fact, when there was no foil with an evaporated platinum film or when platinum was replaced with copper, there was no decomposition of ammonia at $p = 0.1$ Torr and 250 °C. The mass spectra of the gases obtained in these cases were identical with the spectrum of the original ammonia. The absence of the reaction was also confirmed by the fact that the pressure of the reaction products that did not freeze was less than 10^{-3} Torr.

The dissociation of NH_3 in the gaseous phase investigated in [10] occurred when the laser radiation power density was $J > 10^{10}$ W/cm^2 and the ammonia pressure was $p = 10$ Torr, whereas in our experiments, the corresponding parameters were $J < 10^7$ W/cm^2 and $p = 0.1$ Torr.

Since we used CO_2 laser pulses ($t_p = 1.5 \times 10^{-7}$ s) and the ammonia pressure in the cell was $\sim$0.1 Torr (relaxation time $\tau_{VT} = 3 \times 10^{-5}$ s), we concluded that the decomposition of ammonia was stimulated because of radiative excitation of the vibrational levels. This conclusion was drawn from the results of an investigation of the mechanism of the excitation of the NH_3 molecule by CO_2 laser radiation reported in [11].

We shall consider a possible mechanism of stimulation of the decomposition of ammonia on platinum. The main stages of a heterogeneous catalytic reaction [12] are as follows: adsorption, formation of unstable compounds or complexes on the catalyst surface, dissociation of these compounds, and desorption of the reaction products. An increase in the rate of reaction because of CO_2 laser radiation occurs if the rate-limiting stage of the reaction is stimulated. According to [13], ammonia is chemisorbed on platinum in two forms: coordination-bound and dissociative. Infrared spectroscopy methods have established [13] that the absorption bands of NH_3 adsorbed on Pt disappear completely at temperatures above 250 °C and the intensity of the absorption bands corresponding to the NH_2 radicals formed as a result of dissociative adsorption increases. Thus, at 250 °C, the stimulation of the reaction of the NH_3 molecules results in preferential adsorption of the coordinate-bound form. On the other hand, it is shown in [14] that the decomposition of ammonia on platinum at $T > 400$ °C occurs as a result of dissociative adsorption of NH_3 in accordance with the scheme:

$$\begin{aligned} NH_3 &= NH_{2_{ads}} + H_{ads}; \\ NH_{2_{ads}} &= NH_{ads} + H_{ads}; \\ NH_{ads} &= N_{ads} + H_{ads}; \\ 2N_{ads} &= N_2; \\ 2H_{ads} &= H_2. \end{aligned}$$

When the catalyst temperature is $T = 250$ °C so that the adsorption is of the coordination type, there is no decomposition of NH, on Pt. The activation energy of the dissociative adsorption is $E_a = 5.1$ kcal/mol [14]. Since the coordination adsorption of NH_3 occurs at much lower temperatures, it is reasonable to assume that the activation energy of the coordination adsorption is $E_a < E_a$. Then, if the energy of a laser photon hv is of the order $E_a - E_a$, even one photon is sufficient to stimulate the dissociation of ammonia on platinum (if the CO_2 laser photon energy hv corresponds to 2.67 kcal/mol). Thus, under our conditions at 250 °C, the first rate-limiting stage of the decomposition reaction, which is the adsorption of ammonia on platinum, is stimulated.

Our estimates demonstrate that stimulation of the catalytic reaction of decomposition of ammonia cannot be explained by local heating as suggested in [3], This is due to the fact that under chemisorption conditions, the binding energy is much higher than the energy of a vibrational quantum (40 kcal/mol) and the thermal diffusivity is $a = 1$ cm^2/s. Local heating of the surface because of the interaction with vibrationally excited molecules takes place only under physical adsorption conditions at low temperatures. The energy is then transferred to the physically adsorbed layer because of the exchange interaction (see, for example, [15]). Such systems are characterized by $hv \approx Q$ (Q is the adsorption energy) and a low value of the thermal diffusivity ($a = 10^{-2}$ cm^2/s), which localizes the heat evolved on the wall and stimulates desorption.

References

1. M.R. Baklanov, I.M. Beterov, S.M. Repinskii et al., Dokl. Akad. Nauk USSR **216**, 524 (1974)
2. K.S. Gochelashvili, N.V. Karlov, A.N. Orlov, R.P. Petrov, YuN Petrov, A.M. Prokhorov, JETP Lett. **21**, 302 (1975)
3. N.G. Basov, E.M. Belenov, V.A. Isakov, Yu.S. Leonov, E.P. Markin, A.N. Oraevskii, V.I. Romanenko, N.B. Ferapontov, JETP Lett. **22**, 102 (1975)
4. V.D. Borman, B.I. Nikolaev, V.I. Troyan, At. Energ. **40**, 69 (1976)
5. Yu.V. Brzhazovskii, Yu.S. Kusner, A.K. Rebrov, B.I. Troshin, V.P. Chebotaev, JETP Lett. **23**, 260 (1976)
6. N.V. Karlov, A.M. Prokhorov, Sov. Phys. Usp. **19**, 285 (1976)
7. V. I. Gol'danskii, V. A. Namiot, and R. V. Khokhlov, Sov. Phys. JETP 43, 1226 (1976)
8. R.V. Ambartsumyan, V.S. Letokhov, G.N. Makarov, A.A. Puretskii, Sov. Phys. JETP **41**, 871 (1975)
9. H.E. Bass, T.G. Winter, J. Chem. Phys. **56**, 3619 (1972)
10. J.D. Campbell, G. Hancock, J.B. Halpem, K.H. Welge, Opt. Commun. **17**, 38 (1976)

11. R.V. Ambartsumyan, V.S. Letokhov, G.N. Makarov, A.G. Platova, A.A. Puretskii, O.A. Tumanov, Sov. Phys. JETP **37**, 392 (1973)
12. J.M. Thomas, W.J. Thomas, *Introduction to the Principles of Heterogeneous Catalysis* (Academic Press, New York, 1967)
13. D.V. Pozdnyakov, V.N. Filimonov, Kinet. Katal. **13**, 522 (1972)
14. L.O. Apel'baum, M.I. Temkin, Zh. Fiz. Khim. **33**, 2697 (1959)
15. Y.M. Gershenzon, V.B. Rozenshtein, S.Y. Umanskii, Preprint (Institute of Chemical Physics, Academy of Sciences of the USSR, Moscow, 1976)

Chapter 41
Influence of the Pumping Regime on Lasing of an He-Xe Optical-Breakdown Plasma

Abstract An experimental investigation was carried out into lasing of an optical-breakdown plasma in an He-Xe gas mixture exposed to CO_2 laser radiation. A wide range of pump pulse energies and durations and active mixture pressures were used. Lasing was realized on four Xe I transitions (λ = 2.03, 2.65, 3.4, and 3.65 μm). The pump pulse duration was found to exert a strong influence on the lasing characteristics of the optical breakdown plasma. The role of gas-dynamic processes in the interaction of the CO_2 laser radiation, with the gas close to a target during the buildup of inversion, was analysed. A quasi-cw lasing regime of the recombination laser in the optical breakdown plasma was observed.

41.1 Introduction

Special attention is currently being given to the development of new principles for the design of ultraviolet and X-ray lasers. One of the most promising approaches is based on the use of a nonequilibrium intensely recombining plasma as the active medium [1]. Along with the possibility of advancing into the short wavelength region, a recombination pumping system allows creation of an active medium with a high gain in the infrared and visible regions. However, it is quite difficult to realize it experimentally since the plasma has to be strongly supercooled.

One of the methods for creating the active medium of a recombination laser is to cool an optical breakdown plasma during its expansion. This method is convenient in laboratory investigations since an optical breakdown makes it possible to readily obtain plasmas of different chemical and ion compositions.

Infrared recombination lasers utilizing rare-gas transitions pumped in an optical-breakdown plasma produced by CO_2 laser radiation were described in [2, 3]. The experimental conditions in these studies differed mainly in the duration of the CO_2 laser radiation pulses (in [2] a pulse consisted of an initial 70 ns duration spike and a $\sim$1 μs tail, while in [3] it has a bell-shaped profile of overall duration $\sim$250 ns) and in respect of the specific pump energy (E_p/l = 1 and 2.5 J/cm respectively in [2, 3], where l is the length of the active medium of the plasma

© Springer International Publishing Switzerland 2016

V.V. Apollonov, *High-Energy Molecular Lasers*,
Springer Series in Optical Sciences 201, DOI 10.1007/978-3-319-33359-5_41

laser). However, despite the fact that lasing in these studies was due to identical transitions obtained for identical compositions of the active mixture, there were considerable differences between the experimental results. This applies, first of all to the dependence of the He-Xe laser output power on the pressure of the active mixture and, secondly, to the spatial localization of the lasing region. It is natural to assume that the discrepancies between the results reported in [2, 3] were due to the differences in the shape and duration of the pump pulses.

In the present work, the characteristics of an He-Xe laser were investigated in a wide range of pumping conditions (the energy E_p, the pulse duration τ_p, and the active mixture gas pressure p were all varied), including those of [2, 3].

41.2 Apparatus

Figure 41.1 shows a schematic diagram of the apparatus. A CO_2 laser described in [4] was used. The duration of its output pulses could be varied. The laser radiation beam aperture was rectangular with dimensions of 5 × 4 cm. The radiation power density distribution over the cross section of the beam was homogeneous, with an accuracy of 15%. The CO_2 laser radiation pulse shape was recorded with an FP-3 photodetector with a temporal resolution of ~3 ns. The CO_2 laser radiation was focused with a BaF_2 cylindrical lens L (F = 14 cm) onto the surface of an aluminum target M to form a 0.8 mm wide strip with a length of l = 35 mm. The 0.6 m long plasma laser resonator was formed by plane (R_2) and spherical (R_1, R = 5 m) dielectric mirrors made of LiF with reflection coefficients of 95 and 99%, respectively. The vacuum chamber was filled with an He:Xe = 1000:1 gas mixture. This gave the maximum output power in the present work, as it did in the work reported in [2, 3]. The pressure in the chamber was varied in the range 0.1–1 atm. The plasma laser radiation was recorded with a Ge:Au photodetector having a temporal resolution of ~0.1 μs. The spectral composition of the radiation was investigated with an MDR-4 monochromator fitted with a 100 line/mm diffraction grating. The

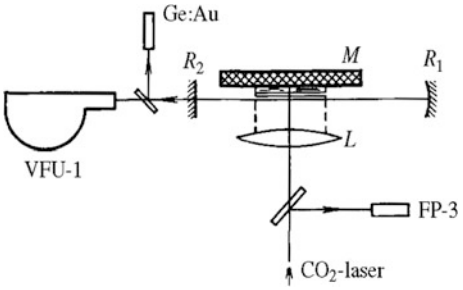

Fig. 41.1 Schematic diagram of the apparatus

dynamics of the expansion of a plasma jet was studied with a VFU-1 high-speed camera.

41.3 Experimental Results

Lasing was obtained for four Xe I transitions: = 2.03, 2.65, 3.4, and 3.65 μ. Since the dependences obtained at all the wavelengths were of an identical nature, the results are given below for λ = 2.03 μ, for which the output power of the He-Xe laser was the highest. Figure 41.2 gives streak photographs of the plasma jet luminescence and oscillograms of the CO_2 and He-Xe laser emission pulses. It can be seen that an increase in the duration of the pump pulses altered the nature of the plasma jet expansion. Under the conditions of the present experiment, the pump radiation intensity q_p slightly exceeded or was less than the threshold intensity q_{OD} for the onset of the optical detonation regime, the magnitude of q_p decreasing with increasing τ_p. Thus, for example, for a mixture at atmospheric pressure and τ_p = 250 ns, 2.5, and 5.2 μs (see Fig. 41.2), q_p had values of respectively 40, 20, and 5 MW/cm^2, whereas the threshold intensity was $q_{OD} \sim 20$ MW/cm^2. It was established that, in the range of pump energies E_p in which lasing was observed from the He-Xe laser, there were three characteristic ranges of the parameter, τ_p, differing with regard to the regimes of plasma jet expansion. For $\tau_p < 300$ ns, we observed the optical detonation regime; for $\tau_p > 4.5$ μs the "laser plasmatron" regime [5]; and for $0.3 < \tau_p < 4.5$ s the optical detonation regime on the spike of the pump pulse and the laser plasmatron regime on its tail. This pattern of behavior remained the same over the whole range of E_p values.

It was established that, depending on E_p and on the pressure of the active mixture, lasing occurred in a certain range of distances Δh from the target. Increasing E_p or decreasing p caused the lasing region to recede from the target. Such a displacement of the lasing region was observed over the entire range of variation of τ_p. Figure 41.3 gives the dependences of the He-Xe laser output power on the distance h from the target for different values of E_p/l and p, but constant τ_p = 2.5 μs. It can be seen that on increasing E_p/l from 1.4 to 2.5 J/cm or on

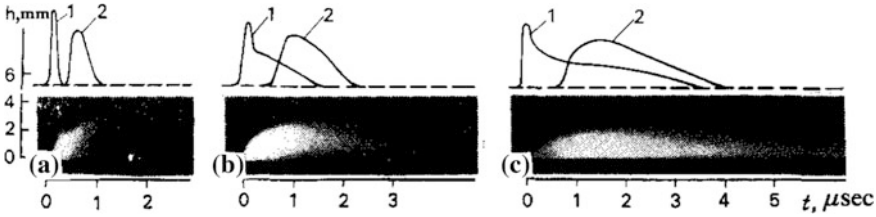

Fig. 41.2 Streak photographs of an expanding plasma jet and oscillograms of the pulses emitted by CO_2 (*1*) and He-Xe lasers (*2*) recorded for τ_p = 250 ns (**a**), 2.5 μs (**b**), and 5.2 μs (**c**). The position of the optic axis of the He-Ne laser resonator is shown by the *dashed line*

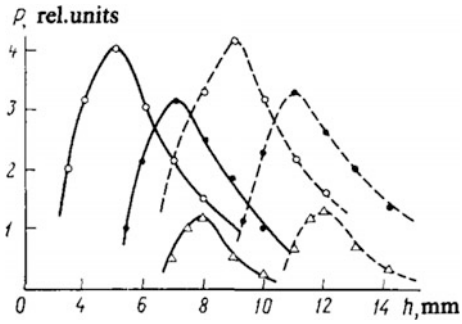

Fig. 41.3 Dependences of the He-Xe laser output power, P, on the distance, h, between the optic axis of the resonator and the target plotted for $p = 1$ (O), 0.5 (•), and 0.25 atm (Δ); $E_p/l = 1.3$ (*continuous curves*) and 2.3 J/cm (*dashed curves*)

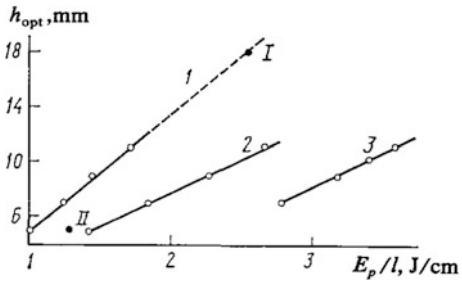

Fig. 41.4 Dependences of h_{opt} on the specific pump energy E_p/l plotted for τ_p = 250 ns (*curve 1*), 2.5 μs (*curve 2*), and 5.2 μs (*curve 3*)

decreasing p from 1 to 0.25 atm, the distance h_{opt} corresponding to the maximum plasma laser power increased from 5 to 9 mm, the magnitude of Δh being ~5 mm.

The dependences h_{opt} (E_p/l) for $p = 1$ atm and different values of τ_p are shown in Fig. 41.4. For the short pump pulses (τ_p = 250 ns), h_{opt} rose with increasing E_p/l more rapidly than for large τ_p values. The minimum values of h_{opt} in Fig. 41.4 correspond to the threshold pump energies $E_{p,th}$. Increasing τ_p led to a rise in $E_{p,th}/l$ from 0.95 J/cm (for τ_p = 250 ns) to 2.75 J/cm (for τ_p = 5.2 μs). Also plotted in Fig. 41.4 are the points I and II corresponding to the experimental conditions of the work reported in [2, 3], where the dependences h_{opt} (E_p/l) were not investigated. It can be seen that these points are in satisfactory agreement with the graphs obtained in the present study.

Figure 41.5 gives the dependences of the He-Xe laser output power on the pressure of the active mixture. The nature of the function $P(p)$ depended strongly on the duration of the CO_2 laser pulses. For τ_p = 250 ns, $P(p)$ had a maximum at p = 0.5 atm, whereas for τ_p = 5.2 μs a monotonic rise in the intensity with increasing pressure was observed in the investigated range of p. For τ_p = 2.5 μs, $P(p)$ reached saturation at p = 1 atm. It must be mentioned that all the graphs in Fig. 41.5 were plotted taking into account the dependences $h_{opt}(P)$.

Figure 41.6 shows the dependences of the duration t_L of the He-Xe laser emission pulses on the pump pulse duration τ_p, obtained for different pressures of the active mixture. An increase in τ_p from 250 ns to 5.2 μs led to a monotonic rise in t_L from 250 ns to 5.5 μs (at the 10% power level) for p = 1 atm. At the same

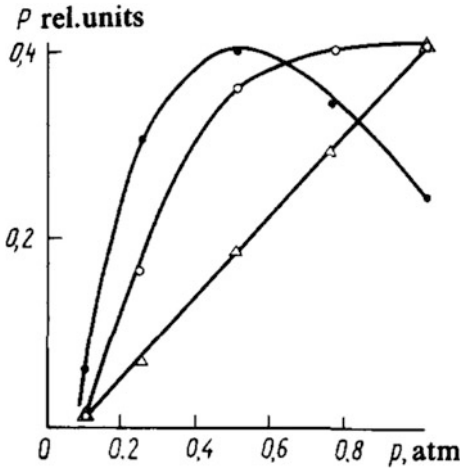

Fig. 41.5 Dependences of the He-Xe laser output power, P, on the active mixture pressure, p, obtained for τ_p = 250 ns (•); 2.5 μs (O); and 5.2 μs (Δ); E_p/l = 0.9 (•); 1.4 (O); and 2.9 J/cm (Δ)

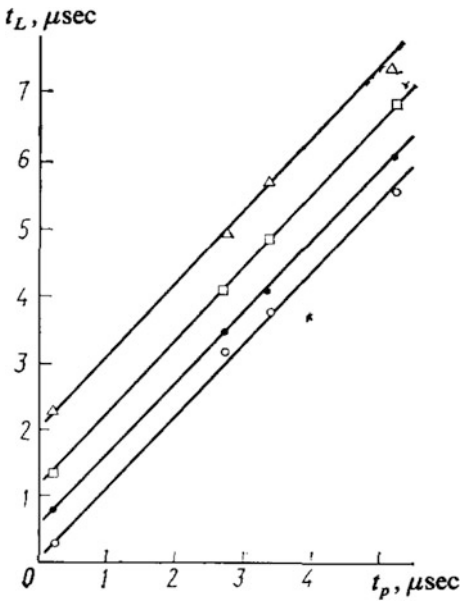

Fig. 41.6 Dependences of the He-Xe laser emission pulse duration t_L on the pump pulse duration τ_p obtained for p = 1 (O); 0.75 (•); 0.5 (O); and 0.25 atm (Δ)

time, a reduction of p from 1 to 0.25 atm at a constant value of τ_p caused an increase in t_L of 2 μs, with the nature of the dependence $t_L(\tau_p)$ remaining the same. The value of t_L was measured at $h = h_{\text{opt}}$.

Figure 41.7 gives oscillograms of the He-Xe laser output pulses obtained for different E_p values (h = const). An increase in E_p at first led to a distortion of the pulse shape and formation of dips, and then to suppression of lasing. When h was

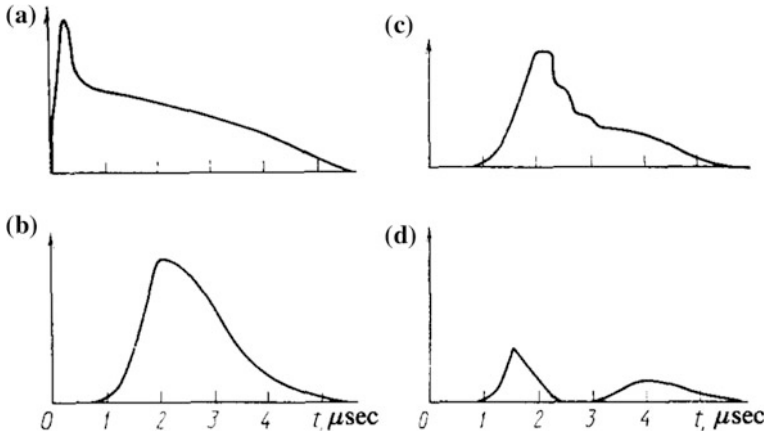

Fig. 41.7 Formation of dips in an He-Xe laser emission pulse: oscillograms of the CO_2 (**a**) and He-Xe (**b**–**d**); laser pulses for E_p/l =1.4 (**b**), 1.7 (**c**), and 2.4 J/cm (**d**)

increased, a similar pattern was repeated at higher values of E_p. It is worth mentioning that behavior of this kind is typical of long pump pulses.

The active medium gain was determined for τ_p = 2.5 μs and an He-Xe mixture at atomospheric pressure. Its value reached 0.1 cm^{-1}, the minimum length of the active medium for which lasing was still observed as being 0.4 cm.

41.4 Discussion of Results

In order to explain the results obtained, it is necessary to consider the gas-dynamic processes that take place when the CO_2 laser radiation interacts with the gas near the target.

The investigations that we carried out made it possible to distinguish (see Fig. 41.2) two main regimes of jet expansion. These are the optical detonation regime (Fig. 41.2a) characterized by adiabatic plasma cooling and the slower laser plasmatron regime (Fig. 41.2b) with two-dimensional plasma expansion from a hot dense nucleus located on the target and its cooling by collisions with the buffer gas [5]. Lasing appears in the He-Xe laser after a delay of >1 μs relative to the instant of gas breakdown. It is natural to relate this to the plasma cooling time. The displacement of the lasing region on varying E_p is a consequence of the dependence of the plasma cooling time on its initial temperature, T_0. The considerable increase in h_{opt} on decrease in p demonstrates the dominant role of collisional plasma cooling, which is more effective at elevated pressures. From the streak photographs of the plasma jet luminescence (see Fig. 41.2), it can be seen that the region where the pump radiation is absorbed and that where lasing takes place are a large distance apart. Therefore, even in the case of the optical detonation regime, supersonic

plasma expansion characterized by adiabatic cooling terminates at a considerable distance from the lasing region. Thus, in all the plasma expansion regimes, plasma cooling mainly occurs as a result of collisions with the buffer gas.

At the same time, the conditions for the pump energy absorption close to the target exert an influence on the rate of rise of h_{opt} when E_p/l is increased (see Fig. 41.4). The larger value of $dh_{\mathrm{opt}}/d(E_p/l)$ in the case of the optical detonation regime, compared with that in the laser plasmatron regime, is determined by the faster rise in the plasma temperature [6].

An increase in the duration of the pump pulse reduces the role played in the processes of inversion by the initial spike. This follows from the identical slope of curves 2 and 3 in Fig. 41.4. It is also clear from Fig. 41.4 that the discrepancy between the results in [2, 3] regarding the localization of the lasing region follows from the dependence $h_{\mathrm{opt}}(E_p/l)$ discovered in the present work.

As assumed, the pump pulse duration exerts a considerable influence on the nature of the dependence $P(p)$ (see Fig. 41.5). The maximum of $P(p)$ for $\tau_p = 250$ ns, which was recorded in the present work, is in good agreement with the dependence $P(p)$ obtained in [3]. At the same time, the difference between $P(p)$ in [2] and in the present work (for similar pumping conditions) is evidently due to the fact that the displacement of the lasing region on varying p (see Fig. 41.3) was not taken into account in [2]. It is also worth noting that the limitation in the He-Xe laser output power on increase in the pressure of the active mixture (for $\tau_p < 4.5$ μs) cannot be explained by the appearance of a supersonic radiation wave, [7, 8] as proposed in [3], since no such wave was observed in the present work over the range of pump intensities investigated.

In view of the considerable spatial separation of the regions of pump energy absorption and lasing of the plasma laser (see Figs. 41.2 and 41.4) the plasma entering the lasing region is transparent to the CO_2 laser radiation and does not interact with it. A lasing regime is thus realized in a recombining optical-breakdown plasma in which the plasma formed near the surface of the target during a pump pulse continuously replenishes the lasing region as it expands (quasi-cw lasing regime).

The appearance of dips in the laser emission pulses of the plasma laser can be explained by taking into account the dependence of the distance h between the target and the lasing region on the initial temperature T_0 of the plasma formed in the vicinity of the target (see Figs. 41.3 and 41.4). The nature of plasma heating by CO_2 laser radiation pulses consisting of a short high-power initial spike and a prolonged tail depends both on the maximum intensity q_p in the spike and on the ratio of the intensities in the spike and in the tail of the pump pulse [9, 10]. For low values of q_p, plasma heating by the radiation in the tail of a CO_2 laser pulse becomes important. The value of T_0 can then reach its maximum in the tail of the pump pulse. The lasing region is also displaced in accordance with the time variation of T_0. Depending on the ratio of this displacement to the dimensions of the He-Xe laser resonator caustic, dips and other distortions of the laser emission pulse shape can appear.

Our investigation of the characteristics of an He-Xe laser was made in a wide range of pumping conditions. It was established that an increase in the duration of the pump pulses reduced the contribution made by the spike in a CO_2 laser radiation pulse in the formation of inversion in the plasma. It was shown that the distance from the target at which the maximum laser emission power was observed depended on the pump energy and on the pressure of the active mix. A quasi-cw lasing regime was discovered in the recombination laser using an optical-breakdown plasma.

References

1. L.I. Gudzenko, S.I. Yakovlenko, *Plasma Lasers* (Atomizdat, Moscow, 1978)
2. W.T. Silfvast, L.H. Szeto, O.R. Wood II, J. Appl. Phys. **50**, 7921 (1979)
3. V.A. Danilychev, V.D. Zvorykin, I.V. Kholin, AYu. Chugunov, Sov. J. Quantum Electron. **12**, 58 (1982)
4. V.V. Apollonov, N. Akhunov, S.I. Derzhavin et al., Sov. J. Quantum Electron. **13**, 1284 (1983)
5. A.I. Barchukov, F.V. Bunkin, V.I. Konov, A.A. Lyubin, Sov. Phys. JETP **39**, 469 (1974)
6. Y.P. Raizer, Laser-Induced Discharge Phenomena (Consultants Bureau, New York, 1977)
7. I.E. Markovich, I.V. Nemchinov, A.I. Petrukhin, YuE Pleshanov, V.A. Rybakov, Sov. J. Plasma Phys. **5**, 560 (1979)
8. V.I. Fisher, Sov. Phys. Tech. Phys. **28**, 1312 (1983)
9. V.A. Danilychev, V.D. Zvorykin, Tr. Fiz. Inst. Akad. Nauk. SSSR **142**, 117 (1983)
10. V.P. Ageev, S.G. Burdin, V.I. Konov, S.A. Uglov, N.I. Chapliev, Sov. J. Quantum Electron. **13**, 483 (1983)

Chapter 42
Formation of the Active Medium in Lasers with Rare-Gas Mixtures Pumped by Optical Breakdown

Abstract A study was carried out into the parameters of the active media of lasers utilizing He–Xe (λ = 2.03 and 2.65 μm) and He–Ar (λ = 1.79 μm) mixtures of gases pumped by optical breakdown due to exposure to CO_2 laser radiation. Lasing was found to be the result of the combined effects of ultraviolet radiation and of a shock wave formed because of optical breakdown.

Optical breakdown is attractive as the means for pumping active media of lasers because it should make it possible to generate stimulated radiation in the far ultraviolet. Lasers pumped by optical breakdown and emitting infrared and visible radiation are already known [1–4]. Nevertheless, the mechanisms responsible for a population inversion in active media of this kind have not been investigated sufficiently thoroughly. For example, it is concluded in [1, 2, 4] that a population inversion in lasers utilizing rare-gas mixtures is established in a recombining optical breakdown plasma as it expands into the surrounding buffer gas. However, detailed investigations of the parameters of the active media that might confirm this mechanism have not yet been carried out.

We carried out an investigation into the mechanisms of a population inversion in lasers utilizing rare-gas mixtures pumped by optical breakdown. We carried out interferometric and spectroscopic investigations of the parameters of the active media of He–Xe (λ = 2.03 μ) and He–Ar (λ = 1.79 μ) lasers.

Our apparatus (Fig. 42.1) was described in [4, 5]. In the present experiments, the length of a plasma strip l was increased to 9 cm. The parameters of the active media were investigated by the method of two-exposure holographic interferometry. The source of light in the interferometer was a ruby laser emitting pulses of $\tau \sim 20$ ns duration. Interferograms of the laser plasma were recorded after various delays, Δt, relative to the moment of the appearance of optical breakdown near a target.

A comparison of the parameters of the plasma laser with the results of an interferometric investigation of its active medium indicated that lasing began at the moment of arrival of a shock wave in the region of the caustic of the resonator, although the optical breakdown plasma did not reach the lasing zone and could not therefore participate directly in the observed population inversion.

© Springer International Publishing Switzerland 2016

V.V. Apollonov, *High-Energy Molecular Lasers*,
Springer Series in Optical Sciences 201, DOI 10.1007/978-3-319-33359-5_42

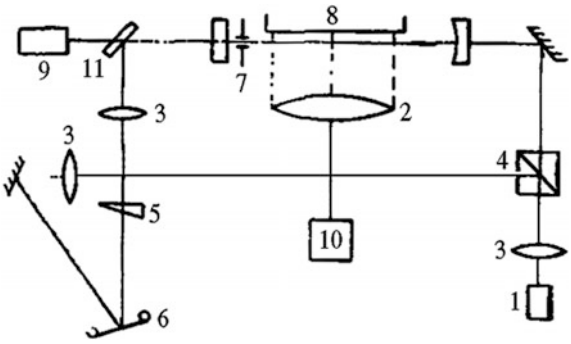

Fig. 42.1 Schematic diagram of the apparatus: ruby laser (*1*); cylindrical lens (*2*); focusing optics (*3*); beam splitter (*4*); wedge (*5*); photographic plate (*6*); stop with an aperture 1 mm in diameter (*7*); aluminum target (*8*); Ge:Au detector (*9*); CO_2 laser (*10*); LiF plate (*11*)

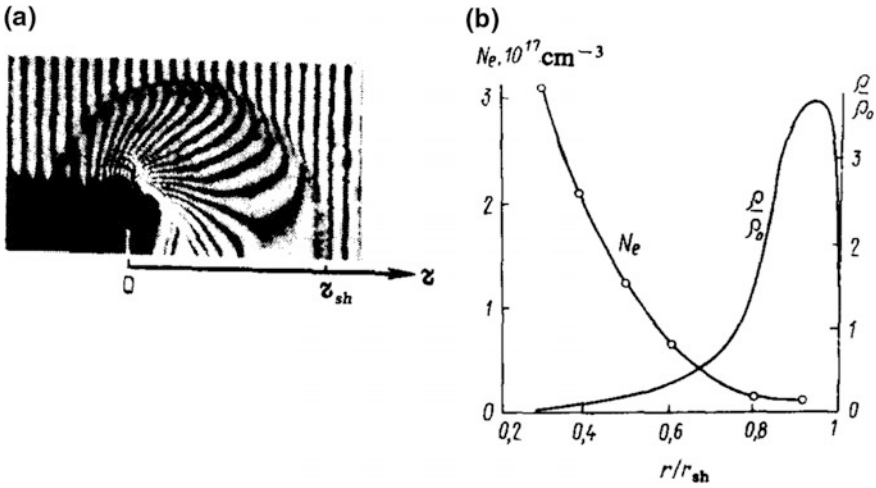

Fig. 42.2 Interferogram of an optical breakdown plasma formed in an He–Xe gas mixture [τ_p (CO_2) = 300 ns, Δt = 1 μs] (**a**); Dependences of the electron density N_e and of the relative density of heavy particles ρ/ρ_0 on the distance r to the target deduced from this interferogram (**b**)

The experimentally determined time dependences of the shock-wave radius obtained in the present study were in good agreement with the model of a cylindrical point explosion. [6] This made it possible to analyze the interferograms, thus allowing for the contribution of heavy particles to the plasma refraction and also to find the shock wave parameters. Figure 42.2 shows an interferogram obtained at Δt = 1 μs, corresponding to the beginning of a pulse emitted by the plasma laser and the distributions of the electron density N_e and of the gas density ρ calculated from this interferogram. The low temperature of the gas behind the shock-wave front $T_g \sim 0.2$ eV indicated that the shock wave could not be the direct source of

pumping of the active medium and particularly could not be responsible for the high electron density $N_e \sim 10^{16}$ cm^{-3}.

It is well known that in lasers utilizing gas mixtures containing helium the formation of an active medium results from the Penning reaction of the active atoms with excited helium, [7] for example:

$$He^* + Xe \xrightarrow{K_p} Xe^+ + He + e.$$

The rate of the Penning reaction $R = K_p/N_{He*}N_{Xe}$ depends on the gas temperature [7, 8] and on the concentrations N_{He*} and N_{Xe} of the particles participating in the reaction. The presence of excited atoms ahead of the shock-wave front was confirmed in our experiments by the emission of the lines of He I, Xe I, and Xe II. In particular, these atoms could form as a result of diffusion of resonant ultraviolet radiation [6] from the hot core of the optical breakdown plasma. The long delay of lasing indicated that the inversion involved atoms in excited states characterized by long lifetimes.

On arrival of a shock wave, an increase in the concentration of the interacting particles (degree of compression) $\eta = \rho/\rho_0 \leq 4$ and heating the gas to a temperature $T_g \sim 0.2$ eV increased the Penning reaction rate sharply. A direct confirmation of the occurrence of this reaction was provided by the absorption of a low-intensity tail of a CO_2 laser radiation pulse by the shock-wave front (Fig. 42.3a) in He–Ar and He–Xe gas mixtures. Such absorption of CO_2 laser radiation was not observed in a similar situation when pure He was employed (Fig. 42.3b). In view of the high concentration of He (He:Xe = He:Ar = 1000:1, $p \sim 1$ atm), the electrons colliding with helium atoms were cooled to the gas temperature in a time $\tau_{coll} \leq 10$ ns. A supercooled plasma with $T_e \sim T_g \sim 0.2$ eV and $N_e \sim 10^{16}$ cm^{-3} was formed,

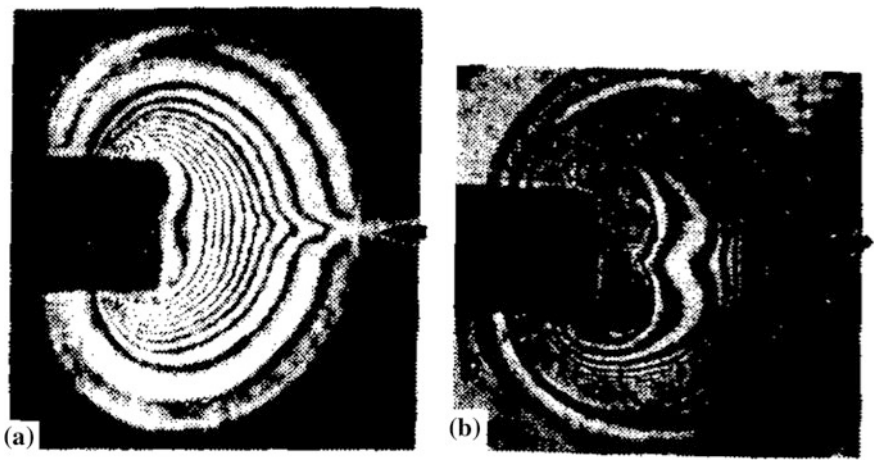

Fig. 42.3 Interferograms of an optical breakdown plasma in an He–Xe mixture (**a**) and in pure He (**b**) pumped by CO_2 laser radiation pulses of τ_p (CO_2) = 3 μs duration. The arrow on the right shows the direction of propagation of CO_2 laser radiation

and a recombination-type pumping occurred in this plasma [$\tau_{rec} \leq$ 5 ns, where $\tau_{rec} \propto (T_e^{-9/2} N_e^2)^{-1}$] [9].

It should also be highlighted that lasing was observed at a fixed distance (for given conditions) from the axis of the plasma strip along any generator of the cylindrical shock-wave front (Figs. 42.2 and 42.3). This was evidence of the cylindrical symmetry of the physical conditions and could be regarded as a confirmation of the validity of using the model of a cylindrical point explosion.

This mechanism of formation of an active medium was confirmed by experiments in which the gas mixture was additionally illuminated with ultraviolet radiation from a spark electric discharge. In the presence of this radiation, which was applied simultaneously with the appearance of optical breakdown, the threshold energy of CO_2 laser radiation, which was still capable of maintaining lasing in an He–Xe mixture decreased considerably [by a factor of 1.5 when the energy deposited in the discharge was $E_d \sim E_p$ (CO_2) $\sim$ 4 J]. The delay between the moments of appearance of optical breakdown and lasing was practically unaffected. Therefore, ultraviolet radiation of the plasma did indeed play a considerable role in the formation of an active medium. The long delay $\Delta t \sim 1$ μs and the fact that the delay was the same in the presence of additional ultraviolet radiation indicated that the population inversion was established under conditions of compression of the gas mixture by the shock wave.

Our experiments therefore demonstrated that lasing in mixtures of rare gases pumped by optical breakdown was due to the combined influence of ultraviolet radiation and a shock wave on the gas mixture. The proposed lasing mechanism accounted for the experimental dependences reported in [1, 2, 4].

References

1. W.T. Silfvast, L.H. Szeto, O.R. Wood II, J. Appl. Phys. **50**, 7921 (1979)
2. V.A. Danilychev, V.D. Zvorykin, I.V. Kholin, AYu. Chugunov, Sov. J. Quantum Electron. **12**, 58 (1982)
3. O.R. Wood II, J.J. Macklin, W.T. Silfvast, Appl. Phys. Lett. **44**, 1123 (1984)
4. V.V. Apollonov, F.V. Bunkin, S.I. Derzhavin, A.M. Prokhorov et al., Sov. J. Quantum Electron. **14**, 1178 (1984)
5. V.V. Apollonov, N. Akhunov et al., Sov. J. Quantum Electron. **13**, 1284 (1983)
6. Y.B. Zel'dovich, Y.P. Raizer, *Physics of Shock Waves and High Temperature Hydrodynamic Phenomena,* 2 vols., (Academic Press, New York, 1966, 1967)
7. Collection: *Plasma in Lasers* [in Russian], (Energoizdat, Moscow, 1976)
8. A.V. Eletskii, B.M. Smirnov, *Physical Processes in Gas Lasers* (Energoatomizdat, Moscow, 1985)
9. L.I. Gudzenko, S.I. Yakovlenko, *Plasma Lasers* (Atomizdat, Moscow, 1978)

Chapter 43
Low-Threshold Generation of Harmonics and Hard X-Ray Radiation in Laser Plasma

Abstract This chapter features an investigation of the generation of hard X-ray radiation possessing multi-spike structure (HXRMS) in a CO_2-laser plasma observed at low intensity of the heating radiation. In the first part of the work, the possibility of applying the principle of low-threshold ($q < 10^{10}$ W/cm^2) generation of hard X-ray radiation (HXR) in single-spike operation resulting from the development of parametric instability (PI) in a homogeneous plasma with the characteristic size L > 1.3 mm was shown experimentally. The schematic of the set-up, plasma parameters and estimates of laser radiation intensity are presented in this chapter.

In this chapter, generation of hard X-ray radiation possessing multi-spike structure (HXRMS) in a CO_2-laser plasma observed at low intensity of the heating radiation is investigated. In the first part of the work, the possibility of applying the principle of low-threshold ($q < 10^{10}$ W/cm^2) generation of hard X-ray radiation (HXR) in single-spike operation resulting from the development of parametric instability (PI) in a homogeneous plasma with the characteristic size L > 1.3 mm was shown experiementally. The schematic of the set-up, plasma parameters and estimates of laser radiation intensity are presented in this chapter.

43.1 Experimental Results and Discussion

The present experiments were carried out with the use of plane targets made of various materials, such as polyethylene-$(CH_2)_n$, aluminum and tungsten. The basic experiments were conducted with the use of an aluminum target. For the purpose of investigeting the HXRMS generation, first discussed in [1, 2], it was essential that the energy distribution in the pulse of CO_2-laser gain switch generation (GSG) and its time structure should be controlled. The simpliest method, the way of varying the CO_2-laser active medium operating mixtures, was chosen in this study. The mixtures of gases of the CO_2:N_2:He = 1:3:6, 1:1:3, 3:1:6 compositions were used.

© Springer International Publishing Switzerland 2016

V.V. Apollonov, *High-Energy Molecular Lasers*,
Springer Series in Optical Sciences 201, DOI 10.1007/978-3-319-33359-5_43

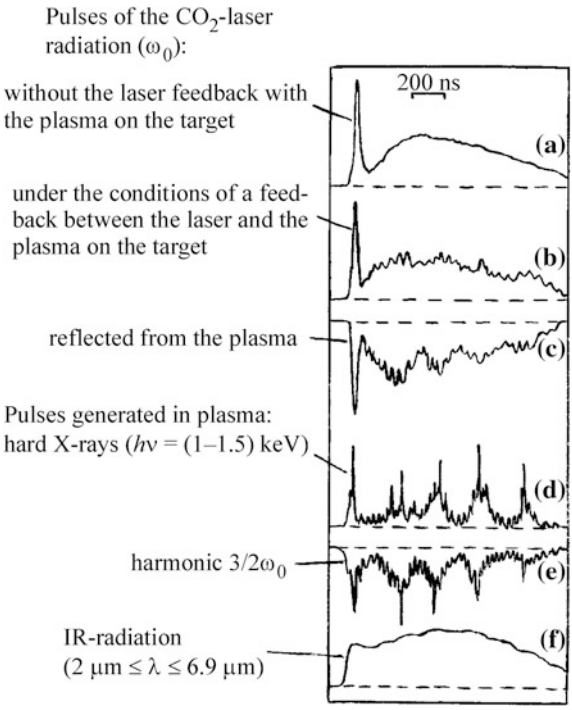

Fig. 43.1 Oscillograms of the pulses of the CO_2-laser radiation (ω_0) (with the laser mixture of the 1:1:3 composition): without the laser feedback with the plasma on the target (the window of the vacuum chamber is closed by the absorbing blank flange) (**a**); under the conditions of a feedback between the laser and the plasma on the target (**b**); reflected from the plasma (**c**). Oscillograms of the pulses generated in plasma: hard ($h\nu \approx$ (–1.5) keV) X-ray radiation (**d**); harmonic 3/2 ω_0 (**e**); infra-red radiation (2 μm $\leq \lambda \leq$ 6.9 μm) (**f**). The target is made of aluminum

The oscillograms of the investigated signals, obtained in the case of CO_2-laser operation on the mixture of gases with the 1:1:3 composition when the aluminum target was located behind the focus (F = 21) of the laser beam (r = (21.1–21.4) cm), are presented in Fig. 43.1. From the comparison of the oscillograms a–c in Fig. 43.1, it transpires that the appearence of spikes with modest amplitudes with the duration of the order of several tens of nanoseconds (regarding the hall-height level) in the pulse "tail" of the incident radiation in case of the laser feedback with the plasma from the effect of "plasma mirror" (PM) [3, 4].

According to [3, 4] the realization of functioning of the CO_2-laser with PM is possible in two different operating conditions: (1) long (in the order of several tens of ns) pulses generation and (2) a train of short pulses (1.8 ns) with the time interval between the pulses of $T = 2l/c$, where l is the length of the resonator of the laser with PM. Due to the fact that only the first type of operation of the CO_2 laser with PM was observed in our experiments, one can draw the conclusion that the threshold of the Brillouin scattering instability participating in short pulses generation [3, 4] has not been achieved.

The oscillograms of the investigated signals, obtained in the process of CO_2-laser operation on the mixture of gases of the 1:3:6 composition when the aluminum target was located behind the laser beam focus (r = (21.1–21.4) cm), are presented in Fig. 43.2. It is noteworthy that, when using the mixture of the 1:3:6 composition, we succeded in HXRMS generation recording both in cases when the

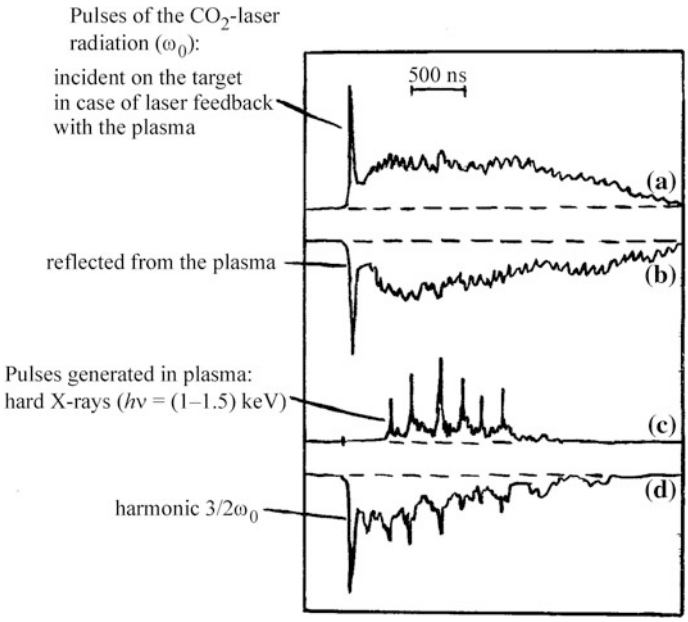

Fig. 43.2 Oscillograms of the pulses of CO_2-laser radiation (ω_0) (with the mixture of the 1:3:6 composition): **a** incident on the target (in case of laser feedback with the plasma), **b** reflected from the plasma; and oscillograms of the pulses generated in the plasma: **c** hard ($h\nu \approx$ (1–1.5) keV) X-ray radiation, **d** harmonic 3/2 ω_0. The target is made of aluminum

target was placed in the focus and even then when it was located in front of it ($r \sim 20.9$ cm), the signal shapes therewith became similar to these observed in the case when the mixture of the 1:1:3 composition was used and the target was placed behind the focus (Fig. 43.1d, e).

The oscillograms, obtained in the experiment with the target made of tungsten and positioned behind the focus ($r = 21.1$ cm) when employing the CO_2-laser operating on the mixture of the 3:1:6 composition, are shown in Fig. 43.3.

Analyzing the results of the experiments, one can draw the following conclusions:

(1) HXRMS is generated from the joint actions of two effects, such as PM and the prepulse effect, in the process of the formation of the homogeneous plasma with a large characteristic size of $L > 1.3$ mm (see p. X of this work) on heating by the long GSG pulse. Thus, it turned out to be possible to maintain and develop PI of a two-plasmon decay type (see p. X of this paper) excited by the laser prepulse (for the case of the target made of aluminum $q_p > 4.6 \times 10^9$ W/cm^2) at the expense of efficient additional plasma heating by the radiation spikes appearing as a result of PM effect and possessing less intensity ($q_t < 10^9$ W/cm^2) in the GSG pulse "tail". It is important to note that the characteristic size of the plasma expanding at the rate of $V_{pl} > 2.6 \times 10^6$ cm/s along the laser beam had achieved the value of

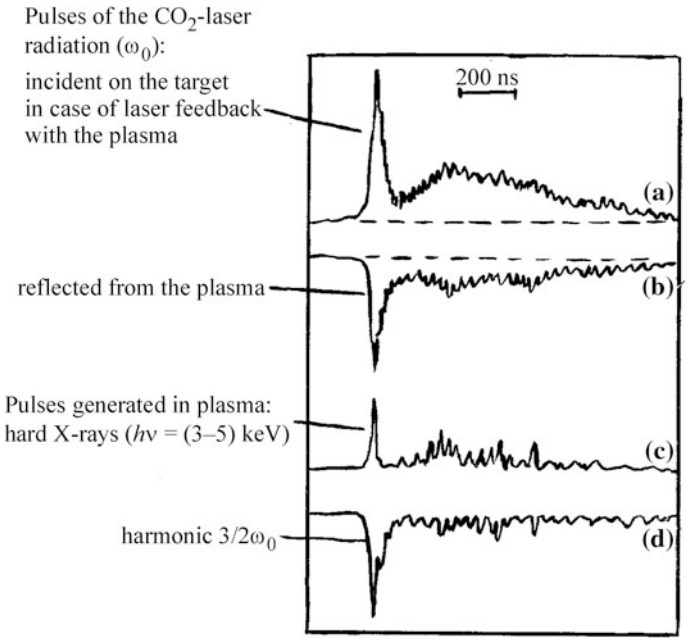

Fig. 43.3 Oscillograms of the pulses of CO_2-laser radiation (ω_0) (with the mixture of the 1:3:6 composition): incident on the target (in case of the laser feedback with the plasma) (**a**); reflected from the plasma (**b**); and oscillograms of the pulses generated in the plasma (**c**); hard ($h\nu \approx$ (3–5) keV) X-ray radiation, harmonic 3/2 ω_0 (**d**). The target is made of tungsten

$L \sim R = V_{pl} \times t \sim 30$ mm by the time when the last HXRMS spikes were generated ($t \sim 1.2$ μs as related to the laser pulse beginning). It is evident that this plasma scale could govern the rather low threshold of the PI development we observed.

(2) Varying the energy distribution in the laser pulse (changing its time shape) and the target position relative to the laser beam locus, one can vary HXRMS energy distribution as needed, and control its time structure. A ten-fold and even higher increase of the HXR time-integrated output has been achieved at the expense of additional spikes in the HXR signals by trial and error of the optimum of the mentioned above experimental conditions. For example, the number of quantums with the energy $h\nu \approx (1–1.5)$ keV, emitted by the plasma into the spatial angle of 4π steradian (under the assumption that the HXR distribution is isotopic) when the target is made of aluminum and the laser mixture has the 1:1:3 composition is equal to $N \approx 4.5 \times 10^{10}$, from where $E_{hv} \approx (1-1.5)\,\text{keV} \approx 1.08 \times 10^{-5}$ J and the relative HXR output is:

$$\eta = E_{hv} \approx (1-1.5)\,\text{keV}/E_{las} \approx 6.85 \times 10^{-7}.$$

(3) HXRMS generation is observed both in the spectral region with $hv \approx (1–1.5)$ keV and in the harder region $hv \approx (3–5)$ keV. As this takes place, it should be empasized that the quantums with the *energy of* $hv \approx (3–5)$ keV were recorded only in case of application of a heavier tungsten target (see Fig. 43.3c), and HXR signals from the plasma of the target made of polyethylene were not recorded at all both in the process of HXRMS generation and in single-spiking generation. These facts are explained in the first part of the present study.

43.2 Conclusion

The phenomenum of HXRMS generation, revealed evidently for the first time in [1, 2] and investigated in the present study, increases the HXR output by a factor of 10 and even higher at the intensity of CO_2-laser radiation of $q < 10^{10}$ W/cm^2. This points to the fact that the CO_2-laser plasma can be a rather efficient source of HXR.

References

1. V.V. Apollonov, S.I. Derzhavin et al., Preprint N.59, IOFAN (Moskov 1991)
2. V.V. Apollonov, S.I. Derzhavin et al., Bull. Am. Phys. Soc. **36**(7), 1959 (1991)
3. I.V. Kholin, *Thesis for a Candidate's Degree* (FIAN, USSR, Moskow, 1979)
4. I.V. Kholin, Trudy FIAN **116**, 118–145 (1980)

Chapter 44
Probe Investigations of Close-to-Surface Plasma Produced by CO_2-Laser Nanosecond Pulse Train

Abstract Investigations of currents in close-to surface plasma, produced by CO_2-laser radiation of different temporal structure have been carried out. The character of evolution of registered currents temporal structure at growing energy density was different when the target was irradiated in air and in vacuum by the train of short (τ = 2.5 ns) pulses. Experiments in vacuum have revealed that the transit from smooth single mode pulse to the nanosecond pulse train of the same total energy was followed by a considerable decrease in plasma formation energy thresholds and by the increase of amplitudes of currents induced by plasma. The current pulses from the target were registered after finishing the laser irradiation; their appearance was probably connected with cumulation effects, caused by the ring form of the irradiated area.

Electromagnetic fields and currents in close-to-surface plasma, produced by successive laser pulses were investigated in [1–5]. In [4] it was determined that the low threshold breakdown of atmospheric air by the train of short (τ = 3 ns) CO_2-laser pulses was followed by generation of high frequency electric fields and currents. Moreover, due to the high peak intensities $I(t)$ in the pulse train, energy breakdown thresholds decreased while the efficiency of plasma—target heat transmission increased in comparison with the irradiation of target by smooth microsecond pulse of the same total energy E = 2.5 J.

In present chapter, analogous experiments have been carried out both in air and in vacuum; moreover, the focusing of pipe-like beam at the sufficiently large irradiation area on the target have been used. That is, laser radiation has not only temporal but also spatial modulation $I(r)$ of intensity, which in some cases significantly influences the currents induced by plasma [6].

© Springer International Publishing Switzerland 2016

V.V. Apollonov, *High-Energy Molecular Lasers*,
Springer Series in Optical Sciences 201, DOI 10.1007/978-3-319-33359-5_44

44.1 The Experimental Set up

The CO_2-laser used in experiments with 20 cm aperture and ~1 kJ output energy [7] had a telescopic resonator of $L = 8.6$ m length and $M = 2.1$ magnification (Fig. 44.1) and generated in two pulse forming regimes:

(a) regime 1—Generation of a smooth single axial mode pulse (Fig. 44.2a) due to injection of cw CO_2-laser radiation
(b) regime 2—Train of nanosecond pulses ($\tau = 2.5$ ns) with $T = 2$ L/c ~57 ns interval (Fig. 44.2c) with injection of nanosecond pulse train produced in a separate CO_2-laser [7].

It is worthy of note that in our experimental conditions, the radiation, reflected by plasma influenced the temporal forr of laser pulse. Moreover, $I(t)$ amplitude increased in regime 1 due to modulation on the smooth pulse "tail" (Fig. 44.2c) and decreased in regime 2 due to generation of a few additional nanosecond pulse trains superimposed on the main one, that is the difference of $I(t)$ amplitude in two regimes decreased. However, the influence of reflection from plasma diminished when the polyethylene attenuators were used for the variation of E.

The laser radiation was focused on a central ring of three-sectional copper target (Fig. 44.3) disposed in air or in vacuum with remained gas pressure of ~10 Torr. Two targets (M_1 and M_2) with external diameters of the irradiated ring of 26 and 10 mm, and internal diameters of 12 and 4.7 mm accordingly were used. The signals $U_1(t)$ and $U_2(t)$ being investigated were taken from two loads $R = 0.33\ \Omega$, which connected the adjacent zones (Fig. 44.3). Moreover, the signal from the

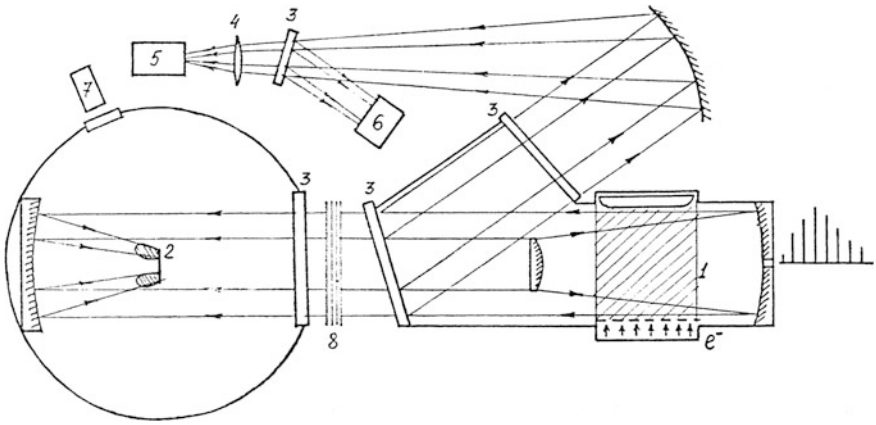

Fig. 44.1 Experimental set up: CO_2-laser 20 × 20 × 125 cm^3 active volume (*1*); the target (*2*), NaCl plates (*3*), lense (*4*), calorimeter (*5*), photon-drag detector (*6*), photo-cathode (*7*), polyethylene attenuators (*8*)

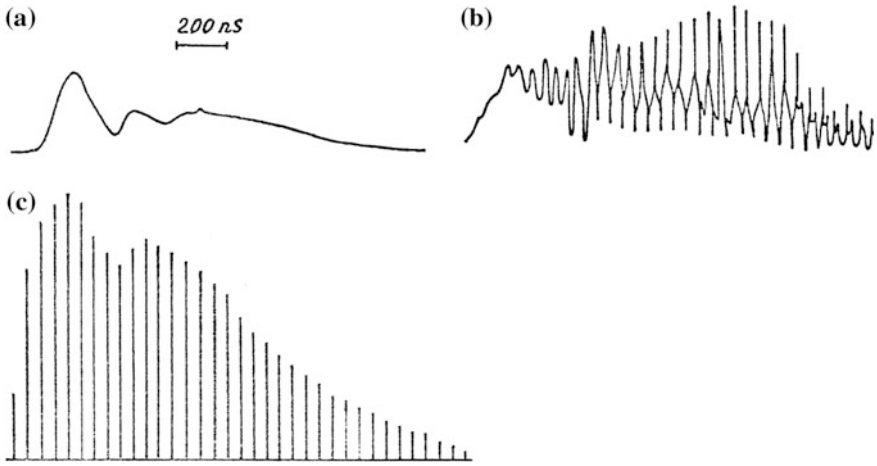

Fig. 44.2 CO_2-laser radiation: regime 1, target is closed (**a**), regime 1, target is opened, E_s = 100 J/cm^2 (**b**), regime 2, target is closed (**c**)

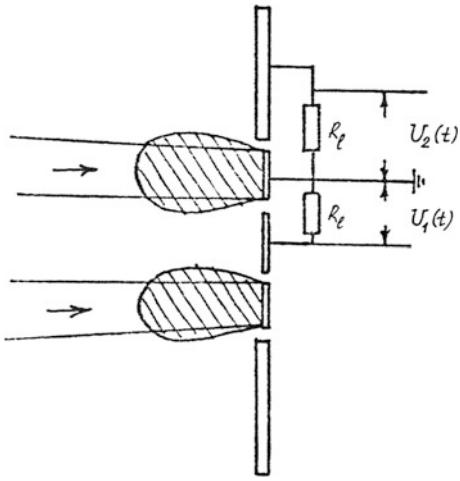

Fig. 44.3 Three sectional target

calorimeter proportional to E as well as signals from 3 termopairs connected with irradiated ring in 3 symmetric points were registered at ligth-beam plotter. The energy Q transmitted to the target was calculated through the average value of three signal amplitudes. $U_1(t)$, $U_2(t)$ signals as well as temporal form of laser radiation (from photon-drag detector) and plasma luminescence were registered on Tektronix 7104 oscilloscope with resolution.

44.2 Experimental Results

The experiments revealed that by the air breakdown at the stage of laser irradiation in regime 2, the temporal form of $U_1(t)$ signal from M_1 target was analogous to that observed in [4]. When the energy density at the target varied in the region E_s = 2–3.5 J/cm^2 close to air energy breakdown threshold E_s. $U_1(t)$ was the train of bipolar nanosecond pulses of current with T period (Fig. 44.4a). At E_s = 3.5–9 J/cm^2 the modulation with T period took place only at $U_1(t)$ front (Fig. 44.4b). The modulation depth diminished with E_s growing and was close to zero at $E_s > 9$ J/cm^2. $U_2(t)$ signal had no modulation at any E_s values.

The signal amplitudes $\Delta U_1, \Delta U_2$ (that is maximum alteration of bipolar signal $U(t)$) were less than 1 V owing to the alienation of plasma from irradiated surface with high E_s [8].

In the present experiments, the maximum value of heat transmission coefficient $A = Q/E$, which took place at $E_s \sim 5$ J/cm (close to E_s^a) increased in regime 2 if compared with regime 1 by 1.4 times [4].

The irradiation of target in vacuum has shown less significant difference of A maximum value in two regimes (Fig. 44.5).

It is interesting to note that rapid growing of $A(E_s)$ in vacuum took place at $E_s \sim 20$ J/cm, which was significantly higher than the E_s value corresponding to the threshold of current and luminescence appearing (Fig. 44.6). In our opinion, the moment that current appears is connected with burning microplasma at separate absorbing centers, which takes an insignificant part of ring square and does not lead to noticeable heating of the target.

The amplitudes of current signals in vacuum were much higher than in air and increased at growing E_s. The evolution of temporal form and amplitude, ΔU_1, of U_1(t) signal at varying E_s in the range E_s = 110 J/cm (with M_1 target) and at $E_s = E_s^{\max} \sim 600$ J/cm (with M_2 target) is shown at Fig. 44.6.

As follows from Fig. 44.6, the E_s value became $\sim$4 times less and the ΔU_1 value was <110 J/cm^2, $\sim$3 times higher in regime 2 compared with regime 1. An even greater difference ($\sim$10 times) in signal amplitudes in the two regimes was registered at $E_s = E_s^{\max}$ (Table 44.1).

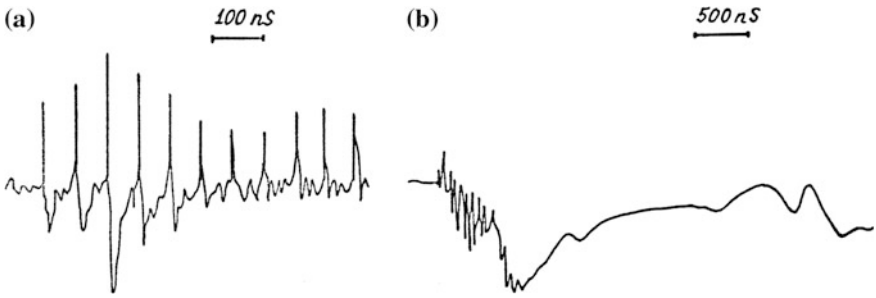

Fig. 44.4 $U_1(t)$ signal oscillograms in air: **a** E_s = 2.8 J/cm^2, **b** E_s = 8.6 J/cm^2 (M_1 target)

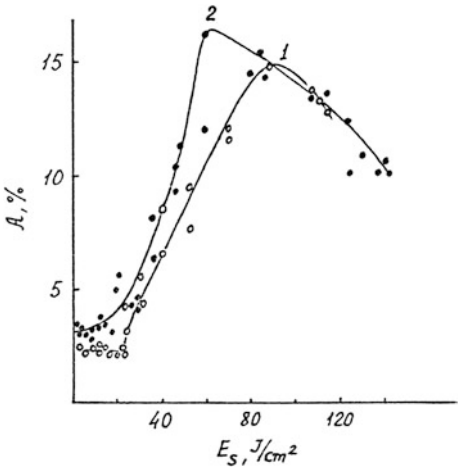

Fig. 44.5 Plasma-target heat transmission coefficient A versus E_s for $M1$ target irradiated in vacuum in two regimes of laser generation

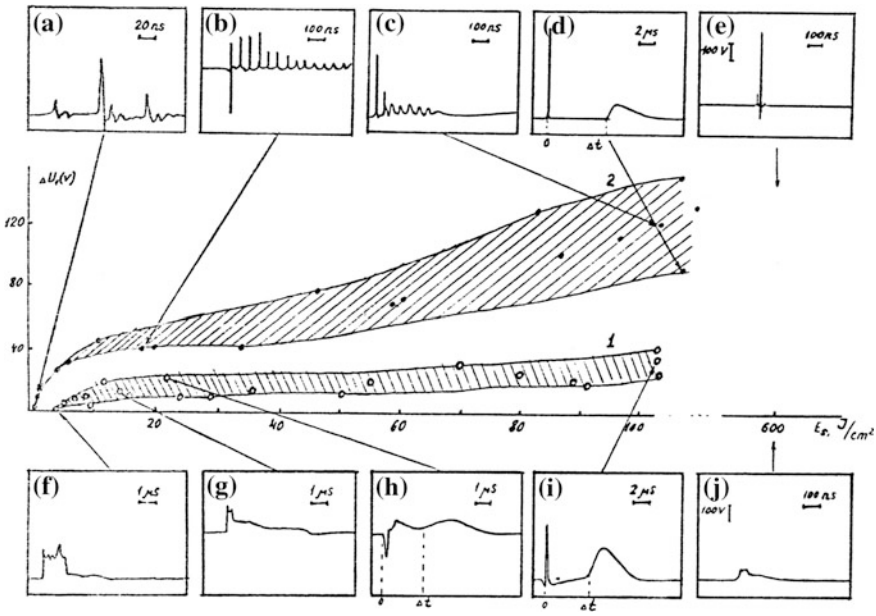

Fig. 44.6 Dependence of ΔU_1 and $U_1(t)$ temporal form on E_s; $U_1(t)$ oscillograms for the train of pulses (**a**–**e**); and for the smooth pulse (**f**–**j**)

Table 44.1 Signal amplitudes in the two regimes

Signals	Signal amplitude (V)	
	Smooth pulse	Train of pulses
U_1	30–70	360–600
U_2	60–100	570–1000

It is worthy of note that significant dispersion of ΔU_1 values at E_s = constant shown in Fig. 44.6 as dashed strip were caused by instability of $I(t)$ due to reflection from plasma and in regime 2 as a result of jitter of master radiation injection moment [7].

Let us discuss the temporal forms of signals registered during the nanosecond pulse train irradiation of target in vacuum. It was determined that, unlike air, in this case the temporal form of U_1(t) and $U_2(t)$ signals had a similar character to nanosecond temporal structure for any E_s value in the range Efe–E_s. $U_1(t)$ evolution at increasing E_s is shown in Fig. 44.6a–c, e. At $E_s = E_s^p$ the signal was the train of 3–4 pulses with $\sim\tau$ duration coinciding in time with a few maximal train pulses (Fig. 44.6a). At growing E_s and correspondingly, $I(t)$, in separate train pulses, which burned plasma at the target number of significant current pulses grows up, the total duration of $U_i(t)$ signal ti increases (Fig. 44.6b). However, from $E_s > E_s \sim$ 60 J/cm ti decreases, reaching $\sim$400 ns at E_s = 100 J/cm and $\sim$100 ns at E_s = 600 J/cm (Fig. 44.6c). Moreover, the nanosecond duration monopulse is distinguished in the $U_i(t)$ front (Fig. 44.6e). This diminishing of ti is probably caused by the alienation of hot plasma area from the target in vacuum that is due to large values of E_s and the small delay T of all pulses in the train after the first one (which is intense enough to produce plasma) initiates the breakdown at the front of spreading plasma of metal vapour. In all cases, the E_s value correlates well with E_s value when $A(E_s)$ begins to decrease (Fig. 44.5), probably owing to the same reason.

Detailed discussion of established regularities demands the study of plasma-spreading dynamics in this regime as well as earring on the analogous measurements at varying T in order to maximize the current amplitudes [2].

The comparison of $\Delta U_1, \Delta U_2$ values with different loads R = 0.33 and 1 Ω have shown that at $E_s = E_s$, the typical resistance of plasma area [8] in current circuit Rpl $\ll R$ that is we registered EMF excited by plasma and limit the circuit current by R value. That is why without load and the gap between target zones, the current density at the target surface from the irradiated ring to the internal zone would be $I\text{ln} = \Delta U_1/\text{Rpl} \gg \Delta U_1/R\text{l} = 2\text{kA}$ and to the external zone $\text{lout} = \Delta U_1/\text{RpL} \gg \Delta U_2/\text{Rpt} = 3.3\text{kA}$.

In conclusion, let us discuss one more feature of current signals. In both regimes of target irradiation in vacuum after the first laser pulse finished and $E_s > E_s$ = 20 J/cm the second pulse of current was registered. Moreover, its amplitude and time delay, At (Fig. 44.6d, h, i), increased at growing E_s. At also increased at growing $I(t)$ amplitude, with E_s = const: at E_s = 100 J/cm, td was $\sim$8 μs in regime 2 and $\sim$6 μs in regime 1. The amplitude of the second pulse was comparable with the main pulse amplitude, although it took place much later than laser pulses (Fig. 44.6d, i). When the M2 target with smaller size was irradiated at $E_s = E_s'' \sim$ At diminished up to 2.2 s. In our opinion, the appearance of that second pulse was connected with ring distribution of $I(r)$, at which cumulation of air breakdown plasma or target vapour plasma took place. Moreover, the hot nuclei is formed in the center of the ionized area giving rise to the current signal analogous to that which arises when the second laser pulse heats preliminary ionized gas [2].

The good correspondence of E_s' and E_s values at which growth of $A(E_s)$ took place (Fig. 44.5), and the decrease of td proportional to target diameter decrease, confirms our supposal. It seems that at particular E_s values, the plasma was burned not at separate inhomogeneities but on the scale of all irradiated ring, giving rise both to effective heating of the target and cumulation. However, in order to unambiguously explain the presence of the second pulse on $U_2(t)$ signal as well as the increase of At at increasing E_s, it is necessary to carry on additional experiments to determine spatial localization of the hot area.

References

1. G.A. Askarian, M.S. Rabinovich, A.D. Smirnova, V.B. Studenov, Currents, induced by light pressure at laser beam interaction with matter. Lett. Sov. J. Exsp. Teor. Phys. **5**, 116–118 (1967)
2. V.I. Konov, P.I. Nikitin, A.M. Prokhorov, A.S. Silenok, Magnetic fields and currents generation in recombinating plasma of optical breakdown. Pis'ma v ZETF **39**, 501–504 (1984)
3. V.I. Konov, P.I. Nikitin, A.M. Prokhorov, Close-to-target air breakdown by two successive CO_2-laser pulses. Magnetic fields, Izv. Sov. Acad, Sci. Ser. Phys. **49**, 1208–1213 (1985)
4. V.V. Apollonov, V.I. Konov, V.R. Sorochenko et al, Plasma formation by the train of nanosecond CO_2-laser pulses. Lett. Sov. J. Techn. Phys. (Pis'ma v ZTF) **ll**(17), 1034–1039 (1985)
5. G.A. Askarian, I.M. Raevsky, Generation of voltage and current quickly alternating pulses when laser pulse train interacting with target in atmosphere. Kvantovaya elektronika **13**(8), 1701–1703 (1985)
6. A.A. Ermakov, V.I. Konov, P.I. Nikitin, A.M. Prokhorov, S.A. Uglov, A.R. Sha- banov, Ligth-induced surface currents. Preprint of General Physics Institute N 357 (1986)
7. V.V. Apollonov, A.N. Prokhorov, V.R. Sorochenko, Y.A. Shakir, Regenerative CO_2-amplifier of a nanosecond pulse train, Kvantovaya elektronika, 15(9), 1766–1769, (1988). Proceedings of the Intern, conference on LASER'S 87 (edited by F.J. Duarte), Lake Tahoe, Nevada, December 7–11, 1987, p 525–530, STS Press McLean, VA (1988)
8. D.A. Dement'ev, V.I. Konov, P.I Nikitin, A.M. Prokhorov, Investigation of currents in air optical breakdown near conducting target, Kvantovaya elektro- nika **8**(7), 1532–1539 (1981)

Chapter 45
Interaction of CO_2 Laser Nanosecond Pulse Train with the Metallic Targets in Optical Breakdown Regime

Abstract Many phenomena accompaning the air optical breakdown (in particular the electric fields and currents arising in breakdown plasma) sufficiently depend on the temporal parameters of laser radiation. For example, utilization of two successive laser pulses results in considerable increase of the magnetic fields and currents. In the present chapter, the electric fields and currents in the air breakdown plasma produced by a train of CO_2 laser nanosecond pulses near the surface of uncharged metallic targets were studied. The breakdown thresholds as well as efficiency of plasma-target heat transmission for different temporal parameters of CO_2 laser radiation were measured. Regenerative amplification (RA) enables transformation of free running mode laser pulses into the train of nanosecond ones with varied duration of the individual pulse and time interval between the pulses. For this reason, we have used RA for carrying out the experiments. The numerical calculations made it possible to predict the influence of RA scheme parameters upon the temporal structure of the nanosecond pulse train and thus facilitate realization of the experimental set up.

45.1 Introduction

Many phenomena accompanying the air optical breakdown (in particular the electric fields and currents arising in breakdown plasma) sufficiently depend on the temporal parameters of laser radiation. For example, utilization of two successive laser pulses results in considerable increase of the magnetic fields [1–4] and currents [2, 3].

In the present paper, the electric fields and currents in the air breakdown plasma produced by a train of CO_2 laser nanosecond pulses near the surface of uncharged metallic targets are studied. The breakdown thresholds as well as efficiency of plasma-target heat transmission for different temporal parameters of CO_2 laser radiation are measured.

Regenerative amplification (RA) enables transformation of free running mode laser pulse into the train of nanosecond ones with varied duration of the individual

© Springer International Publishing Switzerland 2016

V.V. Apollonov, *High-Energy Molecular Lasers*,
Springer Series in Optical Sciences 201, DOI 10.1007/978-3-319-33359-5_45

pulse and time interval between the pulses. For this reason, we have used RA for carrying out the experiments. The numerical calculations made it possible to predict the influence of RA scheme parameters upon the temporal structure of the nanosecond pulse train and thus facilitate realisztion of the experimental set up.

45.2 Numerical Calculation of Regenerative Amplification

In the RA process, growth of self-radiation (SR) from spontaneous omission (developed in the free running mode pulse in lack of injected radiation) is significantly suppressed owing to many-pass nanosecond pulse amplification in saturation regime. The SR level between the train pulses strongly depends on the RA scheme parameters. If these parameters are not optimal, the SR level can be considerable and strongly decreases the peak power of nanosecond pulses, Pi, and their contrast, P_i/P_n, where P_n - is the SR power.

The numerical RA calculation allows the influence of different parameters upon the SR level in the train, and the shape of the train envelope, to be estimated. In the numerical calculations [5, 6], the influence of various parameters on RA process was investigated. However, the time region for RA determined by a ratio of injected pulse power to SR background was determined only in the frame of a strongly simplified point model that did not operate for CO_2 lasers with sufficiently high α_m •LG value, where α_m was the maximum value of low signal gain coefficients, and LG was the active medium length. A more perfect cell model, also used in these papers did not take into consideration SR development.

In [7], the cell model used considered the SR growth. However, for simplicity, only the average value of SR flow density along a resonator axis was calculated. In the present chapter, a more exact model was used to calculate the temporal and space (along resonator axis) SR variation. The active medium and the resonator were divided into cells 10 cm in length and, at each calculation step, two radiation flows moving in opposite directions, including both SR flow and the amplified nanosecond pulse, were determined in each cell.

To determine the amplification coefficient, the rate equation system for the populations of laser levels [8] was solved numerically, considering rotational relaxation [8].

In our calculations, the experimental dependence, ne(t), was used, where ne represented electron density in the active medium of the real CO_2 module. The relaxation rate values used in the calculations were somewhat varied relative to those calculated according to the well-known formula in [8], to obtain maximum coincidence of the calculated and experimental curves of the low signal gain coefficient $\alpha_0(t)$. For simplicity, the transverse mode structure in a resonator was not considered. The begun aperture was considered to be constant along the resonator axis and equal to 6 cm and the energy distribution was considered to be homogeneous across the aperture. Moreover, injected radiation was considered to

also be homogeneous across the aperture, because owing to natural divergency, the injected beam diameter increases up to resonator aperture during the first pass.

In the numerical calculations, the following values of parameters were used: $L = 23$ m; LG = 100 cm; the output mirror reflectivity $R_1 = 0.05$–08; resonator losses were 60% per round trip time (due to absorption in the laser BaF_2 cell windows); injected pulse power P_{inj} = 10-6-10-1 W, its duration $\tau = 3.3$ ns, $T_{inj} = 0$–700 ns, the contrast ratio 'of' the injected pulse to background (due to limited discrimination of electro-optical switch) $K_i = 10^1$–10^6.

These values of parameters correspond (accurately or approximately) to regenerative CO_2 amplifier used in the experimental set up [9].

The main purpose of the numerical calculations was to determine the practically realized (for the given set up) combination of RA scheme parameters to obtain the pulse train with a sufficiently high $A = E_{tr}/E_{tot}$ value, where E_{tr}—is the summary energy of the train pulses, E_{tot}—is the total laser pulse energy.

The calculations showed that, at other fixed parameters, value $A = E_{tr}/E_{tot}$ greatly depends on T_{inj} (Fig. 45.1a), reaching maximum $A = 0.77$ when $T_{inj} = T_{thr}$, where T_{thr} is the time interval from the start of pump to the moment when the gain active medium exceeds the losses in a resonator.

This can be explained as follows. If $T_{inj} < T_{thr}$, then before $T = T_{thr}$ the pulse makes some passes through resonator (when losses exceed the gain) and therefore decreases. That is why value $K = P_i/P_n$ also decreases relative to K_0 at the moment of $t = T_{inj}$. On the other hand, when $T_{inj} > T_{thr}$ $K < K_0$, due to fast SR growth when $t > T_{thr}$. It is important to note that when K_0 is sufficiently high, the SR flow reaches its maximum after the maximum pulse of the train have been formed and therefore does not decrease its energy E_N. However, when K_0 decreases, P_n can approach to P_s before the train maximum pulse is formed and E_N will decrease. Therefore, when T_{inj} differs from T_{thr}, SR level in the resonator will grow and A will decrease. If $K_0 = 1$ the injected pulse is not distinguished at SR radiation and free runnung mode takes place. In Fig. 45.1b $E_N(T_{inj})$, dependence is shown. E_N value variation near T_{thr} can be explained by periodic dependence *of* $E_i(T_{inj})$ where i is the pulse number in the train (Fig. 45.2).

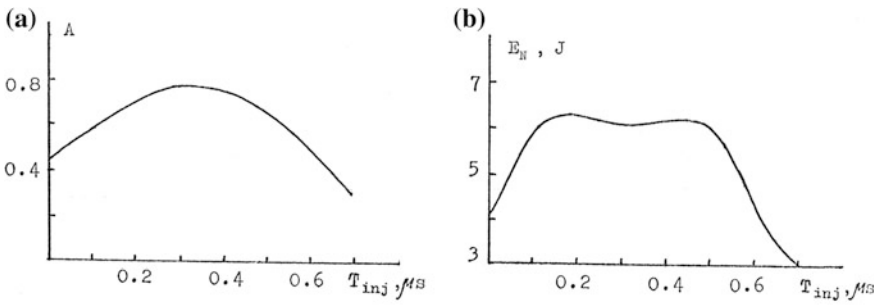

Fig. 45.1 Dependences of $A = E_{tr}/E_{tot}$ (**a**) and E_N (**b**) on T_{inj}, when $R_1 = 0.36$, $P_{inj} = 10^{-3}$ W, $K_i = 104$

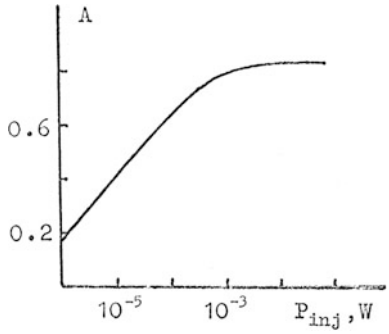

Fig. 45.2 $A(P_{inj})$ dependence when $R_1 = 0.36$, $T_{inj} = T_{tht} = 300$ ns, $K_i = 104$

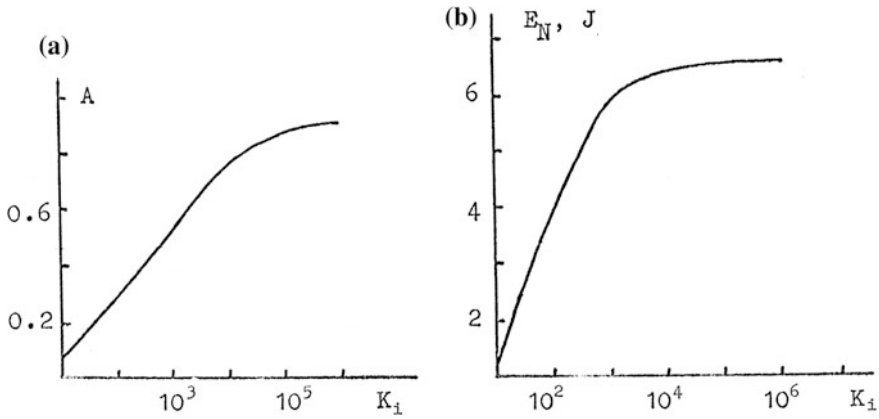

Fig. 45.3 $A(K_i)$ (**a**) and $E_N(K_i)$ (**b**) dependences at $R_1 = 0.36$, $T_{inj} = 300$ ns, $P_{inj} = 10^{-3}$ W

$A(K_i)$ dependence is shown in Fig. 45.3a. When $K_i \sim 106$ A reaches 0.9 and is not changed. This can be explained by the fact that at fixed value of P_{inj} (in our case 10-3 W) there is maximum value of K_i when the injected pulse background is proportional to P_{inj}/K_i and comes into resonator before the injected pulse becomes considerably lower than the SR flow at the moment of $t = T_{inj}$ and therefore does not affect the SR growth. (See $E_N(K_i)$ dependence in Fig. 45.3b).

When R_1 varies from 0.36 (Ge plate with antireflection coating on the one side) to 0.08 (NaCl plate), E_{tr} changes slightly, whereas $E_n = E_{tot} - E_{tr}$ falls almost to 0. The values of R_1 and E_N remain almost constant (Fig. 45.4b).

For this reason, for maximum SR suppression it is profitable to use NaCl plate as the output mirror.

All the calculations were carried out for one gas mixture of the active medium CO_2:N_2:He = 1:1:3 and the constant pump pulse (with base duration $\tau_{pump} = 1.4\ \mu$s) for the real laser module. In these conditions, the train consists of *5–6* main pulses and

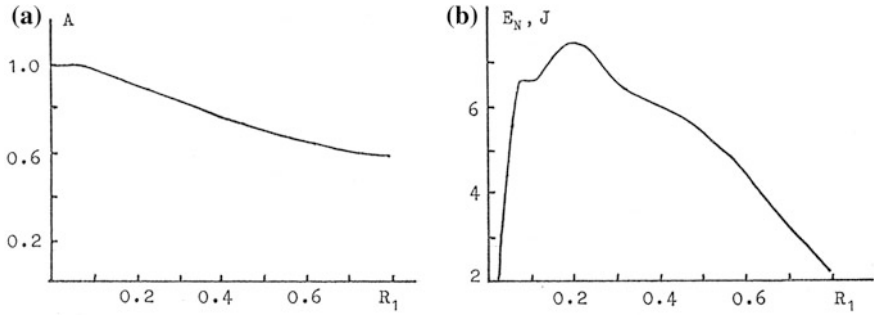

Fig. 45.4 A(R_1) (**a**) and $E_N(R_1)$ (**b**) dependences at $T_{inj} = T_{tht}(R_1)$, $P_{inj} = 10 - 3$ W, $K_i = 104$

at optimal choice of RA scheme parameters, Pn cannot reach Ps in the train "tail" due to the short pulse of pumping. If τ_{pump} increases, Pn approaches the level of Ps after some pulses followed by maximum pulses in the train; in this case SR takes a considerable part of energy of the active medium and the train of pulses at the beginning of radiation pulse turns into continuous radiation in the tail.

For these reasons, we can confirm that in order to obtain high A values, not only high contrast of K but also a sufficiently short pulse of pumping are required.

45.3 Experimental Set up

The results of the numerical calculations mentioned above made it possible to determine an optimal combination of RA scheme parameters that was realised in the experimental set up. The power stabilized CW CO_2 was used as a source of injected radiation. The injected pulses were formed by the electrooptical switch which consists of two successive Pockels cells with GaAs crystals of $7 \times 7 \times 42$ mm^3 dimensions and transmission type Ge polarizers with the contrast $K_i \sim 2.104$ [9].

The electrical pulse applied to the crystals was 5 ns in duration (FWHM). The amplitude was $\sim$6 kV. The halfwave voltage for each crystal was $U_{\lambda/2} \cong 15$kv. Therefore, the high voltage used was not sufficient for the full opening of the switch, but the injected pulse power $P_{inj} \sim 1$ mW was sufficiently great to obtain rather high A (see Fig. 45.2).

The injected optical pulse duration was $\sim$3 ns (FWHM). Compression of the optical pulse relative to electrical pulse is explained by the nonlinear switch transmission and the limited time ($\sim$2 ns) of pulse propagation between the tiyo crystals. The Lamberton-Pearson type TEA-CO_2 module with 50 cm active length, 6×6 cm^2 aperture with Chang profile electrodes and Ti folg strips for preionization was used as regenerative amplifier [10, 11]. The module was placed into three mirror 23 in long resonator (see Fig. 45.5).

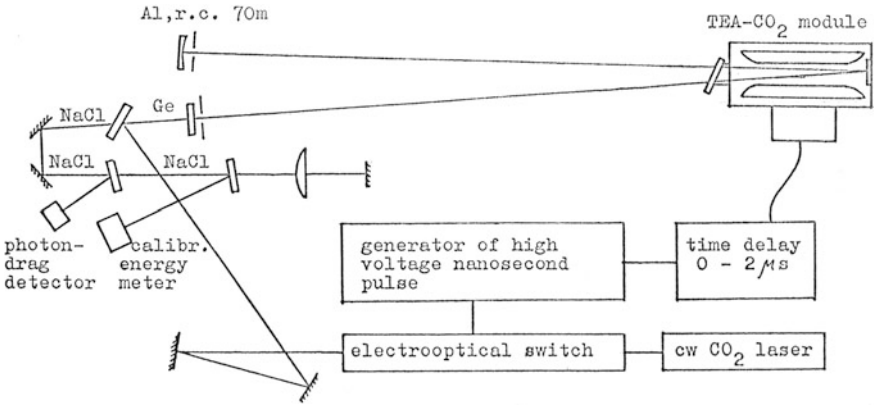

Fig. 45.5 The scheme of the experimental set up

Ge plate with antireflection coating on one side was used as an output mirror. The radius of curvature of the backreflected A_1 mirror was 70 m. To obtain TEMoo mode generation, two diaphragms were placed into a resonator. Beam diameter at the amplifier output was 20 mm.

Ge plate with $R_1 = 0.36$ rather than NaCl plate with $R_1 = 0.08$ was chosen as an output mirror (see Fig. 45.4a) since, in the latter case, the train envelope front becomes more sloping, which makes selection of the individual pulse from the train more difficult [7]. In future, we plan to conduct the experiments on interaction of selected from the train and amplified monopulse with the metallic targets to compare them with the presented experimental setup. The setup parameters such as L and LG were chosen according to the numerical optimization results for the maximum train pulse selection [7].

An autotransformer with the following parameters was used as a pump source for the TEA-CO_2 module: maximum output voltage of 150 kV; maximum current of 20 kA; instantaneous power up to 1 GW; and full duration of the current pulse less than 1 μs [12].

To improve the preionization homogeneity as well as discharge parameters, low-ionizud three-n-propylamin additives were introduced into the working mixture. A scheme of the *L* up is shown in Fig. 45.5. Light pulse of the spark in the autotransformer gap was transported through the optical waveguide to the photodiode and switched on the delay scheme with a tunable delay in the region of 0–2 μs. The delayed pulse switched on a high voltage nanosecond pulse block. The maximum Tinj value was 250 ns and the instability was less than 2 ns.

The injected pulse was introduced into resonator through the output Ge mirror by means of NaCl plate. It was registered by the HgCdTe-type photoreceiver with the time ivimliition better than 7 ns, the output radiation—by the "photon-drag" Go detector.

The TEA-CO_2-laser described above enables realization of three regimes of the target irradiation: I—by the bell-like long pulse (FWHM ~ 400 ns); II—by the

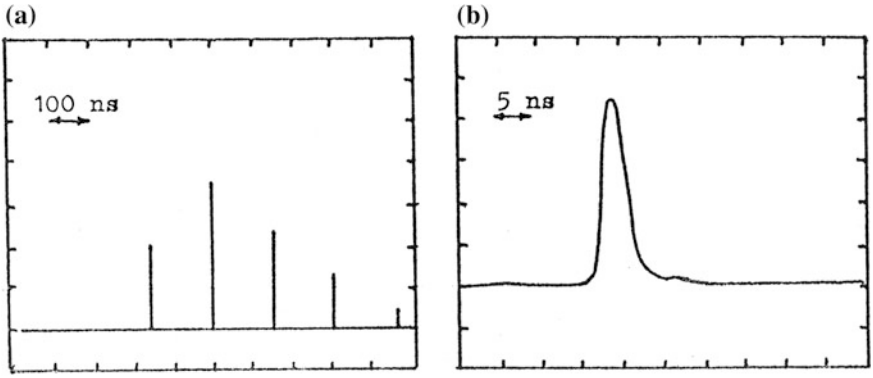

Fig. 45.6 Output radiation of TEA-CO_2 laser in III regime: **a** 100 ns/div, **b** 5 ns/div

train of 5–6 short ($\tau \sim 3$ns) pulses with $\tau \sim 150$ns interval at the SR background; III —by the sruno train of pulses but with P_i/P_n contrast ratio $\sim 10^4$ owing to the nonlinear absorber application (see Fig. 45.6a, b).

In regimes I and II, the radiation energy of E_{tot} was ~ 2.5 J. The experimentally determined A value was ~ 0.7; this value satisfactorily corresponds to the calculated value (see Fig. 45.1a) for the T_{inj} = 250 ns. In regime III, due to nonlinear absorber, E_{tot} was three times as low as before. Radiation was focused into a 1–5 mm diameter spot on the target surface. The electric field potentials near the air breakdown plasma $\varphi(t)$ were measured with the isolated 1 cm long wire probe, loaded on a high frequency emitter repeater [13]; the signal from the later, $U(t)$, was transmitted to the oscilloscope input. Taking the sensitivity into account, $J(t)$ was connected with $U(t)$ by $\varphi[v] = 0.02\ U[v]$. The value of the electric field strength near plasma was $E = \varphi/x$, where x was the nearest distance from probe to plasma front or to the grounded target (where $\varphi = 0$).

To measure the frequency components of E, the emitter repeater signal was transmitted to LC contour whose tunable resonance frequency, f, was varied from 1 MHz to 1 GHz. The amplitude of high-frequency vibrations in the LG contour at the optical breakdown near the antenna-probe was measured by an oscilloscope. Moreover, like in [14], for registration of the electrical field high-frequency components, we have used the wire 1 cm long antenna loaded directly on the LC-contour.

To measure the currents, J, flowing along the irradiated target [14, 15], a probe method was used. The 0.9 mm diameter wire probe was inserted into a 1 mm diameter hole in the copper target so that the probe and target surfaces coincided. A signal for oscilloscope was taken from the load inserted between the probe and target.

Plasma light was registered simultaneously with the current and field measurements by a photocathode. All measurements were carried out by the 50 MHz storage and Tektronix- 7Ю4 oscilloscopes. Time resolution at $\varphi(t)$ measurements were 2.5 ns, and, in other cases, 1 ns.

45.4 Measurements of the Breakdown Thresholds

In our experiments, a moment of plasma formation was determined by registration of plasma light coinciding with the appearance of the electric field and current. The experiments show that at the transition from regime I to III, the threshold energy densities, E_s, required for breakdown near the target are considerably decreased by the factor of 1.7–6 versus a sort of material and level of its cleaning. For example, E_s values for raw copper in the regime I and III are 8.3 and 2.9, respectively, whereas for the diamond copper mirrors they are 100 and 56 J/cm^2, respectively. It is worth noting that without target the air breakdown threshold also decreases from 360 to 90 J/cm^2. It is likely to connect with high peak intensities of laser radiation in the regime II and III, which were 20 times as high as the intensity in the first regime at equal energies.

In regime III, at light intensities of E close to E_s, plasma at metal is ignited by the third and fourth pulse of the train with the intensities approximately half of maximum in the train. This fact is important for analysis of the plasma formation mechanism and is probably connected with the necessity of heating the absorbing inclusions at the surface. Thus, not only the peak radiation intensities play a significant role in the near target air breakdown by the train of nanosecond CO_2 laser pulses but also the energy density at the target.

45.5 The Results of Investigations of the Electric Field and Current

It was revealed that the character of the potential, $\varphi(t)$, and currents, J(t). strongly depend on irradiation regime and energy density values, E_s. In regimes I and II when $E_s > 10$ J/cm^2, at the raw copper target $\varphi(j)$ and J(t) behaviour are similar to those investigated in [13, 15], whereas at E_s = (1–2.5). For E_s in regimes II and III, a considerably different picture takes place. In Fig. 45.7 you can see the oscilloscope

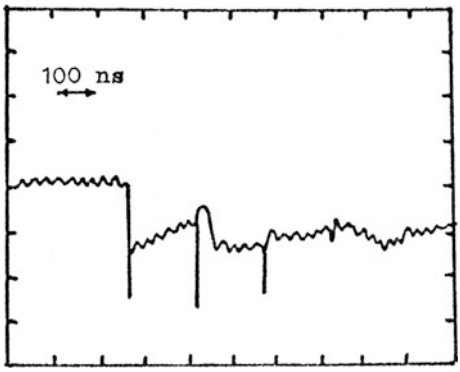

Fig. 45.7 Electrical field potential at 3 mm distance from the spark in regime II at E_s = 8 J/cm^2, 100 ns/div

trace of $\varphi(t)$ at 3 mm distance from the spark ignited by the train of type II with $E = 8$ J/cm^2. (Maximum *measured* value of $\varphi = 6$ V corresponds to E near plasma ~ 20 V/cm). A signal from the current probe centered in the focal spot under the same irradiation conditions and $R_1 = 1\ \Omega$ see in Fig. 45.8a. It is seen from the oscilloscope traces that the electric field and current have high-frequency ($\sim \tau_0^{-1\prime}$) modulation caused by plasma ignition by the different laser pulses. When E further decreases, the amplitude of field and current modulations in regimes II and III strongly increases (Fig. 45.8b) and signal spectrum is broadened to the frequency *region* $\sim \tau_L^{-1}$ (0.33 GHz when $\tau_L = 3$ns). Finally, in regime III, when $E_s < 1.5$, $E_s = 4$ J/cm^2 bipolar noninertial current pulses with duration $<\tau_L$ were observed (see Fig. 45.8c). In the experiments at $E_s \sim E_s^{th}$ the current pulses shorter than $n = 1$ ns (FWNM) (that is close to the time resolution of the measurements) were registered.

Figure 45.9 shows the maximum ΔU amplitude dependence of the bipole current probe signal on E_s for the different regimes. Large values of ΔU for the II and III type intensity are probably determined by the high laser radiation peak intorviity (-6 GY/cm^2) as well as air ionization at its breakdown during the previous train

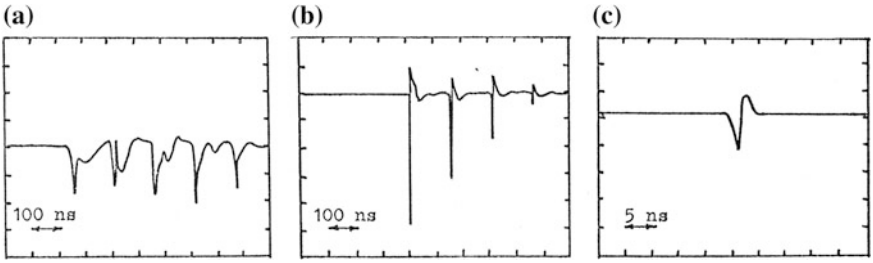

Fig. 45.8 Signal from the current probe load $R_1 = 1\ \Omega$. II regime, $E_s = 8$ J/cm^2, 100 ns/div (**a**); II regime, $E_s = 4$ J/cm^2, 100 ns/div (**b**); III regime, $E_s = 3$ J/cm^2, 5 ns/div (**c**)

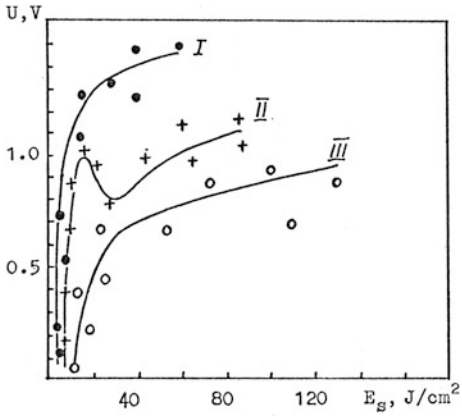

Fig. 45.9 Signal amplitude, U, from the current probe versus E_s at $R_1 = 1\ \Omega$

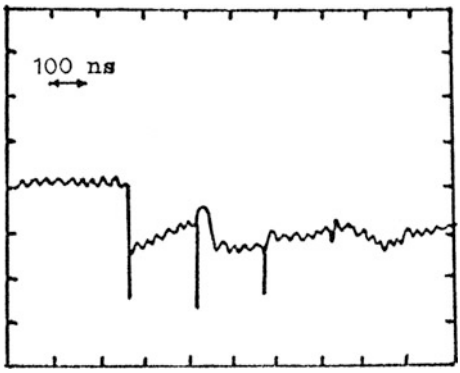

Fig. 45.10 Signal from antenna loaded at LC-contour, 5 ns/dir

pulse [2, 3]. The current density flowing through a probe was 250 A/cm^2. It is worth noting that S_g increasing over 30 J/cm^2 in regimes I and II results in alienation of the optical discharge plasma from target (and decreasing of current $J = \Delta U/R_L$) whereas in regime III, each pulse in the train ignites plasma near the surface. This conclusion corresponds to the results of measurements of plasma target heat transmission, which will be discussed further.

In the experiments with antenna loaded at LG contour, the signals in MHz range were registered in regimes I and III. In the latter regime when $E_a \sim 4$ J/cm^ it was discovered that high-frequency signals with the amplitude ~ 0.1 V were registered in the frequency range up to 1 GHz, (the frequency bandwidth of the measurement system). For the typical oscilloscope trace from antenna see, Fig. 45.10. Let us discuss a possible mechanism of the noninertial current pulses registered in the regime III. The bipolar type of the current pulses as well as transition observed from the long pulses to noninertial ones can apparently be explained by the EMP presence at the plasma border [13, 15]. In this case, fast relaxation of nonequlibrium plasma, which is ignited at $S_s = E_g^{tn}$ only at the separate absorbing centers on the target surface plays an important role.

45.6 The Investigation of Laser-Target Energy Transmission

The copper samples with the surface polished by the abrasive paper just before measurements were used in the present experiments. For the dependence of energy transmission efficiency, B, equal to the ratio of energy, Q, absorbed by the target to the laser pulse energy, E_L, on energy density, $E\sim$, see the Fig. 45.11. The maximum B value for regime III is larger than for regime I, resulting from the close target plasma location during each short pulse of the train III. It is worth highlighting that threshold conditions in the regime III are reached at the lower values of E_s; therefore, in such a regime, high efficiencies of heat transmission are possible if light density is less than the threshold one in the regime I.

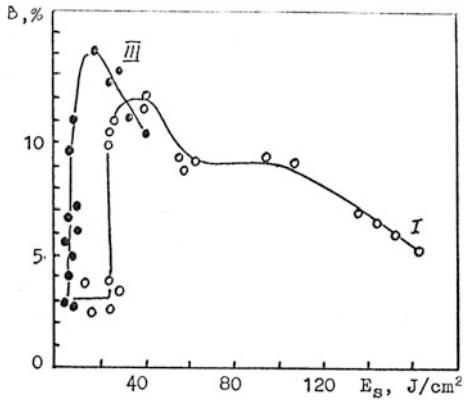

Fig. 45.11 Heat transmission efficiency B versus E_s for the different irradiation regimes

45.7 Conclusion

The main conclusions of this chapter are the following:

I. The numerical calculations allow the time envelope of the nanosecond train of pulses to be determined, as well as the spontaneous emission background between the pulses in a wide range of parameters of the RA scheme. The pulse train with a sufficiently high contrast ratio was experimentally realized while choosing the parameters corresponding to numerical optimization results.
II. The irradiation of the metallic target surfaces by the train of nanosecond laser pulses is followed by a number of interesting phenomena, such as breakdown threshold decrease, increase of energy transmission to the target and excitation of high frequency (1 GHz) electric fields and currents.

Finally, it is important to stress that the present experiments were carried out for the constant temporal parameters of the nanosecond pulse train in order to determine the principle features of interaction of such a radiation with metals. Utilization of regenerative amplification makes it possible to carry out similar experiments in future and to study the breakdown plasma expansion dynamics in a wide range of temporal parameters of laser radiation.

References

1. G.A. Askarian, M.S. Rabinovitch, A.D. Smimpva, V.B. Studenov, The currents, produced by the light pressure when laser beam interacts with matter. Pis'ma v Zh. Eksp. Teor. Fiz. **5**, 116–118 (1967)
2. V.I. Konov, P.I. Nikitin, A.M. Prokhorov, A.S. Silenok, Generation of the magnetic fields and currents at the optical discharge in recombinated plasma. Pis'ma v Zh. Eksp, Teor. Piz. **39**(II), 501–504 (1984)

3. V.I. Konov, P.I. Nikitin, A.M. Prokhorov, Breakdown of air near the target by two sequential CO2-laser pulses. Self-generated magnetic fields. Izvest. AN SSSR, Ser. fiz. **49**(6), 1208 (1985)
4. V.I. Konov, P.I. Nikitin, A.M. Prokhorov, Self-generated magnetic fields of an uir-breakdown plasma produced by two sequental laser pulses. Proceedings of ICPIG-XVTI, Budapest **1**, 237 (1985)
5. K.J. Andrews, Analysis of injection mode locking of high power CO_2 laser systems, International Report, LPI/77/3, May (1977)
6. P.B. Corcum, A.J. Alcock, D.J. James et al., Recent development in high power CO_2 baser mode locking and pulse selection, in ed. by H.I. Schwarz, H. Hora, Laser Interaction and Related Plasma Phenomena, vol. 4 (Plenum Publishing Company, 1977), p. 43
7. V.V. Apollonov, F.V. Bunkin, YuA Shakir, V.R. Sorochenko, Kvantovaya I'Hectronika **9**(4), 832–835 (1982)
8. K.J. Andrews, P.E. Dyer, D.J. James, A rate equation model for the design of tea CO_2 oscillators. J. Phys. E: Sci. Instrum. **8**, 493–497 (1975)
9. V.V. Apollonov, G.G. Baitzur, V.V. Brytkov et al., Generation of the nanosecond pulse of CO_2 laser with the high contrast ratio, Pis*ma v Zh. Techn. Fiz. **10**(19), II92–II95 (1984)
10. H.M. Lamberton, P.R. Pearson, Electron. Lett. **7**, I4I (1971)
11. V.V. Apollonov, F.V. Bunkin, S.I. Derzhavin et al., Amplifier module of many-chain CO_2 laser, Izvest. AN SSSR. Ser. Fiz. f **42**(13), 2488 (1978)
12. V.V. Apollonov, A.I. Barchukov, S.I. Derzhavin, I.G. Kononov et al., Pump source of CO_2 laser at the base of pulsed autotransformer $\gg$. Prib. Techn. Exper. (6), 131 (1978)
13. A.I. Barchukov, V.I. Konov, P.I. Nikitin, A.M. Prokhorov, Probe investigations of electric fields and currents near the laser spark in air, Zh. Eksp. Teor. Fiz. **78**(3), 957–965 (1980)
14. V.I. Konov, P.I. Nikitin, A.M. Prokhorov, Some electrical phenomena following breakdown by laser radiation, Preprint of FIAN *No* 295, Moscow (1982)
15. D.A. Dement'ev, V.I. Konov, P.I. Nikitin, A.M. Prokhorov, Investigation of currents, arising at the air optical breakdown near conducting target, Kvantovaya Electronika, **8**(7), 1532–1539 (1981)

Chapter 46
Wide Aperture Picosecond CO_2 Laser System

Abstract The construction of a CO_2 laser system generating a train of sub-nanosecond laser pulses with total train energy of up to 5 J is reported. *A* record *level* of laser energy was obtained due to utilization of unique 5×5 cm^2 aperture, and 6 atm X-ray preionized CO_2 amplifier. The estimations of individual pulse durations in the train are given. The prospect of upgrading the present configuration of laser systems towards shortening laser pulse duration and increasing the pressure of the working gas mixture of the amplifier and its efficiency are discussed.

46.1 Introduction

The creation of high-power 10 μm picosecond lasers opens new possibilities in fundamental investigations of laser radiation interaction with matter.

One of the potential and very efficient applications of high-power, ultrashort $\lambda = 1.0$ μm pulses is laser acceleration of charged particles. It was shown [1] that relative increase of electrons energy after the interaction with laser field (averaged over electron bunch) is increased with laser radiation wavelength as a square of λ. For the duration of laser pulse 10^{-11} s and its power 10^{12} W (laser pulse energy 10 J) the magnitude of accelerating gradient is 1 GeV/m, which is substantially higher than for modern linear accelerators [2]. 10 μm high power laser pulses can also be utilized in the scheme of supercollider.

The principal parameter of any laser utilized for electrons' acceleration except radiation power and wavelength is its repetition rate. There are many types of modern accelerators that operate with the frequencies 50–60 Hz. It is clear that for high efficiency of a laser acceleration scheme, it is necessary to provide the repetition rate of the laser corresponding to the accelerator frequency. Therefore, in order to obtain a high efficiency of electrons acceleration with 10 μm lasers following values of laser system principal parameters is necessary to achieve:

© Springer International Publishing Switzerland 2016

V.V. Apollonov, *High-Energy Molecular Lasers*,
Springer Series in Optical Sciences 201, DOI 10.1007/978-3-319-33359-5_46

1. Power: 1 TW;
2. repetition rate: <60 Hz.

To date, the methods of 10 μm ps laser pulses generation are well developed and enable production of pulses with τ = 1–10 ps duration and 110 μJ energy [3–6]. In order to amplify these pulses up to energies 1–10 J, it is necessary to utilize many-pass or regenerative high pressure CO_2-amplifiers (CO_2−HPA) with total gain exceeding 10^6 and gas pressure sufficient to provide necessary amplifier's gain bandwidth.

Owing to the facts that the damage threshold of IR-transparent materials utilized for optical windows does not exceed 1 J/cm^2 (e.g., 0.7 J/cm^2 for NaCl and τ = 2.5 ps [7]) and the apertures of commercially available CO_2−HPA do not exceed 1 cm, up to now the maximum achieved energy of amplified picosecond 10 μm laser pulse is was 250 mJ (for $\tau = 2.5$ ps) [7].

That is why *the* only possibility to approach 10 μm ps monopulse energies $\sim$10 J is to increase amplifier's aperture *up* to 5 cm or *even* higher. *To* the beginning of present project (1991), maximum aperture of CO_2−HPA $\sim$3 cm were realized only in e-beam controlled systems, which have well known disadvantages associated with poor quality of laser beam due to large active medium inhomogenity of laser medium as well as necessity of human protection from high current and energy e-beam. *In* our wide aperture, CO_2−HPA we utilized a new approach based on SSVD.

The present report is devoted to the construction of wide aperture picosecond CO_2 laser system generating a train of pulses with sum energy of up to 10 J: present configuration of laser system and the prospect of its upgrading are considered.

46.2 New Approach to the CO_2–HPA Construction

Since the methods of generating picosecond 10 μm laser pulses of microjoule level were well investigated up to the beginning of our project, we concentrated our main efforts into the elaboration and putting in operation high pressure wide aperture CO_2 amplifier.

A vast investigations of physical mechanisms involved in the formation of SSVD in atmospheric pressure CO_2-laser gas mixtures have been carried out in "High power lasers" department of General Physics Institute (GPI) during the last 15 years. These investigations have resulted in the development of a new approach to the SSVD formation. This approach based on the new methods of gas mixture preionization and discharge electric field dynamic profiling enabled us to significantly increase the SSVD stability and to obtain an SSVD in nonprofiled compact electrode systems with interelectrode spacings up to 70 cm and discharge volumes up to 360 L [8].

Except increased SSVD stability, this new approach also provides very uniform excitation of the gas volume and, consequently, very high light energy extraction

and laser efficiency. Thus, in the regime of laser generation on different systems, we have obtained light radiation energies up to 40 J/l/atm for CO_2-mixtures. These results are quite close to those obtained on e-beam controlled systems; moreover, the spatial homogeneity of light energy density distribution and laser radiation divergence were much better for our lasers.

The estimations based on the scaling of laser medium volume and pressure showed that we can try to realize 10 atmospheric pressure CO_2 amplifier with the aperture 5×5 cm^2 and discharge volume $\sim$1.5 1 pumped by SSVD using the concrete scheme of high voltage pulse generator and concrete costructions developed earlier in GPI.

In the beginning of the project of the construction of wide aperture picosecond CO_2-laser system, we decided to use a cooperation with Efremov's Institute of Electrophysics Apparatus in St'Petersberg where, at that time, the technique of X-ray preionization of gas mixtures was developed, tested in wide interelectrode spacing (20 cm) TEA-CO_2-units [9] and seemed to be very effective for supeatmospheric mixtures.

46.3 Description of the Laser System

The main components of laser system are:

1. 10.6 μm picosecond pulse master oscillator (MO), which produces a picosecond laser pulse with duration $\tau_i \approx 120$ ps and power $P = 0.1$–1 MW.
2. CO_2-HPA with $5 \times 5 \times 55$ cm^2 discharge volume and an unstable telescopic resonator to produce a train of subnanosecond laser pulses in a regenerative amplification (RA) regime.

46.3.1 Master Oscillator

Master oscillator consists of:

- TEA-CO_2 laser as a source of 10.6 μm radiation with following laser pulse parameters:
  - FWHM of generation pulse: 100 ns;
  - pulse energy: 30 mJ (TEM_{00});
  - beam aperture: 5 mm;
- a picosecond pulse forming system (PPFS), which is a simplified version of that utilized in [5], which contains 1-plate Ge semiconductor reflection switch to chop *a* $\sim$120 ps 10 μm pulse from initial 100 ns pulse;

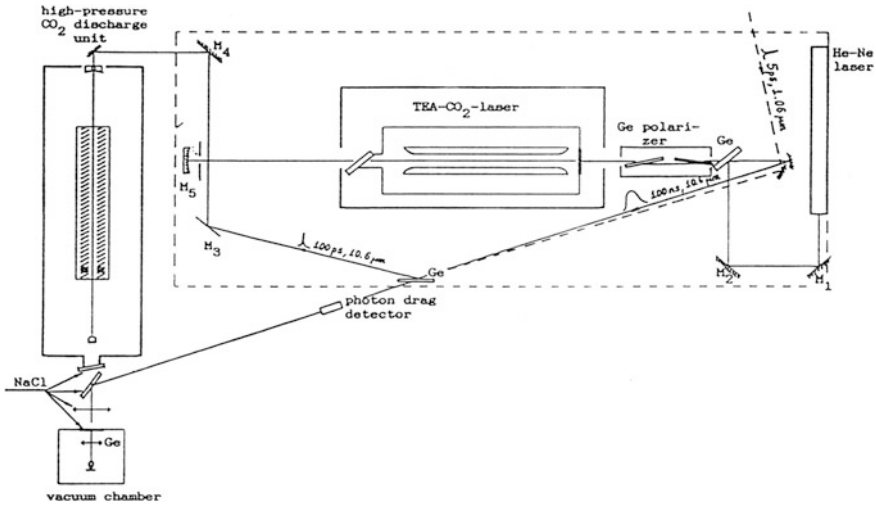

Fig. 46.1 An optical scheme of the laser system

- a 5 ps, 1.06 μm, 10 mJ Nd^{3+}: phosphate glass control laser (CL) intended to control the 10 μm reflectivity of semiconductor plates.

A scheme of PPFS is shown at the Fig. 46.1. The radiation of TEA-CO_2-laser was slightly focused by $R = 3$ m A1 mirror on the surface of plane parallel Ge plate with dimensions $2 \times 18 \times 45$ mm. Ge plate was aligned to Brewster angle (76° for 10.6 μm) relative to falling radiation with accuracy 1′. The contrast ratio of the switch was determined both by the 10.6 μm reflection from the plate (in the absence of 1.06 μm pulse) and the power of the reflected 10.6 μm picosecond pulse. In order to increase the contrast ratio, we install two-plate Ge transmission type polarizer at the exit of TEA-CO_2-laser. Careful adjustment of polarizer's angle of rotation made it possible to minimize the reflected from Ge plate signal up to 10^{-4} from the incident one. The radiation reflected from Ge plate was directed by means of a pair of plane metal mirrors into the resonator of slave laser. The 10.6 μm radiation transmitted by Ge plate was directed to the photon-drag detector.

The radiation of picosecond 1.06 μm laser pulse with the duration $\tau_{cl} = 5$ ps from CL (which was located on a separate optical table) was directed by means of 3 plane 100% reflecting mirrors on the Ge plate with an angle between 10.6 and 1.06 μm beams of <2°. A small angle shift between two laser beams was chosen in order to ensure that the reflection front propagates with the wavefront of the 10 μm laser beam across the reflecting surface of semiconductor.

The duration of the reflected pulse was estimated to be 120 ps (FWHM) according to [10] for absorbed in Ge energy of 1.06 μm radiation 1 mJ/cm^2. According to [5, 10], such a pulse has a sharp front with duration τ_{cl}, flat plato $\sim$100 and $\sim$20 ps (at half maximum) exponential tail.

The further pulse shortening is possible down to τ_{cl} by means of two-step scheme [5]. This scheme as a result of "cutting" the pulse "tail" at the second switch, allows for the smooth variation of 10 μm pulse duration from τ_{cl} up to ~100 ps. In the present set up we limited our short pulse forming scheme by the first step. It was reasonable in the case of our CO_2-HPA discharge unit operating at $P < 6$ atm pressure when broadening the initial ultrashort pulse during RA process up to duration mainly determined by amplifier's bandwidth take place (see paragraph 3).

46.3.2 High Pressure CO_2 Amplifier

The CO_2-HPA consists of three main components: X-ray source (XRS); discharge chamber; and discharge pump pulsed high voltage generator (DPPHVG) to pump SSVD preionized by XRS, and also auxiliary equipment.

46.3.2.1 X-Ray Source

An explosive-emission diode with brake-type shot-through anode was utilized as an XRS. A source schematic picture is shown at the Fig. 46.2. The system of e-beam formation contains an e-beam gun with carbon fiber explosive-emission cathode and anode grid with geometrical transparency 0.8. With 4 cm accelerating gap and operational voltage 70 kV provided by the e-beam gun pulsed high voltage generator, full gun voltage pulse duration was 3.5 μs (at the base) with current peak value of 5 kA. 50 μm thick A1 foil was a source of X-ray. Vacuum diode pressure was 10^{-5} Torr.

46.3.2.2 Discharge Chamber

A schematic picture of the discharge chamber, XRS and DPPHVG scheme of high-pressure amplifier is shown in Fig. 46.2. Glass-plastic cylindrical body of the discharge chamber is terminated from both sides with transparent plexiglas flanges. Chamber's inner diameter is 360 mm, its length −1.3 m. Electrode system of the discharge chamber is formed by profiled solid cathode and plane mesh anode. Discharge area length is 55 cm, interelectrode spacing, d, can be varied in a range of 3–5 cm. XRS radiation is introduced into the discharge area through the extraction window with dimensions 10×60 cm^2, which was a mask of 10 mm in diameter holes (with interhole spacing thickness of 2 mm) drilled inside the wall of the tube normally to the plane surface of the window. Double-side seal of discharge chamber components provided both its evacuation up to 10^{-2} Torr and its safety operation at excess pressures of not less than 6 atm.

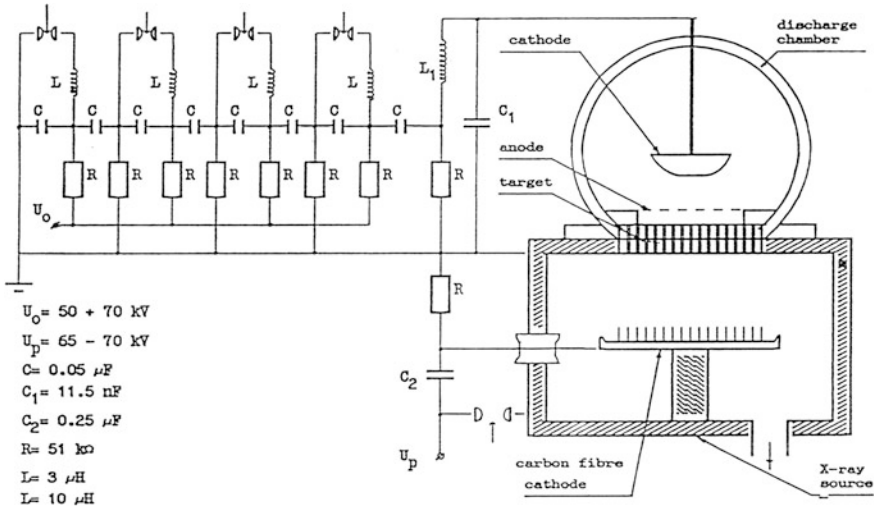

Fig. 46.2 A scheme of X-ray preionized high-pressure CO_2-amplifier

The telescopic resonator of two configurations was used in present work. In the first case: the resonator length $L = 1.4$ m and magnification $M = 2$, and in the second case: $L = 4.25$ m and $M = 1.66$. The variation of resonator's length allowed us to vary the interval between pulses in the train $\Delta T = 2L/c$, which was important for laser-matter interaction experiments.

The main advantage of described construction is a possibility of very quick change in a resonator length from 1.4 to 4.25 m and vice versa.

46.4 Discharge Pump Pulsed High-Voltage Generator

A full electrical scheme of the DPPHVG is shown on the Fig. 46.2. Fitch-Govell type 8 stages generator (FGG) with each stage capacitance $C = 50$ nF and charging voltage $U_0 = 50$–70 kV was utilized as a DPPHVG. The specially elaborated construction of the spark gaps and selective choice of the optimal excess pressure of dry air inside them enables very stable and simultaneous triggering of all spark gaps to occur. Moreover, the jitter of triggering the first spark gap relative to the pulse of multi-channel delayed pulse generator, which in turn triggered multichannel high-voltage triggering unit, turned out to be less than 20 ns. This has a principal significance in the case of picosecond pulse injection into amplifier.

In the given scheme, FGG with shock capacitance $C_{sh} = C/n = 6.25$ nF charged in a pulsed mode through a separating inductance, L_1, a fast capacitor, C_1 (which was a two parallel chains each from 4 in series 23 nF, 100 kV low inductance capacitors located as close as possible to the discharge chamber and parallel to the

discharge gap) up to the voltage determined by C_{sh}/C_1 ratio as well as "separating inductance" value L_1 and the value of breakdown threshold of gas mixture. As a result of detailed experimental measurements it was established that for the effective transfer of energy stored in DPPHVG into discharge, the ratio C_1/C_{sh} should be 1.5–2.5. Moreover, the absolute values of C_1 and L_1 should be thoroughly chosen for concrete pressure and gas components ratio of the mixture. For example, the optimal C_1/C_{sh} value for CO_2:N_2:He = 2:1:17, P = 5 atm mixture was measured to be equal to 2. Such a scheme of the discharge pumping provided a short ($\sim$150 ns at the base) current pulse to pump the gas mixture over generation threshold in the conditions of rapid relaxation of the population inversion typical for the high pressure CO_2 gas mixtures. Simultaneous with mentioned electrical scheme, utilization of low ionizing organic additive to the gas mixture (three-*n*-propylamine) in order to increase initial electron concentration in the discharge as well as to supress some channels of SSVD instabilities associated with metastable N_2 levels enabled stable SSVD to be obtained, as mentioned above; however, P = 6 atm mixture and the specific energy loading density was over 100 J/l/atm.

The parameters C_1 and L_1 previously used for P = 5 atm mixture turned out to not be optimal for 6 atm gas mixture with organic additives. For this reason, the noticeable part of the energy stored in DPPHVG was left inside it after termination of the SSVD and the maximum obtained energy of laser radiation in gain-switched, free-running mode radiation pulse of CO_2-HPA (equal to the energy of the pulse train) was up to 3.5 J (maximal charge voltage = 70 kV and resonator length L = 1.4 m) and less than one earlier obtained at 5 atm organic-free mixture. It was possible to increase the energy of laser generation for 6 atm mixture up to 5 J by means of removing the separating inductance, L_1. In this case, the first main current pulse of SSVD was followed by a few subsequent ones with falling down amplitudes. We can explain the increase of laser generation energy only by the fact that in the subsequent current pulses, the laser medium was pumped over the threshold. It is evident that in this case, the increase of laser radiation energy was due to the appearance of a tail rather than increase of the radiation peak power. Therefore, such mode of CO_2-HPA operation is not very efficient for the experiments on laser radiation interaction with matter when it is necessary to obtain maximum intensity of radiation on the target.

In the very near future, we plan to carry out optimization of DPPHVG scheme in order to better match it with the discharge and therefore to obtain better efficiency of our CO_2-HPA on 6 atm mixture.

Delay of XRS pulse relative to DPPHVG switching on was realized first with cable delay line and in a final version by independent triggering of XRS by the second channel of multi-channel triggering unit. With utilization of organic low-ionizing additives, the mentioned delay turned out to have little effect on SSVD stability and in the majority of experiments was equal to zero.

High U_0 range of SSVD stability indicated the possibility of increasing the mixture pressure up to 7 atm or even to 9–10 atm, but decreasing interelectrode spacing up to 4 cm. In latter case, we shall be able to efficiently amplify the pulses to as short as 1 ps.

46.5 Estimation of the Individual Pulses Duration in the Train

Oscillograms of the trains of pulses for two cases: L = 1.4 m and L = 4.25 m are shown at the Fig. 46.3. The presence of a secondary maximum on the envelope for the case L = 4.25 m can be connected with temporal expanding of the train due substantial increase of ΔT (from 9.3 to 29 ns) when some energy repumping to the discharge directly from Fitch-Goveli generator can take place.

Now the system of direct measurements of the 10.6 μm laser pulses durations based on the up-conversion of 10–0.5 μm radiation and its further registration with fast electroptic streak camera is under development. The combined temporal resolution of the present system of registration of laser radiation temporal structure ($\sim$1 ns rise time photon drag detector + 1300 MHz bandwidth amplifier + 1 GHz, 4 Gs/s digital osciloscope) has $\sim$1 ns rise time and does not enable determination of the real duration of the laser pulses. In this case, in order to make estimations of the individual pulse durations in the pulse train (which is also necessary to estimate the radiation intensity on the target), it is worth using some estimation calculations.

It is well known that during amplification of a laser pulse in a long gain medium (which takes place in RA regime since injected pulse makes a few tens of round trips in the resonator to approach saturation level) with finite bandwidth, the "effective" bandwidth of the medium, which determines the duration of the output pulse, decreases with G (where $G = \sum_{i=1}^{n} \alpha(t_i) \cdot L_g$ total gain increment over n round trips, $\alpha(t_i)$—small signal amplification coefficient, L_g—gain length) due to subsequent multiplication of the spectrum of the amplified pulse by the spectrum of the medium during each pass. When the intensity of the amplified pulse approaches saturation level another effect takes place—modification of the pulse shape, namely sharping of the leading edge end formation of exponential tail due to gain saturation effects. In this case, some compression of the pulse FWHM can take place.

In the case where we can neglect saturation (it take place for the first detectable pulse in the train) it is possible to use estimation from [11]. In this chapter, a

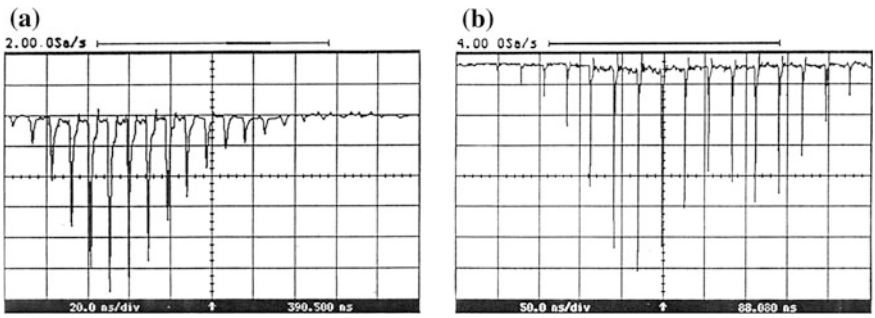

Fig. 46.3 Oscillograms of the 10 μm pulse train for the cases $\Delta T = 9.3$ ns (**a**) and 29 ns (**b**)

broadening of the pulsewidth duration τ_i (this and following designations of pulses duration in [11] corresponds to $1/e$ level of intensity) injected into CO_2-regenerative amplifier in the case $\tau_i \geq \tau_B$ (where $\tau_B = 1/\Delta\nu_H$, where $\Delta\nu_H$—FWHM of the homogeneously broadened line of the laser transition) was investigated. In our case, P = 6 atm, $\Delta\nu_H = 21$ GHz, that is $\tau_B = 50$ ps and condition $\tau_i \geq \tau_B$ is fulfilled.

In the process of multipass amplification of the pulse in the amplifying medium, its spectrum is multiplied on the each pass by the spectrum of the medium:

$$E'(w) = E(w)g(w). \tag{46.1}$$

At significant assumption that both temporal structure of the pulse and Lorentz shape of the homogeneously broadened laser transition line in the vicinity of its center can be approximated by Gaussian function, it is possible to obtain a simplified formulae for the duration, τ_0, of the pulse after n round trips inside the resonator:

$$\tau_0 = \sqrt{\tau^2 + 16G/\Delta w^2} \tag{46.2}$$

where $\Delta w = 2\pi\Delta\nu_H$. In our case, injected pulse had very sharp leading edge (3–5 ps), flat plato $\sim$100 ps and a tail with $\sim$20 ps FWHM. The spectrum of the leading edge covers 4–5 adjacent to $P(20)$ transitions and after a first few passes can be adopted to coincide with these 4–5 independent lines (since at P = 6 atm there are no significant adjacent lines overlapping due to pressure broadening). Since the duration of the pulse tail > reversal of the spectral shift of the adjacent lines for 10 P band (18 ps) the spectrum of the tail covers only $P(20)$ line. Therefore, after a few round trips, the spectrum of all the pulse coincides with the spectrum of 5 adjacent $P(16)$–$P(24)$ lines of the 10 P band of the CO_2 molecule and in further estimations we can use formulae (46.2) for each line. As to the temporal structure of the pulse, it is necessary to add together the Fourier transformations of all these 5 spectrums (after their narrowing due to large G values), which evidently give five Gaussian-shaped pulses separated by the mentioned 18 ps. For simplicity and in order to make an overestimation of the pulse duration, we adopted the equal amplitude of $\alpha(t)$ for all 5 transitions, although in reality the envelope of $\alpha(\nu)$ in 10P band had some sloping from its maximum achieved at $P(20)$ line in spectral range $P(16)$–$P(24)$. The spectrum of the injected pulse-leading edge had similar sloping and was even more sharp.

In order to make an estimation, it is necessary to know G parameter. In our case, the beginning of "injection window" (that is, the temporal range inside which generation of the pulse train takes place rather than gain-switched pulse measured relative to the beginning of the pump pulse of the active medium) coincides with the termination of the discharge current pulse, where the maximum of $\alpha(t)$ for each spectral line $\alpha_{max}(\nu_i)$ takes place. Further $\alpha(t)$ drops down with some time constant due to relaxation processes, but once more for the purposes of making an overestimation we shall adopt $\alpha(t)$ to be constant and equal to α_{max}.

For the case L = 1.4 m the delay, ΔT_1, between the injected pulse and the first detectable (on the oscilloscope) pulse of the train was $\sim$200 ns corresponding to $n = \Delta T/\Delta T_1 \approx 21$ round trips. Threshold value can be determined through the following expression:

$$\alpha_{\text{thr}} = 1/2L_{\text{g}} \ln[1/(R_1 \times R_2)], \tag{46.3}$$

where R_1 and R_2 are efficient reflection coefficients of resonator mirrors, with R_2 including diffraction and other passive losses. For resonator magnification M = 2, R_1 = 0.25 and for $R_2 \sim 1$ $\alpha_{\text{thr}} = 0.0126\,\text{cm}^{-1}$(i.e., we neglect all radiation losses except active losses on the output coupler). In our case, generation threshold corresponded to charging voltage U_{ch} = 45 kV. In the range U_{ch} = 50–70 kV generation energy increased 2.5 times and increased linearly with U_{ch}. Since in saturated amplification regime, which took place in our case, output radiation energy is roughly $\propto \alpha_{\max}$ we can estimate $\alpha_{\max} \approx 0.03\text{cm}^{-1}$ for $U_{\text{ch}} \sim 60$ kV (the most often used U_{ch} value in our experiments). The estimation through (46.2) gives $\tau_0 \approx 200$ ps for a single line and correspondingly $\tau_0 \approx 275$ ps for 5 adjacent lines. In the case L = 4.25 m, ΔT_1 was $\sim$500 ns at $U_{\text{ch}} \sim 55$ kV corresponding to $n \sim 17$. For $\alpha_{\max} \approx 0.025$ cm^{-1} in this case similar estimation gives $\tau_0 \approx 300$ ps (for 5 lines).

There is also another mechanism apart from gain saturation that can also lead to some amplified pulse shortening. Up to now we have considered the pressure broadening of a single gain line only. However, according to [12], large deviation of the experimental points in the dependence of the first detectable pulse in the train duration versus pressure of the gain medium at pressures $P > 4$ atm from the curve computed by assuming a single Gaussian gain profile indicates that the sequence bands have considerable influence on the gain in a high pressure CO_2 amplifier. This deviation is expected since pressure broadening causes significant overlap of P(20) line with sequence P(17) line separated by 10 GHz frequency shift and become important at pressures $P > 3$–4 atm. According to this work, in our case, at P = 6 atm the amplified pulse duration may be $\sim$100 ps for the case when spectrum of the injected pulse covers only P(20) transition (that can be realized by means of increasing of τ_{cl} up to 20–30 ps due to utilization of another dye solution for passive mode-locking with higher relaxation time).

In any case it is evident that in order to prove made above estimations we have to put in operation mentioned system of short 10 μm pulses registration.

46.6 Prospect of the Laser System Upgrading

The possibilities of modification of present MO of laser system to generate initial 10 μm pulses of $\sim$5 ps (and even 2 ps if we shall use methanole solution of absorbing dye in our passive mode-locked CL instead of ethanole) were already discussed (Sect. 2.1). We also discussed the possibility of increasing the efficiency

of our present 6 atm CO_2-HPA as well as possibility of increasing its operating pressure up to 10 atm in order to amplify laser pulses as short as 1 ps (Sect. 2.2). We are planning to realize these possibilities in te very near future since they do not demand principal reassembling of present laser system. We also have some other plans (for longer terms) for our system upgrading:

1. Investigating the possibility of using N_2O:CO:N_2:He mixtures in our CO_2-HPA instead of traditional CO_2:N_2:He ones. It should be noted that owing to lower group of symmetry of N_0 molecule if compared with CO_2 neighboring rotational-vibration transitions in the N_2O molecule are located twice as close to each other compared with CO_2 molecule. Therefore, it is possible to realize smooth gain spectrum of N_2O molecule owing to pressure broadening of laser transitions at the pressures of gas mixtures 5–6 atm, thus considerably decreasing the level of pulsed high-voltage applied to the discharge chamber. It should be also noted that utilization of such a gas mixture is many orders less expensive compared with CO_2 multiisotopic mixtures. Of course we understand that it will not be an easy problem. Owing to the substantially higher attachment of electrons to N_2O molecules compared with that of CO_2 the kinetics of the SSVD in N_2O mixtures strongly differs from that of CO_2. However, we had already realized SSVD in N_2O gas mixtures of 1 atm pressure with record values of SSVD active volume ($20 \times 20 \times 125$ cm^3), efficiency (6.7%) and light energy (465 J) [13] and have a good experience in investigation of kinetics of SSVD in such gas mixtures.
2. We are sure that repetition rates of $\sim$60 Hz can be realized in our laser system. All elements of our present MO scheme can operate at $f \sim 60$ Hz with reasonable upgrading. The e-beam gun utilized in our CO_2–HPA can also operate at such repetition rates if we provide more effective evacuation systems for vacuum diode compared with present one (this necessity is caused by evaporation of graphite into the volume of the diode at each shot of the gun). All elements of our DPPHVG (capacitors and spark gaps) can also operate at such repetition rates; moreover, the spark gaps were elaborated to work at $f < 100$ Hz in the gas flow mode of operation (in the present laser system, there is no need to use this option but it can be put into operation easily). The main problem for 60 Hz operation of CO_2–HPA is to provide gas flow mode of operation of the discharge chamber. It will evidently demand its reassembling and modification or more probable construction of a new one. It should be noted that construction of TEA-CO_2 lasers with f up to 20 Hz and active volumes of 5–10 1 and TEA-CO_2 lasers with f up to 400 Hz and single pulse energy of $\sim$1 J.
3. The utilization of e-beam gun in laser systems demands a high vacuum pump system (to provide 10^{-5} Torr). The presence of this system evidently substantially increases the weight and dimensions of CO_2–HPA as well as making its operation more complicated. It is also evident that additional problems will occur when transitioning to high repirates. As such, we are now searching for alternative systems of gas mixture preionization and one of the possible methods is pulling electrons out of the barrier close-to-cathode discharge and into the

discharge gap. We have a wealth of experience in utilizating this type of preionization in TEA-CO_2 discharge units with interelectrode spacing of up to 60 cm and we hope to use this for superatmospheric pressure gas mixtures [14]. If we are successful in this endeavor, this will considerably simplify the construction and operation of our CO_2–HPA.

46.7 Conclusions

1. We have put a CO_2 laser system in operation with high aperture (5×5 cm^2), 6 atm amplifier, that generates a train of subnanosecond laser pulses with sum energy of up to 5 J.
2. Our estimates based on scaling laws of SSVD stability with pressure indicate that we can obtain SSVD in our CO_2-HPA at $P = 10$ atm for interelectrode spacing =4 cm, present gas mixture (CO_2:N_2:He = 10:5:85) and energy loading densities >100 J/(l atm). Such a discharge unit can effectively amplify 10 μm laser pulses as short as 1 ps.
3. There are no principal limits for upgrading our laser system to operate with repetition rate ~60 Hz. However, such a modification of the setup will obviously demand solutions to a number of technical problems.

References

1. V.V. Apollonov, A.I. Artemyev, Yu.L. Kalachev, A.G. Suzdaltsev, A.M. Prokhorov, M.V. Fedorov, Electrons acceleration by intence laser radiation field in the presence of static magnetic filed. JETF **97**(5), 1498–1510 (1990)
2. J. Amesson, F.K. Kneubuhl, Future laser-driven particle accelerators. Infrared Phys. **25**, 121–130 (1985)
3. S.A. Jamison, A.V. Nurmikko, Generation of picosecond pulses of variable duration at 10.6 μm. Appl. Phys. Lett. **33**(7), 589–600 (1978)
4. P.B. Corkum, High-power, subpicosecond 10 μm pulse generation. Opt. Lett. **8**, 514–516 (1983)
5. P.B. Corkum, Amplification of 10 μm Pulses in Multiatmosphere CO_2 Lasers. IEEE, J. Quantum Electron. **QE-21**, 216–232, (1985)
6. Z.A. Biglov, V.M. Gordienko, V.T. Platonenko, V.A. Slobodyanyuk, V.D. Taranukhin, SYu. Ten, Generation and amplification of phazemodulated picosecond pulses of 10 μm range. Izvestiya AN USSR, Seriya Fizicheskaya **55**, 337–341 (1991)
7. P.B. Corkum, C. Roland, High Energy Picosecond 10 μm Pulses. Proc. SPIE **664**, 212–216 (1986)
8. V.V. Apollonov, G.G. Baitsur et al., SSVD initiated by UV radiation and electrons of plasma of spark discharge on the surface of dielectric (in Russian). Pis'ma v zhurnal telhnicheskoi fiziki **14**, 2107–2110 (1988)

9. A.G. Gordeichik, A.G. Maslennikov, A.A. Kuchinsky, V.A. Rodichkin, V.A. Smirnov, V. P. Tomashevich, I.V. Shestakov, E.G. Yankin, Pulsed CO_2 laser pumped by SSVD and preionized by soft X-ray (in Russian), *Kvantovaya Elektronika* **18**(10), 173–1175 (1991)
10. A.J. Alcock, P.B. Corkum, Ultra-fast switching of infrared radiation by laser produced carrirers in semiconductors. Can. J. Phys. **57**, 1280–1290 (1979)
11. P.E. Dyer, I.K. Perera, Pulse evolution in injection mode locked TE CO_2 lasers. Appl. Phys. **23**, 245–251 (1980)
12. P.B. Corkum, A.J. Alcock, Generation and amplification of short 10 pm pulses. in *Picosecond Phenomena*, Springer Series in Chemical Physics, ed. by C.V. Shank, E.P. Ippen, S.L. Shapiro, vol. 4 (1978), p. 308–312
13. V.V. Apollonov et al., N_2O laser pumped by SSVD. Kvantovaya Elektronika **16**, 1303–1305 (1989)
14. V.V. Apollonov et al, High-power CO_2 and N_2O lasers with SSVD pumping. J. Opt. Soc. Am. B **8**(2), 220 (1991)

Chapter 47
Lasers for Industrial, Scientific and Ecological Use

Abstract This chapter is based on a long-term experience of the development and operation of lasers and contains tested technical solutions on designing separate units as well on the laser on the whole. The best overall dimensions and operation characteristics and the prospects of additional chemical pumping put AMT GDL in the forefront among other powerful industrial lasers. High repetition rate pulse-periodic regime of high power laser radiation generated by AMT GDL on the level of >100 kW of average power is the most important step for effective implementation of many different laser-based technologies of the time. The very near future will highlight the total potential of high-energy lasers, which will be used effectively for processing materials and for the solution of other important challenges faced by future science and technology. However, today it is possible to say that creation of megawatt high-repetition-rate P–P lasers with a large cross section of the active medium will open up an avenue for their use in solving the problems of launching small satellites with lasers, formation of super-long conducting channels in space and atmosphere, and cleaning of the near-Earth space from space debris, etc. Hopefully, the mono-module disk laser will have a lot of advantages in comparison with the many other lasers observed in the present chapter.

47.1 Introduction: The New Era of High Energy Lasers

So, the SDI age is over. The age that was very much influencing research and development in the area of high power and high energy lasers. These days, we have extremely strong demand for the development of very powerful lasers (>100 kW) for civil applications [1]. Now the modern level of laser technology development makes laser methods of materials treatment more and more competitive. In particular, disregarding the higher price of the equipment applied, laser welding of metals provides a significant increase in productivity, a higher quality of the weld practically without any following mechanical processing, and low residual stresses

© Springer International Publishing Switzerland 2016

V.V. Apollonov, *High-Energy Molecular Lasers*,
Springer Series in Optical Sciences 201, DOI 10.1007/978-3-319-33359-5_47

in the welded products. The world market of powerful industrial lasers (average power level 1 ÷ 15 kW) applied for cutting and welding of metal structures of 1 ÷ 10 mm thick has been actively formed.

At the same time, there are a number of technical problems, the solution for which is significantly simplified by the application of industrial powerful lasers (within the range of 50 ÷ 100 kW). In particular, the areas of applications for autonomous mobile technological laser complexes (AMT GDL) are the following:

- Cleaning the coast line from oil products following oil emergency overflow and cleaning of water surface from oil layer including thin iridescent layer that can not be effectively removed by any other methods;
- Remote cutting of metal and armored concrete constructions in a course of demontage and emergency repair on nuclear power plants, oil and gas boring wells, in a process of emergency work after an earthquake and other natural disasters; cutting up ships and submarines to metal scrap;
- Remote treatment of large metallurgical chemical, mining equipment in the course of assembling and repair;
- Special technologies for use at specific conditions of different productions such as cutting of materials and metal constructions, welding and surface treatment;
- Operative struggle with ice-covering of port equipment, constructions and special system;
- Laser-based decontamination of surfaces by peeling in a process of emergency works after natural disasters and different accidents;

The upper level of estimation for output power of laser should be given by:

$$\left[h = \left[\frac{1}{W} \cdot \left(1.26 \cdot \sqrt{v} + 0.126 \cdot v\right) + \frac{0.75 \cdot v}{G} \cdot \left(1 + \frac{0.53}{\sqrt{v}}\right)\right]^{-1}\right]$$

The variables in the expression are given in: h—[cm]; W—[kW]; v—[cm/s]; G—[g/s]. In order to increase cut depth, a simultaneous increase of power and gas flow rate are required and taking into account the losses, the power needed for cutting the samples 35 cm thick should be ≈100 kW (v = 0.3 cm/s; G = 20 g/s).

There are several variants of high-energy laser beams application on removal of a thin oil film from the water surface, removal of the results of disasters, accidents and catastrophes. In these cases, price and work expenses do not play the primary role. The first place is occupied with the requirements for the reliability of high average power lasers; the overhaul period without putting additional components; simplicity in service; and operation and ecological safety. More than this, as the objects of operation are located outside workshops and far away from electric power sources, one of the basic requirements for a powerful high energy laser for such application is its mobility and full autonomy. As such, most attention had been devoted to the discussions and experimental realizations of autonomous mobile technological gas-dynamic laser (AMT GDL) [2].

47.2 Comparison of Some Types of Lasers That Can Be Scaled up to the Average Power Level >100 kW

Among all types of lasers that can be scaled up to the average power level 50 ÷ 100 kW, the following lasers can be taken for industrial applications:

- Gas-dynamic CO_2-laser (CO_2 GDL),
- Chemical HF/DF-lasers,
- Chemical oxygen-iodine laser (COIL);
- Gas-discharge CO laser;
- Gas-discharge CO_2-laser.

Let's make a short comparison of the above-given lasers.

A CW chemical HF-laser can be rather powerful and effective but it is typical of low pressure of the active medium (not exceeding several mm Hg) and a toxic exhaust. Hence, on the ground, this laser can operate only with vacuum vessels, which doesn't satisfy the requirements of a long-term operation.

Intensive development in the latest period chemical oxygen-iodine laser (COIL) does not seem attractive from the point of view of ecology and the exploitation of SCT lasers satisfying the above-given requirements, although the potential of this COIL-laser for the creation of other industrial lasers cannot be stressed highly enough. This laser also has a rather low work pressure; its exhaust gases have iodine vapors. Chemical means of the production of oxygen delta requires components difficult in application (chlorine, alkali, hydrogen peroxide etc.) and rather big chemical reactors. Gas-discharge method of the oxygen delta production does not improve the situation significantly and is yet to be developed perfectly. The price of application of a COIL of such power is assumed by specialists to be 50 ÷ 60 US$ per a kW h of laser, which makes is unprofitable.

A gas-discharge CO laser has a rather high efficiency (of the order of 40%). However, for a long-term operation of the industrial CO laser with an open working cycle and output power of 50 ÷ 100 kW, a rather high consumption of cryogenically cooled CO and N_2 (of the order of 3 ÷ 4 tons/h) will take place. In addition, the bulky store systems of the components, the system of laser gas-dynamic pat cooling as well as complex high-power electric devices will be required. The development of a neutralizing system, which provides ecologically, permitted CO laser exhaust is of a certain difficulty. And the creation of an industrial CO laser of similar power with the closed cycle in a mobile variant seems problematic enough because of high consumption of liquid N_2 for heat pick up from its gas-dynamic path.

The application of gas-discharge CO_2-lasers is discussed in two variants: open and closed cycles. Disregarding a much lower efficiency comprised to a CO laser, a gas-discharge CO_2-laser of the closed cycle is simpler technologically than the analogous CO laser since its gas-dynamic path is not cooled to cryogenic

temperature and heat dissipated by the laser can be removed by means of water heat exchangers. Here the operation of a gas-discharge CO_2-laser of the closed cycle is fulfilled on the mixture of CO_2:N_2:HE with helium content of up to 50%, and the mixture should be renewed in the amount of ≈1% per each one of its rounds over the gas-dynamic path. Hence the laser with the power of ≈100 kW will consume expensive helium for mixture renovation in the amount not less than 35–40 kg/h, which makes its operation much expensive. This laser is a more complex than the analogous one with an open cycle and of much higher weight and overall dimension. That's why it's more advantageous in operation under stationary conditions with a long daily operation cycle where in the first place the level of operation expenses is. At the same time a gas-discharge CO_2-laser of the open cycle is more suitable for the SCT laser creation.

One of the variants of the mobile non-SSVD industrial CO_2-laser of an open cycle developed in Russia with the power of 50 kW, which operates on the mixture of CO_2 and the atmospheric air. This laser is designed for works on recovery after accidents in oil and gas wells, operates from on-board components for 10 min and weights 30 tons. For operation, it requires an external power source of ≥ 600 kW. Work components of this laser consume:

• CO_2 gaseous	1260 kg/h
• Fuel (aircraft kerosene)	2700 kg/h
• Cooling water	15,000 kg/h

The laser is located on two vehicles and requires a powerful electric power source (in the field—a mobile electric station). As such, such a laser is not acceptable for many areas of applications.

47.3 Mobile CO_2-AMT GDL

The experience of the developments show that the best weight & overall dimensions with power levels 50 ÷ 100 kW have gas-dynamic CO_2-lasers (GDL). GDL is not restricted by a stationary power source and does not require intermediate transformers from heat energy into the electric one, it does not need additional systems for spent gases exhaust into the atmosphere, it is rate easy in operation, is highly reliable and has a long service time. All these factors, make GDL most suitable for the creation of SCT laser of full value with the application of air as an oxidizer and sowbelly-spread and low-toxica matter as aircraft kerosene ($C_{12}H_{22}$) and toluene (C_7H_8).

Below can see list of technical parameters of AMT GDL based on reconstructed RD-33 engine.

	AMT GDL	AMT CGDL
Output power, kW	≥ 100	≥ 100
Beam diameter, mm	100	100
Mode of operation	Continuous	Continuous, high repetitive pulsed
Wavelength, μm	10.6	10.6
Angular divergence, rad	$3 \cdot 10^{-4}$	$3 \cdot 10^{-4}$
Fuel consumption		
Laser fuel (toluene), kg/h	1000	$400 \div 500$
Engine fuel (kerosene), kg/h	2800	2800
Sucked air flow rate, kg/s	70	70
Bled off air flow rate, kg	9	5
Compressed air pressure, MPa	20	16
Time of continuous operation, min	30	30
Total service life, h	5000	5000
Power unit and laser device overall dimensions, mm^3	$7000 \times 3000 \times 2500$	$7000 \times 2000 \times 3000$
Setup weight, kg	≤ 7500	≤ 7500

It follows from the list that the cost of 1 kW h of laser power in such AMT GDL are not exceeding 15 US$, which is 4 times lower than for COIL.

It should also be noted that there is a possibility of a more complete reconstruction of RD-33 engine, which allows to bled off up to 14 kg/s of compressed air under the pressure of 2.3 Mpa. Here the output power of AMT GDL with the same operation expenses may reach 100 kW.

The AMT GDL is a module structure mounted in standard container. During the development of this scheme the experience of the creation of autonomous electric stations based on aircraft engines was applied. The container design allows providing its transportation by all types of vehicle as well as comfortable working conditions for the personnel.

It is well know that the specific output in a GDL W_{sp} is determined by the composition of the active medium at the input of the nozzle unit, its stagnation temperature, T_0, and pressure, p_0, the dimension of the restricted section of the nozzle, h_{cr}, as soon as active area width l and optical resonator parameters. All these parameters depend on each other.

The calculations of the specific power output, W_{sp}, of the industrial AMT GDL were made assuming for the application of an unstable optical resonator. Specific output for kerosene constitutes 5 and 7 kW/kg with the expansion ratio values of 15 and 23, respectively, and for toluene 7 and 9 kW/kg.

Table 47.1 gives output power values W for some variants of GDL creation.

Table 47.1 Output power values *W* for some variants of fuel for GDL

Fuel	Nozzle unit parameters			p_0, MPa	T_0, K	Flow rate		W, kW
	h_{kp}, mm	h/h_{kp}	L, m			air, kg/s	fuel, kg/s	
Kerosene	0.4	15	1.5	1.7	1300 ÷ 1400	10.0	0.26 ÷ 0.28	50 ÷ 70
Toluene	0.4	23	2.0	2.3	1400 ÷ 1500	14.0	0.38 ÷ 0.40	100 ÷ 130

As it follows from the given data, the operation of industrial GDL requires the source of compressed air with the pressure ≈1.7 ÷ 2.3 Mpa and the flow rate of 10 ÷ 14 kg/s. Such parameters can be provided by a specially designed compressor driven by the gas-turbine engine (GTE). The advantage of such an approach is in the possibility of optimization parameters of the air fed to the laser. For powerful industrial GDL, operating under stationary conditions, the variant of GTE's feeding from a natural gas source can be discussed. This cuts the operation expenses in half.

At present, the structure on the basis of a serial aircraft engine appears to be more prepared for application. Besides its compressor, it is able to give a portion of the compressed air required for operation of the laser. In such a case, the aircraft engine should not only be able to allow to be bled off the required air portion but also to provide required pressure. A comparative analysis of aircraft engines produced in Russia showed that as a gas-turbine compressor unit of an industrial GDL, a serial RD-33 engine, can be taken. The engine provides sucked airflow rate of up to 80 kg/s and the degree of complete pressure increase $\pi_k \approx 22$. As the studies show, it is quite possible to bled off up to 9 kg/s of air heated to ≈700 K under the pressure of ≈20 Mpa after a rather simple reconstruction of this engine [3].

An input ejector is positioned at the engine input, behind the low-pressure turbine an output ejector is situated that provides the external air pumping through a heat exchanger where heat pick up from the coolant system of units of the laser module (flow part of optical resonator, diffuser, resonator mirrors etc.). The input and output ejectors are of a lobe type because these devices simultaneously fulfil the function of noise suppressors. In a high-pressure compressor, compressed air is fed to the laser device, which is located behind the engine. The exhaust laser and engine gases are sent to the common exhaust device.

The possibility of the application of GDL in the form of industrial laser imposes a number of specific demands on the structure, which were not met by the developers of laser system before. First of all, this concerns the necessity of continuous operation during 6–8 h under conditions of multiple switching OFF and ON with the service life of at least a year without the replacing of any parts and units. This is achieved by the application of materials capable of operation under the temperatures up to 1500 ÷ 1600 K and the application of cooled structures.

47.4 Efficiency Increase of the AMT GDL by Additional Chemical Pumping

The further development of an idea lying in the basis of GDL has yielded appearance of the so-called chemical GDL. The latter approach is based on the optimization of the active medium parameters by the burning process control. Altering the coefficient α (deviation from stoichiometry) in the various stages of the process, feeding the fuel, other components into corresponding areas of the combustion chamber, one may control the portion of chemical energy supplied in the rotational levels and simultaneously decrease the temperature of gas immediately before the nozzle array.

Investigations demonstrated significant growth of specific energy characteristics (in particular gain) compared with the conventional GDL; expected advantages of AMT CGDL are also:

- Smaller consumption of gas and fuel components;
- The temperature of the working gas immediately before the nozzle array may be decreased to 1000 ÷ 1200 K, which essentially simplifies the choice of the materials, cooling of gas flow path; and the entire lifetime of the laser unit significantly grows;
- Due to essential lowering of working gas temperature, the extension ratio of a nozzle and switch pressure of the diffuser (at atmospheric exhaust) may be diminished; hence the blade becomes more manufacturable and of durable;
- Energy consumption, and weight-overall dimension become smaller significantly.

47.5 High Repetitive Pulsed Regime of the AMT GDL

One of the ways of GDL operation mode control and optimization is based on use of active intracavity optics. It enables modulation of transparency of the resonator in the frequency range up to many tens of kHz (30–60 kHz) and thus to form the required temporal modulation of laser radiation. This problem concerns with the high power GDL is of an essential interest. The possibility to accomplish such a mode of operation is considered in details [4].

47.6 New Approach to High Energy Lasers—Mono-Module Disk Laser

The mono-module disk laser concept is an effective design for diode-pumped solid-state lasers, which allows the realization of lasers with a super-high output average power, having very good efficiency and excellent beam quality. Since the

first demonstration of the principle in 1964, the output power of mono-module disk lasers has been increased to the level of a few kW in continuous wave (CW) mode. "Zig-Zag" disk laser geometry is not, in our opinion, promising for scaling up the laser output. The scaling laws for the mono-module disk laser design show that the limits for CW mode are far beyond 100 kW for the output power, and the energy can be higher than 100 J in pulsed mode. Owing to efficient porous cooling technology and possibility of suppressing amplified spontaneous emission (ASE), mono-module disk lasers can operate in CW and pulse-periodic (P–P) regimes at extremely high output powers.

It has long been customary that as new technologies emerge into the light, potential users and experts start wondering whether these new technologies will replace the old, well-established approaches to the solution of known problems. When we look back at the time when the first laser was created, it becomes clear that each new and more advanced technology usually replaces the pre-existing and well-proven technologies. However, a more differentiated and balanced assessment of the many innovations in the field of laser shows that there is no such thing as a perfect design, or an ideal laser. There is always room for improvement and further development. It is possible that in the near future a laser with disk geometry of the active medium will become the dominant technology. However, despite this, a number of existing laser technologies (with some exceptions, of course) will continue to improve for quite a long time. Based on these considerations, we must continue to develop most types of lasers, each time clearly specifying their undeniable technological niche and knowing well their advantages and disadvantages.

High efficiency and excellent beam quality of disk lasers means that they can be widely used in modern science and industry for a very large range of applications, including treatment of the surface of dielectric materials in microelectronics, cutting, drilling, welding, polishing and cleaning of the surface, and other technological operations with superhard and fragile metals and composite materials, etc. Pulse-periodic Q-switched disk lasers and high-average-power, mode-locked laser systems ensure optimal conditions for ablation (sublimation) of a material. A number of advantages of high repetition rate P–P lasers emitting short pulses, as applied to a wide range of industrial technologies, is the basis of many modern concepts of disk lasers. High-intensity light with an insignificant thermal lens effect in the central highly loaded zone of the active medium has led to the lifting of restrictions on the brightness of the pump diode. This has reduced the cost of laser sources, and thus has significantly improved the efficiency of electro-optical conversion, especially in the regime of high average powers. The power of the laser source is varied by scaling the cross sectional area of the generated radiation. It should be noted that its ratio to the thickness of the active material in disk geometry is much larger than the ratio of the cross section of typical core elements of the active medium to their length in any conventional solid-state laser system. This eliminates the problems associated with nonlinear distortions of the geometry of the active medium, and enables realization of super high peak and average powers of laser sources with disk geometry and same parameters of radiation in the far-field region.

It is clear that each laser source has its advantages and disadvantages. The beam quality of modern solid-state lasers (disk and fiber lasers) is pretty excellent, and their efficiency is very high. A fiber laser has significant advantages at low, average and peak output powers, while a disk laser, on the contrary, is preferable in those applications that require high and super-high output powers.

Among high repetition rate P–P sources emitting coherent high average and peak output radiation, disk lasers will undoubtedly dominate today and in the future. They provide the best solution for many industrial applications in the multi-kilowatt power range. A disk is a simple and easily excited laser element, which allows cost-effective generation of radiation with improved parameters. It has a lot of potential for the future. The advantage of a disk laser over a fiber laser is already obvious in the kilowatt power range. Having a large radiating surface, the power density of the disk laser is not critical even at high peak powers. On the contrary, in fiber lasers the increase in the peak power negatively affects the reliability of the resonator. The main disadvantage of the fiber laser is also its high sensitivity to the reflected beam, which often appears in the laser due to the interaction of the generated light with matter. If the radiation reflected from the target affects the fiber laser resonator, then it should be immediately shut down to preserve the cavity.

At the same time, the disk laser resonator is insensitive to the penetration of reflected beams. Even in the case of highly reflective materials, technological operations can be performed without the risk of an emergency switching off of the laser. Another advantage of kilowatt disk lasers is their modular design, which allows one to replace laser modules during after-sales service, thereby ensuring that in the event of failure of the laser, the downtime as well as the cost of repairs will be minimal.

On the contrary, in fiber lasers, the single-unit design of the resonator makes it impossible to easily replace the failed unit without extensive alteration of the system as a whole. At the same time, the use of fiber laser technology offers certain advantages, especially in the power range (up to several hundreds of watts). This laser is suitable for micromachining dielectric surfaces and composite materials. However, only the disk laser has a high potential in the case of high peak powers, i.e., when it is necessary to provide a train of short pulses with the highest peak power. In a typical disk laser, as opposed to a fiber laser, the power density inside the cavity is far below the critical damage threshold of the laser active medium and surfaces of auxiliary optical elements, even at a high peak power. For this reason, a disk laser allows, among other things, a better use of the laser medium in general, and significantly improvement in laser efficiency.

Thus, in the future, solid-state diode-pumped disk lasers will play the dominant role. Laser diode structures are central elements in many new types of lasers. Today, the decisive factor is the acquisition of the necessary experience and skills to design new laser systems most efficiently. Semiconductor-based technologies and applications of laser equipment on new physical principles are key technologies of modern times. For many years, the world has accumulated the experience needed today in this field of knowledge. The challenge is to ensure technological excellence in the application of laser systems, not only today but in the future.

The most difficult problem of solid state lasers is the efficient delivery of pump energy to an active disk media. In cases with a small-signal gain, single-pass absorption of the pump is also low. It follows that the effective utilization of the pump energy is necessary for the effective operation of the laser disk. To scale the output power, the medium must be optically thin, which requires a large number of passes of the pump energy through the medium. In addition, the pump energy coupled in through the lateral side of the disk can also be a possible solution for efficient pumping.

To reduce the effects of the ASE, it was proposed that an optical cover consisting of an undoped material on the surface of the laser disk be used. This cover allows the spontaneously emitted photons to escape from the active layer and prevents their resonance in the bulk of epy active material. Rays cannot be reflected from the surface, as in the case of an open disk. This allows the maximum power achievable by the disk laser to be increased by an order of magnitude. Reflection of the ASE from the disk edge should also be suppressed. This can be carried out through the absorbing layer at the generatrix of the disk cylinder. In the regime when epy output power is close to maximal, much of the energy is used in the ASE; therefore, the absorbing layers must also have heat-accumulating radiators. In the case of the maximum pump density of the disk laser, its efficiency is quite low: most of the pump power is used in the ASE and is absorbed at the edges of the device. In this case, the distribution of the pump energy between several disks can significantly improve the performance of the laser system. Indeed, lasers, consisting of several modules with disk elements in a single cavity, have been repeatedly reported. One of these lasers, fabricated by the TRUMPF Group [5], is a world leader in this class of laser systems.

In the quasi-CW regime, the power can be estimated by scaling the saturation intensity with a duty cycle of the pump and by multiplying the duration of the pump by the pulse repetition rate. At moderate repetition rates (e.g., higher than 1 Hz), the maximum energy of the output pulses is approximately inversely proportional to the cube of background losses. The undoped cover can increase the average output power by an additional order of magnitude, provided that this cover does not increase the background loss. At low pulse repetition rates (in the single-pulse regime) and sufficient pump power, there is no general limitation on the energy, but the required size of the device increases rapidly with increasing pulse energy, thereby establishing a practical limit on energy. One active element, according to the estimates, can generate an optical pulse with the energy of a few thousand joules, depending on the level of internal signal loss in the disk.

Disk lasers, as well as fiber lasers, have a large ratio of the cooling surface area to the gain of the laser. However, these two different concepts of the laser design also differ by the values of the achievable peak power. The beam quality of fiber lasers is determined by properties of waveguides, the core/cladding refractive index difference, and the size of the internal diameter of the fiber that transmits light. On the other hand, the beam quality of disk lasers depends on the resonator design. With increasing size of the optical pump region (its diameter is usually a few millimeters) at a constant optical power density on the disk surface, scaling of the

output power becomes possible. Adjustment of the resonator also has similar features. Self-phase modulation defines the typical limit of nonlinear amplification of ultrashort pulses. It leads to an extension of the spectral line proportional to the ratio of the effective optical path in the material with nonlinear characteristics to the effective cross-sectional area of the beam multiplied by the square of the pulse duration. An electro-optical switch in a regenerative amplifier of the disk laser makes a substantial contribution to the nonlinear characteristics of the gain, which is greater than the contribution from the disk. It must be emphasized that the values of the peak power, achieved today in single disk modules, are much smaller than the values obtained in 'rod' and 'slab' solid-state laser systems. However, the level of the average power generated by a single disk module also leaves much to be desired.

As mentioned previously, the design of the disk laser generating a continuous and relatively high power is ideal for cutting and welding metals, where high optical quality of the beam is required. It is important for industries such as automotive, transportation, aerospace and heavy engineering. However, the design of the disk laser is more suitable for a range of new technologies that are currently in demand. Today, a multi-module laser with a power of up to 30 kW and perfect beam quality is the undisputed leader in this class of laser systems. CW solid-state diode-pumped disk lasers demonstrate high efficiency. The beam quality of the laser disk is outstanding, which makes it possible to work with a target from a large distance, while providing an extremely high concentration of radiation in the interaction region with the help of the focusing optics. In this design of the laser module, the disk size is no more than 10 mm, because at larger sizes the energy loss due to the amplified spontaneous emission increases at an absolutely unacceptable rate. The above-presented laser system consists of a set of disk modules in a single cavity. This geometry of the laser system allows implementation of the P–P regime with a fairly high peak power, but the average power lies within a kilowatt. Parallel operation of disk lasers can increase the peak power of the entire system, but the phase-locking of the disk channels in the P–P regime requires additional investigation. Further expansion of the power to the megawatt level of both the average and peak power in both geometries is very problematic.

At the same time, a different approach is known to the implementation of scalable solid-state laser systems, which consists of a set of active elements in the form of 'slabs', followed by phase-locking of the generated radiation. The team of the Northrop Grumman Corporation has created a laser with a power of >100 kW and high laser beam quality, equal to the diffraction limit of 1.5 (averaged value) with the exposure time of 300 s [6]. The laser efficiency reaches 30%. The authors of the project point to a simple replacement of individual laser channels in case of failure. They also mention some of the advantages of the parallel structure of the amplifying channels in terms of ease of further increasing output power, if necessary, to 100 kW. In addition, the laser assembled according to this scheme provides the divergence at a level of two diffraction limits from the common (composite) aperture. From general physical considerations, we can assume that for a given

power level and a reasonable value of radiation resistance of optical elements, the divergence of the laser radiation at the level of 2×10^{-5} rad can be achieved for the CW generation regime and 0.6×10^{-5} rad for the P–P regime. A further increase in the number of channels in order to obtain an output power of 1 MW will require the coherent summation of the power from at least 80 channels, which seems an elusive task.

The question arises as to how the average power of a few megawatts can be achieved on the basis of solid-state lasers. It is this power that is needed to address the many problems associated with the removal of debris from near-Earth space, with launching of missiles with the help of lasers, with the creation of long-range conducting channels, and others. Fiber lasers are not applicable for these purposes because of the smallness of the area of the exit pupil of the fibers and hence the impossibility of operation of such lasers in the high-frequency P–P regime with high peak powers at an average power of a few megawatts. The laser system based on 'slabs' also seems hard to implement because adjustment of the system and its maintenance in safe operation mode are comparable to the complexity of working with a multi-element system for the solution to the problem of controlled thermonuclear fusion (CTF) at Livermore (USA). Proceeding from the above, the answer is quite clear: such a laser can and should be based on mono-module disk laser geometry!

This is a result of the indisputable advantages of the disk geometry in terms of the minimal thermal lens in the active media and the high radiation resistance of the disk in the P–P regime because of the large area of the optical surface to couple out the radiation. Thus, the necessity of finding a solution to the problem of the ASE suppression along the diameter of the disk was the major problem (matter of patent). In our case, the size of the disk at a megawatt level of the average power output should be at least 50 cm, i.e., at least a hundred times bigger than the size of the disk that is used today in existing systems. Radiation from such a laser, obtained during generation in the active medium of a single disk, does not require additional phase-locking. At the same time, such a laser in mono-module geometry will be very well combined with a large-diameter telescope for ensuring a high peak power density of the laser pulse on space debris. It is well known that the disk geometry of a laser was proposed 52 years ago [7], but it is only now that the solution to the problem of the ASE suppression with increasing transverse dimensions of the active medium in mono-module disk geometry is being found! Thus, the problems of creating of new versions of the mono-module disk lasers for a new class of cutting edge applications still remain to be solved [8–10]. Only the future will show the total potential for mono-module disk lasers, which will be used effectively for the processing of materials and for the solution of other important challenges faced by future science and technology. However, today we can say that creation of megawatt high-repetition-rate P–P disk lasers with a large cross section of the active medium will open up an avenue for their use in solving the problems of launching small satellites with lasers, formation of super-long conducting channels in space and atmosphere, and cleaning of the near-Earth space from the space debris, etc.

47.7 Conclusions

The given overview is based on a long-term experience of the development and operation of lasers and contains tested technical solutions on designing of separate units and the laser on the whole. The best overall dimensions and operation characteristics and the prospects of additional chemical pumping put AMT GDL in the forefront among other powerful industrial lasers. High repetition rate pulse-periodic regime of high power laser radiation generated by AMT GDL on the level of >100 kW of average power is the most important step for the effective implementation of many different laser based technologies of our days. Only the future will show the total potential of high-energy lasers, which will be used effectively for the processing of materials and for the solution of other important challenges faced by future science and technology. However, today we can say that creation of megawatt high-repetition-rate P–P lasers with a large cross section of the active medium will open up an avenue for their use in solving the problems of launching small satellites with lasers, formation of super-long conducting channels in space and atmosphere, cleaning of the near-Earth space from the space debris, etc. Hopefully it will be the mono-module disk laser that shows a lot of advantages in comparison with the many other lasers observed in the present book.

References

1. V.V. Apollonov, S.M. Silnov, *High power P–P lasers* (NOVA, N-Y, 2014)
2. V.V. Apollonov, Laser pulse phenomena and applications, INTECH (2010)
3. V.V. Apollonov, Laser pulses, theory, technology and applications, INTECH (2012)
4. V.V. Apollonov, V.I. Kislov, V.V. Kijko, A.G. Suzdal`tsev, QE **33**(9) (2003)
5. SPIE Events Europe, TRUMPF's R@D (2012)
6. SPIE Events Europe, Nothrop's R@D (2012)
7. N.G. Basov, O.V. Bogdankevich, A.Z. Grasiuk, IEEE J. QE-2 (9) (1966)
8. V.V. Apollonov, Nat. Sci. **4**, 713 (2012)
9. V.V. Apollonov, Symposium HPLS@A-2012, Istanbul 10 September (2012)
10. V.V. Apollonov, Nat. Sci. **4**, 719 (2012)

Chapter 48
Generation of a Submillimeter Half-Cycle Radiation Pulse

Abstract In this chapter, we have suggested the difference frequency generation for producing submillimeter wave packets by means of pulsed CO_2 lasers and nonlinear crystal $ZnGeP_2$. Our experiments were the first to demonstrate the capability of the chosen crystal to generate a submillimeter pulse with the power exceeding 1 W, although the total pumping intensity was limited by the surface break-down threshold of the crystal. It is possible to overcome this limit by reducing the pulse duration of the lasers and obtaining submillimeter pulse power higher than 1 MW. Owing to that we have suggested a new alternative approach for producing high-power half-cycle pulse generation with a terahertz bandwidth significantly exceeding known obtained intensity of coherent radiation, due to lower angular divergence and high pumping intensity avail-able for the crystal $ZnGeP_2$.

Generation of ultrashort laser pulses (ULP) is important in various applications of time-resolved spectroscopy and in powerful laser radiation interaction with matter. Pulses almost as short as a wave cycle T_0 have been obtained [1, 2]. In [1], the 8-fs radiation pulse of Ti: sapphire laser was compressed to 4.3 fs, which corresponds to $1.6 \times T_0$ duration of the median wavelength. The authors [2] subjected nonlinear crystal $LiTaO_3$ to the radiation of a 100-fs laser pulse with the energy of 100 nJ at the wavelength of 625 nm. They obtained Cherenkov radiation pulses slightly exceeding T_0 at a frequency of 1.5 THz. The detected electric field signal corresponds to the calculated frequency spectrum bandwidth ranging from zero to 4 THz. The shape of the spectrum is similar to the curve shown in Fig. 48.1 for a single-cycle case of the function $\sin(2\pi t/T_0)$, where T_0 = 1.3 ps.

Generation of ULP with a duration shorter than the single cycle T_0 of electromagnetic wave is of particular interest. For example, the pulse with duration $\tau = T_0/2$, where the phase of the wave packet changes from 0° to 180°, transfers the total momentum to a charged particle. In such experiments, it is important to precisely measure the phase of the signal. Notice that a half-cycle pulse duration in submillimeter range is of the order of 1 ps.

A method of producing such coherent unipolar pulses was considered in [3], where the author suggests simultaneously accelerating and grouping charged

© Springer International Publishing Switzerland 2016

V.V. Apollonov, *High-Energy Molecular Lasers*,
Springer Series in Optical Sciences 201, DOI 10.1007/978-3-319-33359-5_48

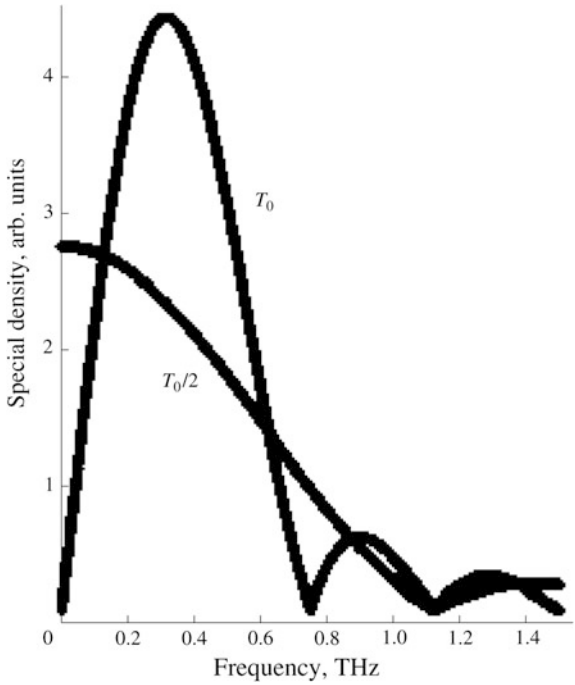

Fig. 48.1 Spectral density of the pulses with the duration equal to the cycle and the half-cycle of the wave packet $\sin(2\pi t/T_0)$, where $T_0 = 2.67$ ps

particles into clusters of length close to the radiation wave-length. If the obtained half-cycle packet affects a charged particle, then the particle acquires a momentum directed perpendicularly to the wave propagation direction. The value of the momentum is a linear function of the electric field strength.

High-power broadband coherent terahertz pulse sources were created [4, 5] as photoconductive antennas. Large-aperture photoconductors were used to generate directional electromagnetic pulses that were con-trolled by laser pulses of 70 and 120 fs. The radiation angle in [4] was 28° and the peak power of the pulses [5] was 1 MW. These sources were used in investigations of Rydberg wave packets in various materials [6].

The differential diffraction loss is found to change the frequency composition of the pulse depending on the propagation distance. As a result, the original pulse shape is altered [5]. The authors [5] correctly used the term "subsingle-cycle pulses" in this case. Then such pulses were called half-cycle pulses [6] although both the presented temporal shape of the electric field and the spectrum correspond to a duration longer than the half-cycle [4, 5].

Figure 48.1 shows the spectral density for the $T_0/2$ and T_0 pulse durations.

We suggest difference frequency generation (DFG) for producing submillimeter wave packets by means of pulsed CO_2 lasers and nonlinear crystal $ZnGeP_2$. Our experiments [7] were the first to demonstrate the capability of the chosen crystal to generate a submillimeter pulse with the power exceeding 1 W, although the total

pumping intensity was limited by the surface break-down threshold of the crystal. One can overcome this limit by reducing the pulse duration of the lasers and obtaining submillimeter pulse power higher than 1 MW. The spectral and the phase-matching characteristics of the crystal in the submillimeter range shown in Figs. 48.2 and 48.3 permit DFG in the range of 100 × 1000 μm and are more correct than data given in [8]. The DFG efficiency in this wavelength range was calculated by the Runge-Kutta method using the classical set of Maxwell differential equations truncated for interacting electric fields. The crystal absorption was taken into account for the infrared input and the submillimeter output waves. In addition, in contrast to our preceding work [9], higher pumping intensity was considered. The difference frequency generation power divided by the total pumping power is shown in Fig. 48.4 as a function of the crystal longitudinal coordinate. It can be seen that the submillimeter radiation intensity can be considerably increased by simultaneously reducing the pulse durations of the lasers and increasing their total intensity at the crystal face. For 804.15 μm wavelength, the maximum possible DFG efficiency is $\eta = 4 \times 10^{-4}$. Hence, for the total laser intensity 15 GW/cm^2 and the crystal length 15 mm, the submillimeter radiation intensity is 6 MW/cm^2. Experimental data on the damage intensity threshold for $ZnGeP_2$ crystal at the wavelength 2.94 μm [10] show that the total intensity of pumping radiation on the crystal face can be increased to 15 GW/cm^2 for laser pulse duration less than 200 ps. In future, we plan to use a complicated laser system with a 4 cm output aperture capable of generating a subnanosecond pulse train with the energy of 3.5 J for DFG with a nonlinear crystal. This laser system was successfully

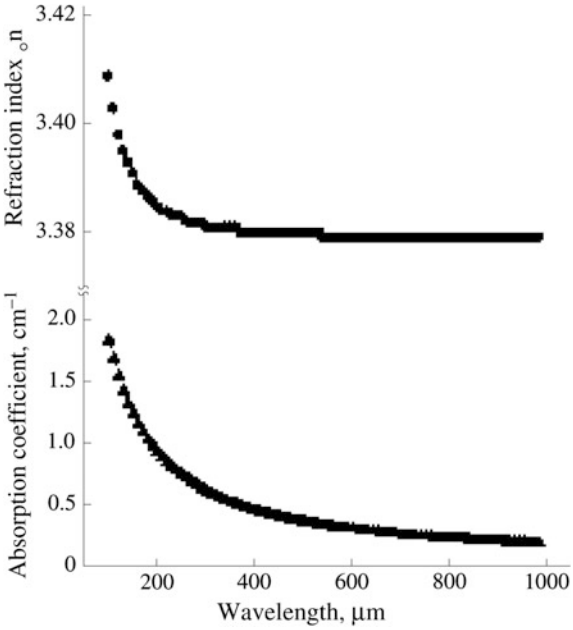

Fig. 48.2 The refraction index n_0 and the absorption coefficient α_0 of $ZnGeP_2$ as a function of the radiation wavelength, λ

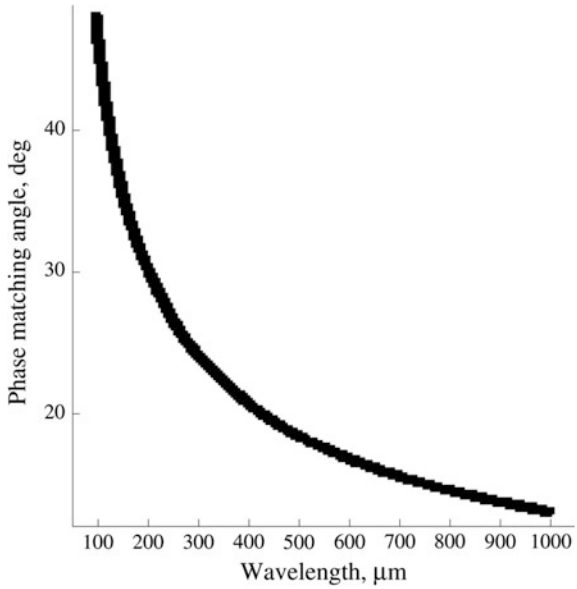

Fig. 48.3 The phase-matching angle for $ZnGeP_2$ as a function of the difference-radiation wavelength λ

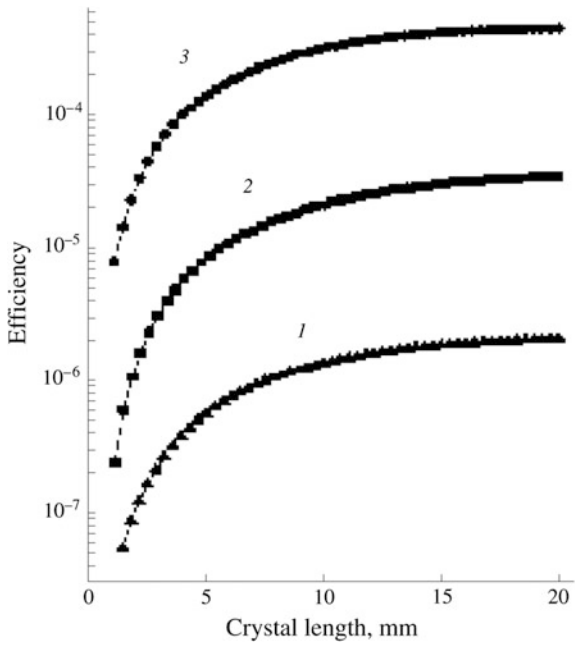

Fig. 48.4 Efficiency η of difference frequency generation of CO_2 laser emission lines in $ZnGeP_2$ versus the crystal length. The pumping radiation intensities are (*1*) 30; (*2*) 500; and (*3*) 7500 MW/cm^2; λ_3 = 804.15 μm

applied to investigations of fast spontaneous magnetic fields [11]. In order to estimate the angular distribution of DFG radiation, we used the equation [12] with the Fraunhofer diffraction and phase mismatch effects taken into account.

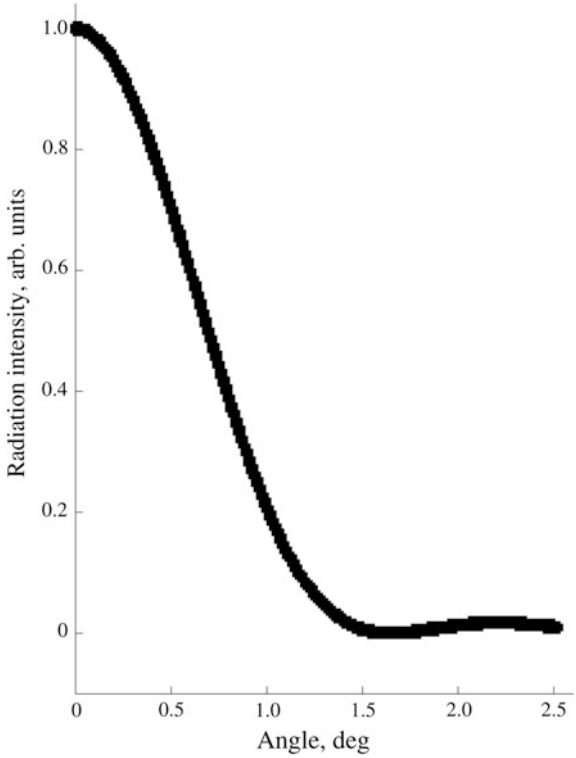

Fig. 48.5 Angular dependence of the spatial distribution for the difference-radiation wavelength 800 μm

We calculated the spatial distribution of DFG for the wavelength 800 μm (see Fig. 48.5) and estimated the angular spread of the beam −0.8° with respect to the level 1/e.

For obtaining 800 μm wave packet generation with pulse duration equal to the wave half-cycle, one should use 1.3-ps pulses of CO_2 lasers. In this case, nonlinear crystal $ZnGeP_2$ can be used for obtaining the difference in frequency generation, because such crystals were used for parametric generation of 1-ps pulses between 5 and 11 μm [13]. Submillimeter pulses of DFG with such duration correspond to a spectral density ranging from 0 to 1 THz (see Fig. 48.1). Efficiency of nonlinear conversion in the case of such broadband radiation requires further theoretical investigations or experiments. However, it is possible to limit the consideration by a minimum pulse duration for which the calculations are still correct (e.g., 200 ps) with a particular high-power DFG. Then, the DFG pulse can be further shortened to a halfcycle by means of laser reflection and absorption switches on semiconductor wafers. This approach was successfully tested for picosecond and femtosecond pulses in the infrared and submillimeter wavelength ranges and demonstrated a high ratio of the peak power to the pulse background [11, 14, 15]. The electric field phase of the ULP can be controlled by electro-optical sampling [16]. Optical methods can control phase characteristics of output signals accurate enough to

obtain unipolar half-cycle pulses. In conclusion, our calculations suggest a method for producing high-peak-power submillimeter radiation. These pulses can be used for investigating interactions of far-infrared, high-intensity radiation with matter or plasma. In such investigations, the submillimeter wavelength range is of particular importance.

Thus, we suggest a new alternative approach for producing high-power, half-cycle pulse generation with a terahertz bandwidth significantly exceeding known obtained intensity of coherent radiation, due to lower angular divergence and high pumping intensity available for the crystal $ZnGeP_2$.

References

1. M. Nisoli, S. De Silvestri, O. Svelto et al., Opt. Lett. **22**, 522 (1997)
2. D.H. Auston, K.P. Cheung, J.A. Valdmanis, D.A. Kleinman, Phys. Rev. Lett. **53**, 1555 (1984)
3. E.G. Bessonov, Zh Eksp, Teor. Fiz. **80**, 852 (1981)
4. B.B. Hu, J.T. Darrow, X.-C. Zhang, D.H. Auston, Appl. Phys. Lett. **56**, 886; B.I. Greene, J.F. Federici, D.R. Dykaar, et al. 1991, ibid, **59**, 893, (1990)
5. D. You, R.R. Jones, D.R. Dykaar, P.H. Bucksbaum, Opt. Lett. **18**, 290 (1993); D. You, P.H. Bucksbaum, J. Opt. Soc. Am. B, **14**, 1651 (1997)
6. C. Raman, C.W.S. Conover, C.I. Sukenik, PH. Bucksbaum, Phys. Rev. Lett. **76**, 2436 (1996); C. Raman, T.C. Weinacht, P.H. Bucksbaum, Phys. Rev. A **55**, R3995; T.J. Bensky, G. Haeffler, R.R. Jones, Phys. Rev. Lett. **79**, 2018 (1997)
7. V.V. Apollonov, Y.A. Shakir, A.G. Suzdal'tsev et al., Quantum Electron. **26**, 469 (1996)
8. A Shakir, V.V. Apollonov, A.M. Prokhorov et al., Proc. SPIE **2842**, 163 (1996)
9. V.V. Apollonov, Y.A. Shakir, Proc. Intern. Conf. "Lasers'97", p. 733 (1998)
10. K.L. Vodopyanov, L.A. Kulevskiy, V.G. Voevodin et al., Opt. Commun. **83**, 322 (1991)
11. V.V. Apollonov, K.K. Kazakov, N.V. Pletnev, V.R. Sorochenko, Proc. Intern. Conf. "Lasers'97", p. 736, (1997)
12. F. Zemike, In *Methods of Experimental Physics*, Ed. by C.L. Tang, vol. 15 (Academic, London, 1979), part B, p. 166
13. V. Petrov, Y. Tanaka, T. Suzuki, IEEE J. Quantum Electron. **QE-33**, 1749 (1997)
14. C. Rolland, P. Corkum, J. Opt. Soc. Am. B **3**, 1625 (1986)
15. F.A. Hegmann, M.S. Sherwin, Proc. SPIE **2842**, 90 (1996)
16. J.A. Valdmanis, G.A. Mourou, C.W. Gabel, IEEE J. Quantum Electron. **QE-19**, 664 (1983); Z. Jiang, X.-C. Zhang, App1. Phys. Lett, **72**, 1945 (1998)

Chapter 49
High Power CO_2-Laser Radiation Conversion with $AgGaSe_2$ and $AgGa_{1-x}In_xSe_2$ Crystals

Abstract In this chapter, the submillimeter spectra of $AgGaSe_2$ and $AgGa_{1-x}In_xSe_2$ crystals investigated for the first time and calculated phase matching tuning characteristic showed the possibility of infrared radiation conversion into a submillimeter one. Computation results showed that it is possible to generate more 10-MW sub-millimeter power values by means of difference frequency generation if we use laser pulses with a reasonable duration and high enough intensity. From the results, it follows that it would be preferable to use $AgGaSe_2$ or the $AgGa_{1-x}In_xSe_2$ to $ZnGeP_2$ for the powerful half-cycle pulse generation.

49.1 Introduction

With different nonlinear crystals, laser radiation can be converted to the submillimeter spectral region by difference frequency generation (DFG) [1]. By means of $ZnGeP_2$ crystal and CO_2 lasers the radiation pulses reached more than 1 W power value for the first time at the 100 μm range [2]. Computation results [3] showed that with the $ZnGeP_2$ of 20 mm length, it is possible to increase output-power value up to 3.3 MW at the wavelength of 804 μm if using laser pulses with a duration less than 200 ps and total intensity up to 10 GW/cm^2. $AgGaSe_2$ and $AgGa_{1-x}In_xSe_2$ crystals were successfully used for second-harmonic generation of CO_2 laser radiation [4, 5]. Some optical characteristics of these nonlinear crystals are described for the infrared spectral region [6, 7]. Both refraction and absorption spectra of these crystals investigated in 4.6–18.5 cm^{-1} range are presented in [8]. The DFG efficiency problem was also investigated in [8].

49.2 Crystal Samples Investigation

In comparison with [8] we considerably expanded the limit of transmission measurements of the $AgGaSe_2$ and $AgGa_{1-x}In_xSe_2$ samples grown by OKB "Amethyst" (x = 0.35) to high frequency direction: up to 39.6 cm^{-1}. These measurements were

© Springer International Publishing Switzerland 2016

V.V. Apollonov, *High-Energy Molecular Lasers*,
Springer Series in Optical Sciences 201, DOI 10.1007/978-3-319-33359-5_49

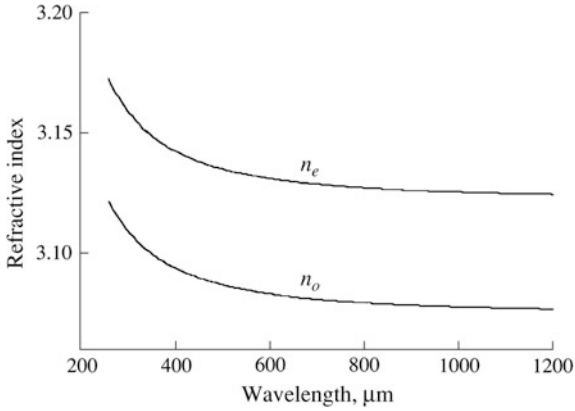

Fig. 49.1 Refractive indices of $AgGaSe_2$ crystal versus wavelength for ordinary and extraordinary waves

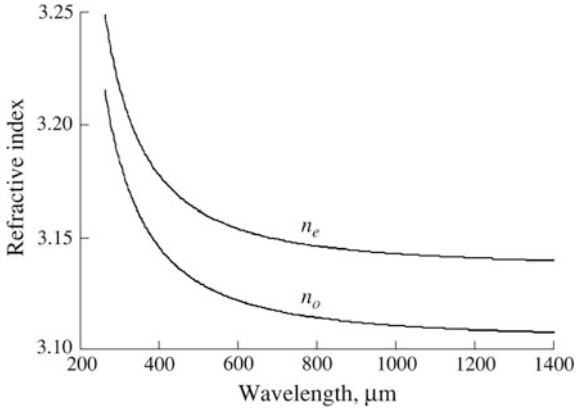

Fig. 49.2 Refractive indices of $AgGa_{1-x}In_xSe_2$ crystal versus wavelength for ordinary and extraordinary waves

realized by laboratory spectrometer "Epsilon" with submillimeter backward wave oscillator [9]. The transmission spectra of parallel-sided plates with a thickness of 0.506 and 1.255 mm were recorded. All measurements were executed for two orthogonal orientations of electric field relative to crystallographic axe of samples: $\mathbf{E} \parallel \mathbf{c}$ and $\mathbf{E} \perp \mathbf{c}$. Both refraction and extinction indices were calculated according to the Fresnel formula for an electromagnetic wave passing through dielectric [9]. These data allowed us to present spectra of refractive (Figs. 49.1 and 49.2) and absorption (Figs. 49.3 and 49.4) coefficients (n and α) corresponding to ordinary and extraordinary submillimeter waves. Relative errors of the presentation equal $\Delta n/n = 2.5\%$, $\Delta\alpha/\alpha = 10\%$.

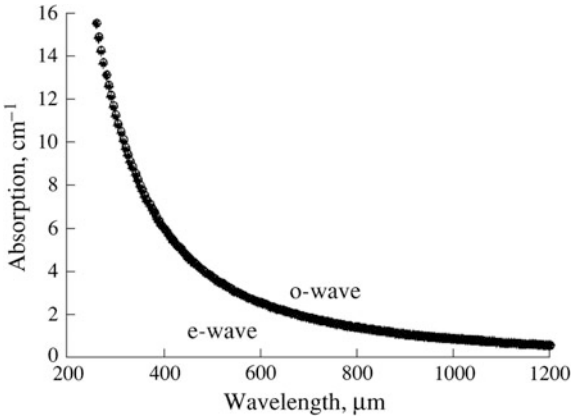

Fig. 49.3 Absorption coefficients of $AgGaSe_2$ crystal versus wavelength for ordinary and extraordinary waves

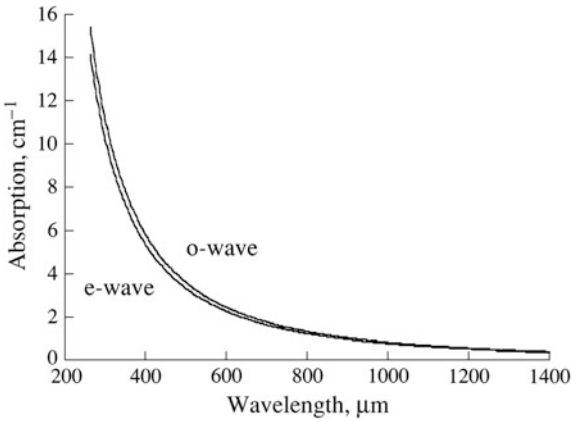

Fig. 49.4 Absorption coefficients of $AgGa_{1-x}In_xSe_2$ crystal versus wavelength for ordinary and extraordinary waves

49.3 Calculations

49.3.1 Phase Matching Characteristic

By means of the refraction data and infrared ones from [7] phase matching, characteristics for $AgGaSe_2$ were calculated when different combinations of CO_2 lines from both 9 and 10 μm branches interact by type "oe → e" (Fig. 49.5). The obtained results highlight the possibility of the infrared radiation conversion into a submillimeter one by these crystals.

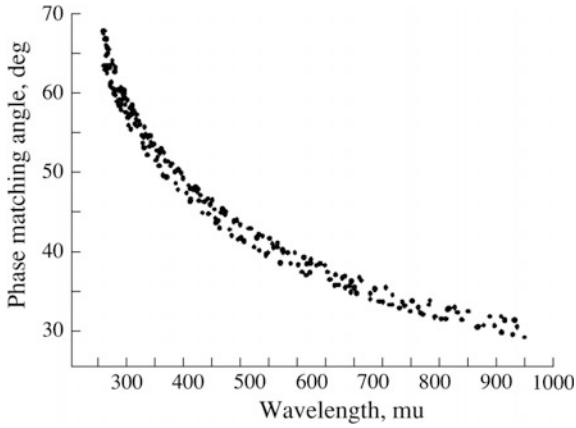

Fig. 49.5 Phase matching characteristics of difference frequency generation with $AgGaSe_2$. Interaction type: oe → e

49.3.2 Efficiency of Difference Frequency Generation

We have performed calculations of an efficiency value of DFG taking into account principal parameters of CO_2 laser radiation and $AgGaSe_2$ crystal investigated. The classical set of Maxwell differential equations, shortened for interacting electric fields, was used for problem solution, as in [2]. Before this set solution, the following assumptions were used: (a) exact phase matching $\Delta k = 0$; (b) series of boundary conditions for laser intensities $J_1(0) = J_2(0)$, and it was assumed ones are equal to 30, 500 and 7500 MW/cm^2 that correspond to damage-free pumping by CO_2 laser radiation with a pulse duration of 100, 2, 100 ps, accordingly; (c) computed values of phase matching angle for the combinations of CO_2 laser emission line pairs that allow the possibility of generating 500.7, 603, 702, and 800.5 μm radiation; (d) submillimeter data of refractive and absorption coefficients from our measurements and the infrared one [1, 7]; and (e) 1 cm^2 area of laser beam aperture. The efficiency value was determined by the correlation $\eta = J_3(z)/(J_1(0) + J_2(0))$. Value η was computed for the given crystal length from 0 up to z_0 and therefore it was possible to observe evolution of DFG along the nonlinear crystal. For coordinate z_0 the condition $J_1(z_0)/J_1(0) = 1/e$ was executed. Computation was realized by the Runge-Kutta method.

The computation results are shown for the above–specified laser intensities in Fig. 49.6 and for the submillimeter wavelength values λ_3 referred to in Fig. 49.7 with $AgGaSe_2$ crystal. In Fig. 49.7, DFG evolution of different λ_3 is not identical because of the difference of absorption values: $\alpha_{1,2} = 0.09{-}0.1$, $\alpha_3 = 1.42{-}3.7$ cm^{-1}. The maximum values of efficiency η_{max} and corresponding crystal lengths are presented in the Table 49.1.

From the results of the calculations, it is possible to see that close values of efficiency are possible with different crystal lengths. When wavelength λ_3 increases, the crystal length of maximum efficiency increases, too. It is necessary to notice that according to our submillimeter measurements and infrared data [5] refractive

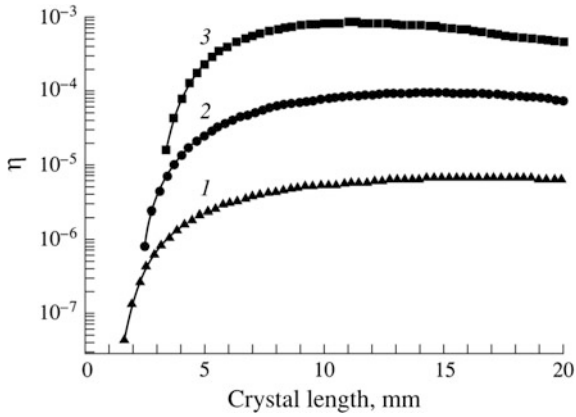

Fig. 49.6 Efficiency η of difference frequency generation of CO_2 laser emission lines with $AgGaSe_2$ versus the crystal length. Pumping radiation intensities equal (*1*) 30, (*2*) 500, and (*3*) 7500 MW/cm^2; $\lambda_3 = 500.7$ μm

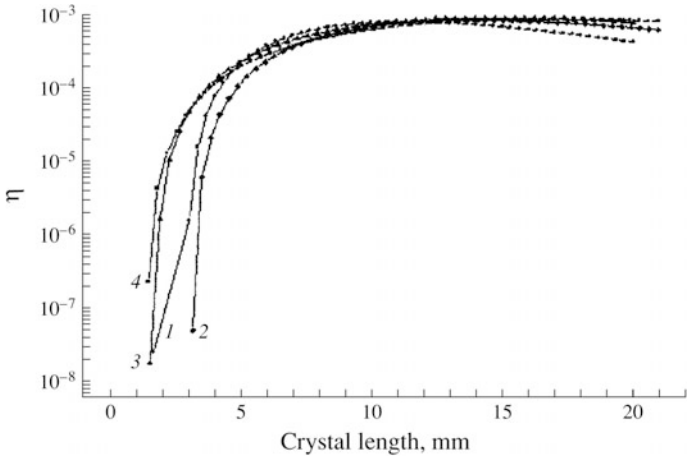

Fig. 49.7 Efficiency η of difference frequency generation of CO_2 laser emission lines with $AgGaSe_2$ versus the crystal length: (*1*) $\lambda_3 = 500.7$, (*2*) 603, (*3*) 702, and (*4*) 800.5 μm, pumping radiation intensities equal to 7500 MW/cm^2

Table 49.1 The maximum values of efficiency g_{max} for corresponding crystal lengths

λ_3 (μm)	η_{max}	Crystal length (mm)
500.7	8.2×10^{-4}	11
603	8.6×10^{-4}	13.9
702	9.2×10^{-4}	14.7
800.5	8.9×10^{-4}	16.6

indices of $AgGa_{1-x}In_xSe_2$ crystal are close to the same indices of $AgGaSe_2$. Since these crystals have close values of absorption, we can assume that the values of DFG efficiency will be close for both crystals, too. Thus with these crystals of a length less than the $ZnGeP_2$ one [3] it is possible to generate 800 μm radiation pulse with power values higher than calculated [3] with $ZnGeP_2$.

49.3.3 Half-Cycle Pulse

The results of calculations allow us to propose $AgGaSe_2$ and $AgGa_{1-x}In_xSe_2$ crystals for powerful half-cycle pulse generation by the method described for the $ZnGeP_2$ crystal [3, 10]. Submillimeter pulse duration would be the same in a half-cycle of a wave if we use ~ 1.3 ps pulses of CO_2 lasers for the 800 μm wave packet generation. However, we suggest the use of pulse duration minimum (for example, ~ 200 ps, for this value our computation results are correct, as yet) with selected power value of DFG and then to reduce submillimeter pulse duration up to half-cycle of 800 μm wave by means of converted radiation reflection and absorption switch of semiconductor wafers. This method has been tested for picosecond and femtosecond pulses at both infrared and submillimetre wave region and demonstrated high values of contrast ratio of peak power to pulse background [11–13]. In our case the method allows us to expect that, after nonlinear crystal, high peak power of radiation produced in correspondence with our calculations data should be saved.

49.4 Conclusion

Submillimeter spectra of $AgGaSe_2$ and $AgGa_{1-x}In_xSe_2$ crystals investigated for the first time and calculated phase matching tuning characteristic showed the possibility of infrared radiation conversion into a submillimeter one. In addition, computation results showed that it is possible to generate more 10-MW submillimeter power values by means of DFG if we use laser pulses with a duration of less than 200 ps and a sum intensity of up to 15 GW/cm^2. From the results, it follows that it would be preferable to use $AgGaSe_2$ or the $AgGa_{1-x}In_xSe_2$ to $ZnGeP_2$ for the powerful half-cycle pulse generation.

References

1. V.G. Dmitriev, G.G. Gurzadyan, D.N. Nikogosyan, *Handbook of Nonlinear Optical Crystals* (Springer, Berlin, 1997), p. 344
2. Y.A. Shakir, V.V. Apollonov, A.M. Prokhorov et al., Proc. SPIE **2842**, 163 (1996)
3. V.V. Apollonov, YuA Shakir, Proc. SPIE **3686**, 145 (1997)
4. J. Heuningsen, S.A. Trushin, T. Mogelberg et al., Appl. Phys. B **61**, 291 (1995)

5. Y.M. Andreev, G.C. Bhar, S. Das, et al., Appl. Phys. Lett. **63**, 1316; G.C. Bhar, S. Das, D.V. Satyanarayan, et al., 1995, Opt. Lett. **20**, 2057, (1993)
6. B.C. Ziegler, K.L. Schepler, Appl. Opt. **30**, 5077 (1991)
7. K. Kiyoshi, S. Tomomi, Oyo Suturi, **50**, 763 (1981)
8. V.V. Apollonov, S.P. Lebedev, Y.A. Shakir et al., Proc. SPIE **3828**, 342 (1999)
9. A.A. Volkov, YuG Goncharov, G.V. Kozlov et al., Trudy IOFAN **25**, 3 (1990)
10. V.V. Apollonov, YuA Shakir, Laser Phys. **9**, 741 (1990)
11. V.V. Apollonov, K.K. Kazakov, N.V. Pletnev, V.R. Sorochenko, Proc. Int. Conf Lasers **97**, 736 (1998)
12. C. Rolland, P. Corkum, J. Opt. Soc. Am. B **3**, 1625 (1986)
13. F.A. Hegmann, M.S. Sherwin, Proc. SPIE **2842**, 90 (1996)

Chapter 50
Subtraction of the CO_2 Laser Radiation Frequencies in a $ZnGeP_2$ Crystal

Abstract Nonlinear conversion of various combinations of the laser lines resulted in generation of FIR radiations at different frequencies that corresponded to the wavelengths λ = 102.60, 106.58, 108.79, 110.76 pm. The energy of the FIR radiation pulses was 180 ± 100 nJ, which corresponded to a power of 1.8 ± 1.00 W when the FIR pulse duration was 100 ns. The discrepancy between the calculated and measured energies of the FIR pulses was primarily due to the losses resulting from mismatch between the dimensions of the crystal and the laser beam cross section. The results of this chapter allow recommendation of $ZnGeP_2$ as an efficient nonlinear crystal for the generation of FIR radiation without recourse to cryogenic temperatures or magnetic fields. The FIR radiation power in excess of 1 W shows that it should be possible to construct an FIR tunable pulse-periodic source on the basis of a $ZnGeP_2$ crystal and characterized by a high output power.

In the far infrared (FIR) range, a difference frequency of the radiation from two CO_2 lasers can be generated in a variety of nonlinear crystals [1]. A crystal of $ZnGeP_2$ has the following advantages: its use does not require cryogenic temperatures or magnetic fields [2], and it has low absorption in the IR and FIR spectral ranges [3, 4]. We investigated subtraction, in a $ZnGeP_2$ crystal, of the radiation frequencies of high-power, pulsed CO_2 lasers.

Collinear phase matching of ordinary and extraordinary IR beams was used to ensure an efficient interaction of radiations in the nonlinear crystal. The spectral characteristics of $ZnGeP_2$ (Fig. 50.1), calculated in accordance with [4] for the ordinary wave, made it possible to determine the phase-matching angle in the FIR range (Fig. 50.2) and to estimate the energy of the FIR radiation. For example, calculations carried out for IR pulses (0.4 and 0.1 J energy, and $\tau \sim 100$ ns duration) gave the $\sim$3.6 μJ energy per pulse at the λ = 100 μm wavelength.

We used two CO_2 lasers with a shared active medium (Fig. 50.3). An active medium (1) was pumped (240 J/2.5 l) by a method similar to that used earlier [5]. basing (with independent frequency tuning) was excited in two three-pass cavities with diffraction gratings (2, 3) and a shared output mirror (5), which was a Ge plate antireflection-coated on one side. The positions of Brewster windows, made of

© Springer International Publishing Switzerland 2016

V.V. Apollonov, *High-Energy Molecular Lasers*,
Springer Series in Optical Sciences 201, DOI 10.1007/978-3-319-33359-5_50

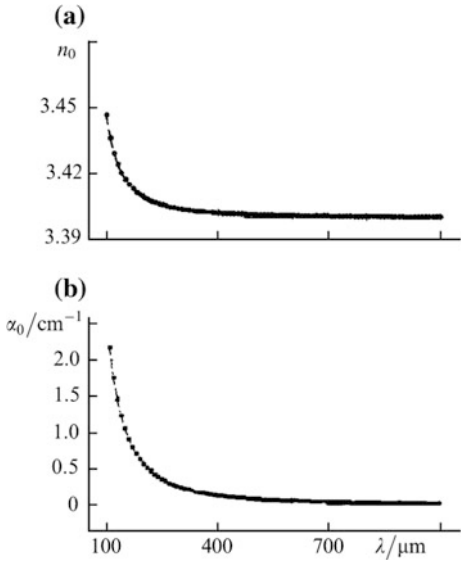

Fig. 50.1 Dependences of the refractive index n_0 (**a**) and of the absorption coefficient α_0 (**b**) of $ZnGeP_2$ on the radiation wavelength, λ

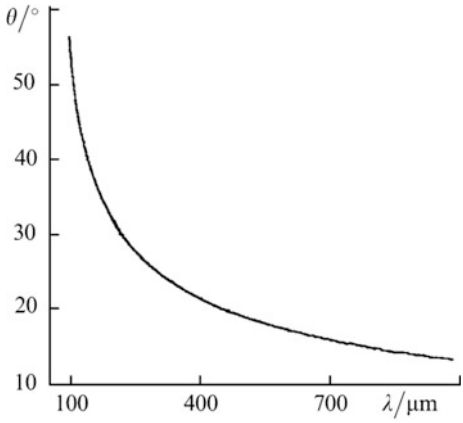

Fig. 50.2 Dependence of the phase-matching angle θ for $ZnGeP_2$ on the difference wavelength λ

KC1, and of gratings (100 and 150 lines/mm) relative to the laser chamber resulted in orthogonal polarization of the rays. The optical length of the cavity was 5.8 m and apertures (6) selected the fundamental mode. The energy of the pulses, measured with an IMO-2 N calorimeter, was 0.2−0.7 J, depending on the emission line. The signals generated in photodetectors (of the FP-1 type) were observed with the aid of S8-14 and Sl-108 oscilloscopes. A radiation pulse had a peak of ~100 ns duration and a gently sloping trailing edge of up to 1.5 μs. The signal was jagged and had nanosecond spikes of longitudinal mode beats. This pulse profile ensured a reduction in the threshold of plasma formation on the surface of a crystal (10) [6], compared with the expected value. Therefore, in our experiments, the total radiation

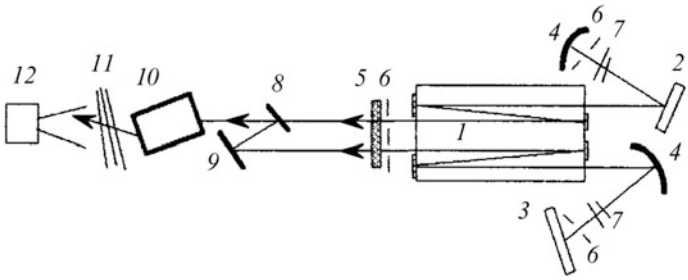

Fig. 50.3 Schematic diagram of the apparatus

energy density at the entry face of the crystal did not exceed 0.6 J cm^{-2}. The rays were made parallel, to within 0.001 rad, by a ZnSe plate (8) and a mirror (9). A time delay between two pulses was the result of differences between the dynamics of growth of the gain for each line of the CO_2 molecule. The pulses were made to coincide by introducing additional Teflon attenuators (7) in the optical field of the line that was generated first. The resultant synchronization of the pulses was characterized by a longterm instability not exceeding 20 ns for a series of 90 pulses. A multichannel synchronization unit [7] with a time instability of the delay $\sim$2 ns was triggered by a spark gap in the pump source of the laser.

The FIR radiation was recorded with a receiver (12), which consisted of a pyroelectric detector of the ELTEC 420M3 type with a cone in front of it and a charge preamplifier of the CAMAC 1005A type. The IR radiation was suppressed by attenuators (11), which were Teflon plates 1 mm thick. The signal amplitude on the oscilloscope screen was proportional to the radiation energy reaching the detector and the duration of the leading edge of the signal was equal to the duration of the radiation pulse.

Nonlinear conversion of various combinations of the laser lines resulted in generation of FIR radiations at different frequencies that corresponded to the wavelengths λ = 102.60, 106.58, 108.79, 110.76 pm. The energy of the FIR radiation pulses was 180 $\pm$ 100 nJ, which corresponded to a power of 1.8 $\pm$ 1.00 W when the FIR pulse duration was 100 ns. The discrepancy between the calculated and measured energies of the FIR pulses was primarily due to the losses resulting from mismatch between the dimensions of the crystal (8 $\times$ 8 11 mm) and the laser beam cross section (diameter $\sim$ 10 mm). The phase-matching angles at the wavelengths just listed were close to those found by calculation.

The results allow us to recommend $ZnGeP_2$ as an efficient nonlinear crystal for the generation of FIR radiation without recourse to cryogenic temperatures or magnetic fields. The FIR radiation power in excess of 1 W, achieved for the first time, suggests that it should be possible to construct an FIR tunable pulse-periodic source on the basis of a $ZnGeP_2$ crystal and characterized by a high output power.

References

1. R.L. Aggarwal, B. Lax, *Nonlinear Infrared Generation,* ed. by Y.R. Shen, (Springer, Berlin, 1977)
2. G.D. Boyd, T.J. Bridges, C.K.N. Patel, Appl. Phys. Lett. **21**, 553 (1972)
3. G.D. Boyd, E. Buehler, F.G. Storz, J.H.Wemick, IEEE J. Quantum Electron. **QE-8** 419 (1972)
4. V.V. Voltsekhovskii, A.A. Volkov, G.A. Komandin, Y.A. Shakir, Phys. Solid State **37**, 1198 (1995)
5. V.V. Apollonov, G.G. Baitsur, A.M. Prokhorov et al., Tech. Phys. Lett. **14**, 241 (1988)
6. V.V. Apollonov, V.I. Konov, P.I. Nikitin, A.M. Prokhorov et al., Sov. Tech. Phys. Lett. **11**, 429 (1985)
7. V.V. Apollonov, V.V. Brytkov, S.I. Zienko, S.V. Murav'ev, Y.A. Shakir, Prib. Tekh. Eksp. **4**, 125 (1987)

Chapter 51
Self-controlled Volume Discharge Based Molecular Lasers Scaling

Abstract The results presented in the Part I for CO_2–N_2–He mixtures pumped by preliminary filling of the gap with an electron flux from an auxiliary discharge plasma source and in the Part II, which are the most interesting due to HF(DF) lasers wavelength for the majority of applications under consideration in Part IV of the book. Both modes of operation (SSVD and SIVD) are suitable for the large distances between electrodes—i.e., big gaps. The total weight of the system can be fixed at the level of a few tones. The size of the system looks very much reasonable for a movable configurations of laser. The main advantage of the system is a non-hazardous nature of components, which means that the usage of such a system could be very much safe and effective.

We presented in the Part I the process of SSVD formation for CO_2–N_2–He mixtures by preliminary filling of the gap with an electron flux from an auxiliary discharge plasma source and SIVD in the Part II, which is the most interesting owing to HF (DF) lasers wavelength for the majority of applications under consideration in the Part IV of the book. As it was mentioned previously, both modes of operation are suitable for the large distances between electrodes—big gaps. The study was made of the characteristics of some type of the discharges that could be used as an auxiliary ones. It was established that the formation of an SSVD is affected significantly by the distortion of the electric field caused by the presence of a space charge of the electron flux in the gap. Dynamic profiling of electrons flux was found to be very much possible, and an SSVD was attained in the systems with a strongly inhomogeneous initial distribution of the electric field in the gap. It was proved experimentally that the technology of filling the discharge gap with an electron flux is a very much scalable technology!

The simplicity of the proposed methods is promising for high-energy CO_2 laser applications. Although the main results of the SSVD investigations for molecular gas mixtures was very impressive. The methods can be applied to other molecular gases such as, for example, N_2O. Owing to our successful investigations, the aperture of SSVD-based lasers and amplifiers was increased by up to 1 m for an electric efficiency of more than 10%. The 30 kJ per pulse laser had been developed

© Springer International Publishing Switzerland 2016

V.V. Apollonov, *High-Energy Molecular Lasers*,
Springer Series in Optical Sciences 201, DOI 10.1007/978-3-319-33359-5_51

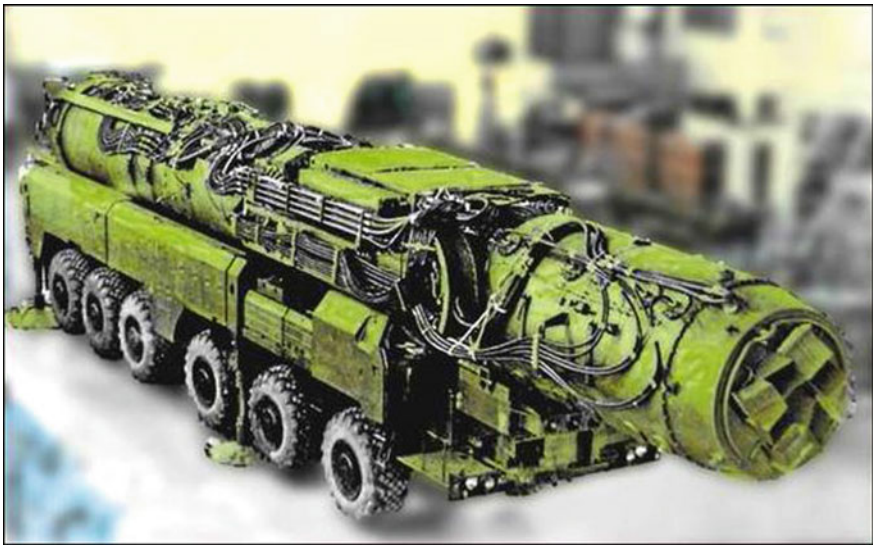

Fig. 51.1 30 kJ CO_2 SSVD based laser

and tested [1]. Operation of the system in the non-SSVD mode was not successful. SSVD as a high energy laser approach is suitable even for realization of MJ scale laser with aperture up to (2 × 2 m) due to the fact that SSVD mode of operation was very efficient for a big scale systems. It is a pity that the prolongation of "Scalable high energy CO_2 laser" project was carried out on a paper only (Fig. 51.1).

A little after this, the SIVD in SF_6-hydrocarbon mixtures, used as an active media for nonchain HF/DF lasers, was also investigated. The following features of the SIVD development had been established. After the primary electrical breakdown of the discharge gap, the SIVD spreads in the gap in the direction perpendicular to that of the electric field as a result of the consecutive appearance of overlapping diffuse channels. As the new channels appear, the current that flows through the channels formed earlier diminishes. The volume occupied by the SIVD increases almost linearly when the energy deposited in the plasma increases and, when the discharge volume is confined by a dielectric surface, the discharge voltage increases simultaneously with an increase in the current. The hypothesis was put forward that mechanisms exist for the limitation of the current in the conducting channel. They are associated with the specific energy released in the plasma, and they prevent the transfer of all deposited energy through a separate channel. It is shown that such mechanisms can be the dissociation of SF_6 and the considered problems of scaling nonchain HF(DF) lasers are discussed in Part II in greater details. This book, is to a large extent a survey of our efforts in this area of high energy molecular lasers research, we touch on the necessary conditions for SIVD in large volumes obtaining:

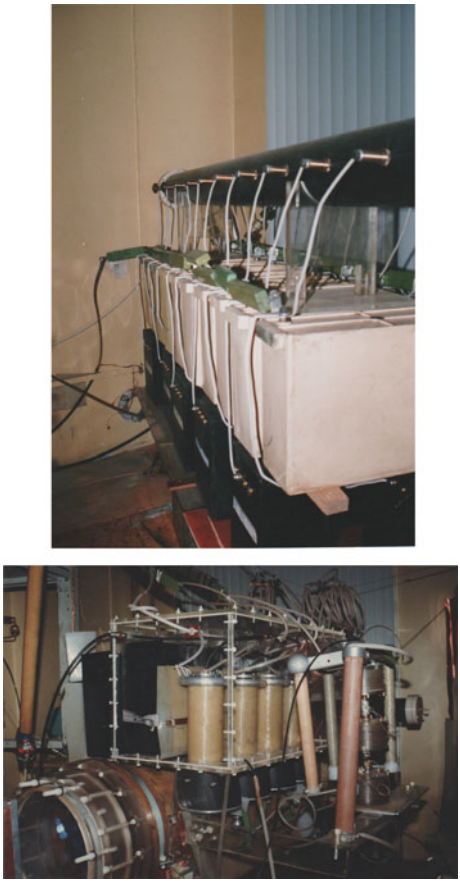

Fig. 51.2 Generator's capacitance and generator

(1) a cathode should posses a small-scale (~50 μm) surface roughness;
(2) to match a circuit wave impedance to the discharge plasma resistance at a given interelectrode distance, a mixture pressure should be chosen in such a way that the discharge burning voltage determined by the conditions of the gap breakdown in SF_6 be two times less than the voltage fed to the gap;
(3) increasing electric energy through increase in the generator's capacitance at a given maximum generator voltage should followed by growth of the discharge volume V as $V \sim C^{3/2}$ where C is the generator's capacitance (Fig. 51.2). On fulfillment of all these conditions, one should also try to maximally decrease the period of time during which the energy is deposited in the discharge plasma.

Maximum generation energy of nonchain HF(DF) laser obtained in our experiments was 407 J on HF and 325 J on DF at electric efficiencies of 4.3 and 3.4%, respectively [2]. The active medium volume was ~60 1 at an aperture of approximately 30 cm (Fig. 51.3).

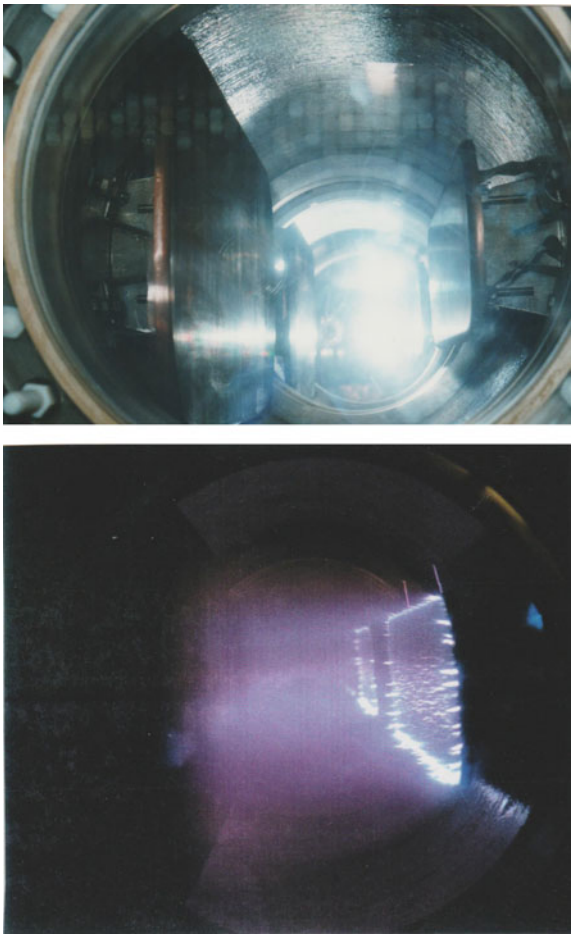

Fig. 51.3 Discharge gap and electric discharge for 400 J HF(DF) laser

Of natural interest is the problem of increasing laser radiation energy. In Fig. 51.4, the dependence is presented of the output HF laser energy, W_{out}, on the energy, W_p, stored in the capacitors of a high-voltage generator. In this figure, are plotted the data we obtained during last few years at the setups with different volumes of active medium. It can be seen that all the points are in good agreement with the directly proportional relationship at electric efficiency of ≈4%. This allows one to predict the possibility of further increase in the output energy of nonchain HF (DF) lasers through creating the setups operating at an energy of about 1 kJ and much more above using the methods we have developed.

As is clear from the above, the main result for SIVD-based HF/DF lasers is very promising for further scaling up, and even a few kJ level for the pulsed energy output could be possible. Such a laser can be realized for the low rate P–P mode of operation (15–20 Hz, which is necessary for the applications under consideration)

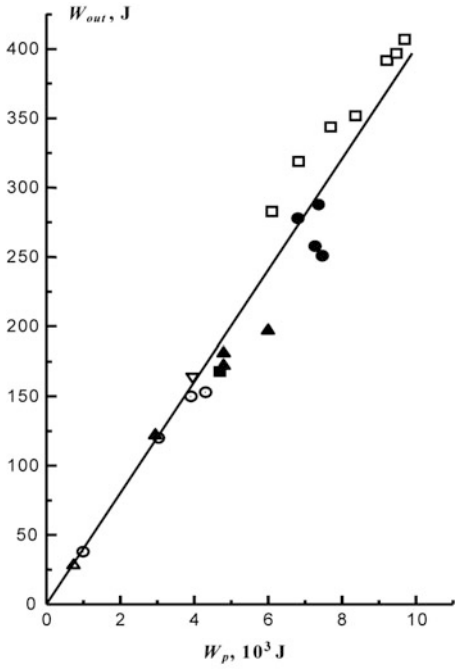

Fig. 51.4 Dependence of the output HF laser energy W_{out} on the energy stored in the generator's capacitors

and cleaning space from debris at the height of up to 400 km. For the telescope with the main mirror, D = 6 m, wavelength of radiation was 3.8 mkm (good for propagation through the atmosphere) and pulses time duration was <1 mks, both of which represent an attainable level of intensity. The total weight of the system can be fixed at the level of few tones. The size of the system looked very reasonable for a movable laser configuration. The main advantage of the system is the non-hazardous nature of components, which means that the usage of such a system could be very much safe and effective.

References

1. V.V. Apollonov, Cent. Eur. J. Phys. **4**, 708 (2003)
2. V.V. Apollonov, S.M. Silnov, *High Power P-P Lasers* (NOVA, New-York, 2014)

Index

A
Absorbing centers, 362
Absorption
  coefficient, 108
  cross section, 290, 292
  properties, 287
  spectra, 117
Accelerating gradient, 379
Acceleration voltage, 4
Activation energy, 339
Active
  media, 12
  medium, 241, 308, 328, 369, 371
  medium gain, 346
  mixture, 344, 347
  volume, 231
Additives, 258
$AgGa_{1-x}In_xSe_2$, 413
$AgGa_{1-x}In_xSe_2$ to $ZnGeP_2$, 418
$AgGaSe_2$, 413, 417, 418
Air breakdown, 367
Aircraft
  engine, 398
  kerosene, 396
Air energy breakdown, 362
Aluminum, 356
Aluminum target, 354
Ammonia
  line, 336
  on platinum, 335
  pressure, 338
Amplification, 308
Amplification coefficient, 368
Amplifier, 319
Amplifier's bandwidth, 383
Amplifying medium, 387
AMT GDL, 397
Anisotropically resistive cathode, 204
Anode-directed waves, 148
Anode layer, 211
Antireflection-coated, 44
Antireflection coating, 370
Aperture edge, 238
Apertures of up to 70 cm, 132
Arkad'ev-Marx, 15, 29
  generator, 36, 83, 98
  voltage, 44
Arkadiev-Marks generator, 277
ASE, 402
ASE suppression, 404
Attaching electrons, 256
Attachment, 105, 132, 192
Attachment of electrons, 192, 210
Attenuation, 315
Attenuators, 423
Auxiliary discharge(s), 58, 64, 80, 158, 167
Avalanche, 271
Avalanche multiplication, 49
Average power, 395, 399

B
Barrier discharge, 65, 70, 74, 76, 99, 126
Barrier discharge plasma, 73, 74
Beam quality, 400
Beam splitter, 301
Bias voltage, 120
Big gaps, 425
Big scale systems, 426
Bipolar signal, 362
Bipole current, 375
Blumlein line, 330
Boltzmann equation, 161
Boltzmann factor, 221
Breakdown, 228, 266
  of the gap, 185
  plasma, 364
  voltage, 36, 262
Brewster angle, 382

© Springer International Publishing Switzerland 2016

V.V. Apollonov, *High-Energy Molecular Lasers*,
Springer Series in Optical Sciences 201, DOI 10.1007/978-3-319-33359-5

Brillouin scattering, 354
Bruce, 271
Buffered SF_6, 288
Buffer gas(es), 288, 290, 292, 294, 295, 349
Burning
  process, 399
  voltage, 136

C
Calorimeter, 361
Capacitance, 239
Cathode-directed
  ionization, 81, 146, 151
  wave, 147
Cathode
  edge(s), 236, 264
  fall layer, 151
  layer, 40
  preionizer, 28
  spot(s), 175, 191, 234, 235, 260, 261, 272, 274
  structure, 46
  surface, 251, 259
Chang, 271
Chang profile, 17, 59, 243
Channel glow, 227
Channel glow intensities, 230
Characteristic current density, 211
Charged particle(s) , 379, 408
Charge kinetics, 203
Charge neutrality, 159
Charging capacitor, 66
Charging voltage, 167
Chemical pumping, 399
Chemical reaction, 179, 247
Cherenkov radiation, 407
Circuit inductance, 261
Circuit oscillation, 169
Cleaning space, 429
Clusterization, 208
CO_2
  discharge units, 390
  laser, 132, 351, 355, 336, 353, 421
    plasma, 357
    radiation, 416
Coefficient for electron attached, 193
Collisional ionization, 40
Collisional quenching, 136
Collision-induced absorption, 290
Compact
  cathode, 124
  cathode system, 125
  electrodes, 127
Composite materials, 401
Compression of the pulse, 386
Computer modelling, 229
Concave mirror, 315
Conducting channel, 192, 224, 426
Continuous operation, 397, 398
Contrast, 308
  enhancement, 290, 294
  ratio, 282, 382
Conventional electric circuit, 75
Cooled structures, 398
Cooling surface area, 402
Copper target, 373
Corona, 66, 233
Cost-effective, 401
Critical field strength, 209
Cryogenically cooled, 395
Crystal length, 416
Cumulation, 365
Current
  density, 230, 244
  density distribution, 239
  filaments, 224
  limitation, 235
  pulse(s), 364, 372
Cylindrical point explosion., 352

D
Damage intensity threshold, 409
Decaying plasma, 203, 205, 210, 211
Decaying SF_6 plasma, 207
Decomposition products, 192
Density distribution, 277
Detachment, 145, 222
Detachment instability, 216, 224
Deuterated carbon, 173
Dibutylamine, 16
Dielectric surface, 191
  discharge, 249
Difference frequency generation, 408, 410, 416
Diffraction gratings, 421
Diffraction-limited value, 127
Diffuse
  channel(s), 175, 184, 191, 194, 227, 228, 234, 249, 251, 252, 259, 264
  glow, 228
  plume, 186
Dimethylamine, 16
Dimethylaniline, 20
Direct ionization, 110
Dirichlet and Neumann, 142
Discharge, 3, 325
  area, 383
  capacitance, 47
  chamber, 174, 383, 389

circuit, 10, 248
circuit inductance, 173
column, 123, 124
contour, 241
contraction, 217
cross section, 16
current, 4, 6, 143, 185, 199, 235, 272, 275, 328, 387
development, 38, 239
electron source, 99
gap, 58, 63, 75, 79–81, 87, 88, 124, 151, 174, 201, 206, 232, 233, 239, 2553, 276, 331, 385
glow, 218
homogeneity, 46, 149
ignition, 102, 141, 164, 217
inductance, 272
instability, 252
plasma, 67, 117, 121, 132, 183, 190, 253, 264, 267, 376
plasma load, 169
ringing, 166
sizes, 246
stability, 115, 120, 121
stabilization, 115
uniformity, 266
voltage, 165, 188, 259
volume, 174, 243, 427
zone, 79, 113
Discrimination, 284
Discrimination ratio, 302
Disk rounded, 251
Dissociation, 192, 193
constant, 192
of SF_6, 194, 426
thresholds, 256
Dissociative
adsorption, 338
attachment, 136, 149
attachment of electrons, 207
attachment reaction, 149
charge exchange, 207
electron attachment, 118
electron-ion recombination, 203
Distortion, 68, 92, 323
Double-pass amplifier, 285
Double-pulse excitation, 161, 168
Drag detector(s), 282, 386
Drift velocity, 121, 193
Dumanchin, 114
Duration of the current, 187
Dynamic profiling, 79, 87, 122, 159, 238, 425
Dynamic profiling phenomenon, 151
Dynamics investigation, 250

E
Earthquake, 394
Easily ionizable, 102
elements, 79
substance, 53
Easily ionized substance, 88
Edge inhomogeneity, 38, 184
Edge nonuniformity, 237, 238, 255
Effective detachers, 132
Effective ionization, 39
Efficiency, 32, 131, 330
Electrical
circuit parameters, 162
efficiency, 157, 166, 169, 264
spark breakdown, 190
Electric
conductivity, 256
discharge, 15, 25, 26, 305, 428
efficiency, 242, 267, 428
energy, 267
Electric field(s), 35, 57, 62, 70, 75, 244, 373, 408
and currents, 377
distribution, 149
enhancement, 245
intensity, 326
strength, 207
Electrode
curvature, 17
profiles, 75
system, 181, 265
Electroionization, 128
devices, 113
systems, 132
Electron
acceleration, 379
attachment, 190, 258
attachment mechanism, 176
avalanche, 147
beam, 3, 9, 43, 48, 128
beam-controlled, 135, 137
concentration, 116, 122, 193
current, 64
density, 61, 89
drift velocity, 145
losses, 22
temperature, 329
Electron-depletion, 89
Electron energy distribution, 101
function, 105
Electron-filled part, 98
Electron flux, 58, 62, 84, 149
current, 67
Electron-impact, 256

Electron-impact (*cont.*)
destruction, 221
detachment, 215, 220, 221, 223, 224, 258
ionization, 219
Electron-ion recombination, 142, 230, 257
Electronegative
components, 105
gases, 209, 239, 243, 246, 249, 255
impurity, 215
molecules, 222
Electronegativity, 176, 222
Electro-optic switches, 300
Electroptic streak camera, 386
Elementary processes, 197
Emergency works, 394
Energy
absorption, 347
consumption, 399
density, 374
deposited, 274
deposition, 68
meter, 301
relaxation length, 212
transfer, 331
Envelope, 313
Equivalent
charging voltage, 161
electric circuits, 200
impedance, 328
Evaporating platinum, 336
Evaporation of graphite, 389
Evolution of SSVD, 232
Excitation circuit, 331
Excitation of the SF_6, 192
Expansion ratio, 397
Explosive-emission, 383

F
Far-field region, 400
Far-infrared, 412
F-atom production, 229
Few kJ level, 428
Fiber laser, 401
Field
distribution, 17
enhancement, 274, 277
measurements, 373
strength, 212
Filling the discharge gap, 97
Fitch generator, 36, 328
Fitch-Howell, 161
Fixed contrast, 308
Flashlamp-pumped, 108
Flashlamps, 90
Formation of inversion, 348
Fourier transformations, 387
Free runnung mode, 369
Fresnel, 414

G
Gain increment, 386
Gap breakdown, 250, 251, 427
Gap conductance, 58
Gas concentration, 192
Gas-discharge, 395
Gas-discharge plasma, 102
Gas-dynamic, 394, 395
Gas-dynamic processes, 346
Gas temperature, 351
Gaussian spatial profile, 303
Ge
Au photodetector, 342
detector, 283
transmission, 382
Generation energy, 242
Glass tube, 251
Glow discharge, 219
Gradually filling, 184
Grating-tuned, 299

H
Half-cycle pulse, 407, 418
Hard X-ray radiation, 353
Heat transmission, 363, 376
Heat transmission efficiency, 377
Helium-free mixtures, 68
Heterogeneous, 335
He-Xe
laser, 342
laser output, 345
mixture, 352
HF/DF-lasers, 395
HF-laser characteristics, 212
HgCdTe-type photoreceiver, 372
High-contrast, 282
High efficiency, 403
High electronegativity, 255
High energy CO_2 laser, 426
High-frequency signals, 376
High-power CO_2 laser, 281
High power GDL, 399
High-power laser, 85
High-power pulses, 305
High pressure, 380
High-pressure CO_2, 384, 385
High-repetition-rate, 404
High-speed camera, 342
High-speed electron-optic, 228

High vacuum pump, 389
High-voltage generator, 329
High-voltage pulse, 28, 179
Homogeneity, 37, 92, 129, 138
Homogeneity of the discharge, 41
Homogeneous, 128
  electric field, 87, 173
  excitation, 137
Hot area, 365
HXR, 357
Hydrocarbons (deuterocarbons), 173, 186, 198, 240, 244, 261, 276

I
Ice-covering, 394
Identical compositions, 342
Ignition, 39
Ignition of the discharge, 140
Illumination, 262, 275
Impact ionization, 210
Impedance matching, 162, 167, 169
Incomplete streamers, 38
Independent triggering, 385
Induced absorption, 291
Inductance, 239
Industrial GDL, 398
Industrial lasers, 405
Industrial powerful lasers, 394
Infrared radiation, 418
Inhomogeneities, 84, 92, 179, 365
Inhomogeneous, 70
Inhomogeneous electric field, 27
Initial diffuse channel, 184
Initial distribution, 70
Initiating
  conductor, 253
  electrode, 185
  wire, 234
Initiation of electrons, 180
Injected power, 318
Injected pulse, 306–308, 368–370
Injection, 282
  mode locking, 299
  window, 312, 315, 316, 387
Instability, 39, 105, 117
Insufficient uniformity, 132
Insulator, 75
Integro-differential equation, 221
Intensive saturation, 313
Interaction, 317
Interelectrode distance, 209
Interelectrode gaps, 155
Intracavity spectroscopy, 117
Intrinsic conductance, 10
Ion-current, 337
Ion density balance, 212
Ion-ion recombination, 204, 206, 208, 229, 256, 257
Ion-ion recombination coefficient, 204, 212
Ionizable
  additives, 11
  organic additive, 142
  substance, 44, 48, 54, 77, 91, 98, 103
Ionization, 116
  and attachment, 221
  coefficient, 191, 192, 199
  flux, 107
  instability, 215, 222, 224
  of hydrocarbons, 235
  potentials, 54
  processes, 65, 76, 84
  sources, 49
  wave(s), 149
Ionized substance(s), 20, 22, 26
Ion mobility, 145, 209
Ion-source chamber, 337
IR and FIR spectral ranges, 421
Irradiation in vacuum, 364
Isolated conductors, 251

K
Kerosene, 397
Kirchoff's equation, 143

L
Lagrangian interpolator, 161
Lamberton-Pearson system, 93
Langevin approximation, 209
Large active volumes, 114, 239
Large-aperture(s), 54, 83, 122, 278
Large-aperture systems, 152
Large-volume devices, 155
Large volumes, 242, 271
Laser
  beams application, 394
  emission, 344
  generation energy, 385
  pulses, 374
  radiation, 377
Laser-matter interaction, 384
Lasing, 346
Lasing region, 347
Launching small satellites, 405
Leading and rear edges, 184
Leading edge, 309, 321, 322, 387, 423
Lens telescope, 319, 322
Level population, 108
Limitation of the current, 194

Livermore (USA), 404
Local heating, 339
Lo-current beam, 135
Longitudinal mode beats, 422
Long pulse, 313
Long resonator, 309
Low-current spark, 181, 262
Low-energy electron beam, 151
Lower ionization potential, 47
Low-inductance capacitors, 48
Low-ionization additive, 315
Low-lying laser level, 131
Low signal gain, 368
Low threshold, 356
Low-toxica, 396
Luminosity, 250

M
Magnetic compression, 330
Magnetic field, 113
Marks generator, 240
Marx, 161
Marx pulse generator, 4
Mass spectrometer, 337
Mass-spectrometric measurements, 207
Master oscillator, 320, 322
Maximum efficiency, 416
Maximum intensity, 347
Measurement accuracy, 316
Measuring circuit, 205
Mechanisms
  of limiting the current, 228
  preventing, 184
  restricting, 190
Mesh anode, 272
Metallic target, 377
Metastable kinetics, 164
Metastable N_2, 150
Micromachining, 401
Microsecond pulse, 359
Mining equipment, 394
Mirror reflection, 47
Mixture composition, 115
Mixture renovation, 396
Mobile, 394
Mobility and recombination, 208
Mode-locked, 288
Mode-locked train, 285
Mode-locking, 294, 388
Modulated transmission, 305
Molecular gases, 30
Mono-module disk, 400
Monopulse, 372
Monte Carlo method, 204
Multi-channel, 385
Multistage ionization, 107
Multistep-ionization instability, 151
Mylar attenuators, 289

N
N_2O
  device lasing, 131
  electron-beam-controlled, 135
  laser, 132
  molecule, 389
Nanosecond CO_2, 305
Nanosecond pulse(s), 281, 293–295, 312, 360, 372
  train(s), 315, 360, 364
  transmission, 293
Nanosecond train, 377
Near-cathode zone, 121
Near-Earth space, 404
Near-electrode layers, 210
Needle-plane geometry, 218
Negative
  bias, 58
  charge, 62
  ions, 60, 206, 208, 210, 223, 229, 257
  space charge, 46, 50, 84
Neumann boundary condition, 144
Neutral gas, 109
Nitrogen lasers, 325
Noise suppressors, 398
Nonchain, 247
  chemical lasers, 244
  HF (DF), 194, 231, 426
Non-hazardous nature, 429
Noninertial current, 376
Nonlinear absorber, 373
Non-self-sustained microwave discharge, 107
Non-SSVD, 3
Northrop Grumman Corporation, 403
Nozzle array, 399
Nozzle unit, 397
Number of passes, 307
Number of spots, 184
Numerical calculation, 311
Numerical optimization, 372

O
Optical
  breakdown, 319, 341, 350, 351, 367
  breakdown plasma, 351
  detonation, 343, 346
  pulse, 371
Ordinary and extraordinary waves, 414
Organic additives, 385

Organic-free mixture, 385
Oscillator, 301
Oscilloscope, 321
Oscilloscope traces, 375
Output
  coupler, 300
  energy, 32, 128
  power, 342
Overheating-ionization, 104
Overlapping the channels, 274
Overvoltage, 68
Oxygen delta production, 395
Oxygen-iodine laser, 395

P

Peaking capacitance, 11
Peaking capacitor, 330
Peak power, 315
Penning
  collisions, 159
  discharge, 9
  ionization, 21, 45, 53, 55, 104, 115, 144, 147, 151
  process, 21, 140, 198
  reactions, 139
Phase, 233
Phase distortion, 295
Phase-matching, 415, 423
  angle, 422
Photoelectric effect, 278
Photoelectron density, 74, 88
Photoelectrons, 22
Photo initiation, 263
Photoionization, 63, 64, 73
Photoionization processes, 119
Photon-drag detector, 361, 382
Photoplasma, 89
Photo triggered discharge, 263
Physical efficiency, 176
Picosecond and femtosecond pulses, 411, 418
Picosecond laser(s), 379, 381
Picosecond pulse, 381
Pipe-like beam, 359
Planar anode, 59
Planar layer, 210
Plane electrode(s), 248
Plane electrode system, 183, 187
Plasma
  channels, 219
  cooling, 346
  formation, 374
  homogeneity, 167
  jet luminescence, 343
  laser power, 343
  parameters, 353
  resistance, 4, 266
Plasma-target, 367
Pockels cells, 371
Poisson's equation, 38, 142
Polarisation limit, 209
Polished anode, 232
Polyatomic molecular, 295
Polyethylene attenuators, 360
Polyethylene-insulated copper wire, 216
Population, 109, 116, 118, 131
Population inversion, 349
Positive ions, 229
Postpulses, 303
Potential drop, 211
Powerful high energy laser, 394
Powerful lasers, 393
Power of 1 MW, 404
P–P regime, 403
Prebreakdown currents, 175
Prefilling, 128
Preionization, 26, 27, 29, 92, 114, 128, 177, 180, 232, 272
  and ignition, 150
  discharge, 10
  phase, 141, 164
  process, 160
Preionizer, 28
Preliminary
  bias, 59, 62
  filling, 70, 92, 140, 155
  ionization, 50
Pressure broadening, 388
Primary electrons, 57, 248
Pulse
  compression, 330
  forming network, 158
  generator, 50, 325
  injection, 384
  repetition frequency, 338
  train, 311, 386
  transmission, 283
  voltage generator, 4
Pulse-periodic, 265
Pulse-periodic regime, 262
Pulse-selection, 299, 303
Pump diode, 400
Pumping
  active media, 349
  conditions, 127
  regime, 328
Pump pulse, 370
Pure resistances, 258
Pyroelectric detector, 175

Q
Quality of the laser, 236
Quartz bulb, 232
Quasi-dc bias, 156, 164
Quasi-equilibrium conditions., 148
Quasi-periodic current, 223
Quasi-periodic structures, 223
Quasi-stationary
  approximation, 212
  phase, 198, 212, 259
  SSVD, 216
  value, 252
  voltage, 201
Quasisteady, 233
Quasisteady phase, 175
Quasisteady-state, 183
Quasisteady-state phase, 19
Quiescent period, 169

R
Radiation
  energy, 6, 88, 249, 265–267, 312, 327, 328, 385
  energy distribution, 32
  intensity, 39
  pulse power, 247
Rate-of-attachment, 239
RD-33, 397
Readily ionized substance(s), 23, 30
Recirculating-flow, 147
Recombination, 208
  coefficient, 212
  kinetics, 209
  plasma, 209
  processes, 256
Reflection from plasma, 364
Regenerative amplification, 317, 377
Regenerative amplifier(s), 311, 320–322, 371
Removal of debris, 404
Repetitively pulsed regimes, 180
Residual voltage amplitude, 166
Resistance, 66
Resistive losses, 199
Resonance frequency, 373
Resonator, 403
Resonator mirrors, 109
Restriction mechanisms, 244
Rise-time pulse, 169
Rod-plane electrode system, 188
Rod-plane geometry, 253
Rogovski coils, 233
Rogowskii, 271
Rogowski loops, 198
Rogowski profile, 43
Rotational relaxation, 291
Round trips, 387
Runge-Kutta algorithm, 144

S
Sandblasted, 180
Sandblasting, 232, 240
Sand jet, 173
Sand-jet scouring, 174
Saturable absorber(s), 284, 287, 306
Saturated amplification regime, 388
Saturation, 66, 85
Saturation level, 386
Scalability, 114, 128
Scaling, 244
Scaling characteristics, 240
Screened by a space charge, 79
Screened by electrons, 98
Screening, 98
  conditions, 70
  of the cathode, 75
Secondary discharge plasma, 80
Secondary electrons, 256
Second-harmonic generation, 413
Sectioned cathode, 181
Selection technique, 281
Self-organization, 223
Self-radiation, 368
Self-sustained equilibrium, 145
Semiconductor-based technologies, 401
Semiconductor plates, 382
Separate channel, 194
SF_6 dissociation, 257
SF_6-hydrocarbon, 197
SF_6-hydrocarbon mixtures, 426
Shaped electrodes, 126
Sharp edges, 182
Shock wave, 217, 352
Shunting a capacitor, 205
Significant overlap, 388
Simultaneous cathode, 148
Single axial mode, 360
Single-discharge unit, 115
Single-frequency radiation, 322
Single-pulse excitation, 163, 169
Single-spiking generation, 357
SIVD, 180, 185, 227, 425
SIVD dynamics, 227
Slowly rising voltage pulse, 167
Small-curvature electrodes, 17
Small-scale inhomogeneities, 62
Small-signal gain, 60, 62, 77, 81, 91, 99, 125
Small-signal transmission, 303
Smooth gain spectrum, 389

Soft x-ray radiation, 243
Soft x-rays, 57, 271
Solid state lasers, 402
Source of X-ray, 383
Space charge, 80, 125
Space-charge layer, 157
Space-charge screening, 140, 141
Spark breakdown, 102
Spark channel, 103
Spark channel length, 115
Spark gap(s), 241, 384
Spark illumination, 228
Spark source(s), 80, 234
Spatial separation, 347
Spatial-temporal evolution, 232
Spatio-temporal evolution, 147
Specially profiling, 248
Specific
  deposited energy, 12
  energy, 6, 190
  input, 30
  input energy, 51, 100, 186
  output, 44, 48
  output energies, 31
Spectrometer Epsilon, 414
Spherical mirrors, 320
Spots on the cathode, 183
SSVD, 9, 30, 35, 38, 40, 49, 67, 91
  current, 109
  formation, 425
  in N_2O mixtures, 389
  instability, 220
  stability, 152, 235, 380
Stability, 110, 261, 265
Stabilization, 277
Stable
  discharge(s), 116, 118
  ignition, 56
  time delay, 232
Static breakdown, 80
Stationary conditions, 396
Steady-state, 62
Steady-state discharge, 130
Stimulated decomposition, 338
Stimulates desorption, 339
Stored energy, 169, 255
Strong
  electronegativity, 245
  gas heating, 216
  quenching, 150
Strongly inhomogeneous, 425
Sublimation, 400
Submillimeter range, 409
Subnanosecond laser pulses, 390
Substantially, 145
Subtraction, 421
Super-long conducting channels, 405
Surface-discharge, 26, 98, 165
Surface-discharge plasma, 169
Surface profile, 97
Synchronization unit, 423

T
Tail, 383
Target alignment, 303
Target in vacuum, 364
Temporal expanding, 386
Temporal structure, 288
Tens of nanoseconds, 354
Terahertz pulse, 408
Threshold value, 388
Time resolution, 375
Toluene, 397
Toxic exhaust, 395
Train, 306
Train of pulses, 322
Translational relaxation time, 109
Transmission, 293, 302
  measurements, 289
  switch(ing), 284, 299
Transport coefficients, 212
Transverse discharge, 41
Transverse mode, 312, 368
Trapping coefficient, 60
Triethylamine, 16, 84, 93, 103, 118
Tri-*n*-propylamine, 20
Tri-*n*-propylamine and triethylamine, 21
Tripropylamine, 63
Tripropylamine and triethylamine, 45, 60, 74
TRUMPF Group, 402
Tungsten, 356
Two CO_2 lasers, 421

U
Ultrashort laser pulses, 407
Ultraviolet, 341
  illumination, 49
  radiation, 21, 25, 35, 43, 53, 57, 89, 102, 352
  radiation source, 89
Ultraviolet-preionized, 320
Uncontracted confined SIVD, 188
Uniform
  discharge, 266
  electric field, 114
  energy deposition, 246
  excitation, 380
  fields, 124

preionization, 139
SSVD, 265
Uniformity, 248, 258
Unilateral illumination, 30
Unprofiled electrodes, 152
Unstable resonator(s), 283, 301
Unstable telescopic resonator, 262, 381
Upper edge, 181
UV illumination, 274, 278
UV radiation, 325

V
Vacuum, 362
Vacuum chamber, 354
Very-large-aperture, 155
Vibrationally excited, 194, 257
SF_6, 192
SF_6 molecules, 194
Visible homogeneity, 50
Voltage, 58
and the current of the SSVD, 200
oscillograms, 244
pulse generators, 15
rise time, 36, 39
Volume discharge, 59, 126, 140, 190, 247
VUV preionization, 144, 146

W
Wave half-cycle, 411
Weak-current electron beam, 130
Welding, 394
Wide-aperture, 227, 380
Wide-aperture nonchain, 177
Winding inductance, 331
Without preionization, 242
With repetition rate $\sim$60 Hz, 390
Working mixture(s), 261, 237, 276

X
X-ray
lasers, 341
preionization, 271, 381
radiation, 354–356

Z
$ZnGeP_2$, 409, 418